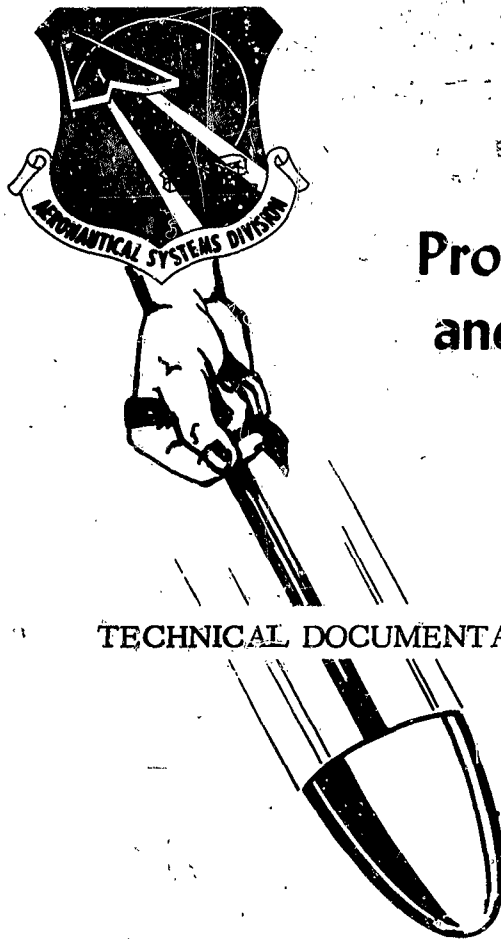


63-4-2

CATALOGED BY DDC
408 772
AS AD No. _____

408 772

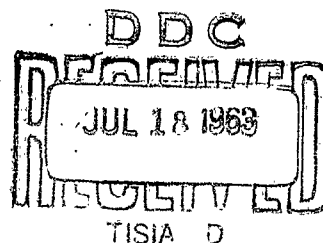


Proceedings of Retardation and Recovery Symposium

TECHNICAL DOCUMENTARY REPORT NO. ASD-TDR-63-329

May 1963

Flight Accessories Laboratory
Aeronautical Systems Division
Air Force Systems Command
Wright-Patterson Air Force Base, Ohio



NOTICES

When Government drawings, specifications, or other data are used for any purpose other than in connection with a definitely related Government procurement operation, the United States Government thereby incurs no responsibility nor any obligation whatsoever; and the fact that the Government may have formulated, furnished, or in any way supplied the said drawings, specifications, or other data, is not to be regarded by implication or otherwise as in any manner licensing the holder or any other person or corporation, or conveying any rights or permission to manufacture, use, or sell any patented invention that may in any way be related thereto.

Qualified requesters may obtain copies of this report from the Armed Services Technical Information Agency, (ASTIA), Arlington Hall Station, Arlington 12, Virginia.

This report has been released to the Office of Technical Services, U.S. Department of Commerce, Washington 25, D.C., in stock quantities for sale to the general public.

Copies of this report should not be returned to the Aeronautical Systems Division unless return is required by security considerations, contractual obligations, or notice on a specific document.

FOREWORD

The Retardation and Recovery Symposium held at the Imperial House Motel, Dayton, Ohio, 13 - 14 November 1962, was sponsored by the Flight Accessories Laboratory, Aeronautical Systems Division. The Retardation and Recovery Branch initiated, organized and conducted the symposium. Mr. P. R. Murray, Technical Director of the Aeronautical Systems Division, served as Chairman and Lieutenant Colonel L. E. Winebrenner, Chief of the Flight Accessories Laboratory, as Deputy Chairman.

Acknowledgement is made on behalf of the Flight Accessories Laboratory to Brigadier General F. J. Ascani, Deputy Commander, B-70, for his support of the symposium and his welcoming address, and to the Session Chairmen and the Speakers for their presentations and contributions to this report. We also thank the many organizations who contributed directly or indirectly to the overall success of the symposium.

ADDRESSES OF SESSION CHAIRMEN AND SPEAKERS

MR. R. J. BERNDT
Chief, Advanced Technology Sec.
Aeronautical Systems Division

MR. M. L. BUCK
Chief, Hypersonic Flight Section
Aeronautical Systems Division

MR. J. K. BUCKNER
General Dynamics Corporation
P. O. Box 748
Fort Worth 1, Texas

MR. G. CHERNOWITZ
American Power Jet Co.
705 Grand Avenue
Ridgefield, N. J.

MR. R. C. FREDETTE
Hayes International Corporation
Birmingham, Alabama

MR. A. M. HEGELE
Chief, Parachute Branch
Aeronautical Systems Division

DR. H. G. HEINRICH
University of Minnesota
Institute of Technology
Department of Aeronautical Eng.
Minneapolis 14, Minnesota

MR. S. K. IBRAHIM
University of Minnesota
Institute of Technology
Department of Aeronautical Eng.
Minneapolis 14, Minnesota

MR. E. G. JOHNSON
Chief, Fluid Dynamics Facilities Br.
Aeronautical Systems Division

MR. T. W. KNACKE
Northrop Ventura
8000 Woodley Avenue
Paradynamics Section
Van Nuys, California

MR. S. R. METRES
Chief, Application Criteria Sec.
Aeronautical Systems Division

LT. COL. J. E. MURRAY
Hq. USAF(AFRDP)
Washington, D. C.

DR. J. N. NIELSEN
Vidya, Inc.
2626 Hanover Street
Palo Alto, California

MR. F. M. ROGALLO
NASA - Langley Research Ctr.
Langley AFB, Va.

MR. P. H. ROSE
AVCO-Everett Research Lab.
2385 Revere Beach Parkway
Everett 49, Mass.

MR. J. H. ROSS
Fibrous Materials Branch
Aeronautical Systems Division

DR. A. J. SHINE
Air Force Institute of Technology
Head/Mechanical Engineering Dept.
Wright-Patterson AFB, Ohio

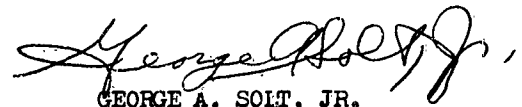
MR. G. A. SOLT, JR.
Chief, Retardation & Recovery Br.
Aeronautical Systems Division

ABSTRACT

This report contains the proceedings of the Retardation and Recovery Symposium sponsored by the Aeronautical Systems Division on 13 and 14 November 1962. The Introductory Session was opened with the Keynote Address which reviewed the use and applications of deployable aerodynamic decelerators throughout the past fifty (50) years and noted the areas in which additional work had to be accomplished. The four Technical Sessions deal with the latest significant developments in the retardation and recovery area. The Technical Sessions begin with presentations and discussions of investigations in the hypersonic and supersonic flight regimes followed by a technical analysis of transonic and supersonic flow phenomena. In addition, new aerodynamic decelerator designs and discussion of the wind tunnel tests pertaining to these designs, as well as overall reliability of recovery systems, are presented. The final Technical Session concludes with a discussion of the military, scientific, and general objectives for decelerators intended for future use.

PUBLICATION REVIEW

This report has been reviewed and is approved:



GEORGE A. SOLT, JR.
Chief, Retardation and
Recovery Branch
Flight Accessories Laboratory

TABLE OF CONTENTS

| | Page |
|--|------|
| GENERAL SESSION I | |
| OPENING REMARKS Peter R. Murray | 1 |
| WELCOME ADDRESS Brig. Gen. F. J. Ascani | 3 |
| KEYNOTE ADDRESS Warren P. Shepardson and George A. Solt, Jr. | 6 |
| TECHNICAL SESSION I: HYPERSONIC SESSION | 13 |
| HEATING PROBLEM FOR SUPERSATELLITE RE-ENTRY Peter H. Rose | 14 |
| HYPERVELOCITY RE-ENTRY CONFIGURATIONS Alfred C. Draper and Melvin L. Buck | 34 |
| HYPERSONIC DRAG DEVICES Solomon R. Metres and Stanley McFarland | 86 |
| TECHNICAL SESSION II: SUPERSONIC SESSION | 111 |
| SUPERSONIC PARACHUTE RESEARCH Rudi J. Barrett and Charles A. Babish, III | 112 |
| APPLICATION OF AXISYMMETRIC FLOW ANALYSIS TO IN- FLATION STABILITY OF SUPERSONIC FLEXIBLE PARACHUTES J. K. Buckner | 158 |
| ROGALLO WING F. M. Rogallo | 194 |
| HIGH TEMPERATURE FIBROUS MATERIAL Jack H. Ross | 215 |
| TECHNICAL SESSION III: DECELERATOR INVESTIGATIONS SESSION | 234 |
| VELOCITY AND PRESSURE DISTRIBUTION IN THE TRANSONIC AND SUPERSONIC WAKE Dr. H. G. Heinrich | 235 |

| | Page |
|--|------|
| RELIABILITY OF RECOVERY SYSTEMS G. Chernowitz | 280 |
| WATER SURFACE WAVE ANALOGY S. K. Ibrehim | 316 |
| PARAVULCOON RECOVERY AND LANDING SYSTEM A. J. Oberg, S. S. Sopczak and M. A. Sutton | 368 |
| TECHNICAL SESSION IV: GENERAL CONSIDERATIONS SESSION | 417 |
| SYSTEMS CONSIDERATION T. W. Knacke | 418 |
| NEW PARACHUTE DEVELOPMENT ASPECTS A. M. Hegele, C. E. Carroll and H. Engel, Jr. | 442 |
| TECHNICAL AREA OUTLOOK George A. Solt, Jr. | 461 |
| GENERAL SESSION II | |
| CLOSING REMARKS L. H. Hildebrandt | 471 |
| QUESTION AND ANSWER PERIOD - HYPERSONIC SESSION | 472 |
| - SUPERSONIC SESSION | 479 |
| - DECELERATOR INVESTI- GATIONS SESSION | 489 |
| - GENERAL CONSIDERATIONS SESSION | 491 |
| APPENDIX - LIST OF ATTENDEES | 494 |

| | Page |
|--|------|
| RELIABILITY OF RECOVERY SYSTEMS G. Chernowitz | 280 |
| WATER SURFACE WAVE ANALOGY S. K. Ibrahim | 316 |
| PARAVULCOON RECOVERY AND LANDING SYSTEM A. J. Oberg, S. S. Sopczak and M. A. Sutton | 368 |
| TECHNICAL SESSION IV: GENERAL CONSIDERATIONS SESSION | 417 |
| SYSTEMS CONSIDERATION T. W. Knacke | 418 |
| NEW PARACHUTE DEVELOPMENT ASPECTS A. M. Hegele, C. E. Carroll and H. Engel, Jr. | 442 |
| TECHNICAL AREA OUTLOOK George A. Solt, Jr. | 461 |
| GENERAL SESSION II | |
| CLOSING REMARKS L. H. Hildebrandt | 471 |
| QUESTION AND ANSWER PERIOD - HYPERSONIC SESSION | 472 |
| - SUPERSONIC SESSION | 479 |
| - DECELERATOR INVESTI- GATIONS SESSION | 489 |
| - GENERAL CONSIDERATIONS SESSION | 491 |
| APPENDIX - LIST OF ATTENDEES | 494 |

OPENING REMARKS

by

MR. PETER R. MURRAY
Technical Director
Deputy for Technology
Aeronautical Systems Division

—Lady and gentlemen, I would like to point out that I heard, at breakfast this morning, a comment which I thought most appropriate. Somebody said it's about time retardation and recovery did stand on its own feet and have its own symposium, and I heartily agree with this. I'd like to point out that my barber led me into this feeling. The other day I was talking about space. He knows very little about it, but I queried him on whether he would like to go to the moon or not, when the Apollo gets up there. Instead of giving me the idiot treatment about not going -- or going to the moon, it didn't bother him a bit. In fact, I got the feeling that he would go but what was bugging him was the return trip. In other words, if you could give him a guarantee that he could get back, you could very easily talk him into going. Now, when you hear all the things about the Mercury coming in and everything, you always get that sigh of relief from the Astronauts as they see their parachute come out. Gentlemen, I think you're on the verge of a space age discovery in retardation and recovery. If it just weren't for that name. If you could get across in the next symposium, wherever it's held, that we are having a symposium known as the "Bring 'em Back Alive Symposium", I think you'd have it hacked and the place would be filled to overflowing with people very keen on this fact. They sympathize with getting people back alive.

The barber story also reminds me of the fact that the meeting has some very excellent papers and the scope is outstanding. This reminds me of the story of the barber in Wichita, and he was a lousy barber. He -- In fact, they were about to run him out of town when the state decided that barbers had to be licensed. Now, the people that patronized this particular barber knew this was going to do it. This fellow could never hack the course; he just plain couldn't do it, so they shipped him off to Kansas City to get a license, knowing full well that he would never return to set up shop. He just wasn't going to make it. Believe it or not, gentlemen, he did get back to Wichita and he did open up his shop.

Well, they drew straws to see who was going to take his life in his hands to get a shave and to find out how this guy did it. The guy walked in and got in the chair and said, "Well, I see you're back."

"Yes."

He said, "Did you take the exam?"

"Sure did."

"Did you pass it?"

"See my license up there on the wall?"

"Well, for old time's sake, would you tell me how you did it?"

And the guy said, "Well, I'll tell you. The shaving part, it was pretty tough; I got 50%, but I got 100% on blood stoppage."

Now, I know that in this particular series of papers there are more papers associated with the shaving part of this retardation and recovery than there is on blood stoppage, and I think this is the mark of success of any symposium.

Now, a little bit of commercial, and commercial I'd like to point out that there is going to be a lot of material presented here, some of it quite new to everybody, and that the responsibility for this particular material is certainly that of the presenter and company representative when it comes to classification, security, and so forth, since this is an unclassified symposium. And, finally, you all know that everybody in the Air Force, the Army and the Navy, NASA and everywhere wears several hats. In fact, historians looking back to the 60's will determine that this was the decade of the two-hat or four-hat management. You just can't be anybody now unless you wear almost a revolving hat. At this time, I want to introduce to you for the welcome, a gentleman who is the acme at ASD in wearing multiple hats. He is the Vice Commander of the Aeronautical Systems Division, and in his spare time serves as Deputy Commander for the RS-70 program. General Fred J. Ascani.

WELCOME ADDRESS

by

BRIG. GEN. F. J. ASCANI
Deputy Commander/B-70
Aeronautical Systems Division

Thank you, Pete. You forgot to mention another one we work on in our spare time that has to do with reorganization.

I am quite impressed with the group that has shown up this morning, and before I read some prepared comments here which I think are appropriate to the symposium, I would like to express my personal interest in the specific area of retardation and recovery. Going back several years, it became quite evident to a good number of us that a good amount of operations in space were completely meaningless unless we devised reliable systems for getting capsules, manned or unmanned, back within the atmosphere and have them recovered at a suitable location. I think we all marveled at the early successes of the Soviets. It is obvious that they devoted a great deal of time and effort to this specific phase of overall space operations. I certainly don't mean to imply that we did not, but it would appear to me that a great deal more emphasis should have been placed on this portion of the overall effort than actually was, because there is a tremendous amount of room for new techniques and new methods of successfully recovering, retarding and recovering any type of space capsule that we may employ. So, I feel that all of you gentlemen that work in this area and are dedicating your efforts in this particular phase really represent quite a key operation in the overall success of our space effort.

Now, it is obvious, in going from there to what the nature of this symposium is, that we are all interested, naturally, in the security of our nation, and the security of our nation is not necessarily governed by any one area of activity. It is the result of many things - military, economic, political, as well as the moral fiber of the people involved. It is with the feeling that each of us is a member of this team, responsible for our national security, that I take great pleasure in welcoming you to this symposium. Today, our national security is dependent on many operational systems in being - the B-52, B-58 and so forth. Tomorrow's security is

obviously going to be greatly dependent on operational systems which result from the scientific advancements of today. In order to advance, we obviously have to shed the blinders of the horse and carriage era and replace them with peripheral vision in order to insure a greater number of revolutionary rather than evolutionary strides in scientific knowledge, particularly in this technical area. These advancements in technology must take place so that we, as free people, may operate the aerospace vehicles of tomorrow with the confidence that our equipment is beyond any doubt the most effective and reliable available. Although the individual human mind, in many cases, will enhance the equipment's capability, he is limited by the equipment with which he has to operate. In other words, at the present time, we couldn't expect the Mercury Astronauts to land their vehicle on a pre-selected landing strip. The knowledge and talents to make these future systems a reality are enormous. There are many technical disciplines involved - flight dynamics, propulsion, aeromedical, guidance and control, all interrelated, and all of these constitute a major part of this technology. There are other smaller technical areas, however, very important ones, such as retardation and recovery, which we are here to discuss today, and these obviously form very important supplements to the major areas.

In order to realize our maximum capability, we must take advantage of each technical area to enhance the overall system performance. The three R's of the space age might well be "Recoverable, Re-usable, and Reliable", so that in terms of the thrifty buyer, the Government, we may obtain maximum dollar value. Therefore, as the military sphere of influence extends itself into the space age, the systems of tomorrow will be evaluated on performance and capability, of course, but also on the economy of overall operation. The concepts of retardation and recovery will increase in importance as a military space requirement is formulated, and the influence of these concepts on the economy is recognized by all responsible people. The application of a recovery concept to any mission requirement may take many forms, from the basic ballistic type shapes with associated recovery hardware and aerodynamic decelerators to the lifting vehicle.

The necessity for recovery in its broadest interpretation, from sea level to outer space, requires the knowledge of many technical disciplines. However, it is not the aim of this symposium to review the entire recovery field, but to present some of the retardation and recovery concepts and the allied research efforts. In familiarizing you with these programs, we are fostering the generation, we hope, of new and bold concepts

resulting from your combined technical talents. Again, it is my pleasure to welcome you to this Aeronautical Systems Division symposium. We have with us today distinguished speakers representing Government, industry and educational institutions.

Now, our keynote speaker was to have been Mr. Warren Shepardson, Chief of the Crew Equipment Division of the Aeronautical Systems Division. However, he is home ill with the flu, and, in my opinion, we have a real fine substitute, Mr. George A. Solt, who is Chief of the Retardation and Recovery Branch of the Flight Accessories Laboratory. Mr. Solt has had extensive experience in this area and is probably one of the most articulate disciples in this technical area designated 720F.

KEYNOTE ADDRESS

PROGRESS IN AERODYNAMIC DECELERATOR
RESEARCH AND DEVELOPMENT

by

MR. W. P. SHEPARDSON
Chief, Crew Equipment Division
Aeronautical Systems Division

INTRODUCTION TO KEYNOTE ADDRESS AS PRESENTED BY

MR. G. A. SOLT, JR.
Chief, Retardation & Recovery Branch
Aeronautical Systems Division

Thank you, General Ascani. Gentlemen, as dedicated as Mr. Shepardson is to his work and to the retardation and recovery area, I know that he is greatly disappointed that he couldn't be here with us today. I am going to give his paper for him. I know I can't do the justice that he could. I know most of us know Mr. Shepardson, "Shep" as most of us know him, and we know he has been dedicated throughout the years since 1931 in work directly or indirectly associated with parachutes. As such, I feel humble in the fact that I can give his paper, although I certainly wish he were with us this morning.

In this talk, I plan to define deployable aerodynamic decelerators as the technical area is presently titled, since this is the subject of the majority of papers being presented at this Symposium. I then plan to give a brief description of significant events in the development and use in this country of the most common such decelerator, the parachute. I then plan to close with some personal observations on work in this area that I feel still needs to be accomplished on an urgent basis.

A deployable aerodynamic decelerator is a collapsible or foldable device which can be stowed in or on a body in flight so that it will be capable of being deployed from the body to its operating shape to increase the drag of the body thus achieving a preplanned effect such as retardation, stabilization, trajectory control or recovery. Some examples of such decelerators are parachutes, balloons and rotors.

In the United States, parachutes were used in exhibition jumps from balloons as early as the late 18th century and this continued to be practically their only use until World War I. During the early days of that war, both the Allies and Germany quickly learned that observation balloons could be easily destroyed by enemy planes. As a consequence, these balloons were soon equipped with parachutes so the observers could escape when this happened. When it entered the war, the United States similarly equipped balloons with parachutes.

Although exhibition parachute jumps had been made from planes as early as 1912, apparently no serious thought was given to their use in planes as a life-saving device until the Germans and Austrians started using them rather widely during the war, the first known use being in 1916. Shortly after our entry into the war, the pleas of General Mitchell, Commander of U. S. Air Forces in Europe, for parachutes for his men resulted in the establishment in early 1918 at McCook Field, Dayton, Ohio, of an organization to develop such a parachute.

The McCook group tested all types of parachutes then available and ultimately decided that the attach types used with balloons were unsuitable for use from aircraft and that most were too weak. Their efforts were then concentrated on what was called a free type or manually operated type worn on the man and on increasing the strength. The original parachute they developed was a back type with a flat circular canopy made with silk cloth and lines. It was first jumped by Leslie Irving at McCook Field on 28 April 1919. Additional jumps by members of the McCook development group led to the standardization of this parachute for the Air Corps and in June 1919, parachutes were ordered to equip the Air Corps. The first emergency use of this parachute by an Air Corps pilot was that of Lt. Harris in October 1922.

During the early 1920's, evaluation of design improvements was continued to improve the performance and reliability of the parachute. These efforts resulted in the award of the Collier Trophy to Major E. L. Hoffman in 1926 for his leadership and guidance of these efforts.

From the mid-twenties until 1940, development efforts by both government and industry involved further improvement of all personnel parachute components and the commercial development and sale of a variety of canopies, pack and harnesses. Back, seat and chest type parachutes, both attached and attachable were available with canopies of silk or pongee. For private planes, parachutes were even built into the seats with harnesses designed for quick donning in an emergency. Quick-release harnesses were also designed to facilitate removal after landing in water or on land. In the Air Corps, a change to the seat type parachute was made for most applications. A triangular shaped canopy with a new design of pack and harness was standardized in 1934 and remained standard until 1937 when the flat circular canopy was restandardized due to its greater strength, reliability and simplicity of manufacture. During this period also, parachutes were developed for illuminating shells and flares and also used to a limited extent for cargo delivery.

In 1940, following the example of the Russians and later the Germans, the U. S. Army established its first paratroop training program at Ft. Benning, Ga. The first troop parachute was a static line deployed flat circular 28' diameter canopy.

Our entry into World War II accelerated the development and use of parachutes for many purposes. Rayon and nylon parachutes were developed in a variety of sizes and colors for cargo delivery. All personnel parachutes were converted from silk to nylon and back and attachable chest types came into common usage. Clustering of cargo parachutes for delivery of heavier cargo items was developed. A technique was developed to air deliver an amphibious vehicle for the invasion of Norway and a similar technique was used to air deliver a rescue boat to survivors in the water. For the delivery of munitions, parachutes were developed for fragmentation bombs, sea mines and high explosive bombs for low altitude delivery. Gliders were fitted with a parachute for faster descent after separation from the towing aircraft. In general, none of these applications involved significant advancements in the state-of-the-art. In general, the loads to be decelerated or recovered did not exceed 3000 lbs. and the speed at which parachutes were deployed did not exceed 300 knots in the extreme cases.

At the end of the war in Europe, in recognition of advances made by the Germans in parachute development, the Air Corps initiated action to bring a team of parachute development personnel to Wright Field under Project Paper-Clip. As a result of these efforts, a team of seven men who had worked together at the Graf Zeppelin Institute at Stuttgart were assigned to the Parachute Branch at Wright Field early in 1946.

The first task assigned to this group was the preparation of reports on the various uses to which FIST ribbon parachutes and guide surface parachutes had been put in Germany and also on the design information and details which had been derived. They were also used as consultants on a number of missile recovery tasks which arose as a result of our missile development programs and the upper air research programs being carried out using Aerobee sounding rockets and captured V-2 rockets. A constantly recurring problem in connection with these recovery tasks was the lack of proper space for a recovery system primarily due to the fact that recovery had never been intended until after failures occurred during development flights. In many instances, these failures could not be explained due to complete destruction of the missiles and inadequate or inoperative instrumentation on board the missiles. It was only after such failures that the need for a recovery system was recognized and then the need was immediate.

In an effort to alleviate at least a portion of this problem, a joint program was established between the Navy Bureau of Aeronautics and the Parachute Branch at Wright Field that the Navy undertake, on contract, a study of subsonic recovery concepts while the Air Corps would undertake a similar program for recovery in the transonic and supersonic regime. The Air Corps agreed to prepare and publish a Parachute Handbook which would include as much design detail on parachutes for all types of applications as was known at that time with supplemental data on test equipment and methods, instrumentation, accessory and control devices, etc. This Handbook was written completely in-house with major input from the German specialists. The original edition was published in 1947. This Handbook and succeeding editions have been widely used and is currently distributed in about one thousand copies for each revision. It is probably the most widely referenced parachute publication in the United States today.

In my opinion, this Handbook has been the most significant accomplishment in the area of parachute development and use in this country.

Other developments in 1947 were the design and installation of a brake parachute in the B-47. This and the subsequent in-flight approach chute for this same aircraft set the pattern for brake parachute application to nearly all Air Force and some Navy

jet aircraft. Development of the ring slot parachute as a substitute for the more expensive ribbon parachute was also started at this time.

In 1949 and 1950, the Navy and Air Force standardized on the 28 ft. diameter ripstop nylon canopy for emergency parachutes. Included in the assembly was a quick adjustable harness and in the Air Force an automatic feature to permit free fall from altitude with automatic parachute opening at a pre-set altitude. Also standardized in 1950 was a new troop parachute, the Type T-10 which has proven to be the most reliable parachute known.

1951 was the year in which a new aerial delivery method was standardized. In this system, loads were extracted from the rear opening of C-82 and C-119 aircraft and recovered by a whole new family of cargo parachutes of 30, 64 and 100 ft. diameters. This provided a capability for aerial delivery of vehicles and weapons weighing up to 22,000 lbs., the maximum that could be carried in the aircraft. This year also saw the Air Force follow the Navy's lead and transfer most of its parachute testing to the Naval Air Station at El Centro, California and the Lockheed Company finalize the design of the first supersonic parachute recovery system. This system for the X-7 ramjet test vehicle was a very advanced system for its time and was used many times before successful parachute was demonstrated in track tests.

In 1953, development was completed on a completely new back type emergency parachute. This assembly consisted of the guide personnel canopy and a more easily adjustable harness with integral pack. The new canopy provided lower opening forces and descent with less oscillation. For its development, Dr. Heinrich received the Thurman Bane award in 1954.

1954 also saw the standardization of the first nuclear weapon retardation parachute, the first of a growing family of parachute systems designed for operation under very high opening force conditions.

In 1956, the first successful supersonic sled test of both ribbon and guidesurface parachutes was conducted at Mach 1.15.

In 1957, the first successful ballistic missile nose cone recovery was accomplished by the Army. In this same year the Air Force decided to withdraw the guide personnel canopy from service since its lower opening shock features were obtained at the cost of a fraction of a second longer opening time which penalized low altitude escape.

In 1958, a successful free flight test of a parachute at Mach 2.2 was accomplished.

In 1960, NASA recovered the first unmanned Mercury capsule. The first Discoverer capsule was recovered from orbit and Capt. Kittinger successfully accomplished a parachute stabilized free fall from 102,000 ft. with a special two-stage parachute designed for his jump.

In 1961, the first manned Mercury capsule was successfully recovered and in 1962 a live test of the B-58 capsule escape system was accomplished. This system is designed to provide both on the deck recovery and recovery at altitude up to Mach 2.2. Recent tests on small scale self-inflating and inflated balloon type drag devices have demonstrated successful operation in the wind tunnel at least to Mach 4.0.

From the above applications and test programs it is evident that a considerable capability exists to develop reliable recovery systems for various types of vehicles. In essence, this capability includes Mach numbers to 2.5 or 3.0 so long as dynamic pressure does not exceed about 4000 lbs. per sq. ft. and altitude does not exceed 100,000 ft. A new textile fibre is now available which is capable of withstanding 500° F for significantly long periods or higher temperatures for shorter periods. It should be suitable for any system within present decelerator capabilities where aerodynamic heating is a problem. In addition, the fibrous materials program of Materials Central is showing good progress on metal fibres and ceramic fibres. What then do we lack?

First, the ability to predict the performance of decelerators. At the present time, we are able to do this only for heavily loaded subsonic and transonic textile parachutes using available empirical data. Such data or analytical information for all other decelerator applications is not available.

Second, model laws to enable the prediction of performance of full scale decelerators based upon either model test in wind tunnels or in free-flight are non-existent or completely unproven.

Third, the ability to design parachute canopies which will inflate in a uniform and consistent manner. The uneven inflation characteristics, particularly of lightly loaded final descent parachutes and our consequent inability to predict load distribution within such canopies, forces us to build such canopies much more heavily than would be required if we could achieve uniform load distribution.

Fourth, designs for single and cluster parachute systems which will be steerable and provide glide ratios of at least one or more so that a greater degree of landing point control can be achieved.

Fifth, the design and demonstration of a steerable gliding re-entry drag device which can be used throughout the re-entry process preferable with drag modulation.

Session I

HYPERSONIC SESSION

Chairman: MR. E. G. JOHNSON
Aeronautical Research Laboratory
Wright-Patterson AFB, Ohio

HEATING PROBLEM FOR SUPERSATELLITE RE-ENTRY

Peter H. Rose

Avco-Everett Research Laboratory, Everett, Mass.

ABSTRACT

Our knowledge of the heating environment of re-entering missiles and space vehicles has been closely paralleled by our ability to reproduce the proper re-entry conditions in the laboratory. The recent development of the arc-driven shock tube has extended our capability of experimental simulation to velocities as high as 50,000 ft/second.

The present state of research in the main sources of heating at supersatellite velocity is discussed. Various theories and experimental measurements of convective heat transfer of partially ionized air, as well as the present controversy about this phenomenon are discussed. New data on the radiative properties of high temperature air are interpreted in terms of the heat transfer problem. Finally, the relative magnitude of these phenomena will be evaluated in terms of typical re-entry situations.

HEATING PROBLEM FOR SUPERSATELLITE RE-ENTRY

When a vehicle re-enters the earth's atmosphere at the high velocities associated with space flight, some of the atmosphere is accelerated to the vehicle velocity either by friction or by collisions with the body. A shock wave forms in the air around the vehicle to accomplish this acceleration. In this process, the air is heated by the shock wave to very high temperatures. This high temperature air, in turn, imparts heat to the vehicle both by radiation and aerodynamic convection. This, in essence, is the re-entry heating problem.

The problems of re-entry heating and hypersonic flight first became imminent in 1954, when the development of ballistic missiles was accelerated and re-entry vehicles were a necessity. At that time, shock tubes were available capable of simulating the re-entry environment for flight at velocities up to 25,000 ft/sec; sufficient for studying ballistic missile and satellite re-entries. Our present knowledge of re-entry physics is largely due to the data collected from shock tube experiments in this velocity range.

The shock tube is a simple device, consisting essentially of a long tube divided by a diaphragm into a long test section and a shorter driver section. Shock tube lengths have ranged from a few feet up to over a hundred, and inside diameters of the order of one or two inches have been used commonly, although much larger tubes are no longer rare.

The test section of a shock tube is filled with the gas in which an experiment is to be performed; air for most re-entry studies. The driver section, as its name implies, provides the force that generates the shock wave which heats the test gas. Early shock tubes employed high pressure light gases as a driver. In order to utilize shock tubes in re-entry studies the combustion energy of hydrogen and oxygen gas was employed to generate the driver force. The mixture, usually moderated by an inert gas, such as helium, to prevent detonation, was pumped into the driver section under high pressure and then ignited by an exploding wire or another suitable means. The sudden increase in pressure due to the energy release bursts the diaphragm separating the two sections, and a shock wave surges through the test gas.

Although shock tubes capable of simulating re-entry conditions for missiles and satellites existed in 1954, their full potential was not immediately realized and the necessary diagnostic instrumentation and techniques were not available. By 1956, meaningful measurements of both convective and radiative heating had been carried out. Re-entry heating was defined phenomenologically and quantitatively;

the convective heating problem by the theory of Fay and Riddell¹ and the experiments of Rose and Stark.² Radiative effects were defined from the work of Keck, et al.³ Upon these foundations rest much of our present knowledge of re-entry physics.

The re-entry problem at supersatellite velocities represents a logical extension of the research in re-entry technology developed during the missile program. However, there are differences—both of kind and degree—between the supersatellite re-entry from a lunar mission (with a velocity of at least 36,000 ft/sec) and those of the lower satellite and missile velocities.

Missile and satellite re-entries involved, for the most part, departures from perfect gas behavior due to energy invested in dissociation and the internal degrees of freedom of the gas molecules. In the higher re-entry velocity regime, as exemplified by a lunar re-entry, as much as 50 percent of the energy of the gas may be invested in ionization, creating new problems of energy transfer by ions and electrons. Thus, just as it was necessary to produce dissociated air to simulate missile and satellite re-entry problems involving the new phenomenon of dissociation, it is now necessary to produce ionized air to investigate supersatellite re-entry.

Combustion-driven shock tubes are able to produce air in which only a fraction of a percent of the gas is ionized. A new type of shock tube with an arc-heated driver has been developed⁴ to push shock tubes into the regime of higher velocities and ionization problems. Arc-driven shock tubes, such as shown in Fig. 1, have been able to shock-heat air by shocks travelling at velocities of 43,000 ft/second. This shock velocity provides simulation of stagnation conditions, i. e., enthalpy and density, for flight velocities as high as 60,000 ft/second. In an arc-driven shock tube, electrical energy is discharged from a capacitor bank into helium or hydrogen gas in the driver section. The discharge of the capacitors is fast compared to the opening time of the high-pressure diaphragm and thus, even though the heating of the driver gas is due to electrical currents (joule heating), the expansion of the driver gas is a purely gas dynamic phenomenon. The arc-driven shock tube operates in a completely analogous manner to the conventional combustion-driven shock tube. Practical present operating limits of arc-driven as well as conventional shock tubes are shown in Fig. 2.

The stagnation conditions which can be produced in an arc-driven shock tube are shown in Fig. 3 in terms of the flight velocities and altitudes which particular shock conditions simulate. An envelope of possible lunar re-entry trajectories for a $W/C_D A = 50 \text{ lb/ft}^2$, $L/D = 0.5$ vehicle is also shown in the figure. The range of stagnation conditions of interest in this type of re-entry are seen to be easily achievable in this type of device. In fact, simulation of conditions at much higher re-entry velocities, such as suggested by Riddell¹² is seen to be achievable.

Utilizing the new capability of this type of shock tube, a number of investigations have been carried out to study the effects of the

ARC DRIVEN SHOCK TUBE

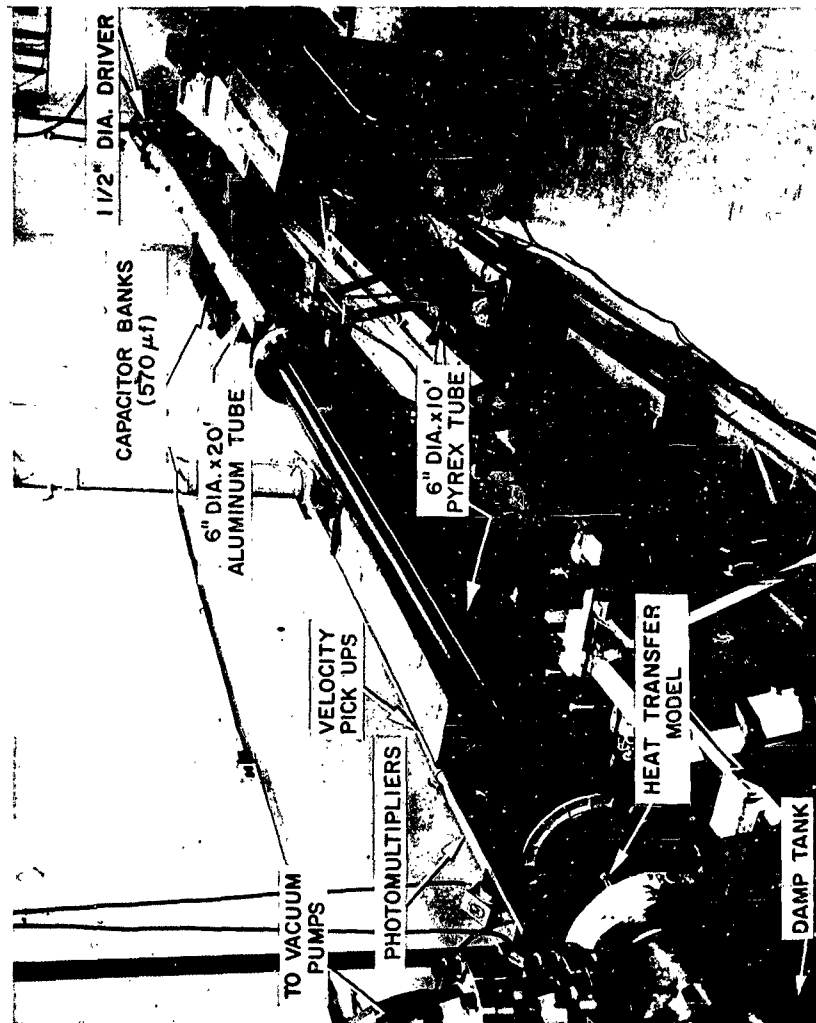


Fig. 1 Photograph of arc-driven shock tube opened to show heat transfer experiments.

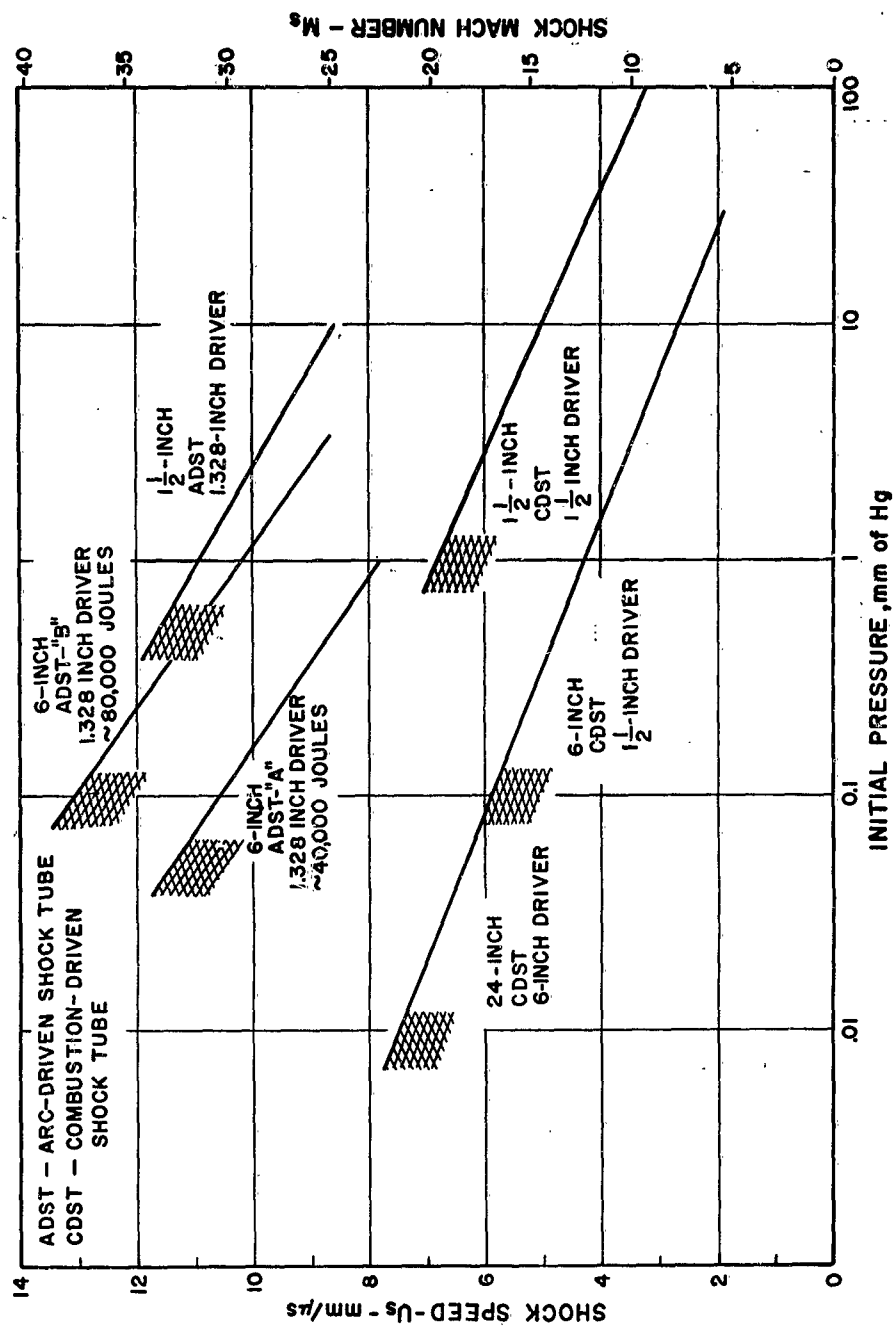


Fig. 2 Operating limits of combustion and arc-driven shock tubes (10,000 psi driver limit).

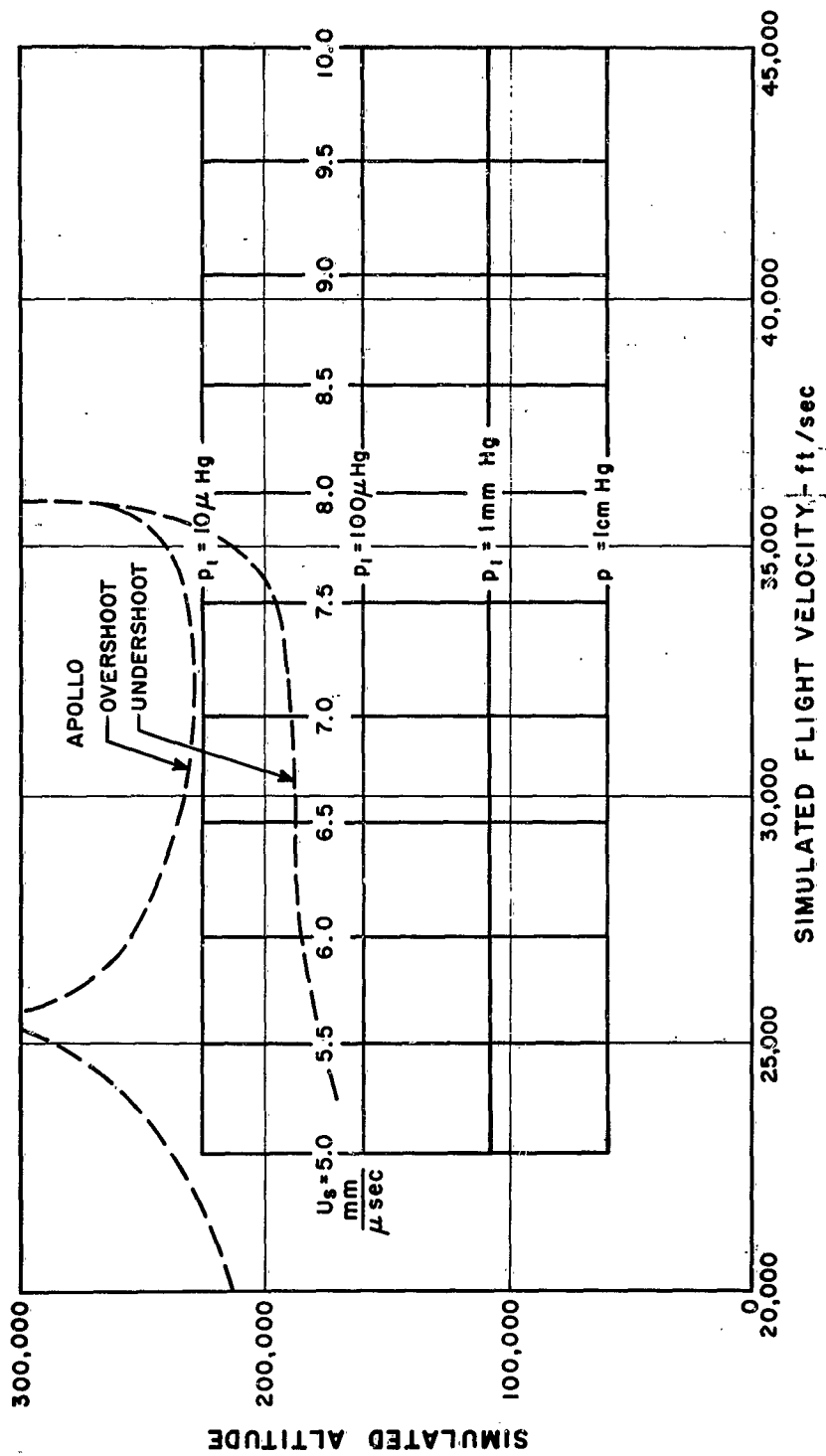


Fig. 3 Grid of hypersonic flight regime showing the shock tube conditions which produce exact simulation at the stagnation point of blunt bodies.

presence of electrons and ions in high temperature air on convective and radiative heating. From these investigations, some limits on the severity of the heating problem at supersatellite re-entry velocities can be established, particularly for the lunar re-entry case. However, much work remains to be done, both in shock tubes and other facilities, before our knowledge is refined to the degree desirable from the engineering and design point of view.

Heat transfer measurements have been made by utilizing resistance thermometers to measure the temperature response of a point on a surface as had been done at lower velocities.² From a temperature response, a heat transfer rate can be inferred. Either a thin film, which measures the temperature history of the substrata, or a calorimeter which absorbs all the incident heat energy, can be utilized in shock tube heat transfer measurements. The high heat transfer rates which occur at high velocities and the high conductivity of the ionized gases both favor the use of the latter type of instrument in measurements in partially ionized air. Measurements of stagnation point heat transfer rates have been made with calorimeter gages at conditions simulating flight at velocities up to 45,000 ft/sec at simulated altitudes between 100,000 and 140,000 feet.¹⁶ In order to isolate the resistance thermometer circuitry from the ionized gases, the gage element was covered by a thin evaporated layer of silicon monoxide. By this technique electrical artifacts, observed in earlier experiments, were largely eliminated.

The results from this series of experiments are shown in Fig. 4. Contrary to the predictions of Scala⁵, the presence of significant numbers of electrons does not produce a radical departure from the result which would be predicted without differentiating between the electrons and ions as opposed to the atoms and molecules. The theories of Hoshizaki⁶ and Cohen⁷, as well as extrapolations of Fay and Riddell¹, show reasonable agreement with the data. It must be concluded from these results that the transport properties of air, i.e., the thermal conductivity, as calculated by Hansen⁸ and used in these theories to predict the heat transfer rates, must be approximately correct. The same statement can be made for the collision cross section used in the calculations of the transport properties as summarized by Fay.⁹ The engineering accuracy to which the above data defines the convective heat input is estimated to be about 20 percent.

It appears that Scala⁵ has achieved his erroneous results by incorrect assumptions regarding the collision cross section for nitrogen ions diffusing through nitrogen atoms. This cross section is needed in the calculation of the transport properties of the ionized high temperature air. Scala calculates a thermal conductivity which is a factor of 20 larger than Hansen's⁸ value at 15,000°K, due to using a cross section for the above diffusion process which is two orders of magnitude smaller than the value suggested by Fay.⁹ Fay's value was derived from analogy to the value for argon ions diffusing through argon atoms which had been both calculated and measured. A recent calculation for nitrogen, following the method successfully employed in argon, has been performed by Yos.¹³

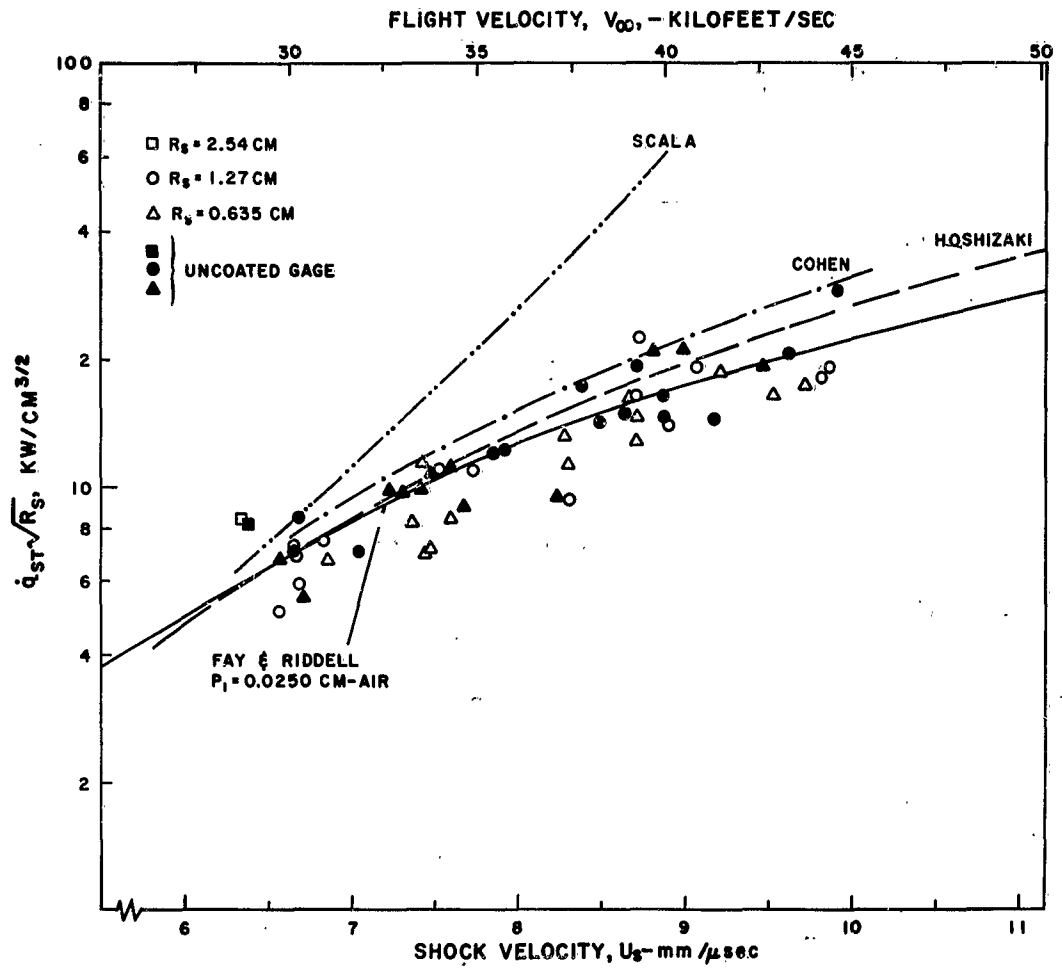


Fig. 4 Stagnation point heat transfer rate measurements in partially ionized air.

The experiments of Warren⁵ supporting the calculations of Scala are more difficult to explain. Here one must consider the extreme difficulties involved in producing any data in this regime, i.e., the operation of the shock tube, the effects of ionization on the gage performance, as discussed in detail in Refs. (4) and (16). The weight of the evidence of three separate investigations,^{14,15,16} carefully considering the experimental difficulties encountered in each of these investigations, must speak for the validity of the data presented in this paper.

The other prime source of re-entry heating is heat transfer by radiative processes. Shock tube experiments have shown the radiative properties of air to be extremely sensitive to temperature.^{3,10} In fact, air is a transparent gas in the regions of interest to most re-entry applications, and for such a gas the temperature dependence of radiant emission intensity is considerably stronger than the familiar black body, fourth-power relationship. Thus, it has been anticipated that even though at missile re-entry velocities radiative heating has proven to be only about 10 percent of the convective heating contribution, the radiative heating process may dominate at the higher velocities.

Two different gas radiation phenomena have been observed to be significant for the heating problem. First, the radiative properties of the high temperature gas in thermodynamic equilibrium are an important consideration. Secondly, the radiative emission during the relaxation process by which the shock-heated gas approaches its equilibrium state must be considered. These two phenomena are shown in a schematic form in Fig. 5. As air flows through a shock wave, the kinetic energy is rapidly invested in the translational and rotational degrees of freedom of the air molecule. The translational temperature rises almost instantaneously in the shock-front to a very high value. Somewhat later, vibrational and dissociative equilibration sets in and the translational temperature drops as energy is transferred to these modes.

The radiative properties of a gas are proportional to the concentration of the radiating species and an electronic temperature characterizing the radiation process. Experiments have shown this electronic temperature to lag the translational temperature in the early part of the shock front. Radiation appears to follow some path related to a temperature intermediate between the translational temperature and the final, equilibrium value, overshooting the equilibrium value considerably under certain conditions.

The radiative properties of both the equilibrium and non-equilibrium regions behind strong air shocks were studied thoroughly in the pursuit of the missile re-entry problem. The main contributors to radiative emission in both regions were found to be the molecular bands of nitrogen, oxygen, and nitric oxide.^{3,10} Extrapolations of this data to higher temperatures have indicated the possibility of serious heating problems from both these sources of radiation. It was expected that at the higher temperatures involved in supersatellite re-entries the dominant equilibrium radiation should be due to

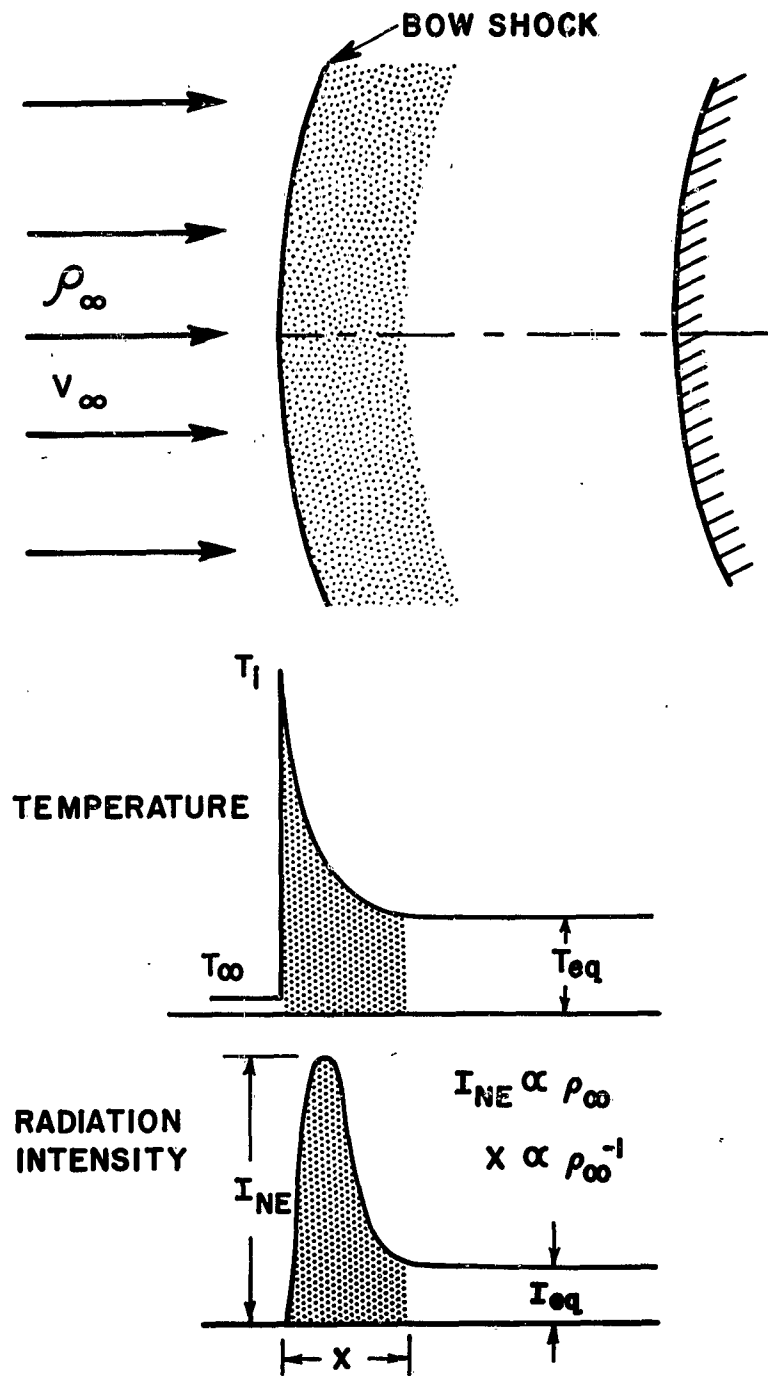


Fig. 5 Schematic diagram showing the time histories of temperature, T , and non-equilibrium radiation intensity, I_{NE} , behind a strong normal shock.

recombination of electrons with atomic ions, and atomic lines of nitrogen and oxygen. Early estimates of the non-equilibrium radiation indicated that if the excitation process were fast, i. e., if the electronic temperature were to equilibrate with the local translational temperature early in the shock front, before relaxation processes had proceeded to a large degree, the radiative energy transfer during the relaxation process could be extremely large.¹⁷

Shock tube experiments in the arc-driven, high velocity shock tube have provided some answers regarding both the equilibrium and non-equilibrium radiation problems. From observations with calibrated monochromator-photomultiplier combinations, we have been able to observe the radiation history behind strong shock fronts with excellent time resolution. Typical observed radiation profiles behind strong shocks are shown in Fig. 6. Both the equilibrium radiation level and the non-equilibrium overshoot are clearly identifiable.

Narrow bandwidth, absolute intensity monochromator-photomultiplier measurements over a large wavelength region have allowed us to estimate the absolute magnitude of the energy under the non-equilibrium radiation overshoot. Wavelength traverses of absolute radiation intensity have been made by performing many repetitive experiments at a given shock velocity. Figure 7 shows such a result for a 33,000 ft/sec shock. The envelope surrounding the experimental points and connecting this data with the unknown wavelength regions, gives a conservative estimate for the total energy involved in the non-equilibrium radiation overshoot. The results from integrating under such curves, plus other available data,¹⁸ are shown in Fig. 8. The good agreement between the two sets of data is not entirely fortuitous. Ballistic range data are generally corrected in accordance with spectral distributions either theoretical or observed in shock tubes, due to the limited wavelength coverage available in range experiments. The non-equilibrium radiation, because of the binary nature of the chemical reactions which dominate the shock structure, is independent of density and, consequently, a function of velocity only. In such binary processes, the radiative intensity will decrease with decreasing density due to the lesser number of collisions, but the reactions will also slow down, thereby broadening the reaction zone. These two effects cancel the density dependence of the non-equilibrium radiation.

The same shock tube experiments have also produced new data on equilibrium radiation. By analyzing the level portion of a radiation profile from a monochromator-photomultiplier experiment, the absolute value of equilibrium radiation in a given wavelength region can be established. Such results taken over a considerable wavelength regions are shown in Fig. 9. The estimates from the tables of radiative properties of high temperature air of Kivel and Bailey¹⁰ are also shown. It is evident that radiation considerably in excess of the predictions is being measured in a region where atomic nitrogen lines are present. It can also be seen that the estimate of Kramer's radiation, i. e., $N^+ + e \rightarrow N + h\nu$, is probably somewhat high in Kivel and Bailey and that the more sophisticated estimate by Lindenmeier¹¹ shows a better fit to the available data. The present knowledge of these sources is yet too uncertain to make precise

NORMAL AIR SHOCKS

$P_1 = 0.1 \text{ mm Hg}$

TOP TRACE [55—1.0 μ]

BOTTOM TRACE [40—42 μ]

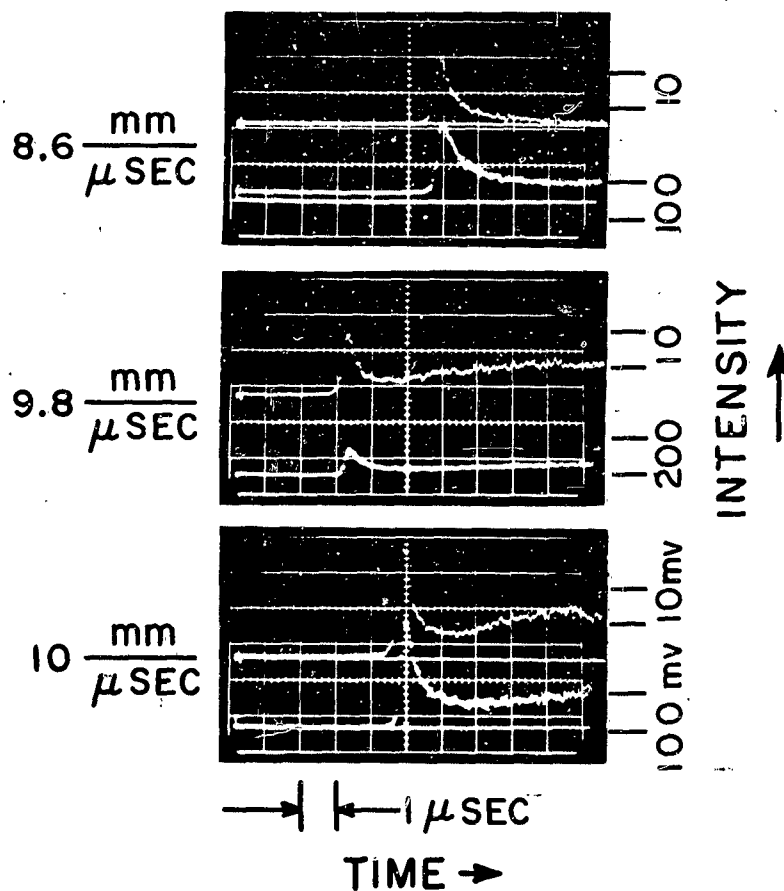


Fig. 6 Measured radiation intensity profiles behind strong normal shocks.

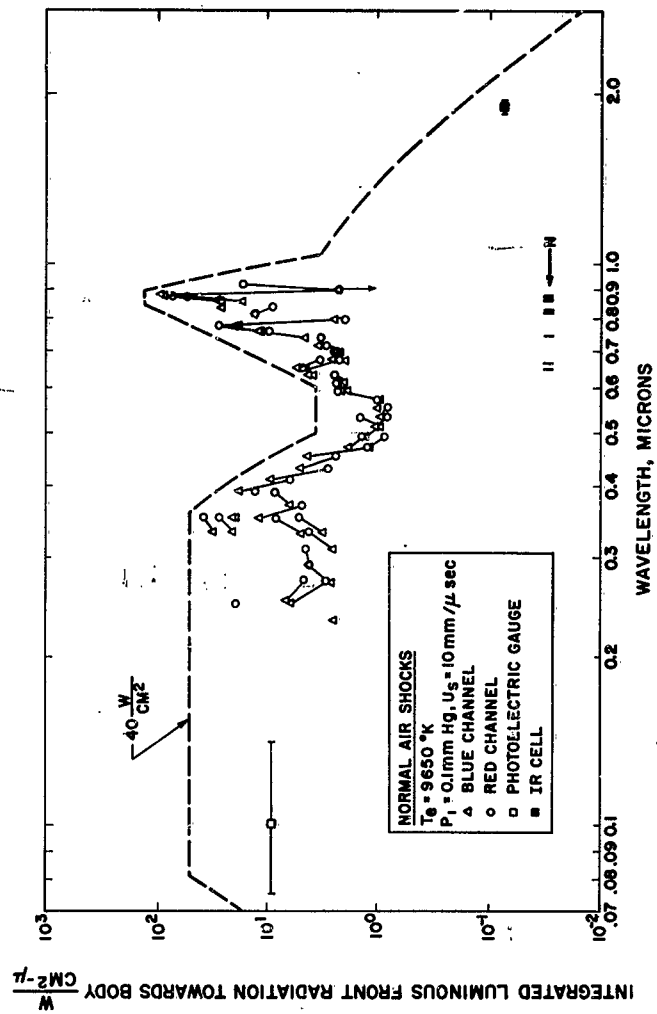


Fig. 7 Measured spectral distribution of integrated non-equilibrium radiation intensity.

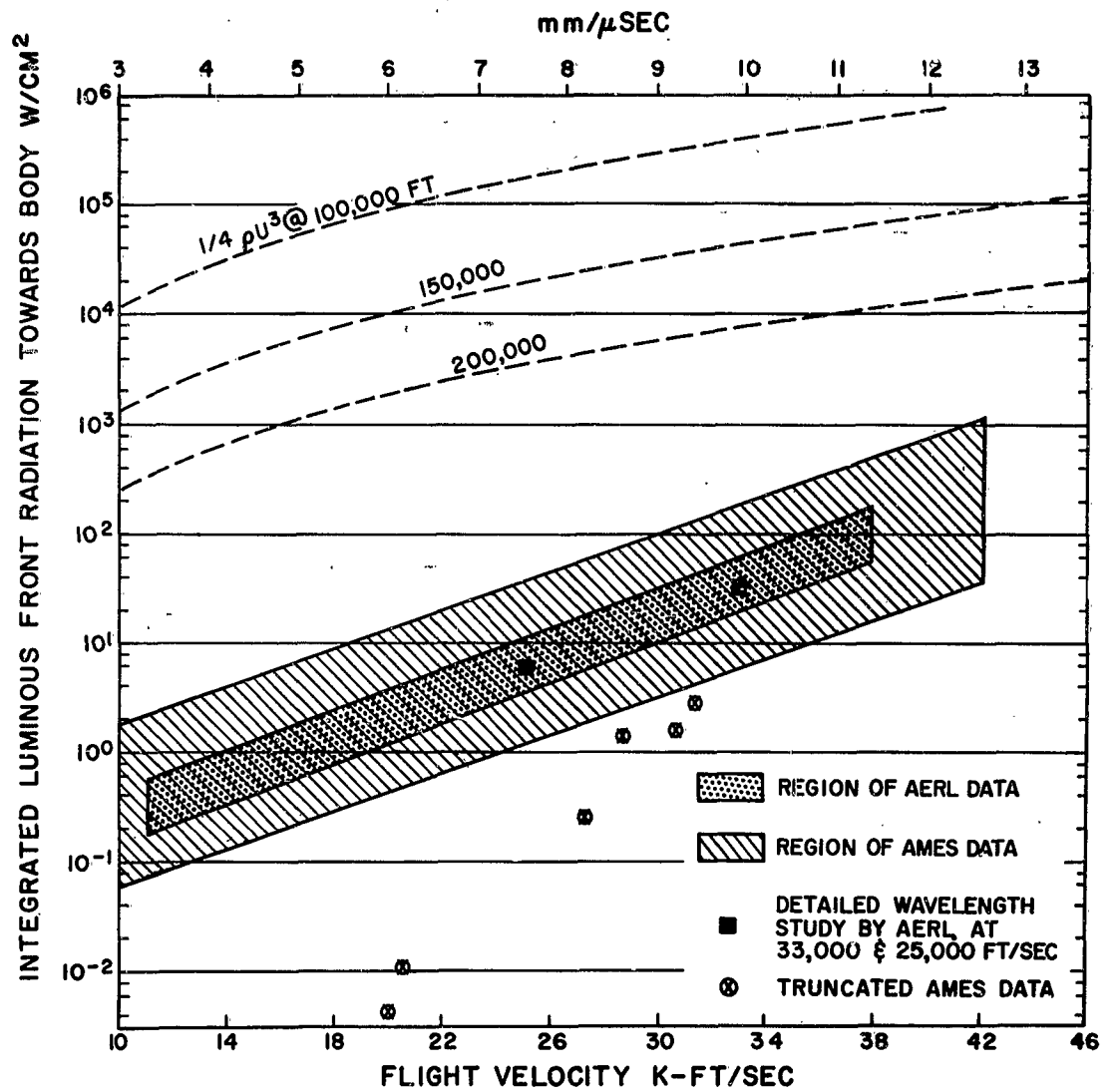


Fig. 8 Velocity dependence of total integrated non-equilibrium radiation intensity.

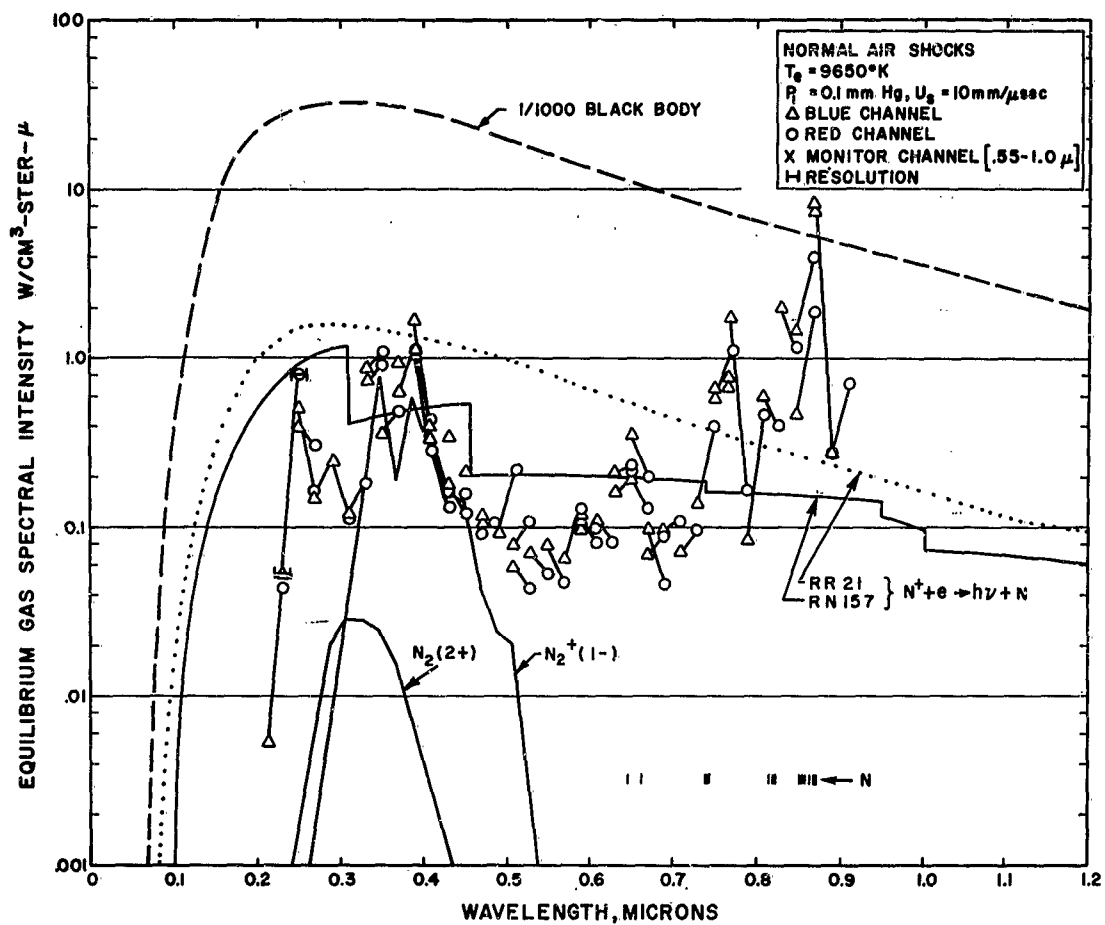


Fig. 9 Measured spectral distribution of equilibrium radiation behind a strong normal shock.

predictions, but new limiting estimates of this source of radiation can be derived from these measurements.

The data obtained from the recent shock tube studies discussed can be used to assess the heating problem for supersatellite re-entry velocities. Velocities of the greatest immediate interest are in the range of 36,000 ft/sec, typical of a lunar re-entry mission. By fitting the experimental or theoretical data available, simple equations for the convective and radiative heating can be developed. Hoshizaki⁶ arrived at the expression

$$q = \frac{1.54 \times 10^4}{R^{0.5}} \rho_{\infty}^{0.5} \left(\frac{U_{\infty}}{10^4} \right)^{3.19} \text{ Btu/ft}^2\text{-sec} \quad (1)$$

from fitting the results of his boundary layer calculations. As we have seen in Fig. 4, this theory adequately describes the experimental results. The above expression is not very different from the earlier correlation equation of Detra¹⁹ which was formulated to fit the results of Refs. 1 and 2.

The radiative emission intensity of equilibrium air can be expressed in a similar form by fitting the data of Ref. 10.

$$q = 49.2 R \rho_{\infty}^{1.6} \left(\frac{U_{\infty}}{10^4} \right)^{15} \text{ Btu/ft}^2\text{-sec} \quad (2)$$

The absolute value of the above is probably uncertain by a factor of two or three due to the uncertain magnitude of de-ionization (Kramer's) radiation and atomic line radiation, and is applicable in the speed range of 25,000 ft/sec and up.

Recognizing this uncertainty, we can establish the relative magnitudes of these two effects by plotting

$$\frac{q_{\text{AERO}}}{q_{\text{RAD}}} = \frac{313}{R^{1.5}} \rho_{\infty}^{-1.1} \left(\frac{U_{\infty}}{10^4} \right)^{-11.81} \quad (3)$$

Lines of constant values of the above parameter can be drawn in a velocity altitude (or density field) as shown in Fig. 10. The relative importance of the non-equilibrium radiation contribution can also be shown on such a plot. As long as the binary chemistry of the shock front dominates the shock structure, the non-equilibrium radiation will be independent of density. Thus an approximate expression for this contribution valid in the velocity range of 25-40,000 ft/sec would be

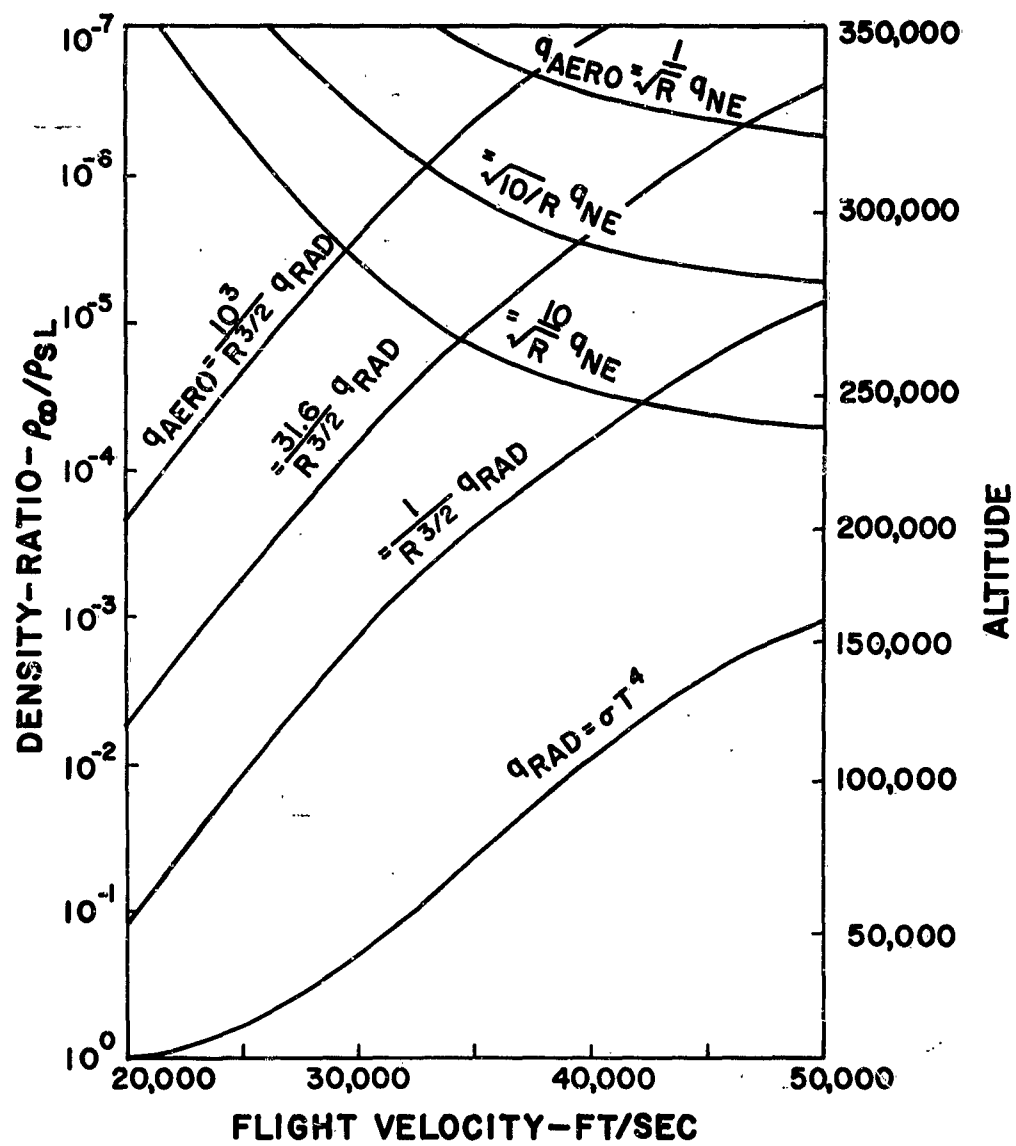


Fig. 10 Comparison of the importance of the various heating mechanisms for the supersatellite flight regime.

$$q_{\text{RAD N.E.}} = 35.2 \left(\frac{U_{\infty}}{33,000} \right)^8 \quad \text{Btu/ft}^2\text{-sec} \quad (4)$$

and the ratio of the above to the convective heating is

$$\frac{q_{\text{AERO}}}{q_{\text{RAD N.E.}}} \sim \left(\frac{\rho_{\infty}}{R} \right)^{0.5} U_{\infty}^{-4.81} \quad (5)$$

This effect is also shown in Fig. 10. Due to the stronger velocity dependence of the non-equilibrium radiation, the severity of this effect increases rapidly with velocity and is only weakly dependent on the density and body size.

Thus, it can be seen that at high altitudes and high velocities non-equilibrium radiation should dominate. For low altitudes and high velocities, equilibrium radiation will be the largest contributor to heating. For low speeds convective heating will still be dominant. The approximate borders of these regimes are shown in Fig. 10 for one, ten, and 100 ft nose radius bodies.

Figure 10 can be a useful tool for preliminary estimates when used with consciousness of the assumptions which entered the calculations. The convective heat transfer relationship used is good for continuum flow and caution must be exercised at very high altitudes where free molecule effects are present. The correlation used is based on an equilibrium calculation but experience has shown frozen boundary layers to make only small perturbations to the heat transfer. The equilibrium radiation is probably overestimated in this plot as previously discussed. It must also be borne in mind that as the width of the non-equilibrium region increases, the equilibrium contribution, as commonly defined, diminishes. Finally, the non-equilibrium radiation has been derived assuming binary scaling. Thus, the effects of collision limiting at low densities and truncation of the radiation profile when the shock stand-off distance is much smaller than the width of the relaxation zone, have not been accounted for and should be considered.

REFERENCES

1. Fay, J. A. and Riddell, F. R., "Theory of Stagnation Point Heat Transfer in Dissociated Air," J. Aero Sci., Vol. 25, No. 2, February 1958.
2. Rose, P. H. and Stark, W. I., "Stagnation Point Heat Transfer Measurements in Dissociated Air," J. Aero. Sci. Vol. 25, No. 2, February 1958.
3. Keck, J. C., Camm, J., Kivel, B. and Wentink, T., Jr., "Radiation from Hot Air - Part II, Shock Tube Study of Absolute Intensities," Annals of Phys., Vol. 7, No. 1, 1959.
4. Camm, J. C. and Rose, P. H., "Electric Shock Tube for High Velocity Simulation," Avco-Everett Research Laboratory Research Report 136, July 1962. (Submitted to Physics of Fluids for publication).
5. Scala, S. and Warren, W., "Hypervelocity Stagnation Point Heat Transfer," ARS Jour., Vol. 32, No. 1, January 1962.
6. Hoshizaki, H., "Heat Transfer in Planetary Atmospheres at Supersatellite Speeds," ARS Preprint No. 2173-61, December 1961.
7. Cohen, N., "Boundary Layer Similar Solutions and Correlation Equations for Laminar Heat Transfer Distribution in Equilibrium Air at Velocities up to 41,100 Feet per Second," NASA Technical Report R-118, 1961.
8. Hansen, C. F., "Approximations for the Thermodynamic and Transport Properties of High Temperature Air," NASA Technical Report R-50, 1959.
9. Fay, J. A., "Hypersonic Heat Transfer in the Air Laminar Boundary Layer," Avco-Everett Research Laboratory AMP 71, March 1962.
10. Kivel, B. and Bailey, K., "Tables of Radiation from High Temperature Air," Avco-Everett Research Laboratory Research Report 21, December 1957.
11. Lindenmeier, C. W., "Kramer's Radiation from Hot Air," AFBMD-TN 59-28, Avco-Everett Research Laboratory Research Note 157, September 1959.

12. Riddell, F.R. and Winkler, H.B., "From ICBM Re-Entry to Meteorite Entry," National IAS-ARS Joint Meeting Preprint 61-113-1807, June 1961.
13. Yos, J.M., "Transport Properties of Nitrogen and Hydrogen to 30,000°K," AVCO-RAD-SR-62-11, February 1962.
14. Hoshizaki, H., "Convective Heat Transfer Measurements at Superorbital Speeds," Lockheed Missiles and Space Company, Technical Report: Flight Sciences 6-90-62-50, June 1962.
15. Offenhartz, E., Weisblatt, H. and Flagg, R.F., "Stagnation Point Heat Transfer Measurements at Super-Satellite Speeds," J. Roy. Aeronaut. Soc., January 1962.
16. Rose, P.H. and Stankevics, J., "Measurements of Stagnation Point Heat Transfer in Partially Ionized Air," to be published.
17. Teare, J.D., Georgiev, S. and Allen, R.A., "Radiation from the Non-Equilibrium Shock Front," Avco-Everett Research Laboratory Research Report 112, October 1961.
18. Canning, T.N. and Page, W.A., "Measurements of Radiation from the Flow Fields of Bodies Flying at Speeds up to 13.4 Kilometers per Second," presented at Fluid Mechanics Panel, AGARD, Brussels, Belgium, April 3-6, 1962.
19. Detra, R., Kemp, N.H., Riddell, F.R., Addendum to "Heat Transfer to Satellite Vehicles Re-Entering the Atmosphere," Jet Propulsion, Vol. 27:1256, December 1957.

**SOME CONSIDERATIONS FOR RE-ENTRY CONFIGURATIONS
RELATIVE TO MISSION AND TECHNICAL CONSTRAINTS**

Alfred C. Draper and Melvin L. Buck

**Flight Branch
Flight Dynamics Laboratory
Directorate of Aeromechanics
Deputy for Technology
Aeronautical Systems Division
Wright-Patterson Air Force Base, Ohio**

ABSTRACT

A review is made of the various types of configurations considered suitable for re-entry at hypervelocity speeds. These configurations are viewed relative to a series of mission applications increasing in complexity from pure weapon delivery to sophisticated manned re-entry. Design trends and considerations peculiar to the various regions of re-entry flight from hyperbolic to the terminal phases are outlined with proposed methods for solution. Particular emphasis is placed on delineating the constraints peculiar to re-entry from superorbital velocities and the advantages and requirements associated with certain aerodynamic designs are discussed in detail. Future design requirements and long term goals are viewed from the separate considerations of mission applications, technical constraints, optimization parameters, and growth potential. It is shown that a common design point is suggested for future re-entry configurations which will simultaneously satisfy these separate considerations. Several advanced configuration concepts are then proposed and weighed against the more significant design problems. The latter portion of the paper directs its attention to various supplemental aids which appear attractive for advanced applications with emphasis on expandable surfaces as aerodynamic augmentors and the use of aerodynamic decelerators at parabolic velocities. Finally, a promising technique for aid during superorbital re-entry is proposed and the design constraints and advantages are delineated.

SYMBOLS

| | |
|--------------------------|------------------------------------|
| \dot{q} | Heat Flux, BTU/ft ² sec |
| \dot{q}_{conv} | Convective Heat Flux |
| \dot{q}_{hgr} | Heat Flux Hot Gas Radiation |
| \dot{q}_{total} | Total Heat Flux |
| ρ_{∞} | Free Stream Density |
| ρ_{stag} | Stagnation Density |
| V_{∞} | Free Stream Velocity |
| h_w | Enthalpy at Wall |
| h_{st} | Stagnation Enthalpy |
| R | Radius |
| σ | Density Ratio |
| C_f | Friction Coefficient-Drag |
| S | Wetted Area |
| C_D | Drag Coefficient |
| A | Reference Area |
| W | Weight |
| γ | Flight Path Angle |
| C_L | Lift Coefficient |
| L/D | Lift-to-Drag Ratio |
| ϕ | Bank Angle |
| $\sqrt{1-k}$ | Velocity V (Satellite) |
| y | Lateral Range |

SOME CONSIDERATIONS FOR RE-ENTRY CONFIGURATIONS RELATIVE TO MISSION AND TECHNICAL CONSTRAINTS

SECTION I

INTRODUCTION

During recent months, there has been considerable discussion concerning the type of re-entry configuration which should be selected for a specific mission. The technical discourses have embodied practically all types of vehicles from pure ballistic to complicated lifting vehicles and the assets and liabilities associated with each class of vehicle have been debated enthusiastically and with considerable vigor. To many, however, no clear conclusion is readily obvious and may, perhaps, not even exist in view of the many possible missions associated with space exploitation. This paper will attempt to delineate as a function of various missions, technical constraints and requirements for growth potential; the various configurations which show promise. The possible missions will be outlined and then viewed relative to vehicle requirements for increased sophistication and complexity. The technical problems and constraints associated with suborbital, orbital, and superorbital re-entry will be outlined and examined in an effort to determine a trend in vehicle design. It will be shown in this paper that for sophisticated operational flexibility, the requirements demanded by both the mission and physical constraints are not at all paradoxical, but, indeed, suggest a common design point for future re-entry vehicles in terms of aerodynamic efficiency. In view of the high costs of re-entry devices, a composite analysis of growth potential has also been made which again demonstrates the tie-in between the mission and technical requirements and further amplifies the common design goal.

The problems associated with optimization are analyzed and the parameters which have been suggested for optimization such as weight, volume, lateral range, etc. are discussed in detail. The paper views these optimization parameters relative to their potential order of importance and draws conclusions as to which parameters will be of real significance for future systems. The question of pseudo optimization for current vehicles such as volumetric efficiency is discussed and its relative importance to the actual physical constraints on the total design problem is shown. A survey is then made of the various re-entry configurations which for the purpose of this paper have been grouped into two major categories, ballistic and lifting vehicles. Specifically, the vehicles which are considered and analyzed relative to their application for various missions have been further delineated into the subcategories of pure ballistic, controlled ballistic, modified ballistic, winged gliders, lifting bodies; and, finally,

variable geometry configurations. The design details and problems peculiar to the regions of flight from the hyperbolic to the landing phases are discussed and various methods for solution are recommended. Particular emphasis has been placed on the constraints peculiar to re-entry from supercircular velocity and an attempt is made to delineate the lifting configurations as a function of the re-entry speed. Relative to the variable geometry concepts, the potential and modulation possibilities of such configurations are analyzed.

Having approached the design requirements and long term goals from these four separate approaches, i.e., mission considerations, technical constraints, optimization parameters and growth potential, and having analyzed the broad spectrum of re-entry configurations; the problems associated with the design of the most promising configuration concepts are then considered in detail. Several techniques to achieve highly efficient aerodynamic re-entry configurations are outlined and weighed against the more significant design obstacles.

The final portion of this paper directs its attention to the various supplemental aids which appear especially attractive and which hold promise for application to advanced configuration concepts. In particular, the use of expandable surfaces as aerodynamic augmentors and aerodynamic decelerators are investigated and their potential applications are outlined. A unique technique for aid during superorbital re-entry is proposed by the authors and the design constraints and advantages are delineated.

SECTION II

CONFIGURATIONS AND MISSIONS

It would be most difficult, if not presumptuous to attempt to postulate the missions for advanced Air Force systems and no such attempt will be made here. It is possible, however, to outline in a general way the broad spectrum of unmanned and manned missions for future space exploration. The design requirements for various configurations can then be outlined in terms of increased mission sophistication and complexity to give some indication of the problems which are involved and to suggest the most probable evolutionary goal for future vehicles. No attempt will be made to build a case for an absolute optimum configuration for it is felt no such vehicle currently exists for all probable missions; rather an effort will be made to demonstrate a trend in configuration design as a function of various mission requirements, and then to concentrate on several specific design considerations which demonstrate promise for a particularly complex set of mission constraints.

Prefaced with these initial remarks, it seems appropriate for the subsequent discussions, to divide the potential missions, as previously stated, into two major categories; i.e. Unmanned/Sustained Missions and Manned Missions. The Unmanned or Sustained Missions will further be delineated into those which are primarily oriented towards weapons, recoverable payloads and permanent satellites. In a similar manner but with more completeness the manned missions will be classified in an ascending order of complexity as being missions requiring (a) recovery from restricted orbits, (b) recovery from selected orbits, (c) recovery from arbitrary orbits and (d) tangential landing. The latter two possibilities will then be compounded in order to review configuration concepts which can best satisfy a complicated manned mission requiring recovery from arbitrary orbits at any time, with a tangential landing capability. Various classes of configurations which show promise will be then discussed relative to these mission possibilities and the most promising configuration will be outlined for each mission concept.

A. Unmanned and Sustained Missions

The unmanned and sustained missions, for this paper, will be postulated as being missions which are concerned with pure weapons, recoverable unmanned payloads, and permanent or long term orbital vehicles which do not re-enter.

1. Weapons

The weapon oriented missions can be best typified by the current ICBM and advanced versions of this concept. Ballistic shapes have been and are still generally quite attractive for use when weapon delivery is the prime function of the vehicle. These shapes have by evolution, essentially followed two broad design concepts -- the heat sink designs and the low drag concepts.

Initially, all work tended to center around the H. Julian Allen blunted nose concept as a heat sink. The technique, simply was that the total convective heat input could be maintained at reasonably low levels since the fraction of the total kinetic energy change which had to be accepted as convected heat to the vehicle could be expressed: $C_f S / 2 C_D A$ where C_f is the frictional drag coefficient per unit of wetted area S and C_D the total drag coefficient. In other words, when the friction drag is small relative to the total drag, a large fraction of heat is yielded to the atmosphere and the actual convection to the vehicle is small. This particular technique was demonstrated by the first generation of nose cones by both General Electric and AVCO.

Recent advances in ablative type material has enabled the design of lower total drag vehicles and consequently the evolution of the sphere-cone-cylinder-flare type of body employed in the Minuteman design. The use of ablation techniques has permitted much higher values for the ballistic coefficient, $W/C_D A \sim 1000$. This design breakthrough reduced the problems associated with transonic instability, wind, and atmosphere density gradient effects, and thereby permitted less dispersion and greater impact accuracies. The Newtonian drag of a sphere-cone-cylinder-flare shape can be written in approximate form as being:

$$C_D = \left(\frac{R_{B1}}{R_{B2}} \right)^2 \left[2 \sin^2 \theta_{c1} + \left(\frac{R_n}{R_{B1}} \right)^2 \cos^4 \theta_{c1} \right] + 2 \sin^2 \theta_{c2} \left[1 - \left(\frac{R_{B1}}{R_{B2}} \right)^2 \right]$$

where: R_{B1} = radius of base of cone - inches

R_{B2} = radius of base of flare - inches

R_n = radius of nose - inches

θ_{c1} = half angle of cone-degrees

θ_{c2} = half angle of flare-degrees

Of course, it is reasonably obvious that a combined design i.e., heat sink plus ablation, represents a rational approach for many applications. If on the other hand a small degree of maneuvering is desired, or for that matter required; the controlled ballistic appears quite attractive. This configuration is normally defined as being a conventional ballistic shape with some sort of aerodynamic control surface or surfaces attached, e. g. a flap. Its use is particularly attractive if the maneuver capability is restricted to the terminal phase. An alternate approach which has been suggested would be a modified ballistic shape which is generally characterized as a high drag lifting vehicle with moderate to low values of lift to drag ratio normally in the range of 0.3 to 0.6

hypersonically. The choice of this particular configuration would enable some reasonable hypersonic maneuverability and could improve both the selectivity and accuracy of the weapon. Cross range or lateral maneuverability of this type of vehicle can be expressed in approximate form as being

$$y = 875 \left(\frac{L}{D} \right)^2 \sin \phi \cos \phi \left\{ L(1-L) \frac{1}{2} + \frac{1}{4}(1-L)^2 + \frac{1}{9}(1-L)^3 + \dots \right\}$$

For $\phi = 45^\circ$ which maximizes y we have $y = 660 \left(\frac{L}{D} \right)^2$ where $\frac{V}{V_c} = \sqrt{1-L}$

Consequently, it can be seen that these vehicles could adjust their cross ranges from 60 to 220 miles depending on the specific configuration design and the resulting lift-to-drag ratio.

Perhaps the aeroballistic or extended length axially symmetric configuration offers the most promising growth potential for advanced weapon delivery applications. This configuration is generally characterized by a conical or ogive fore body with a large fineness ratio cylindrical afterbody. Conical surfaces or pressure panels are generally used for control. Depending on the velocity altitude environment involved, some degree of bluntness is required to withstand the aerodynamic heating during the hypervelocity portion of flight. If appropriate advances are made in transpiration and mass transfer coolant techniques, however, it may be possible to design these vehicles with extremely high hypersonic lift-to-drag ratios. Current designs are limited to lift-to-drag ratios of approximately 2.5, however, depending upon the bluntness, it should be possible to achieve lift-to-drag ratios of 3.0.

It can be readily seen that this would result in extremely large cross ranges depending upon when the turning flight was initiated.

Perhaps some of the most significant and attractive possibilities of the aeroballistic vehicle are those which are associated with the maneuverability and evasive action capabilities that might be employed in order to avoid detection and to reduce the chances of predicting the point of impact of the vehicle when functioning as a weapon system. In order to reduce the possibilities of a successful head-on defensive shot, the aeroballistic vehicle could enter the atmosphere miles from the target and glide to the target at reasonably low altitudes and at very high velocities. Pre-programmed turns or changes in direction would enable the vehicle to maneuver on the final approach to the target which would aid in complicating the detection and interception from an anti or defensive missile firing. The trajectory of the ballistic missile is very easily determined and the launch point itself located, particularly, if the launch point is on the earth's surface. This can lead to the destruction of subsequent vehicles and the launch point after only a few launchings. The aeroballistic vehicle because of its lateral maneuvering capabilities and with the unpredictable point of "dive-in" to the target would reduce the possibilities of detection of the launch point as well as the vehicle itself. The point of "dive-in" could be pre-programmed as suggested for the turn or dog leg maneuver and high impact Mach numbers could be obtained.

This particular configuration has been analyzed in considerable detail in Reference 1 & 2 by Allen, Eggers, and Niece of the NASA and Draper of ASD. In summary, if weapon delivery is the prime objective of a mission, it can be concluded that the ballistic, controlled ballistic, modified ballistic and aeroballistic vehicles all have attractive applications. The actual configuration selection would be dependent upon the accuracy, maneuvering, evasive action, and range extension requirements. Figure I shows the evolution of these vehicles in this context as a function of time.

2. Recoverable Payloads

This particular mission application requires, to a degree, slightly different configurations than those which have been proposed for pure weapons. Depending upon the location accuracy required, several choices are available. If the prime desire is to generate the largest payload to re-entry weight ratio then the ballistic configuration would currently represent the most expeditious approach. The pure ballistic concept has the associated disadvantages, however, of requiring the accurate tolerances for firings of retro rockets, and the re-entry trajectories can be influenced by winds and density gradients. No maneuverability is available during re-entry and flight path corrections are difficult which can result in greater dispersions and impact errors. These factors, of course, limit the orbits available - if recovery is desired in the zone of the interior. Location problems after impact are aggravated and are of some concern. The retrieval approaches employed for such systems as Mercury, Discoverer, etc., would have to be used. In any event, low values of the ballistic coefficient, W/CDA , are generally required in order to reduce approach and impact velocity. Supplemental aids such as decelerators can be extremely useful for such application and auxiliary landing devices are normally required such as parachutes, impact cushions etc.

In view of the advantages associated with low values of the ballistic coefficients, an approach which has merit for such application would be the variable drag type configuration, such as the AVCO drag chute. This type of configuration is characterized by low ballistic coefficients and because of the drag modulation capability some down range adjustment in the impact point is possible. The drag modulation is normally made prior to maximum heating. Consequently, any subsequent adjustments required may not be possible. This configuration approach does, however, offer some advantages over the pure ballistic shape.

Perhaps one of the more promising configurations for this application is the high lift/high drag shape or modified ballistic. This type of vehicle can best be represented by the Eggers M - I shapes. Hypersonically, this type of configuration can generate lift-to-drag ratios of approximately 0.5 therefore has a reasonable degree of lateral maneuverability, e.g. 160 miles. Other more efficient configurations can, of course, be chosen but may not be necessary if recovery from a series of selected orbits is the only requirement. Work performed both in NASA and ASD with expandable surfaces indicate that by deploying such aids during the terminal portions of flight reasonably soft-landings can

be accomplished at predesignated points with such configurations. It must be clearly understood, however, that such configuration approaches will restrict the orbit selectivity and if a completely versatile system is required, then configurations with higher lift-to-drag ratios must be chosen. Perhaps it would be appropriate to mention one additional approach for future application which may prove useful; the inflatable configuration. This concept is certainly not new but if the materials used for heat protection could be extended to approximately 2000°F then it is felt that this approach would have merit. Recent studies, which admittedly are somewhat incomplete, indicate that the return payload to re-entry weight ratio could be extended to 0.4 or even higher.

In summary, it is the conclusion of the authors that the modified ballistic configuration would represent the most promising configuration for the unmanned recoverable missions for some lateral maneuverability does exist with reasonable ratios of payload to re-entry weight. These configurations have an added advantage of simplicity and do not require the use of gross modulations or inflations; the advantages over the pure ballistic are significant as stated previously.

3. Permanent Satellites

Very little will be said concerning this type of configuration for by definition, re-entry is not a requirement. It is reasonably obvious that the vehicle selected would be one which tended to minimize launch weight, launch stability problems, generate total compatibility and assure sufficient volume for satisfying the payload and mission requirements. Various approaches from the module tank concept to huge spheres have been proposed and advantages have been cited for each concept. It is neither the purpose nor the scope of this paper to pursue or attempt to resolve the questions concerning the choice of configuration for this application for it is felt that in confining the discussion to re-entry vehicles more than sufficient problems exist for meaningful discussion. Suffice it to say that if the proverbial "barn door" will satisfy the mission requirements then, by all means, the "barn door" should be orbited as the permanent satellite.

B. Manned Missions

The major emphasis of this paper will be directed toward the manned mission, for it is felt that such applications are of primary interest for future investigation.

1. Recovery From Restricted Orbits

If it is desired to locate the re-entry vehicle at some predesignated point on the earth's surface in terms of latitude and longitude, some lifting efficiency will be required. The particular class of applications of which we are concerned here will be represented by orbital applications which are

constrained in terms of both inclination angle, number of passes and launch site. It will be assumed that the launch site is located within the ZI and that orbital inclination angles are between 28° and 90° , or the restricted polar orbit. The number of orbital passes initially, if restricted to three, will always allow passage over the Continental United States. Under these particular stringent constraints, it appears that most missions of this type can be satisfied with hypersonic lift-to-drag ratios of 1.5 through 1.8 and that some particular missions within this category can be satisfied with hypersonic lift-to-drag ratios of 1. This should be more than sufficient to guarantee enough lateral maneuverability to allow some selectivity in the choice of landing site. If the restriction on the number of passes is removed, it is still possible to accomplish return to the Zone of the Interior for approximately 50% of the orbits with hypersonic lift-to-drag ratios of 1 and the percentage of orbits from which return can be accomplished with L/D's in the order of 1.8 will be greater. Early papers by Eggers, Allen, Niece and other authors concentrated heavily on the pure boost-glide mission, but in view of the difficulties experienced in obtaining high hypersonic lift-to-drag ratios, the general tendency in recent years has been to no longer emphasize this particular application. This decision, of course, was not without its justification, for the energy requirements with low lift-to-drag ratios were essentially the same as those required for complete orbital vehicles.

Now as for the types of configurations which will best satisfy these mission requirements for manned return from restricted orbits, there are a number of possible choices. Since we are talking in terms of lift-to-drag ratios from approximately 1.0 through 1.8, no significant state-of-the-art improvements are required and either winged gliders such as the Dyna-Soar or lifting bodies from modified lenticular through M-2 type of configurations will be quite satisfactory. For that matter, if conventional landing is not a requirement and if restricted orbital inclinations similar to those used in Project Mercury, $1-33^\circ$ are used, then simple blunted elliptical cone configurations could be used which would guarantee enough lateral maneuverability to allow some selectivity in the choice of landing site. Figure 2 indicates some of the possible configurations which would satisfy the design requirements of this class of missions.

Now we have been discussing orbital applications which are clearly extremely restricted and which, indeed, do not offer much flexibility; for the constraints such as inclination, number of passes, launch site, if stringent enough, can be satisfied by a pure ballistic vehicle such as the Mercury capsule. Indeed, we have removed some of the restrictions such as number of passes and we have added an additional requirement of selectivity in choice of landing site requiring lateral maneuverability and hence corresponding hypersonic efficiency in terms of lift-to-drag ratios. We have established a trend toward the lifting vehicle in order to assure some degree of versatility for manned operations even for these restricted applications, nevertheless, severe limitations are still apparent relative to orbit selectivity and return interval in hours required, for even in the case of the $L/D \approx 1.8$ it may be necessary to delay re-entry up to as much as seven hours to achieve touchdowns at certain given locations within the ZI.

2. Recovery From Selected Orbits

In order to assure even greater versatility in terms of orbit choice and availability, it seems desirable to employ higher aerodynamic efficiency and hence generate a corresponding increase in the lateral capabilities of the re-entry vehicle. If we remove the restrictions relative to both the launch point and the orbital inclination angle and address ourselves to orbits which may have inclinations from 0 to 90 degrees, then it will be necessary to generate hypersonic lift-to-drag ratios greater than 2.0 to assure one pass return from at least 60 percent of the orbital possibilities. As the lift-to-drag ratio increases, this value, of course, rapidly improves to say, for an L/D of 2.5, something in excess of 80 percent. For certain orbital inclinations, the return interval still may be in excess of five hours, however, a large operational capability is now available in the vehicle.

Now the achievement of these higher lift-to-drag ratios is not an easy task for low density effects in the regions of high maneuverability $V \sim 23,000$ fps can influence such configurations in terms of a large increase in the friction drag, in other words, for certain re-entry paths, the configurations can be viscous controlled and may not be wave drag dominated. Figure 3 gives some inclination of the magnitude of this problem and it can be readily seen that hypersonic L/D ratios can drop from 5.0 to approximately 2.0 in the strong viscous regime. The highest known lift-to-drag ratio generated in a relatively strong viscous regime to date has been 2.6 on the FSL-I configuration tested by ASD, but this was on a high fineness ratio asymmetric elliptical cone with a low bluntness ratio presenting the optimum flat surface to the impinging air. It is believed to be currently possible, however, with careful configuring to generate lift-to-drag ratios of this magnitude for practical configurations - that is to say that it is within the state-of-the-art although some advanced cooling techniques most probably would be required.

3. Recovery From Arbitrary Orbits

We have indicated that a considerable amount of increased operational flexibility can be realized with an increase in the hypersonic lift-to-drag ratio. If the previously mentioned restrictions in orbital applications are completely removed and if we now address ourselves to the problem of return from an arbitrary orbit from an arbitrary point along the orbit, we will have considered the most completely versatile operational case. It can be shown that return can be accomplished to the Zone of the Interior for all orbital cases with a hypersonic lift-to-drag ratio of 3.5 or greater. Now, as we have previously suggested, this represents quite a difficult task and is not currently within the state-of-the-art, however, it is felt that this represents a worthwhile goal for design of future vehicles for re-entry from close proximity orbits.

Now it can be seen from Figures 4 and 5 that not only can return be made from all orbital cases, but that the return interval would reduce only to the time required for re-entry itself and that no lingering or waiting time would occur. The most probable configuration choice for such an application is a difficult conjecture at this point in time for only recently has an attempt been made to deliberately obtain very high hypersonic lift-to-drag ratios. Since extreme aerodynamic efficiency is required, very little bluntness can be tolerated and the configuration obviously will have to employ advanced cooling techniques such as transpiration or film ejection. In addition, fairly compact shapes will have to be chosen to minimize the surface area, for heat protection weight increases sharply with area as well as the friction drag which, in the strong viscous regime, most adversely affects the lift-to-drag ratio. Since volumetric efficiency is generally desirable, it would appear that an extremely carefully designed lifting body employing optimized geometry would represent the most likely candidate for these mission requirements. Perhaps the salient thing to emphasize here is that the trend is clearly towards increased aerodynamic efficiency in terms of lift-to-drag ratio and at least at this point in time toward the optimized lifting body requiring breakthroughs in cooling. It may not be possible to aerodynamically achieve the total lift-to-drag ratio requirement of 3.5 because of the previously mentioned strong viscous effects in the region of high maneuverability, nevertheless, it is felt that such an attempt will be worthwhile for, if successful, significant operational dividends can be realized. Several detail design approaches will be discussed later in this paper, and Figure 6 summarizes the trend toward the increased aerodynamic efficiency as a function of mission complexity.

4. Tangential Landing Requirements

In the previous section, we have established the hypersonic lift-to-drag ratios required for recovery from restricted, selected, and arbitrary orbits. Considering, now, the low and mid speed portion of the velocity spectrum, we are confronted with the requirement for a tangential or conventional landing capability. At this point in time, this requirement cannot be treated lightly, for historically the Air Force has always consisted of manned vehicles. Even though the sphere of operation of these manned vehicles is currently being extended and the vehicle has radically changed in appearance, we cannot expect the requirement for tangential landing to disappear in the future. Current operational aircraft generate subsonic lift-to-drag ratios which provide reasonable landing characteristics. But even with these more conventional aircraft there is a trend toward lower subsonic lift-to-drag ratios. This trend is particularly evident in the case of the X-15 which displays a poor subsonic lift-to-drag ratio and which, consequently, results in high rates of sink and landing speed. The high speed re-entry vehicle is usually even more unconventional in design and the subsonic lift-to-drag ratio is generally quite poor because of the high sweep, low aspect ratios and broad base areas normally characteristic to such vehicles.

These vehicles must ~~possess~~ subsonic lift-to-drag ratios on the order of five and with wing loadings not much in excess of 50 to provide good landing and sink speeds which increase the time available for pilot reactions and provides a vehicle with improved handling qualities. In addition to the high lift-to-drag ratio, a high lift curve slope is required to provide good lifting characteristics at low angles of attack. This enables the pilot to make only minor adjustments when drag is increased due to lowering of landing gear and other landing aids. In addition, the high lift curve slope decreases touchdown velocity and since high lift is provided at low angles of attack, it is easier to stay within the structural limits, when touchdown occurs, for the angular rate of the nose gear about the main gear is more easily controlled; hence, decreasing the impact loads on nose gear and fuselage.

Figure 7 shows the distinction between landing characteristics as a function of lift-to-drag ratio. Superimposed are the various classes of configurations and it is readily apparent that the re-entry vehicles designed to date have poor landing characteristics. To obtain good low speed characteristics, those portions of the vehicle's geometry which contribute most to the low speed aerodynamics must be optimized for subsonic flight. For instance, the upper surface should be contoured to resemble efficient low speed airfoils, for the lifting efficiency is dependent on this geometry; the leading edge should tend toward the conventional low speed geometry; and the base area should be minimized to reduce the base drag contribution.

With these thoughts in mind, a re-entry vehicle with a lift-to-drag ratio of the order of five can be obtained thus giving acceptable landing characteristics.

5. Compounded Requirements

The previous discussions have established the requirements for high lift-to-drag ratios at both ends of the velocity spectrum, that is, at hypersonic and at subsonic velocities. This immediately imposes on the designer two boundary conditions which, at first thought, seem to be incompatible. The features which are desired hypersonically are not generally beneficial at subsonic speeds. As an approach to this problem, the MDF-1 was designed for superorbital re-entry and tangential landing. This vehicle employs, essentially, a dual design approach to accommodate both the high and the low ends of the velocity spectrum. The lower surface is flat for hypersonic aerodynamic efficiency as dictated by Newtonian Theory; the nose and leading edges are contoured for heating with a consideration given to the performance potential at the lower speeds; the sweepback is dictated by the heating with an aspect ratio selected which would be compatible with the landing phase. The upper surface is contoured for subsonic velocities and the large base has been deliberately minimized. Employing these design features, the hypersonic lift-to-drag ratio of approximately two is complimented with a subsonic lift-to-drag ratio of about 6. The hypersonic lift-to-drag ratio is, of course, below the 3.5 which was previously suggested; but the concept itself, that is

the dual design approach, does provide a point of departure for additional investigations. The MDF-1 is not meant to be an optimum, but only a new design concept. Hence, we see that the possibility of successfully combining the compounded design points into one re-entry vehicle is not only required, but is indeed possible.

6. Optimization Parameters and Configurations

In considering the over-all design of the vehicle one must be aware of the compromises involved to obtain certain ingredients within the design concept to successfully fulfill the specified mission or to enable a vehicle to have the growth potential to advance to a higher degree of sophistication. Listed below and shown in Figure 8 are a few of the optimization parameters to be considered which have a direct bearing on the over-all design of re-entry vehicles.

- a. Weight
- b. Volume
- c. Wetted area for volume
- d. Launched stability
- e. Low speed characteristics
- f. Lateral maneuverability

Considering, for the moment, the first optimization parameter of weight; from past experience and analysis we have found that by decreasing the exposed wetted area there is a considerable decrease in the requirements for heat protection resulting in a decrease in the over-all weight of the vehicle. The configuration which lends itself best to this optimization parameter is the lifting body type of configuration. This result goes hand and hand with the second parameter of volume for it is readily apparent that a body configuration will have a higher internal volume to exposed wetted area ratio than a winged glider configuration. Hence, one is able to obtain more useful volume per wetted area which describes the third parameter. In optimizing for these first three parameters the trend is toward the lifting body. Using a lifting body on a booster system it now becomes apparent that this configuration more readily adapts itself to our present day booster systems. The booster system does not require large fins to overcome destabilizing moments created by the body as in the case of the winged vehicle as represented by the Dyna Soar configuration. As a result of employing the lifting body on a booster system the desired launch stability can be readily and economically achieved. In addition, it should be pointed out that by reducing the wetted area to volume ratio an increase in the hypersonic lift-to-drag ratio would result since the wetted area would decrease which would, in turn, result in a decrease of the skin

friction drag. This increase in the hypersonic lift-to-drag ratio makes itself apparent in an increase of lateral maneuverability. After consideration of the optimization parameters, with the exception of low speed characteristics, the trend is toward higher aerodynamic efficiency and a lifting body configuration. It is appropriate to mention that current vehicles are not volume limited but are, rather, weight limited because of the available boosters. On the other hand, as new launch systems such as the Saturn and Titan III are developed, the limitations on vehicle weight will be reduced and, may no longer represent a significant obstacle.

SECTION III

CONFIGURATIONS AND TECHNICAL CONSTRAINTS

The problems which must be solved and the constraints which must be considered vary somewhat throughout the velocity spectrum from very low to hypervelocity speeds and at the various altitudes from sea level to in excess of 400,000 ft. There are quite a number of compromises which must be made in the associated disciplines of aerodynamics, structures, and dynamics to provide a complete capability within the entire flight spectrum. Figure 9 is a typical altitude velocity map showing a re-entry from high energy orbit or a lunar mission to the earth's atmosphere. An attempt has been made to indicate the areas and at least some of the major problems which have to be solved relative to the various velocity regimes. In the superorbital regime, we can say that the largest percentage of problems are those associated with very critical heating, both the convective and radiation effects, and, of course, the problems associated with developing efficient structures, including the dynamic effects, to perform in this extreme operating environment are perhaps the most difficult. At the suborbital velocities experienced during return from orbital applications, we note that the problems again are largely associated with high heating and the stability of the vehicle, although reusable and efficiently designed structures still represent a major problem. At the interim speeds; essentially supersonic and hypersonic velocities, we are concerned with a host of problems; generally at the supersonic speeds to improve the aerodynamic efficiency or at hypersonic speeds to develop configurations which can operate in a semisustained flight or a mode with large degrees of maneuverability, sufficient stability, and still generate reasonable total performance characteristics. At the low speed, of course, the problems are those which are quite obvious, such as that of the low speed aerodynamics of new candidate designs, and the actual landing problems such as sink rate, approach, and touchdown.

With the advent of this possibility of re-entry from supercircular, parabolic, or hyperbolic velocities, the design constraints associated with the selection of one fixed configuration become overwhelming and, for that matter, even paradoxical. It is immediately obvious that if a manned vehicle re-enters at supercircular velocities, it must perform reasonably well at the circular, suborbital, and low speed regions of the corridor. If the vehicle is to be landed in a conventional manner, the problem of total vehicle design becomes most complex, for many design compromises have to be made. The following table and Figure 10 summarizes desirable vehicle characteristics as a function of speed regime.

| <u>Low Speed and Landing</u> | <u>Hypersonic and Orbital</u> | <u>Superorbital and Hyperbolic</u> |
|---------------------------------------|---|---|
| High Aspect Ratio | Low Aspect Ratio | Low Aspect Ratio |
| Low Sweep | Medium Sweep | High Sweep |
| Moderate or Conventional Leading Edge | Very Blunt Leading Edge and Noses | Less Bluntness |
| Small Base Area | Large Base Area | Large Base Area |
| Contoured Upper Surfaces | Flat Bottom (Cylindrical Bottom Reduces Lift 40%) | Low Curvature Bottom (To Reduce Radiation Heating) |

The actual bluntness required at superorbital and hyperbolic speeds may be, of course, dictated by the requirement of minimizing the stand off distance of the shock and thereby reducing the heating due to hot gas radiation.

It is readily apparent that to design all these constraints into one fixed configuration is a monumental task and that even if the vehicle can be made to function reasonably well through the entire speed range, it represents, at best, a compromised configuration for any particular velocity portion of the flight. If any optimization is to occur, it immediately suggests that a variable geometry configuration should be considered and various concepts will be discussed later in the paper.

In view of the supercriticality of the problems associated with superorbital re-entry, it is considered appropriate to discuss this particular region in some detail. It should be pointed out here, that at sub-orbital and circular orbit re-entry, the convective heating dominates and the heat flux is given by Lester Lees as being:

$$\dot{q}_{\text{conv.}} = \frac{[21.9 \rho_{\infty}^{1/2} (\frac{V_{\infty}}{1000})^3] [1 - \frac{hw}{hst}]}{\sqrt{R}}$$

At supercircular re-entry velocities the hot gas radiation becomes significant and at certain altitudes of re-entry may even become dominant. Lees' hot gas radiation heating equation (based on the works of Kivel) can be expressed:

$$\dot{q}_{\text{ngr}} = 7.5 R \sigma^{1.5} (\frac{V_{\infty}}{1 \times 10^4})^{12.5}$$

The total aerodynamic heating of the re-entry vehicle becomes:

$$\dot{q}_{\text{total}} \sim \dot{q}_{\text{conv}} + \dot{q}_{\text{hot rad.}}$$

The amount of heat radiated depends upon the depth of the radiating layer and hence the shock detachment distance and $\dot{q} \propto R$. The heating is increased by increasing the body radius or, in other words, the degree of bluntness. At lower speeds, however, $\dot{q} \propto \frac{1}{\sqrt{R}}$ and the heating was reduced by blunting the configurations.

We have here two competing design constraints which must be considered when a vehicle is to re-enter from supercircular speeds and still perform efficiently through the suborbital portions of flight.

At supercircular re-entry velocities, we have quite substantial values of dynamic pressure which again make aerodynamic control surfaces appear extremely attractive. The heating problems associated with such surfaces are, however, most severe and unique or sophisticated heat protection schemes will have to be developed before they can become a reality. Lift values will be, to a large extent, modulated during supercircular re-entry which will, again, cause some rather serious design problems associated with stability throughout a large range of angles. Certainly, at this point in time, it also appears to be desirable to have a large lift capability. It can also be shown that lift-to-drag ratios around 1.0 to 1.2 are quite satisfactory at these speeds relative to "pull-out" points and corridor widths. No practical gains should be anticipated for first generation superorbital vehicles for lift-to-drag ratios in excess of these, for, again, at this point in time, they would not be practical because of the long term re-entry and exposure times which would result. As shown in Figure 11 however, considerable gains in corridor widths can be achieved with increased lift-to-drag ratios when modulation is employed consequently, the trend is to the high lift-to-drag ratio with breakthroughs in advanced cooling techniques such as film ejection and transpiration for second generation superorbital designs. This, of course, is particularly true at suborbital speeds where lateral maneuvering would be accomplished. Figure 9 shows a typical altitude -- velocity relationship for supercircular re-entry as well as the broad aerodynamic problems associated with each re-entry regime. The "pull-out" points are shown for typical values of the flight path angle. The values of γ are taken as occurring at 400,000 ft. altitude. It is readily apparent that as steeper entry angles are employed, the "pull-out" points fall deeper in the atmosphere and further compound the heating problem. The heat flux lines for both convective and radiation are indicated, the significance of the hot gas radiation is shown for $\dot{q} = 1000 \text{ BTU/ft}^2/\text{sec}$. The re-entry times at velocities above the circular orbital velocity are of a reasonably short or medium duration, 2 1/2 to 12 minutes; consequently, the ablation techniques appear quite promising. At suborbital speeds, however, where re-entry times are much higher and heat flux peaks are significantly lower; the radiative techniques are most efficient because of the large weight penalties associated with ablation. It is obvious that if a vehicle must perform efficiently throughout the complete corridor; the composite approach will be highly desirable.

Figure 12 shows the design trend in hypersonic configurations as a function of velocity ratio. One additional comment should be made relative to the flight mechanic techniques at supercircular re-entry. Shallow re-entry angles with negative lift now appear quite promising; however, if an extremely steep re-entry is employed, positive values of lift may be used through the high velocity portions of flight. It may be advisable, after the "pull-out" point is reached, to employ either negative lift or to roll over and direct the lift towards the earth. These particular maneuvers will enable higher altitude re-entries and the peak heating should be reduced. Longer re-entry times will occur, however, and consideration will have to be carefully given to the total integrated heating. Figure 13 shows the variation in re-entrant characteristics for both the shallow, $-C_L$, and steeper, $+C_L$, initial entry conditions. Again, the precise choice of re-entrant mode still is opened to legitimate question. If a continuous modulation of the lift is followed, it will be possible to execute a wide range of flight paths, but dynamic pressure limits must be carefully considered.

SECTION IV

CONFIGURATIONS AND GROWTH POTENTIAL

Perhaps one of the most serious problems associated with the expanding technology of re-entry dynamics and the resulting specific system implementation is the alarmingly increasing costs. A general realization has occurred that the costs of highly sophisticated systems can rapidly become prohibitive and that design and mission goals must be carefully evaluated and delineated before large expenditures are committed. It is readily apparent, then, that the particular concepts selected for future emphasis should be those which inherently possess the largest flexibility and versatility. In other words, in the case of a manned re-entry system, it appears desirable to pursue a design procedure that will enable a large number of mission applications and which will, in fact, perform many different jobs with an explicit potential for reusability. Prefaced with these remarks relative to costs and performance flexibility, additional comments pertinent to growth potential can now be made. Since the payload to gross weight ratio also is a factor which must be considered relative to growth potential, it is appropriate to consider such parameters again, such as volumetric efficiency and weight. Figure 14 clearly demonstrates that the payload to gross weight ratio favors the choice of the lifting body configuration over, say, the winged glider. In addition, the lifting body designs normally have inherently large usable volume capabilities and as previously mentioned, wetted surface areas are minimized thereby more efficiently employing the heat protection weights and reducing the skin friction drag contribution. With the increased launch capability soon to be realized with the Saturn and Titan III booster systems, a much wider range of possible mission applications will be worthy of serious consideration and increased velocity potentials will be complemented with reduced restrictions on vehicle weight. This will reflect itself by requiring vehicle designs with much broader performance capabilities than those currently being pursued. In particular, it has recently been shown by some investigators that considerable advantages are associated with vehicles which have the capability of operating in high energy orbits beyond the Van Allen belts, for detection and interception problems are significantly reduced. This, of course, implies that if it is desired to re-enter the earth's atmosphere on a single pass to avoid exposure to radiation as well as the other psychological and military disadvantages associated with multi-pass re-entry, then the resulting re-entry velocities can be easily in the order of 35,000 fps. In order to assure a large corridor capability for a second generation system of this type, a vehicle with high aerodynamic efficiency with modulation capabilities would be advantageous. In addition, the large lift-to-drag ratio capability of such a vehicle would enable significant maneuvering potential for return to the ZI. As mentioned in a previous section, however, advanced cooling techniques such as transpiration or film ejection would be required but this factor in itself, would contribute significantly to the reusability of such vehicles which we have already mentioned as a highly desirable requirement for the future manned lifting re-entry system. In summary then, in view of

the projected growth potential requirements such as volume, high energy orbital applications, large corridor widths, maneuverability, increased booster capabilities and, most assuredly, costs, the trend clearly appears to be toward the highly aerodynamic efficient lifting body design concept.

SECTION V

CONFIGURATIONS AND SUPPLEMENTAL AIDS

It has been shown, in a previous section, that if it is desired to assure a capability throughout the complete corridor, then it may be worthwhile to consider the use of some sort of variable geometry. Now the configuration can be made to vary its geometry in many different fashions. The various possibilities which are listed are only representative and no effort has been made to perform an exhaustive survey of all potential variations.

1. Variations in nose shape and wing characteristics
2. Control surface configurations and locations
3. Aft section geometry (modulation or mutation)
4. Modulated nose canting
5. Mass ejections
6. Magnetogasdynamics
7. Lift augmentation devices
8. Drag control techniques
9. Inflatables

From this very brief listing, it is clear that there are several different types of variable concepts involved, some, such as magnetogasdynamics, which can be termed pseudo variations, would be employed only at the very high velocities; others, such as modulated nose cantings might be used at interim velocities, still others, such as mutation or modulation of aft section geometry or variations in the wing characteristics such as sweep would probably be logically accomplished at the lower speeds.

A. Expandables

Perhaps one of the more promising areas to explore, however, regarding the use of variable geometry is at the low speed or landing phases of flight. The judicious use of expandable structures appear to offer significant pay-off. Specifically, the use of expandable structures applied to re-entry type vehicles would offer large dividends in the terms of aerodynamics and performance augmentation. These expandable surfaces could be deployed after the vehicle has slowed to subsonic speeds. In this case, the heating would not present a problem and it would permit crew escape in the event of malfunction. It would be possible, of course, to use inflation

to produce a basic vehicle optimized specifically for the subsonic speed regime, however, many practical design problems would be involved and it is difficult to say the pay-off would be as significant as one might postulate. Rather, the expandable structures, in terms of wings, could be used to decrease the sweep of the wing, increase the effective aspect ratio, and to optimize the leading edges, thereby producing a much more efficient lifting vehicle and a reduction in the wing loading, Figure 15 indicates the effect. Further, subsonic optimization can be obtained with the use of afterbody fairings. This, in effect, would boattail the base and would result in a sizable reduction of the base drag which, at subsonic velocities, is a large portion of the total drag.

It should be clearly recognized, however, that aerodynamic control of these expandable structures may be rather difficult to achieve and much effort would logically be required in this area. Another problem area would be the actual in-flight deployment of the expandable structure and control and safety considerations involved.

B. Decelerators

Another area in which variable geometry could achieve significant pay-off would be that of the superorbital velocity re-entrant vehicle. Specifically, the use of aerodynamic drag devices in order to independently modulate the drag relative to the lift of the re-entrant vehicle appears to offer considerable promise. This drag control technique could take the form of many different types of configurations. It may be the final stage of the booster which is retained in order to augment the drag during initial portions of the superorbital re-entry. On the other hand, it may be a variable geometry drag device which could modulate its drag as penetration occurred within the superorbital corridor. The device most probably would either be allowed to burn off or disconnect prior to the interim re-entrant portions of flight, that is, after the superorbital portion of the flight had been terminated or perhaps even after the "pull-out" point into the corridor had occurred. Figure 16 shows two different drag brakes considered for superorbital applications as suggested in Reference 9 by Alexander, while Figure 17 clearly indicates the performance advantages associated with their use during superorbital re-entry.

It is not a difficult task to make conjectures as to the nature of the configuration changes, it is quite a different problem to apply such concepts, however, on a practical design basis. Nevertheless, it is felt that as re-entry technology improves, a natural evolution to the variable geometry configuration can be anticipated. The extent of predicted success for such configurations is, of course, somewhat nebulous and will, by nature, be altered as more information is obtained. It is safe to say, however, that as additional knowledge is gained, new and perhaps even more challenging ideas will be evolved for technical exploitation relative to the variable geometry concept.

C. Advanced Design Concepts

It has been shown, in a previous section of this paper, that a concept which has considerable promise is that where the upper surface of the re-entry configuration is designed in an effort to try to optimize or increase the efficiency of the aerodynamic lift at low speed while designing a lower surface for the other major constraints of the vehicle adequate for re-entry conditions such as a flat surface in order to generate high hypersonic efficiency. This particular concept, as indicated in Figure 18, is being pursued with the development of MDF-1 configuration at the Aeronautical Systems Division.

It has also been shown that considerable promise now seems to exist for use of variable geometry for new configuration concepts. For, indeed, any effort or any attempt to optimize a configuration for the broad flight regime could only be accomplished by the use of such methods. But perhaps the most significant design trend is that for a vehicle which is capable of re-entering at superorbital velocities, generating a wide corridor, a large amount of lateral maneuverability, and finally, possessing a tangential landing capability. This appears to offer considerable promise for a future system to be developed by the United States Air Force. The configurations which best lend themselves for re-entering at these extreme conditions are essentially lifting bodies. It can also be stated that the configurations should have reasonable useable volume and every effort should be made to reduce the wetted surface area and the resulting skin friction drag particularly for the regions that are viscous controlled.

A particular design approach which appears to show considerable promise is for an operational vehicle with a high degree of reusability and maneuverability and which could re-enter the earth's atmosphere from an arbitrary point in an arbitrary orbit and still land within the Zone of the Interior of the United States. The lift-to-drag ratio requirements for such a mission would be hypersonically in the order of $3 \frac{1}{2}$, as previously mentioned. This indeed, presents a formidable design problem. As previously mentioned, the vehicles within the region of high maneuverability, that is, velocities in the order of 24,000 feet per second can be viscous controlled and to date, the highest known lift-to-drag ratio obtained within the strong viscous regime has been in the order of 2.6. Consequently, studies are currently being pursued at the Aeronautical Systems Division to determine just what the limiting hypersonic lift-to-drag ratio will be over practical configurations and whether, indeed, it is at all possible to aerodynamically obtain a lift-to-drag ratio of $3 \frac{1}{2}$. Such configurations obviously would not and could not be blunt. Consequently, it would be necessary to use sophisticated cooling techniques such as transpiration cooling or mass transfer cooling if such configurations were ever to become a reality. Nevertheless, it appears to be a reasonable design goal for the Air Force to obtain the capability of designing a vehicle which could, as previously mentioned, orbit the earth in an arbitrary orbit, deorbit at an arbitrary point, and still return to the Zone of the Interior.

Figure 19 shows an approach to such a configuration. It can be seen that every effort has been made to minimize both the wave drag and the skin friction drag while still producing a lifting configuration of some efficiency. Work performed at both NASA and ASD has indicated that the optimum planform of such a vehicle will, in general, be a cross between that dictated by the wave drag and that dictated by friction considerations. The flat lower surface is dictated as being optimum by the Newtonian Theory. On the other hand, it can be shown that an isentropic surface, if designed properly for viscous considerations, could potentially offer significant gains in terms of lifting efficiency. One additional comment is appropriate relative to the selection of the particular planform. If no bluntness is used and the chord and span are set as constraints, then it would appear that the rectangular planform would offer a promising choice, as shown in References 12 and 13. Again, however, it is tied intimately in to the reduction of wave or pressure drag and the reduction of friction drag in the viscous controlled regimes. Hence, a compromised planform has been selected with hopes that both the pressure as well as the skin friction drag can be minimized. This figure also shows representative experimental data from a series of high lift-to-drag ratio configurations. It can be seen that to obtain hypersonic lift-to-drag ratios of 3.5, a major design breakthrough appears to be required; and additional applied research obviously will have to be pursued relative to the nonconventional or sophisticated cooling techniques. In other words, large bluntness cannot be tolerated for the highly efficient hypersonic vehicle.

D. A New Technique

An auxiliary relief method for use during the superorbital portion of flight has been considered at ASD. The technique is to incorporate a small propulsion unit within the re-entry vehicle located, for initial study purposes, at the center-of-gravity of the configuration. The device is used primarily as an additional lift generator with the propulsive force directed toward the earth, in other words, to help "hold the vehicle at higher altitudes". It appears to be particularly attractive for use immediately prior to the "pull-out" portion of the flight path into the corridor. By employing such a technique, it now appears possible to significantly tailor the flight path and to avoid the rather deep penetrations into the atmosphere which normally occur at the "pull-out" point. The device enables, in essence, the elimination of the "pull-out" point by decelerating the vehicle at a higher altitude and a gradual transition to the subsequent flight path as shown in Figure 20.

Of course, the initial re-entry was assumed to use positive lift for entry to the corridor, the technique could also be employed for different re-entries using negative lift. The propulsive force in this case would then be generated in the opposite direction. Treating the example case, however, that of positive lift, initial investigations seem to indicate that by modulating the propulsive force for a smooth transition to the latter flight path and elimination of the "pull-out" points, the requirements for such a device in terms of propulsive and weight requirements do not appear to be severe. This is true largely because the actual time for application is quite short, not in excess of 70 seconds, and the altitudes at which the technique is employed are reasonably high with relatively low densities involved. It can be seen from Figure 21 that by eliminating the "pull-out" point considerable reductions can be made to the heating experienced by the vehicle. The impact of this, of course, is the possible reduction of the critical structural and heat protection requirements associated with the severe environments experienced during the superorbital portions of flight. It may be possible to avoid the use of ablation techniques over certain portions of the vehicle. Now, it is true that the reduction of the "pull-out" point can also be achieved, by say, initiating re-entry with small negative values of the flight path angle, $\gamma \sim -5^\circ$, and by employing negative lift during the initial re-entry. Use of small values of the flight path angle, however, tend to approach the skip limits of such vehicles and the requirements imposed on the flight control system are usually extremely severe. It appears, at this point in time, that it would be desirable to negotiate re-entry with path angles somewhere between the skip limitations and those imposed by the aerothermodynamic-structural limits of the vehicle, for it should also be clearly understood that large values of the flight path angle $\gamma \sim -10^\circ$ are accompanied by extremely large increases in the dynamic pressures. The use of these interim path angles $-6^\circ \leq \gamma \leq -9^\circ$ would enable more unplanned deviations from the nominal and we would normally expect a reduction in the control requirements, consequently, it appears that the use of such a lift augmentation could be, indeed, beneficial. This technique has also another possible use as a recovery device in the event of a possible failure in the heat protection of the vehicle, for, again, if some preknowledge is had of, say, a fracture, then it may be possible for the astronaut to adjust and tailor his re-entry trajectory with the use of this lift augmentor to limit the maximum temperature to that of the basic structure, or at least to some value that can be accommodated by the ruptured system.

SECTION VI

CONCLUDING REMARKS

In conclusion, it seems appropriate to summarize our findings relative to the trends of hypervelocity vehicles. For the unmanned missions of weapon delivery and recoverable payloads from orbital applications, it appears that considerable dividends can be achieved with use of the aeroballistic and lifting body design concepts. In the case of pure weapon delivery, considerable gains in terms of lateral maneuverability, range augmentation and terminal control can be realized with this choice of the aeroballistic type of vehicle. The lifting body configurations seem to offer sufficient flexibility for the return of recoverable payloads although it appears that various sorts of landing aides should be used for the terminal and impact phases of flight. The payload to re-entry weight ratio definitely favors this choice over a winged glider, and in view of lateral maneuvering requirements, the ballistic vehicle does not appear particularly promising.

In the case of the manned lifting re-entry vehicle, we have viewed the trend from the four considerations of mission requirements, technical constraints, optimization, and growth potential and have attempted to demonstrate that these factors are not at all paradoxical, but indeed, suggest a common design point for advanced configurations. The advanced design trend clearly indicated by an individual and simultaneous analysis of these considerations is, definitely, to a vehicle with higher aerodynamic efficiency in terms of lift-to-drag ratio as shown in Figure 22. In view of the volumetric efficiencies, structural, and aerodynamic advantages associated with lifting bodies, a significant trend is to these types of configurations for advanced applications. Initially, for first generation superorbital re-entrant vehicles, it appears desirable to have reasonably substantial drag levels and the capability of independently modulating the drag from the lift in order to decelerate the vehicles at higher altitudes, reduce the exposure time, and consequently the heating which will occur during re-entry. On the other hand, for second generation manned lifting re-entry vehicles, either from circular or high energy orbits, it has been concluded that significant gains can be realized with an increase in the aerodynamic efficiency as reflected in the hypersonic lift-to-drag ratio. It has been shown that considerable gains can be achieved in the superorbital corridor width with modulated and increased lift-to-drag ratios and that with lift-to-drag ratios of approximately 3.5 it will be possible to generate a sufficient lateral maneuvering capability to effect a single pass return from an arbitrary point along an arbitrary orbit to the Zone of the Interior. The difficulties of achieving this aerodynamic efficiency because of the strong viscous effects have been recognized and, in fact, sufficient efficiencies may not be completely possible. Certainly, the need for advanced cooling techniques such as transpiration or film ejection has been delineated and were included in the new design approach employed with the MDF-4 configuration. We have also considered the problems associated

with landing such vehicles in a conventional sense and have proposed two techniques as possible solutions. The dual design approach of contouring the upper surface as reflected with the MDF-1 configuration and the judicious use of expandable surfaces in terms of variable wings and base fairings show particular promise for the augmentation of the vehicles characteristics during the terminal flight phases. Finally, a new technique for use during the superorbital portion of flight and as a possible solution to catastrophic eventualities has been proposed by the authors. The technique is to employ a small propulsive force primarily as a lift augmentor to eliminate the deep penetrations which occur in the atmosphere during the corridor "pull-out" and thereby reduce the total heating experienced by the re-entrant vehicles.

REFERENCES

1. Allen, H. Julian - "Hypersonic Flight and the Re-Entry Problem", Journal of Aeronautical Sciences Vol 25, Nr. 4, April 1958.
2. AEDC ARC Project Nr 311240, Preliminary Data, "ASD Re-Entry Configuration Evaluation", May 1962.
3. Draper, Alfred C. - "Possible Applications of the Aeroballistic Vehicle to Some Advanced System and Research Concepts", ASD TM 61-2, January 1961.
4. Eggers, A. J. Jr. - Ames Research Center, Moffett Field, California, NASA Unpublished Data, January 1960.
5. Boeing Unpublished Data "Why L/D" 1962.
6. Lees, L. - "Recovery Dynamics - Heat Transfer at Hypersonic Speeds in a Planetary Atom", Space Technology, John Wiley and Sons, Inc. 1961.
7. Kivel, B. - "Radiation From Hot Air and Its Effect on Stagnation Point Heating", Journal Aerospace Sciences, February 1961.
8. Chapman - "An Analysis of the Corridor and Guidance Requirements for Supercircular Entry into Planetary Atmospheres", NASA TR-55.
9. Alexander, Hankey, Belcher, Neumann and McLaughlin - "On Manned, Lifting Vehicle Entry into the Earth's Atmosphere from Supercircular Trajectories", ASNRFA Technical Memo, August 1961.
10. Dasken, W., and Seidman, M. H. - Investigations of Hypersonic Viscous and Inviscid Effects (Pressure and Heat Transfer Distributions on Lifting Configurations) (U), WADD TR 61-74, May 1961, CONF Rpt.
11. Adams, M. C. - "A Look at the Heat Transfer Problem at Super-Satellite Speeds", ASR Paper 1556-60, 1960.
12. Resnikoff, M. M. - "Optimum Lifting Bodies at High Supersonic Air-Speed", NACA RM 454B15, May 1954.
13. Ridyard, H. W. - "The Aerodynamic Characteristics of Two Series of Lifting Bodies at Mach Number 6.86", NACA RM L54C15, May 1954.
14. Eggers, A. J., Jr. and Wong, T. J. - "Motion and Heating of Lifting Vehicles During Atmosphere Entry", ARS Journal, Vol 31, Nr. 10, Oct 1961.

15. Sieron, T. - Unpublished data, "Estimation of the Aerodynamic Characteristics of a high L/D Configuration", ASD, Sept 1962.
16. Benson, B. and Neumann, R. - Unpublished data "Performance and heating Data on Auxiliary Aides During Superorbital Re-Entry", ASD, Aug 1962.
17. "Results of the Second United States Manned Orbital Space Flight"
NASA SP-6, May 24, 1962.

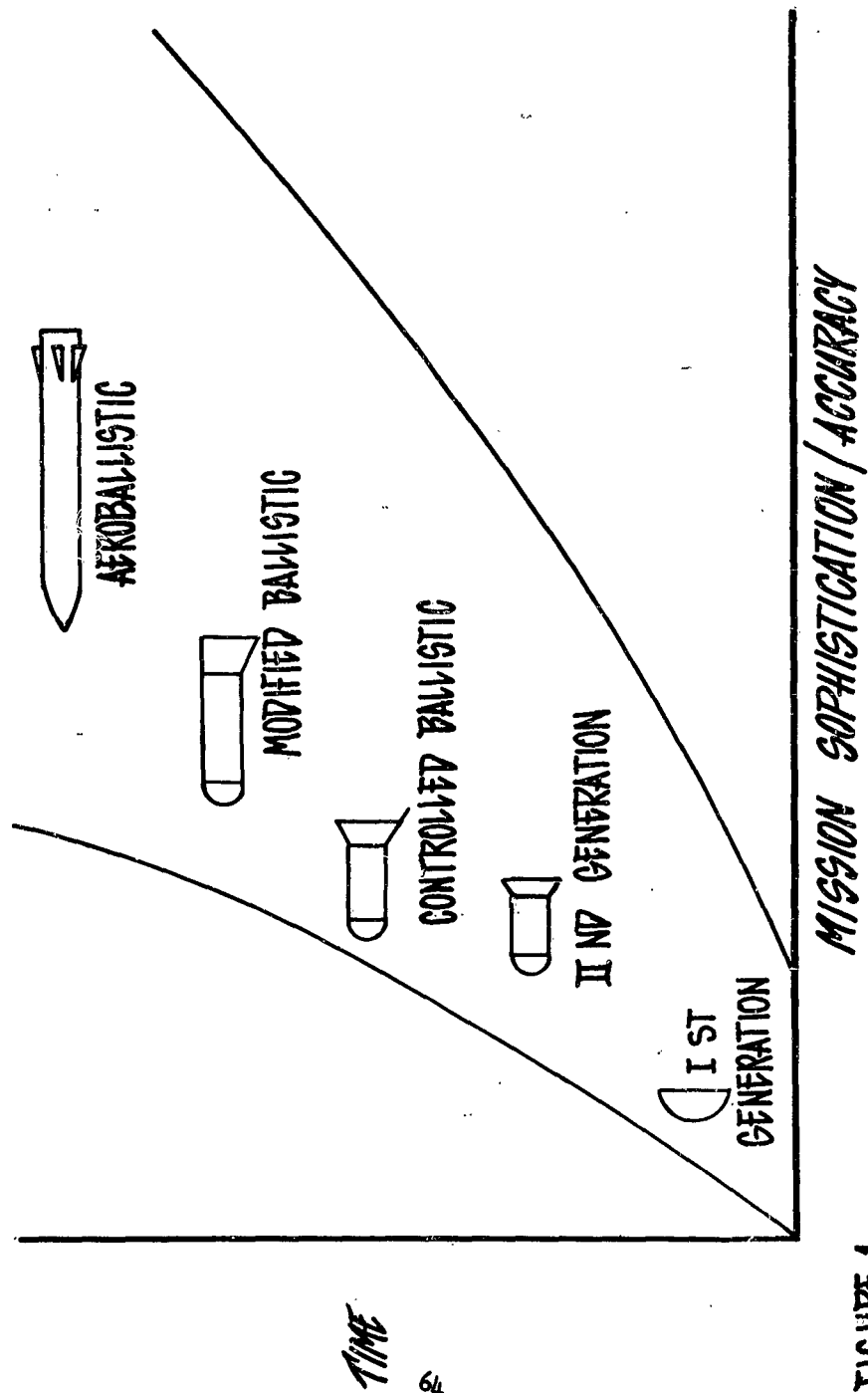
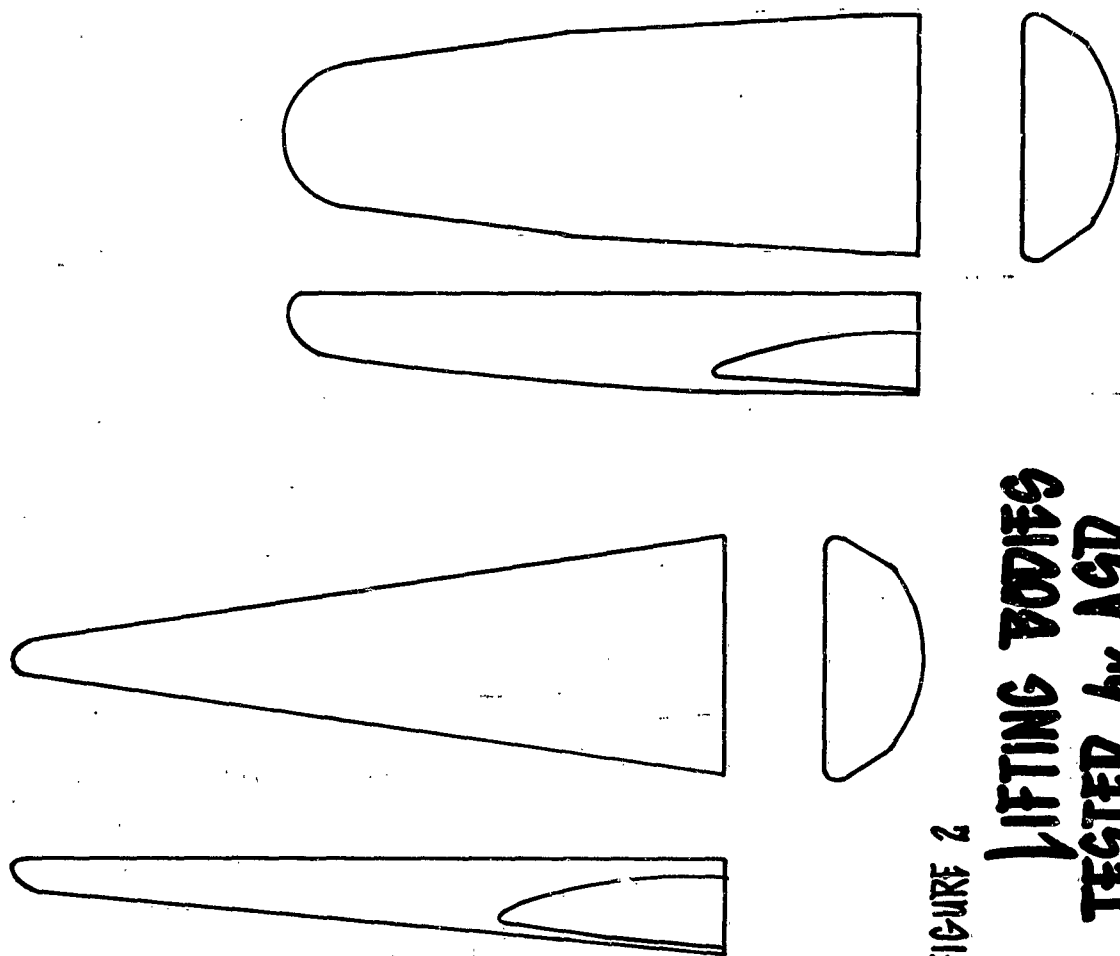
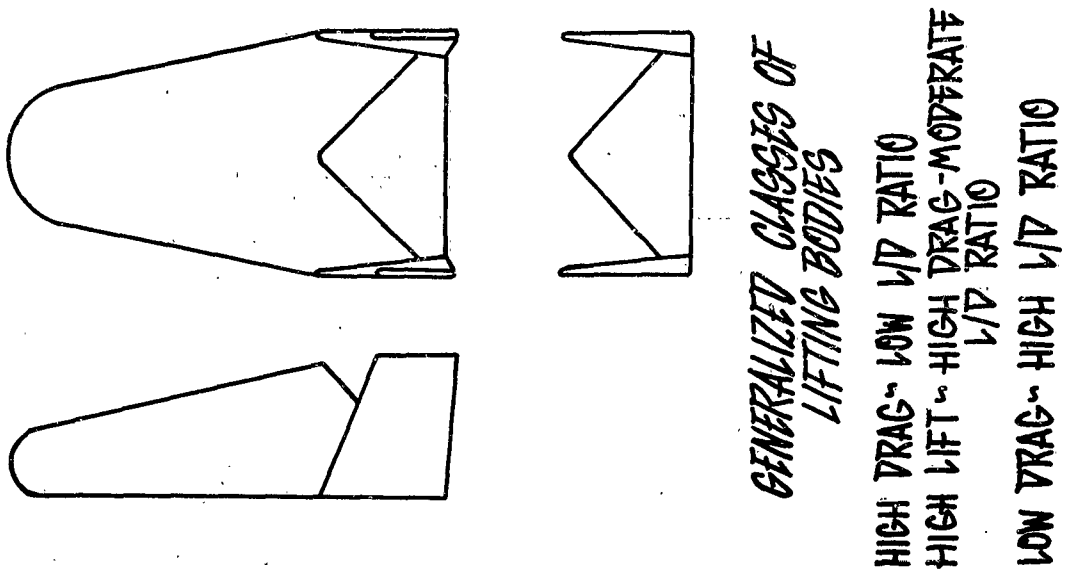


FIGURE 1

EVOLUTION of CONFIGURATIONS SUITABLE for WEAPONS



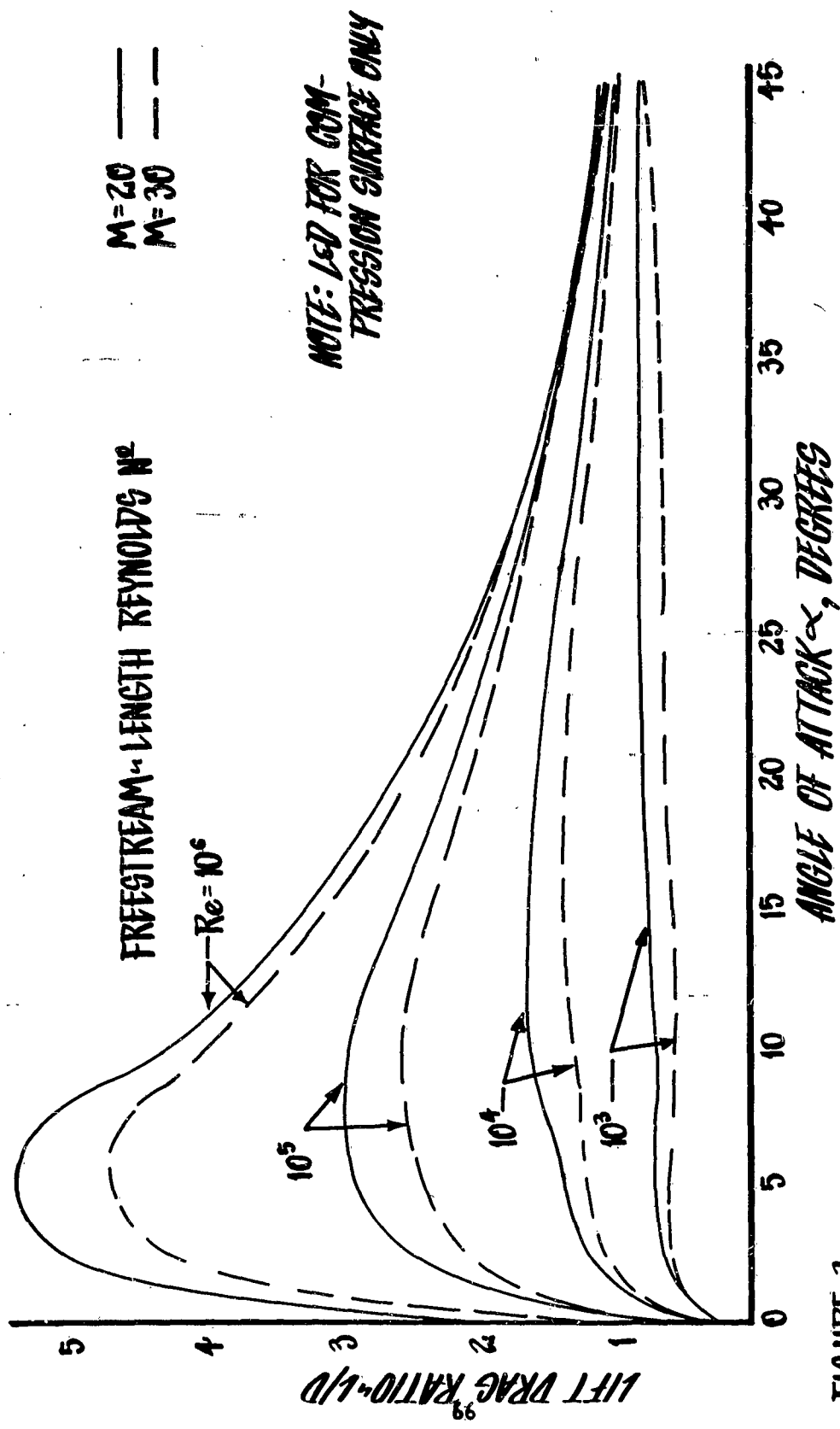


FIGURE 3

Viscous low density effects on the hypersonic lift-to-drag ratio

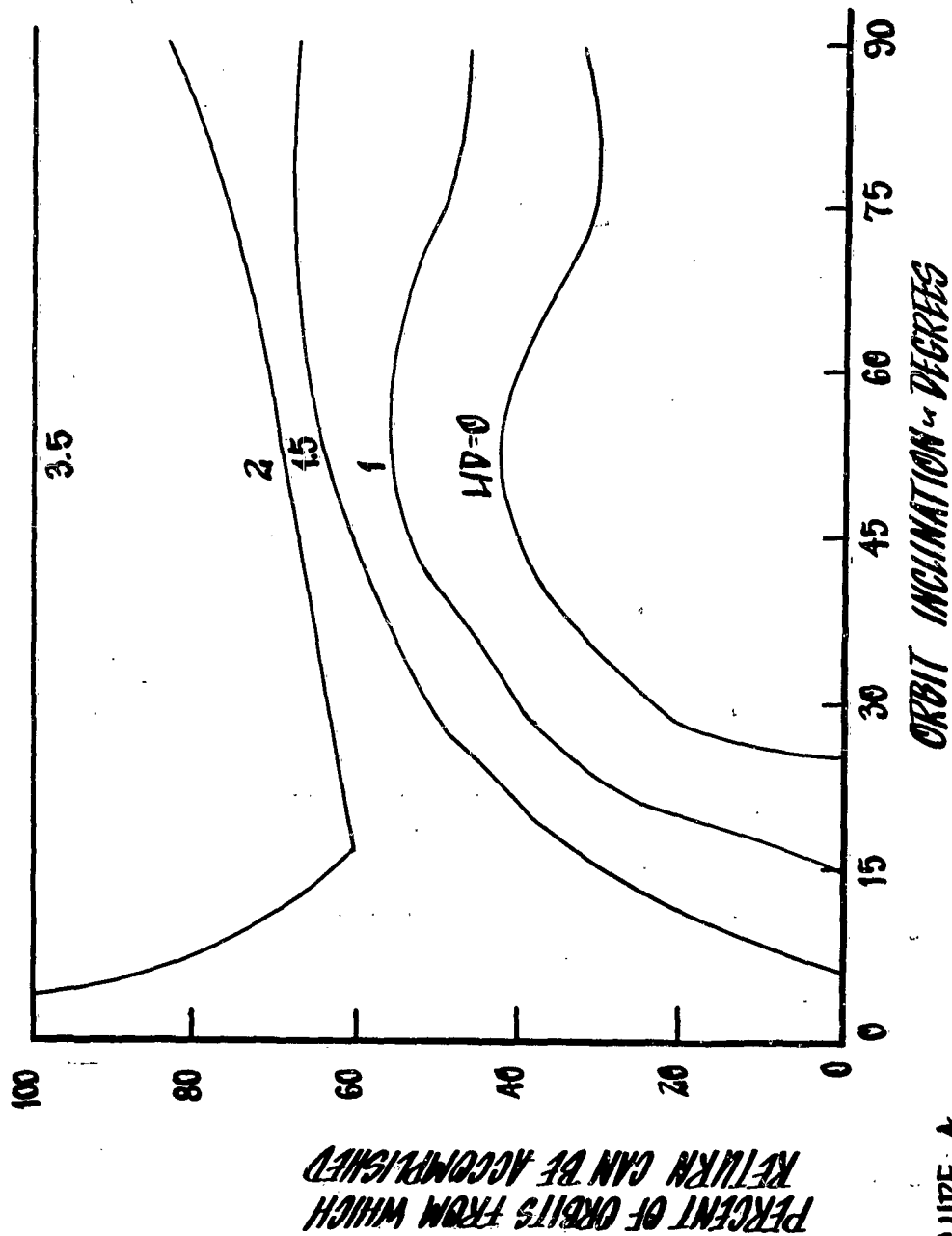
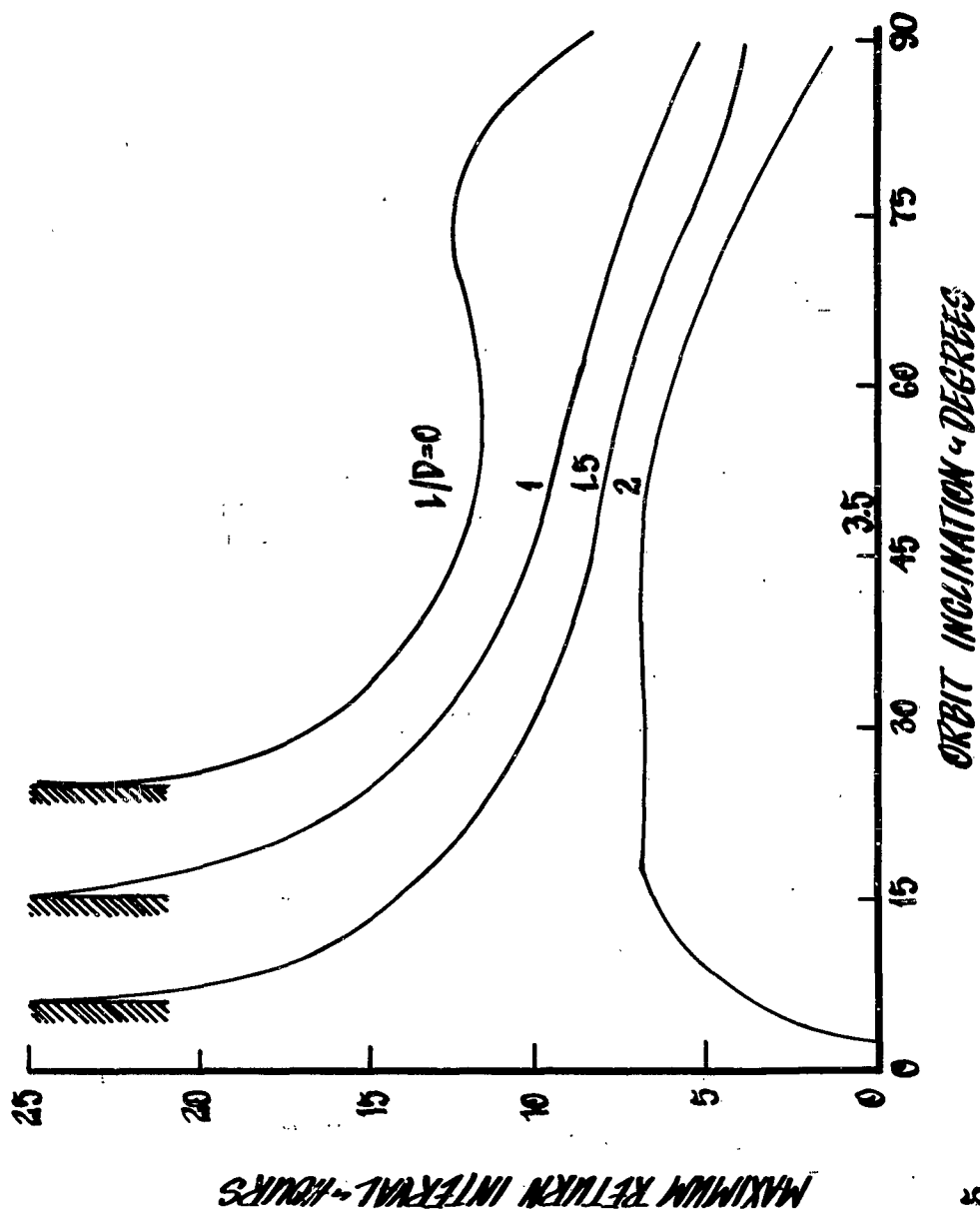


FIGURE 4

**% OF ORBITS WHICH RETURN IN ONE PASS
EFFECT OF L/D RETURN TO CONTINENTAL U.S.**

MAXIMUM HOLDING TIME RETURN TO CONTINENTAL UNITED STATES EFFECT OF Δ/D

FIGURE 5



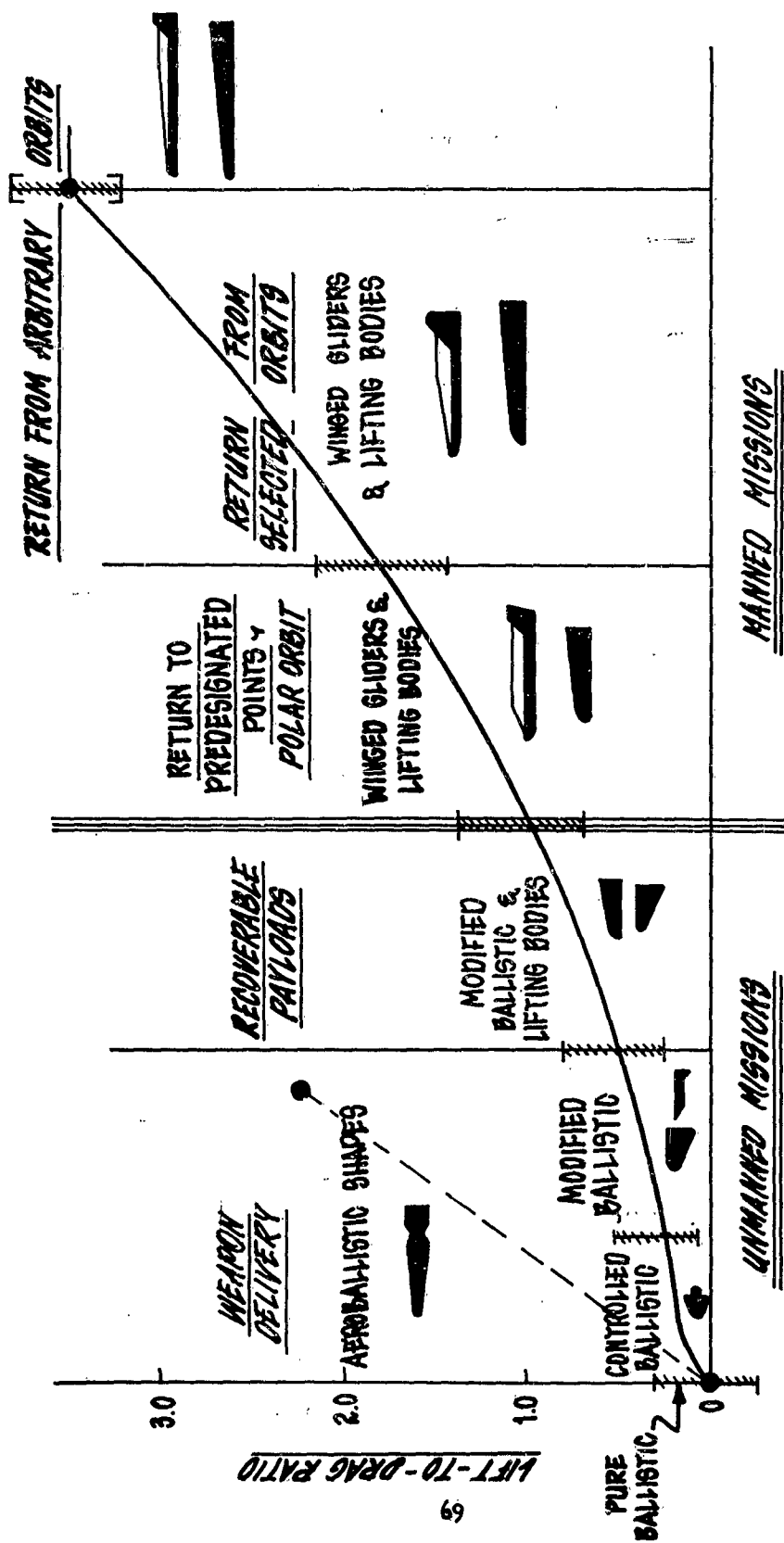


FIGURE 6
HYPERSONIC LIFT-TO-DRAG RATIOS AS A FUNCTION OF
CONFIGURATION AND POTENTIAL MISSIONS

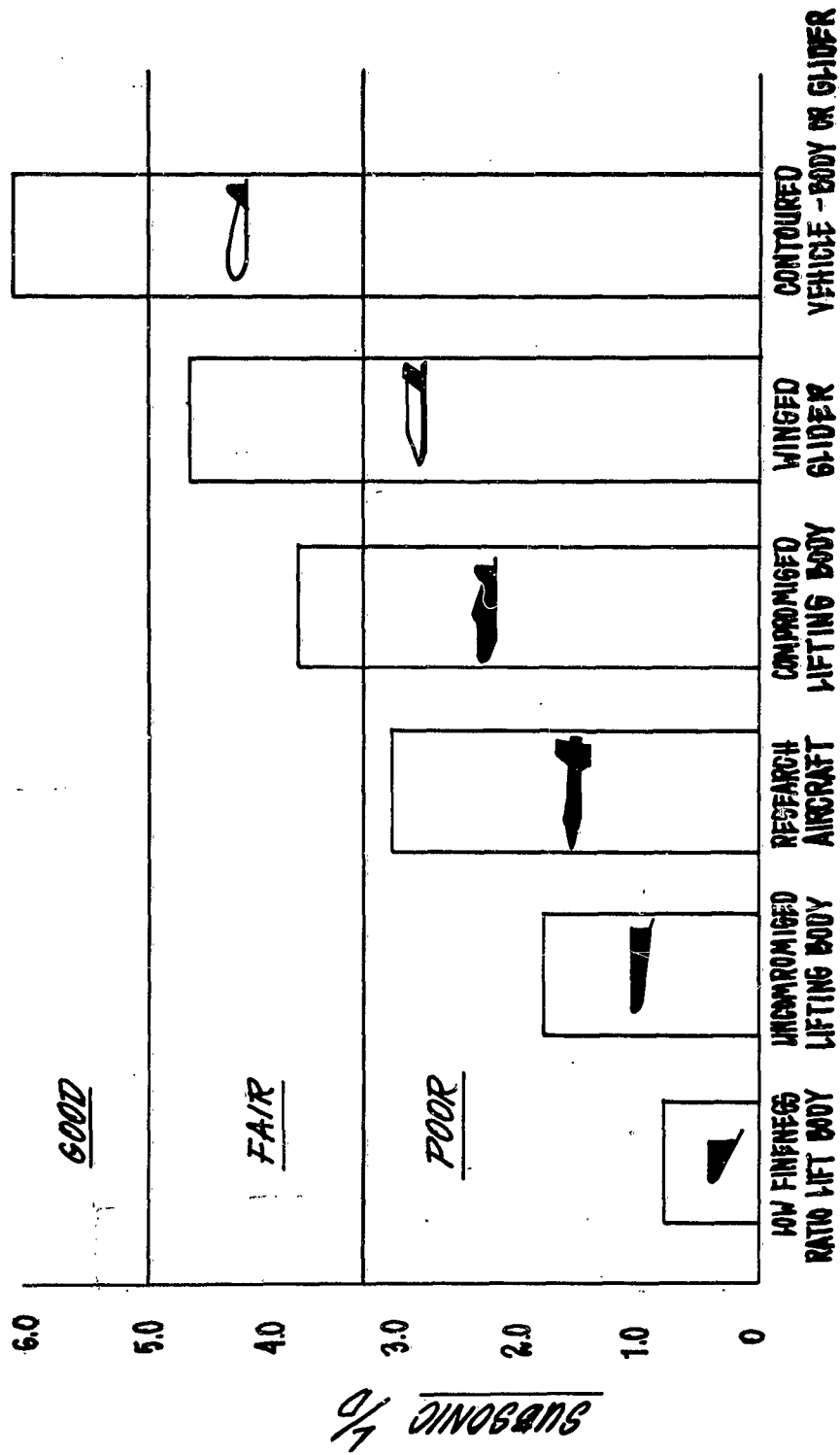


FIGURE 7

SUBSONIC % RE-ENTRY CONFIGURATIONS

CLASS OF CONFIGURATIONS

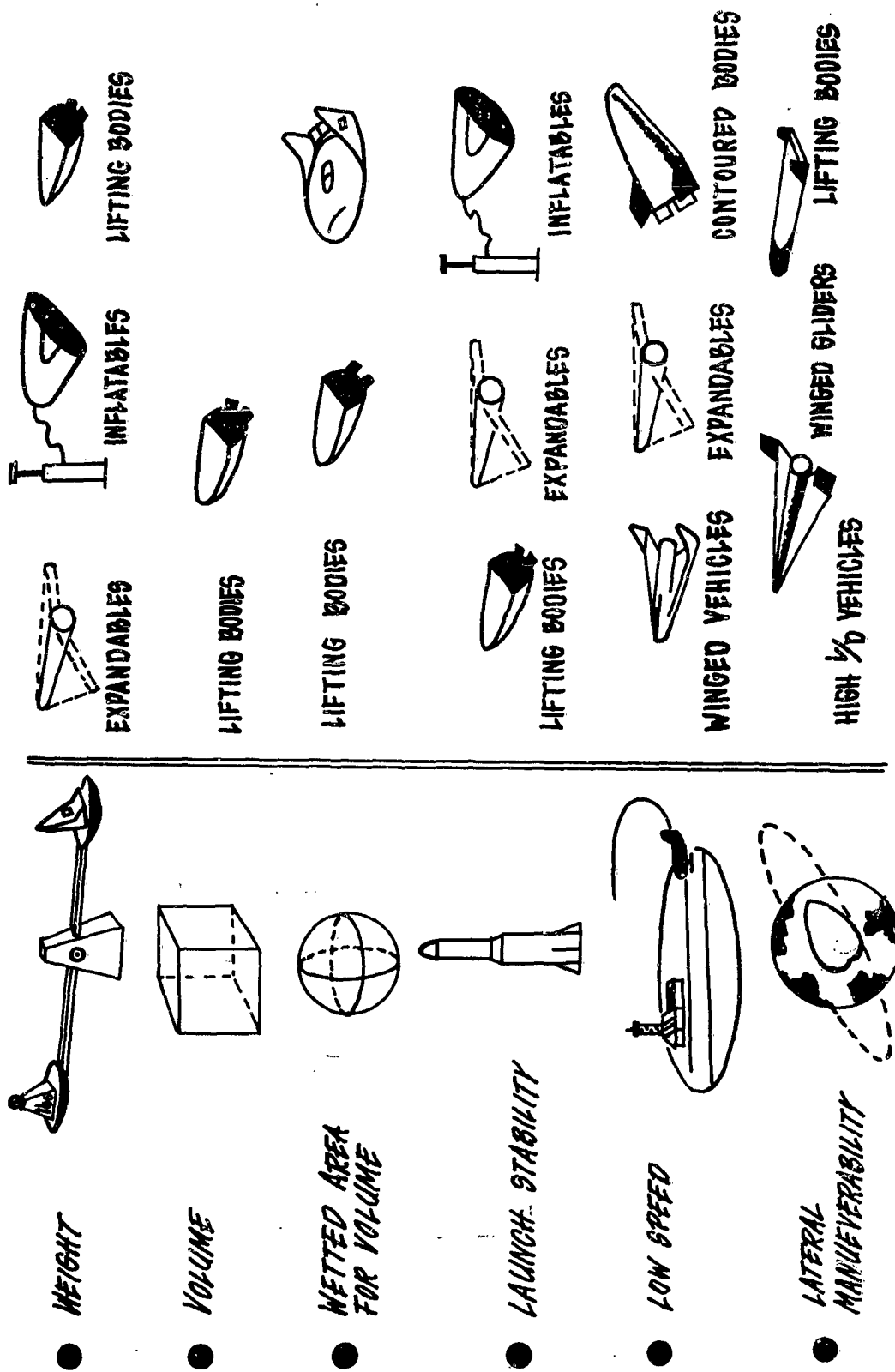


FIGURE 8

OPTIMIZATION PARAMETERS

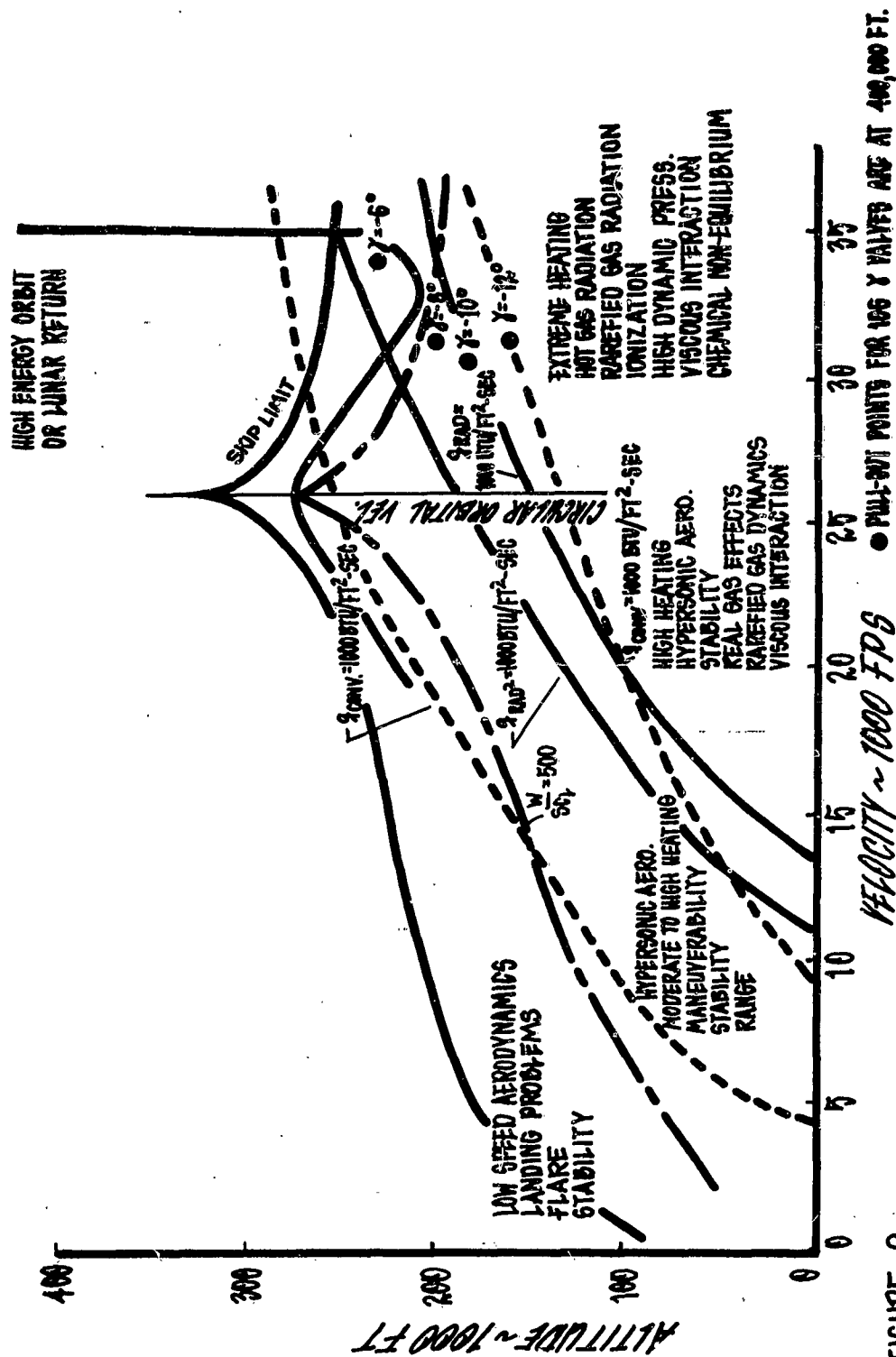

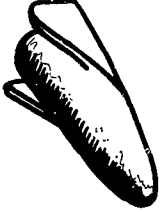



FIGURE 9

PROBLEM AREAS AS A FUNCTION OF SPEED REGIME and SUPERORBITAL PULL OUT POINTS

| | | |
|---|--|---|
|  <ul style="list-style-type: none"> ● HIGH ASPECT RATIO ● LOW SWEEP ● SMALL BASE ● CONVENTIONAL LEADING EDGE ● CONTOURED SURFACES |  <ul style="list-style-type: none"> ● LOW ASPECT RATIO ● MEDIUM SWEEP ● LARGE BASE ● VERY BLUNT LEADING EDGE ● FLAT BOTTOM (CYL. BOTTOM REDUCES LIFT 40%) |  <ul style="list-style-type: none"> ● LOW ASPECT RATIO ● HIGH SWEEP ● LARGE BASE ● POSSIBLE LESS BLUNTNESS ● LOW CURVATURE BOTTOM (TO REDUCE RADIATION HEATING) |
|---|--|---|

LOW SPEED & LANDING HYPERSONIC & ORBITAL SUPERORBITAL & HYPERBOLIC

FIGURE 10
Angle

VEHICLE CHARACTERISTICS AS A FUNCTION OF SPEED

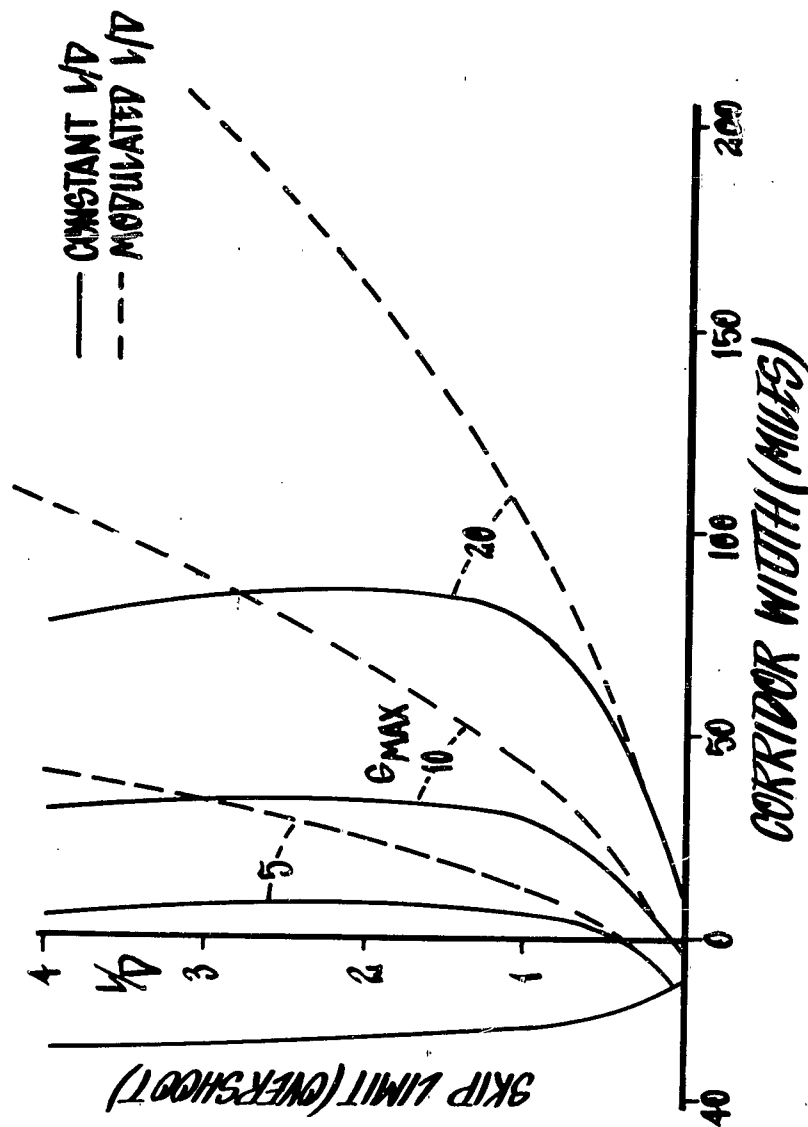


FIGURE 11

EFFECT OF LIFT-TO-DRAG RATIO ON CORRIDOR WIDTH AT SUPERORBITAL VELOCITIES

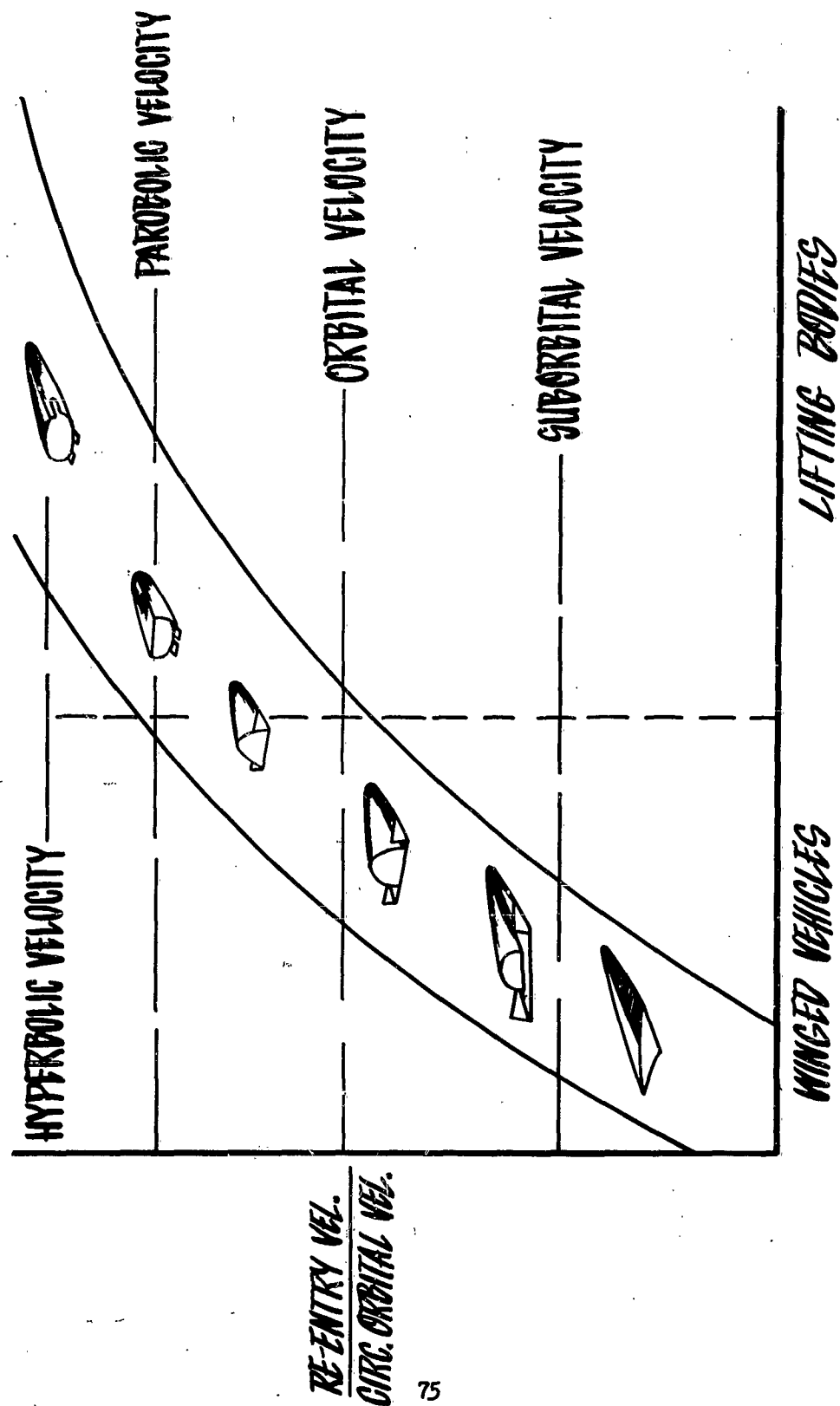


FIGURE 12
DESIGN TRENDS IN HYPERSONIC LIFTING CONFIGURATIONS

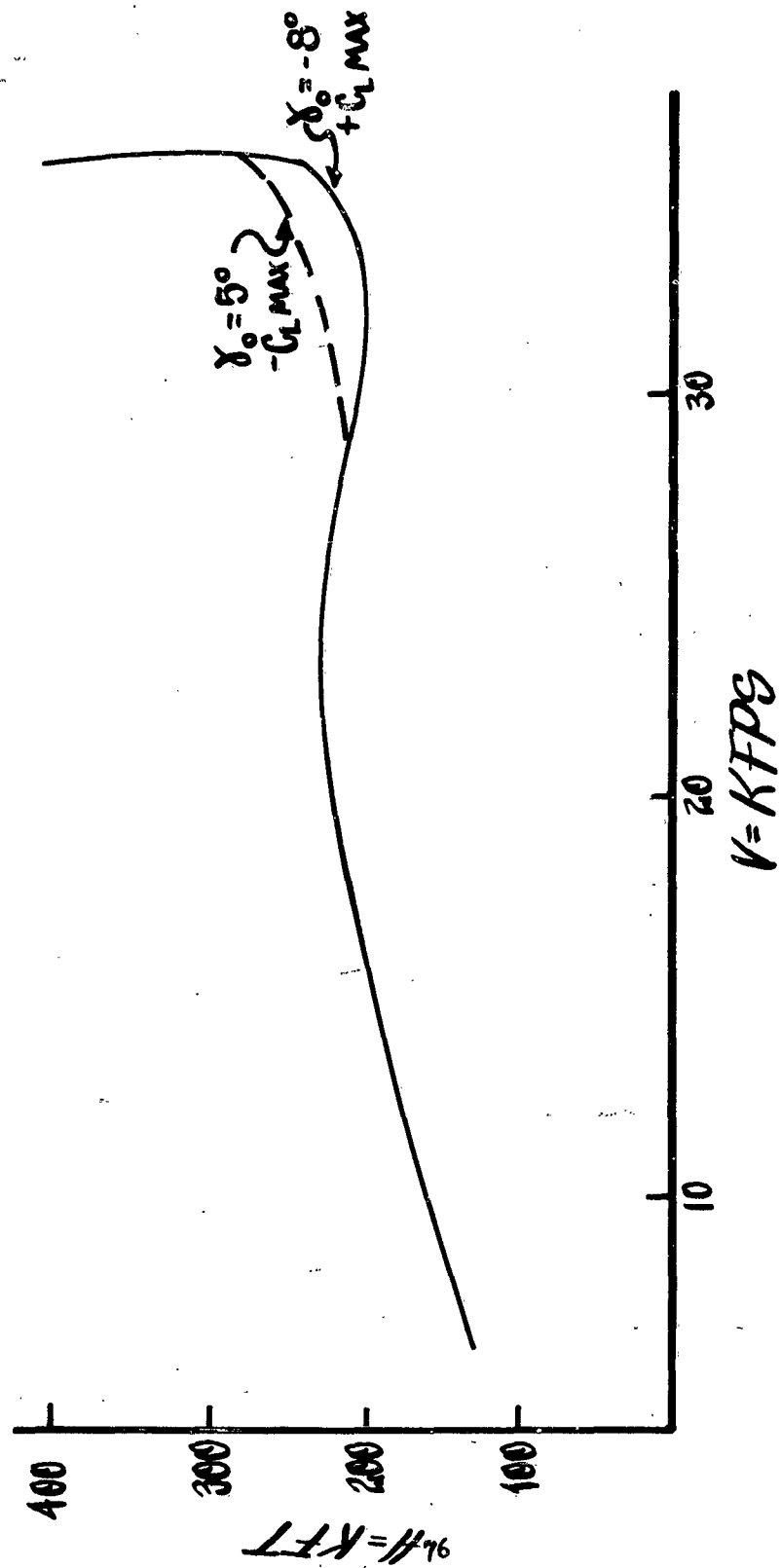


FIGURE 13

A

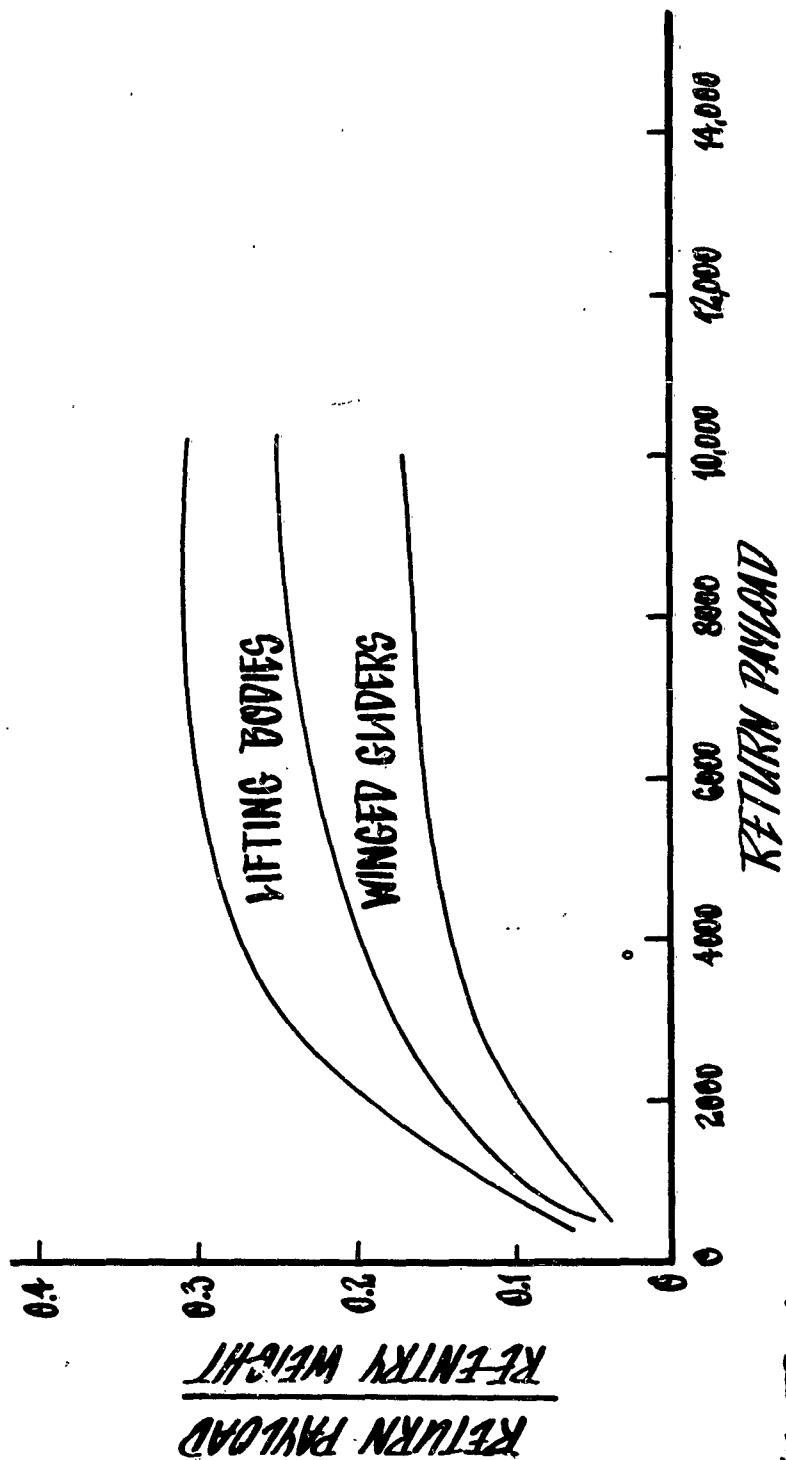


FIGURE 14

RE-ENTRY VEHICLES PAYLOAD FRACTIONS

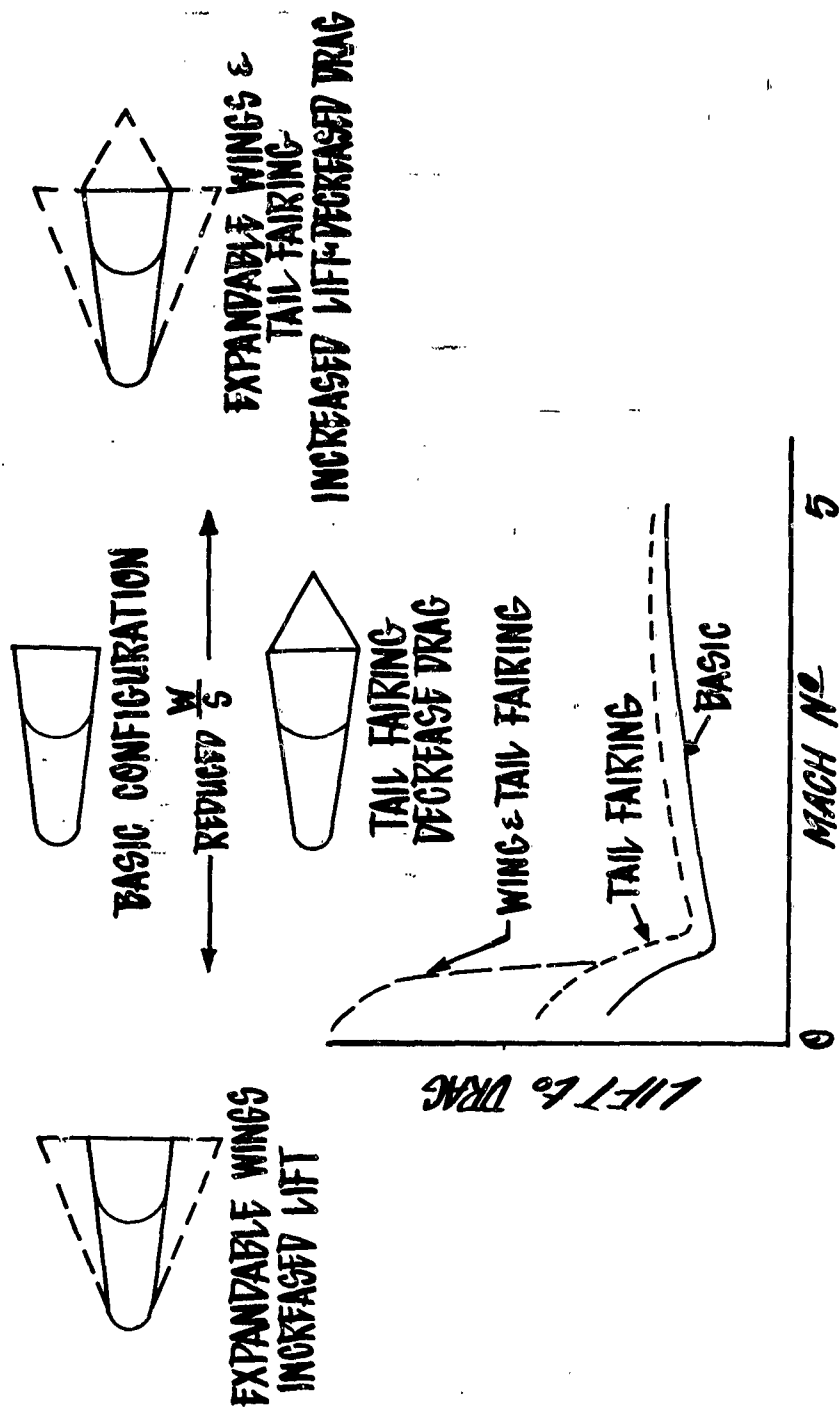
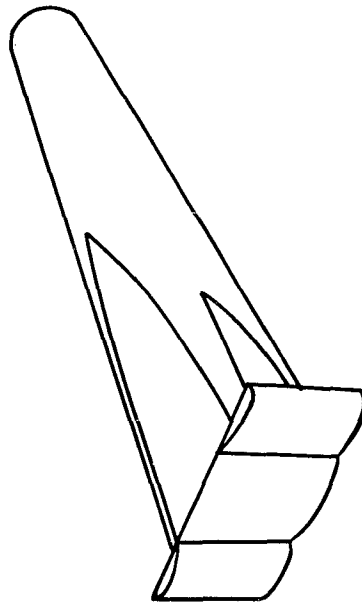


FIGURE 15

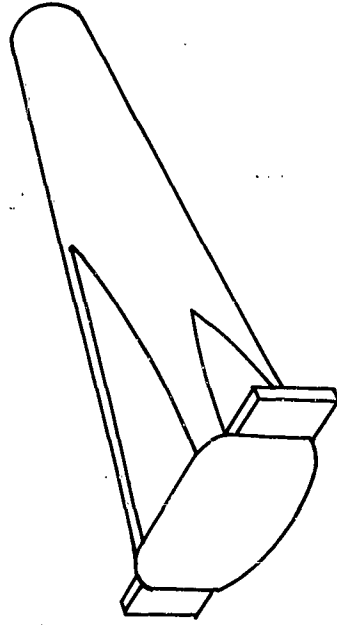
VARIABLE GEOMETRY for RE-ENTRY VEHICLES at LOW SPEEDS

AUXILIARY DRAG DEVICES

FIGURE 10



EJECTABLE
DRAG BRAKE



SLIDE-TROLLE
DRAG BRAKE

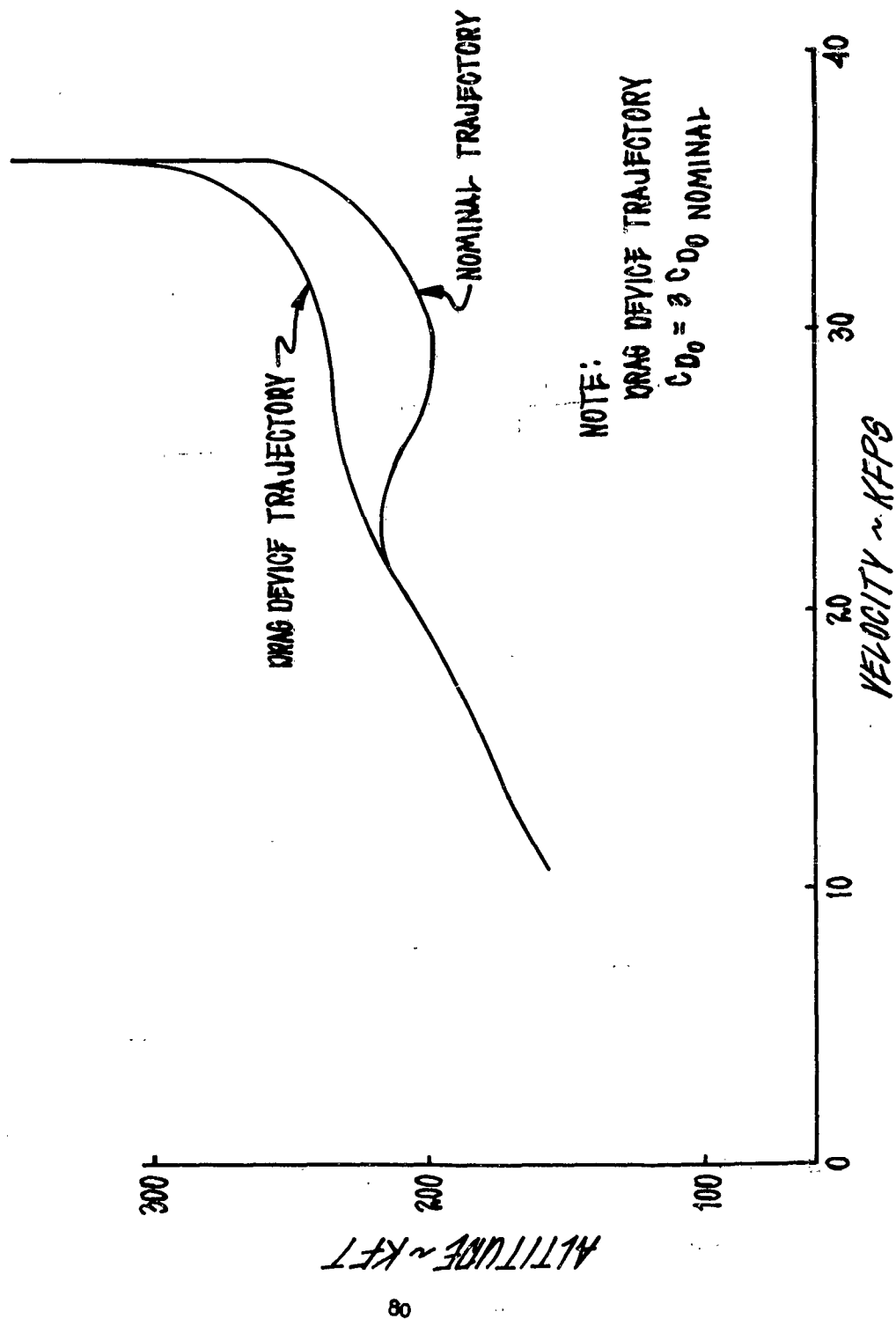
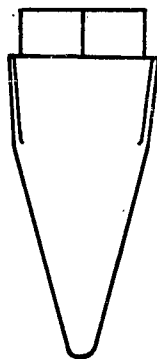


FIGURE 17

THE EFFECT OF DRAG DEVICES



MDF-1 CONFIGURATION

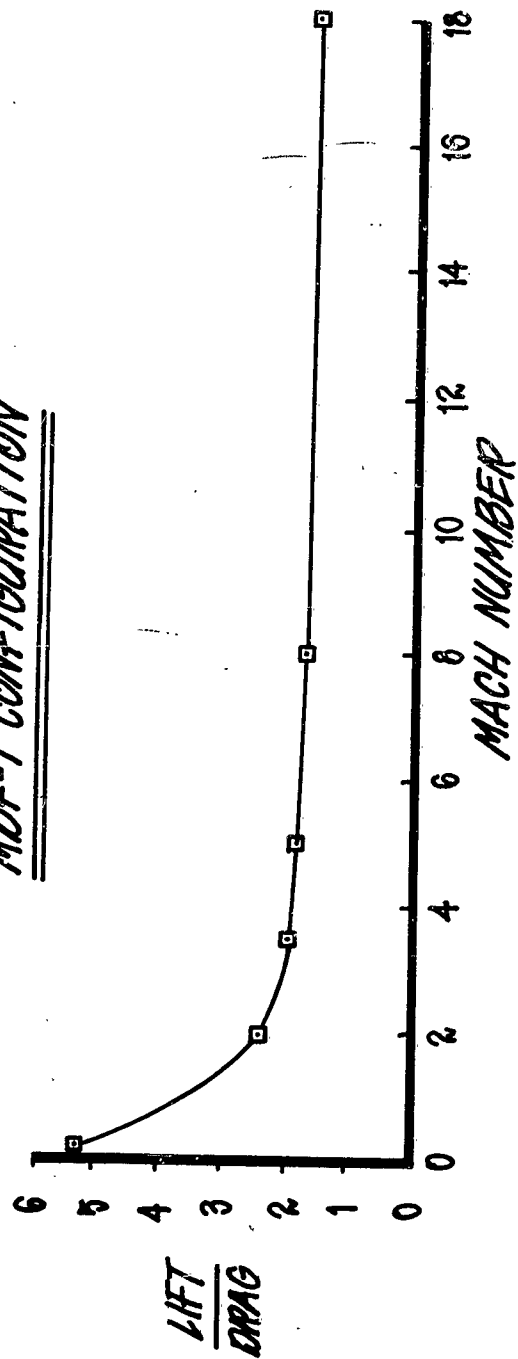


FIGURE 18

MDF-1 LIFTING BODY & EXPERIMENTAL DATA

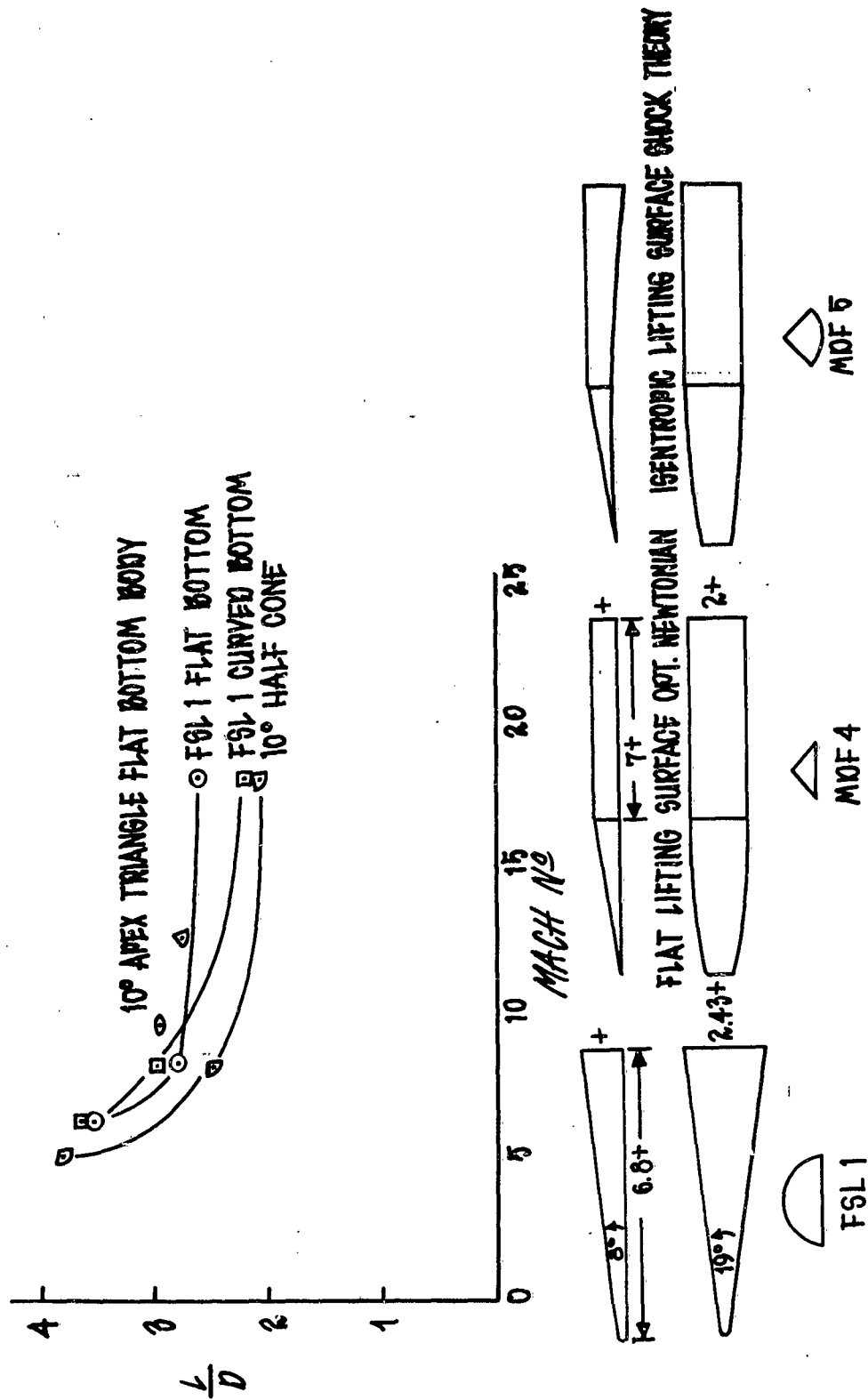


FIGURE 19

A DESIGN APPROACH for VERY HIGH LIFT-TO-DRAG RATIO VEHICLES

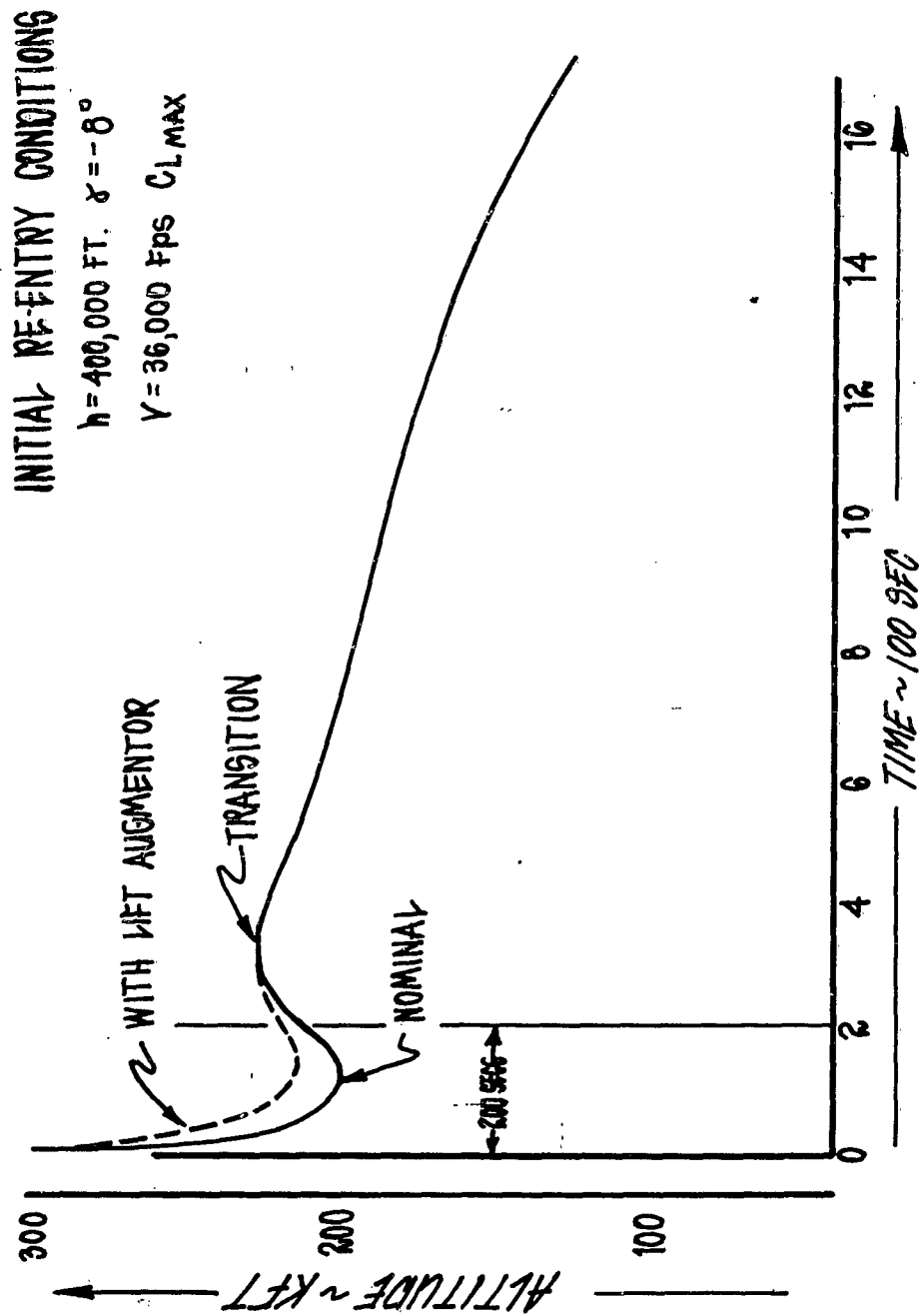


FIGURE 20
PROJECTED GAIN IN PULLOUT ALTITUDE

INITIAL RE-ENTRY CONDITIONS

$h = 400,000 \text{ FT.}$ $\alpha = -8^\circ$

$V = 36,000 \text{ FPS}$ $C_{L \text{ MAX}}$

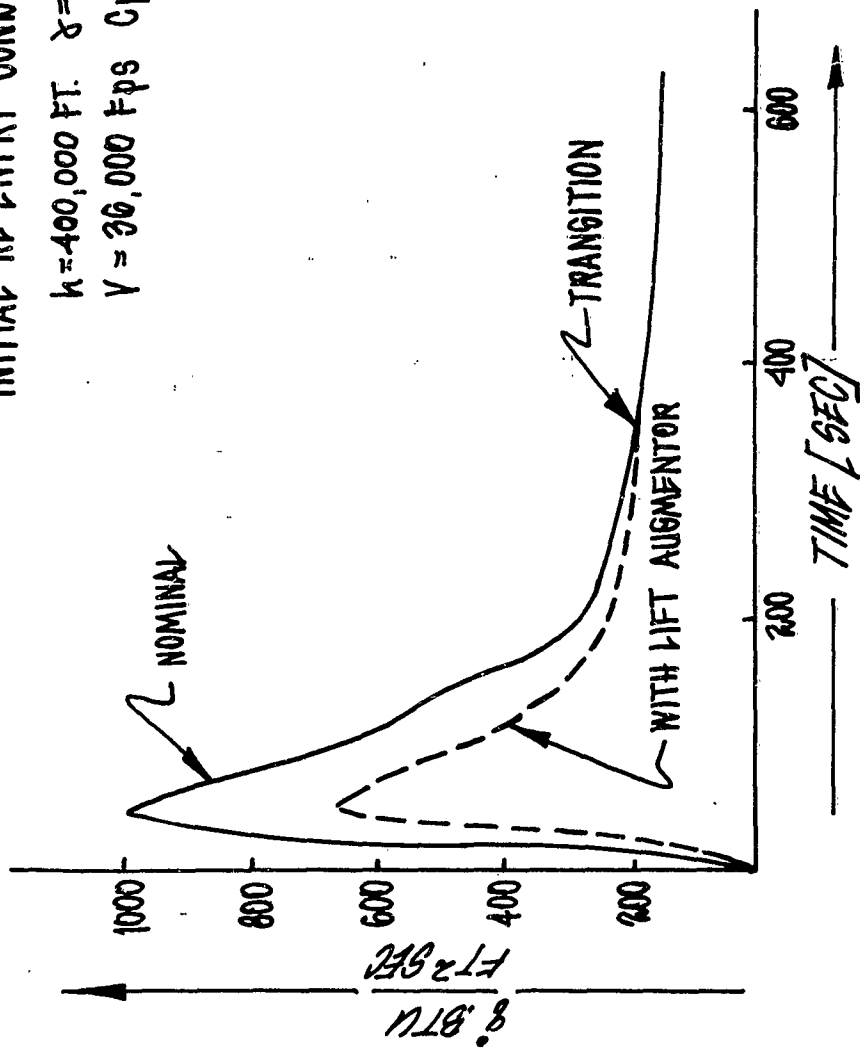
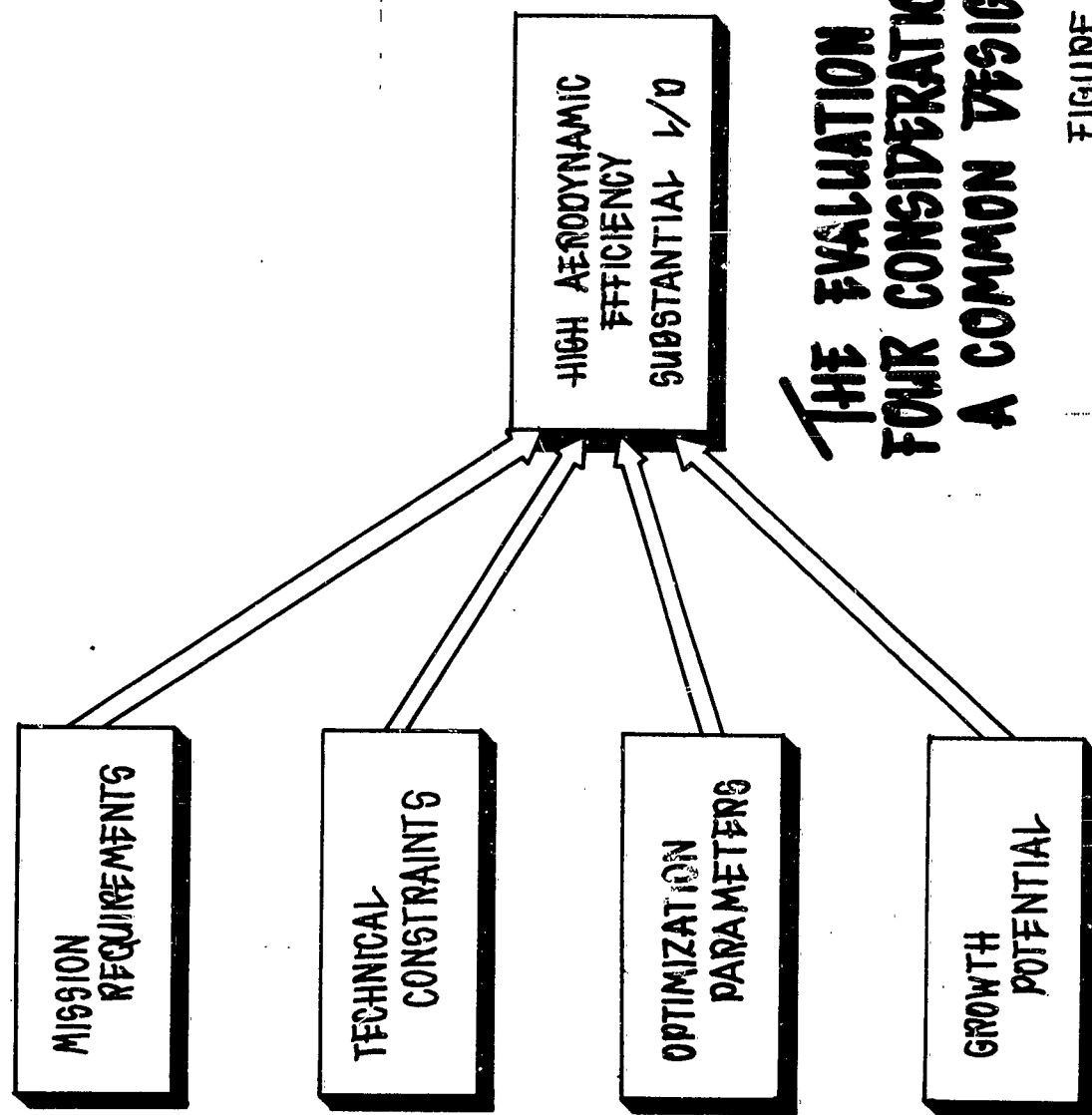


FIGURE 21

POTENTIAL RELIEF IN PEAK VALVES OF HEAT FLUX



**THE EVALUATION FROM
FOUR CONSIDERATIONS TO
A COMMON DESIGN GOAL**

FIGURE 22

HYPERSONIC DRAG DEVICES

SOLOMON R. METRES and STANLEY McFARLAND

This paper will be published
at a later date. Copies of
the paper will be mailed to
all registered attendees of
the Retardation and Recovery
Symposium.

Session II

SUPERSONIC SESSION

Chairman: MR. R. O. FREDETTE
Hayes International Corporation
Birmingham, Alabama

SUPERSONIC PARACHUTE RESEARCH

**RUDI J. BERNDT
CHARLES A. BABISH, III**

**RETARDATION AND RECOVERY BRANCH
FLIGHT ACCESSORIES LABORATORY
DIRECTORATE OF AEROMECHANICS
AERONAUTICAL SYSTEMS DIVISION
WRIGHT-PATTERSON AIR FORCE BASE, OHIO**

ABSTRACT

The background, experimental phases, and the results of two parallel investigations leading to the evolution of flexible parachute canopy configurations for potential applications as first stage aerodynamic deceleration devices at high supersonic velocities are presented.

Generalized drag data and high speed Schlieren photographs obtained during supersonic wind tunnel tests on the most promising canopy configurations are included to illustrate the performance characteristics of both supersonic aerodynamic decelerator concepts.

SUPERSONIC PARACHUTE RESEARCH

INTRODUCTION

Considerable emphasis has been and is being placed upon efforts to develop trailing aerodynamic decelerator devices capable of stabilizing and decelerating aerospace vehicles or payloads discharged therefrom while moving at supersonic speeds through the atmosphere. A variety of devices is being considered for this purpose; among this group of potential devices are balloons, cones, toroids, rotors, parachutes, and combinations thereof. All of these aerodynamic deceleration devices have certain advantages and disadvantages, and the final selection for a particular application will have to be based upon a number of considerations. Consideration must be given to the range of dynamic pressures at which the deceleration device is required to operate, the drag producing capability of the device, stability, weight, stowability, state-of-the-art of materials to be utilized in the fabrication of the device, simplicity of design and construction, and predictability and reliability of aerodynamic decelerator performance. This assumes that for each of the devices a sufficient state of basic knowledge has been generated.

Among this group of trailing aerodynamic deceleration devices, the self-inflating parachute type device is considered to be most suitable for applications in the supersonic and relatively high dynamic pressure regime of the flight spectrum. This type of trailing aerodynamic decelerator has the least weight and, in a majority of cases, requires the least storage volume for a given drag area. In addition, the self-inflating parachute canopy is relatively simple in design and does not require complex accessories, other than deployment aids, to insure its operation. Thus, with proper systems design, a high operational reliability may be attained.

Although textile parachute canopies have demonstrated reliable and predictable performance in stabilizing and decelerating manned and unmanned aerospace vehicles operating at subsonic, transonic, and low supersonic velocities, efforts to extend the operational capabilities of conventionally shaped textile type parachute canopies into the high supersonic speed regime have not been too successful. As a consequence, the state-of-the-art of textile parachute canopies for high supersonic applications has not kept pace with projected requirements.

Only recently, applied research investigations sponsored by the United States Air Force in the area of self-inflating textile type parachute canopies have yielded data of sufficient significance as to raise hopes of achieving a "breakthrough" towards the evolution of flexible canopies for high supersonic speed operations. The following discussion represents the results of two of these applied research efforts which are part of an overall program to advance the state-of-the-art of aerodynamic decelerator technology consistent with known or projected requirements.

BACKGROUND

Several research investigations have been conducted in the past with the objective of determining the inflation, stability, and drag characteristics of conventional parachute canopies operating in the supersonic speed regime. These investigations included exploratory wind tunnel and free-flight tests on the two types of parachute canopies judged to have the greatest potential for a supersonic speed capability extension, the ribbon and the guide surface type canopies.

Analysis of data obtained during these investigations revealed a typical canopy behavior at free-stream velocities above Mach 2. This behavior is characterized by a rather violent breathing tendency or alternate inflation and deflation of the drag producing surface, considerably reduced drag, and failure of cloth, ribbons, and suspension lines at a fraction of their rated strength due to violent oscillation of the material (Reference 1).

Violent breathing tendencies prevailed in the case of ribbon type canopies over a considerable range of geometric porosities and porosity distribution in the drag producing surface. Although the extremes in pulsing were not as pronounced in the guide surface type canopies as they were for the ribbon type, over-inflation of the roof section and indentation of the guide surface panels resulted in nearly immediate failure of the guide surface type canopy at the intersection of the roof and guide surface panels.

In order to determine whether this pulsing phenomena was associated with the flexibility of textile type canopies or could be attributed to an unstable flow field ahead of the canopy, rigid canopies with and without simulated suspension lines were tested in undisturbed flow. During this test series, the existence of unsteady flow conditions and Mach number effects was confirmed (Reference 2).

It was postulated by Maynard (Reference 3) that the action which initiates the fluctuations or pulsing of a flexible canopy in supersonic

flow is caused by the interaction between the boundary layer on the individual suspension lines and the shock wave generated by the drag producing surface. In addition, however, an analysis conducted by Fredette (Reference 4) concluded that the nature of the flow field and shock wave pattern upstream of the parachute canopy is greatly dependent upon the wake of the forebody or towing body, and that the canopy configurations are greatly affected by the interaction of the canopy shock wave with velocity gradients existing in the wake of the towing body.

Subsequent further analysis of Schlieren photographs of conventionally shaped ribbon type parachute canopies in supersonic flow has substantiated, to a degree, the existence of significant shock wave-boundary layer interactions. It has appeared from observation of parachute test data that for those configurations which exhibited low or marginal inflation characteristics the effect of the shock wave-boundary layer interaction has a significant influence on the inflation stability of the canopy. This shock wave-boundary layer interaction has been shown to be somewhat associated with cyclic canopy collapse.

However, in other instances it has been demonstrated that this phenomena does not have a significant effect upon canopy performance, suggesting that certain configurational characteristics of the drag producing surface may have a strong influence upon the suppression of the unfavorable interaction effects. For example, Reference 5 reports the testing of a canopy configuration consisting of a 15° half angle conical frustrum, fabricated of non-porous material and with a vent which provided an exit to inlet area ratio (S_v/S_i) of 0.29. Extremely high inflation characteristics were observed at a Mach number of 2.0, and very little canopy breathing or pulsation was evident.

It has also been postulated by Heinrich (Reference 6) that the primary cause of the general disorder of the flow field ahead of a drag producing surface of conventionally shaped parachute canopies immersed in undisturbed flow is located within the inflated surface itself. Although the interference from the suspension lines may be detrimental, it was not considered to be the primary cause of the general disturbance. This opinion was supported by the fact that rigid models of conventionally shaped canopies without suspension lines generally show the same unsteady flow pattern as those which do incorporate suspension lines (Reference 2). This postulation was further strengthened by the results of an analysis accomplished by Heinrich (Reference 6) wherein the flow pattern ahead of, inside of, and surrounding flexible two-dimensional models of conventionally shaped drag producing surfaces in simulated supersonic flow were visualized and explained by means of the water surface wave analogy.

It was evident, then, that phenomena exist which have a detrimental effect upon textile parachute canopy performance in uniform and, to some extent, in non-uniform supersonic flow. However, it was also apparent that certain configurational characteristics of the flexible canopy together with the existence of a wake field of finite boundaries ahead of the canopy could suppress, if not negate, these detrimental effects or that a change in the momentum of the air by a series of smaller pressure changes and flow deflections could produce conditions conducive to the inflation stability of flexible structures.

Therefore, parallel systematic investigations were initiated and sponsored by the Aeronautical Systems Division, AFSC, USAF, resulting in the evolution of two new textile parachute concepts for supersonic operation: the so-called "Hyperflo" canopy and the "Cone-Cup" canopy concepts. The "Hyperflo" canopy concept was the result of analytical and experimental studies conducted under Contract AF33(616)-8459 by Cook Research Laboratories, Morton Grove, Illinois, with Mr. Lee Sims the principal investigator, whereas the "Cone-Cup" canopy concept was one of the products of research investigations accomplished under Contract AF33(616)-6372 by the Institute of Technology of the University of Minnesota, Minneapolis, Minnesota, with Dr. Helmut G. Heinrich the Principal Investigator.

The following discussion presents the results obtained to date on these two independent investigations. Although it is realized that all trends and data obtained were generated on small scale models, configurational details for textile parachute canopies have been established which appear to have a sufficiently high potential for predictable supersonic operations as to warrant full scale free-flight validations. This experimental investigation is currently being conducted.



FIG.1 CHARACTERISTICS OF A 15° CONICAL
CANOPY $s_v/s_i = 0.29$ $M = 2.0$

THE HYPERFLO CANOPY CONCEPT

The results of an analysis of tests conducted in supersonic flow on a flexible parachute canopy of a 15° half-angle conical frustum shape with an exit to inlet area ratio of 0.29 (Reference 5) revealed a configuration with extremely strong inflation and inflation stability characteristics. More significantly, this configuration demonstrated these characteristics in the presence of unfavorable flow conditions, i.e., unstable shock wave patterns.

Various shock wave patterns observed during these tests are depicted in Figure 1, which represents a reproduction of Schlieren photographs obtained. These changes in shock pattern were suspected to have been caused by the shock wave-suspension line boundary layer interaction, resulting from excursions of the canopy skirt about the point of suspension (Reference 4). For the case of a canopy normal bow shock wave, which exists in the first frame of the Schlieren sequence in Figure 1, wherein this wave intersects the suspension line at a right angle, the heavy boundary layer existing on the suspension line is subjected to a sharp pressure rise. In this case, a shock wave-boundary layer interaction may be expected to occur similar to that of a shock wave impinging upon a flat plate. If this takes place, there is no choice but for an adjustment of the flow to take place by pressures transmitting through the subsonic layer and causing an upstream separation of the boundary layer. At high Mach numbers, the minimum pressure ratio required for separating the boundary layer is considerably less than the pressure rise associated with a normal shock wave. This separation of the boundary layer is seen to occur whenever a suspension line becomes normal to the shock wave. As a consequence, the separated flow region extends upstream of the undisturbed normal shock wave position, generating conical waves. This conical shock pattern is shown in the second and third frames of the Schlieren sequence in Figure 1. Since the pressure rise is large compared to the minimum required for separation, the region of separation extends far upstream. A similar situation arises when the canopy oscillates relative to the shock front and when the canopy skirt approaches the shock wave itself. When the shock detachment distance required by the edge of the skirt exceeds the distance available between it and the shock wave, the shock breaks locally into a normal shock intersecting the suspension line and causing a shock wave-boundary layer interaction, as shown in Figure 1.

Although this phenomena was observed, and a postulation as to its occurrence was made, the major significance of these test results was believed to be the fact that a specific canopy configuration had displayed strong inflation tendencies and excellent inflation stability at Mach 2, even in the presence of unfavorable flow conditions. However, this canopy configuration exhibited an instability about the point of

suspension which resulted in oscillation angles as high as 20°. This instability was attributed to the ring airfoil type lift inherent in this type of canopy configuration. Nevertheless, a basis for further configurational and performance analysis appeared to have been established.

In the design of the conical frustrum shaped canopy configuration, three features differed significantly from those of conventional canopy designs. One, a much lower exit to inlet area ratio had been employed. Whereas in conventional ribbon type canopies with geometric porosities between 15 and 28 per cent the exit to inlet area ratio, assuming full hemispherical shape inflation would be 0.30 to 0.56, the conical canopy had an area ratio of 0.29. Two, a non-porous material was used extending back from the inlet or skirt of the canopy to the vent. In conventional ribbon type canopies, the porosity adjacent to the skirt is normally greater than near the vent. And three, a much lower total porosity was employed. Considering that the canopy was fabricated from non-porous material, the total porosity for this canopy may be expressed as the ratio of open area to total surface area and was only 9.5 per cent. Although it is well known that for a given canopy configuration the stability about the point of suspension varies directly with porosity, and it might be argued that the stability characteristics of the conical canopy configuration might be improved by increasing its total porosity, it must be pointed out that in the case of the Guide Surface type parachute canopy the total porosity is very low and canopy stability about the point of suspension is extremely good. The stabilizing effect of the forward guide surface is apparent in that type of canopy. Therefore, it appeared essential that in order to improve the stability characteristics of the conical canopy and still maintain its inflation stability, the overall canopy porosity should be maintained and that stabilizing surfaces should be added to the configuration. Based upon these considerations, an investigation of the effects of canopy porosity distribution in producing good inflation, of the stabilizing surface angles and surface length for proper inflation and stability, and of the overall geometric shape of the canopy for optimum drag to weight ratio appeared to prescribe the direction of effort during the initial program phases. In addition, the dependence of satisfactory parachute canopy performance upon the presence of a non-uniform flow or wake was to be investigated.

CONFIGURATION AND FLOW FIELD STUDIES

Initial wind tunnel tests were conducted at velocities between Mach 1.5 and 3.0 on a number of variations of the basic 15° half-angle conical frustrum shape described above (Reference 7). These variations consisted primarily of the addition of conical inlet sections of various length and inlet angles, the addition of roof sections with various geometric porosities, and changes in suspension line length. All parachute canopy models were deployed in the wake of a conical forebody which was strut-mounted to the tunnel side wall. The canopies were tested with riser

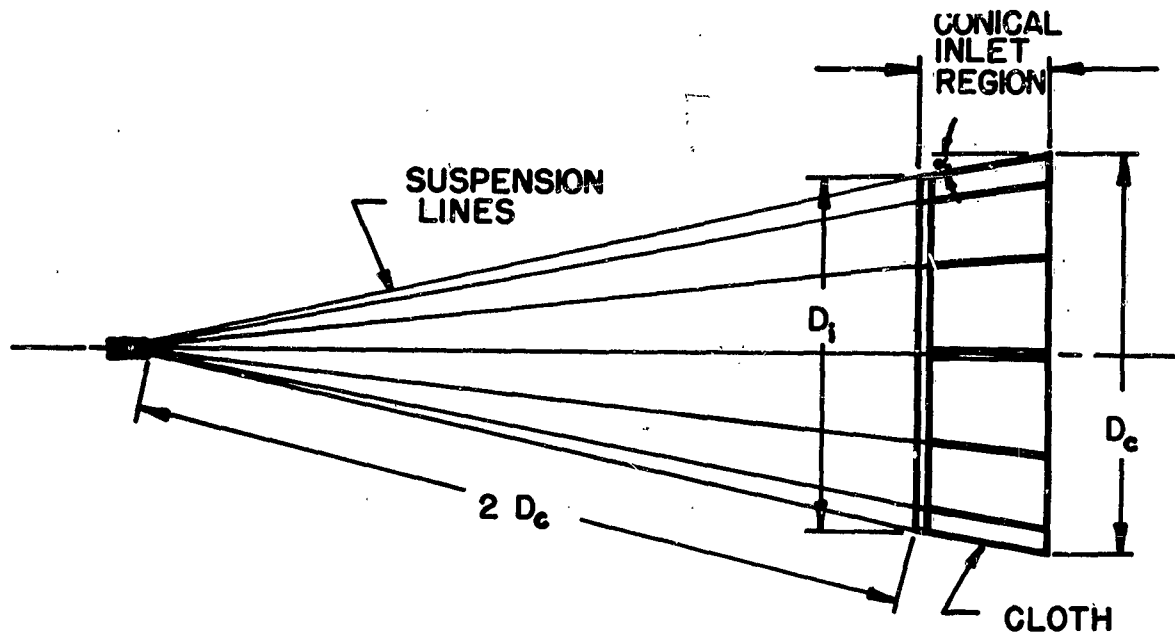


FIG.2 HYPERFLO CANOPY

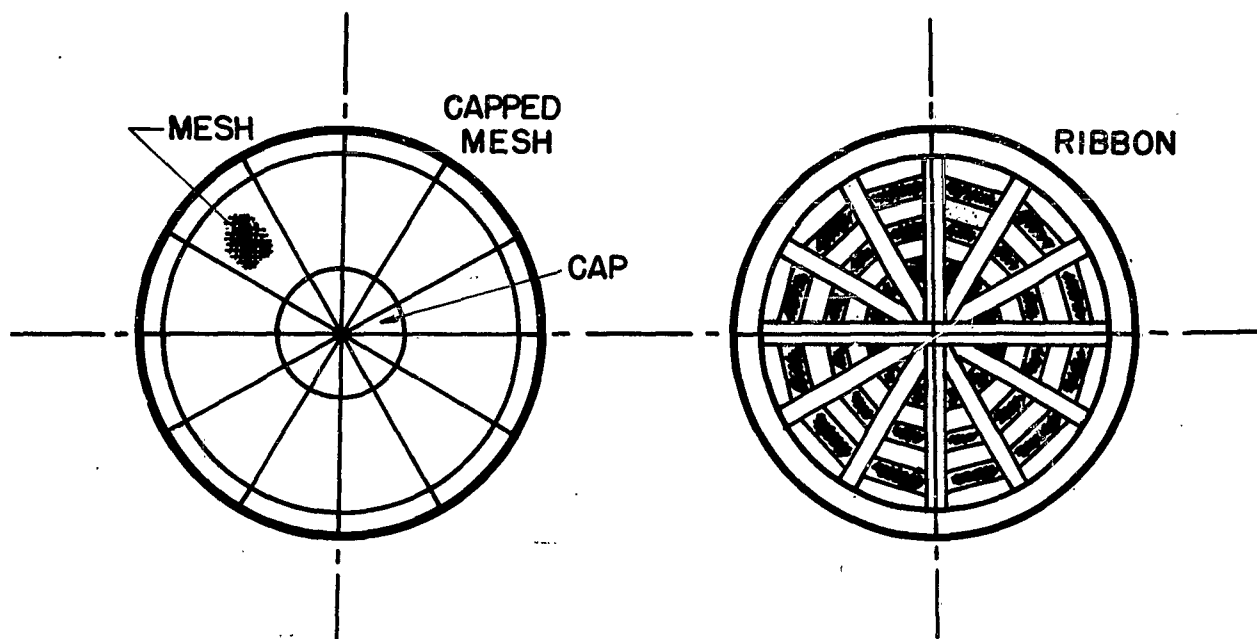


FIG.3 CANOPY ROOF DESIGNS

lengths which located the plane of the inlet of the canopy at approximately 10 forebody base diameters aft of the forebody base.

It was the primary purpose of these initial investigations to determine trends in canopy inflation stability, static canopy stability about the suspension point, and drag producing capability as a function of the configurational design variables chosen. Therefore, no exact performance measurements were attempted but data acquisition was limited to direct motion photography, Schlieren movies, and, in some cases, drag force measurements. Since the direct motion photography and the Schlieren movies made possible the analysis of various phenomena at short frame-time intervals, changes in canopy inlet opening, degree of canopy inflation, steadiness of shock geometry, and canopy stability characteristics were readily discernible.

In analyzing the data obtained, an attempt was made to isolate the contributing factors causing both the desired and detrimental performance characteristics. The results of this analysis can be summarized as follows: one, strong inlet inflation tendencies of canopies may be attributed to a low porosity conical inlet region wherein the conical surface is positioned at a positive angle of attack to the airflow immediately upstream of the plane of the inlet area; two, good roof inflation tendencies are the result of utilizing the least amount of material to provide the proper amount and location of the exit area. Low overall porosity, especially in the center of the roof, provides ideal opening tendencies; three, large inlet to maximum diameter ratios and low overall porosity combine to produce large drag forces; four, canopy instability about the point of suspension may be attributed to the ring airfoil type lift generated by the conical inlet region and to low exit to inlet area ratios; and five, instability about the center of gravity of the canopy may be attributed to the slightly negative "flat plate" lift generated by the conical roof region and to poor inlet inflation characteristics.

In an effort to analyze the flow field ahead of and around the canopy, and perhaps explain the need for particular parachute canopy geometry for satisfactory performance at supersonic speeds, the effects of the wake of a forebody on a trailing parachute canopy configuration were studied. Fredette (Reference 4) performed calculations to determine the effects of the non-uniform flow field, produced by the wake, on a shock wave ahead of a blunt trailing decelerator. Significant shock diffraction was verified by employing empirical wake theory for the determination of the wake flow ahead of the canopy shock wave. Diffraction of the typical near normal shock wave, which would exist under free stream conditions ahead of an inflated canopy, into a conical type shock wave was indicated by these calculations. To illustrate this diffraction, one may consider the following. Let us assume that the wake velocity profile is described by a descending velocity gradient

from free stream toward the wake centerline (Figure 2). If a normal shock were to exist across the wake, the static pressure rise across that portion of the shock wave on the centerline would be smaller than the pressure rise existing away from the centerline. This would result in a convergence of the flow toward the centerline. Since the flow in back of the normal shock wave is subsonic, the convergence of the streamlines toward the centerline would further produce a reduction in the static pressure, P , requiring a further convergence toward the centerline. Such a situation cannot exist unless a sink is located on the centerline. This is impossible and implies that the rate of change of pressure be zero at the centerline and be less than zero for short distances away from the centerline. Consequently, it is necessary for the shock wave to curve and deviate from a normal shock across the wake. This diffraction, resulting in the formation of a conical type detached shock wave, has been confirmed by numerous Schlieren photographs of canopies operating in a forebody wake.

One such confirmation is presented in Reference 7. The sketch in Figure 3 represents a trace from a Schlieren photograph of a well inflated and stable canopy configuration which was tested at Mach 2.13 and was located downstream of a conical forebody at a distance of 10 forebody diameters. A wake width equal to the forebody diameter was assumed ahead of the shock wave. It may be seen from this Figure that a subsonic outflow, resulting from the deflection through the shock, has a very favorable effect in maintaining full canopy inflation. Canopy inlet angles, below the horizontal, of up to 25 degrees will provide a positive "angle of attack" of the canopy inlet with respect to the local flow direction. It is also apparent that the flow deviation angle based upon the free stream Mach number, M_∞ , is sufficient to spread the wake in such a manner that the wake width at the canopy skirt is approximately equal to the inlet diameter. Wake flow divergence is indicated to be required, since the static pressure rise across the normal portion of the shock wave on the centerline is greater than the pressure rise across the oblique portion of the shock wave at the free stream Mach number. Divergence of the wake flow is further encouraged by the high (near stagnation) pressures existing in the canopy.

As a result of this analysis, it may be postulated that satisfactory supersonic operation of parachute canopies of the general shape described and tested is dependent upon the presence of non-uniform or wake flow ahead of the canopy. In this particular case (Figure 3), the wake width was sufficient to produce and sustain a favorable flow condition around the canopy. In the event that the ratio of inflated canopy diameter to the wake width would be significantly increased, and assuming a similar shock geometry, the flow deviation through the shock wave would not be adequate to spread the wake to the skirt of the canopy if the shock standoff distance remained the same, and the flow aft of the shock at greater distances from the wake centerline would be supersonic. A lip

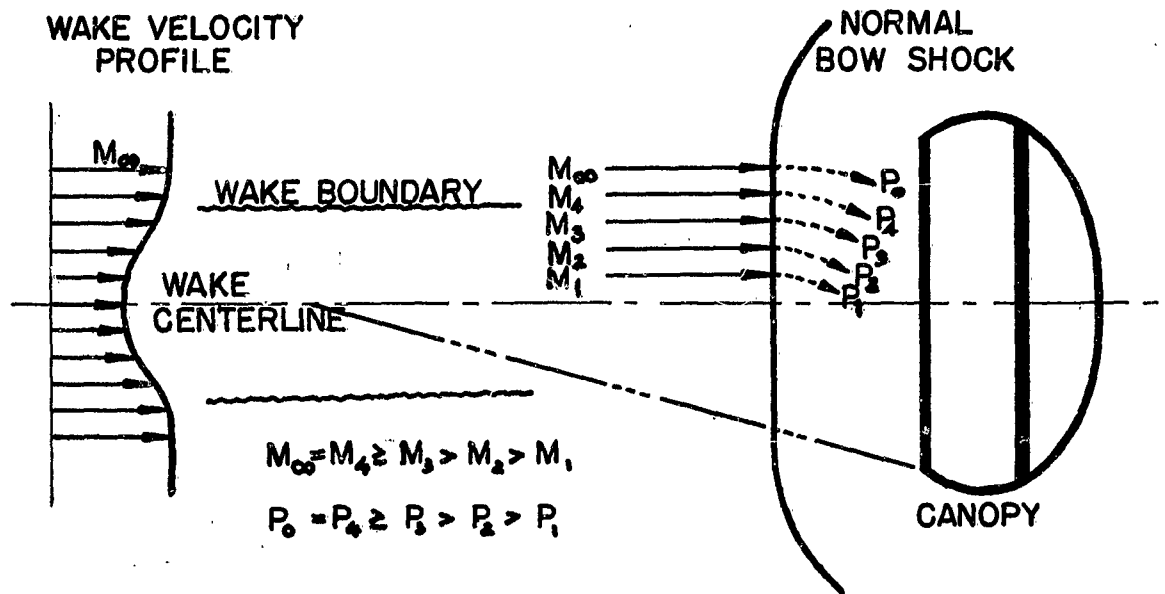


FIG.4 CANOPY SHOCK PATTERN

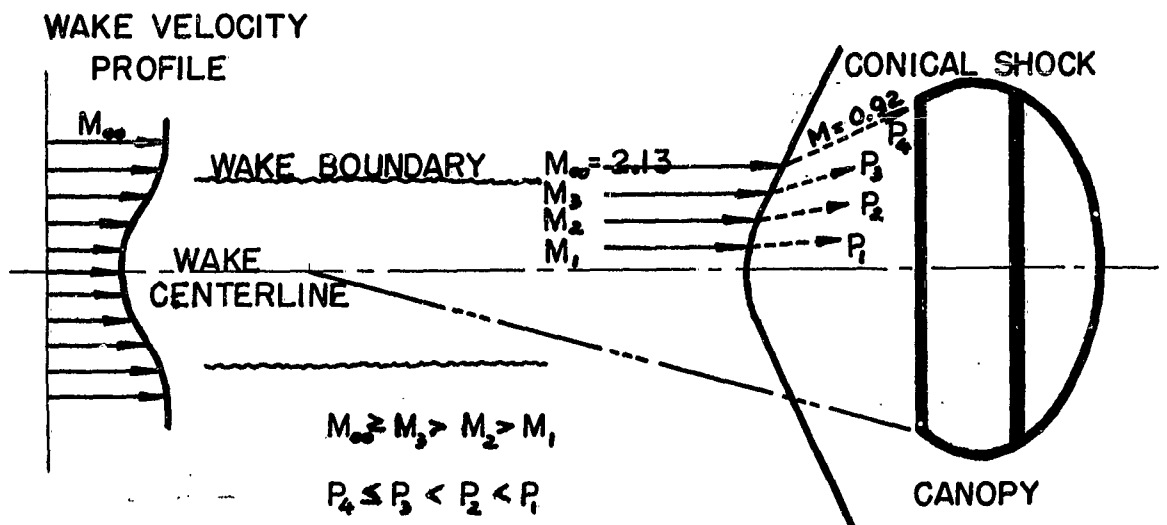


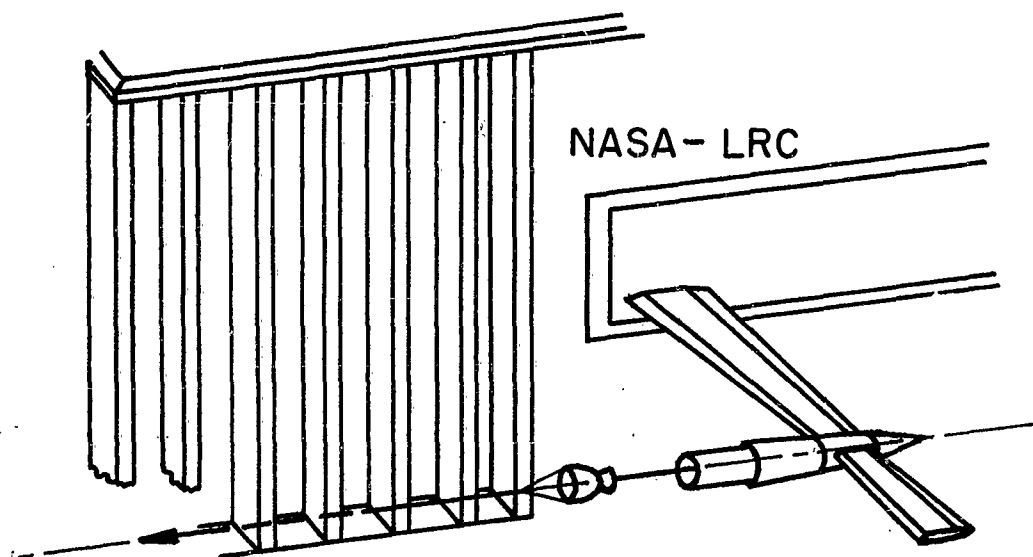
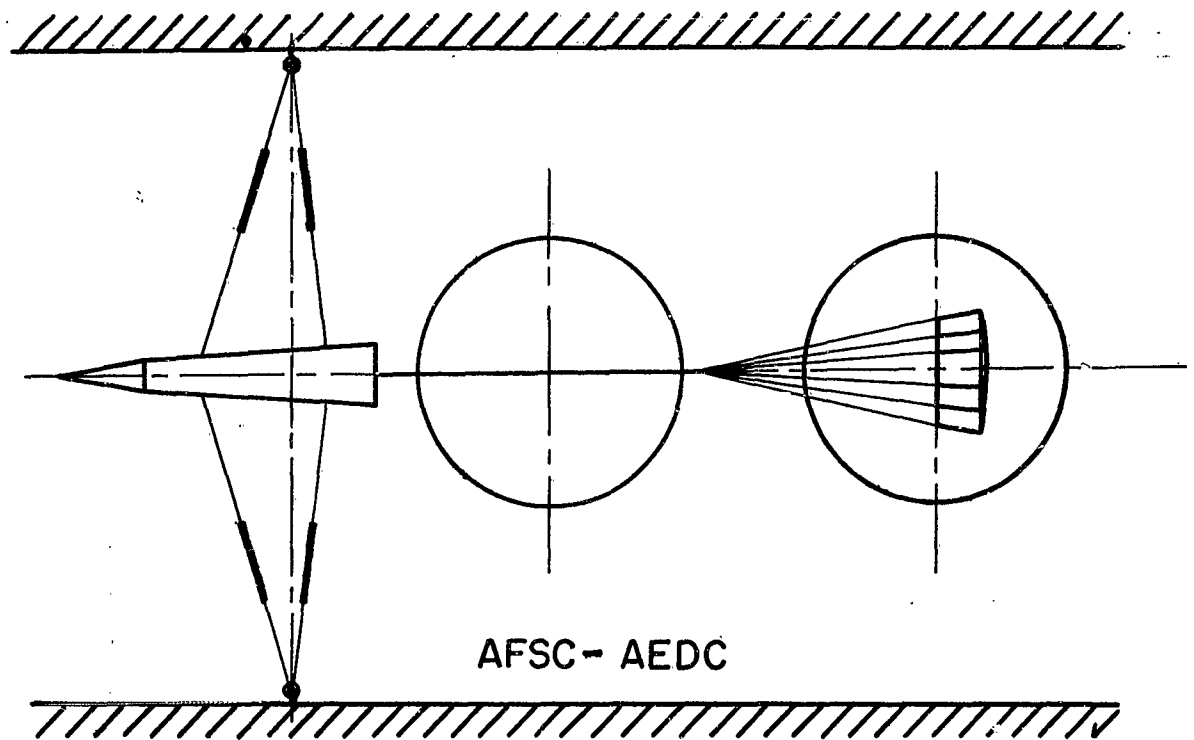
FIG.5 CANOPY SHOCK PATTERN

shock would then be produced which may, as results of past tests indicate, further spread the wake upon intersecting the boundary layer until the entire canopy is in subsonic flow. This would possibly lead to a fluctuating flow condition and reduction in canopy performance. In consideration of this and other associated phenomena, it may be expected that a practical canopy to forebody diameter ratio limit exists for the efficient operation of flexible textile type parachute canopies of configurations similar to those described and tested.

Recognizing the configurational variables as well as the flow phenomena which may cause both the desired and the detrimental canopy performance characteristics and incorporating trade-offs in configurational component designs, a canopy configuration was proposed by Sims (Reference 7) as a possible solution to the problem of obtaining efficient flexible parachute canopy performance in the supersonic flow field behind a primary or towing body. A schematic view of this canopy configuration is shown in Figure 4. This configuration incorporates a low porosity material in the conical inlet region which provides for the necessary strong inflation characteristics when the maximum inlet cone angle, α , is limited to that corresponding to the local flow direction ahead of the plane of the canopy inlet. The roof is of flat design and of relatively high porosity, thus minimizing the surface area of the roof region. This results in a low ratio of total cloth area to projected frontal area which for this configuration is in the order of 2.0. The ratio of inlet diameter to maximum diameter is large (approximately 0.9). In order to obtain the desired amount and distribution of flat roof porosity, a variety of means may be considered. Two practical designs are shown in Figure 5. The first sketch represents a flat roof consisting of a 35 percent porosity mesh monofilament, with suspension lines carried over the roof and an effectively non-porous disk positioned in the center of the roof. The diameter of this disk is dictated by the desired total canopy porosity. A second flat roof design may incorporate ribbon gores, much the same as found in flat circular ribbon type canopy designs. This roof may be constructed with or without a center vent. A third possible roof design may incorporate an all mesh roof covering the entire exit area. Parachute canopies of these general designs, called the "Hyperflo" family of parachute canopies, were designed and subjected to further supersonic testing to establish more specific canopy performance characteristics.

HYPERFLO CANOPY CONFIGURATIONS, WIND TUNNEL TESTS

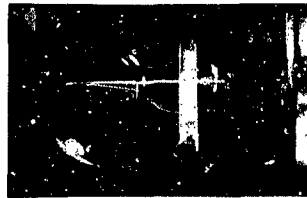
Experimental investigations were conducted on flexible models of Hyperflo canopy configurations utilizing the supersonic wind tunnel facilities at the National Aeronautics and Space Administration, Langley Research Center (LRC) and at the Air Force Systems Command, Arnold Engineering Development Center (AEDC). Testing was accomplished in the Mach number range between 2.3 and 6.0. Canopy models of 6 and 8 inches



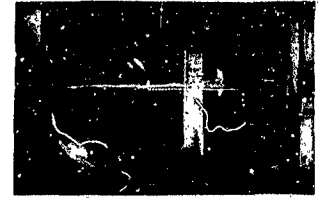
**FIG.6 WIND TUNNEL MODEL
INSTALLATION**



$T + 0.0 \text{ sec}$



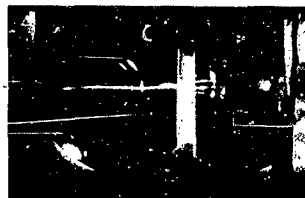
$T + 0.004 \text{ sec}$



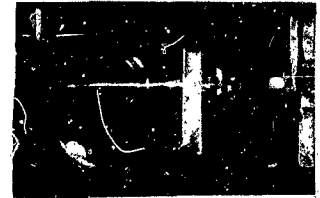
$T + 0.008 \text{ sec}$



$T + 0.012 \text{ sec}$



$T + 0.016 \text{ sec}$



$T + 0.020 \text{ sec}$

FIG.7 CANOPY DEPLOYMENT SEQUENCE



FIG.8 INFLATED CANOPY SHAPE

design diameter were deployed in the wake of a cone-cylinder type forebody of 2.375 inches diameter during the tests at NASA-LRC. These test configurations resulted in ratios of secondary to primary body diameter of approximately 2.5 and 3.37. During the test series conducted at AFSC-AEDC, canopy models of 8 inches design diameter were deployed behind a conical body of 3.72 inch base diameter, resulting in a diameter ratio of 2.15. All canopy models were initially stowed in a deployment bag placed in or near the forebody base. The deployment bag was connected to a deployment line rigged for axial movement. To deploy the canopy model, the deployment bag was moved downstream by an externally controlled deployment line. Figure 6 shows schematically the model installation arrangements at the two test centers. The general performance characteristics of the canopies and their drag characteristics were recorded by 16 mm high speed motion picture cameras and computer readout from a strain gage type drag link, respectively. One camera, operating at approximately 1000 frames per second, was installed in the Schlieren system and recorded the shock wave patterns in the flow field about the canopy models. An additional camera, operating at approximately 500 frames per second, was utilized during the tests at AFSC-AEDC to record a side view of canopy excursions about the point of suspension and about the canopy center of gravity as well as to record the canopy deployment sequence. The final stages of the test canopy deployment sequence is depicted in Figure 7. At the NASA-LRC test facility, the canopy models were tested at various distances downstream of the base of the forebody. Due to the suspension line-riser configuration used, x/d ratios between 6.5 and 12.6 were obtained, where d equals the forebody base diameter. An x/d ratio of 9.2 was maintained during tests at the AFSC-AEDC test facility. In general, the canopy models were deployed at the Mach number which corresponded to the upper Mach number of a given wind tunnel mode, with Mach number successively reduced while the canopy was inflated. Several canopies survived several hours of tunnel testing without damage; and in particular, one canopy configuration survived with no damage after four hours of continuous exposure to Mach numbers above 2.3. This in itself attests to the excellent behavior of this family of parachute canopies, since conventionally shaped canopies operating above this Mach number would probably survive only minutes of operation without major damage resulting from the dynamic loadings associated with the typical inflation instabilities which are characteristic of such canopies at Mach numbers in excess of 2.

Three basic designs of Hyperflo canopies were tested: an all mesh roof, a mesh roof and center solid cloth cap, and a ribbon roof configuration. An identical conical inlet configuration was utilized in all three designs. Design details and specific performance characteristics of canopies of the Hyperflo family are still classified. Therefore, only generalized performance characteristics and performance trends arrived at as a result of the supersonic wind tunnel tests will be presented hereafter.



$M = 2.5, x/d = 7$



$M = 3.0, x/d = 7$



$M = 3.75, x/d = 7$



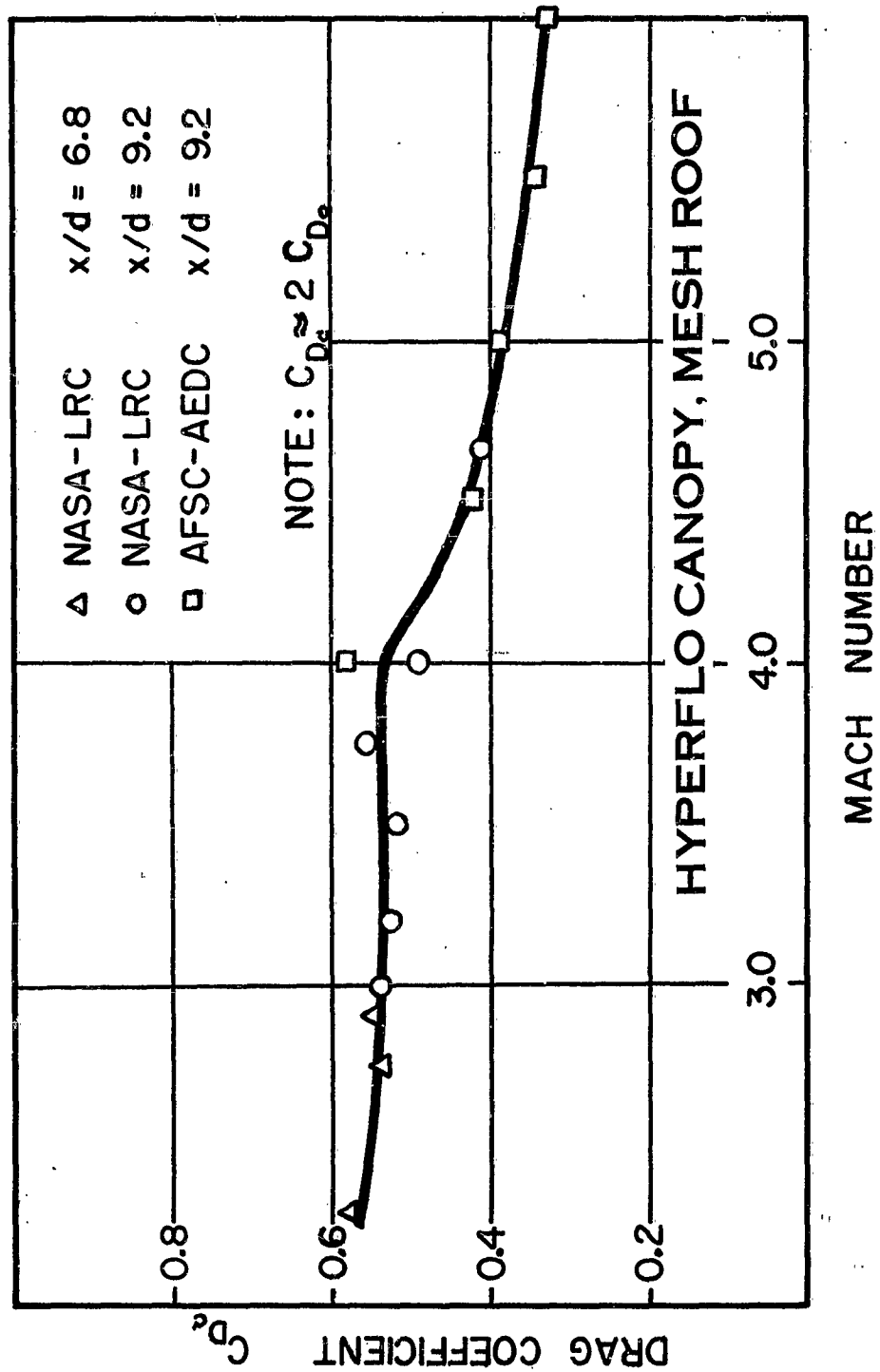
$M = 4.65, x/d = 9$

**FIG.9 SCHLIEREN PHOTOGRAPHS OF
MESH ROOF CANOPY**

TEST RESULTS, WIND TUNNEL TESTS

In general, all Hyperflo canopy models tested in the Mach number range between 2.3 and 4.65 at the NASA-LRC test facility exhibited good inflation characteristics, inflation stability, and stability about the point of suspension. In particular, the 6 inch constructed diameter canopy models displayed outstanding inflation and stability characteristics. The typical inflated shape of an all mesh roof Hyperflo canopy and the attendant shock wave pattern is presented in Figure 8. Very little breathing or pulsing of the canopies were observed. The few inflation instabilities that did occur were due to the excursion of the canopy toward the relatively fixed shock wave. As the canopy touched this wave, it collapsed in the region nearest the shock wave. As soon as this occurred, a large radial pressure gradient was established along the inlet region which drove the canopy away from the shock wave and toward the equilibrium position on the centerline of the wake. Figure 9 shows Schlieren photographs of a mesh roof with central cap canopy configuration at several Mach numbers. Full canopy inflation is evident. The inflated diameter to constructed diameter ratios for almost all of the configurations tested were 0.90 and greater.

The majority of the canopy configurations were highly stable with respect to the point of suspension. A trend, however, was noted in the stability of the canopy as a function of canopy location downstream of the forebody. Observations made at the time of tests and also the analysis of Schlieren and direct motion pictures indicated a general trend of increased stability with decreasing x/d canopy positions from an x/d near 13 to an x/d of 7. An optimum canopy location appeared to be in the region of 8 calibers aft of the forebody. Measurements of oscillation angles for the test canopies were found to be complicated by the introduction of secondary oscillations along the riser line, particularly at the larger x/d canopy positions. These oscillations were possibly caused or aggravated by the large mass of the riser and, in some cases, of the swivel used and located at the suspension line confluence. These secondary oscillations included oscillations with two, three, and even four nodes over the length of the riser. As a consequence, accurate quantitative measurements of oscillation angles of the canopy models about the point of suspension were only possible for the smaller x/d canopy positions. The all mesh roof configuration exhibited oscillation angles below 6 degrees and an average angle of oscillation of 2.5 degrees at Mach numbers up to 4.65. During the tests at AFSC-AEDC over a Mach number range between 4.0 and 6.0, a slight deterioration of canopy stability as compared to that observed at NASA-LRC was noted. However, this may be attributed to the fact that all canopies were placed at a distance of 9.2 forebody diameters downstream of the base of the forebody and that canopy design details differed somewhat from those tested at NASA-LRC. In general, it appeared that under identical conditions a somewhat greater degree of



**FIG.10 DRAG COEFFICIENT versus MACH NUMBER
HYPERFLO CANOPY, MESH ROOF**

stability was attained by canopies with higher roof porosities. No instabilities about the center of gravity of the canopy were observed.

The best overall performance characteristics were obtained with the all mesh roof Hyperflo canopy configuration. Since a considerable number of tests were conducted on this particular canopy configuration, it also yielded the majority of the drag data acquired during this test series. The trend of drag coefficient of the all mesh roof Hyperflo canopy configuration is presented in Figure 10 as a function of Mach number. The drag coefficient plotted is based upon the finished constructed diameter (D_c) and is obtained from the equation

$$C_{D_c} = \frac{D}{q S_c} \quad (1)$$

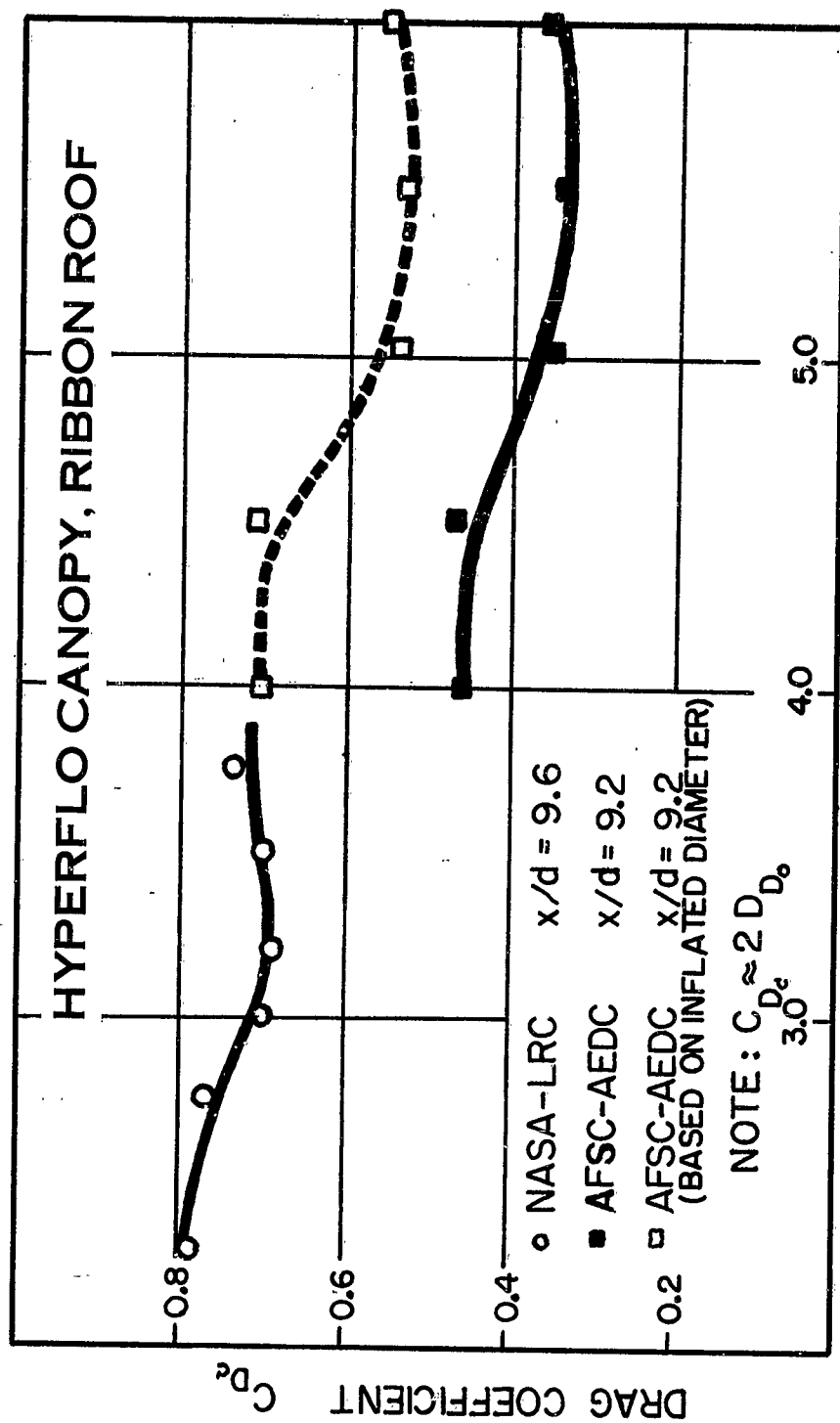
wherein

- D = Average drag reading, lb
- q = Free stream dynamic pressure, psf
- S_c = Constructed area, sq ft

The value for the constructed area, S_c , is obtained from

$$S_c = \frac{\pi}{4} D_c^2 \quad (2)$$

where D_c is the actual finished (measured) constructed diameter across the roof of the canopy. The drag coefficient values plotted in Figure 10 were calculated from the average drag readings taken at canopy positions at or near an x/d ratio of 9.2 with the exception of those points at the three lowest Mach numbers. These points were included since the drag coefficient appeared to be independent of the canopy position within the x/d range tested at the lower Mach numbers. As is evident from Figure 10, there is a marked decrease in the value of the drag coefficient at Mach numbers above 4.0. Since all tests above Mach 4 were conducted at approximately the same dynamic pressure (95 to 110 psf), a dynamic pressure effect cannot be suspected. Analysis of motion pictures taken during these tests indicates full inflation of the canopies at all Mach numbers with the ratio of inflated to constructed diameter remaining constant at approximately 0.9. In addition, a detailed study of all drag readings obtained suggests an apparent downward trend in drag coefficient, reaching a low value at



**FIG.11 DRAG COEFFICIENT versus MACH NUMBER
HYPERFLO CANOPY, RIBBON ROOF**

Mach 3, followed by an upward trend until Mach 3.75 is reached, and then decreasing sharply, leveling off at the higher Mach numbers. It must be pointed out, however, that the dynamic drag traces of all Hyperflo configurations indicated large amplitude, high frequency oscillations in the drag loadings (Reference 8). Therefore, the curve drawn in Figure 10 represents an average of all values obtained for the particular forebody-canopy configuration. In general, there also appeared to be a trend in drag coefficient increase with decreasing x/d ratios at free stream Mach numbers above 3.0. This trend was particularly pronounced at Mach numbers between 3.0 and 4.0 and was found to be true for all three Hyperflo canopy configurations as well as canopy to forebody diameter ratios investigated. At the present time, sufficient data are not available to either substantiate these apparent trends or explain their causes.

Comparing the drag coefficient values obtained on the mesh roof and solid cloth cap Hyperflo canopy with those of the all mesh roof canopy configuration, value increases of approximately 10% were realized throughout the Mach number range tested. This increase in drag coefficient is explainable since the incorporation of a solid cloth cap in the roof region lowered the total canopy porosity to some extent. At the same time, however, canopy stability about the point of suspension was slightly less than that observed on the all mesh roof canopy configuration.

A plot of drag coefficient versus Mach number for the ribbon roof Hyperflo canopy configuration is presented in Figure 11. This canopy achieved only partial inflation during tests in the Mach number range between 4.0 and 6.0 due to suspension line wrap-up. Upon canopy deployment, the canopy began to rotate causing the suspension lines to wrap-up to the extent that the unwound length of the lines was about half of the total length. It remained in this condition throughout the Mach number range tested. However, an approximately constant ratio of maximum inflated to constructed canopy diameter of approximately 0.8 was maintained. The solid curves in Figure 11 represent an average of the drag coefficient values based upon the actual constructed canopy diameter, D_c . The broken curve shows an average of the drag coefficient values based upon the actual inflated canopy diameter. The same general drag coefficient trends as those discussed above for the all mesh roof canopy configuration are in evidence.

The ribbon roof Hyperflo canopy configuration exhibited a significantly higher drag coefficient than both the all mesh roof and the mesh and cap roof canopy designs. This was true over the entire Mach number range tested. Consideration of the effective total porosity values of each of the three canopy configurations may provide an explanation for this increase in drag coefficient. For example, the total design porosity of the all mesh roof canopy configuration was

approximately 18 percent, and the incorporation of a solid cloth cap in the roof region lowered this value to approximately 14 percent. However, cursory calculations indicate that under the dynamic pressures at which the canopy models were tested, the mesh roof will be stretched which may result in an effective canopy porosity of 20 to 23 percent. On the other hand, the ribbon roof canopy configuration incorporated a total canopy design porosity of approximately 14 percent. The roof was constructed of ribbons which are not expected to stretch under the dynamic pressures encountered during tests. Therefore, the effective canopy porosity for the ribbon roof configuration may be assumed to be equivalent to the design canopy porosity. In view of the lower effective canopy porosity of the ribbon roof configuration, a higher drag coefficient must be expected.

All canopy models which were constructed using the basic Hyperflo canopy geometry performed in a comparable manner when designed with equivalent total canopy porosity. Observation of these canopies under the subsonic conditions during wind tunnel shut down has indicated maintenance of good stability and inflation characteristics.

THE CONE-CUP PARACHUTE CONCEPT

Investigations of the flow field ahead of, inside of, and surrounding a conventionally shaped drag producing surface immersed in uniform supersonic flow have indicated that the kinetic energy of the air captured by the inflated surface is too high to be converted to a body of calm air with a steady and uniform pressure distribution. (Reference 6) In subsonic flow, the drag producing surface of a parachute canopy includes a large volume of air, the pressure of which is essentially constant within the inflated surface. This air mass is carried along inside the surface and no significant relative motion of air within the drag producing surface nor a pronounced in and out flow occurs. In supersonic flow, however, the same drag producing surface is not filled with relatively calm and homogeneous air. Instead, there is a continuous in and out flow associated with moving pressure ridges which form a disorderly and unpredictable flow pattern. Under these conditions, a flexible parachute canopy varies its shape in accordance with the state of the pressure and flow. This motion, which represents the inflation in the form of breathing or pumping, was observed on flexible canopies operating in uniform and, to some extent, in non-uniform supersonic flow.

An approach towards a flexible drag device configuration for operation in essentially undisturbed supersonic flow was proposed

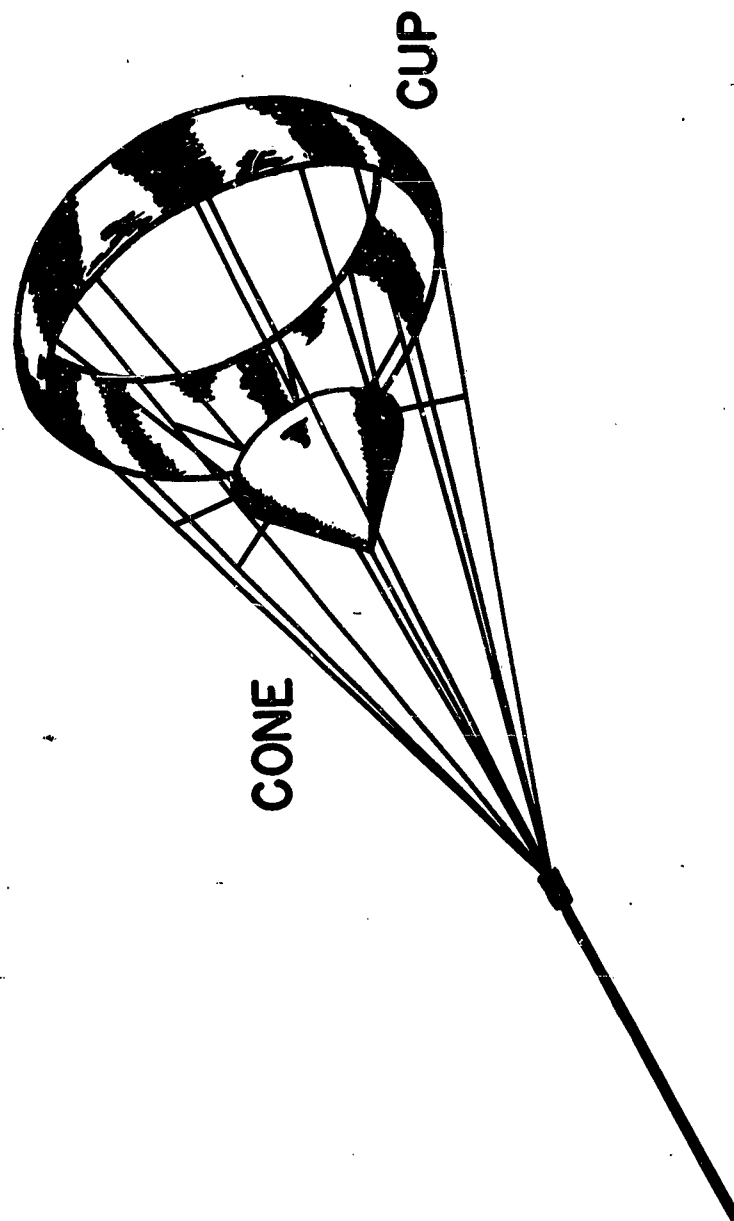
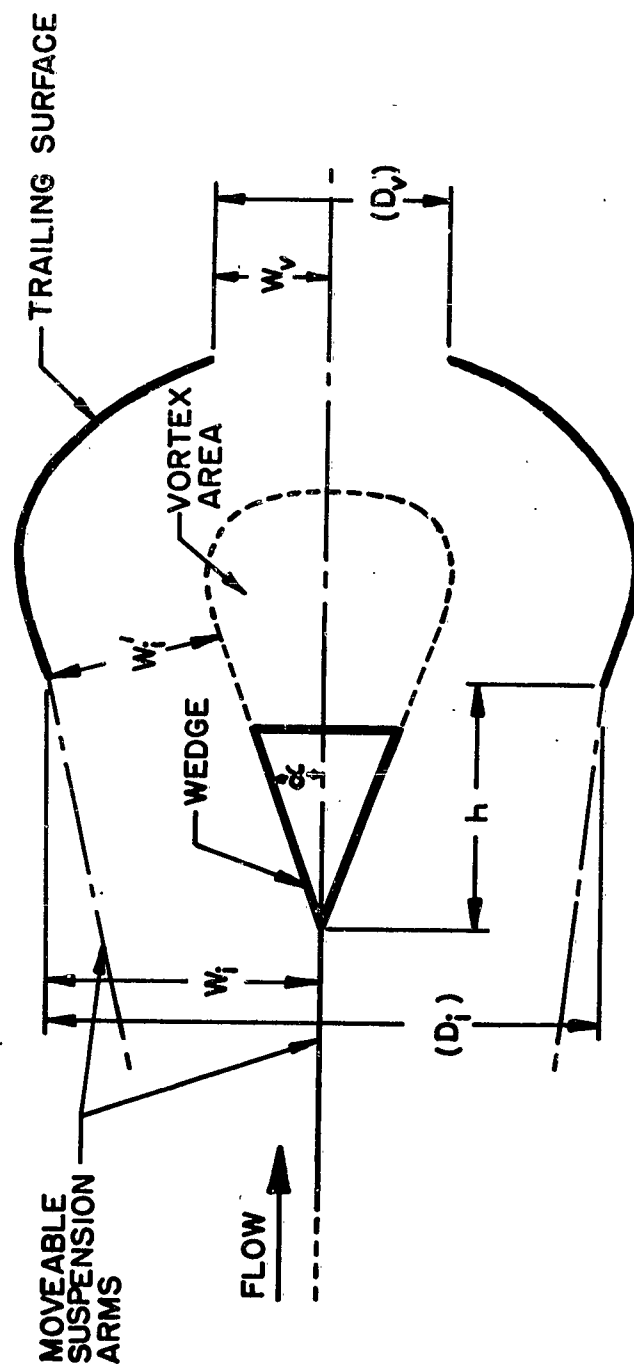


FIG.12 CONE-CUP PARACHUTE CONCEPT



**FIG.13 TEST CONFIGURATION
TWO-DIMENSIONAL MODEL**

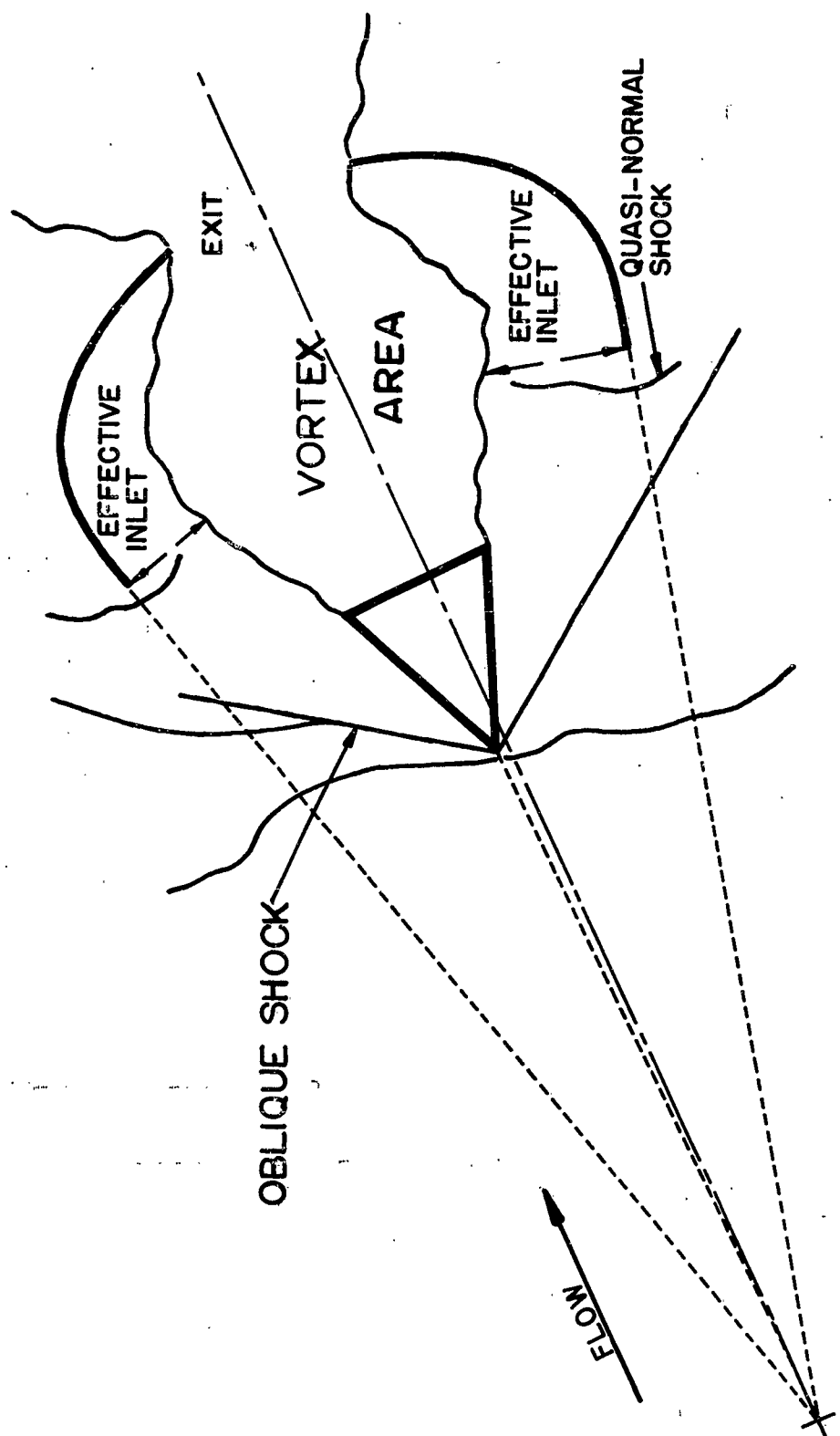
by Heinrich (Reference 9). This approach, which has some similarity to a spiked inlet diffuser, embodies a concept under which the momentum of the air is converted in a series of smaller pressure changes, by a certain amount of flow deflection, and finally allowed to escape through an enlarged vent. The inlet and outlet cross sections of the decelerator would be adjusted in such a manner that all air entering the inflated drag device would flow through it in an orderly and controlled manner. Physically, a practical aerodynamic deceleration device of this type would consist of a textile type "cup" forming in its inflated state a body of revolution having the shape of a conical frustrum joined by a spherical segment, and a cone, the base of which is located some distance ahead of the plane of the inlet area of the "cup". The cone and the "cup" would be positioned with respect to each other and to the forebody attachment point by means of a suitable suspension line system. A possible configuration of such a supersonic aerodynamic deceleration device is shown in Figure 12.

FLOW FIELD AND CONFIGURATIONAL STUDIES, TWO-DIMENSIONAL FLEXIBLE MODELS

In order to study the flow field surrounding such a configuration in simulated supersonic flow and in order to analyze the flow through the "cup", two-dimensional tests were conducted by the University of Minnesota (Reference 10), utilizing as test facilities both a shallow water tow channel and a flowing water channel. A two-dimensional water tow model may be visualized as a section of a body of revolution cut along the axis of symmetry. Thus, in the two-dimensional model of the cone-cup configuration the cone is simulated by a wedge and the "cup" is simulated by a strip of material. In order to obtain an attached shock with a proper angle for a simulated Mach number of 2, a wedge half-angle of 20° was chosen. The "cup" was simulated by a flexible strip of mylar film suitably suspended to maintain the desired configurational dimensions. Hereafter, this strip of material will be called the trailing surface. The wedge and the trailing surface were mounted in such a manner as to allow free oscillation of both bodies, either in unison or independently. A schematic view of the test configuration is shown in Figure 13.

For the flow conditions under consideration, namely, that the flow velocity at the exit area of the cone-cup configuration is sonic, and that no flow spillage occurs at the inlet area, the critical area ratio can be calculated by employing the inlet diffuser theory as derived by Herman (Reference 11):

$$\left(\frac{S_v}{S_1} \right)_{\text{critical}} = \frac{f(M)}{\eta} \quad (3)$$



**FIG.14 STABLE CONFIGURATION
TWO-DIMENSIONAL MODEL TEST**

where S_v is the exit area, S_i is the inlet area, M is the Mach number or average Mach number, depending on whether the flow is two or three dimensional, immediately ahead of the normal shock and η is the total pressure ratio across the subsonic region. This critical area ratio in turn determines the stability of the configuration. The configuration is stable if

$$\frac{S_v}{S_i} > \left(\frac{S_v}{S_i} \right)_{\text{critical}} \quad (4)$$

and unstable if

$$\frac{S_v}{S_i} < \left(\frac{S_v}{S_i} \right)_{\text{critical}} \quad (5)$$

Applying this relationship to the two-dimensional configuration, the critical area ratio, $(S_v/S_i)_{\text{critical}}$ becomes a critical width ratio, $(W_v/W_i)_{\text{critical}}$. In view of the expected formation of a large wake field downstream of the base of wedge, an "effective" inlet width must be considered (Figure 13). This "effective" inlet width, W_i' , can be assumed to be the section between the leading edge of the trailing surface and the wake boundary behind the wedge. As a first approximation, the wake boundary was assumed to be an extension of the wedge to the plane of the inlet area.

Initial water analogy studies were conducted to determine the effects of two configurational variables upon the flow field and general behavior of the configuration at a simulated Mach number of 2. These variables are the "effective" width ratio, W_v/W_i' , and the standoff distance of the wedge, h , ahead of the plane of the inlet area.

It was found immediately that certain configurations displayed steady and orderly flow patterns, with attendant inflation stability of the flexible trailing surface, as well as static stability, while others were statically unstable and had disorderly flow patterns. In all cases of a stable configuration (Figure 14), that is a configuration exhibiting both static stability and orderly flow, a large wake or vortex region is formed immediately behind the wedge. This wake region is symmetrically located and no significant mass transfer between this region and the surrounding much faster moving fluid was observed to occur. The symmetrical bow shock is always attached to the wedge and

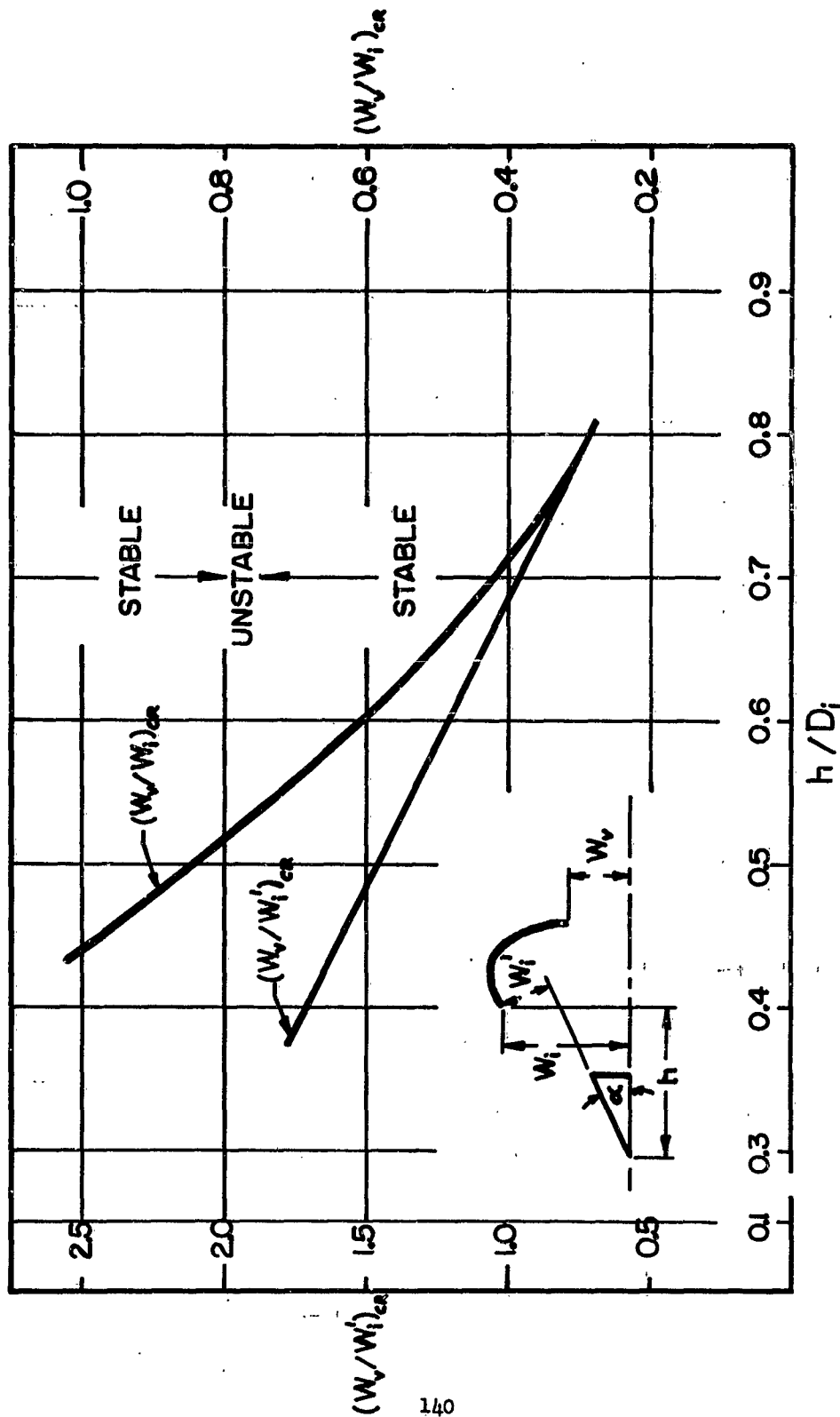


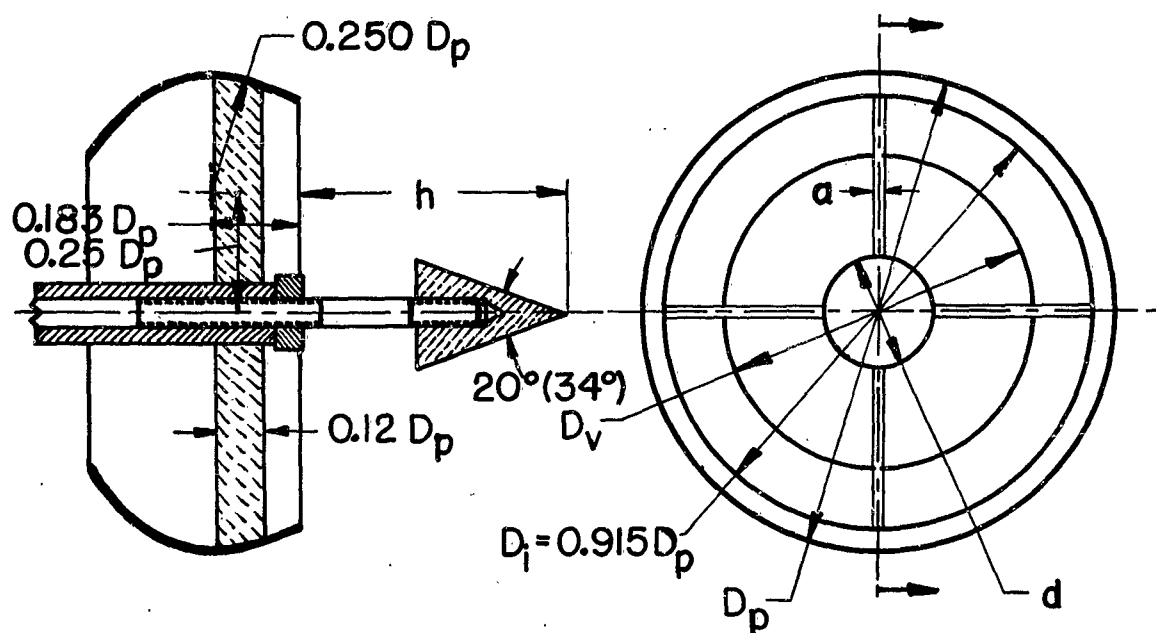
FIG. 15 CRITICAL WIDTH RATIO versus STAND-OFF DISTANCE TWO-DIMENSIONAL MODEL TEST

located upstream of the leading edge of the trailing surface. If this shock wave touches the leading edge, unsteady flow patterns and irregular flow velocities occur and the configuration becomes statically unstable. In general, it was found that the configuration is stable when there is a normal shock originating steadily at the leading edge of the trailing surface, with no spillage occurring around the entrance. In unstable configurations, the normal shock is detached from the leading edge and its point of origin varies.

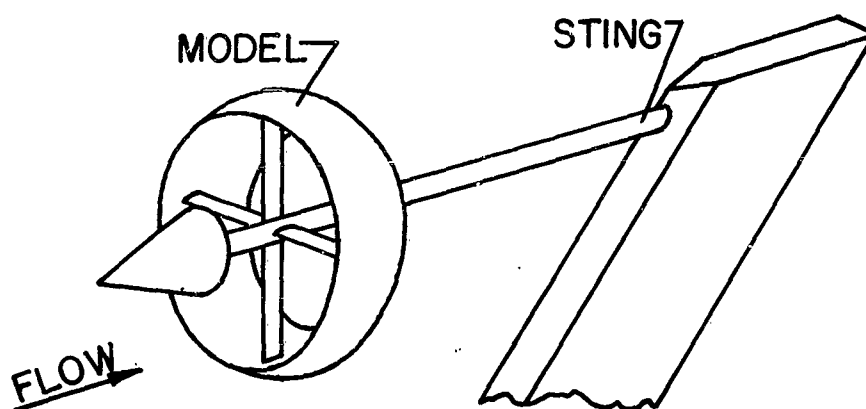
It was also found that the stand-off distance of the wedge ahead of the plane of the inlet has rather finite boundaries for a given width ratio. If the wedge is placed too close to the inlet, the shock wave of the trailing surface precedes the wedge, undefined flow patterns occur within the trailing surface, and the configuration becomes unstable. If the stand-off distance becomes too great, the shock wave of the cone develops into the form of Von Karman's vortex sheet, and the configuration again becomes unstable.

As a result of these initial tests, the existence of stable flow patterns ahead and inside of the trailing surface as well as static stability of configurations was confirmed for width ratios larger than critical and related wedge stand-off distance. A stable system of symmetrical shock waves attached to the wedge and to the leading edge of the trailing surface was observed to be present for all stable configurations. Although some relationship between wedge stand-off distance, critical "effective" width ratio, and stability of the configuration was established during these tests, as shown in Figure 15, a ratio of stand-off distance to inlet diameter of the trailing surface, h/D_i , of 0.7 was selected for subsequent investigations as being the optimum based upon observed flow field and configuration stability. The fineness ratio of the wedge was selected to be 1/1.375.

For practical applications, i.e. for the design of three-dimensional configurations, area ratio in terms of the actual constructed inlet area, S_i , or inlet diameter, D_i , should be considered, rather than the "effective" inlet area, S_i' , since the actual constructed inlet diameter, D_i , will be one of the design parameters for the complete configuration. For the geometric relationship which was established for the entrance to the trailing surface for two-dimensional analogy, namely, that the wedge stand-off distance, $h/D_i = 0.7$, that the half-angle of the wedge = 20° , and with the assumption that the "effective" inlet width, W_i' , is bounded by the leading edge of the drag producing surface and by the linear expansion of the wedge, a relationship between "effective" exit to inlet width ratios (W_v/W_i') and actual exit to inlet ratios (W_v/W_i) can be established as a function of wedge



$$D_v/D_i = 0.814, 0.856, 0.898, 0.982$$



**FIG.16 RIGID MODEL CONFIGURATION
THREE-DIMENSIONAL TEST**

stand-off distance. This relationship is also shown in Figure 15.

In order to determine the range of width ratios for the selected wedge stand-off distance ($h/D_1 = 0.7$) within which the configuration exhibits flow and static stability, additional water analogy experiments were conducted. The results of these experiments showed that if the width ratio is increased significantly above the critical ratio, an additional range exists wherein the flow within the trailing surface is unstable (Figure 15). Stable flow conditions were observed within a range of width ratios between critical and approximately 0.75. Increasing this ratio further to a value of approximately 0.85 results in the generation of unstable flow. The shock wave generated by the surface becomes somewhat swallowed and unsteady. As the width ratio is increased beyond this range, the flow once again becomes steady; however, the wedge and the trailing surface behave as a primary secondary body combination with relatively independent flow patterns. Because of the higher drag produced, it is logical to assume that an optimum stable configuration should be one with a width ratio near the critical. Based upon the tests conducted, a width ratio of 0.55 was selected as the optimum and was taken as the basis for the design of three-dimensional models for wind tunnel test validation.

AIR FLOW VALIDATION STUDIES, THREE-DIMENSIONAL RIGID MODELS

As a result of the water analogy experiments and data analysis, cone-cup configurations have been established which showed steady flow patterns and static stability characteristics in two-dimensional water flow. To validate these findings for three-dimensional air flow, the behavior of related model configurations was studied by the University of Minnesota in supersonic wind tunnels (Reference 11). For this purpose, the configurational geometry had to be adjusted from two-dimensional to three-dimensional units, and the changes in flow phenomena from water to air had to be taken into account.

The purpose of the exploratory test series was two-fold: one, analyze the flow stability around rigidly mounted models as affected by variations in diameter ratio and cone stand-off distance; and two, to determine the degree of static stability of model configurations which were found to exhibit a stable shock pattern during fixed model tests. This determination was made by allowing the rigid model to freely oscillate or rotate about a suspension point to which the model was attached by means of a steel cable. All models tested during this phase consisted of cone-cup configurations only, and did not include suspension line systems. Configurational details of the models are shown schematically in Figure 16.

For the three-dimensional models, diameter ratios, D_v/D_1 , between 0.8 and 0.98 were chosen for the "cup". To obtain these ratios, the



$D_1/D_2=0.898$ $h/D_1=0.821$ $\alpha=20^\circ$ $D_1/D_2=0.898$ $h/D_1=0.681$ $\alpha=20^\circ$

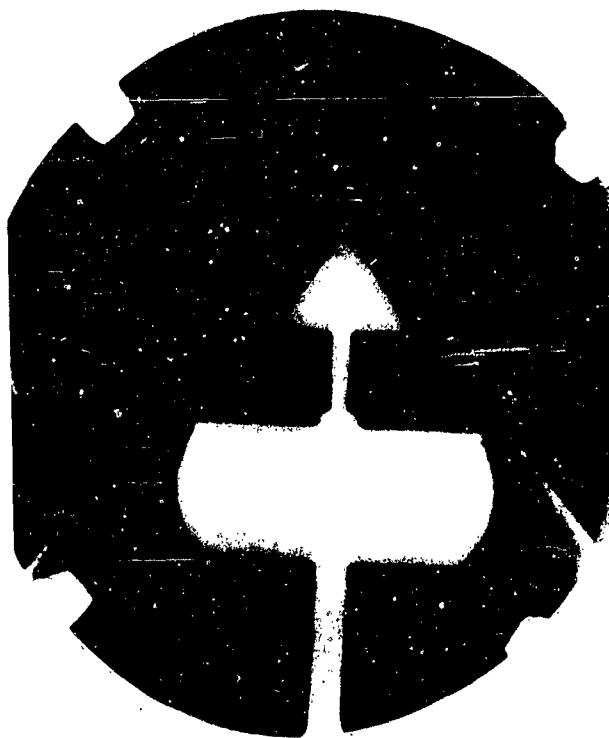
**FIG.17 STABLE CONFIGURATIONS
AT MACH 2.0**

inlet diameter was kept constant while the exit diameter was made variable in the model. To maintain the proper shock wave angle from the cone for the same Mach number of testing, the cone angle should be changed from that of the wedge angle; however, it was felt that a change of this angle would adversely affect the vortex area downstream of the cone. Therefore, the half-angle of 20° was maintained for the cone during the initial wind tunnel tests at a free-stream Mach number of 2.0.

The results of this test series which was conducted at a free-stream Mach number of 2.0 revealed that a rather limited stability region exists for given diameter ratios and cone stand-off distances. In general, it was observed, as it was the case in the two-dimensional tests, that the configuration is statically stable once stability of the flow pattern has been achieved. The results also verified the existence of a narrow range of optimum cone stand-off distances for which the shock wave pattern exhibited excellent stability. This range of stand-off distance was similar to that found during the two-dimensional water flow experiments, $0.65 < h/D_1 < 0.85$. One diameter ratio, $D_v/D_1 = 0.898$, yielded best results for this range of cone stand-off distances. Schlieren photographs of typical shock wave patterns for the two configurations found stable at a free-stream Mach number of 2.0 are shown in Figure 17.

Subsequently, tests were conducted with the same model configurations at a free-stream Mach number of 3.0, and violent instability of those models found to be stable at a free-stream Mach number of 2.0 was observed. An analysis of the flow patterns generated by the unstable configurations revealed that the cone shock wave fluctuated at a high frequency near the entrance to the "cup", suggesting that mass spillage occurred around the leading edge. The wake region behind the cone fluctuated in size with the same frequency as the shock wave pattern. Occurrence of this phenomena was believed to have been caused by the fact that the mass flow behind the cone shock wave and immediately ahead of the leading edge of the "cup" was too large to be accommodated. To decrease the mass flow into the "cup", the Mach number of the incoming flow had to be reduced. This was accomplished by increasing the half-angle of the cone from 20° to 34° . With a 34° half-angle cone, the same Mach number is achieved behind the shock wave at a free-stream Mach number of 3.0 as at Mach 2.0 with a 20° half-angle cone. The fineness ratio of the 34° half-angle cone was selected to be 1/1.186. All other configurational details of the models were identical to those sketched in Figure 16.

Repeated tests at free-stream Mach number of 3.0 with configurations incorporating a 34° half-angle cone confirmed the existence of a stable shock wave pattern. The results revealed that those model configurations which were found to be stable at a free-stream Mach



$D/D_i = 0.898$ $h/D_i = 0.681$ $\alpha = 34^\circ$



$D/D_i = 0.821$ $h/D_i = 0.898$ $\alpha = 34^\circ$

FIG.18 STABLE CONFIGURATIONS
AT MACH 3.0

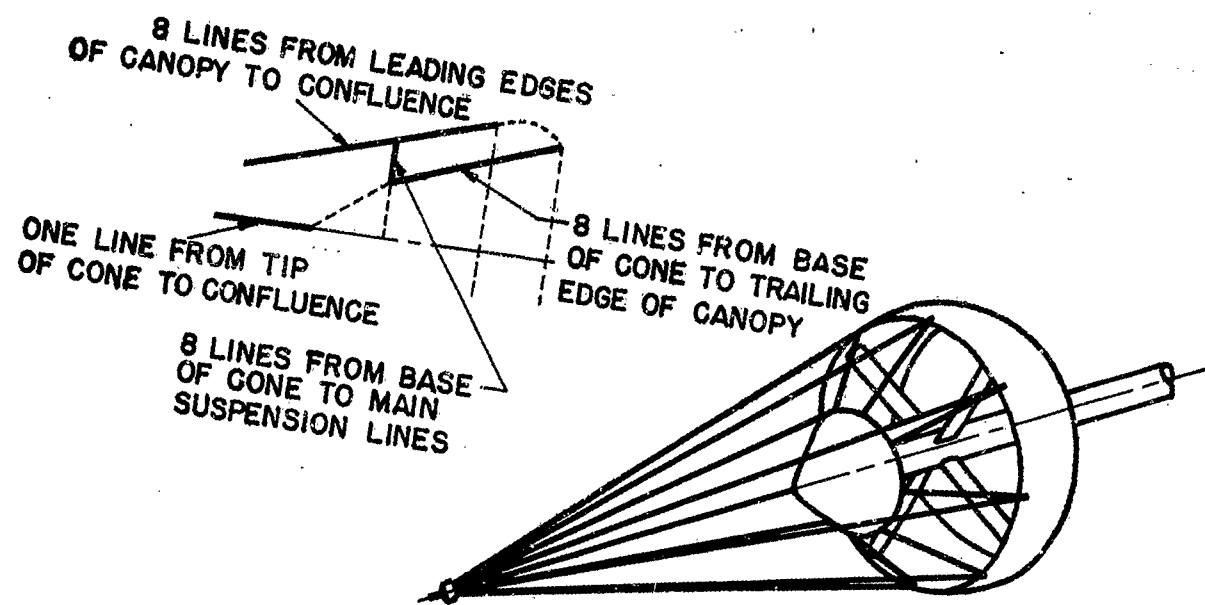


FIG.19 SUSPENSION LINE SYSTEM

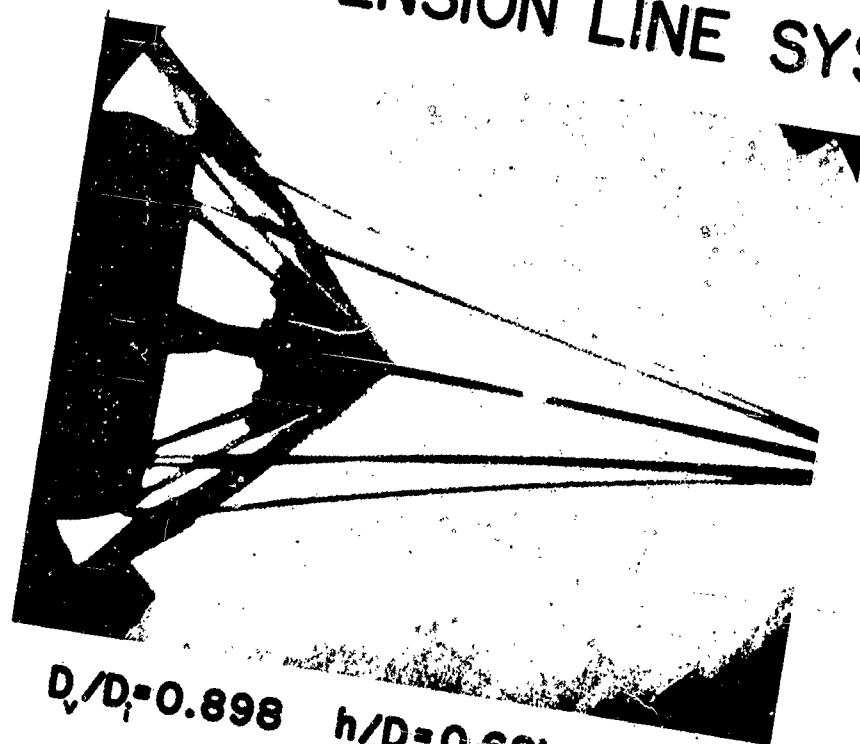
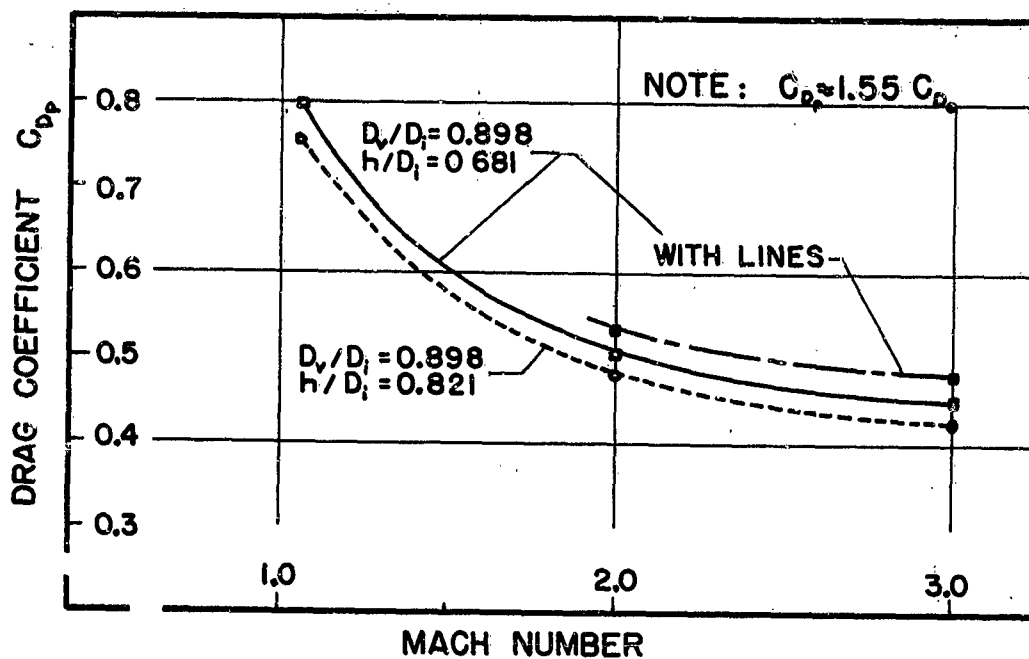
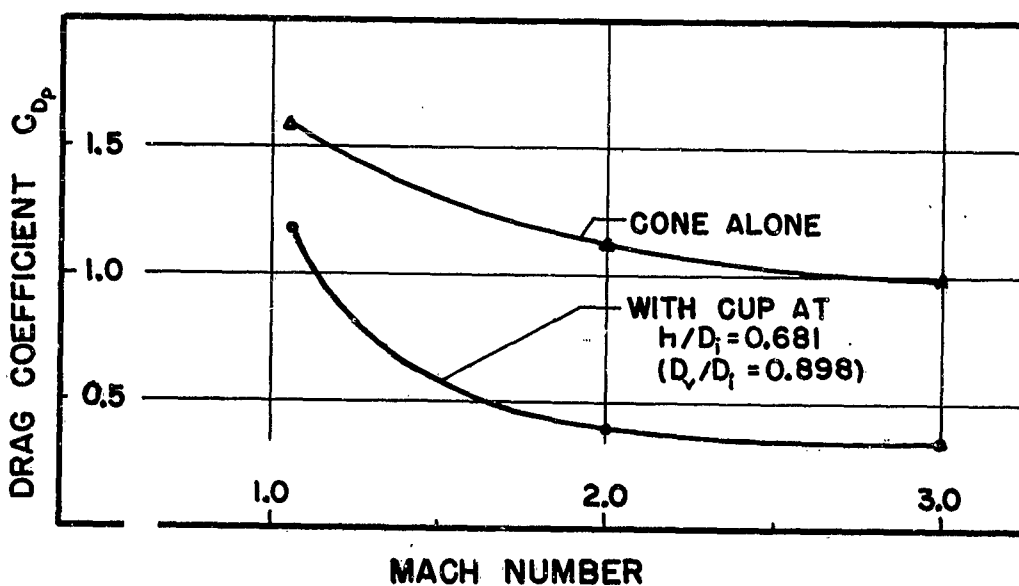


FIG.20 STABLE CONFIGURATION WITH
SUSPENSION LINES AT $M=3.0$



**FIG. 21 DRAG COEFFICIENT versus MACH NO.
RIGID MODEL, CONE HALF-ANGLE 34°**



**FIG 22 DRAG COEFFICIENT versus MACH NO.
 34° HALF-ANGLE CONE**

number of 2.0, namely, for configurations with $D_v/D_1 = 0.898$ and $h/D_1 = 0.821$, and $h/D_1 = 0.681$, but with the cone half-angle increased to 34° were also stable at Mach 3.0. Schlieren photographs of typical shock wave pattern for these configurations at a free-stream Mach number of 3.0 are shown in Figure 18. Although the model configurations were designed for operation at a Mach number of 3.0, flow stability, and with it, static stability of the configurations was observed to exist at all free-stream Mach numbers between 1.06 and 3.0.

Finally, a suspension line system of the configuration and dimensions shown in Figure 19 was added to the models. As can be seen from Figure 20, which represents Schlieren photograph of the shock wave pattern at a free-stream Mach number of 3.0, the suspension lines do not significantly influence the air flow pattern. No deterioration in model stability was observed. This was found to be true for all free-stream Mach numbers at which tests were conducted ($1.06 < M < 3.0$).

DRAG COEFFICIENT AND PRESSURE DISTRIBUTION, THREE-DIMENSIONAL RIGID MODELS

The drag coefficients for the two stable configurations of the 34° half-angle cone-cup model without suspension lines (Figure 16) are shown in Figure 21 for the range of Mach numbers between 1.06 and 3.0. The drag coefficients plotted are based upon the projected area of the "cup", S_p . For this particular configuration, the drag coefficient, C_{D_o} , based upon the total surface area of the cup is approximately $0.645 C_{D_p}$. As can be seen from this Figure, the drag coefficient drops sharply after having reached the characteristic peak at transonic Mach numbers and tends to level off at the higher Mach numbers. Adding suspension lines to the model, a slightly higher drag coefficient is obtained.

As illustrated in Figure 22, the presence of the "cup" behind the cone greatly reduces the drag of the cone. It may be concluded that the presence of the "cup" downstream of the cone produces a relatively high base pressure on the cone, thus causing a reduction in drag.

In order to gain information as to the degree of inflation stability which might be expected for a flexible model, the external and internal pressure distribution over the "cup" surface as well as the pressure distribution in the wake of the cone were determined for free-stream conditions at a Mach number of 3.0. All pressure measurements were reduced to coefficient form with the pressure coefficient, c_p , defined as

$$c_p = \frac{P_L - P_\infty}{q} \quad (6)$$

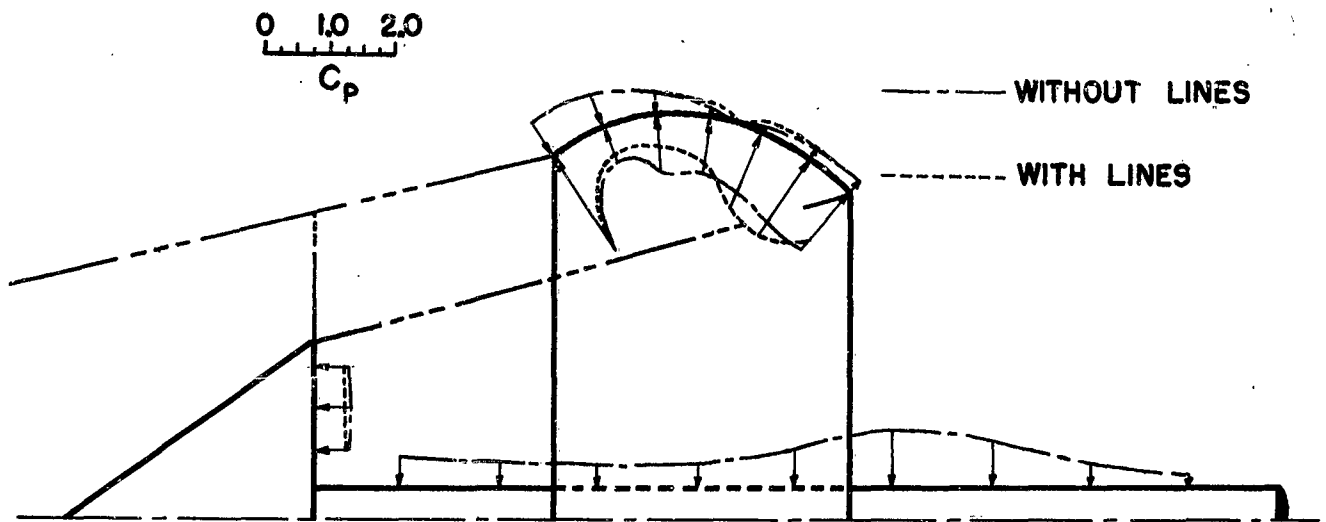


FIG.23 SCHEMATIC PRESSURE COEFFICIENT DISTRIBUTION, RIGID MODEL

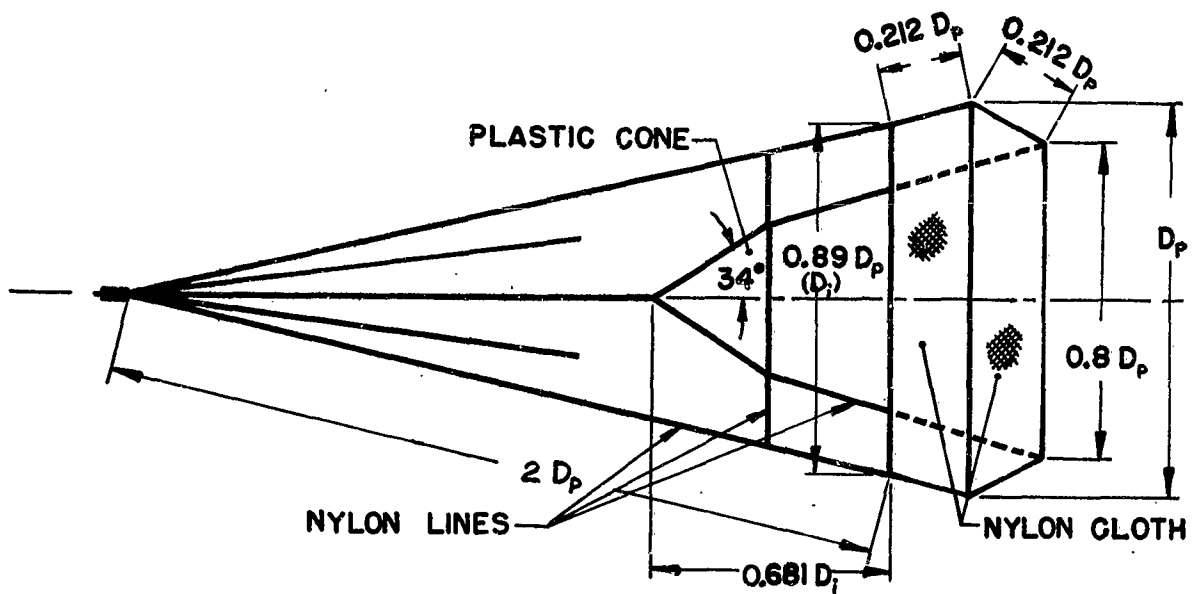
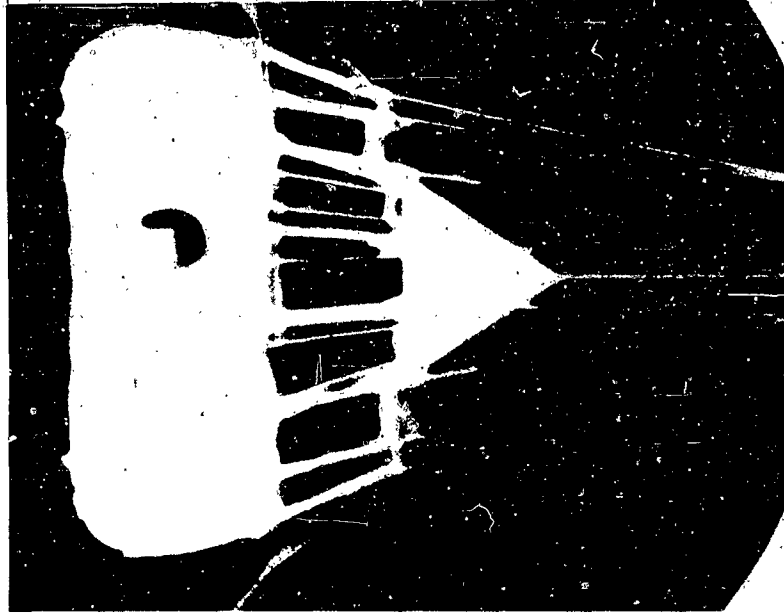


FIG.24 DESIGN, FLEXIBLE MODEL



$D_v/D_i = 0.898$ $h/D_i = 0.621$ $\alpha = 34^\circ$

FIG.25 FLEXIBLE CONE-CUP CANOPY
MODEL AT MACH 3.0

where P_L is the local pressure on the surface of the model, P_∞ is the free-stream static pressure, and q the free-stream dynamic pressure. The pressure coefficients for the model with and without suspension lines are plotted in Figure 23. These measurements show that, in general, the pressure distribution on the "cup" is of a form required to insure inflation and inflation stability. The suspension lines have very little effect upon the external pressure distribution; however, a change of the internal pressure distribution is evident. In addition to a slight and uniform decrease of the base pressure on the cone and of the pressure in the wake, the suspension lines have the effect of decreasing the internal pressure adjacent to the inlet area of the "cup" while increasing it towards the exit area. This change in pressure distribution tends to explain the increase in drag coefficient obtained on identical configurations with suspension lines as compared to those without lines.

VALIDATION TESTS ON FLEXIBLE CONE-CUP CONFIGURATIONS

Flexible models of the configuration shown in Figure 24 were fabricated and tested without a forebody at a free-stream Mach number of 3.0. In order to simplify model fabrication, the "cup" was constructed of two conical segments joined together at the maximum diameter. The "cup" diameter ratio and cone stand-off distance determined as optimum during the rigid model tests were maintained. The "cup" was fabricated of MIL-C-8021A, Type II nylon cloth (300 lb/inch), whereas the cone was made of polystyrene foam molded within a nylon cloth cone to which the suspension lines had previously been sewn.

During deployment tests, this configuration showed very good inflation characteristics as well as good shock wave and inflation stabilities. A Schlieren picture of the typical shock wave pattern generated by the flexible cone-cup configuration is presented in Figure 25.

Only preliminary investigations have been completed to date to determine the performance characteristics of the cone-cup configuration in the wake of a forebody. Initial results indicate, however, that the flexible "cup" of the configuration shown in Figure 24 does not display the same degree of inflation observed during the free-stream model tests. Design changes are currently being made to the "cup" configuration, which may include the reduction and shaping of the exit area in order to obtain a more favorable pressure distribution as well as a reduction in the steep pressure gradient of the exit observed during water analogy investigations. It is believed that these modifications will result in better "cup" inflation as well as higher drag, and improved stability characteristics of the cone-cup configuration when operating in the wake of a forebody.

SUMMARY

Two independent investigations were conducted under contract for the Aeronautical Systems Division, Air Force Systems Command, United States Air Force, by Cook Research Laboratories, Morton Grove, Illinois and by the University of Minnesota, Minneapolis, Minnesota, which led to the evolution of flexible parachute canopy concepts for potential high supersonic speed applications.

In one case, the approach taken was to consider the wake field generated behind a towing body travelling at supersonic speeds and the effects of the non-uniform flow field produced by the wake on the shock wave ahead of a trailing decelerator configuration. It was determined that a significant shock diffraction occurs and that a subsonic outflow and spreading of the wake, resulting from flow deflections through the shock to near the skirt of the canopy, will have a favorable effect in maintaining full inflation of flexible and suitably shaped canopy configurations. To take advantage of this phenomena, the canopy inlet geometry must exhibit inlet angles of sufficient magnitude to provide a positive angle of attack of the inlet region to the local flow direction. To assure reliable canopy inflation, the inlet region should be non-porous or of low porosity; to obtain static stability of the canopy about the point of suspension, the conical surface may be considered as a "guide surface" and must be of a length capable of generating a sufficient restoring moment; to generate desired high drag, the overall total porosity of the canopy must be kept low. These considerations resulted in a new family of flexible parachute canopy configurations, called the "Hyperflo" design.

Basically, the drag producing surface consists of a truncated cone fabricated of low porosity material to which is added a flat roof of suitable geometry to yield the desired total canopy porosity.

Experimental wind tunnel tests conducted on Hyperflo canopy models of different roof designs have verified the assumptions made in selecting this particular design geometry. Testing was accomplished in the wake of symmetrical forebodies and in a Mach number range between Mach 2.3 and 6.0. Throughout this Mach number range, the Hyperflo canopy configurations generally exhibited strong inflation tendencies, excellent inflation stability as well as good static stability and drag characteristics.

The drag coefficient, C_{Dc} , was found to be a function of Mach number, total canopy porosity and canopy position in the wake. A Reynolds Number effect may also be present.

The canopy location downstream of the base of the forebody appeared to significantly affect the overall performance of all configurations. The most favorable location appeared to be at the lower x/d positions, although no quantitative evaluation has been made at this time.

The effects of the diameter ratio of canopy to that of the forebody was not clearly established, although there are indications of a reduction in canopy performance at ratios larger than 2.5. A practical limit of canopy to forebody diameter ratio may exist for efficient operation of this canopy configuration at a prescribed supersonic Mach number. It might be postulated that for the case where the canopy diameter to wake width ratio becomes significantly great, and assuming a similar shock geometry, the flow deviation through the shock wave would not be adequate to spread the wake to the skirt of the canopy, if the shock stand-off distance remained the same. Consequently, the flow aft of the shock at greater distances from the wake centerline would be supersonic. A lip shock would be produced which may, as past tests indicate, further spread the wake upon intersecting the boundary layer until the entire canopy is in subsonic flow. This would possibly lead to a fluctuating flow condition and result in the type of inflation instability observed on conventionally shaped flexible parachute canopies.

The approach taken during the second investigation was to consider supersonic free stream conditions and attempt to convert the momentum of the air by a series of smaller pressure changes, by a certain amount of flow deflection, and finally allowing the air to escape through an enlarged vent. The inlet and outlet cross section of a decelerator embodying this principle would need to be adjusted in such a manner that all air entering the inflated drag device would flow through it in an orderly and controlled manner. As a result of these considerations, a drag device configuration was evolved which consists basically of a textile type "cup" forming in its inflated state a body of revolution having the shape of a conical frustrum joined by a spherical segment, and of a cone, the base of which is located some distance ahead of the plane of the inlet area of the "cup".

Two- and three-dimensional flow field and configurational stability studies were accomplished to determine the effects of configurational variables upon the performance characteristics of this drag device. The results showed that if the half-angle of the cone is adjusted so that the symmetrical shock generated by the cone is located upstream of the leading edge of the "cup" and a normal shock originates steadily at the leading edge of the "cup", the configuration is stable. In the case of a stable configuration, a large vortex region is formed immediately behind the cone. This

wake region is symmetrically located and no significant mass transfer between this region and the surrounding much faster moving air through the "cup" was observed to occur.

Configurations incorporating a 34° half-angle cone, a vent to inlet diameter ratio of 0.898, and a cone stand-off distance of 0.70 were tested over a Mach number range between 1.06 and 3.0 in uniform flow. These configurations displayed very strong inflation tendencies, excellent inflation stability, and good static stability and drag characteristics.

As a result of the limited tests conducted, effects of Mach number, exit to inlet diameter ratio of the "cup", and cone stand-off distance were observed.

Although some deterioration of static and inflation stability of the cone-cup configuration was detected when operating in the wake of a symmetrical primary body, lowering of the exit to inlet diameter ratio and shaping of the exit area may assure inflation stability of the flexible "cup" as well as static stability of the configuration.

Additional tests have indicated the possibility of eliminating the suspension lines which connect the leading edge of the "cup" and the confluence point. This would leave a suspension line system consisting of only a single line connecting the cone to the forebody and a line system for the positioning of the "cup" behind the cone. Such a configuration may be considered to have the potential of a two-stage drag device, where the cone would be deployed at higher Mach numbers to initially decelerate a towing vehicle, and the "cup", stowed inside the cone, would be forcefully ejected and deployed to generate increased aerodynamic drag at supersonic Mach numbers.

All test results obtained and presented above were acquired on small scale models. Both supersonic parachute configurations have exhibited performance characteristics and performance trends which may be expected to extend also to larger diameter configurations. Verification, however, can only be accomplished under full scale free-flight conditions. These efforts are currently being conducted.

REFERENCES

1. Meyer, R. A., Wind Tunnel Investigation of Conventional Types of Parachute Canopies in Supersonic Flow, WADC TR 58-532. Cook Research Laboratories for Wright Air Development Center, December 1958
2. Engstrom, B. A., Performance of Trailing Aerodynamic Decelerators at High Dynamic Pressures, Phase III, WADC TR 58-284, Part III. Cook Research Laboratories for Wright Air Development Center, December 1959
3. Maynard, J. D., Aerodynamic Characteristics of Parachutes at Mach Numbers from 1.6 to 3, Technical Note D-752, Langley Research Center, National Aeronautics and Space Administration, May 1961
4. Fredette, R. O., Parachute Research Above Critical Aerodynamic Velocities, Cook Research Laboratories, May 1961 (Unpublished Report)
5. Supersonic Tests Conducted at the Cook Technological Center Wind Tunnel on Parachute Type Decelerator Models. Cook Research Laboratories, October 1960 (Unpublished Report)
6. Progress Report Nr. 12, Contract AF33(616)-6372, Theoretical Parachute Investigations, University of Minnesota (H. Heinrich et al)
7. Sims, L. W., Analytical and Experimental Investigation of Supersonic Parachute Phenomena (Unclassified Title), ASD TDR 62-844. Cook Research Laboratories for Aeronautical Systems Division, October 1962 (CONFIDENTIAL REPORT)
8. Deitering, J. S., Investigation of Flexible Parachute Model Characteristics at Mach Numbers from 1.5 to 6, (Unclassified Title), AEDC TDR 62-185. Von Karman Gas Dynamic Facility, ARO, Inc. October 1962 (CONFIDENTIAL REPORT)
9. Progress Report Nr. 13, Contract AF33(616)-6372, Theoretical Parachute Investigations, University of Minnesota (H. Heinrich et al)
10. Progress Reports Numbers 14 through 16, Contract AF33(616)-6372, Theoretical Parachute Investigations, University of Minnesota (H. Heinrich et al)

11. Herman, R., Inlet Diffuser Theory and Introduction to Internal Aerodynamics, Minneapolis Honeywell Regulator Co., 1956
12. Progress Report Numbers 17 through 22, Contract AF33(616)-8310, Basic Aerodynamic Decelerator Investigations, University of Minnesota (H. Heinrich et al)

APPLICATION OF AXISYMMETRIC FLOW ANALYSIS
TO INFLATION STABILITY OF SUPERSONIC FLEXIBLE
PARACHUTES

J. K. BUCKNER

GENERAL DYNAMICS/FORT WORTH

ABSTRACT

An axisymmetric flow analysis is performed on supersonic porous parachutes utilizing available data from tests of three different parachute designs. Photographs of the flow field near various parachute models have been studied to establish a hypothesis concerning the nature and causes of inflation instability. With careful consideration given to the uniqueness of each parachute geometry and the assumptions necessary to establish the flow field, the upper porosity-Mach number limit for stable operation of a 30° Conical, a 15% Skirted Equiflo, and a 10% Skirted Hemisflo parachute is calculated.

LIST OF SYMBOLS

| | |
|-------------|---|
| A_i | Inlet area of parachute ($= S_i$) |
| A_s | Total slot area |
| A_s' | Slot area excluding slots in skirt |
| C_i | Circumference of inlet |
| $C_{i\max}$ | Maximum possible circumference at inlet |
| $C_{i\min}$ | Minimum circumference at inlet |
| D | Diameter of cone base |
| $-D_i$ | Inlet diameter |
| D_o | Nominal chute diameter $(4S_o/\pi)^{1/2}$ |
| D_p | Inflated chute maximum diameter |
| d | Length across main parachute fabric (see Appendix) |
| M_∞ | Free stream Mach number |
| M_1 | Mach number ahead of shock |
| M_2 | Mach number behind shock |
| M_i | Mach number at inlet |
| M_s | Mach number through slots |
| P_B | Base perimeter of cone |
| R | Radius at cone base ($D/2$) |
| R_i | Inlet radius |
| S_i | Inlet area of parachute ($= A$) |
| S_o | Total chute surface area |
| δ | Deflection of ribbon to local stream ("+" tending to open) |
| λ_G | Porosity (A_s/S_o) |
| λ_G | Partial porosity (A_s'/S_o) |

APPLICATION OF AXISYMMETRIC FLOW ANALYSIS TO INFLATION STABILITY OF SUPERSONIC FLEXIBLE PARACHUTES

INTRODUCTION

In the development of a stabilization parachute for the B-58 escape capsule, it was found that the particular geometry of each parachute has a profound effect on the upper stability limit of the device. Through a trial and error process, a final design was chosen to be used on the escape capsule. This design has demonstrated stable operation throughout the Mach number range in which it has been tested. It became desirable then to know why one geometry demonstrates stable operation at a given Mach number while another is highly unstable at the same Mach number. If the answer could be found, it might reveal the conditions under which the most stable geometry would become unstable.

The study represented by this report began as an effort to find the dependence of inflation stability on parachute geometry so that the upper Mach number limitation of the B-58 escape capsule could be predicted. The resulting method can be applied to any parachute design so long as sufficient consideration is given to the uniqueness of the design geometry.

REVIEW OF PAST WORK

General

A review of some of the work to date on supersonic flexible parachutes has been made, and the results have been used to arrive at an analytical means for solving the upper porosity limit of stable operation for three different types of parachute designs. Each of the three designs presents a different problem which must be considered unique; however, the same basic flow picture is assumed for all designs.

Three methods have been employed to date to test parachute characteristics: that is, the testing of flexible chutes suspended by shrouds and harness; the testing of sting supported rigid chutes with no shroud lines; and the testing of sting supported rigid chutes with shroud lines. A limited number of Schlieren pictures has been published from each type of test.

The testing of flexible models (reference TND-752) indicates that there is usually a strong pressure disturbance standing in front of the chute inlet but behind the shroud lines' confluence point as shown in Figure 1a. There appears to be no oblique shock associated with the shroud lines originating at the confluence point; however, the shrouds probably do affect the strong shock ahead of the chute mouth distorting it from normal in nature to combined normal and oblique. This distortion would increase the local Mach number behind the shock.

The testing of rigid models without shrouds revealed much the same as the flexible models except that there is no distortion of the strong pressure disturbance ahead of the inlet. This disturbance was clearly a normal shock, which moved closer to the chute mouth with increasing porosity. A typical schematic is shown in Figure 1b.

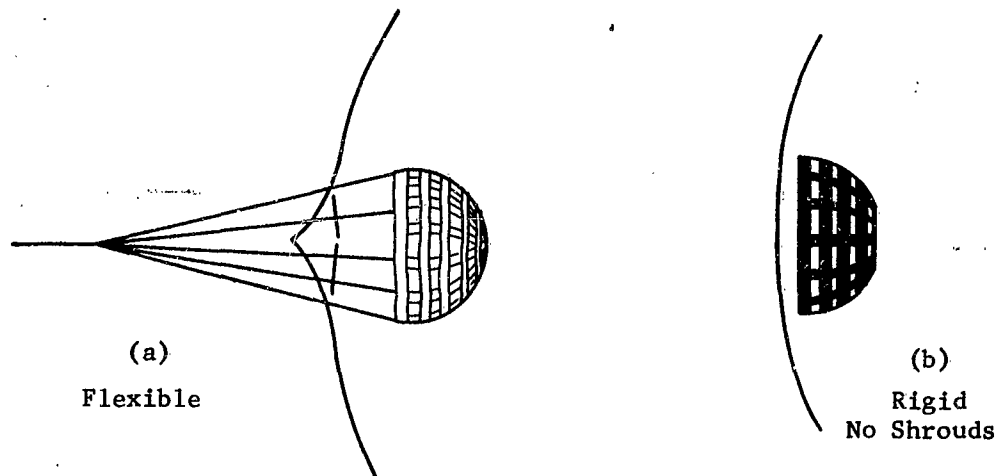
The tests of rigid models with shroud lines converging into a cone at the confluence point have all shown a distinct oblique shock originating at the cone. These models usually experienced unsteady flow similar to the inlet buzz phenomenon of spiked inlets. That is, the normal shock appeared to move out of the chute mouth toward the oblique shock, overtake the oblique shock, and finally disappear. A schematic of this phenomenon is shown in Figure 2. There has been some speculation that inflation instability of flexible parachutes is due to this unsteady flow observed on rigid parachutes with shrouds.

Establishment of Flow Field

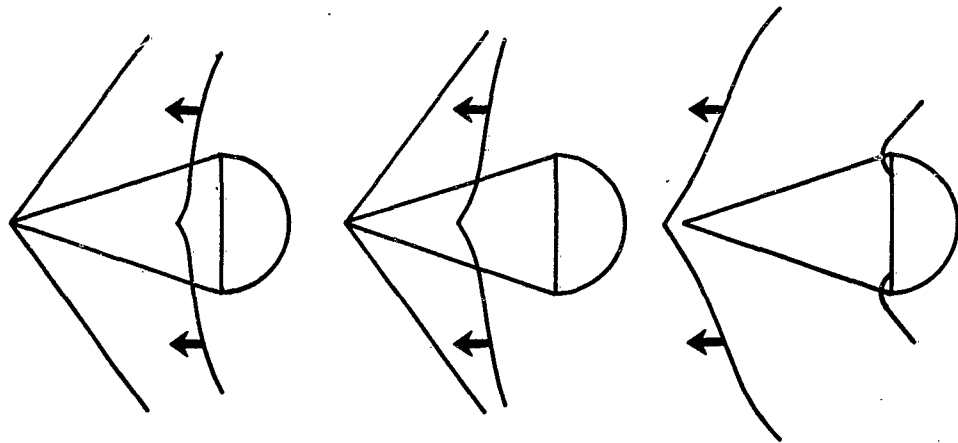
It is the purpose here to present a method for calculating the upper porosity limit as a function of Mach number for stable parachute operation. To do this a flow picture ahead of the chute mouth must be established.

The flow picture obtained from the rigid models with shrouds can be eliminated for two reasons. First, the contention here is that inflation instability is not closely related to the inlet "buzz" phenomenon because there is no strong oblique shock associated with the confluence point of the shroud lines in the flexible parachute case. Second, the unsteady flow demonstrated in these rigid model tests has been observed at conditions in which some flexible parachutes have demonstrated stable operation.

The flexible parachute tests would be the ideal with which to establish a flow picture; however, the distortion of the normal shock renders the problem extremely difficult. If a normal shock is assumed ahead of the inlet, the Mach number behind the shock will be lower than we would expect in the real case; and we will see later that this assumption



SCHEMATIC OF SHOCK PATTERNS
Figure 1



UNSTEADY FLOW ON RIGID MODELS WITH SHROUDS

Figure 2

will result in a conservative estimate of the region of stable operation for the device.

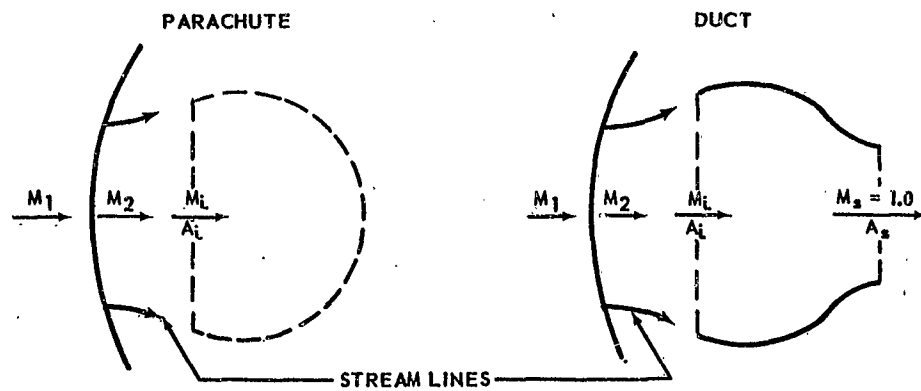
Consequently, to completely establish the flow picture from which the stable operating region can be calculated the following assumptions are made:

- (1) A normal shock stands in front of the chute inlet.
- (2) This normal shock is not distorted by the presence of the shroud lines.
- (3) There is no oblique shock originating at the shroud line confluence point.
- (4) Porosity is low enough to give Mach one flow through the slots, that is, the flow through the chute is choked.
- (5) Inflation instability will begin when the porosity is such that the normal shock attaches to the inlet of the chute.

Inflation Instability

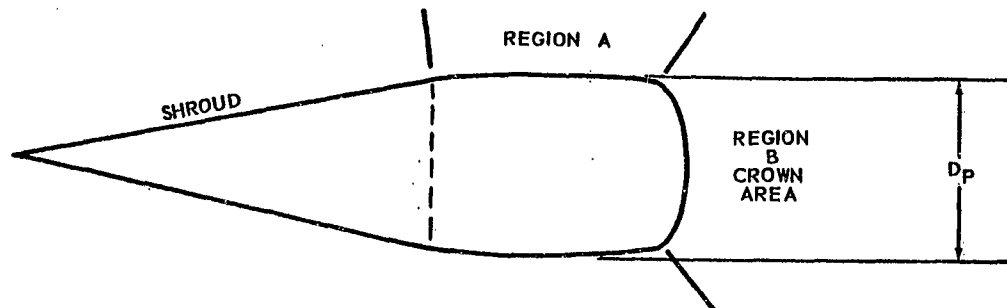
From Figure 3 it can be seen that the area ratio A_1/A_s controls the Mach number at 1 as long as the flow is choked. The normal shock is a result of the choked flow and its position is dependent upon the ratio of M_2 to M_1 . If M_2 is greater than M_1 the shock will remain detached and the streamlines from 2 to 1 will be divergent tending to hold the chute open by creating a "lip-suction" on the leading ribbon. As M_1 increases M_2 will decrease, and the shock will move closer to the inlet until $M_2 = M_1$, at which point the shock will become attached. With the shock attached there is no region 2 to 1; therefore, "lip-suction" created by diverging streamlines is not available. The chute inlet may then tend to close causing the shock to form entirely within the chute where it probably becomes partly normal and partly oblique. This form of shock inside the chute will tend to elongate the chute causing it to close even further. The same sequence of events can be said to occur if M_1 is held constant and A_1/A_s decreased until M_1 becomes equal to M_2 . In either case (varying porosity or Mach number), inflation instability would begin at the lowest M_1 possible if the shock were actually a normal because this would produce the lowest M_2 attainable. Thus, assumption (1) above gives a conservative region of stable operation.

Recent diameter data taken during inflation instability indicate that there is a minimum value of D_p during this period. To explain the minimum, we must examine the shape of the chute when it reaches the minimum observed inflation.



ANALOGY OF PARACHUTE FLOW WITH ONE-DIMENSIONAL DUCT FLOW

Figure 3



TYPICAL CHUTE SHAPE AT MINIMUM INFLATION DURING INFLATION INSTABILITY

Figure 4

As the normal shock moves inside, the canopy elongates and closes until the chute assumes a shape similar to that shown in Figure 4. If the flow is entirely supersonic in the chute, we can perhaps explain why the chute, after reaching a minimum inflation, begins to open. We may again assume that the flow through the slots is at Mach 1.0; however, the outflow primarily occurs through the portion of the canopy which is nearly normal to the flow. It may be noted here that if the chute has a large vent which covers nearly all of the region B, it is likely that the flow will leave the chute supersonically and the chute will stabilize at this condition with low drag. However, if (as in our case) the porosity in region B is as low as or lower than the total porosity, we may expect Mach 1.0 through the slots.

To illustrate a possible occurrence let us examine the picture for a 20%, 30° Conical chute. The vent of this chute is sufficiently small to assume the porosity in region B to be .5 the total porosity. Thus, the area ratio A/A^* from just ahead of the slots to the slots would be 10.0. This area ratio would require an upstream Mach number of 3.92 to hold the shock in the slots. Thus at Mach numbers less than 3.92 the shock would begin moving upstream or toward the mouth of the chute. As it moves, the increased pressures behind the shock would begin influencing the aft portion of region A thus tending to open the chute. Inflation would continue as the shock proceeds upstream until it leaves the chute, and then the original flow picture of Figure 3 would occur again.

ANALYSIS OF THREE PARTICULAR PARACHUTES

General

With the flow picture established, the various chute geometries may now be considered. Three different designs will be discussed, all of which were tested behind a bomb dropped from an F-104. A brief description of the test and parachutes is presented in the Appendix. The drop tests have provided drags and parachute inlet diameters as functions of free stream Mach number. Using the diameter data and a careful consideration of the parachute geometry with the above assumed flow picture, a critical Mach number may be calculated, above which inflation instability is likely.

30° Conical Design

The first design is a so-called 30° Conical parachute. A schematic of this design appears in Figure A3 of the Appendix. A description of the particular chute used in the drop test follows:

30° Conical, 20% λG

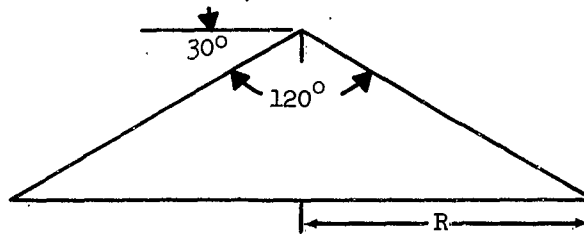
$$S_0 = 8.41 \text{ Ft}^2; D_0 = 3.272 \text{ Ft}$$

$$A_S = \lambda G S_0 = 1.682 \text{ Ft}^2$$

The critical ratio is A_1/A_S , for it can be shown that if this ratio falls below a certain value at a given M_1 , the chute will lose its tendency to stay open. Therefore, we must investigate the inlet geometry of the parachute.

For a flexible chute, it is always possible for A_1 to vary. The maximum inlet diameter may be determined as follows:

$$S_0 = \text{Surface Area} = (1/2 \text{ Base Perimeter})(\text{Slant Height})$$



$$P_B = 2\pi R; \text{ Slant Height} = \frac{R}{\cos 30^\circ} = 1.155 R$$

$$\text{Therefore: } S_0 = (1/2 \ 2\pi R) (1.155R) = 1.155\pi R^2$$

$$\text{From which: } R = 1.524 \text{ (in our case) or,}$$

$$D = 3.05 \text{ Ft.}$$

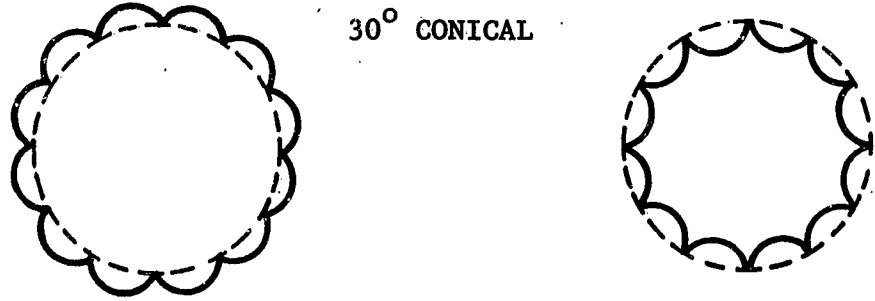
Therefore the maximum possible diameter at the mouth of the chute is 3.05 feet; however, the maximum observed diameter was 2.32 feet. It is obvious that if 3.05 π feet of ribbon is available at the mouth of the chute, and the diameter observed is 2.32 feet, there is excess ribbon present which must either blossom out or in. The two possible inlet shapes are shown in Figure 5.

In the interest of conservatism and simplicity, let us assume the chute mouth takes one of the shapes shown in Figure 6. Figure 6(A) illustrates the blossom out case, and Figure 6(B) shows the flop-in case. Further let us assume that the average inlet radius, R_{avg} , at any time during instability is as shown in Figure 6.

With the D_1/D_0 versus Mach number data of Figure 7, an average value of D_1 can be found for a given Mach number. Knowing D_1 it is a simple matter to find the amount of excess ribbon available at the mouth of the chute at this average

A. BLOSSOM-OUT

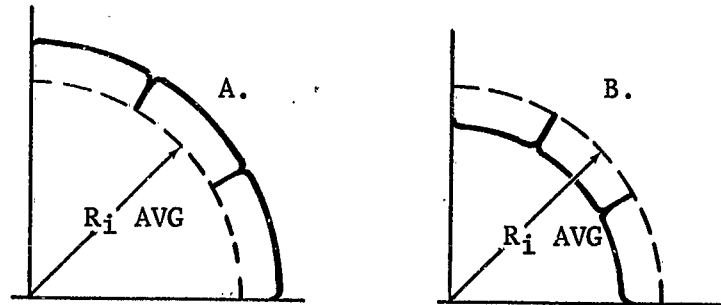
B. FLOPPED-IN



TWO POSSIBLE CHUTE MOUTH SHAPES

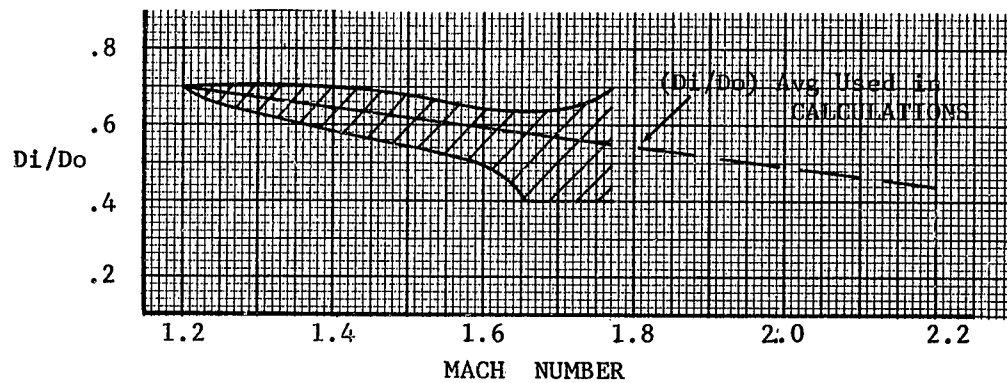
Figure 5

30° CONICAL PARACHUTE



ASSUMED CHUTE MOUTH SHAPES

Figure 6



30° CONICAL MEASURED INLET DIAMETER

Figure 7

inflation condition. The circumference is known; thus, the excess ribbon at the inlet is the difference ($\pi D - \pi D_1$). The chute in question is a twelve gore pattern; therefore, if the excess ribbon were to flop-in as shown in Figure 6(B), then

$$\Delta R_1 = (R_{1avg} - R_{1n}) = \frac{\pi D - \pi D_1}{24}.$$

From this expression, R_{1min} and A_{1min} may be found.

The value of A_{1min} as calculated by the above reasoning will be used to arrive at a theoretical critical porosity for a given Mach number. This choice of inlet area is made for the following reason. Due to the conical design of the chute, it is observed that the ribbons near the inlet will always have a deflection to the free stream. In the blossom out condition, the deflection will be positive (tending to open the chute); whereas, in the flopped-in condition the deflection will be negative (see Figure 8). In addition, it is observed that if the drag of the ribbons causes them to fall aft, an unstable ribbon ensues which could have a positive or negative deflection to the stream. When the deflection is negative, it would tend to close the chute; or it may tend to flop the ribbon inward. It is assumed in the choice of A_1 above that near and during inflation instability the ribbons do fall aft where they are unstable, and violent inflation instability ceases when the minimum A_1 exceeds a critical value as Mach number decreases.

From the above reasoning it is postulated that inflation instability of a conical shaped parachute is caused by the flopping of excess ribbon in the region of the chute inlet. When the excess flops inward it presents a negative deflection to the stream which tends to close the inlet. Once the inlet has closed below a critical value, it tends to continue to close regardless of the shape the ribbons assume at the mouth. The closing chute will reach a minimum inflation after which it will begin to open again unless the free stream Mach number is high enough to support a shock at the exit slots of the elongated chute. In the latter case the chute will remain semi-inflated, and it will experience low drag.

With the above considerations it is now possible to calculate the critical Mach number versus porosity curve. The local Mach number in the wake of the bomb, M_1 , is calculated using reference 1. This calculation yields $M_1 = .954M_\infty$. M_2 is taken from shock tables. A critical porosity is then calculated knowing A_{1min} , $M_1 = M_2$, and $A_1/A_8 = A/A^*$ for the Mach number M_1 . Then knowing the value of S_0 for the particular design, $(A_8/S_0)_{CR}$ is easily calculated.

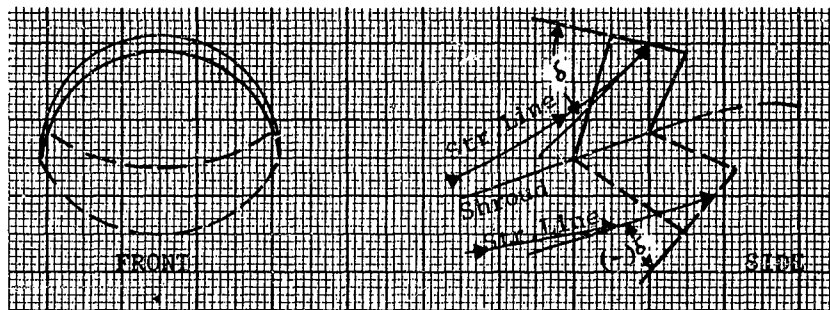


ILLUSTRATION OF POSSIBLE RIBBON DEFLECTIONS TO THE LOCAL STREAM

Figure 8

The resulting curve of porosity versus Mach number is plotted in Figure 9, and the calculations are tabulated in Table 1.

| <u>M_∞</u> | <u>M₁</u> | <u>M₂</u> | <u>(S₁/A_s)_{CR}</u> | <u>(D₁/D₀)_{AVG}</u> | <u>R₁_{AVG}</u> | <u>C₁_{AVG}</u> |
|----------------------|----------------------|----------------------|---|--|------------------------------------|------------------------------------|
| 1.3 | 1.24 | .8183 | 1.0311 | .675 | 1.105 | 6.95 |
| 1.5 | 1.43 | .7274 | 1.0759 | .622 | 1.017 | 6.39 |
| 1.7 | 1.62 | .6625 | 1.1243 | .570 | 0.932 | 5.85 |
| 1.9 | 1.81 | .6143 | 1.1720 | .520 | 0.850 | 5.34 |
| 2.1 | 2.00 | .5774 | 1.2164 | .466 | 0.762 | 4.79 |

| <u>ΔC₁</u> | <u>ΔR₁</u> | <u>R₁_{MIN}</u> | <u>S₁_{MIN}</u> | <u>(A_s)_{CR}</u> | <u>(A_s/S₀)_{CR}</u> |
|-----------------------|-----------------------|------------------------------------|------------------------------------|-------------------------------------|---|
| 2.62 | .109 | 1.0 | 3.14 | 3.05 | .362 |
| 3.18 | .1325 | .8845 | 2.46 | 2.285 | .272 |
| 3.72 | .155 | .777 | 1.896 | 1.685 | .200 |
| 4.23 | .176 | .674 | 1.425 | 1.217 | .1447 |
| 4.78 | .199 | .563 | 0.995 | .819 | .0974 |

$$S_0 = 8.41 \text{ Ft.}^2$$

$$C_{1\text{MAX}} = 9.57 \text{ Ft.}$$

$$D_0 = 3.272 \text{ Ft.}$$

$$\Delta C_1 = C_{1\text{MAX}} - C_{1\text{AVG}}$$

$$(A_s)_{\text{CR}} = \frac{S_{1\text{MIN}}}{(S_1/A_s)_{\text{CR}}}$$

$$\Delta R_1 = \Delta C_1 / 24$$

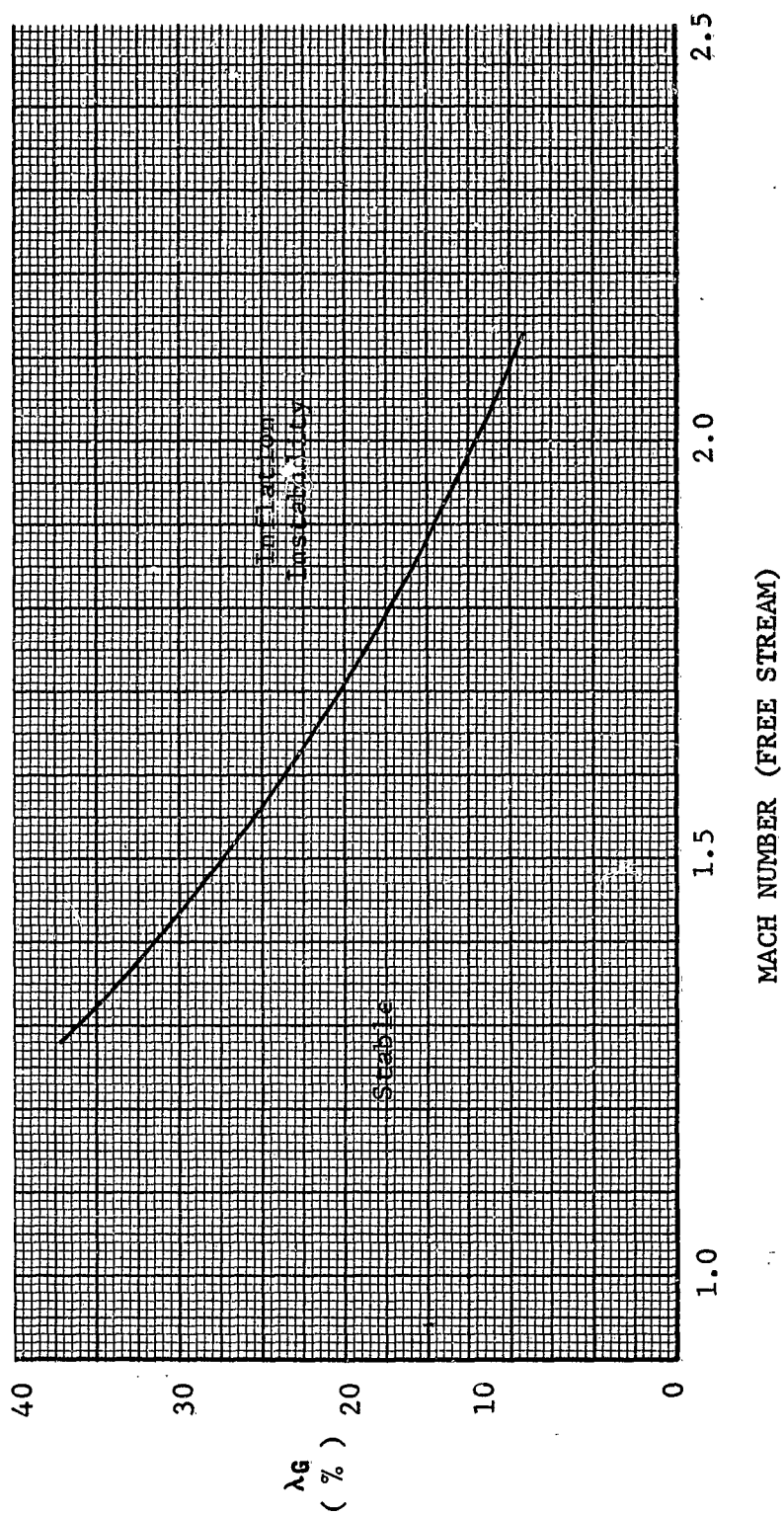
$$M_1 = .954 M_\infty$$

$$R_{1\text{MIN}} = R_{1\text{AVG}} - \Delta R_1$$

Table 1. 30° CONICAL PARACHUTE

30° CONICAL STAB CHUTE BEHIND BOMB

Figure 9



15% Skirted Equiflo

The previous section has shown that a 20% porous, 30° Conical chute is unstable above 1.7 Mach number. However, since the Equiflo chute has a skirt (see Appendix) and in light of the previous examination of inflation instability, the skirted Equiflo chute would not be expected to demonstrate the same instability as the Conical chute. To be sure, it will have excess ribbon in the fully inflated condition, and assuming that the excess has a tendency to flop-in at high Mach numbers, there would remain basic differences in the two chute designs. The primary difference lies in the effective deflection of the inlet ribbon to the local stream in the flopped-in case. Figure 10 illustrates that the deflection of the mouth ribbon to the free stream could be negative; however, as long as there is a slight divergence of streamlines at the mouth, the deflection of the local stream will be zero or positive whether the excess ribbon is blossomed out or in.

If we now attempt to find a reason for the excess ribbons to flop-in, we find it a difficult task. The geometry of the skirt is such that there is always little or no deflection of the ribbons to the free stream; therefore, the local streamlines would have to be highly convergent in order to force the excess ribbon inward. If, however, the flow were convergent at the inlet, inflation instability would have already begun, and the flopping-in would have no significance.

From these considerations it appears that the theoretical critical porosity versus Mach number should be calculated without regard to the flopping of excess ribbon at the mouth or inlet of the skirted Equiflo chute.

Examination of the inflated parachute in the assumed flow field reveals another consideration which should be included in the calculation of the stable region of operation. If we say that inflation instability begins when the shock attaches to the mouth of the chute, then with the help of Figure 11 another observation typical of skirted chutes can be made. That is, there can be little or no flow through the slots of the skirt when the conditions are critical or near critical. In fact, it appears that any flow through these slots will be into rather than out of the chute. A calculated critical porosity should therefore be applied to the area ratio A_g'/S_o where A_g' is the area of only the slots in the main chute not including any slots in the skirt.

The diameter data of a typical F-104 bomb drop with the skirted Equiflo chute are shown in Figure 12. Again

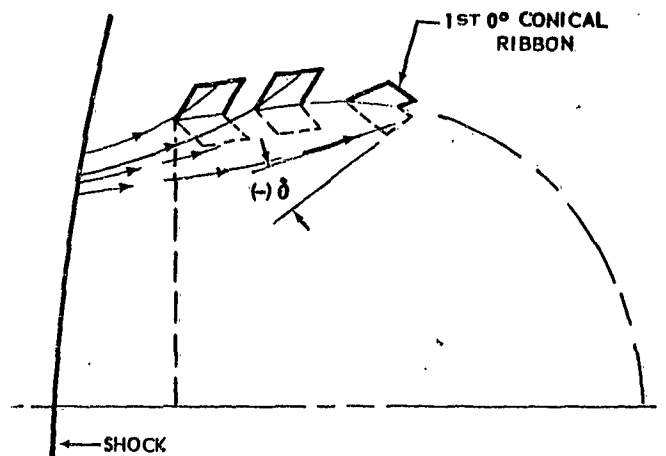


Figure 10 SKIRTED EQUIFLO-LOCAL FLOW DEFLECTION TO RIBBONS

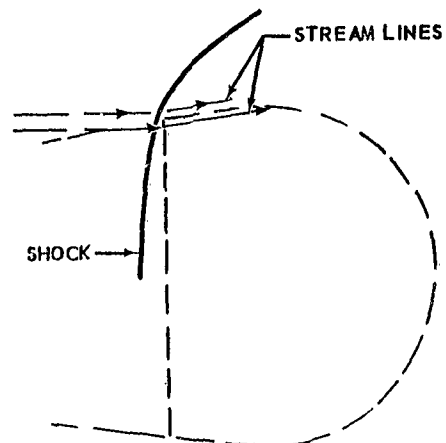


Figure 11 FLOW DIAGRAM OF SKIRTED EQUIFLO AT MACH NUMBERS APPROACHING CRITICAL

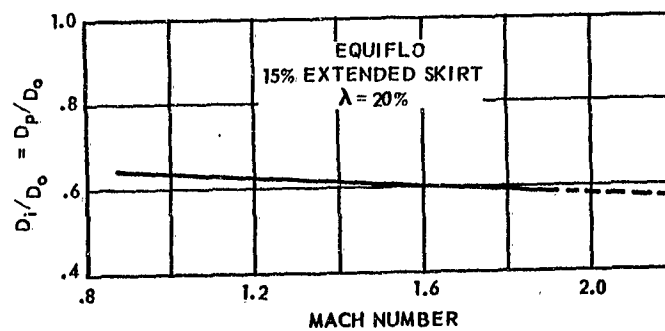


Figure 12 EQUIFLO AVERAGE MEASURED INLET AREA

the data may be used to find the variation of D_1 with Mach number.

The same general method as was used for the Conical chute is then applied to the skirted Equiflo with two exceptions: (1) that A_1 is used directly rather than a minimum inlet area as calculated by taking into account the excess ribbon, and (2) that the porous area is only that of the main portion of the chute, $A_{S'}$.

The results of the calculation of critical partial porosity ($A_{S'}/S_o$) versus Mach number for a skirted Equiflo chute are shown in Figure 13, and the calculations are tabulated in Table 2.

| M_∞ | M_1 | M_2 | $(S_1/A_{S'})_{CR}$ |
|------------|-------|--------|---------------------|
| 1.3 | 1.24 | 0.8183 | 1.031 |
| 1.7 | 1.62 | 0.6625 | 1.124 |
| 2.1 | 2.00 | 0.5774 | 1.216 |
| 2.5 | 2.38 | 0.5253 | 1.295 |
| 2.9 | 2.765 | 0.4907 | 1.359 |
| 3.3 | 3.145 | 0.4672 | 1.407 |
| 3.7 | 3.53 | 0.4500 | 1.449 |

| $(D_1/D_o)_{AVG}$ | $(S_1/S_o)_{AVG}$ | $(A_{S'}/S_o)_{CR}$ |
|-------------------|-------------------|---------------------|
| 0.620 | 0.384 | 0.372 |
| 0.600 | 0.360 | 0.320 |
| 0.580 | 0.337 | 0.277 |
| 0.560 | 0.314 | 0.242 |
| 0.540 | 0.292 | 0.215 |
| 0.520 | 0.270 | 0.192 |
| 0.500 | 0.250 | 0.173 |

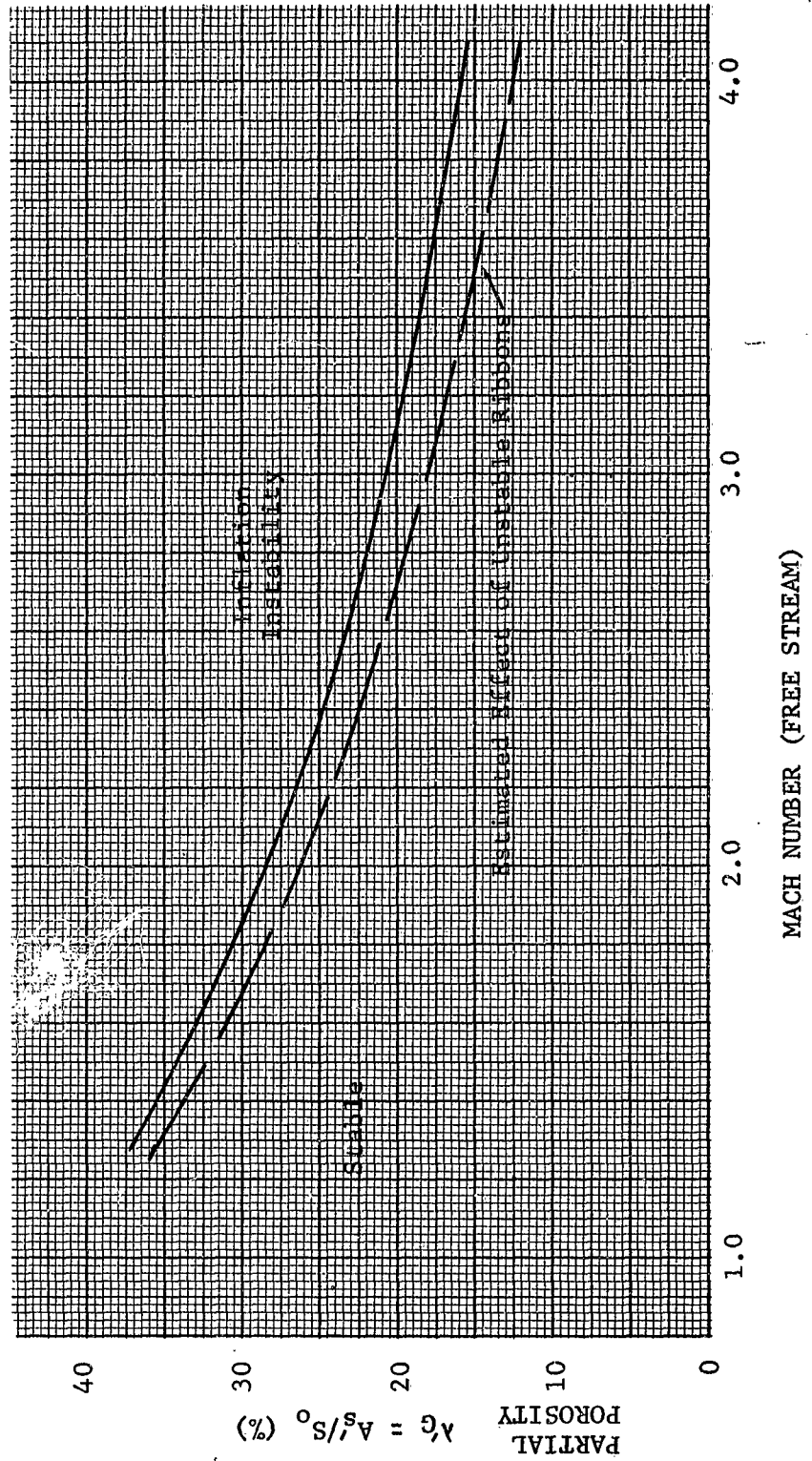
$$M_1 = 0.954 M_\infty \text{ (Bomb Configuration)}$$

$$\lambda = \frac{A_{S'}}{S_o} \times \frac{A_S}{A_{S'}} \quad (A_{S'}/S_o)_{CR} = \frac{(S_1/S_o)_{AVG}}{(S_1/A_{S'})_{CR}}$$

Table 2. 15% SKIRTED EQUIFLO CHUTE

15% SKIRTED EQUIFLO STAB CHUTE
BEHIND BOMB

Figure 13



There are two considerations which could reduce the Mach critical of the skirted Equiflo chute from its above calculated theoretical value. The first is that even though the ribbons in the skirt have little chance of presenting a negative deflection to the free stream there remains a significant amount of excess ribbon at the mouth which would allow the inlet area to fluctuate freely. If any fluctuations occur, the stable region of operation would be reduced.

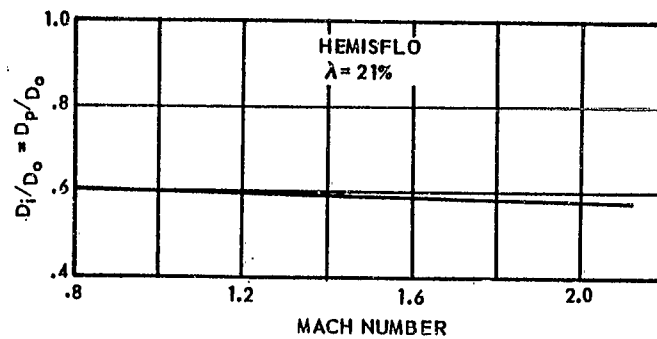
The second unaccounted for consideration is the variation of Mach critical with skirt length. Immediately aft of the skirt the chute is essentially a 0° Conical design. Consequently, there are ribbons in this region which could have a negative deflection to the local stream if the skirt were not sufficiently long. Figure 10 illustrates this possibility. If the skirt is shortened, the first 0° Conical ribbon, as shown in Figure 10, takes a position relatively closer to the mouth of the chute and any closing effect due to its possible negative deflection becomes of increasing importance. Conversely, lengthening the skirt, decreases any closing effect of the first 0° Conical ribbon.

A preliminary estimate of the effect the first 0° ribbon has on the 15% skirted chute is shown in Figure 13. This estimate is based on test observations of D_1 fluctuations.

10% Skirted Hemisflo

The final design to be considered is a Hemisflo chute with a skirt similar to that of the Equiflo. Design details of the Hemisflo are given in the appendix. A stability analysis of this chute can be made using essentially the same method applied to the skirted Equiflo design; however, the results will not be influenced by excess ribbons in the skirt or by deflected ribbons immediately aft of the skirt.

Again values of D_1/D_0 as a function of Mach number are available from F-104 drop tests, and typical data are shown in Figure 14. All other assumptions made in calculating the stability region of the skirted Equiflo design are applicable to the Hemisflo including that of no flow through the skirt slots. The Hemisflo calculations are tabulated in Table 3, and the resulting inflation stability curve shown in Figure 15.

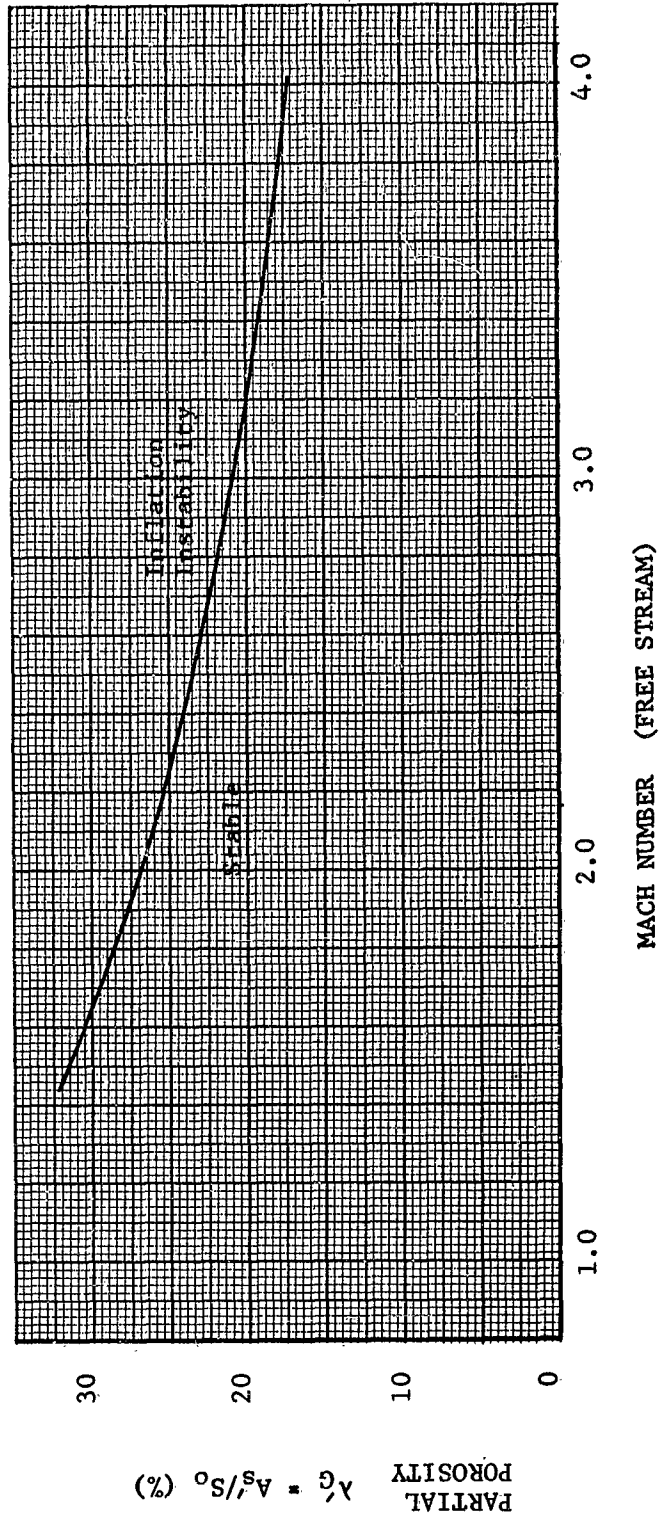


HEMISFLO MEASURED INLET AREA

Figure 14

10% SKIRTED HEMISFLO CHUTE
BEHIND BOMB

Figure 15



| M_∞ | M_1 | M_2 | $(S_1/A_{S'})_{CR}$ |
|------------|-------|--------|---------------------|
| 1.5 | 1.43 | 0.7274 | 1.0759 |
| 2.0 | 1.91 | 0.5937 | 1.196 |
| 2.5 | 2.38 | 0.5253 | 1.295 |
| 3.0 | 2.86 | 0.4840 | 1.372 |
| 3.5 | 3.34 | 0.4578 | 1.430 |
| 4.0 | 3.815 | 0.4403 | 1.474 |
| 4.5 | 4.29 | 0.4279 | 1.507 |

| D_1/D_0 | S_1/S_0 | $(A_{S'}/S_0)_{CR}$ |
|-----------|-----------|---------------------|
| 0.583 | 0.340 | 0.316 |
| 0.5675 | 0.322 | 0.2695 |
| 0.5519 | 0.3045 | 0.235 |
| 0.5363 | 0.288 | 0.21 |
| 0.521 | 0.272 | 0.19 |
| 0.5050 | 0.255 | 0.173 |
| 0.4893 | 0.240 | 0.159 |

$$\frac{A_S}{A_{S'}} = 1.288$$

$$M_1 = 0.954 M_\infty \text{ (Bomb Configuration)}$$

$$(A_{S'}/S_0)_{CR} = \frac{S_1/S_0}{(S_1/A_{S'})_{CR}}$$

Table 3. 10% SKIRTED HEMISFLO CHUTE

DISCUSSION OF RESULTS

The results of this study indicate that there is a profound effect of chute geometry on the useful operating range of flexible parachutes. The basic reason for this effect is the variation of inlet diameter with Mach number which was observed during the bomb tests. The various designs have different ratios D_1/D_0 both in level and in slope as a function of Mach number.

A comparison of the three designs is shown in Figure 16. The Equiflo curve is taken from the dashed curve of Figure 13. Every effort has been made to show a conservative region of stable operation for each chute design. Therefore, it is believed that these boundaries represent an upper porosity limit below which inflation instability is not probable.

The Hemisflo demonstrates the largest range of stable operation. This conclusion has been reached by testing; in fact, unpublished data from tests of 21.2% porous Hemisflo chute indicate that this design is stable up to at least a Mach number of 2.5.

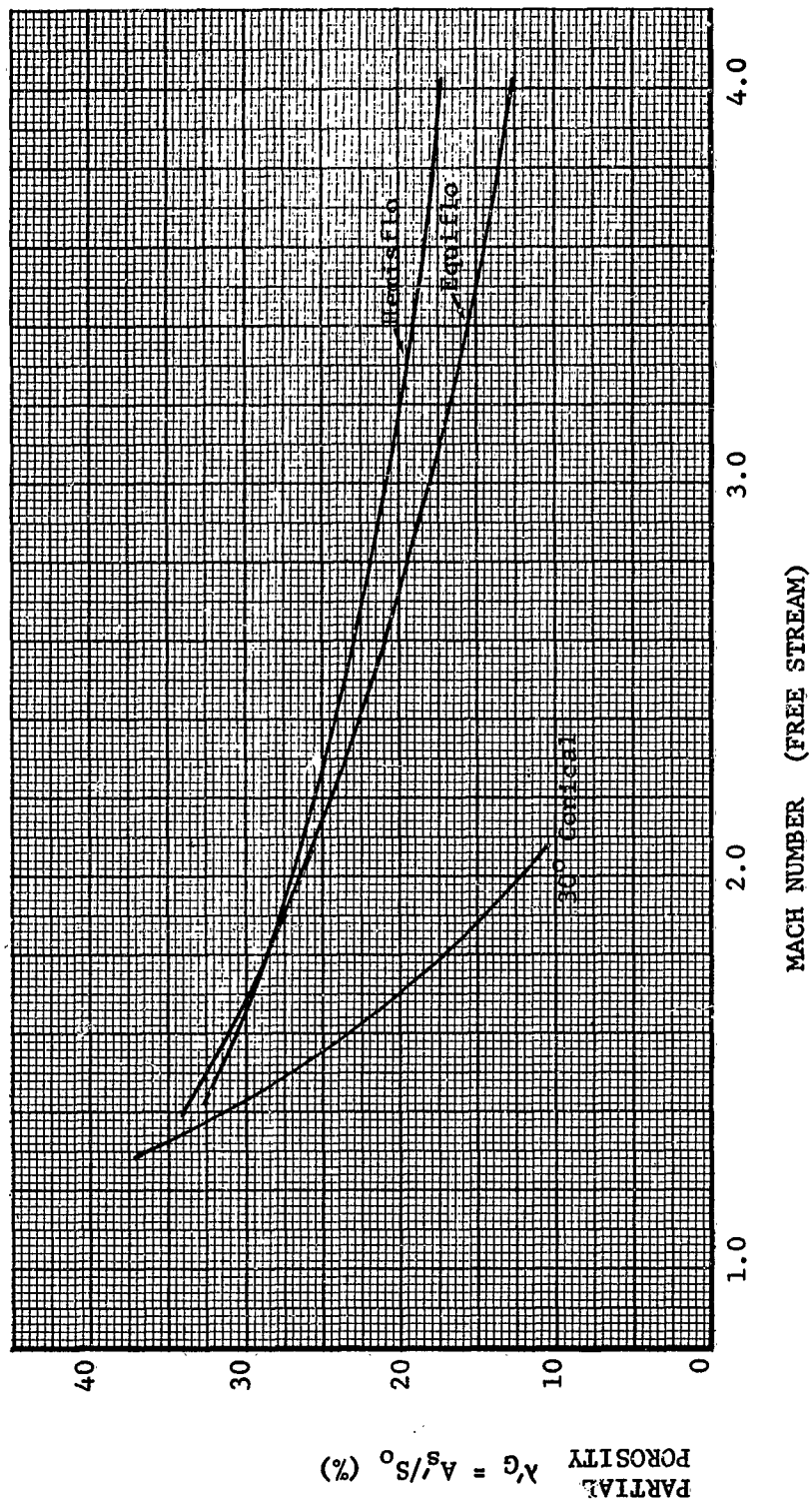
The Conical and Equiflo designs are inferior to the Hemisflo primarily because of the presence of excess ribbons in these designs. A secondary effect is the variation of D_1/D_0 with Mach number. However, it appears that the amount of excess ribbon in addition to the deflection of the ribbons near the chute mouth may be factors contributing to a rapidly decreasing inlet area with increasing Mach number.

Since the curves of Figure 16 apply only to the performance of parachutes behind a particular payload configuration (in this case F-104 bomb), the results have been generalized in Figure 17 as functions of the local Mach number (M_1). These curves may be used to find the local Mach number (M_1) above which one of the three parachute designs considered herein becomes unstable. The free stream Mach number corresponding to the local Mach (M_1) number would depend entirely on the payload or vehicle being stabilized.

Any parachute design which has a so-called skirt would have to be analyzed independently from these results unless it happened to be one of the two skirted designs studied here. This fact is evident because S_0 and S_1 will vary with skirt length. For example, if the skirt lengthens, S_0 increases and S_1 probably decreases while As' remains unchanged. Thus, the ratio S_1/S_0 would decrease and $(As'/S_0)CR$ would be reduced proportionally. For small

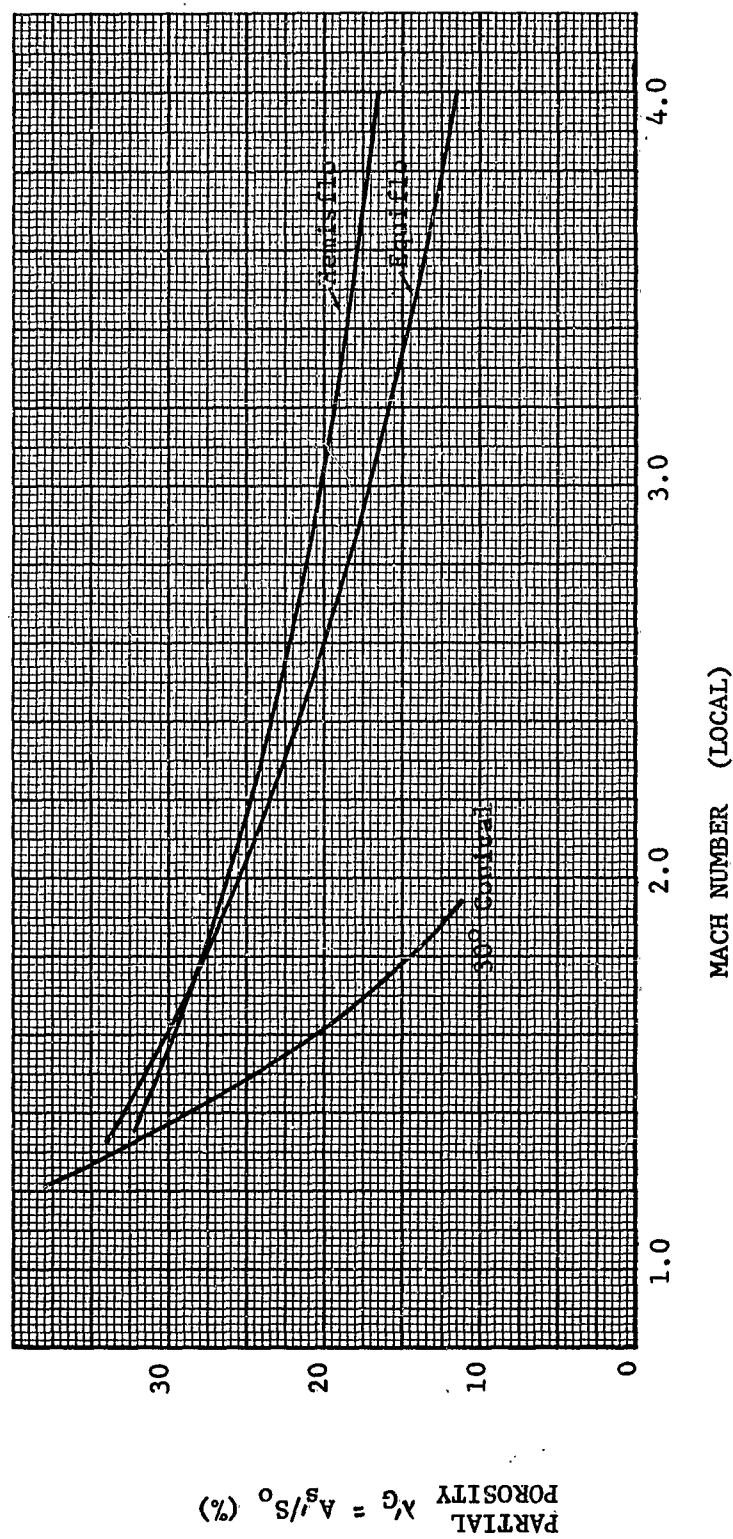
COMPARISON OF THREE STAB CHUTE DESIGNS
BEHIND BOMB

Figure 16



COMPARISON OF THREE STAB CHUTE DESIGNS
PARTIAL POROSITY VERSUS LOCAL MACH NUMBER

Figure 17



changes in skirt length it may be possible to simply correct the curves for changes in S_0 thus assuming no change in inlet area.

The final curves are left in terms of partial porosity ($A_{S'}/S_0$) due to the fact that the relation between porosity (A_S/S_0) and partial porosity ($A_{S'}/S_0$) is dependent upon the porosity distribution of the design. Since only the slot area in the main chute ($A_{S'}$) is used in the calculation of critical Mach number, leaving the final curves in terms of ($A_{S'}/S_0$) allows them to be more useful in application to other parachutes.

The curve for the 30° Conical parachute is more useful than the others since it is not complicated by a skirt; therefore, its partial porosity is equivalent to the total porosity ($A_S = A_{S'}$) and it may be used to estimate the stability of 30° Conical designs which have good porosity distributions and reasonable suspension line lengths. The 30° Conical test article analyzed here had 1-d suspension lines (see Appendix), and the degree to which the suspension line length affects the inlet diameter ratio D_1/D_0 is not yet known.

All the results of this study are based on the analysis of parachutes which have good porosity distributions. It has been found that excessive porosity in either the crown or near the leading edge can cause poor performance. The curves in Figures 16 and 17 are not valid for parachutes with poor porosity distributions.

RECOMMENDATIONS

An experimental study of the Equiflo and Hemisflo designs needs to be performed to locate the deployment conditions at which significant inflation instability will occur. Dependence of the stable region on the following variables could be determined:

- (1) variations with Mach number,
- (2) variation with porosity.
- (3) variation with skirt length,
- (4) variation with dynamic pressure.

A theoretical and experimental study of the lower porosity limit for stable chute operation is desirable for the purpose of determining the slope of this limit with Mach number.

Further work may become desirable in order to define the region of stable operation in which a parachute remains semi-inflated experiencing low drag. It may be found that this

region overlaps the stable region of the Hemisflo design considered herein rendering the Hemisflo chute usable under any conditions.

REFERENCES

1. Heinrich, Helmut G., Analytical and Experimental Consideration of the Velocity Distribution in the Wake of a Body of Revolution, WADD Technical Report 60-257, December 1959.
2. Maynard, Julian D., Aerodynamic Characteristics of Parachutes at Mach Numbers from 1.3 to 3, NASA TN-D-752, May 1961.

BIBLIOGRAPHY

- Engstrom, B. A. and Meyer, R. A., Performance of Trailing Aerodynamic Decelerators at High Dynamic Pressures, Part III Wind Tunnel Testing of Rigid and Flexible Parachute Models, WADC TR 58-284, 1959.
- Meyer, R. A., Wind Tunnel Investigation of Conventional Types of Parachute Canopies in Supersonic Flow, WADC Technical Report 58-532, December 1958.
- Roberts, B. G., "An Experimental Study of the Drag of Rigid Models Representing Two Parachute Designs at $M = 1.40$ and 2.10 ," Ministry of Aviation C.P. No. 565, London, 1961.
- Etherton, B. D., Burns, F. T., and Norman, L. C., "B-58 Escape Capsule Stabilization Parachute System Development," GD/FW Report FZA-4-408, 19 February 1962.

APPENDIX

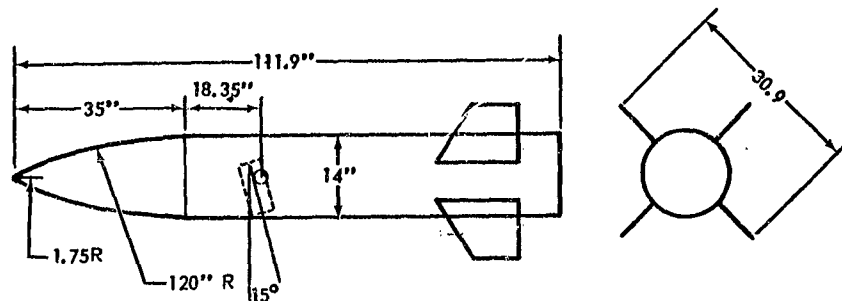
F-104 Bomb Drop Program

The F-104 bomb drop program from which the data for this study were obtained consisted of 14 full-scale stabilization parachute tests behind a bomb-shaped test vehicle launched from an F-104 aircraft. The test program was conducted by Radioplane in conjunction with NASA under a sub-contract from Stanley Aviation Corporation. The tests began in April 1961 and were completed in October 1961. Out of the 14 tests, the data from the 3rd, 6th and 8th tests were chosen to represent the 30° Conical, the 10% skirted Hemisflo, and the 15% skirted Equiflo designs respectively. A photograph of the launch airplane is shown in Figure A2,

and details of the bomb are given in Figure A1.

Stabilization Parachute Designs

The three basic parachute designs considered in this report are shown schematically in Figure A3. From the figure, it can be seen that the skirt length is defined in terms of the total length (d) taken over the main portion of the chute fabric. Photographs of one-third scale models which are similar to the full-scale parachutes used in the bomb-drop tests are shown in Figures A4 through A6. The gore patterns of these scale models are shown in Figures A7 through A9.



F-104 BOMB CONFIGURATION

Figure A1

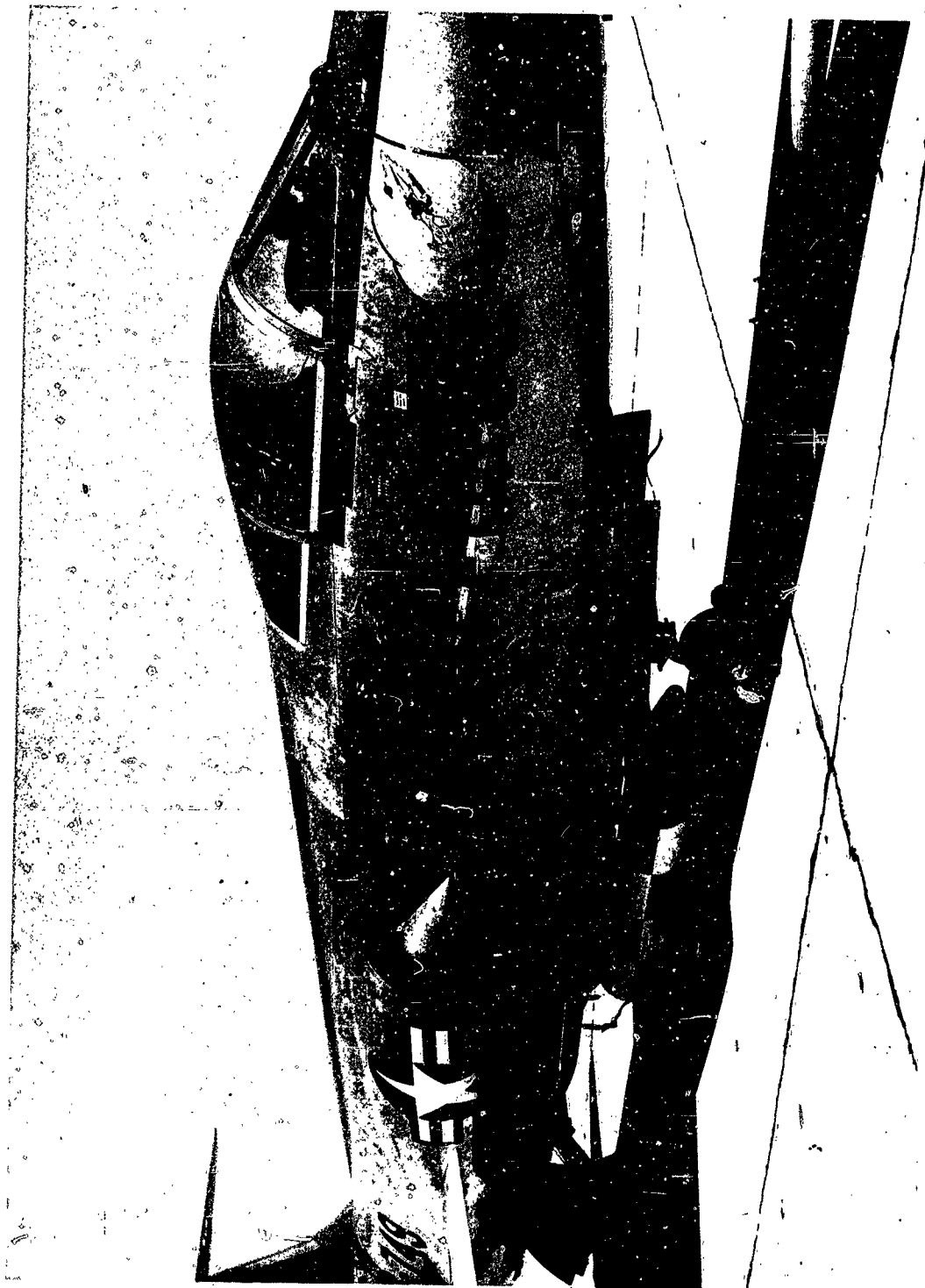
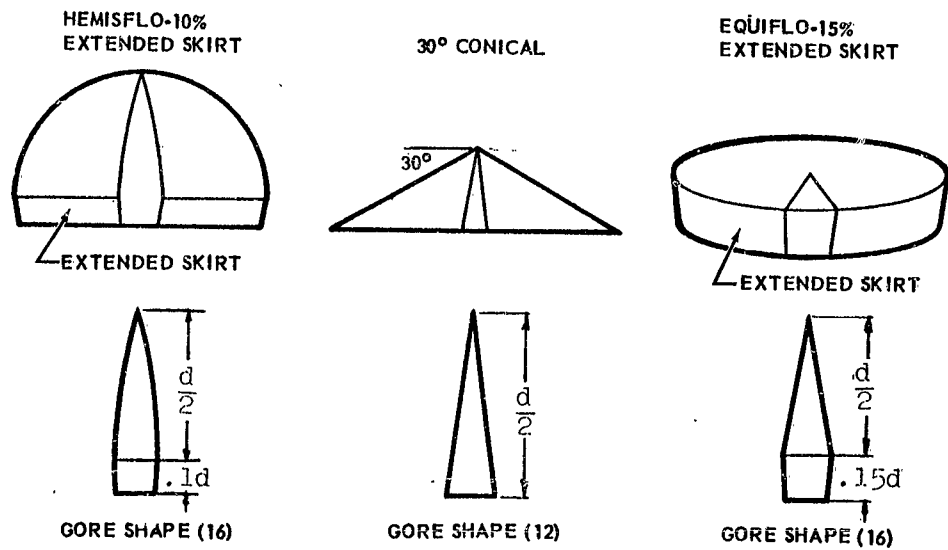
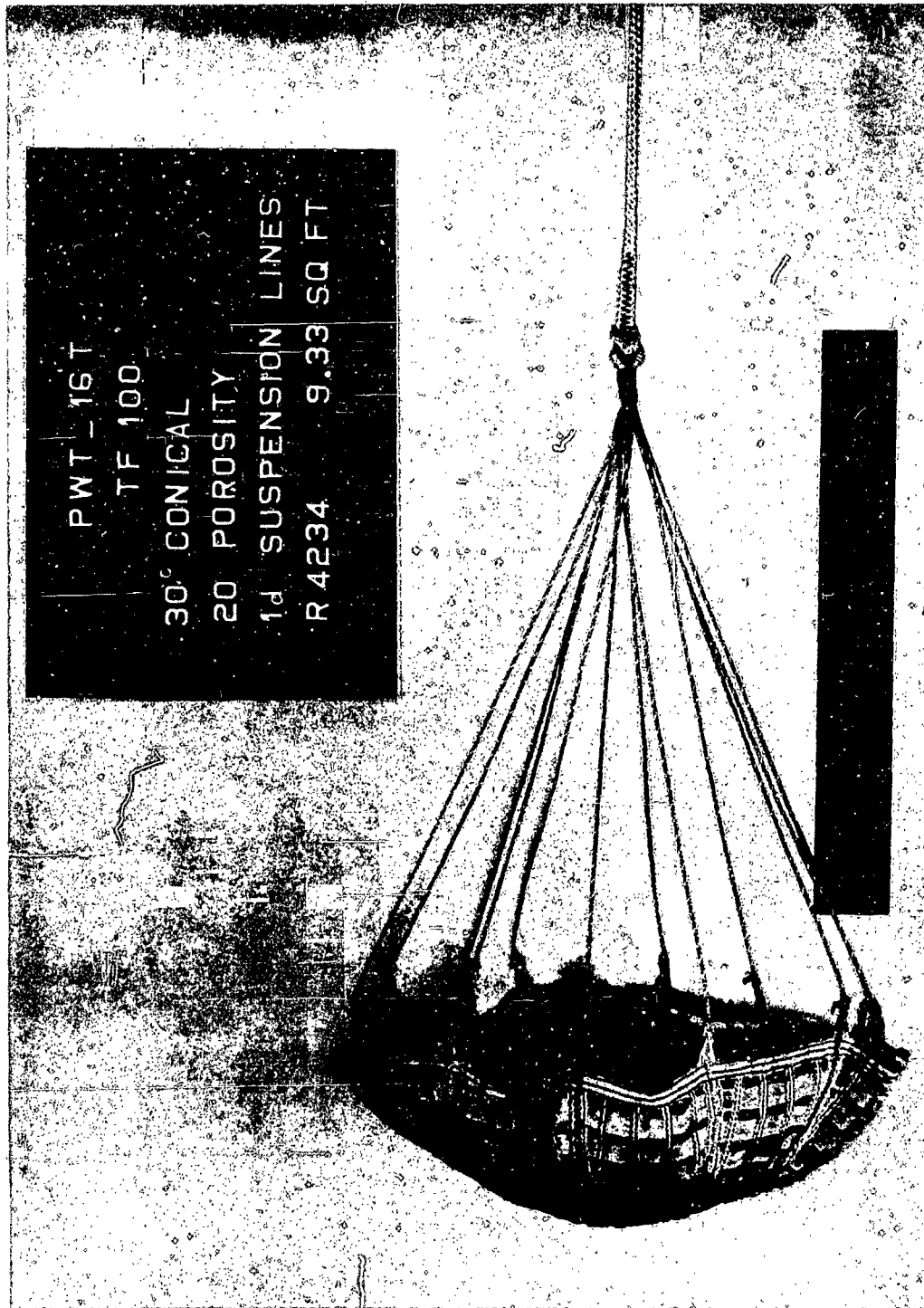


Figure A2. Test Bomb Loaded on F-104



BASIC STABILIZATION PARACHUTES
CONSTRUCTED SHAPES

Figure A3



PWT_16T

TF 100

30° CONICAL

20 POROSITY

1d SUSPENSION LINES

R 4234 9.33 SQ FT

Figure A4. One-Third Scale Test Specimen

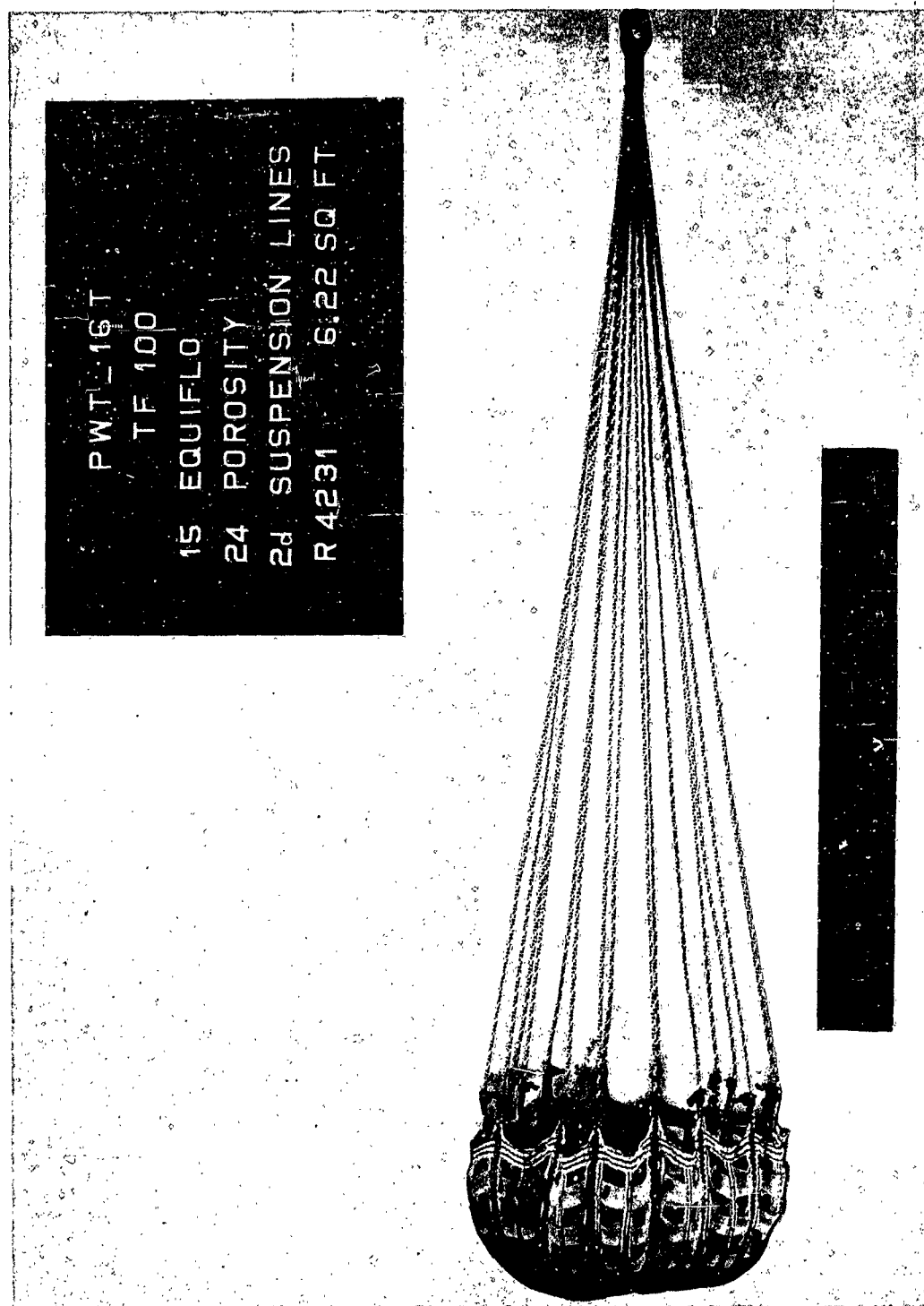


Figure A5. One-Third Scale Test Specimen

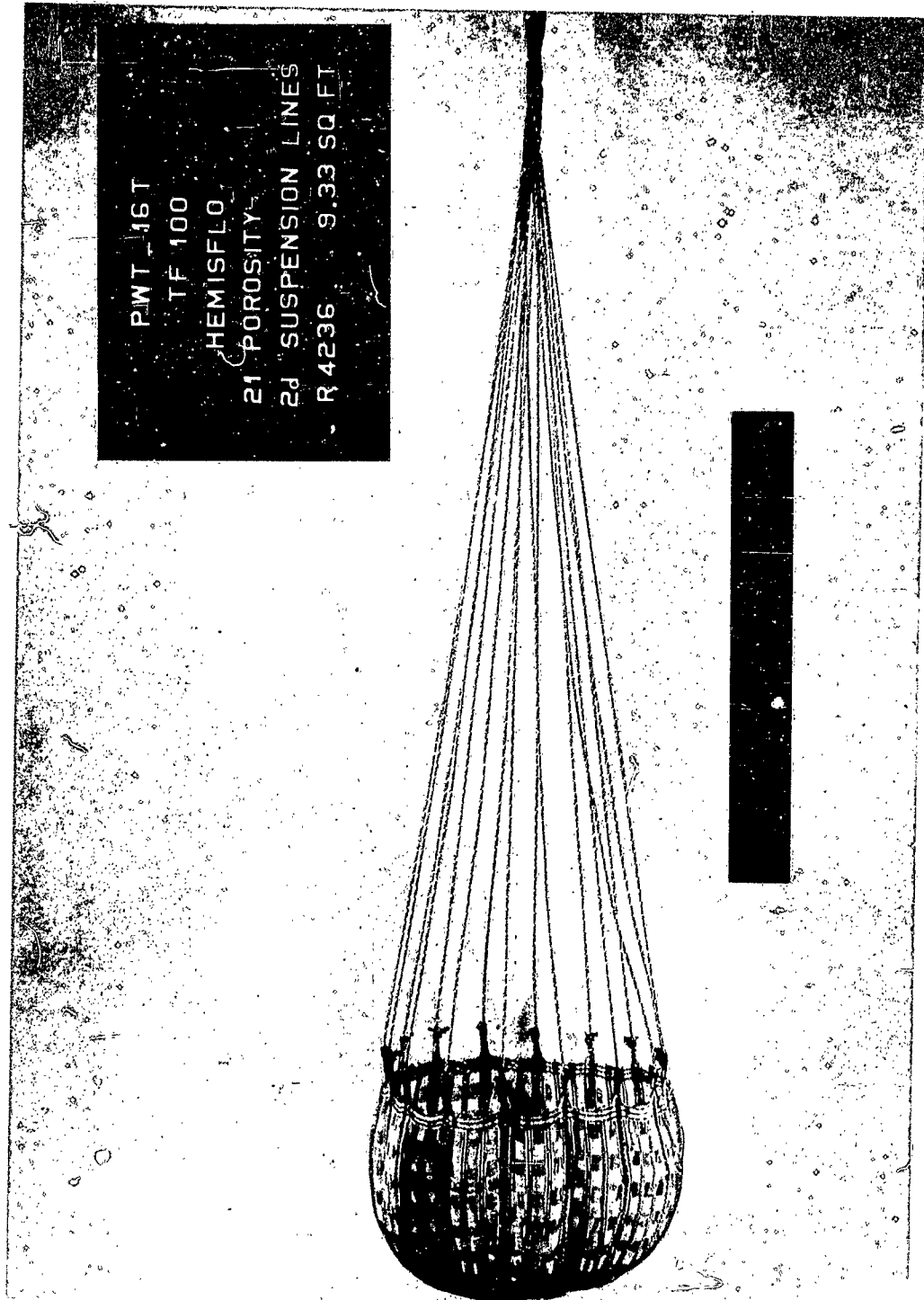


Figure A6. One-Third Scale Test Specimen

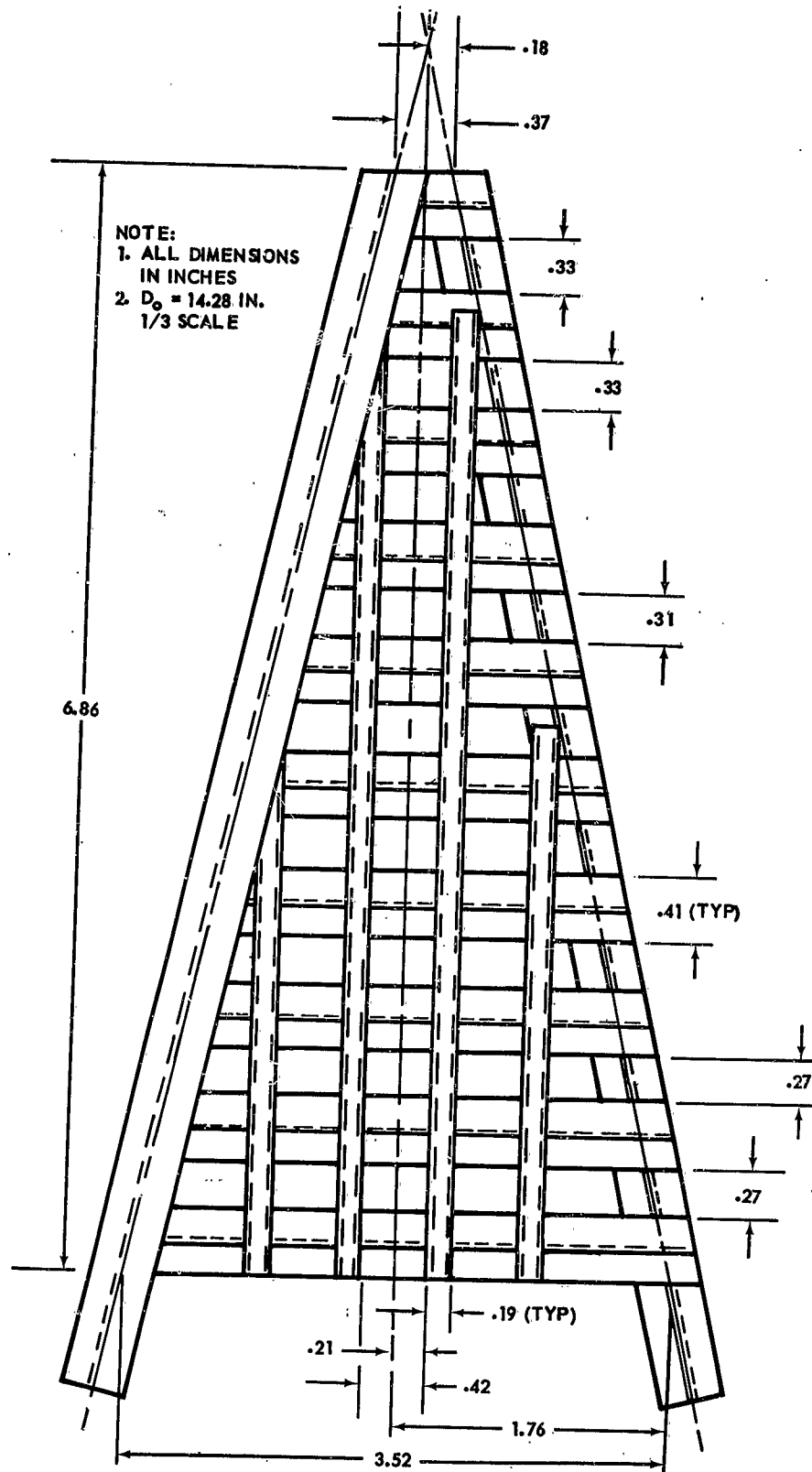


Figure A7. Typical Gore - One-Third Scale, 30 Degree Conical,
 24 Percent Porosity

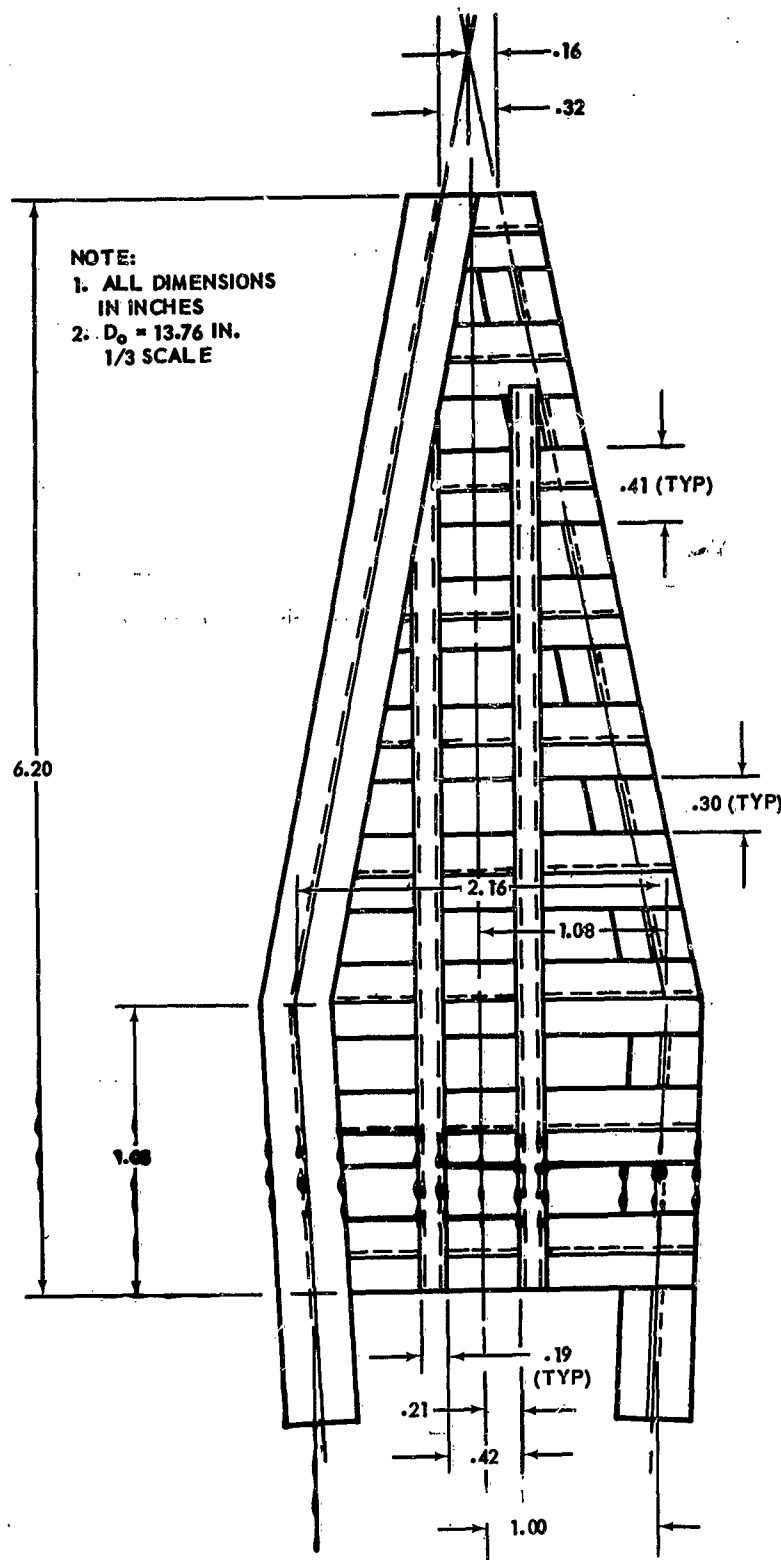


Figure A8. Typical Gore - One-Third Scale, 15 Percent Extended Skirt
 Equiflo, 24 Percent Porosity

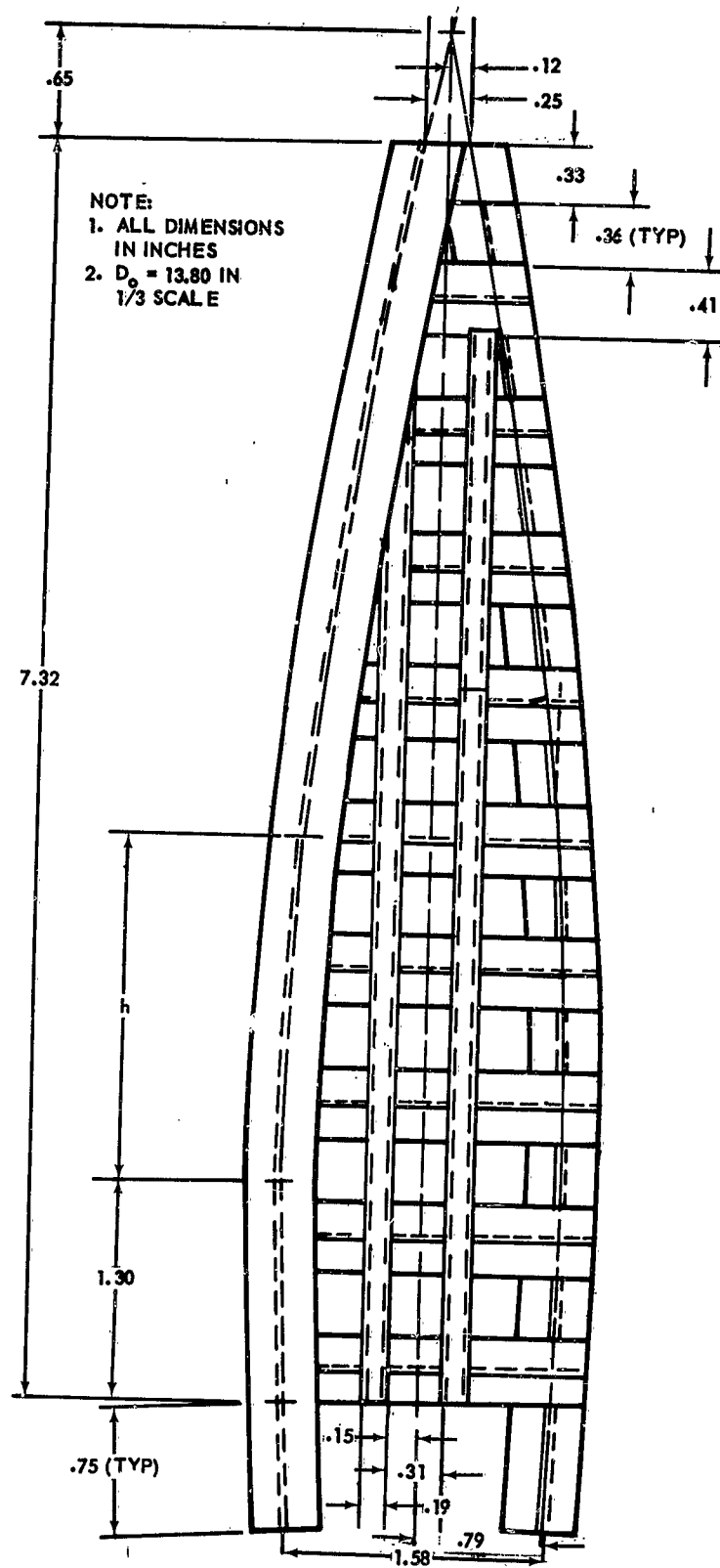


Figure A9. Typical Gore - One-Third Scale, 10 Percent Extended Skirt
 Hemisflo, 21 Percent Porosity

FLEXIBLE WING RESEARCH AND DEVELOPMENT

By F. M. Rogallo

NASA Langley Research Center
Langley Station, Hampton, Va.

ABSTRACT

This paper reviews flexible-wing research and development projects recently completed or now in progress by the National Aeronautics and Space Administration or by the industry under contract to NASA or the Department of Defense.

FLEXIBLE WING RESEARCH AND DEVELOPMENT

INTRODUCTION

When I was invited to present a paper on the subject "Rogallo Wing" I assumed that your program committee had in mind what has been called the "Paraglider," "Parawing," "Flexikite," "Flex-wing," "Flight-Sail," etc., or more broadly, the flexible-wing concept. Because nearly all of our publicized flexible-wing research and development has pertained to only one of the many possible configurations, the impression may sometimes be given that we are not considering other configurations or that they do not fall within the flexible-wing concept. To emphasize that this is not so, figure 1 of reference 1 is repeated herein, and attention is called to the two-lobe, single curvature configuration on which so much work has now been done simply because that configuration was arbitrarily chosen for a beginning. In preparing this paper I am assuming that you have seen my St. Louis paper (ref. 1) and the film shown there (Langley film L-688) and the earlier film shown in my 1961 IAS Presentation (Langley film L-593). The present paper will cover new projects or additional work on those of the previous papers.

THE 50-FOOT INFLATED-FRAME PARAGLIDER

Work has continued on the 50-foot inflated-frame paraglider discussed in reference 1. (See fig. 2.) Flights have been made with the full-size boiler-plate Mercury capsule at total weights of 2,000, 2,500, and 3,000 pounds using a particular rigging that provided nearly straight flight and a rather low angle of attack. Radio-control equipment is under construction that should allow investigations of the stability, control, and performance of this wing over a wide lift range in both straight and turning glides and during the landing maneuver. In addition to being the largest flexible wing yet built and having the heaviest payload yet carried, this wing has a very limber frame that will allow it to increase its span during the flare, which may improve its landing characteristics relative to gliders with a more rigid frame.

THE NASA FLIGHT RESEARCH CENTER MANNED PARAGLIDER

The NASA Flight Research Center at Edwards, California has built and flown two additional versions of the manned paraglider previously discussed in reference 1. The I-A version shown in figure 3 has been flown numerous times by four different pilots of varying backgrounds and experience, and the general consensus is that the craft maneuvers and

handles quite well at a w/s of 4.25 and a L/D maximum of 3.8, according to Victor W. Horton of the Flight Research Center.

When I was at Edwards in August of this year I witnessed several flights of the I-B version which had 100 square feet of cloth area and a flying weight of 660 pounds for a w/s of 6.6 and an estimated L/D maximum of about 3, values of these parameters very near those estimated for the Gemini paraglider landing system to be discussed later. All the landings I was privileged to witness were very good.

GEMINI PARAGLIDER

The Gemini paraglider landing system is shown in figure 4. The deployment sequence is shown at the bottom of the figure. Models of this configuration have been investigated in wind tunnels at the Langley and Ames Research Centers, and flights of radio-controlled models are being made at NASA Flight Research Center. I saw one of the early flights of a 1/2-scale model in August of this year. As mentioned, many manned flights have already been made at Edwards with a paraglider having approximately the wing loading and lift-to-drag ratio expected for the full-scale version of the Gemini-paraglider landing system. Development of this system is being done by North American, McDonnell, and Goodyear under contract from the NASA Manned Spaceflight Center.

THE INFLATED MICROMETEOROID PARAGLIDER

A full-scale model of the inflated micrometeoroid paraglider is shown in figure 5. This model was investigated in the Langley full-scale tunnel, mounted as shown in figure 5, and was investigated in gliding flight after release from a helicopter. In these latter studies it was released from a cable attached successively to the nose, tail, wing tip, and the bottom of the instrument pack. In all drops it attained its normal steady glide attitude after a very few oscillations. Inflated micrometeoroid paragliders, which are being built by Space-General under contract to NASA will be lofted to an altitude of 700,000 feet by means of an Aerobee rocket at Whitesands. Micrometeoroid impacts on the 200 square feet of instrumented wing surface will be telemetered to the ground receiver. The micrometeoroids and their effect on the wing will be studied after recovery of the paraglider subsequent to its landing.

RYAN FLEX-WING AND FLEEF

Reports are now available covering wind-tunnel and flight investigations of model and full-scale versions of the Ryan flex-wing shown in figure 6. (See refs. 2 and 3.) Although flown successfully for 25 hours (ref. 3.), the full-scale machine did not have entirely satisfactory

flying and handling qualities, and a NASA flight research program was initiated that was expected to remedy these deficiencies. At the beginning of this program, while a check flight was being made of the machine in its previously flown condition, the machine was wrecked. The Ryan Aircraft Company is at present under Army contract to build several more machines of this general configuration, called the "Fleep," a contraction of the words "flying jeep."

MARINE RECONNAISSANCE DRONE

The Ryan Aircraft Company built for the Marine Corps several small photo reconnaissance drones like that shown in figure 7. Photographs of particular objects on the ground were taken from these radio-controlled drones.

INDIVIDUAL DROP AND PRECISION CARGO DROP

An artist's conception is shown in figure 8 of an individual drop paraglider that I saw under development at Yuma, Arizona last August. The payload at that time was a dummy, but after completion of developmental work using radio-controlled dummies it is anticipated that these paragliders will be investigated in flight by men who will control them to the desired landing spot by direct manipulation of the harness lines. Prior to deployment, the wing is carried in a backpack like a parachute. This work and a parallel development of a radio-controlled precision cargo-drop paraglider using essentially the same wing are being done by Ryan under contract to the Army.

TOW GLIDERS

Although the towing of manned paragliders has been demonstrated by NASA Flight Research Center as previously discussed, by Flight Dynamics, Inc., of Raleigh, North Carolina, and by others, the towing of uncontrolled paragliders has been limited as yet to rather small models. The Ryan Company is now under contract to the Army to design, build, and fly several unmanned cargo-tow gliders to carry 1,000 pounds of payload when towed behind a helicopter as shown in figure 9. These gliders can be kept on the tow line during the landing, or they can be cut loose in flight and landed under radio control from an aircraft or a ground station. After this technique is developed it may have very wide applications for both military and civil uses whenever surface transportation is impractical.

PARAWING L/D VERSUS C_L

Results of an exploratory study of some effects of parawing geometry on performance are shown in figure 10. The lift-to-drag ratio L/D , which is an indication of the glide ratio or of the thrust required, is plotted as a function of the lift coefficient C_L , which is an indication of the lifting capability of the wing. The four wings investigated had cloth surfaces attached to rigid leading edges and keels. The two wings with lowest $(L/D)_{max}$ had straight leading edges and conical surfaces as shown in the lower part of figure 11 and the two wings with highest $(L/D)_{max}$ had curved leading edges and cylindrical surfaces as shown in the upper part of figure 11. In addition to the improvement in maximum L/D , the cylindrical wings exhibited flyable characteristics to much lower values of C_L than the conical wings, indicating a much greater speed range potential. The conical wings were superior at high values of C_L . The performance and stability parameters obtained in this exploratory investigation are being prepared for publication, and a more complete investigation is under way.

STABILITY AND CONTROL

Aerodynamically a nonporous flexible wing is identical with a rigid wing of the same shape. Much of the wealth of aerodynamic information and experience on rigid wings is therefore applicable to flexible wings, including the methods for obtaining stability and control. Proper account must be taken of the flexibility of the wing surface and of the frame. In some designs in order to simplify the design problem a very rigid frame has been used, but this expedient increases the structural weight and the difficulty of packaging or stowing the wing. Other advantages of a flexible frame are a reduction of fragility and the possibility of obtaining control by flexing the wing without need for hinges. A wide variety of shape and location of stabilizing and control surfaces and other devices may be used with flexible wings as is done with rigid wings if desired, but many applications, as for example, the NASA Flight Research Center manned glider have proved that a single piece of cloth can be made to provide lift, stability, and control.

PACKAGING AND DEPLOYMENT

Several methods of packaging and deploying paragliders with rigid-tube frames have been developed and demonstrated by the NASA. A long slender package was attained by merely hinging the tubes at the apex for an early investigation involving gliders rocket launched from Wallops Island. In the Saturn booster recovery investigation the length of the package was reduced to half by adding another set of hinges in the middle of each tube. And in the investigation of a space-capsule recovery system an even shorter package was effected by use of telescoping tubes of many segments.

The packagability of inflated-frame paragliders is obvious. Several methods of deploying such gliders are available. Some have been demonstrated and others are under investigation by NASA and others.

The packaging and deployment capability of spring-edge paragliders is utilized by the recently marketed "Friendship-7 Paraglider Toy," and this system should find more serious application.

MATERIALS

Although nylon, dacron, Mylar, and other fabrics and plastics are adequate for construction of flexible wings for moderate temperature applications, a substantial effort is needed to develop better materials designed especially for this use to have the greatest possible strength-to-weight ratios and dependability under all operating conditions to which they might be subjected, even after years of use and exposure to the elements.

In some applications, for example, the recovery of space capsules and boosters, paraglider membrane material capable of operating at high temperature is needed. Even with presently available materials a paraglider suitable for coming all the way from orbit to earth is possible, but may not yet be practical. An improvement in materials could make it practical.

CONCLUDING REMARKS

In this paper I have done no more than mention the parawing research and development projects that are actually under way or recently completed by the NASA or by the industry under contract to NASA and the Department of Defense. Time and/or security restrictions do not allow mention of the many other applications that have come to our attention, some of which are now under serious consideration.

After more than 15 years of study and experiment with flexible wings I have come to the conclusion that many things that can be done with rigid wings or parachutes can be done better with flexible wings. Flexible wings are a new, important, and fascinating field of aerospace research. It's big enough for all of us. Come on in.

REFERENCES

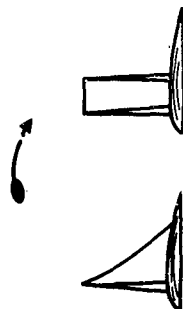
1. Rogallo, Francis M.: Paraglider Recovery Systems. For Presentation at IAS Meeting on Man's Progress in the Conquest of Space. St. Louis, Mo., April 30, May 1-2, 1962.
2. Johnson, Joseph L., Jr.: Low-Speed Wind-Tunnel Investigation to Determine the Flight Characteristics of a Model of a Parawing Utility Vehicle. NASA TN D-1255, 1962.
3. Flexible-Wing Manned Test Vehicle. Prepared by Ryan Aeronautical Company, San Diego, Calif. U.S. Army, Transportation Research Command, Fort Eustis, Va., TCREC Tech. Rep. 62-25, August 1962.

LIST OF ILLUSTRATIONS

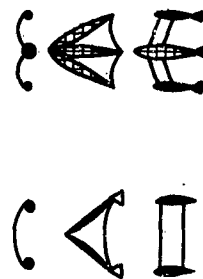
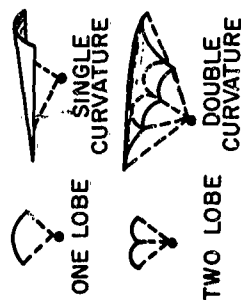
| Figure | Page |
|--|------|
| 1. Flexible-wing concept as presented to Langley Committee on General Aerodynamics, December 19, 1958. | 203 |
| 2. Fifty-foot inflated-frame paraglider with boiler-plate Mercury Capsule lifted by a helicopter. | 204 |
| 3. Paraglider research vehicle I-A, built and flown at NASA Flight Research Center, Edwards, California. | 205 |
| 4. Artist's conception of Gemini paraglider landing system. | 206 |
| 5. Inflated micrometeoroid paraglider in Langley full-scale wind tunnel. | 207 |
| 6. Ryan flexible-wing research vehicle. | 208 |
| 7. Experimental reconnaissance drone built by Ryan for the Marine Corps. | 209 |
| 8. Artist's conception of individual drop paraglider being developed by Ryan for the Army. | 210 |
| 9. Artist's conception of cargo tow glider being developed by Ryan for the Army. | 211 |
| 10. Lift and drag characteristics of parawings with conical and cylindrical surfaces. | 212 |
| 11. Parawing models under investigation in a Langley 7- by 10-foot wind tunnel. | 213 |

WHY A MEMBRANE WING ?

1. VERY LIGHT WING WEIGHT PER UNIT AREA
MAKES POSSIBLE VERY LOW WING LOADING
2. ABILITY TO BE ROLLED UP OR FOLDED LIKE
A PARACHUTE
3. RADIATION FROM BOTH SURFACES REDUCES
AERODYNAMIC HEATING AND FLEXIBILITY
REDUCES THERMAL STRESS
4. VERY THIN WINGS REDUCE WAVE DRAG AT
HIGH SPEED

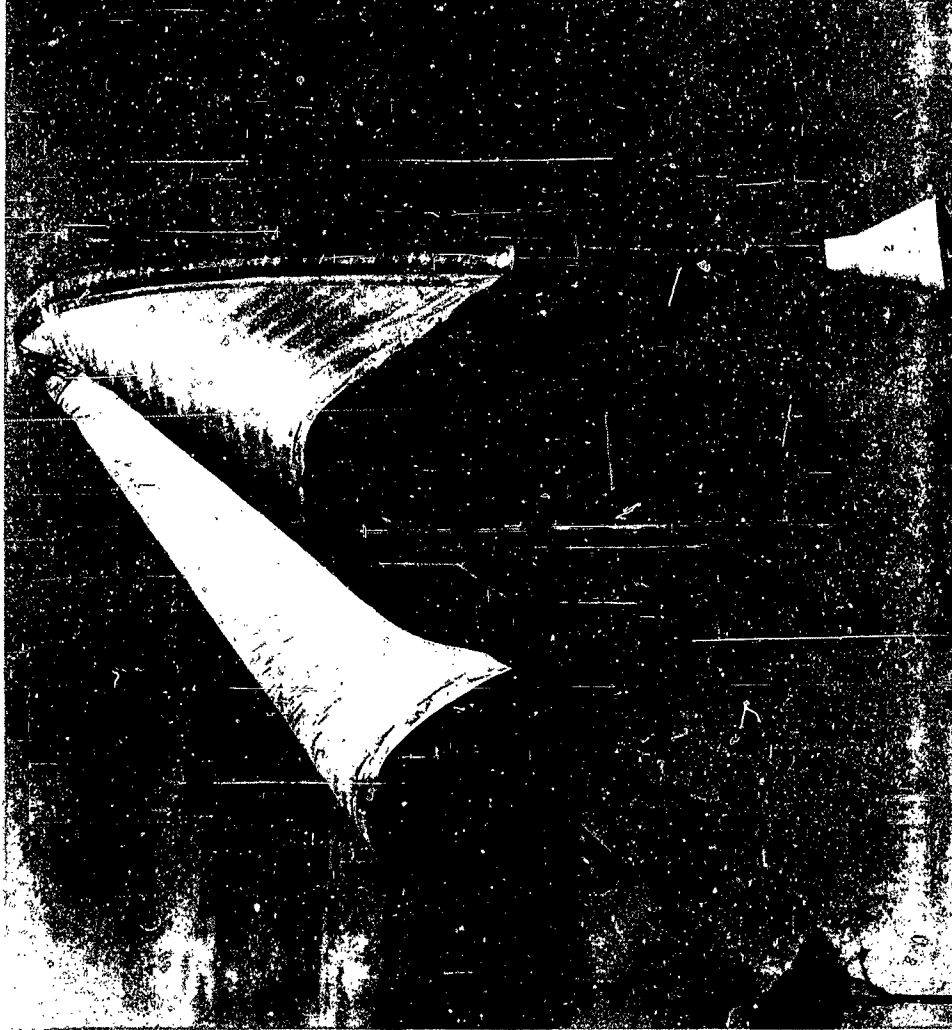


1. REENTRY
2. SPACE SHIP LANDING
3. SOLAR SAILING
4. HIGH ALTITUDE CRUISE (POSSIBLY
DISSOCIATED OXYGEN PROPULSION)
5. PERSONNEL AND/OR CARGO GLIDING
PARACHUTE AS SUBSTITUTE FOR
CONVENTIONAL PARACHUTE
6. WINGS FOR STOL (COULD BE ROADABLE)
7. LANDING AID FOR CONVENTIONAL
AIRPLANE (LIFT ADVANTAGE OVER DRAG)

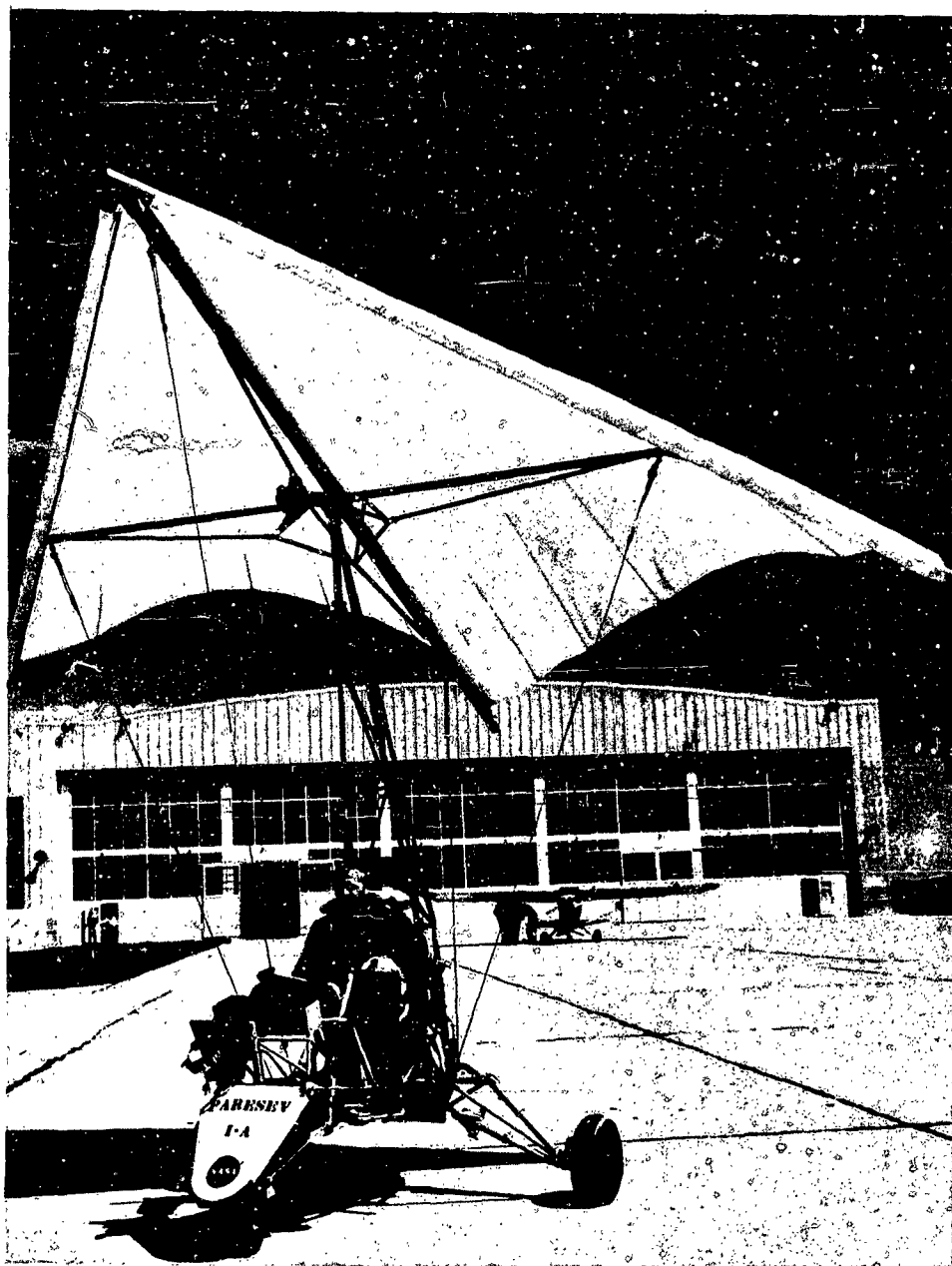


NASA

Figure 1.- Flexible-wing concept as presented to Langley Committee on General Aerodynamics, December 19, 1958.



NASA
L-62-2680
Figure 2.- Fifty-foot inflated-frame paraglider with boiler-plate Mercury Capsule being lifted
by a helicopter.



NASA

Figure 3.- Paraglider research vehicle I-A, built and flown at NASA Flight Research Center, Edwards, California.

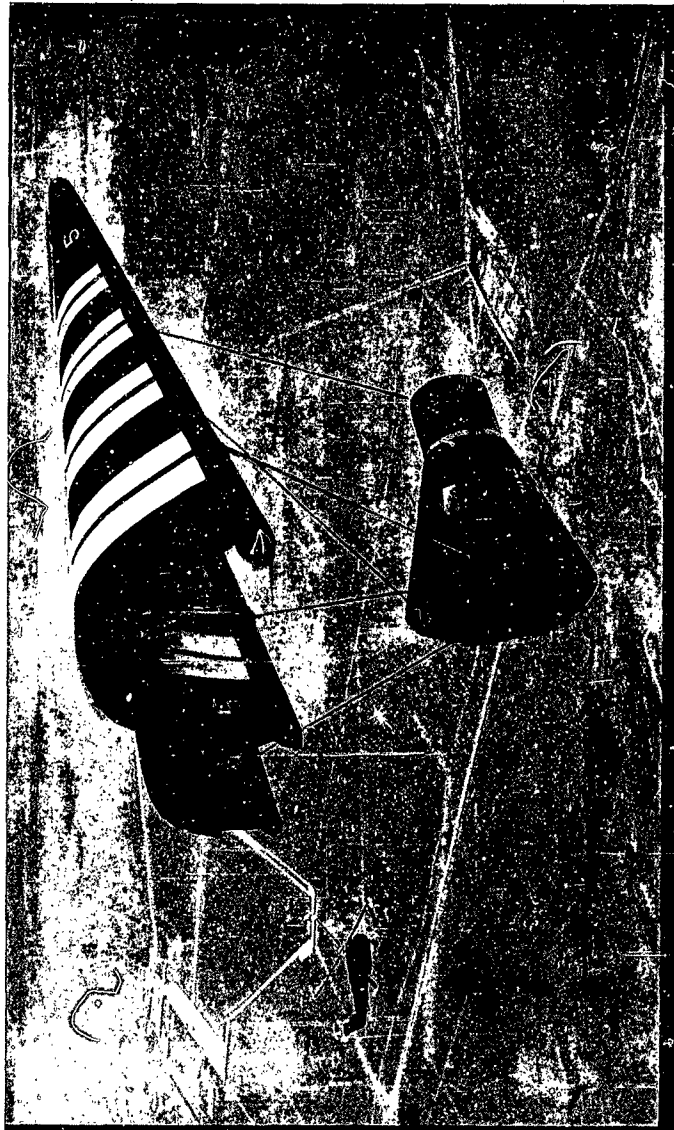


Figure 4.- Artist's conception of Gemini paraglider landing system.



NASA
L-62-5996
Figure 5.- Inflated micrometeoroid paraglider in Langley full-scale wind tunnel.

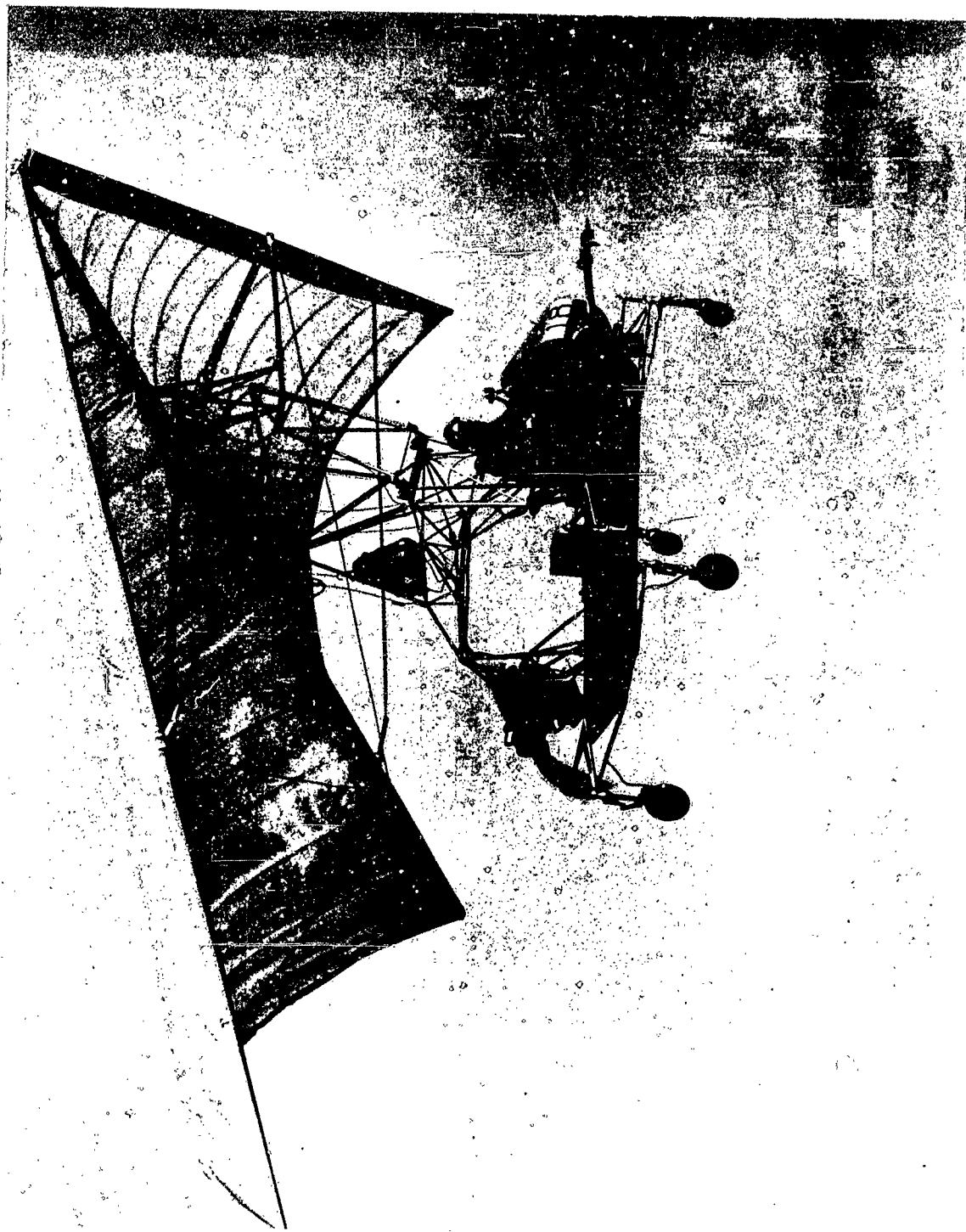


Figure 6.- Ryan flexible-wing research vehicle.

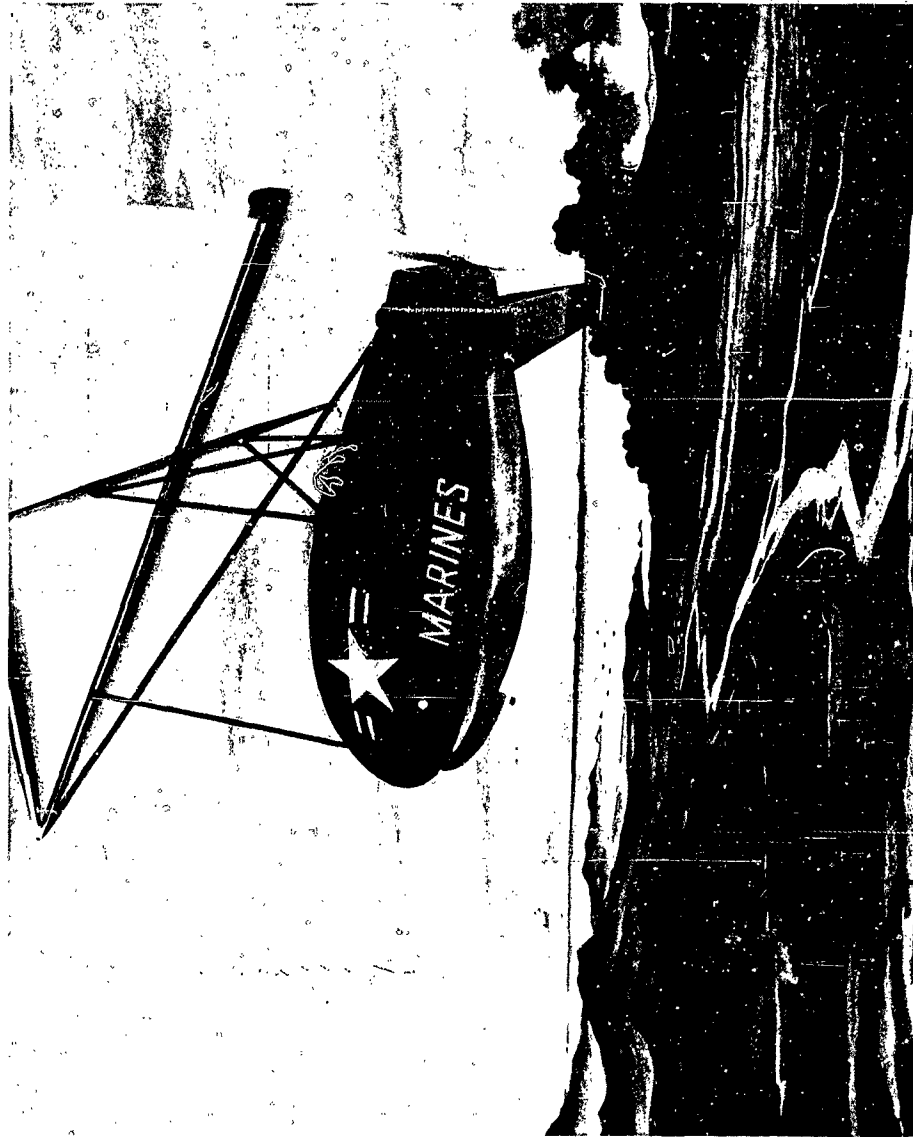


Figure 7.- Experimental reconnaissance drone built by Ryan for the Marine Corps.



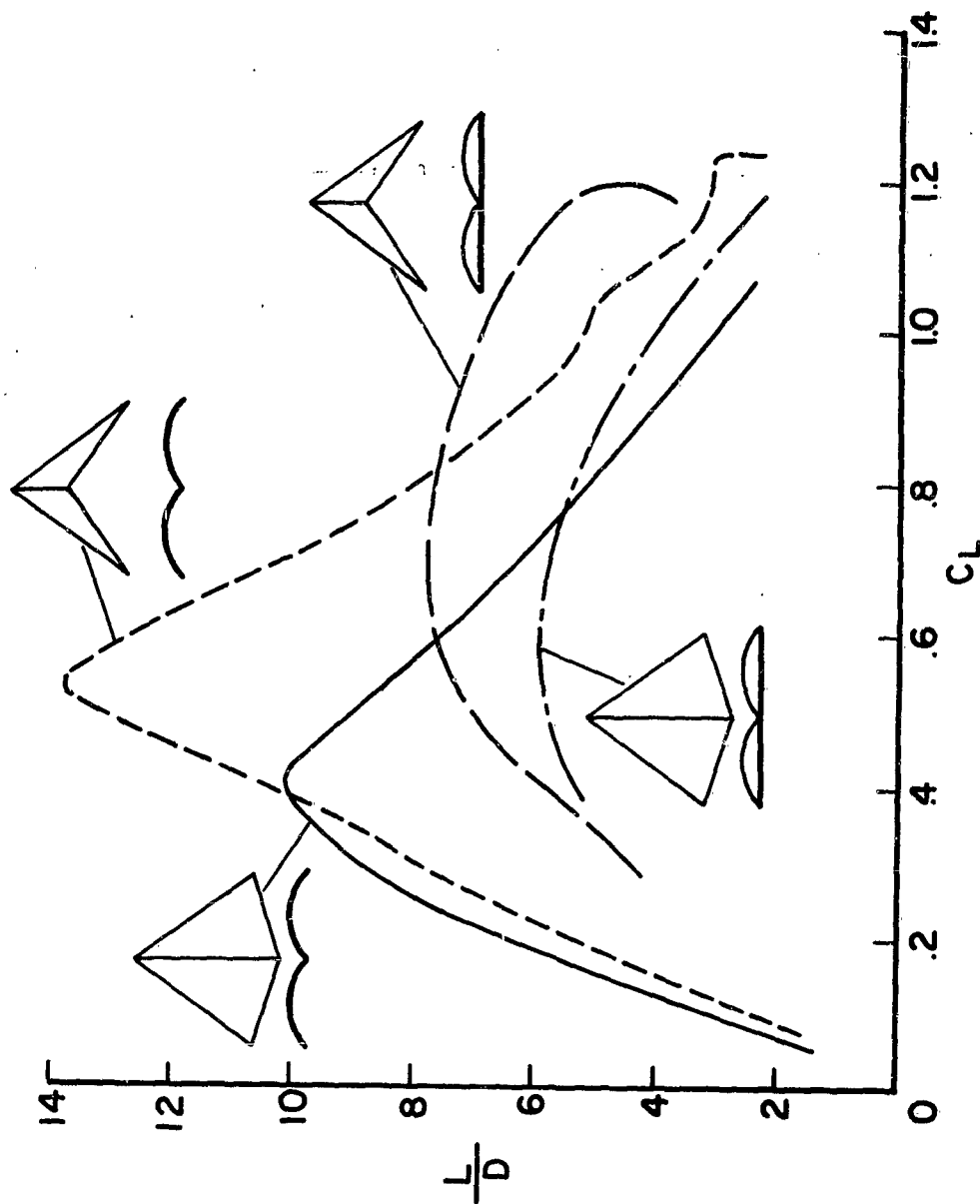
Figure 8.- Artist's conception of individual drop paraglider being developed by Ryan for the Army.



Figure 9.- Artist's conception of cargo tow glider being developed by Ryan for the Army.

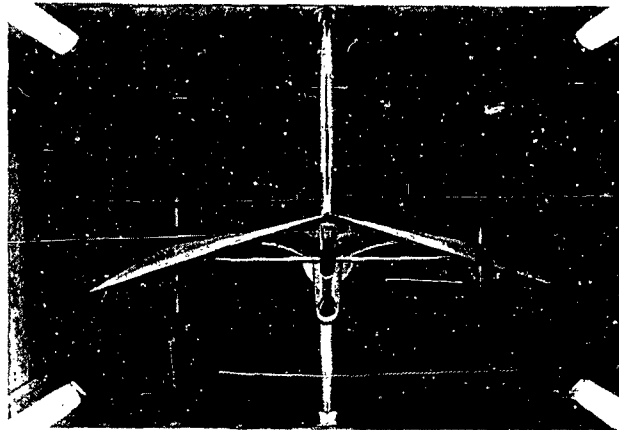
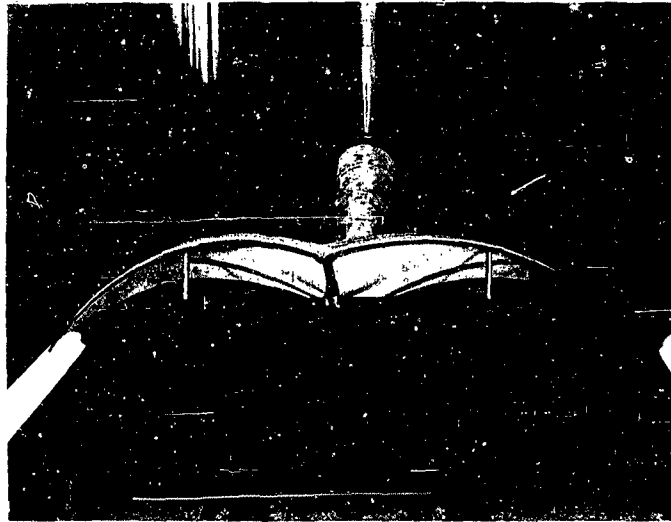


Figure 9.- Artist's conception of cargo tow glider being developed by Ryan for the Army.



NASA

Figure 10.- Lift and drag characteristics of parawings with conical and cylindrical surfaces.



NASA

Figure 11.- Parawing models under investigation in a Langley 7- by 10-foot wind tunnel.

**HIGH TEMPERATURE FIBROUS MATERIALS
FOR DECELERATORS**

**JACK H. ROSS
Fibrous Materials Branch
Nonmetallic Materials Laboratory
Directorate of Materials and Processes**

ABSTRACT

As the role of decelerators expands into supersonic and hypersonic regimes and ultimately into the recovery of aerospace vehicles, the need for flexible fibrous materials looms larger and larger. The major environment to be encountered in these new areas of decelerator applications is that of temperature. The successful use of recovery systems, then becomes dependent on advances in the State-of-the-Art of Fiberology, - the forming of fibers and characterization of their behavior - and Fabric Geometry - the design of highly efficient flexible structures from yarn bundles and their characterization. This paper reviews that applied research which has been accomplished toward the achievement of fibers and flexible structures capable of operation over a broad temperature range.

HIGH TEMPERATURE FIBROUS MATERIALS FOR DECELERATORS

INTRODUCTION

Through the course of recent history, since the advent of the airplane and its subsequent rapid coming of age, decelerators in various forms have been used to first provide a safe means of escape, then to recover various loads all the way to the present day when a deceleration system is used to stop aircraft, lower manned space capsules and even provide a strategic means of delivering weapons of all sizes and shapes. The rapid expansion of the deceleration system to so many diverse uses has been brought about only through the versatility of the flexible fibrous materials which in many forms are joined together to form the actual structure which effect deceleration. During this growth period of the decelerator, many fibers have been used successfully, yet each fiber used has ultimately been displaced by new, improved fibers as the textile industry has made technological gains. As an example many of us can remember when nylon first replaced silk, when rayon replaced cotton. As the speed of aircraft increased, as the use altitude increased, as loads increased the ability of present day synthetic fibers to fill the bill has become questionable and in many cases out of the question. Unfortunately in most cases when environment causes a system to fail we seldom are able to obtain the residue to analyze. However in the two examples represented by Figures 1 and 2, it was possible to attribute failure to high temperature in the first instance, and either supersonic buffeting or subsonic flutter in the second instance. Thus the stage has been set for major advancements in the State-of-the-Art in Flexible Fibrous Materials.

Obviously one fiber cannot fulfill all the needs and requirements for woven forms to be used in decelerators. In this day of re-entry devices, aerospace and aeronautical vehicles, the deceleration devices will take shapes never seriously thought of except in Science fiction paperbacks. Therefore the flexible woven forms may have many variations. They may be low strength, high porosity, or high strength, low porosity, or the reverse, or they may be high strength coated forms which will have a zero porosity. Each decelerator system will have its own requirements for the flexible material involved and subsequently this will decide the fiber type to be utilized.

This then brings us to High Temperature fibrous materials for Decelerators. Since this paper will be concerned with many fibers types and their behavior in various environments, it becomes logical to discuss them in some sequence. It becomes apparent that if they are broken down by composition (polymeric, ceramics or glass, and metallic), they also



Figure 1. MELTED PARACHUTE

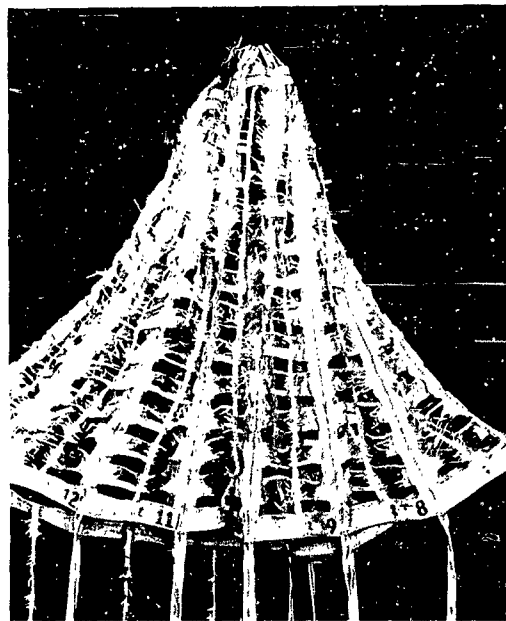


Figure 2. FRAYED PARACHUTE

fall into temperature categories (Polymeric - up to 900°F, glass or ceramic - 700°F to 1100°F, and metallic - 1200°F up). Therefore the following sections will cover high temperature fibrous materials by compositions.

POLYMERIC FIBERS

There is little need in this paper to discuss nylon as a fiber for deceleration systems, rather it is best to review the deficiencies in nylon and why other superior fibers are required. Basically nylon's prime deficiency is poor temperature resistance. The low melting point of 482°F results in damage to the fiber as shown in Figure 1 previously. Actually this is the only real deficiency that concerns us. However the use of decelerators at super and hypersonic speeds results in sufficiently high aerodynamic loads to create heat enough to melt nylon. When the problem first came up other available fibers of the polyester class were even considered, but one of the major drawbacks of organic fibers has been their low melting point and resulting low temperature at which strength deteriorates.

Starting in recent years, our research has been aimed at development of polymer systems which would have increased melting point as well as the ability to be formed into fibers. Even as research progressed, a variation of nylon was introduced, known as HT-1, this modified nylon became the first polymeric fiber which would retain a considerable percentage of its original tenacity (or strength) when evaluated either at or after exposures of 600°F. Figures 3, 4, represent a cross section of the behavior of this fiber under various environments. One of the intriguing results of laboratory studies has been that the strength at temperatures to 600°F could be improved through a gamma-thermal treatment such as shown in Table 1. As our work on the behavior of this fiber progressed, studies of weavability were initiated. A few decelerators of various shapes and constructions were assembled for drop tests, see Figures 5 and 6. At the same time, studies of the behavior of HT-1 in woven form were initiated. The primary purpose was to develop comparative data using nylon as a base. Of prime concern have been those environments to which decelerator materials are normally exposed. These included strength at temperatures, ultraviolet radiation resistance, impact behavior and pressure packing. Figures 7, 8, and Table 2 and 3 present data comparing HT-1 vs. nylon in these four environments. The advantages of HT-1 are apparent in two of the four areas. In the case of ultraviolet exposure the two fibers are on an equal basis, although initial reports received indicated HT-1 should have extremely poor ultraviolet radiation resistance. Impact behavior of HT-1 is not as good as for nylon. Although the fiber is tougher than nylon, its higher modulus 3.4×10^6 to 1.1×10^6 psi has an effect on this characteristic. From the data it can be seen that through logical use of engineering principles we can design HT-1 webbings with fairly high impact energy absorption. Then actual evaluation in recovery systems will

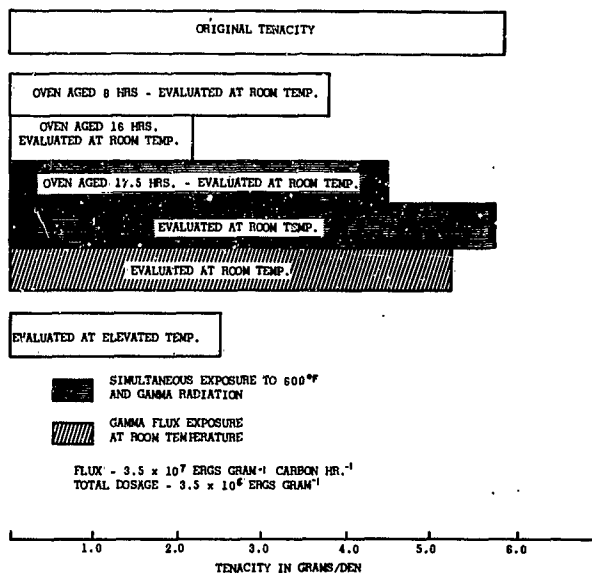


Figure 3. EFFECTS OF GAMMA RADIATION ON HT-1 AT 600°F

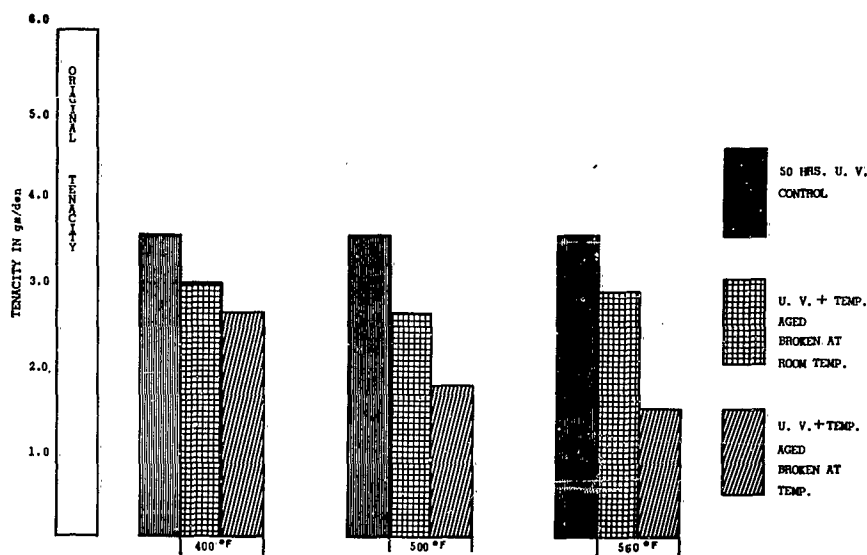


Figure 4. DEGRADATION OF HT-1 AFTER EXPOSURE TO ULTRA VIOLET RADIATION AND ELEVATED TEMPERATURES

Conditions

Oven Aged At Indicated
Temperatures For 8 Hrs.

1. Subjected Simultaneously To Gamma
Radiation Plus 400°F.
(Tot. Dosage 1.4×10^6 Ergs/gm.-Carbon-Hr)
2. Oven Aged At Indicated Temp.
For 8 Hours.

| | % Of Original Strength Retained | |
|-------|---------------------------------|------|
| 400°F | 96.3 | 96.3 |
| 500°F | 85.1 | 89.5 |
| 600°F | 58.6 | 78.2 |

Table 1. BREAKING STRENGTH DATA OF HT-1

| MATERIAL | INSTRON | IMPACT | | |
|----------------|---------|----------------------------|------------|------------|
| | | 200 FT/SEC | 500 FT/SEC | 700 FT/SEC |
| | | FORCE-LBS. | | |
| NYLON-1 1 INCH | 6,000 | 4,900 | 8,640 | 4,900 |
| HT-1 1 INCH | 5,500 | 7,500 | 5,700 | 0 |
| NYLON 1 INCH | 9,100 | 7,500 | 8,300 | 6,400 |
| HT-1 1 INCH | 8,200 | 10,000 | 12,000 | 0 |
| | | EXTENSION-% | | |
| NYLON | 14.0 | 12.0 | 11.0 | 12.0 |
| HT-1 | 18.0 | 11.0 | 10.0 | 0 |
| NYLON | 19.0 | 15.0 | 14.0 | 14.0 |
| HT-1 | 18.0 | 8.0 | 6.0 | 0 |
| | | ENERGY ABSORPTION-FT.-LBS. | | |
| NYLON | 1,190 | 1,469 | 2,258 | 1,694 |
| HT-1 | 2,718 | 1,840 | 2,945 | 472 |
| NYLON 8 INCH | 1,232 | 2,013 | 2,960 | 1,822 |
| HT-1 OVERLAP | 1,736 | 1,159 | 790 | 692 |

Table 2. IMPACT BEHAVIOR, HT-1 VS. NYLON

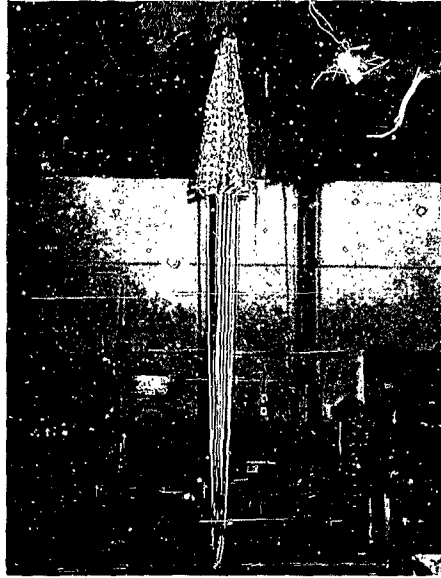


Figure 5. HT-1 RIBBON PARACHUTE



Figure 6. RING SLAT PARACHUTE OF HT-1

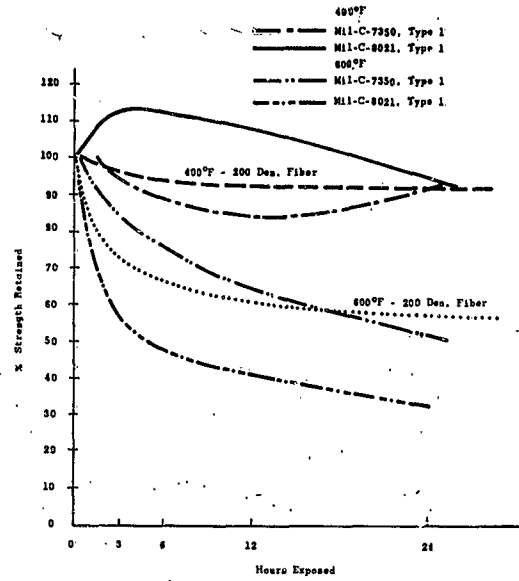


Figure 7. COMPARATIVE DATA OF HT-1 MATERIALS AFTER EXPOSURE TO ELEVATED TEMPERATURE

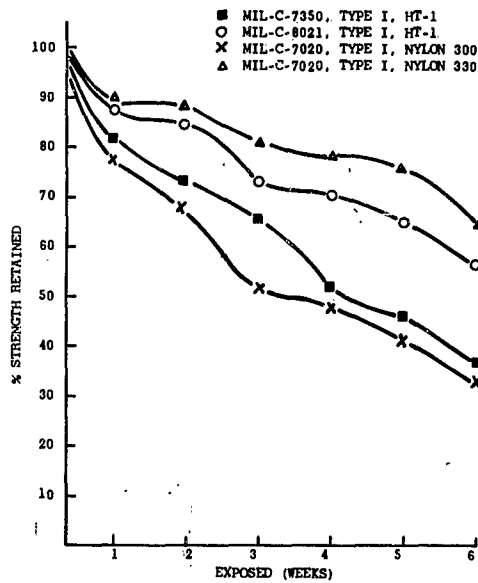


Figure 8. COMPARISON OF NYLON AND HT-1 FABRICS AFTER OUTDOOR EXPOSURE

verify whether the impact behavior will continue to be a problem area. Other studies of this fiber in woven form included the application of elastomeric coatings for the purpose of creating impermeable, heat resistant materials. One very interesting coating that has been given preliminary evaluation is a glass frit filled silicone rubber. When applied to a 7.25 ounce/sq. yard plain woven fabric, it was determined that temperatures as high as 1000°F had no qualitative effect for as long as 30 seconds.

Even as this fiber has been put through exhaustive Laboratory evaluations, our research on new polymer families has continued, of most interest to date have been that of the polybenzimidazole (PBI) polymer. Dry spinning (the polymer dissolved in an easily evaporated solvent is extruded into a column at elevated temperatures) techniques have been used to form fibers and yarn having strengths up to 4.5 grams per denier. Table 4 summarizes data obtained on very limited quantities of fiber and yarn. Preliminary studies of yarn exposed to simulated Florida sunlight for 220 hours indicated that 91% of the original 4.5 grams/denier was retained. As of now we have not had sufficient quantities of yarn to initiate extensive weaving studies. One attempt has been made to weave a PBI yarn into fabric. The PBI was used as the filling of a warp composed of HT-1 yarn. Considering that the PBI yarn was at least 5 times the denier of the HT-1 yarn, some success was achieved. Presently a small scale-up program has been initiated to produce enough yarn to allow extensive weaving studies so that we can characterize the behavior of the PBI yarn in anticipated environments in the same manner HT-1 has been characterized.

Another fiber type which is under consideration at the present could be classed as an organic or could be placed in a separate grouping. These are the fibers which are converted from an organic to a carbon or graphite structure. They will be discussed under this group since the majority of the fibers now being so converted are of cellulose, being rayon or Fortisan. These carbonized and graphitized fibrous materials are

TABLE 4

PBI STRENGTH GPD

| | | AT °F FOR 15 MIN. | | | | |
|-------|----------|-------------------|------|------|---------------------|-----|
| | ORIGINAL | 300 | 450 | 650 | 750 | 850 |
| FIBER | 4.1 | 4.4 | 3.2 | 2.6 | 1.0 | 0.4 |
| YARN | 4.1 | 3.46 | 2.85 | 2.22 | AFTER 24 HRS. AT °F | |
| | | 572 | | 662 | 752 | |
| FIBER | 4.5 | 4.1 | | 2.4 | | 1.0 |

| | CONDITIONS | | | STRENGTH | |
|--------------------------|------------|-----|------|----------|--------|
| | °F | Hr. | psi. | lbs. | % LOSS |
| HT -1 | 500 | 2 | 250 | 142 | 0 |
| | 600 | 2 | 250 | 118 | 16 |
| | 650 | 2 | 250 | 52 | 63 |
| | 700 | 2 | 250 | 43 | 69 |
| GLASS, LIGHT | 500 | 6 | 250 | 295 | 24 |
| GLASS, HEAVY | 500 | 6 | 250 | 454 | 32 |
| METAL (316 STAINLESS) | 1000 | 6 | 250 | 56 | 0 |
| | 1000 | 72 | 250 | 50 | 11 |

Table 3. PRESSURE - HIGH TEMPERATURES

| MATERIAL | 1000°F | | 1600°F | | 2000°F |
|---|------------------------------|-------------|---------------|------------------------------|------------------------------|
| | AIR | NITROGEN | AIR | NITROGEN | NITROGEN |
| GROUP 101-B, TYPE A, 3 OZS., 17.0 LBS/IN | NO STRENGTH 75% SHRINKAGE | 25.0 LBS/IN | DISINTEGRATED | NO STRENGTH 70% SHRINKAGE | DISINTEGRATED |
| GROUP 101-B, TYPE B, 6 OZS., 12.9 LBS/IN | NO STRENGTH 40% SHRINKAGE | 15.0 LBS/IN | DISINTEGRATED | 0.2 LBS/IN | NO STRENGTH 85% SHRINKAGE |
| GROUP 102, TYPE D, 45.8 LBS/IN | 18.0 LBS/IN | 21.3 LBS/IN | DISINTEGRATED | 2.3 LBS/IN | 19.0 LBS/IN |
| GROUP 103, TYPE F-1, 17.1 LBS/IN | DISINTEGRATED | 1.0 LBS/IN | DISINTEGRATED | DISINTEGRATED | DISINTEGRATED |

Table 5. EFFECT OF HEAT ON THE STRENGTH OF CARBONIZED FIBERS

generally obtained through a pyrolysis reaction. The major reasons for selecting cellulosic fibers are their high initial strength and capability of undergoing thermal decomposition without melting. In addition pyrolyzed rayon yields a strong yet flexible carbonaceous residue. The reaction must be accomplished in an inert, reducing atmosphere, or low pressure bone dry atmosphere. Atmospheric oxygen must be excluded, since its presence will increase decomposition by thermochemically oxidizing the polymeric carbon or even result in ignition of the volatile matter. The resulting fibers are classified into three categories based on the content (%) of elemental carbon, described as follows:

1. Partially carbonized fiber: Contains carbon content of up to 90%.
2. Carbon Fibers: Contains elemental carbon of between 91 and 98%.
3. Graphite fibers: Contains elemental carbon in excess of 98%

Many problems exist which must be overcome before we can even consider this type fiber. The major problem is strength. In addition, the material must be pyrolyzed in woven form (in most cases) resulting in inefficient constructions, lack of porosity control, and handling difficulties. Techniques to join the woven structures together also constitute a problem area. Much has been made of the resistance of these type materials to extremely high temperatures. However, when we review the data presented in Table 5, the supposed potential of this type fiber is rapidly diminished. Further, the weight loss that occurs at elevated temperatures (Table 6) indicates the shrinkage that can be expected in the fabrics.

TABLE 6
EFFECT OF HEAT ON WEIGHT OF CARBONIZED FABRICS

| FABRIC | 1,500°F NITROGEN ATMOSPHERE WEIGHT LOSS (%) |
|-----------------------------|--|
| GROUP 101, TYPE A, 5 OZS. | 84.3 |
| GROUP 101, TYPE B, 8 OZS. | 85.7 |
| GROUP 101, TYPE C, 12 OZS. | 58.3 |
| GROUP 101-B, TYPE A, 3 OZS. | 100.0 |
| GROUP 101-B, TYPE B, 6 OZS. | 64.3 |
| GROUP 102, TYPE D | 32.8 |
| GROUP 102, TYPE E | 29.2 |
| GROUP 103, TYPE F-1 | 51.9 |
| GROUP 103, TYPE F-2 | 55.7 |

Although it appears that this type of material has little possibility of being used in decelerators, it is entirely feasible that an adequate research program will result in graphitic fibers with more interesting characteristics.

This is especially true if the research is concerned primarily with forming of graphite type fibers and their conversion into woven forms.

This pretty well covers the recent advances in the field of polymeric fibers and their capabilities. We can say in brief summary of this group that use to 600 - 700°F bare and possibly to 900°F with proper coating is possible and should be given thorough evaluation in prototype systems.

Glass or ceramic type fibers which constitute the next area of study always involve, a two prong attack to obtain usable textile like structures. That is (1) research to obtain high strength fibers and (2) to develop suitable protective chemical systems to provide improved abrasion resistance and flexibility. In many instances the latter is far more important than the former. Until recently, very little consideration was given to the use of glassy fibers in flexible applications. Their sensitivity to fiber on fiber abrasion, stress concentrations due to moisture and temperature change, always has dictated the use of glassy type fibers as reinforcements where flexibility and abrasion resistance were not required. In any attempt to utilize glassy type fibers in flexible structures, techniques for evaluation must be developed. In the case of glass or ceramic fibers, it was necessary to achieve a method of evaluation which would simulate the most critical degradation of this type fiber. In this case it was combination of flexing and packing pressure in conjunction with temperature. To thoroughly characterize flexible structures of glass fibers, a procedure was developed which at one time applied 250 psi pressure at 500°F to specimens of woven ribbon, tape, or webbing either flat, folded 90° on itself or 180° on itself. This was used in evaluating typical glass fibers in forms that could be used in decelerators. Table 7 shows the results of some recent developments.

TABLE 7
BEHAVIOR OF FIBERGLAS RIBBONS & TAPES

| CONDITION | 1" WIDE | | 2" WIDE | |
|--|-------------|----------------|-------------|----------------|
| | B.S. (lbs.) | ELONGATION (%) | B.S. (lbs.) | ELONGATION (%) |
| GRIEGE | 7864 | 6.7 | 2639 | 6.3 |
| HEAT TREAT & FINISHES | 8660 | 6.0 | 2824 | 4.0 |
| 500 DEG. F-5 HRS. | 7864 | 6.7 | 2611 | 4.1 |
| FOLD-I | 7158 | 6.2 | 2801 | 5.3 |
| FOLD-II | 7428 | 6.8 | 2493 | 4.5 |
| FOLD-III | 8042 | 5.3 | 2703 | 5.6 |
| FOLD I-FLAT-250 PSI-500 DEG. F-5 HOURS | | | | |
| FOLD II-180 DEG. FOLD-250 PSI-500 DEG. F-5 HOURS | | | | |
| FOLD III-90 DEG. FACE-250 PSI-500 DEG. F-5 HOURS | | | | |

By changing the method of heat cleaning the woven glass materials and adding a silicone finish these results were obtained. Specifically the materials

were passed through an oven at 1000°F to partially remove the size, or to caramelize the size. As the tape came from the oven it was passed through the silicone finish and then cured at 300°F. This partial heat cleaning did not lower the basic strength of the materials, therefore higher strength to weight ratios could be obtained. Even seamability of these materials have been improved. Where previously 60% was maximum attainable in the past, four of six constructions yielded seams having 90% efficiency. This has only been done with E Glass fibers, whose temperature capability is really not much better than HT-1 or the forthcoming polybenzimidazole fibers. However the techniques used here obviously will be useful in forthcoming research programs.

Another research program, involving glassy type fibers concerns development of a suitable chemical finish for fused silica fibers. Produced in multifilament form, these fibers have good strength to 1800°F. However when woven into flexible forms, characterization showed that at 1200°F, no strength was left. This gives a good indication that really what is needed is a protective cover for each filament or fiber. Initial studies resulted in a magnesium acetate finish which was very effective at room temperature (flexibility and abrasion resistance being improved by a factor of 9 at the peak). However, this finish was not effective at elevated temperatures. Fabrics woven of fused silica yarn treated with the magnesium acetate has good room temperatures however the strength dropped to approximate 15% of original at 1200°F and 10% of original at 1800°F. If the material was loaded at room temperature to 25% of rupture load and then raised to 1200°F, the fabric would continue to take the preload, however as soon as additional load was applied the fabric failed. This indicated that the elevated temperature was volatilizing the magnesium acetate in a short time (less than 5 minutes). Present research is aimed at high temperature additives which will overcome this deficiency.

The last grouping is that of metals or the temperature range of 1500°F and higher. The ability to form metals into fine filaments constitutes problems of considerable complexity, therefore this discussion will not become involved in that area, but simply assume the availability of the fine metallic fibers.

Since the fine filament of a metal might behave differently than the sheet or bar of the same metal, thorough characterization of these fine fibers would be essential at the very beginning of research. It has been found that as in the case of many organic fibers the tensile strength increases and elongation decreases as metal fibers are drawn to successively finer diameters. Table 8 shows this effect very graphically as René 41 is reduced to the diameter considered optimum for use in forming multifilament yarns.

TABLE 8

EFFECT OF METAL FIBER DIAMETER ON STRENGTH AND ELONGATION

| Diameter In Mils | Tenacity-GPD | Elongation-% |
|------------------|--------------|--------------|
| 10 | 1.69 | 33 |
| 8 | 1.88 | 27 |
| 5 | 2.01 | 24 |
| 3 | 2.14 | 19 |
| 1.5 | 2.41 | 16 |
| 0.5 | 2.69 | 17 |

To accomplish this characterization of fine metal fibers, a series of varying diameter fibers of three (3) super alloys were drawn. These diameters were 5, 2, 1, and 0.5 mils. The alloys initially chosen were Rene 41, and Elgiloy, and Inconel 702. However, it was found that Inconel 702 could not be drawn to less than 1.0 mil diameter due to work hardening and embrittlement. Tensile strength, ductility, increase in weight due to oxidation, and creep effects were investigated on the various diameters of the previously mentioned alloys. Other super alloys such as Karma, Nichrome V and Chromel R - all Nickel Chromium alloys - were given cursory study as their high temperature behavior were reported - in sheet form - to be not quite as good as the first three alloys referred to. Since we could not draw the Inconel 702 to less than 1.0 mil, data are not shown here. With respect to oxidation at elevated temperatures the following trends became apparent for Rene 41 and Elgiloy:

1. The oxide film grows most rapidly in the first minute, increases at a reduced rate from 1 to 5 minutes and levels off between 5 and 10 minutes.
2. The rate of oxide growth (average absolute penetration depth) is less with decreasing fiber diameter.
3. The rate of oxide growth is greater with increasing temperature.

Temperatures have considerable effect on these fibers, as shown in Table 9. These data were obtained after exposing the fibers in static air. If, however, we were to obtain tensile after exposure in an inert atmosphere, the results are completely different as shown in Table 10. The question arises - if we are using these metal fibers in applications for aerospace recovery, why the concern about exposure to temperature in air? A simple explanation unconfirmed to date, is that as a device pushes through a low density atmosphere, oxygen molecules will collect along the leading edge or behind a shock wave, thus creating an atmosphere which could cause oxidation damage. The major advantage on our side at this point is that we will be using the ultra fine 0.5 mil fibers in multiple filament yarns having overall diameters of more than 4.0 mils. Then we can be more concerned with, say, 5 mil diameter yarns in getting an idea as to the tensile properties after exposure to elevated temperatures. We have

| TEMP. TO WHICH FIBERS WERE EXPOSED °F | HEATING TIME MINUTES | | | | | |
|---|----------------------|---------|---------|-------------|---------|-------------|
| | 1 | 5 | 10 | | | |
| | Elgiloy | Rene'41 | Elgiloy | Rene'41 | Elgiloy | Rene'41 |
| ULTIMATE TENSILE STRENGTH p.s.i. × 10 | | | | | | |
| NOT HEATED | 200 | 169 | 200 | 169 | 200 | 169 |
| 1500 | 194 | 203 | 179 | 207 | 169 | 200 |
| 1800 | 155 | 146 | 118 | 114 | 85 | 66 |
| 2000 | 113 | 130 | 87 | Too Brittle | 77 | Too Brittle |
| ELONGATION % | | | | | | |
| NOT HEATED | 28 | 23 | 28 | 23 | 28 | 23 |
| 1500 | 21 | 13 | 13 | 13 | 7 | 8 |
| 1800 | 6 | 6 | 3 | 1 | < 2 | 1 |
| 2000 | 6 | 3 | 5 | 0 | 3 | 0 |

Table 9. COMPARISON OF STRENGTH OF TWO ALLOYS
AFTER HEATING IN STAGNANT AIR, 1 MIL FIBERS

| WIRE DIAMETER MILS | 1 MIN | | | | 10 MIN | | | |
|-----------------------|-----------|----|-----------|-----|-----------|----|-----------|-----|
| | ELGILOY | | RENE'41 | | ELGILOY | | RENE'41 | |
| | Air Argon | | Air Argon | | Air Argon | | Air Argon | |
| | | | 1500°F | | | | | |
| 5.0 | 5 | 1 | +7 | +9 | 8 | 1 | +32 | +18 |
| 1.0 | 3 | 0 | +20 | +3 | 16 | 2 | +18 | +2 |
| 0.5 | 9 | 0 | +15 | +12 | 22 | 0 | 12 | +18 |
| | | | 1800°F | | | | | |
| 5.0 | 6 | 1 | 1 | +3 | 15 | 1 | 5 | +24 |
| 1.0 | 23 | 1 | 14 | +11 | 58 | 8 | 61 | +8 |
| 0.5 | 30 | 0 | 54 | +10 | 53 | 12 | | 30 |
| | | | 2000°F | | | | | |
| 5.0 | 14 | 2 | 23 | +13 | 25 | 7 | 24 | +8 |
| 1.0 | 44 | 12 | 23 | +7 | 62 | 36 | | 4 |
| 0.5 | 54 | 22 | | 26 | | 38 | | |

Table 10. PERCENT LOSS OF STRENGTH DUE TO
HEATING TWO ALLOYS IN ARGON-AIR

found also that elongation, or ductility is very seriously effected by temperatures over 1500°F. For any temperature from 1500°F - 2000°F, Rene' 41 was found to lose practically all ductility, while Elgiloy retains some ductility to 1800°F. Again this is with 0.5 mil fibers and it is conceivable that a multifilament yarn will react quite differently after exposure to the same environment.

In considering materials that will withstand temperatures in excess of 1800 - 2000°F, one thinks first of the refractory metals. It is well known that refractory metals such as tungsten are used as filaments for light bulbs, in extremely fine diameters. However, with the problem of catastrophic oxidation (Molybdenum burns at 1400°F), alloys of or coatings for refractory metal fibers are required. A study of metal coatings has been conducted with little real success. Many coating materials and methods of application to fine molybdenum and tungsten fibers were investigated, but none of these whether organic or metallic, or whether applied by vapor deposition, electroplating, electrodeless plating, cladding, or dipping, gave adequate protection in air at 2000°F.

Recently a new approach has been given considerable study and indicates a possible break through. This new approach has involved the passage of the refractory metal fiber through a molten solution of tin - aluminum. Initial studies were with a 90-10 solution. Coating thicknesses of .05 to .5 mils have been obtained on 1 mil tungsten wires. Some of these coated wires withstood 2000°F for 27 minutes. Further studies of solution concentration have been conducted and an 80-20 coating enabled a 1 mil wire to withstand 2000°F for 39 minutes.

To this point the discussion of metal fibers has been centered on those drawn individually. This is really a slow, costly process which needs to be eliminated.

One unique method of forming ultra-fine fibers of the super alloys is to draw a large number of wires through a single die. Although the equipment used is that for drawing single metal fibers, the ability to draw any number of fibers through a single opening would eliminate the need for dies with, say, 1/2 mil diameter openings, yet make possible individual fibers with diameters of less than 1/2 mil. Initial drawings were made with 7 Hastelloy B filaments of .004 inches diameter. When drawn bunched and uncoated filament breakage was excessive. Further drawings were made after inserting the bunched filaments in lead or nickel tubing. The major success has been obtained when using a nickel tubing. With annealing after each reduction, the bundle was reduced to a final diameter of .0027 inches. Polished metallographic specimens revealed the individual filaments were still discernible and the diameter of each filament was quite uniform. Drawing of 37 filaments of Elgiloy in a Chromel C tube has been conducted with a final diameter of .0027 inches being reached. In this case the individual filaments are less than .0004 inches in diameter. Figure 9. A study was made of the bending recovery of the drawn

37 filament bundle versus a monofilament wire of the same diameter and alloy. (It must be recognized that the 37 filament bundle was still sheathed). It was found, that even with the sheath still in place, the 37 filament bundle showed an improvement in bending recovery over the monofilament yarn. Although the bending recovery is not as good as would be experienced with a stranded bundle of .0005 inch filaments, it is conceivable that after removing the sheath, a major improvement in bending recovery can be accomplished.

This is so stated because we have been successful in removing the sheath, however bending recovery studies have not as yet been conducted. Figure 10 shows the 37 strands of Elgiloy after removing the Chromel C sheath by pickling in acid. In the beginning it was found that drawing and pressure welded these filaments together, however annealing in a slightly oxidizing atmosphere prevented a recurrence of this. Tensile data has not been noteworthy, however fiber breakage could account for this as the individual fibers are in the order of .0003 inches in diameter and are very weak if compared to a 1.0 or 1.6 mil fiber. High temperature tensile data on Elgiloy and Rene' 41 37 strand bundles revealed that the stranded Elgiloy retained more strength than a monofilament of .0027 inches diameter, where the Rene' 41 retained approximately the same strength.

Up to this point only preliminary weaving studies have been made using the multifilament metal yarns. Both 49 and 100 filament yarns of Chromel C have been woven into one and two inch ribbons for permeability and bending recovery tests. With respect to permeability, a 49 filament yarn in a 109 X 117 construction had a permeability of 72 cu ft/min./sq. ft, while a monofilament wire fabric having the same calculated porosity had a permeability of 883 cu ft/min./sq. ft. This demonstrates the effect of flattening that occurs in multifilament yarns when woven and can be expected regardless of whether the fiber is metallic or polymeric. These same two fabrics had a bending recovery of 55% and 35%, when the bending curvature was 12 inches, again revealing the advantage of multifilament yarns.

Much broader studies of optimum filaments per yarn, and twist for 0.5, 0.7 and 1.0 mil fibers has been initiated with weaving of broad goods to follow utilizing the best yarn constructions developed. This will be followed by behavior characterization and then studies of techniques to be used to join these fabrics together.

A tremendous amount of research is still necessary before we achieve true first and second generation flexible fibrous materials for decelerators. The work accomplished to date has been the result of excellent joint effort with our contractors. This joint internal - contractual research program must continue to attain the goals established so that the materials required will be available when the decelerator research scientist decides the time has come for full wind tunnel or field evaluation of a design concept.

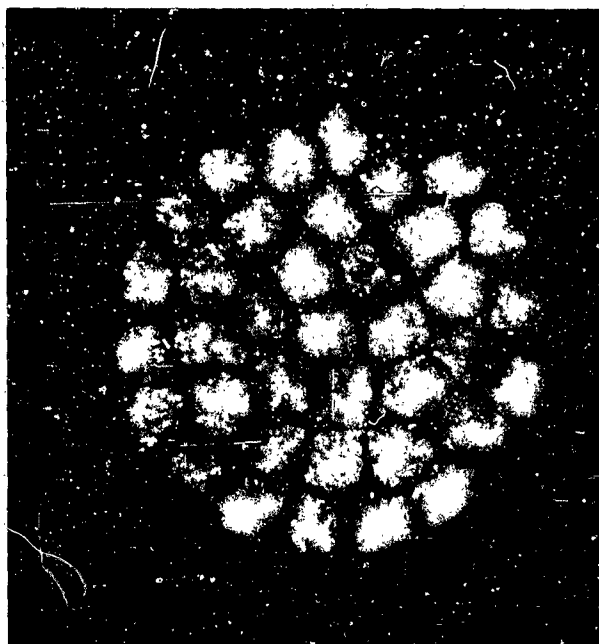


Figure 9. CROSS SECTION OF 37 STRANDS OF ELGILOY
DRAWN TO FINAL DIAMETER OF .0027 INCH INCLUDING SHEATH.

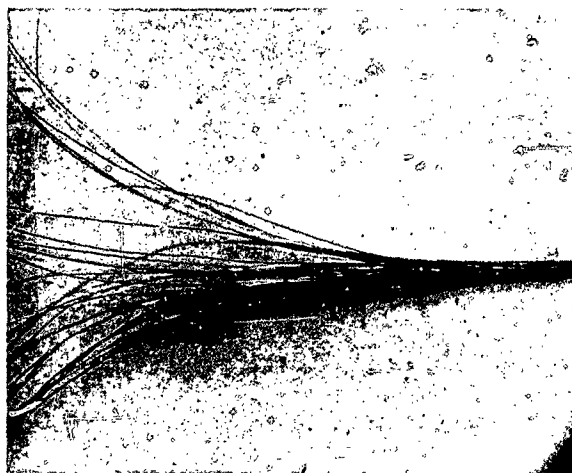


Figure 10. 37 STRANDS OF ELGILOY AFTER REMOVAL OF
CHROMEL C SHEATH

REFERENCES

1. WADD TN 60-299, Thermal and Gamma Radiation Behavior of New High Temperature Organic Fiber, C. O. Little, Jr., June 1961.
2. ASD TR 60-511, Part II, Impact Characteristics of Parachute Materials, R. J. Coskren and C. C. Chu, February 1962.
3. WADD TR 60-588, Some Effects of Compression and Heat on Decelerator Materials, N. J. Abbott, June 1961.
4. ASD TR 61-677, Flexible, Low Porosity, Woven Metallic Materials, M. J. Coplan, W. D. Freeston Jr., and D. H. Powers, Jr., November 1961.
5. ASD TR 62-180, Metal Filaments For High-Temperature Fabrics, D. E. Johnson, et al, February 1962.
6. ASD TDR 62-518, High Strength, Glass Fiber Webbing, Tapes and Ribbons for High Temperature Pressure Packaged Decelerators, E. S. Cobb, Jr., July 1962.
7. ASD TDR 62-542, New and Improved Materials for Expandable Structures, D. M. Marco, June 1962.
8. Ross, J. H, "High Temperature Fiber Research," 32nd Annual Meeting, Textile Research Institute, March 1962.
9. Ross, J. H, "Prospects for Use of Fibrous Metals," Metal Progress, April 1962.

Session III

DECELERATOR INVESTIGATIONS SESSION

Chairman: DR. A. J. SHINE
Air Force Institute of Technology
Mechanical Engineering Department
Wright-Patterson AFB, Ohio

THE VELOCITY AND PRESSURE DISTRIBUTION
IN THE WAKE OF A BODY OF REVOLUTION
AT TRANSONIC AND SUPERSONIC SPEED*

Helmut G. Heinrich
and
R. Sheldon Hess**

Department of Aeronautics and Engineering Mechanics
University of Minnesota

The basic problems of the flow field analysis of the wake in subsonic flow are discussed and the principles of the analytical approaches are reviewed. Experimental results of the distribution of static pressure and Mach number along the axis and the total pressure profiles across the wake in transonic and supersonic flow are presented.

*The work was sponsored jointly by the U.S. Air Force, Army, and Navy. Messrs. R. J. Berndt and J. H. DeWeese, WADD, were the Project Engineers.
**Messrs. J. G. Ballinger and G. Stumbris and students of the University of Minnesota also participated in the experimentation and data reduction.

LIST OF SYMBOLS

| | |
|---------------|--|
| b | Half-width of wake |
| C_D | Drag coefficient of body |
| $C_{D\infty}$ | Drag coefficient of body in free stream |
| C_H | $= \frac{H - H_0}{q_\infty}$ = Total pressure coefficient in transonic wake |
| C'_H | $= \frac{H - H'_\infty}{q_\infty}$ = Total pressure coefficient in supersonic wake |
| C_P | $= \frac{P - P_\infty}{q_\infty}$ = Static pressure coefficient |
| D | Maximum body diameter |
| H | Total pressure in wake as recorded by total pressure tube |
| H_0 | Wind tunnel stagnation pressure |
| H'_∞ | Total pressure which would exist behind a normal shock in free stream |
| M | Calculated Mach number in wake |
| M_∞ | Free stream Mach number |
| P | Static pressure in wake as recorded at surface of support sting or wire |
| P_∞ | Free stream static pressure |
| q_∞ | Free stream dynamic pressure |
| r | Radial distance from centerline of body |
| R | $= \frac{D}{2}$ = Maximum body radius |
| Re | Reynolds number (based on D) |
| S | $= \frac{\pi D^2}{4}$ = Projected frontal body area |
| u | Velocity defect in wake |
| u_0 | Free stream velocity |
| X | Distance downstream from body base |
| * | Factor of porportionality |

THE VELOCITY AND PRESSURE DISTRIBUTION IN THE WAKE OF A BODY OF REVOLUTION AT TRANSONIC AND SUPERSONIC SPEED

INTRODUCTION

The turbulent wake is one of the most common phenomena in the aerodynamics of real flow; but its mechanics have never been very well understood. However, in problems of aerodynamic deceleration, in which a secondary body is located in the wake of a forebody for the purpose of reducing the speed of the combination of the two bodies, the knowledge of the velocity and pressure distribution in the wake is one of the fundamental requirements.

The drag of the secondary body, also called aerodynamic decelerator, is of course well known for free stream flow conditions. When, however, such a decelerator is totally or partially immersed in the turbulent wake of the primary body, the force which the decelerator exerts upon the primary body differs from its free stream drag. One may expect that the useful drag of the decelerator will depend on its size relative to the primary body, its location in the wake of the primary body, its characteristic form, and the flow regime in which the deceleration is performed, subsonic, transonic, supersonic, or hypersonic. But for performance calculations of aerodynamic recovery systems, it is necessary to know the drag of the system as well as the specific drag of the decelerator.

The relationship of the drag in the wake to the free stream drag of a number of bodies related to commonly used aerodynamic decelerators is illustrated in Figs 1 through 3 (Ref 1). These figures indicate that the useful drag of these decelerators is in all cases significantly reduced from the free stream drag when the decelerator has to operate in the turbulent wake of the primary body. Furthermore, it can be observed that the drag reduction depends indeed on the relative size between decelerator and primary body, the location of the decelerator, and the flow regime.

These figures indicate the significance of the wake effect and it may be concluded that the knowledge of the velocity and pressure distribution in the turbulent wake is one of the principal problems which must be investigated in order to analyze and to understand the drag reduction which aerodynamic decelerators suffer when they are placed in a turbulent wake. Therefore, an analysis of the wake shall be attempted as the first step in this general effort.

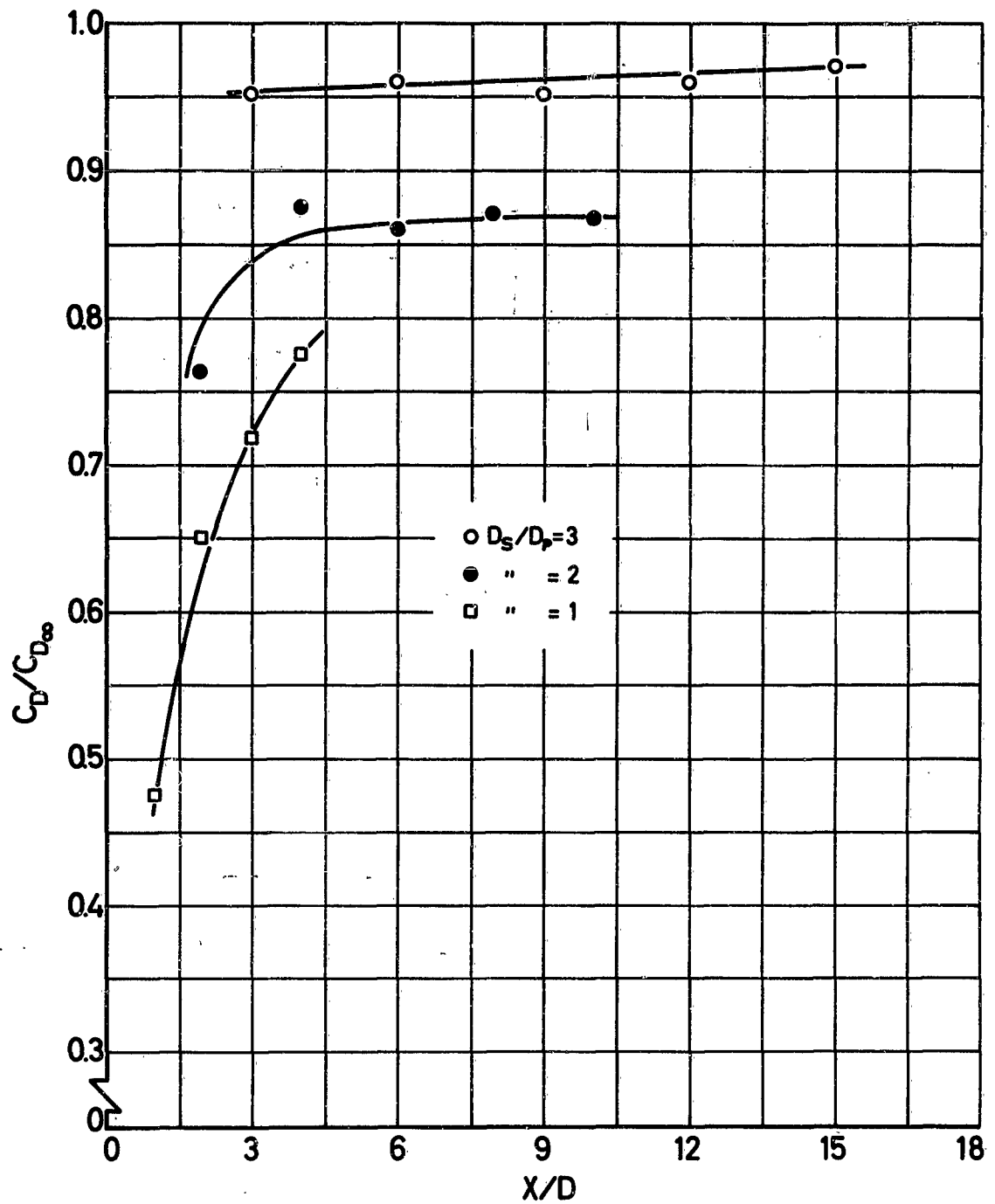


FIG 1. DRAG COEFFICIENT OF A FLAT PLATE IN WAKE OF OGIVE CYLINDER AT SUBSONIC SPEED ($M_\infty=0.2$, Ref 1)

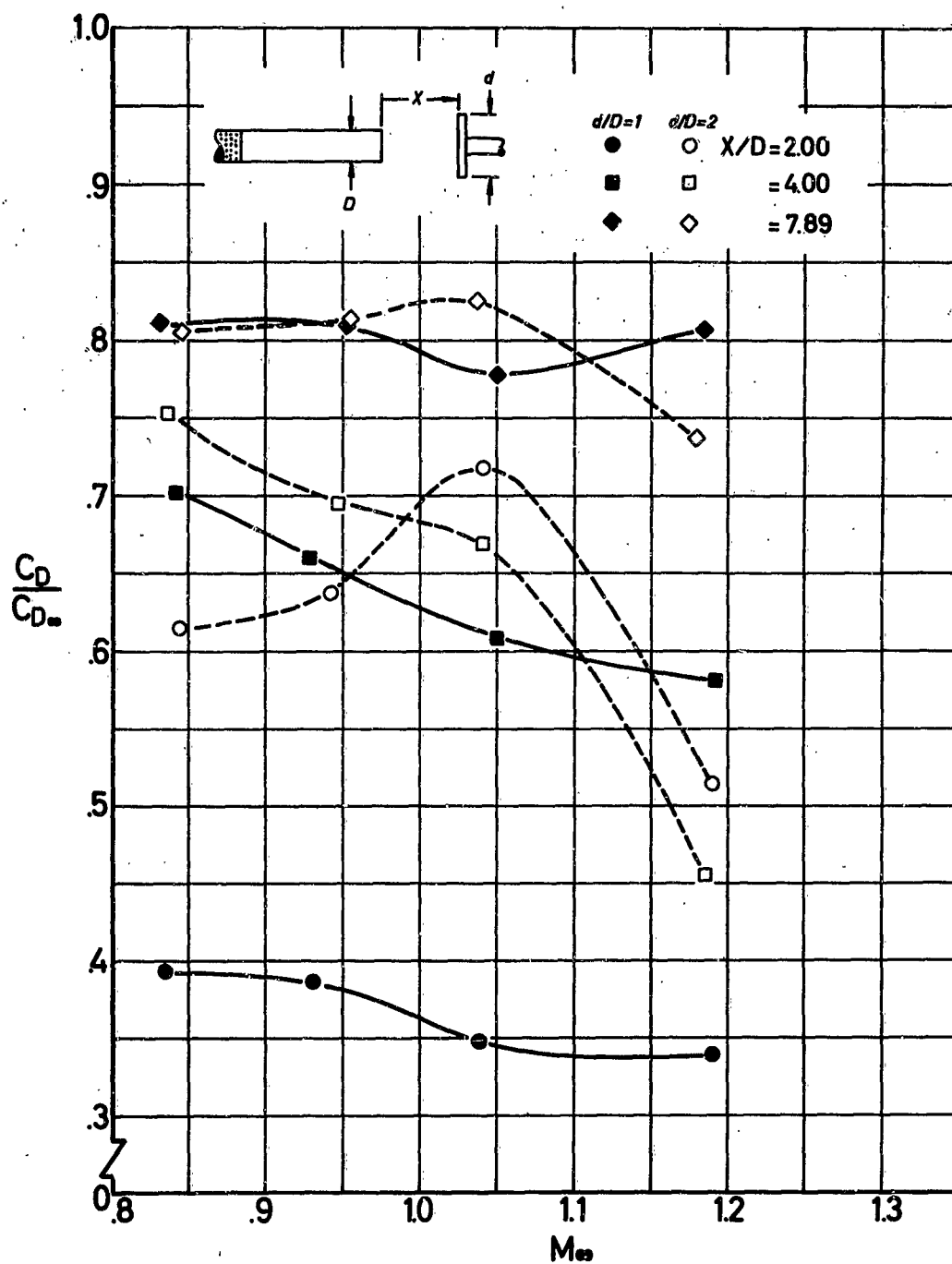


FIG 2. DRAG COEFFICIENT OF A FLAT PLATE IN WAKE OF OGIVE CYLINDER AT TRANSONIC SPEEDS ($M_\infty = 0.85$ to 1.18)

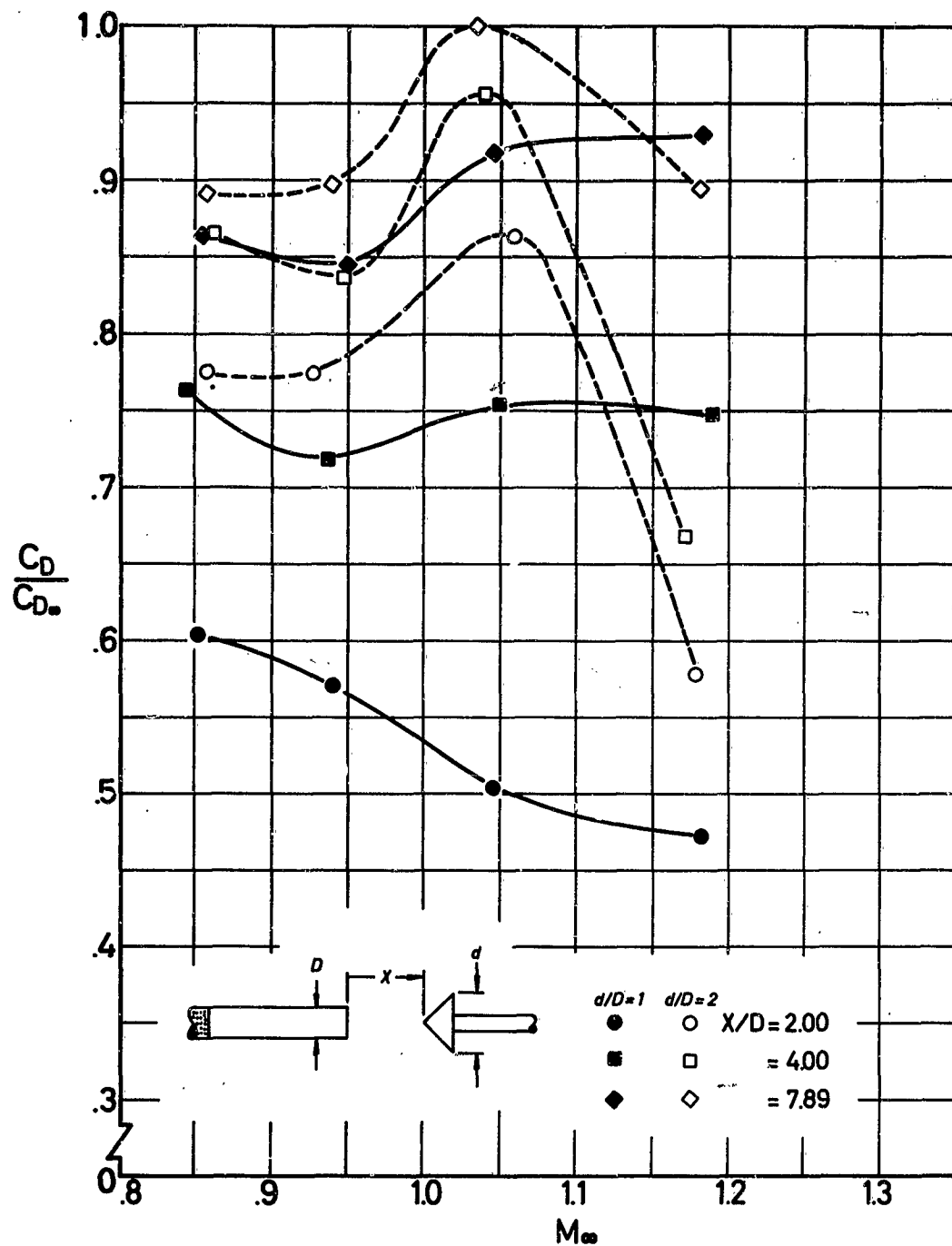


FIG 3. DRAG COEFFICIENT OF A 45° HALF-ANGLE CONE IN WAKE OF OGIVE CYLINDER AT TRANSONIC SPEEDS ($M_\infty=0.85$ to 1.18)

THE TURBULENT WAKE IN SUBSONIC FLOW

In spite of being commonplace, the flow field in the wake does not lend itself to accurate mathematical analysis, as indicated by the varied solutions and treatments by the authors listed under Refs 2, 3, and 4. These treatments give satisfactory solutions for distances of 20 or more diameters downstream of the primary body. For aerodynamic deceleration, however, the range from three to ten diameters becomes more important since this is the distance at which one usually wishes to deploy the aerodynamic decelerator. Therefore, a new attempt was made by the authors of Ref 5 with the specific objective to establish the flow characteristics of the wake closer to the primary body. Figure 4 is taken from Ref 5 and illustrates the pressure distribution in the wake of a body of revolution at a distance from two to twelve diameters downstream. This body of revolution, an ogive cylinder, was chosen because similar bodies have been investigated in Refs 2 through 4, and such bodies also appear in problems of aerodynamic deceleration.

The analysis presented in Ref 5 was based on the coordinate system shown in Fig 5, and the basic assumptions as to the composition of the turbulent shearing stress, the width of the wake, and the related mixing length, as well as the widening of the wake with increasing distance, were made in agreement with the classical treatments. The end result of the studies under Ref 5 is shown in Eqn 1.

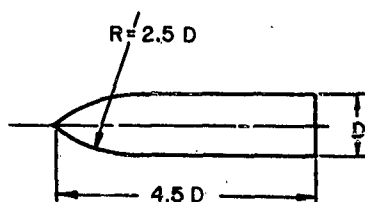
$$\frac{u}{u_0} = \frac{0.105}{\chi^{2/3}} (C_D S / \chi^2)^{1/3} e^{-\frac{r^2}{1.525 (C_D S \chi)^{2/3}}} \quad (1)$$

The results of the theories of Refs 2 through 5 are compared in Fig 6. One observes that the various theories agree rather well; however, it should be noted that the assumptions on which these theories are based are valid only for great distances behind the primary body.

Equation 1 includes the drag area of the body, $C_D S$, and an experimental parameter, χ , which first appeared in Prandtl's expression for turbulent shearing stress,

$$\tau = c \chi b (u_{max} - u_{min}) \frac{du}{dr} \quad (2)$$

The significance of this factor of proportionality χ is that it is connected with the width of the wake, b . Furthermore, in the term for the turbulent shearing stress, the ratio of the mixing length, l , and the half-width of the wake, b , is assumed to be constant throughout the wake. This is, in accordance with Ref 2, acceptable for the wake region of



RELATED TO D, FREE
STREAM VELOCITY AND
AIR DENSITY. REYNOLDS
NUMBER = 2.74×10^5
MACH NUMBER ≈ 0.2

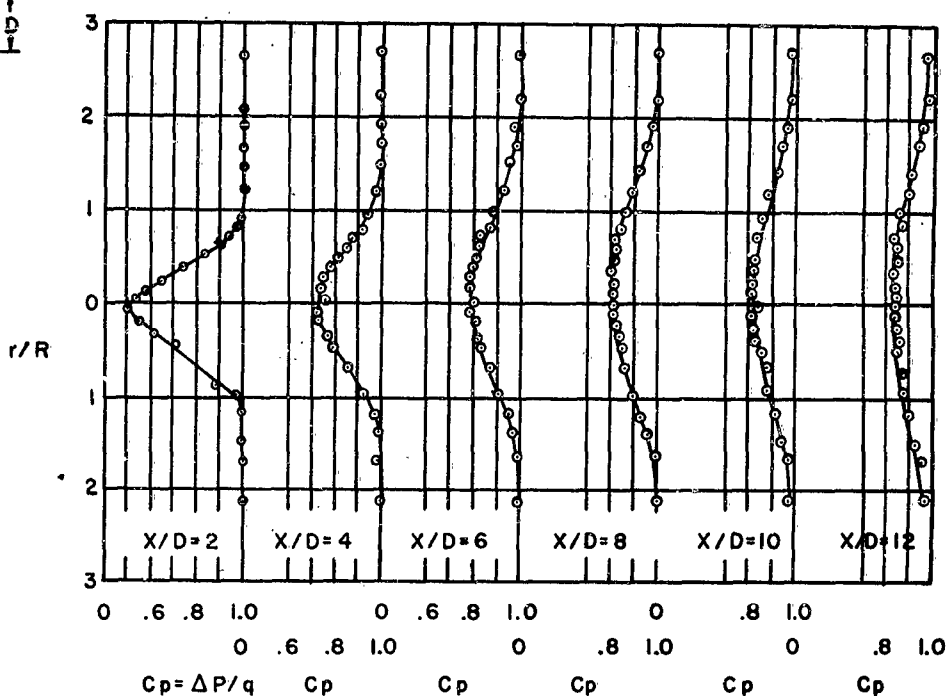


FIG 4. PRESSURE DISTRIBUTION IN THE WAKE OF A
BODY OF REVOLUTION ($C_D = 0.35$, REF 5)

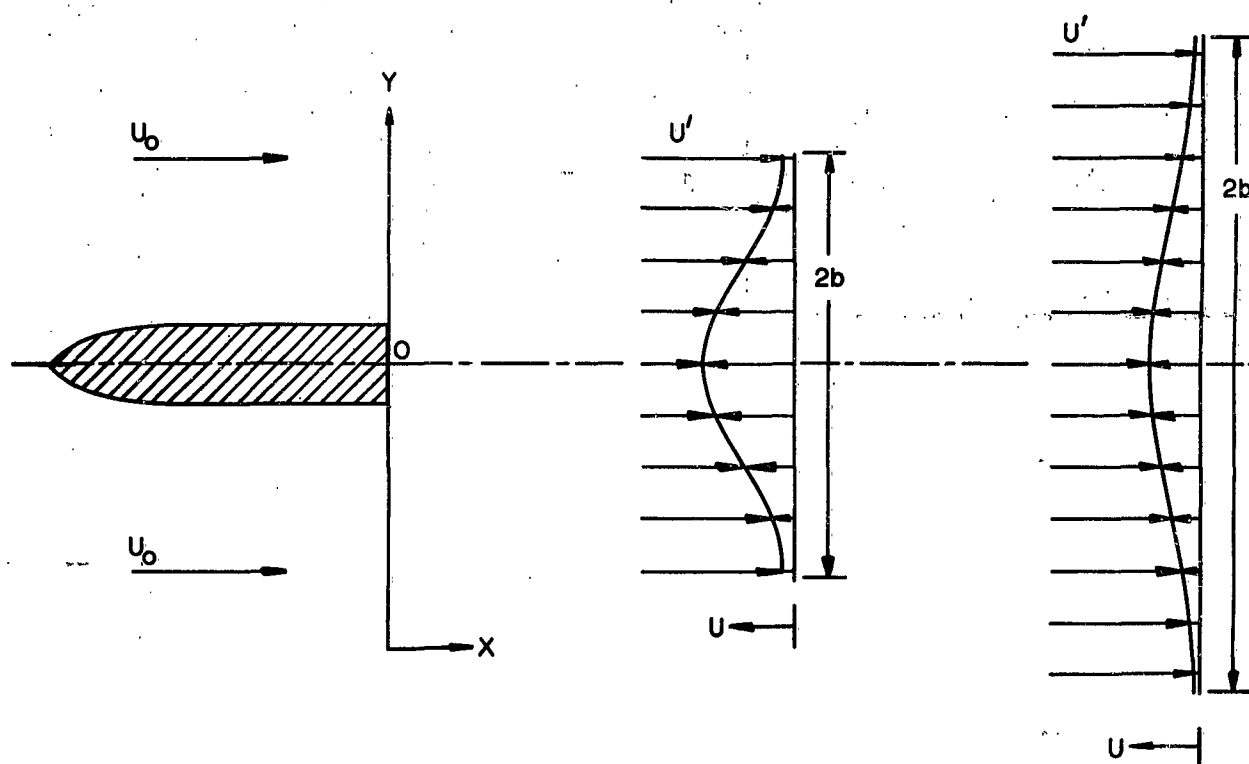


FIG 5. VELOCITY DISTRIBUTION FOR A BODY AT REST AND A MOVING FLUID

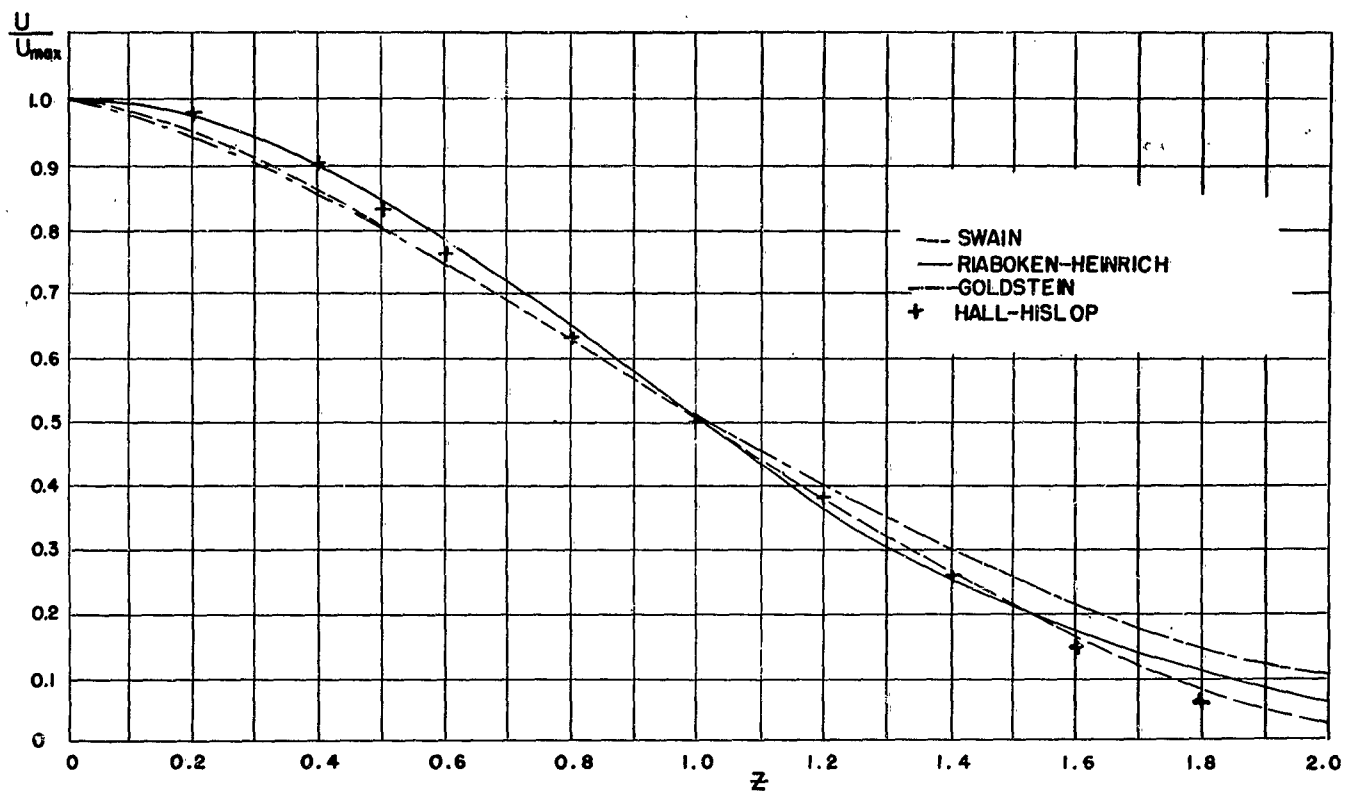


FIG 6. VELOCITY DISTRIBUTION IN ACCORDANCE WITH ANALYTICAL AND EXPERIMENTAL STUDIES (REF 5)

larger distance behind the primary body. Experiments also indicate that at great distances the value of λ approaches asymptotically a constant value.

However, in the region important for aerodynamic deceleration, the classical assumptions concerning wake width, mixing length, etc., are probably not valid. Therefore, the parameter, λ , in Eqn 1 was determined from the experimental velocity distribution in such a way that the measured and the calculated velocity distribution were matched at the centerline of the wake. The factor of proportionality so determined is shown in Fig 7, and the velocity distribution in the wake, calculated from Eqn 1 using λ values from Fig 7, is shown in Figs 8 and 9.

From these figures, it can be seen that the agreement between measured and calculated flow characteristics appears to be acceptable as far as one may expect in view of the underlying assumptions and modifications. For example, the theory which provided Eqn 1 encompasses the assumption that the width of the wake increases with the $1/3$ power of the distance, x . This is a good approximation for large distances, but one knows from experience that the wake close to the body is significantly influenced by the body form. For example, the outer boundary of the wake of a flat plate close to the plate is considerably different from the one of the ogive cylinder. Therefore, one must assume that λ values close to the base of the primary body as derived and presented in the preceding paragraph will be characteristic only for bodies somewhat similar to the ogive cylinder. In view of these circumstances, Rubbert (Ref 6) investigated the wake of a flat plate, applied the methods as described above, and extracted λ values for the flat plate. These values, shown in Fig 10, were introduced in the basic Eqn 1 and provided the experimental and calculated relationship of pressure distribution as shown in Fig 11.

Similar efforts are now being pursued (Ref 7) with the objective to establish certain generalized values which will enable one to calculate pressure and velocity distribution in the wake of a considerable variety of bodies of interest for aerodynamic deceleration. In summary, it may be said that sufficient information is available to predict the flow characteristics of a subsonic wake for a variety of bodies of revolution.

THE TRANSONIC WAKE

In the transonic flow regime several phenomena occur in the field of the wake flow which are not encompassed by the

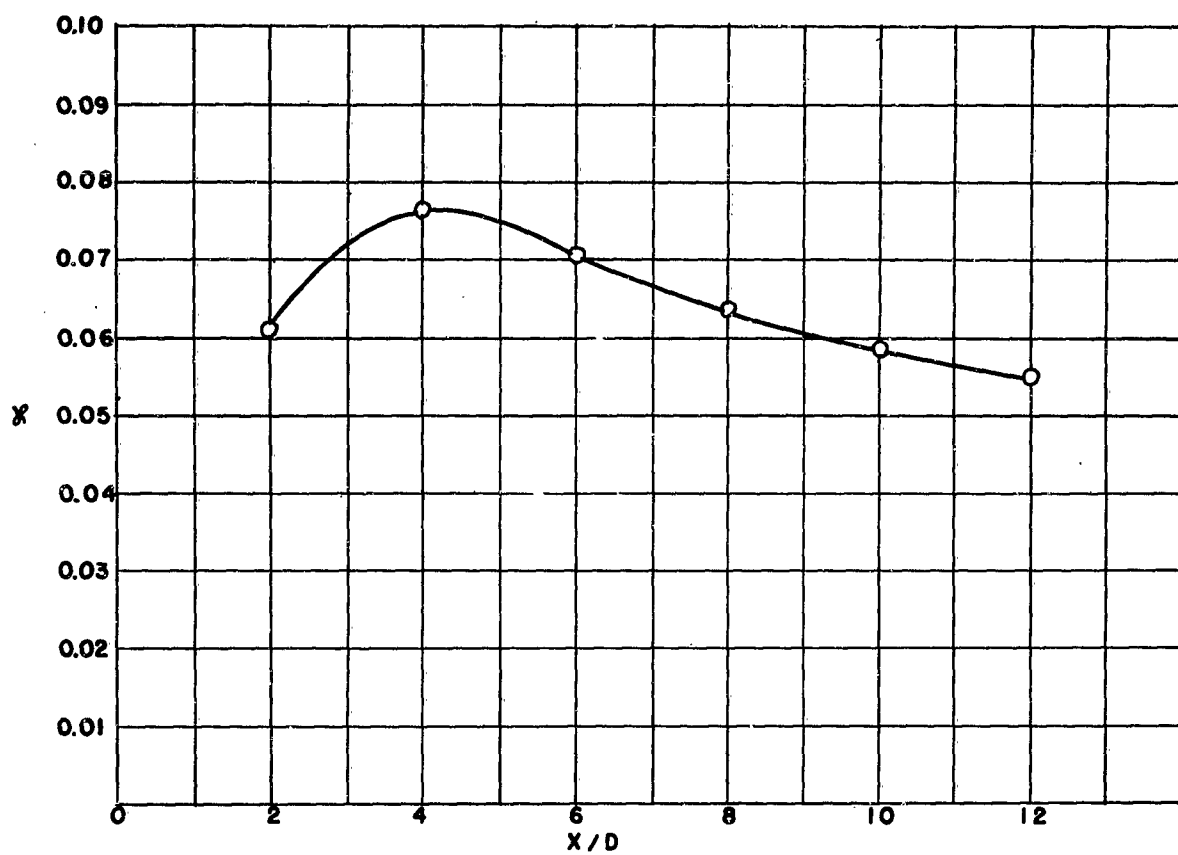


FIG 7. x VS. x/D AS DETERMINED FROM EXPERIMENTAL DATA
(REF 5)

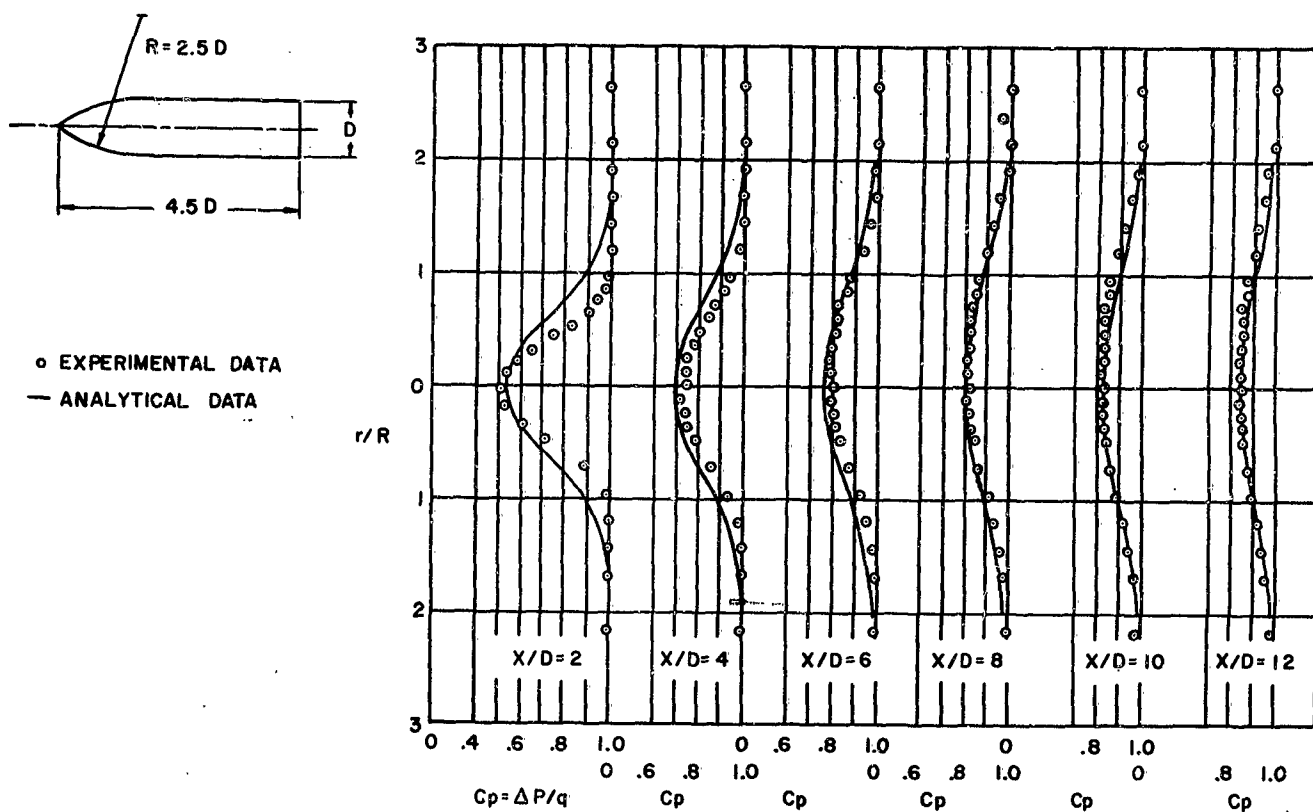
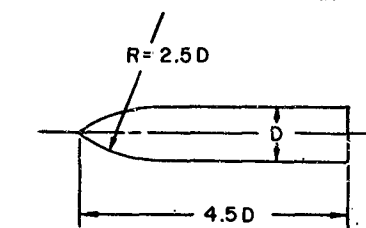


FIG 8. EXPERIMENTAL AND ANALYTICAL DATA FOR A BODY OF REVOLUTION (BASED ON $\alpha = 0.0633$ RELATED TO C_p AT $X/D = 8$, REF 5)



○ EXPERIMENTAL DATA
— ANALYTICAL DATA

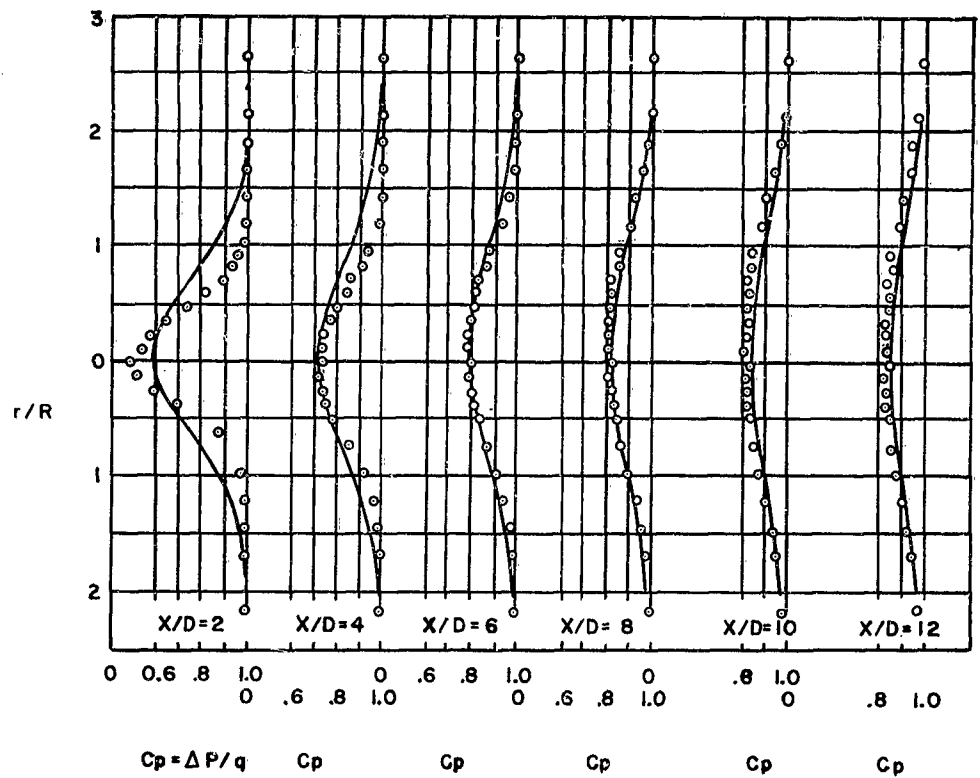


FIG 9. EXPERIMENTAL AND ANALYTICAL DATA FOR A BODY OF REVOLUTION
(BASED ON $\alpha = 0.0764$ RELATED TO C_p AT $X/D = 4$, REF 5)

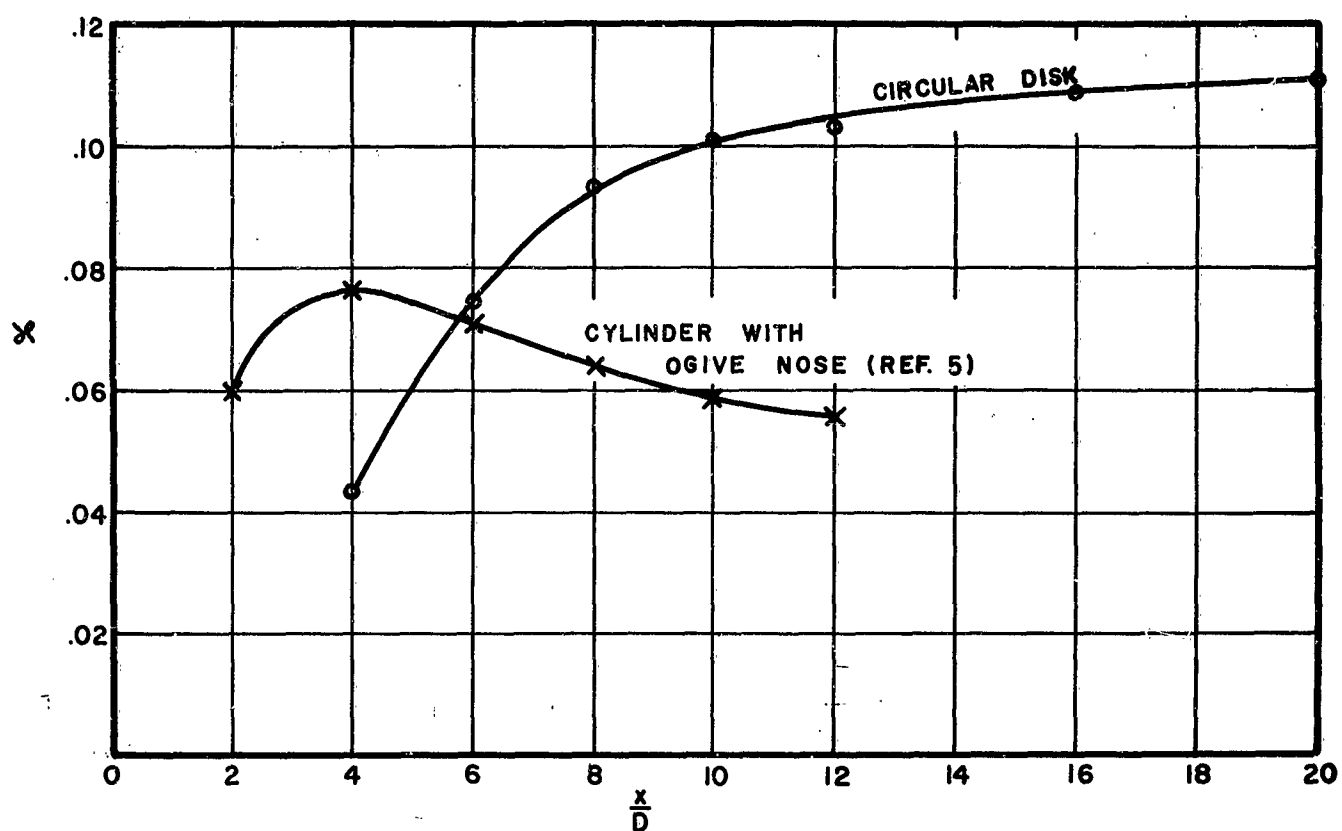


FIG 10. X VS $\frac{x}{D}$ AS DETERMINED BY EXPERIMENT (REF 6)

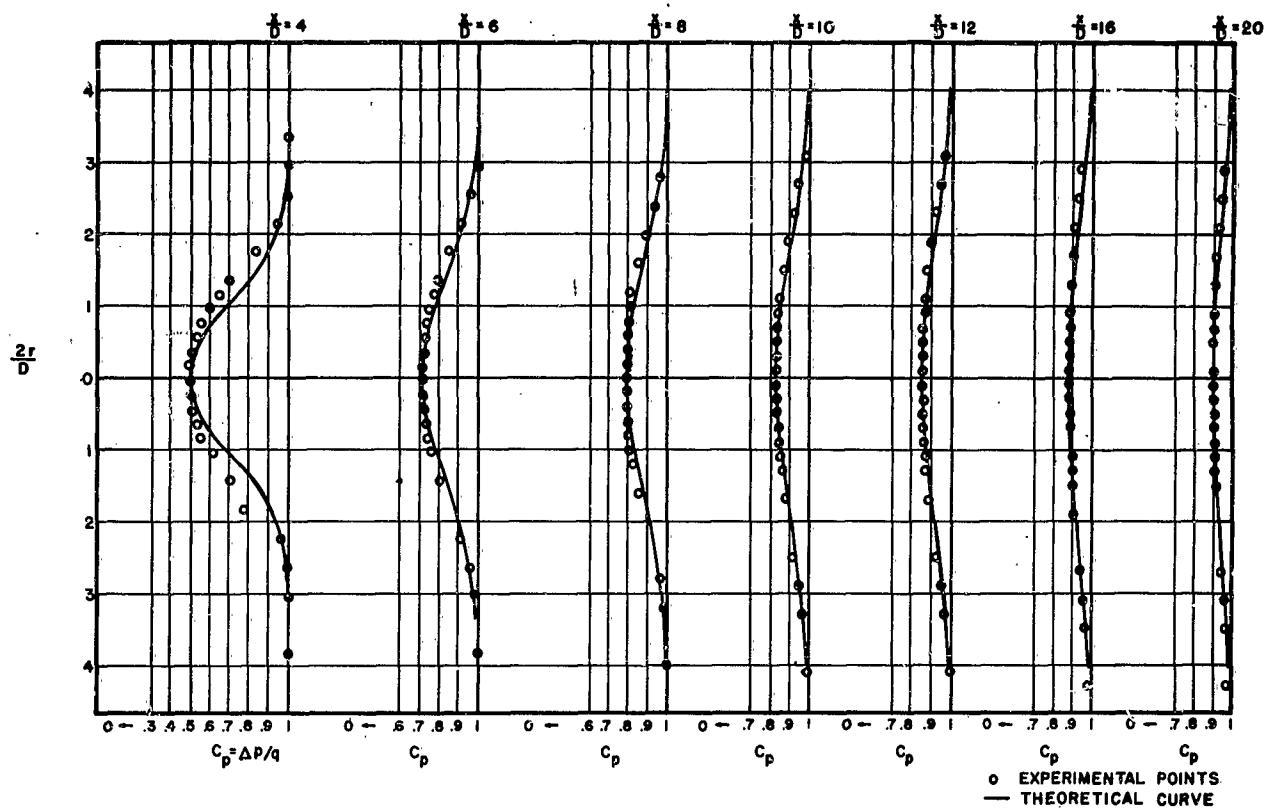


FIG II. EXPERIMENTAL AND THEORETICAL PRESSURE DISTRIBUTION IN THE WAKE OF A FLAT, CIRCULAR DISK
(REF 6)

theory which gave satisfactory results in subsonic flow. This is particularly true for the region close to the base of the primary body. A few of these phenomena which are not accounted for by theory are energy losses in the formation of compressive shock waves, the existence of regions of flow expansion, the formation of trailing shock waves, and a significant variation of the density in the wake. Also, the back and the cross flow velocity components are in the transonic more influential than in the subsonic flow regime. Therefore, in the following, merely the results of the measurements in the wake will be presented.

Two bodies of revolution have been selected as the primary bodies, one of which is the ogive cylinder already investigated in the subsonic flow. The second body is the so-called skirted hemisphere being of particular practical interest. Both primary bodies are shown in Fig 12. Because of the more complicated circumstances of transonic and supersonic wind tunnel operations, the investigation had to be limited and in the following the wake shall be characterized through the static pressure along its approximate centerline, the distribution of total pressure at various radially oriented locations, and the approximate Mach number in the neighborhood of the wake centerline.

Reviewing first the static pressure near the wake axis as illustrated in Fig 13 (numerical values are given in the Appendix, Tables 1 and 2), one observes that the static pressure varies considerably from the base of the body in the direction downstream of the flow. This variation is also dependent on the Mach number and it is interesting to note that the static pressure of the wake is considerably higher than the free stream static pressure at a relatively short distance from the base.

The dependency of the local static pressure at any given position downstream of the base on the free stream Mach number is very clearly indicated in Fig 14. The lowest static pressure coefficient for all wake locations occurred when the free stream Mach number was approximately unity. There is, however, one exception for X/D of 6 which is an unexplained observation. Furthermore, the graphs indicate that the static pressure coefficient in the wake of the skirted hemisphere is considerably lower than in the wake of the ogive cylinder.

In summary, these graphs indicate that an aerodynamic decelerator located at X/D positions between 3.5 and 6.0 would experience a considerable variation of static pressure when the primary-secondary body system passed through the transonic range.

The distribution of the total pressure in the wake of the ogive cylinder is shown in Fig 15. This pressure was

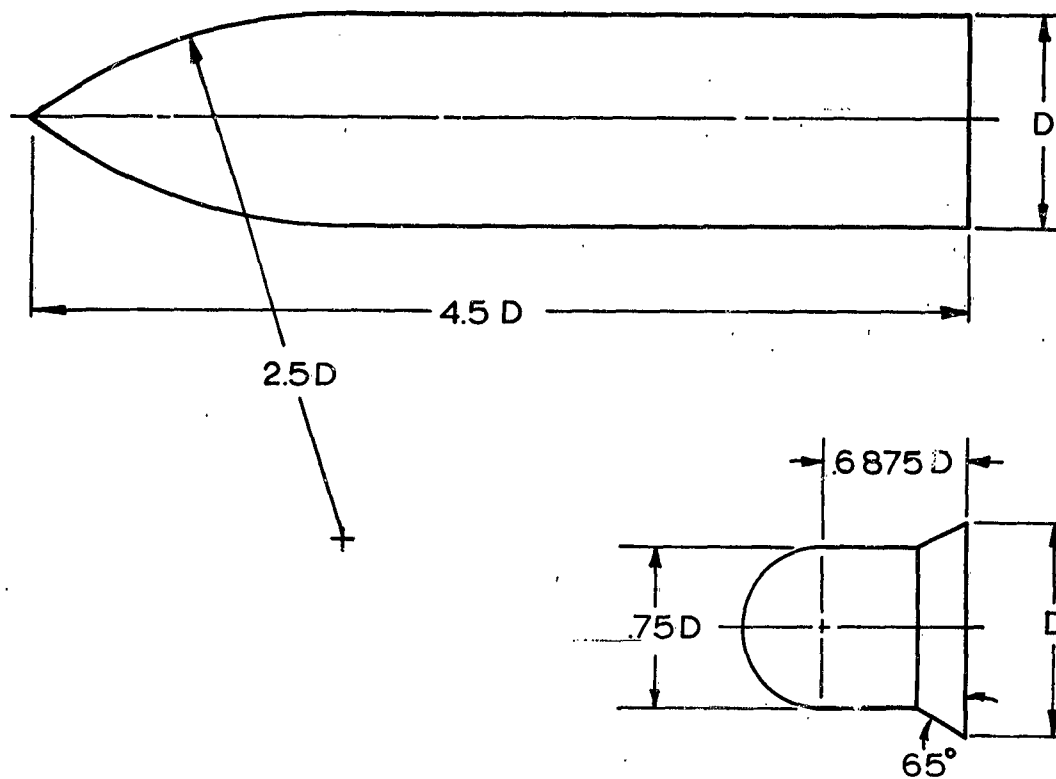
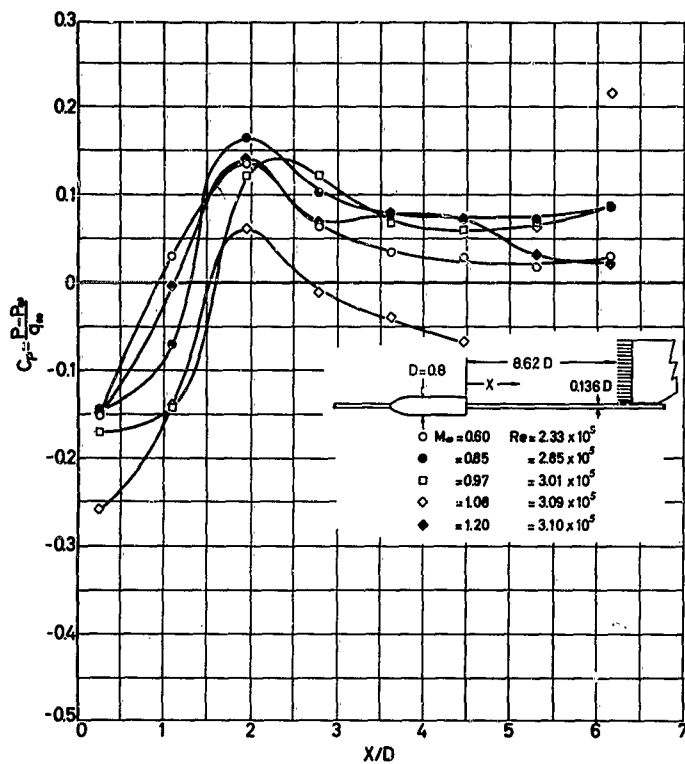
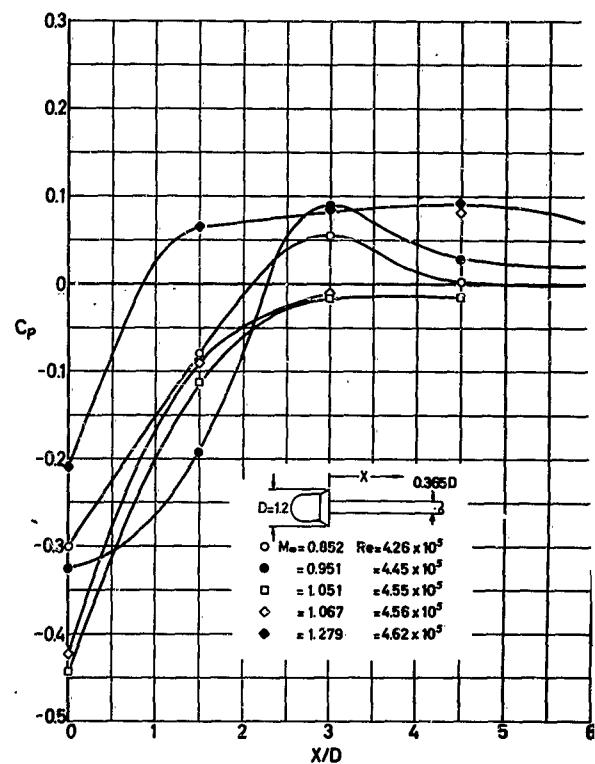


FIG 12. OGIVE CYLINDER AND SKIRTED HEMISPHERE

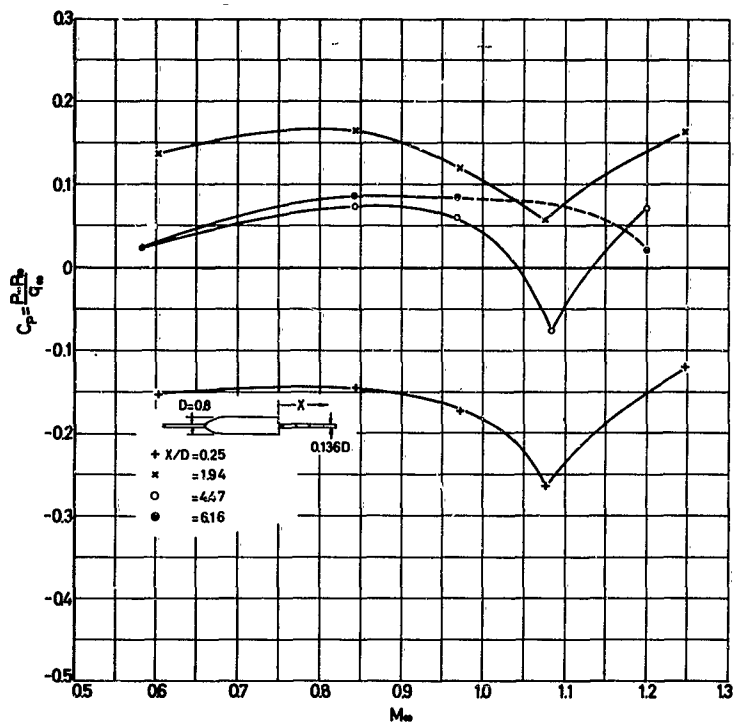


A. OGIVE CYLINDER

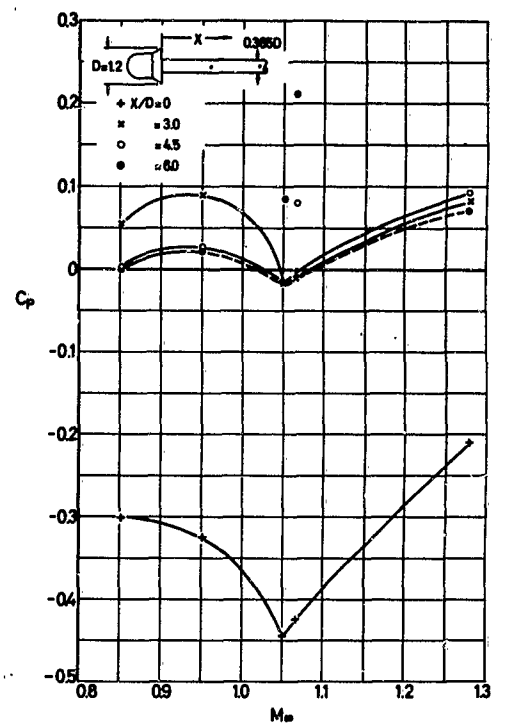


B. SKIRTED HEMISPHERE

FIG 13. STATIC PRESSURE COEFFICIENT NEAR THE AXIS OF THE WAKE AT TRANSONIC SPEEDS



A. OGIVE CYLINDER



B. SKIRTED HEMISPHERE

FIG 14. VARIATION OF STATIC PRESSURE COEFFICIENT WITH MACH NUMBER AT FIXED POINTS IN WAKE

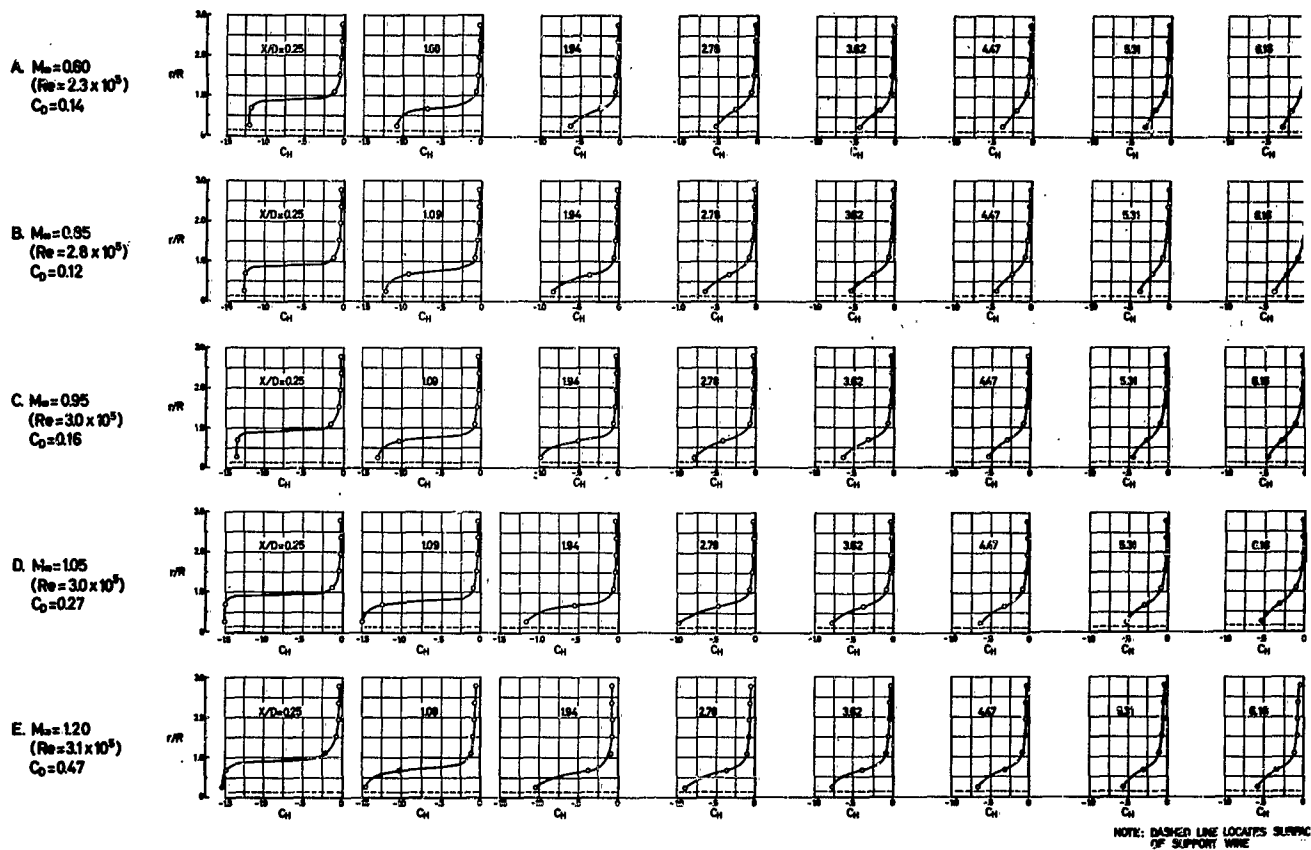


FIG 15. TOTAL PRESSURE COEFFICIENT* IN WAKE OF OGIVE CYLINDER. AT TRANSONIC SPEEDS

(MODEL SUSPENDED ON CENTERLINE WIRE)

$$*C_{H1} = \frac{H_1 - H_\infty}{\frac{1}{2} \rho V_\infty^2}$$

measured by means of a pitot tube with the opening directed towards the free stream velocity. Therefore, these measurements probably do not incorporate the total energy, since the components of the back and cross flow are not registered by such a tube. This is particularly significant close to the base of the body. Considering the total pressure as measured and described, one observes that the wake total pressure shows appreciable reduction from the free stream total pressure and that the pressure recovers towards the free stream total pressure as the downstream distance increases. At the same time the wake width increases as expected and as known from the study of the subsonic wake. Numerical values of these measurements are shown in Table 5 of the Appendix.

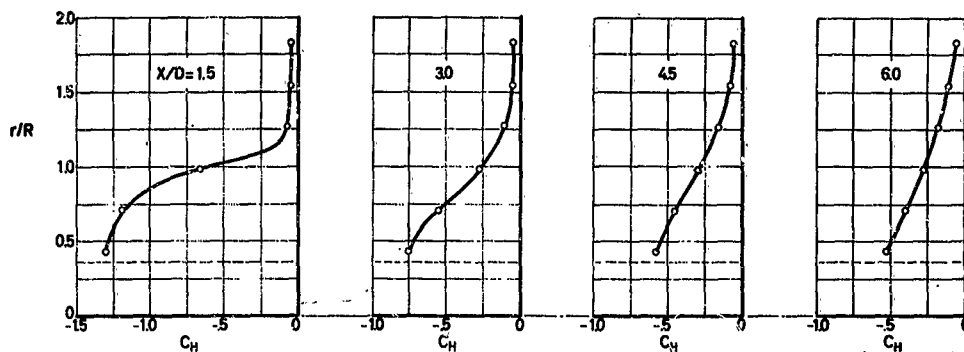
It may be pointed out that the total pressure curves of Fig 15 do not approach the zero line, which would indicate that even at considerable radial distances the energy in the wake is still smaller than in the undisturbed flow. This phenomenon may be explained as follows. In accordance with standard wind tunnel practice, the total pressure of the undisturbed flow has been assumed to be equal to the total pressure in the stilling chamber. However, wind tunnels have energy losses over the distance from the stilling chamber to the test section. This would account for one part of the observed deficiency. Secondly, measuring the total pressure at supersonic speeds is connected with energy loss in the shock wave standing ahead of the opening of the pitot tube. For undisturbed flow certain corrections can be introduced which would account for these deficiencies. However, in view of the uncertainties existing in the wake flow, it appears to be unjustified to apply corrections. Thirdly, the wake widths must increase with the downstream distance with energy from the free stream transferred into the wake area. This transfer of energy is, of course, reflected in the relatively slow approach of the total pressure line towards the zero line.

The numerical deviation as explained under the first two points in the above paragraph represent, however, a small portion of the total pressure level. An inspection of Fig 15 indicates a possible deficiency in the order of 2.5%. In view of the uncertainty of the real flow pattern of the wake and the small numerical amount of the pressure deficiency, it is suggested to adapt Fig 15 as shown.

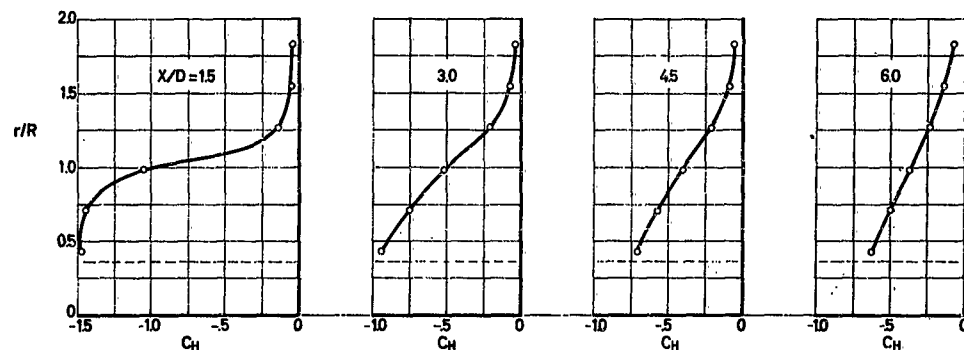
The distribution of the total pressure in the wake of the skirted hemisphere is illustrated in Fig 16. In general the pressure profiles have the characteristic forms of pressure distribution in a turbulent wake.

Comparing the profiles of the ogive cylinder with those of the skirted hemisphere, one notices that the wake of the skirted hemisphere has a stronger tendency of flattening out with increasing downstream distance. Also, the profiles at

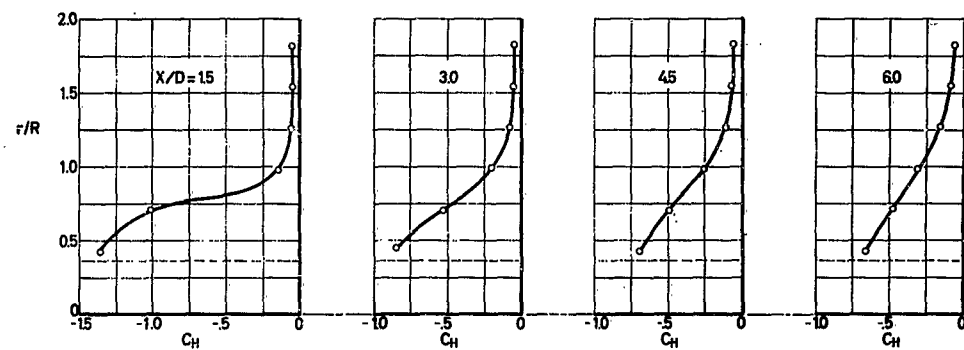
A. $M_\infty = 0.85$
 $(Re = 4.4 \times 10^5)$
 $C_D = 0.46$



B. $M_\infty = 0.95$
 $(Re = 4.6 \times 10^5)$
 $C_D = 0.50$



C. $M_\infty = 1.07$
 $(Re = 4.8 \times 10^5)$
 $C_D = 0.68$



NOTE: DASHED LINE LOCATES
 SURFACE OF STING

D. $M_\infty = 1.28$
 $(Re = 4.8 \times 10^5)$
 $C_D = 0.76$

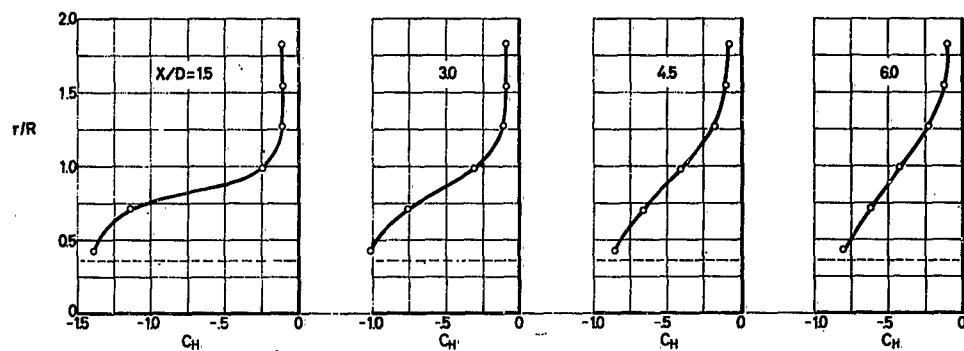


FIG 16. TOTAL PRESSURE COEFFICIENT* IN WAKE OF SKIRTED HEMISPHERE AT
 TRANSONIC SPEEDS

$$* C_H = \frac{H - H_0}{q_\infty}$$

any given downstream distance behind the skirted hemisphere seem to change their form more significantly with Mach number than the similar profiles for the ogive cylinder under the same speed conditions.

Comparing the difference between the total pressure in free stream and in the wake, the pressure losses, of the skirted hemisphere with those of the ogive cylinder, one notices that the skirted hemisphere has in general more pressure loss than the ogive cylinder. Both the stronger widening tendency and the more severe pressure losses of the skirted hemisphere may be understood as a consequence of the higher drag coefficient of the skirted hemisphere. This was also experienced in the studies of the subsonic wake of bodies of various drag coefficients, as may be seen in Ref 7.

The results of the pressure measurement on the skirted hemisphere are subject to the same errors and deviations caused by deficiencies in wind tunnel operations and pressure measurements as explained for the ogive cylinder.

In general, however, it can be seen that the pressure profile of the ogive cylinder and the skirted hemisphere in transonic flow have certain similarities with those observed in the subsonic flow regime.

Based on the recordings of the static and the total pressure, the Mach number in the region near the centerline of the wake was determined. For this purpose, the total pressure was measured as close as possible to the point at which the static pressure was sensed. However, the points are not absolutely identical. On the other hand, it may be assumed that the total and the static pressure at points close to each other can be correlated and a corresponding Mach number may be derived.

The results of these efforts for the ogive cylinder are shown in Fig 17. One observes that the Mach number throughout the entire range of investigation remains subsonic, but the velocity in the wake significantly changes its downstream gradient and its magnitude with the free stream Mach number. Figure 18 shows the same information in dimensionless form for the ogive cylinder and the skirted hemisphere. Comparing these figures, one observes that the Mach number in the wake of the skirted hemisphere is in general lower than in the wake of the ogive cylinder. The increase of the Mach number with downstream distance is, however, about the same for both bodies. The speed in the wake remains in both cases subsonic while the range of the free stream extends from high subsonic to low supersonic velocities.

In view of the back and cross flow components near the base of the primary body, calculated Mach numbers in the near base region appear to be somewhat unrealistic and it is suggested to assume that the values presented in Fig 18

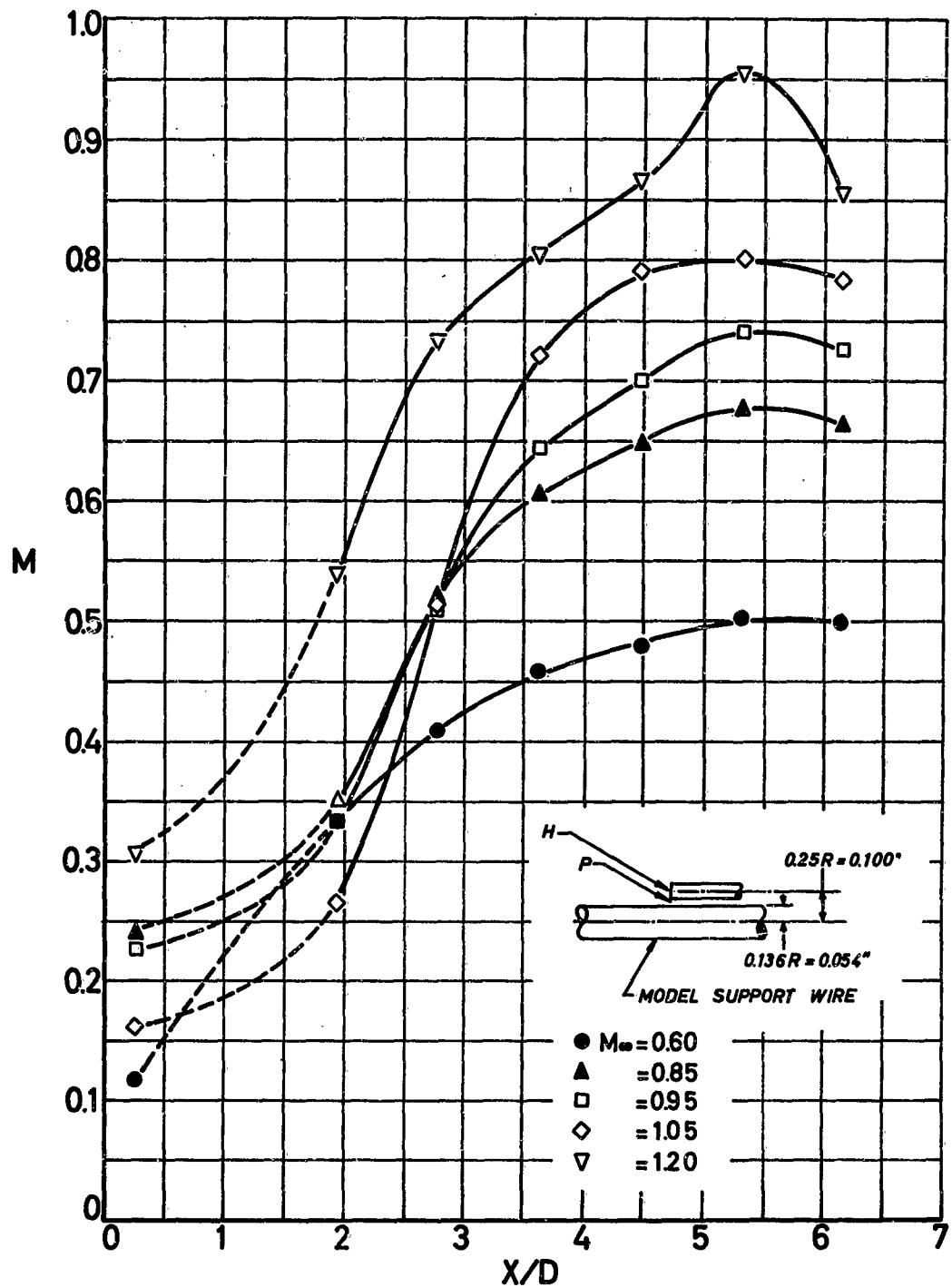


FIG 17. VARIATION OF LOCAL MACH NUMBER NEAR WAKE AXIS OF OGIVE CYLINDER

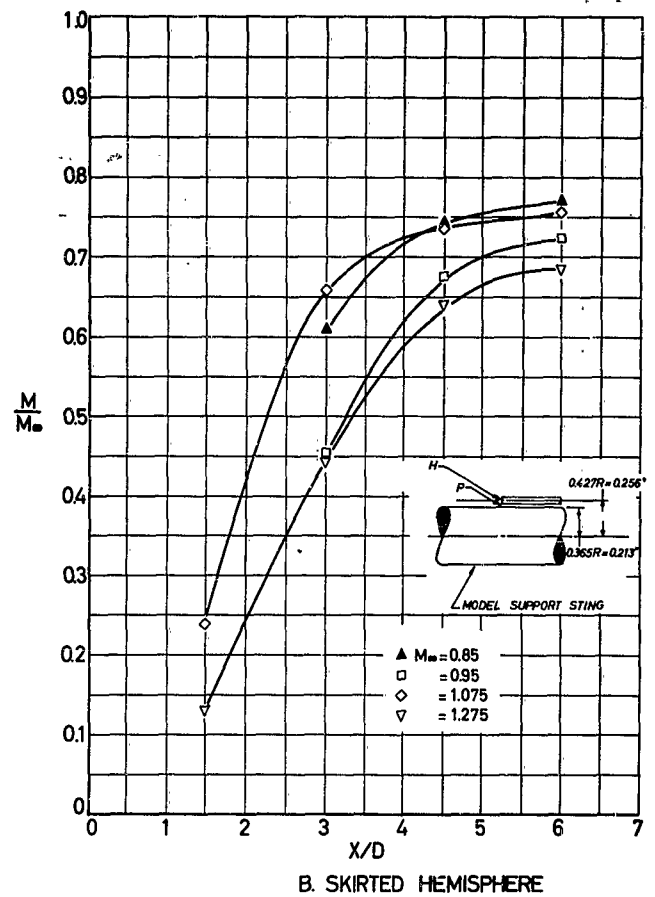
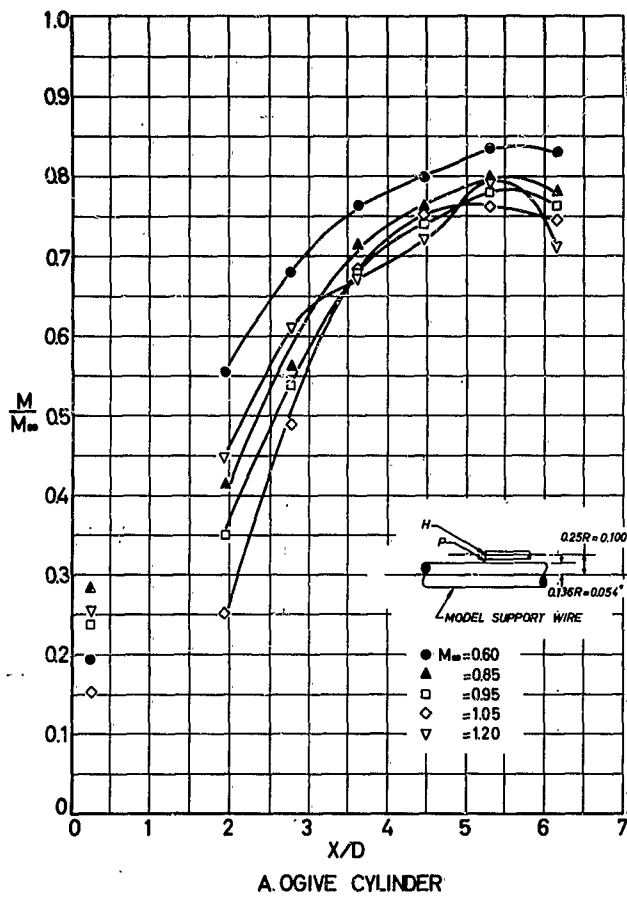


FIG 18. MACH NUMBER NEAR CENTERLINE OF WAKE AT TRANSONIC SPEEDS

indicate the true conditions beginning at approximately 1.5 diameters downstream.

In view of the fact that the Mach number of the wake in both cases stays in the subsonic region and that the subsonic and transonic wakes showed somewhat similar profiles, one may assume that the methods which were successfully applied for the subsonic wake may possibly be useful for the prediction of the velocity and pressure distribution in the wake under transonic flow conditions. For this purpose, it may be necessary to devise a second order approximation, whereas the basic theory is merely based on a number of first order approximations.

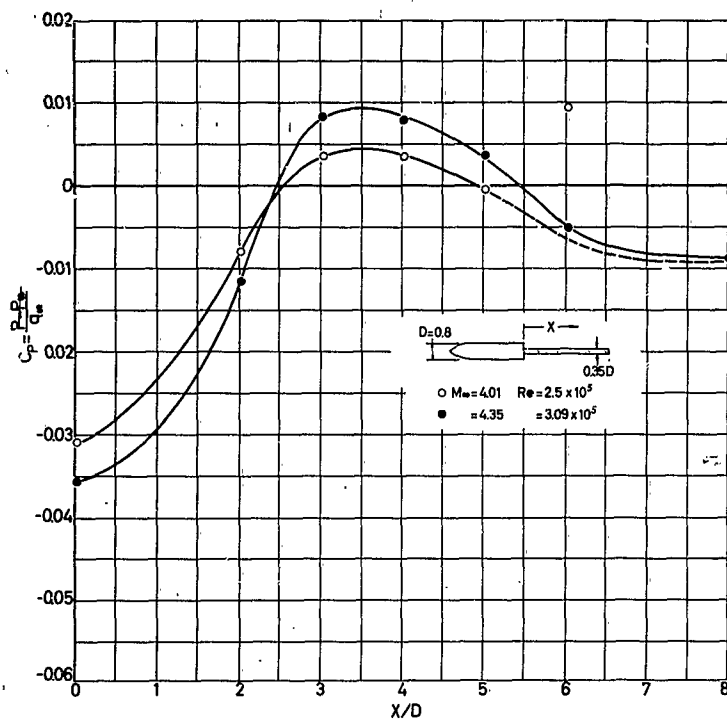
THE SUPERSONIC WAKE

In the supersonic flow regime a reliable interpretation of the measured velocity and pressure distributions is even more difficult because of the flow expansion near the base of the primary body and the trailing shock, both of which show their effect very pronouncedly in the near base region of the wake. In the following, an attempt shall be made to discuss static and total pressure, and the Mach number registered in the downstream region between 0.5 and 8.0 body diameters related to the ogive cylinder and the skirted hemisphere.

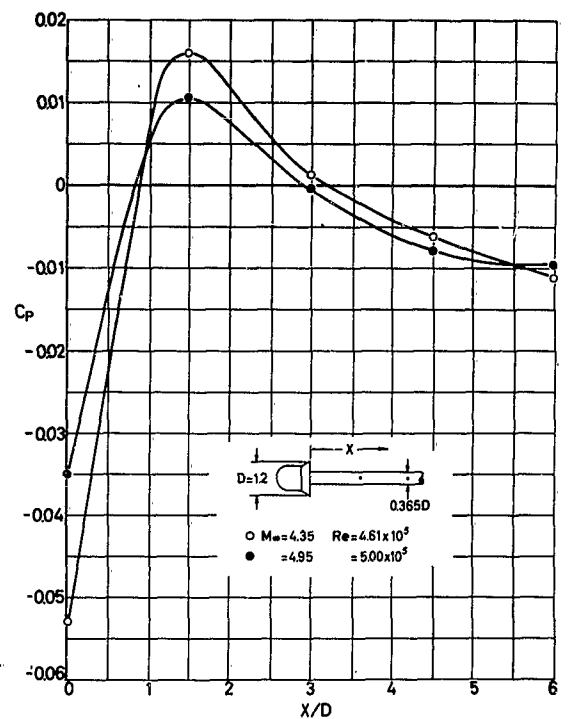
The static pressure coefficient in the wake of the ogive cylinder and the skirted hemisphere at Mach numbers of 4.01 and 4.35, and 4.35 and 5.0 respectively are shown in Figs 19A and B. The numerical values are presented in the Appendix, Tables 3 and 4. In one case the downstream pressure in the wake of the ogive cylinder at $M_\infty = 4.01$ shows an interference from a sting enlargement which was located at $X/D = 8$. This measuring point should be neglected and the curve shown by the dotted line assumed to reflect a more realistic condition.

Comparing the static pressure in the transonic region previously shown in Fig 13 with that in the supersonic region, one notices certain similarities with, however, some changes caused by conditions characteristic for supersonic flow.

The measurements for the ogive cylinder and the skirted hemisphere have the common Mach number of 4.35 which allows an interesting comparison. The skirted hemisphere shows a lower base pressure than the ogive cylinder and a more rapid static pressure increase with downstream distance which causes the pressure maximum to be located closer to the base



A. OGIVE CYLINDER



B. SKIRTED HEMISPHERE

FIG 19. STATIC PRESSURE COEFFICIENT IN CENTERLINE OF WAKE AT SUPERSONIC SPEEDS

of the skirted hemisphere than the observed pressure maximum on the ogive cylinder. This may be understood in view of the flow photographs in Fig 23 which indicate that the origin of the trailing shock wave is closer to the base of the skirted hemisphere than the origin of the trailing shock to the base of the ogive cylinder. Obviously then, the point of shock wave origin is related to the location of the pressure maximum. At a further distance, the static pressure at the centerline of the wake of both bodies appears to approach approximately the same value.

The total pressure in the wake of the ogive cylinder and the skirted hemisphere is illustrated in Figs 20 and 21, respectively, while the related tables with numerical values can be found in the Appendix, Tables 7 and 8.

The pressure curves shown in Fig 20 may be organized in a region close to the body, an intermediate region, and a further downstream region. The close region, from $X/D = 0.5$ to 2.0 , Figs 20B and C, shows near the centerline of the body a relatively low pressure, which also can be found farther downstream. Thereafter, there follows at the position $X/D = 2$, a region of transition in which the expansion following the base of the body is probably reflected. In the intermediate region between $X/D = 2$ and $X/D = 4$, a reversal in the pressure gradient in the radial direction can be observed. This is probably caused by the trailing shock which originates in this range as indicated in Fig 23A. The further out regions, $X/D = 6$ to 8 , show a certain regularity and a monotonous increase of total pressure in the radial direction.

The region close to the base is of minor interest for the functioning of aerodynamic decelerators, but of great importance for the successful operation of compartment and deployment devices. From Figs 20B and C it can be seen that the total pressure close to the body is markedly reduced, but increases quite fast with downstream distance.

It should be noted that Figs 20A, B, and C represent results obtained at slightly different Mach numbers. However, certain similarities and a basic agreement among findings under the various Mach number conditions as well as various locations can be recognized.

The total pressure coefficients were derived from measurements with pitot tubes, but Rayleigh's correction for measurements in the wake was not applied. The free stream total pressure, however, has been corrected for shock wave losses, and therefore the results presented in Fig 20 may be considered a first approximation.

Essentially the same pressure characteristics can be seen from Fig 21 for the skirted hemisphere. Comparing these two graphs for the common Mach number of 4.35 , one notices

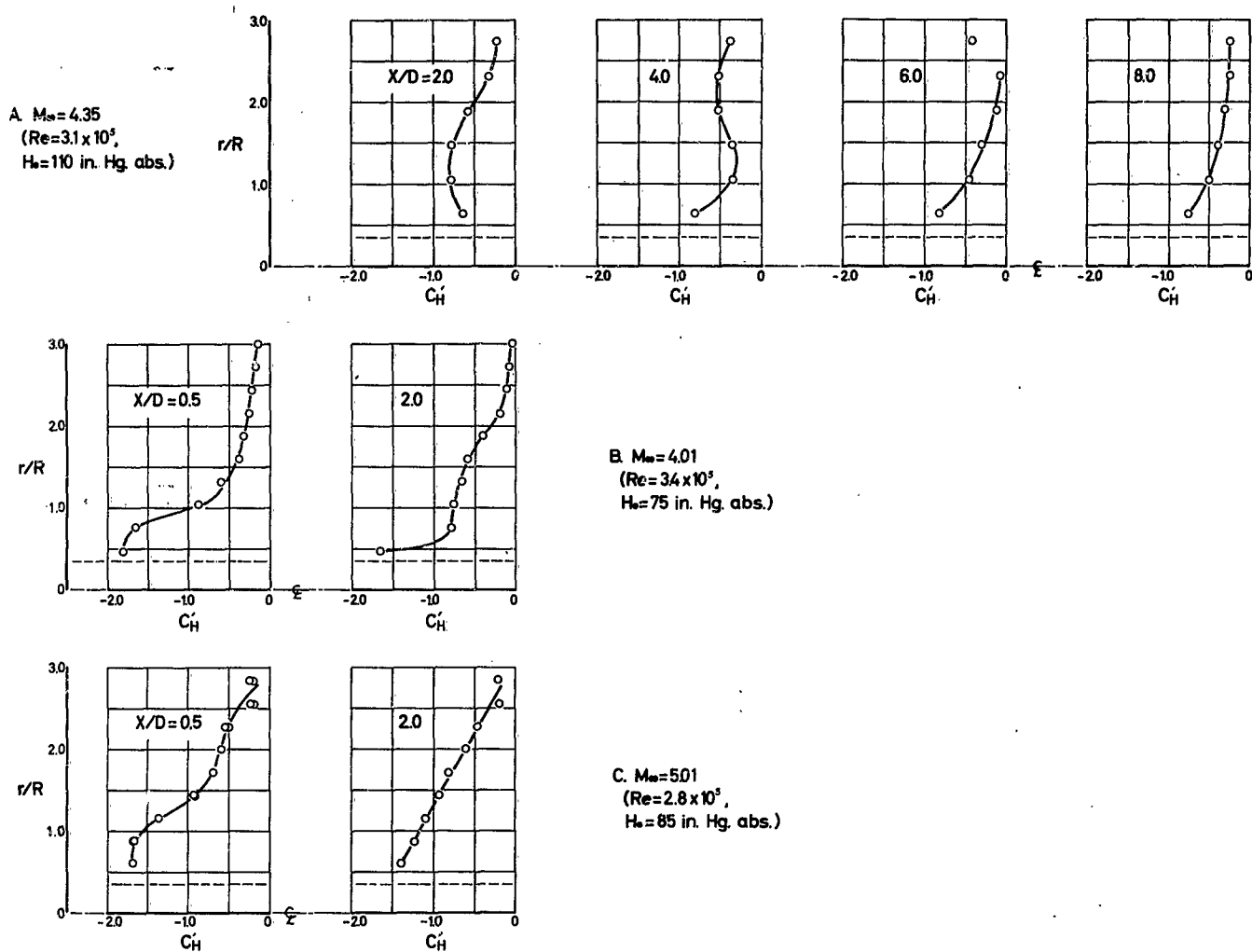
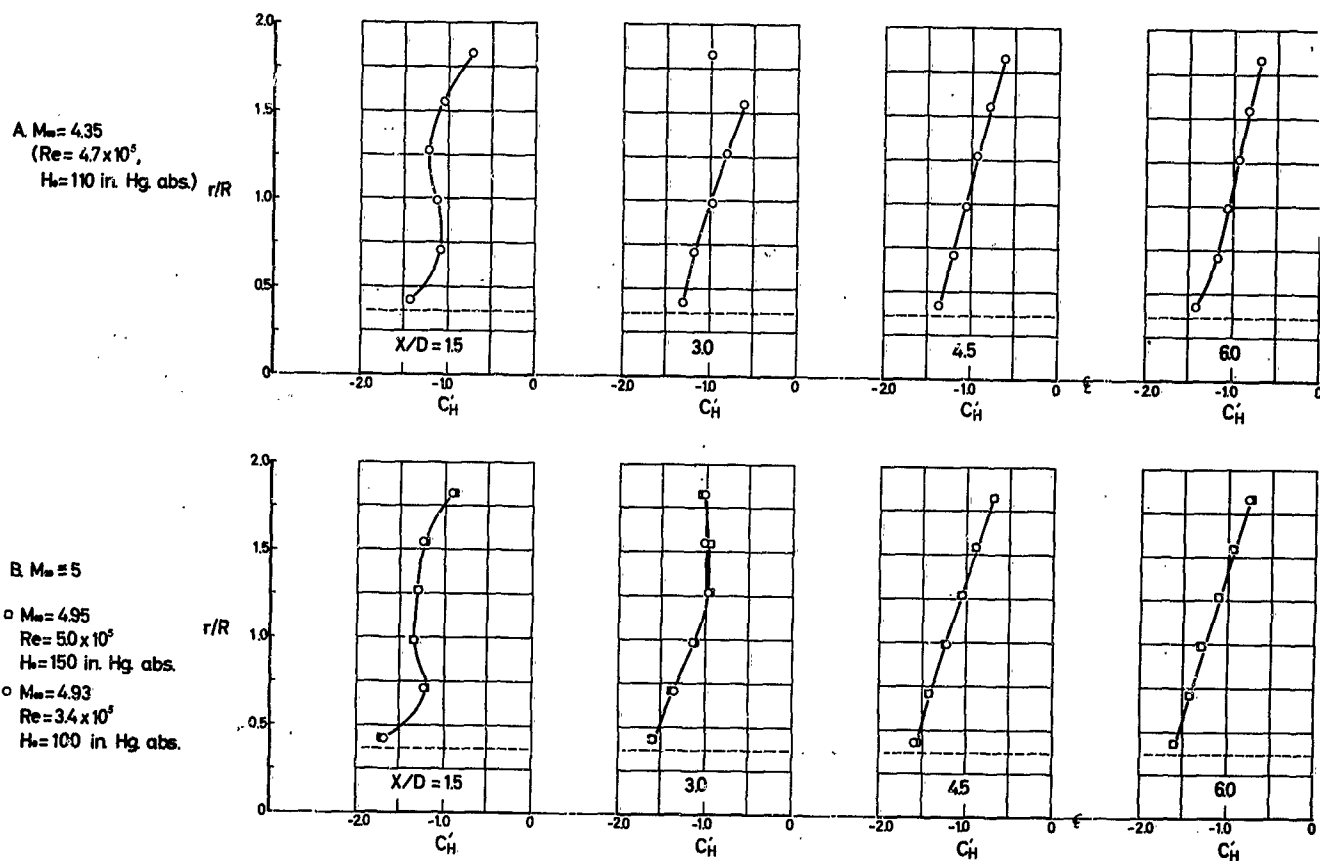


FIG 20. TOTAL PRESSURE COEFFICIENT* IN WAKE OF OGIVE CYLINDER AT SUPERSONIC SPEEDS

$$*C_H = \frac{H - H_\infty}{q_\infty}$$



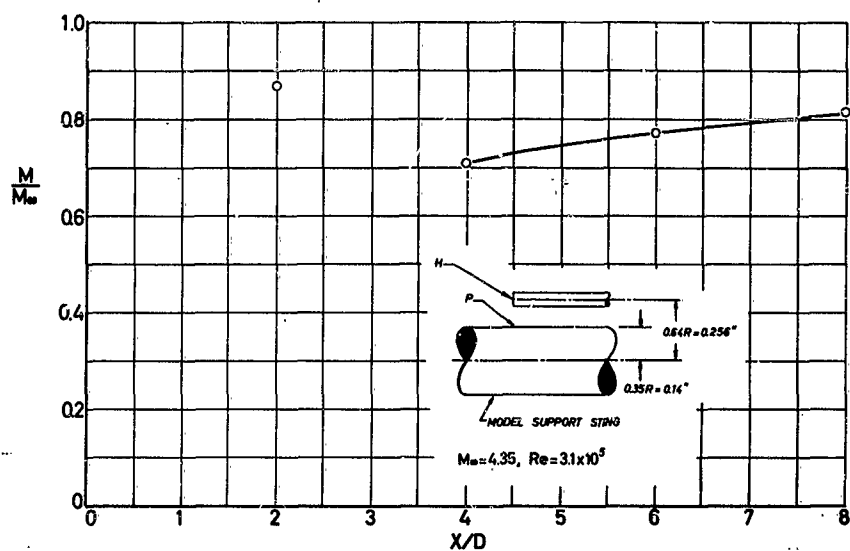
certain similarities in the pressure curves; however, the interferences caused by the trailing shock do occur at different downstream distances.

Furthermore, the total pressure behind the skirted hemisphere is throughout the entire wake lower than the pressure in the wake of the ogive cylinder. In particular, at the comparable position, $X/D = 6$, the total pressure in the wake of the skirted hemisphere amounts to approximately 50% of the pressure at the comparable position behind the ogive cylinder. This statement, however, shall apply only to the regions which are not affected by the trailing shock.

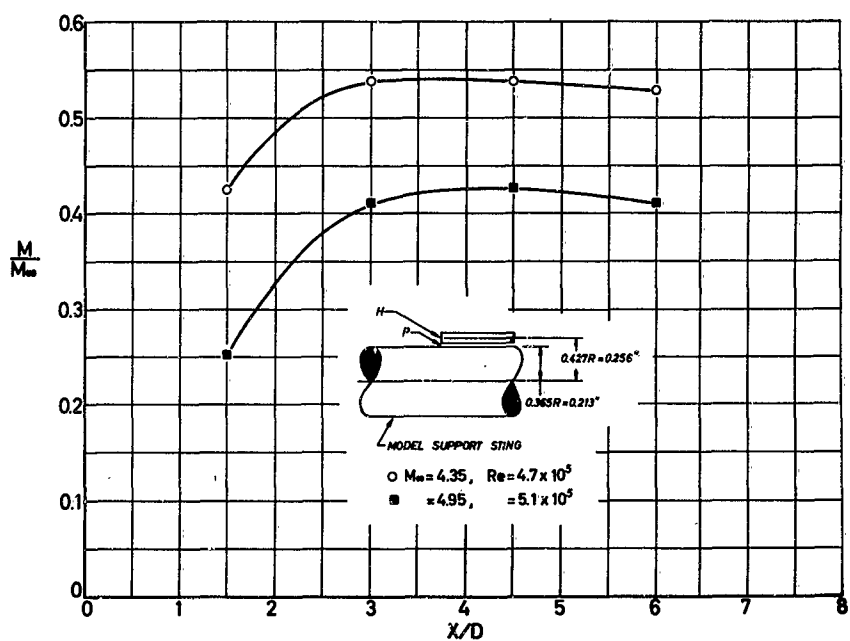
The curves in Fig 21B are for slightly higher Mach numbers, but in principal they show the same conditions with merely minor modifications. It may be pointed out that the results of Fig 21B were also obtained from flow conditions with different Reynolds number. However, it can be seen that the Reynolds number influence apparently is insignificant.

From the static and total pressures, the Mach numbers near the wake axis were calculated and are shown in Fig 22. It can be seen that in the range at which these measurements were made, the velocity in the wake of the skirted hemisphere is in general lower than the velocity behind the ogive cylinder. Furthermore, the velocity increase in the central wake region shows some similarity to those recorded at transonic speeds; however, the wake velocities for supersonic free stream flow are supersonic as well, whereas the velocities in the wake under transonic conditions remained subsonic at these downstream distances.

The Mach numbers presented in Fig 22 do not represent the velocity at the centerline but merely in the central region of the wake, and thus their significance should not be overestimated. On the other hand, since the velocity in the wake is supersonic, principal difficulties for the development of a flow theory do occur because satisfactory assumptions for the shearing stress for compressible fluids as well as the relationship between mixing length and wake widths have not been established as yet. Furthermore, the expansion, the trailing shock wave, and the back and cross flow components in the near body region impose considerable complications. If in an analytical effort these conditions are disregarded, the method may not produce very useful results. Therefore, it appears that at present a thorough experimental investigation of the near body wake region is the only possibility to provide information needed for problems in aerodynamic deceleration.



A. OGIVE CYLINDER



B. SKIRTED HEMISPHERE

FIG 22. MACH NUMBER NEAR CENTERLINE OF WAKE AT SUPERSONIC SPEEDS

THE BOUNDARY LAYER

The results described in this study were compared with findings in Ref 8, which is concerned with the establishment of characteristics indicating the existence of a laminar or turbulent boundary layer. These comparisons showed that the experimental data presented in this study are related to a laminar boundary layer on the primary bodies.

Two flow pictures at supersonic speeds are given in Fig 23 which show the characteristic head waves and the trailing shock waves as well as an indication of the wake boundaries.

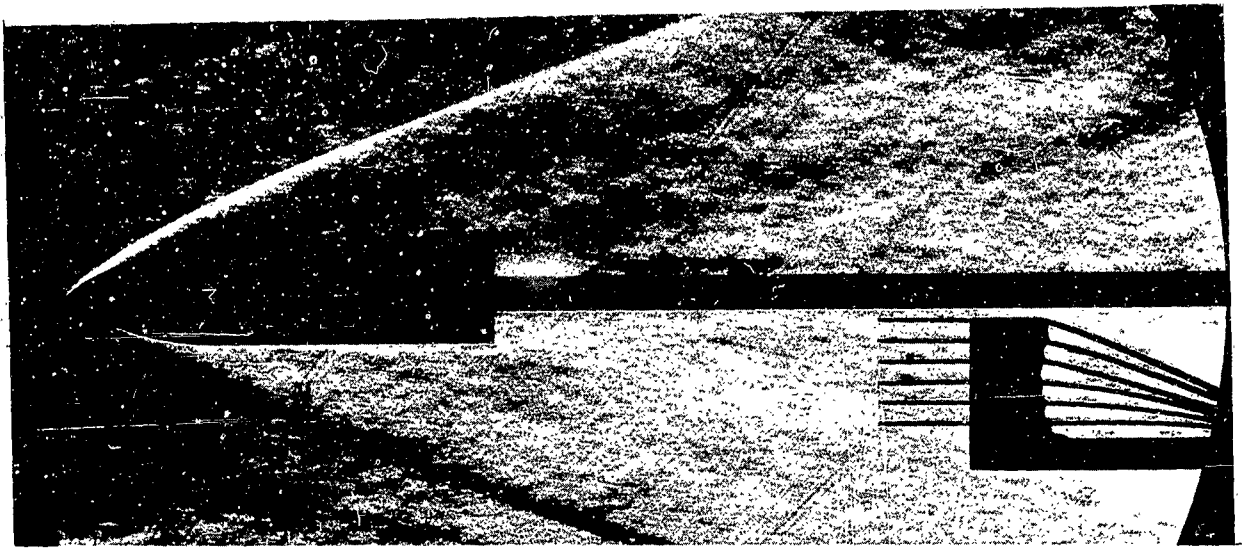
SUMMARY

Experiments indicate that objects which carry a certain resemblance to aerodynamic decelerators suffer a loss in drag when located in the wake of a forebody. The drag deficiency depends on the location of the decelerator, its size relative to the primary body, and the free stream Mach number.

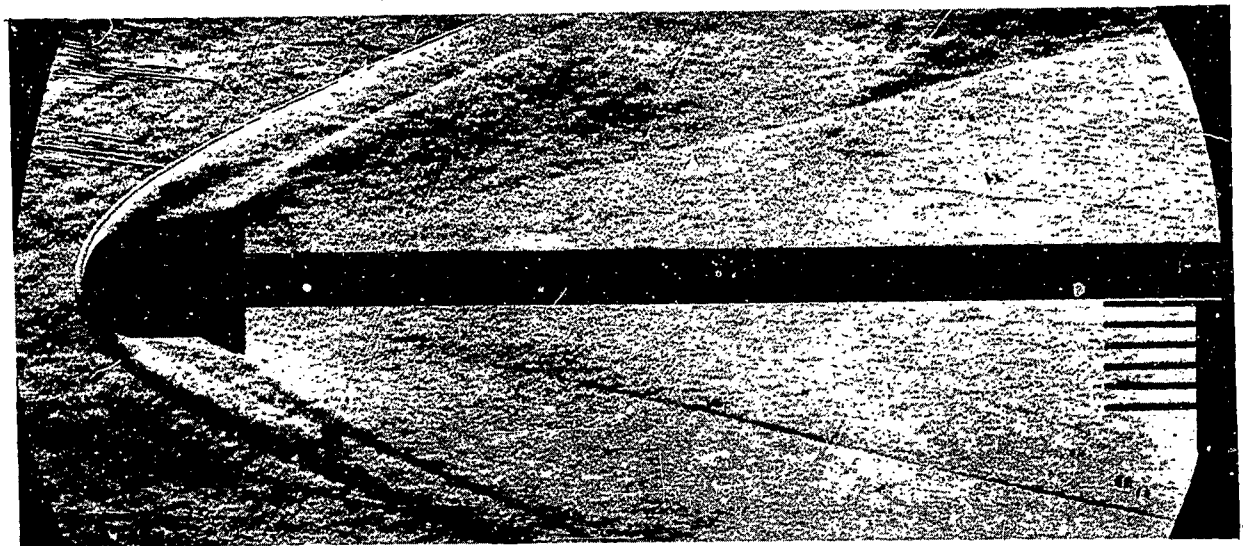
Experimental and theoretical efforts have been made to predict the velocity and pressure distribution in the wake near the body in subsonic flow, and the results of calculations agree satisfactorily with experimental findings.

At transonic free stream velocities the wake near the body is somewhat similar to the wake in subsonic flow regime. It appears that the theoretical approaches which gave very satisfactory results in the subsonic flow regime may be modified and may become useful for the prediction of flow characteristics in the transonic flow regime.

At free stream supersonic Mach numbers the wake in the near body region suffers considerable interferences from flow expansion, a trailing shock, and variation of density. The intensity of these interferences differ with the form of the forebody. In view of the non-existence of the basic assumptions for turbulent shearing stress, mixing lengths, wake widths, and back and cross flow components, an analytical method to predict velocity and pressure distribution in the near body region in supersonic flow is not visualized at present.



A. OGIVE CYLINDER



B. SKIRTED HEMISPHERE

FIG 23. FLOW PATTERNS OF OGIVE CYLINDER AND SKIRTED HEMISPHERE
AT $M_{\infty} = 4.35$

REFERENCES

1. Heinrich, H. G. and Haak, E. L.: The Drag of Cones, Plates, and Hemispheres in the Wake of a Forebody in Subsonic Flow, ASD TR 61-587, December, 1961.
2. Schlichting, H.: Boundary Layer Theory, McGraw Hill, New York, 1955.
3. Swain, L. M.: Turbulent Wake Behind a Body of Revolution Proceedings of the Royal Society of London, Series A, Vol. 125, 1929.
4. Goldstein, S.: On the Velocity and Temperature Distribution in the Turbulent Wake Behind a Heated Body of Revolution, Proceedings of the Cambridge Philosophical Society, Vol. 34, 1938.
5. Heinrich, H. G. and Riabokin, T.: Analytical and Experimental Considerations of the Velocity Distribution in the Wake of a Body of Revolution, WADD TR 60-257, December, 1959.
6. Rubbert, P. E.: Investigation of the Velocity Distribution in the Wake of an Axially Symmetric Body, Master's thesis submitted to the Graduate School of the University of Minnesota, July, 1960.
7. Theoretical Parachute Investigations, Progress Report No. 21, AF 33(616)-8310, Project 6065, Task 60252, 31 May 1962:
8. Reller, J. O., Jr. and Hamaker, F. M.: An Experimental Investigation of the Base Pressure Characteristics of Nonlifting Bodies of Revolution at Mach Numbers from 2.73 to 4.98, NACA TN 3393, March, 1955.

APPENDIX

NUMERICAL VALUES OF PRESSURE COEFFICIENTS

| M_∞ | 0.603 | 0.583 | 0.845 | 0.843 | 0.973 | 0.970 | 1.077 | 1.083 | 1.248 | 1.201 |
|-----------------------------|--------|-------|--------|-------|--------|-------|--------|--------|--------|-------|
| $\frac{Re \cdot 10^5}{X/D}$ | 2.34 | 2.29 | 2.85 | 2.85 | 3.01 | 3.01 | 3.09 | 3.09 | 3.12 | 3.12 |
| 0.25 | -0.152 | | -0.144 | | -0.173 | | -0.263 | | -0.122 | |
| 1.09 | 0.029 | | -0.066 | | -0.145 | | -0.141 | | 0.049 | |
| 1.94 | 0.137 | | 0.165 | | 0.119 | | 0.057 | | 0.164 | |
| 2.78 | 0.064 | | 0.101 | | 0.122 | | -0.011 | | 0.090 | |
| 3.62 | | 0.031 | | 0.077 | | 0.069 | | -0.046 | | 0.079 |
| 4.47 | | 0.025 | | 0.073 | | 0.060 | | -0.076 | | 0.073 |
| 5.31 | | 0.013 | | 0.072 | | 0.068 | | 0.064 | | 0.032 |
| 6.16 | | 0.025 | | 0.087 | | 0.085 | | 0.215 | | 0.021 |

TABLE 1. STATIC PRESSURE COEFFICIENTS* NEAR CENTERLINE OF OGIVE CYLINDER WAKE
AT TRANSONIC SPEEDS

$$* C_p = \frac{P - P_\infty}{q_\infty}$$

| M_∞ | 0.852 | 0.951 | 1.051 | 1.067 | 1.279 |
|----------------------------|--------|--------|--------|--------|--------|
| $x/D \quad Re \times 10^5$ | 4.26 | 4.45 | 4.55 | 4.56 | 4.62 |
| 0 | -0.301 | -0.325 | -0.444 | -0.424 | -0.210 |
| 1.5 | -0.079 | -0.191 | -0.112 | -0.091 | 0.065 |
| 3.0 | 0.055 | 0.090 | -0.016 | -0.010 | 0.083 |
| 4.5 | 0.002 | 0.028 | -0.015 | 0.081 | 0.092 |
| 6.0 | 0 | 0.022 | 0.085 | 0.210 | 0.071 |

TABLE 2. STATIC PRESSURE COEFFICIENTS* NEAR CENTERLINE OF SKIRTED HEMISPHERE WAKE AT TRANSONIC SPEEDS

| M_∞ | 4.01 | 4.35 |
|----------------------------|---------|---------|
| $x/D \quad Re \times 10^5$ | 2.50 | 3.09 |
| 0 | -0.0310 | -0.0357 |
| 2.0 | -0.0079 | -0.0114 |
| 3.0 | 0.0037 | 0.0084 |
| 4.0 | 0.0036 | 0.0079 |
| 5.0 | -0.0002 | 0.0037 |
| 6.0 | 0.0095 | -0.0051 |
| 8.0 | 0.0807 | -0.0087 |

TABLE 3. STATIC PRESSURE COEFFICIENTS* NEAR CENTERLINE OF OGIVE CYLINDER WAKE AT SUPERSONIC SPEEDS

| M_∞ | 4.35 | 4.95 |
|----------------------------|---------|---------|
| $x/D \quad Re \times 10^5$ | 4.61 | 5.00 |
| 0 | -0.0530 | -0.0351 |
| 1.5 | 0.0160 | 0.0106 |
| 3.0 | 0.0012 | -0.0004 |
| 4.5 | -0.0062 | -0.0079 |
| 6.0 | -0.0111 | -0.0094 |

TABLE 4. STATIC PRESSURE COEFFICIENTS* NEAR CENTERLINE OF SKIRTED HEMISPHERE WAKE AT SUPERSONIC SPEEDS

$$* C_p = \frac{P - P_\infty}{q_\infty}$$

A. $M_\infty=0.60$ ($Re=23 \times 10^5$)

| $\frac{x/d}{r/R}$ | 0.25 | 1.09 | 1.94 | 2.78 | 3.62 | 4.47 | 5.31 | 6.16 | 8.62 |
|-------------------|--------|--------|--------|--------|--------|--------|--------|--------|--------|
| 0.25 | -1.202 | -1.078 | -0.622 | -0.531 | -0.439 | -0.383 | -0.330 | -0.324 | -0.286 |
| 0.67 | -1.185 | -0.702 | -0.247 | -0.280 | -0.204 | -0.200 | -0.196 | -0.198 | -0.200 |
| 1.09 | -0.122 | -0.073 | -0.060 | -0.077 | -0.063 | -0.076 | -0.082 | -0.083 | -0.111 |
| 1.52 | -0.050 | -0.051 | -0.043 | -0.043 | -0.042 | -0.052 | -0.056 | -0.047 | -0.057 |
| 1.94 | -0.034 | -0.035 | -0.030 | -0.032 | -0.030 | -0.040 | -0.041 | -0.034 | -0.031 |
| 2.36 | -0.032 | -0.033 | -0.028 | -0.028 | -0.030 | -0.036 | -0.038 | -0.031 | -0.027 |
| 2.78 | -0.026 | -0.033 | -0.027 | -0.023 | -0.016 | -0.026 | -0.031 | -0.023 | -0.020 |

B. $M_\infty=0.85$ ($Re=28 \times 10^5$)

| $\frac{x/d}{r/R}$ | 0.25 | 1.09 | 1.94 | 2.78 | 3.62 | 4.47 | 5.31 | 6.16 | 8.62 |
|-------------------|--------|--------|--------|--------|--------|--------|--------|--------|--------|
| 0.25 | -1.260 | -1.222 | -0.841 | -0.660 | -0.540 | -0.452 | -0.382 | -0.395 | -0.338 |
| 0.67 | -1.246 | -0.925 | -0.374 | -0.350 | -0.265 | -0.245 | -0.230 | -0.256 | -0.265 |
| 1.09 | -0.116 | -0.077 | -0.064 | -0.082 | -0.077 | -0.079 | -0.087 | -0.108 | -0.138 |
| 1.52 | -0.047 | -0.045 | -0.043 | -0.042 | -0.046 | -0.046 | -0.046 | -0.051 | -0.066 |
| 1.94 | -0.034 | -0.032 | -0.031 | -0.031 | -0.034 | -0.033 | -0.033 | -0.035 | -0.034 |
| 2.36 | -0.029 | -0.027 | -0.029 | -0.029 | -0.024 | -0.028 | -0.027 | -0.031 | -0.027 |
| 2.78 | -0.033 | -0.029 | -0.030 | -0.026 | -0.021 | -0.023 | -0.024 | -0.024 | -0.025 |

TABLE 5. TOTAL PRESSURE COEFFICIENTS* IN WAKE OF OGIVE CYLINDER AT TRANSONIC SPEEDS

$$*C_H = \frac{H-H_\infty}{q_\infty}$$

C. $M_{\infty}=0.95$ ($Re=30 \times 10^5$)

| r/R | x/D | 0.25 | 1.09 | 1.94 | 2.78 | 3.62 | 4.47 | 5.31 | 6.16 | 8.62 |
|-------|-------|--------|--------|--------|--------|--------|--------|--------|--------|--------|
| 0.25 | | -1.360 | -1.312 | -0.985 | -0.790 | -0.641 | -0.540 | -0.450 | -0.466 | -0.397 |
| 0.67 | | -1.342 | -1.041 | -0.508 | -0.421 | -0.325 | -0.286 | -0.271 | -0.304 | -0.298 |
| 1.09 | | -0.146 | -0.080 | -0.060 | -0.078 | -0.079 | -0.087 | -0.094 | -0.122 | -0.165 |
| 1.52 | | -0.046 | -0.042 | -0.040 | -0.041 | -0.046 | -0.047 | -0.045 | -0.051 | -0.071 |
| 1.94 | | -0.034 | -0.031 | -0.031 | -0.031 | -0.035 | -0.036 | -0.034 | -0.033 | -0.032 |
| 2.36 | | -0.031 | -0.027 | -0.030 | -0.030 | -0.031 | -0.031 | -0.032 | -0.028 | -0.027 |
| 2.78 | | -0.032 | -0.032 | -0.030 | -0.030 | -0.030 | -0.029 | -0.028 | -0.026 | -0.028 |

D. $M_{\infty}=1.05$ ($Re=30 \times 10^5$)

| r/R | x/D | 0.25 | 1.09 | 1.94 | 2.78 | 3.62 | 4.47 | 5.31 | 6.16 | 8.62 |
|-------|-------|--------|--------|--------|--------|--------|--------|--------|--------|--------|
| 0.25 | | -1.503 | -1.498 | -1.172 | -0.975 | -0.769 | -0.638 | -0.533 | -0.538 | -0.442 |
| 0.67 | | -1.498 | -1.250 | -0.547 | -0.480 | -0.381 | -0.328 | -0.300 | -0.325 | -0.291 |
| 1.09 | | -0.123 | -0.090 | -0.056 | -0.072 | -0.087 | -0.087 | -0.088 | -0.108 | -0.121 |
| 1.52 | | -0.042 | -0.050 | -0.036 | -0.035 | -0.043 | -0.043 | -0.039 | -0.043 | -0.048 |
| 1.94 | | -0.029 | -0.038 | -0.029 | -0.025 | -0.033 | -0.031 | -0.029 | -0.029 | -0.028 |
| 2.36 | | -0.024 | -0.035 | -0.030 | -0.023 | -0.030 | -0.028 | -0.027 | -0.025 | -0.029 |
| 2.78 | | -0.026 | -0.036 | -0.034 | -0.030 | -0.029 | -0.028 | -0.027 | -0.027 | -0.029 |

TABLE 5. (CONTINUED)

E. $M_\infty=1.20$ ($Re=3.1 \times 10^5$)

| r/R | x/d | 0.25 | 1.09 | 1.94 | 2.78 | 3.62 | 4.47 | 5.31 | 6.16 | 8.62 |
|-------|-------|--------|--------|--------|--------|--------|--------|--------|--------|--------|
| 0.25 | | -1.515 | -1.462 | -1.050 | -0.890 | -0.765 | -0.667 | -0.561 | -0.580 | -0.482 |
| 0.67 | | -1.490 | -1.024 | -0.366 | -0.360 | -0.356 | -0.313 | -0.303 | -0.334 | -0.301 |
| 1.09 | | -0.217 | -0.122 | -0.089 | -0.098 | -0.088 | -0.085 | -0.100 | -0.122 | -0.142 |
| 1.52 | | -0.042 | -0.100 | -0.077 | -0.080 | -0.066 | -0.054 | -0.069 | -0.091 | -0.096 |
| 1.94 | | -0.029 | -0.084 | -0.075 | -0.069 | -0.051 | -0.041 | -0.052 | -0.085 | -0.083 |
| 2.36 | | -0.024 | -0.070 | -0.076 | -0.059 | -0.044 | -0.037 | -0.041 | -0.075 | -0.074 |
| 2.78 | | -0.026 | -0.059 | -0.075 | -0.049 | -0.038 | -0.032 | -0.036 | -0.050 | -0.064 |

TABLE 5. (CONCLUDED)

A. $M_\infty=0.85$ ($Re=4.4 \times 10^5$)

| x/D r/R | 1.5 | 3.0 | 4.5 | 6.0 |
|----------------|--------|--------|--------|--------|
| 0.43 | -1.258 | -0.727 | -0.590 | -0.535 |
| 0.71 | -1.130 | -0.522 | -0.457 | -0.407 |
| 0.99 | -0.567 | -0.240 | -0.302 | -0.297 |
| 1.27 | -0.053 | -0.079 | -0.157 | -0.185 |
| 1.55 | -0.047 | -0.047 | -0.080 | -0.107 |
| 1.83 | -0.045 | -0.045 | -0.057 | -0.065 |

C. $M_\infty=1.075$ ($Re=4.8 \times 10^5$)

| x/D r/R | 1.5 | 3.0 | 4.5 | 6.0 |
|----------------|--------|--------|--------|--------|
| 0.43 | -1.355 | -0.840 | -0.693 | -0.668 |
| 0.71 | -1.004 | -0.533 | -0.490 | -0.468 |
| 0.99 | -0.170 | -0.201 | -0.260 | -0.307 |
| 1.27 | -0.052 | -0.078 | -0.106 | -0.157 |
| 1.55 | -0.050 | -0.056 | -0.060 | -0.083 |
| 1.83 | -0.053 | -0.049 | -0.054 | -0.060 |

B. $M_\infty=0.95$ ($Re=4.6 \times 10^5$)

| x/D r/R | 1.5 | 3.0 | 4.5 | 6.0 |
|----------------|--------|--------|--------|--------|
| 0.43 | -1.463 | -0.939 | -0.708 | -0.627 |
| 0.71 | -1.428 | -0.782 | -0.572 | -0.496 |
| 0.99 | -1.041 | -0.506 | -0.398 | -0.378 |
| 1.27 | -0.140 | -0.207 | -0.205 | -0.237 |
| 1.55 | -0.040 | -0.075 | -0.088 | -0.134 |
| 1.83 | -0.041 | -0.048 | -0.056 | -0.070 |

D. $M_\infty=1.275$ ($Re=4.8 \times 10^5$)

| x/D r/R | 1.5 | 3.0 | 4.5 | 6.0 |
|----------------|--------|--------|--------|--------|
| 0.43 | -1.390 | -1.007 | -0.851 | -0.795 |
| 0.71 | -1.148 | -0.757 | -0.669 | -0.615 |
| 0.99 | -0.259 | -0.306 | -0.411 | -0.429 |
| 1.27 | -0.113 | -0.108 | -0.175 | -0.228 |
| 1.55 | -0.113 | -0.088 | -0.098 | -0.125 |
| 1.83 | -0.115 | -0.085 | -0.085 | -0.096 |

TABLE 6. TOTAL PRESSURE COEFFICIENTS* IN WAKE OF SKIRTED HEMISPHERE AT TRANSONIC SPEEDS

$$*C_H = \frac{H-H_0}{q_\infty}$$

A. $M_\infty=4.35$ ($Re=31 \times 10^5$)

| $r/R \backslash x/D$ | 2.0 | 4.0 | 6.0 | 8.0 |
|----------------------|--------|--------|--------|--------|
| 0.64 | -0.659 | -0.810 | -0.823 | -0.756 |
| 1.06 | -0.791 | -0.342 | -0.454 | -0.502 |
| 1.48 | -0.786 | -0.352 | -0.297 | -0.383 |
| 1.90 | -0.586 | -0.515 | -0.124 | -0.303 |
| 2.32 | -0.321 | -0.509 | -0.069 | -0.234 |
| 2.74 | -0.220 | -0.371 | -0.424 | -0.232 |

B. $M_\infty=4.01$ ($Re=34 \times 10^5$)

| $r/R \backslash x/D$ | 0.5 | 2.0 |
|----------------------|--------|--------|
| 0.47 | -1.812 | -1.660 |
| 0.76 | -1.650 | -0.796 |
| 1.04 | -0.871 | -0.770 |
| 1.32 | -0.602 | -0.661 |
| 1.60 | -0.385 | -0.597 |
| 1.88 | -0.322 | -0.406 |
| 2.16 | -0.256 | -0.200 |
| 2.44 | -0.220 | -0.117 |
| 2.72 | -0.181 | -0.078 |
| 3.00 | -0.147 | -0.043 |

C. $M_\infty=5.01$ ($Re=2.8 \times 10^5$)

| $r/R \backslash x/D$ | 0.5 | 2.0 |
|----------------------|--------|--------|
| 0.60 | -1.673 | -1.392 |
| 0.88 | -1.665 | -1.239 |
| 1.16 | -1.360 | -1.103 |
| 1.44 | -0.940 | -0.946 |
| 1.72 | -0.706 | -0.820 |
| 2.00 | -0.612 | -0.620 |
| 2.28 | -0.548 | -0.470 |
| 2.56 | -0.230 | -0.197 |
| 2.84 | -0.249 | -0.215 |
| | | |

TABLE 7. TOTAL PRESSURE COEFFICIENTS* IN WAKE OF OGIVE CYLINDER AT SUPERSONIC SPEEDS

$$*C_H' = \frac{H-H_\infty}{q_\infty}$$

A. $M_\infty=4.35$ ($Re=4.7 \times 10^6$)

| $r/R \backslash x/D$ | 1.5 | 3.0 | 4.5 | 6.0 |
|----------------------|--------|--------|--------|--------|
| 0.43 | -1.427 | -1.296 | -1.353 | -1.406 |
| 0.71 | -1.080 | -1.176 | -1.190 | -1.166 |
| 0.99 | -1.124 | -0.979 | -1.045 | -1.055 |
| 1.27 | -1.223 | -0.809 | -0.938 | -0.935 |
| 1.55 | -1.044 | -0.605 | -0.786 | -0.828 |
| 1.83 | -0.729 | -0.994 | -0.615 | -0.702 |

B. $M_\infty=4.93$ ($Re=3.4 \times 10^6$)

| $r/R \backslash x/D$ | 1.5 | 3.0 | 4.5 | 6.0 |
|----------------------|--------|--------|--------|--------|
| 0.43 | -1.680 | -1.599 | -1.597 | -1.606 |
| 0.71 | -1.235 | -1.354 | -1.423 | -1.433 |
| 0.99 | -1.346 | -1.144 | -1.214 | -1.302 |
| 1.27 | -1.297 | -0.969 | -1.050 | -1.095 |
| 1.55 | -1.255 | -1.028 | -0.896 | -0.944 |
| 1.83 | -0.911 | -1.014 | -0.693 | -0.766 |

C. $M_\infty=4.95$ ($Re=5.0 \times 10^6$)

| $r/R \backslash x/D$ | 1.5 | 3.0 | 4.5 | 6.0 |
|----------------------|--------|--------|--------|--------|
| 0.43 | -1.692 | -1.532 | -1.553 | -1.582 |
| 0.71 | -1.207 | -1.387 | -1.418 | -1.413 |
| 0.99 | -1.343 | -1.126 | -1.248 | -1.291 |
| 1.27 | -1.300 | -0.960 | -1.056 | -1.095 |
| 1.55 | -1.217 | -0.951 | -0.884 | -0.931 |
| 1.83 | -0.888 | -1.053 | -0.674 | -0.744 |

TABLE 8. TOTAL PRESSURE COEFFICIENTS* IN WAKE OF SKIRTED HEMISPHERE AT SUPERSONIC SPEEDS

$$* C_p = \frac{H - H_\infty}{q_\infty}$$

**RELIABILITY OF RECOVERY SYSTEMS --
EVALUATION AND ATTAINMENT**

by

George Chernowitz

Director, American Power Jet Company

ABSTRACT

The factors which must be considered in evaluating the reliability of a proposed recovery system, and the appropriate mathematical methods and models for this purpose are discussed. Key points of engineering and critical components, as well as sources for reliability assessment, will be covered. Additional topics will include: Component versus system reliability; the roles of design, checkout and human factors; the attainment and demonstration of reliability.

RELIABILITY OF RECOVERY SYSTEMS-EVALUATION AND ATTAINMENT

INTRODUCTION

During recent years, the lead time required to bring new weapon systems into the field has become a matter of deep concern to all members of the weapons development community. No small contributor to this problem has been that of reliability; a system is not judged to be truly "operational" unless it meets acceptable standards of reliable performance. Since reliability in the mission is the essential criterion for determining when a system is satisfactory, steps which can help select the required level of reliability and to speed its attainment and demonstration are desirable.

This is particularly true in the early stages of a weapon system development. The more complicated the system, and the greater the required advance in the state-of-the-art, the more important does the reliability specification and preliminary assessment during the design phases become. In the extreme case, the reliability required by the specification may be shown to be so difficult to attain that the system becomes obsolete before the acceptable reliability level is reached.

The advancement in the scope of application, in the sophistication of aerodynamic decelerators from the World War II cargo and personnel parachute to present day satellite recovery systems, have extended and taxed the ingenuity of science and technology in the fields of aerodynamics, thermodynamics, textiles and other materials, equipment design and operation. The place of reliability in the structure of progress is of the greatest interest and has major implications for research, design and development, and application.

UNIFIED DESIGN FOR WEAPONS SYSTEM RELIABILITY

Reliability design begins with the very statement of the operational mission and a consideration of the technology available to accomplish it. It is futile to speak of missions and goals without considering the means available to attain them. They are in a feedback relationship.

The mission specifies a function and the natural and induced environments within which they occur; a state-of-the-art produces a capability in that same envelope of environments. If the mission is well within the state-of-the-art, then it may be reconsidered to take advantages of capabilities not otherwise utilized. On the other hand, if major state-of-the-art development is necessary in order to meet the mission requirement, then a decision must be reached as to whether there are sufficient funds and time available to undertake the development, or whether the means selected to achieve the mission must be reconsidered.

Reliability design begins with an analysis of the mission requirements, the envelope of natural and induced environments which are encountered, and the technology which is applicable. By matching the levels of effort which are available with the mission requirements, balancing factors such as cost, development time, facilities and trading against a level of reliability that can be achieved in each of these directions, a reliability level can be chosen which is within the practical realm of possibility. A unified design philosophy therefore "previews" the decelerator life history including the phases of design, test, manufacture, storage and transportation and application. For each of these stages the reliability specification must cover:

1. The specific natural environments which will be encountered by the decelerator system. This must include not only density-altitude, temperature and the other factors encountered in use, but specify these in terms, so far as possible, of the probability of encounter so that adequate weight can be given in the analysis.
2. The induced environment, i.e., that environment which is caused by the functioning of the system, may then be superposed on the natural environments. Care must, of course, be taken to combine these properly, taking account of the interactions of environments and combined environmental effects. For example, shock loading depends not only on the design of the parachute, but also on altitude, release velocity, and loading. A change in

these factors for a given parachute has changed the induced environment which it sees.

There is advantage in separating the natural and induced environments for analysis purposes since the same decelerator may be used in several missions in the same natural environment.

Finally, the criteria of "success" must be clearly specified, particularly the areas in which degraded performance or variability in performance is acceptable. It should be pointed out that under actual conditions, both natural and induced environments have a statistical uncertainty, frequently of considerable extent. These measures are the initial steps in the reliability analysis and evaluation procedure.

RELIABILITY DEFINED

The assessment of parachute reliability, either from design or from test data gathered during a developmental and test program, is a problem which must be approached in a logical step by step manner if meaningful results are to be obtained. A number of key concepts are involved which facilitate our consideration of this.

Reliability is inversely related to the expected rate of failure. It is defined as:

Reliability = $1 - \text{Expected Rate of Failure}$.

The important concept is the term "expected rate of failure": The calculated reliability of the system cannot be used to forecast the performance of a single example of that system in a single use. It gives the "odds", but does not foretell the result of any single event.* / It refers to the number of successful uses to be expected when a large number of identical systems are to be used, or when a given system is used a large number of times. Thus,

* / Of course, if the "odds" are high enough in practical life situations, we behave as though we are dealing with certainty.

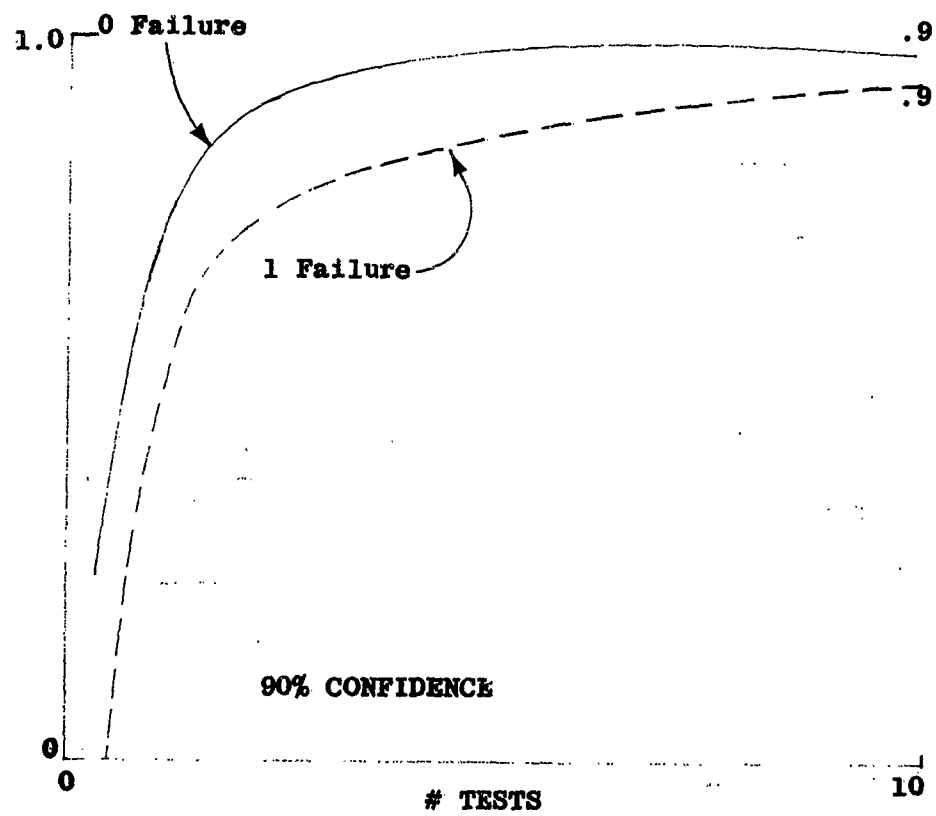


FIG. 1 PRACTICAL VIEWPOINT - ONE SHOT RELIABILITY

reliability may be defined as the probability of successful operation of a decelerator system under given conditions in the long run.

However, the definition as specified requires emphasis on three terms: (1) "successful operation", (2) "given conditions", and (3) "long-run".

The "successful operation" depends on the specific mission of the decelerator in the application under analysis. Thus, the basic function of a parachute may be merely to land a load without damage in a general area. In such a case, the loss of a panel from a canopy may scarcely affect the reliability of a parachute in the mission.

On the other hand, in cases where both the deceleration of the load and the achievement of a reasonable precise touchdown point are vital, failure of the single panel may so change the trajectory of the parachute system and load that the mission might be a failure even though the decelerator functions of the parachute have been accomplished successfully. Thus, mission analysis is a vital factor in determining specific requirements which dictate a "successful operation" of a parachute system.

The "given conditions" which must be specified for any set of reliability data can also vary radically for given missions. For example, a significant contribution to the success or failure of a parachute system is the release conditions. A study of the stresses which are placed on the various canopy members during parachute deployment and descent has indicated that for each given portion of the decelerator system deployment and operation, a given range of stresses will be seen by each component of the canopy. Factors which contribute towards this are the specific conditions of each deployment; tumbling of the load, gusts, specific manner in which the canopy unfolds, etc. Superimposed on all these factors are, of course, the velocity of the delivery vehicle, details of release, and aircraft attitude. Release conditions which have proven highly satisfactory for one application have resulted in operational unreliability in another.

The "long-run" specifies the total population (in theory, infinite) which is being considered. For either single or repeated-use systems, reliability does not specify the performance of a single example in a single use, but is the limiting proportion of successes over a series of missions; the required number depends on the variability which we are willing to accept.

DECELERATOR RELIABILITY MODEL

Granting a sound definition of each of the qualifying terms of reliability, an appropriate reliability model may be selected. * / This, as we shall see, consists of dividing the system under analysis into a series of individual non-interacting components. Such non-interacting "building blocks" may properly be combined in a multiplicative model. Inasmuch as operational factors, e.g., packing, release conditions and the like, are involved, a term or series of terms must also be inserted for these factors. (Reference 1) The resulting reliability model may then be stated as follows:

$$R = R_p (R_{c_1} \cdot R_{c_2} : \dots \cdot R_{c_n})$$

Where R = System Reliability
 R_p = Operational Reliability
 R_c = Component Reliability

The multiplicative model has the great advantage of close correspondence to the actual decelerator components under analysis; e.g., canopy, reefing line cutters, etc. Therefore, component data from a diversity of sources may be used (with suitable judgment) for preliminary assessment or prediction. The component approach also has the advantage that it can utilize laboratory test data, engineering computations or actual field use experience with identical components in other systems, to compute the reliability of

* / By "sound definition" we mean one which is clearly specified and verifiable and which applies unambiguously to each stage of the decelerator life history.

a complete system prior to the availability of test data on the new assembly.

SINGLE USE RELIABILITY

In any given parachute mission, the performance of the parachute depends on the success or failure of each operation in sequence rather than repeated use. In reliability terminology, it is characterized as a "one shot or single use". That is to say, at each stage we choose between two mutually exclusive events (success and failure). This is appropriately described by the Binomial Distribution, which expresses mathematically the probability that failure will occur exactly x times in n independent trials of the system, where p is the expected probability of failure (Figure 2).

The application of the Binomial Distribution involves calculating factorials and although increasingly extensive tables are available (Reference 2), it is highly convenient to use the Poisson Approximation (Figure 2). The Poisson Approximation is excellent when the expectation of failure is very small. Only one factorial is involved and numerical manipulations are considerably simplified (Reference 3).

REPEATED USE RELIABILITY

Discussion thus far has implied that the parachute is used once in its lifetime. While this is true for a system used to decelerate a weapon, the usual man-carrying parachute, aircraft decelerator and cargo parachute may be used for several missions. In this case, it is necessary to establish the effect of prior use on reliability. Such factors as wear, age, damage on landing, weakening of fabric by number of previous loadings, effects of exposure to sunlight, etc., during previous usage must be evaluated.

This problem is basically one of determining whether the inspection or repair process which follow the parachute use prior to packing for the next mission returns the parachute to the equivalent of new condition. This can usually be determined by the facts of individual cases. If it is known that the re-used parachute is equivalent from a reliability viewpoint to a new parachute, then the

BINOMIAL DISTRIBUTION

$$F(x) = \frac{N!}{x!(N-x)!} p^x (1-p)^{N-x}$$

POISSON DISTRIBUTION

$$F(x) = \frac{\theta^x e^{-\theta}}{x!}$$

X = Number of Events

θ = Expected Value of x

FIGURE 2. FAILURE PROBABILITY DISTRIBUTIONS

analysis proceeds as if the parachute were a single use item. If it is found that inspection or repair does not return the parachute to its as new condition, then allowance must be made for the deteriorating effect of prior use in assessing parachute successive use.

SERIES VS. PARALLEL ELEMENTS

Redundancy and parallel functions are powerful means available to increase reliability. If a given function can be performed independently by two non-interacting mechanisms, then the functioning of the system no longer depends on a single component but rather on the assembly. It is therefore necessary to consider those functions which are performed by components which operate in series or in parallel.

A series component is defined as one which must operate successfully if the parachute system is to operate successfully in its mission and is represented by a single term in the reliability model (Figure 3). One example of such a component is a riser; another, generally, is a suspension line, since experience has shown that the breaking of one suspension line throws so great a load on the neighboring lines that they usually break also.

Parallel components (those which are designed as redundant subsystems) have more than one component performing the same function with the design such that the operation of any one will insure system success. Such arrangements in parachute systems are often found in reefing line cutters, where two or even four may be used on the same canopy, and the functioning of any one will cut the reefing line. A second example is that of the interstage disconnects, where two disconnect mechanisms are often installed, and a functioning of either will serve to separate the stages. The entire redundant system is represented in the model by a single term. In such a case, the component reliability term is calculated from the redundant reliability formula. For any number of parallel components, the reliability term of the parallel subsystem will be shown by the following:

$$R_b = 1 - (1 - R_{b_1}) (1 - R_{b_2}) \dots (1 - R_{b_n})$$

$$R = R_{C_1} \cdot R_{C_2} \cdot R_{C_3} \cdot R_{C_4} \cdot R_{C_5} \cdot R_{C_6} \cdot R_{P_1} \cdot R_{P_2}$$

C₁ - 1st CANOPY LINES

C₂ - REEFING CUTTERS

C₃ - DISCONNECT

C₄ - 2nd CANOPY LINES

C₅ - 2nd CANOPY RISERS

C₆ - REEFING CUTTERS

P₁ - 1st CANOPY PACKING

P₂ - 2nd CANOPY PACKING

FIG. 3. PARACHUTE COMPONENTS - SERIES INTERACTION

where the reliability of the parallel system, R_p , will be dependent on the reliability of each of its n parallel components.

RELIABILITY ASSESSMENT

The simplest method to evaluate the reliability of a decelerator system which has been tested numbers of times under the actual conditions of operations is to calculate the failure rate observed, i.e., the number of failures observed divided by the total number of drops. The best single numerical estimate of the reliability of this system is the observed failure rate subtracted from unity.

Although this is satisfactory under some conditions, the accuracy of such a point estimate depends on the number of trials which were made and the distribution of the failure rates about the average. It must be realized that the single number value gives no information about the degree of confidence that may be placed in this number as a true measure of the potential performance of the system. Thus, it is quite possible that the true reliability is either lower or higher than the point estimate obtained from experiment.

To take into account the possibility that the true reliability may be lower or higher, a more refined measure of reliability is needed. The basis for this type of reliability value, the confidence-interval estimate, asserts that the true reliability value will be found in an "interval" with a given probability.

To present a little clearer illustration of the significance of point estimate as opposed to confidence interval, Figure 4 shows a typical example of the evaluation of a given set of data. The reliability point estimate is measured as approximately .94. However, an evaluation of the data on the basis of a 90% confidence interval indicates that we have a 90% chance of finding the true value between 86% and 100% in a series of tests; a 95% chance of finding the value between 84% and 100%. The

higher the confidence insisted upon, the wider the interval. */ Of course, the relative magnitude of the confidence interval depends on the sample size being tested; The larger the sample size, the shorter the interval for any level of confidence.

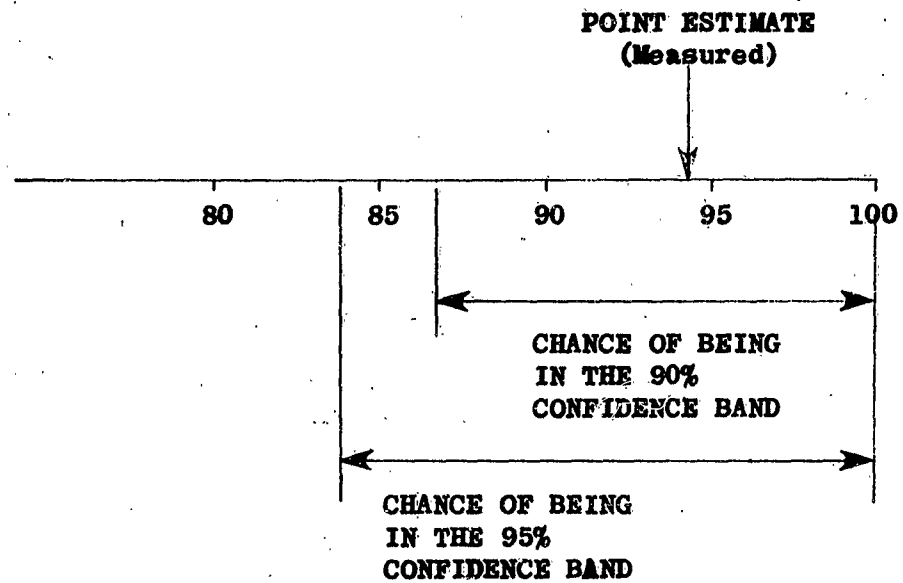
STRESS-STRENGTH RELATIONSHIPS

The preceding discussion describes a reliability philosophy and a model which is applicable to decelerators. The primary input is, of course, test results and observed performance. **/ However, it is both feasible and sound to use the results of design analysis. This procedure we may call "Stress-Strength Technique". It consists in determining the probability that the stress placed on the component will not exceed the strength of the component.

Even in theoretically repetitive situations, the actual stress placed on a component from one event to another will vary. Similarly, the characteristics of components of given design will differ from one unit to another because of manufacturing tolerances, materials variability, quality control, and specification tolerances. The purpose of stress-strength analysis is to determine the distribution of strengths and the distribution of stresses in commensurate terms and to consider the degree of overlap of the two distributions. This is considered the failure probability area and is a measure of the risks occasioned by placing the stress and strength values

*/ For a clear discussion of the confidence interval see "The Advanced Theory In Statistics", M.G. Kendall, A. Stuart, London, 1948-1962 (Reference 4). For an elementary discussion, "Introduction to Mathematical Statistics", Hoel, 1954 (Reference 5).

**/ Observations are available by both formal and informal means. The writer recalls watching a movie travelog of parachute resupply of a New Guinea exploring party in which low altitude drops resulted in six perfect, two streamers and one unopened!



THE SAMPLE SIZE DETERMINES
THE CONFIDENCE BAND

FIG. 4 RELIABILITY ESTIMATES POINT
VS CONFIDENCE INTERVAL

in a given relationship. This approach appears in other fields of engineering as "margin of safety" or, less properly, safety factor design philosophy. Thus, when a design is completed and the results of calculations are multiplied by a safety factor or "taking the next larger size", the designer is implicitly introducing the stress-strength approach, but without giving a quantitative measure of its meaning. Reliability analysis converts this intuitive procedure to values that can be used as a consistent part of the decelerator reliability assessment technique. There is a considerable body of experience which suggests that the random failures are well described by a normal distribution. (For that is precisely what we mean when we say that we are considering variability due to a very large number of causes, each of which is insufficiently important to be taken into account, but which are important when taken together).

To characterize the normal distribution for the purpose of this analysis, it is necessary to have the mean and variance both of the stress and the strength. From the point of view of reliability analysis, the variance or standard deviation is of extreme importance. Considering only the distribution of the strength for the moment, we may inspect Figure 5. In those cases where the standard deviation is high, the probability that some values will fall below the maximum stress level becomes exceedingly important, indicating that the component will fail under these conditions. Only where the standard deviation is sufficiently small, will the system being analyzed have a relatively high reliability.

A starting point in a stress-strength reliability analysis is the determination of the form of the distribution of the strength of a component with respect to the most likely modes of failure and the determination of the distribution of the stresses which will cause these failures. Figure 6 shows the stresses and strength of a single component measured in the same physical dimensions. In this example, the overlap between the two distributions represents the probability that the stress will be greater than the strength and that the system will fail. The probability that the strength (S) of a given component item will lie between any two given points, for example,

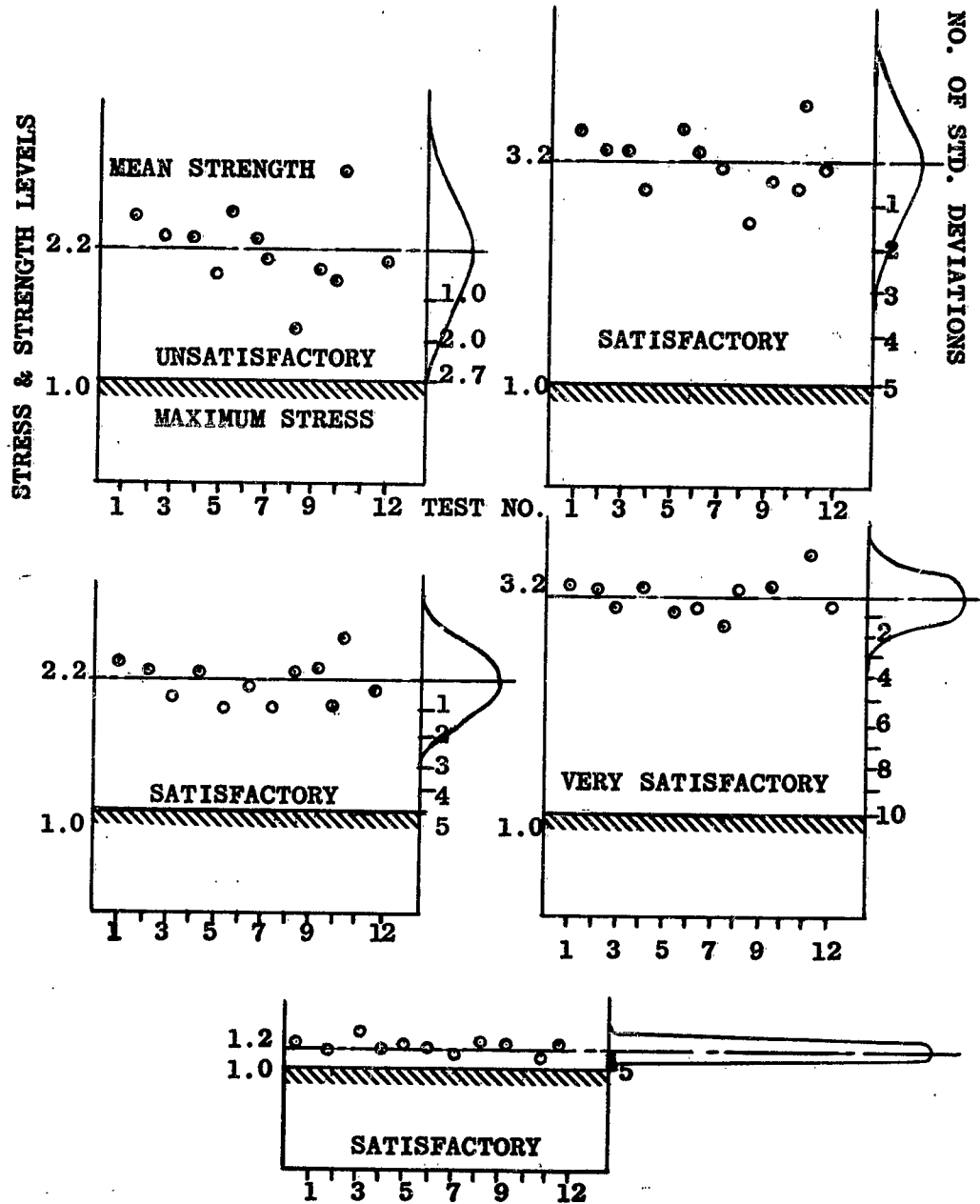


FIG. 5 EFFECT OF STANDARD DISTRIBUTION OF STRENGTH
ON RELIABILITY

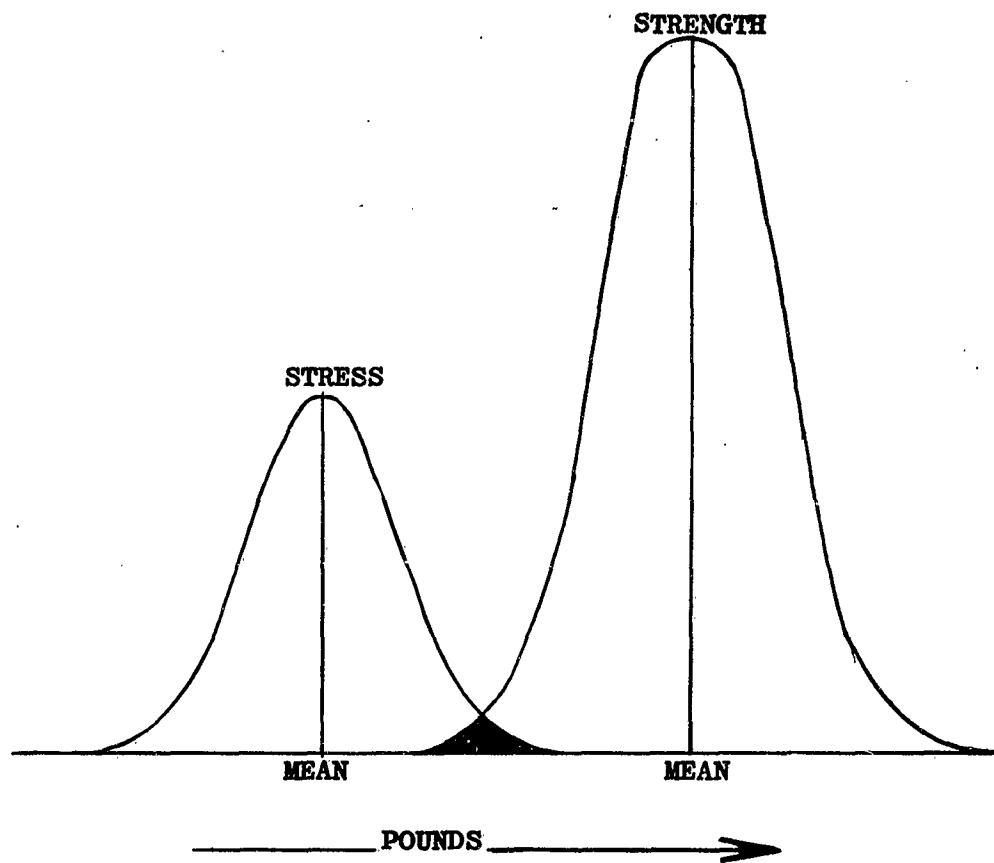


FIG. 6 TYPICAL STRESS-STRENGTH DISTRIBUTION

x_1 and $x_1 + dx$, is given by:

$$P(x_1 < S < x_1 + dx) = g(x_1) dx$$

where $g(x_1)$ = Strength probability density function

The probability that the stress (E) on a given trial does not exceed x_1 is:

$$P(E < x_1) = \int_0^{x_1} f(x) dx$$

where $f(x)$ = Stress probability density function.

The reliability of the component when subject to the stress will then be the integral of the two products over all possible values of x :

$$R = \int_0^{\infty} \left[\int_0^{x_1} f(x) dx \right] g(x_1) dx$$

where R = Reliability

This expression is the probability that a given strength is experienced, and that the stress is not greater than this value. The reliability can, of course, be calculated, in the order of integration with appropriate changes in limits.

These integrals generally cannot be solved directly; however, a graphical method may be employed. The integrals can be evaluated by letting

$$F(x) = \int_0^x f(x) dx, \quad G(x) = \int_0^x g(x_1) dx$$

so that

$$dG(x) = g(x_1) dx$$

and

$$R = \int_0^1 F dG$$

To evaluate this equation, F is plotted as a function of G, as shown on Figure 7, both being functions of the independent variable x. The area under the curve is equal to the reliability. This area may be measured by a planimeter or by counting squares.

For phenomena which are normally distributed, the respective functions may be evaluated in a straightforward manner. Here, the failure probability is designated as the probability that the strength will be less than the stress. The probability density functions can thus be expressed as:

$$g(x) = \frac{1}{\sqrt{2\pi} \sigma_1} \exp -\left(\frac{(x_1 - \mu_1)^2}{2 \sigma_1^2}\right)$$

σ_1 = Standard deviation of strength

μ_1 = Mean Strength

and the stress probability distribution as

$$f(x) = \frac{1}{\sqrt{2\pi} \sigma_2} \exp -\left(\frac{(x - \mu_2)^2}{2 \sigma_2^2}\right)$$

σ_2 = Standard deviation of stress

μ_2 = Mean Strength

The distribution of the difference between the two:

$$D = x_1 - x_2$$

is in itself a normal distribution with mean given by:

$$\mu = \mu_2 - \mu_1$$

and standard deviation by:

$$\sigma = \sqrt{\sigma_1^2 + \sigma_2^2}$$

The distribution of the difference will be given by:

$$f(D) = \frac{1}{\sqrt{2\pi} \sigma} \exp -\left(\frac{(D - \mu)^2}{2 \sigma^2}\right)$$

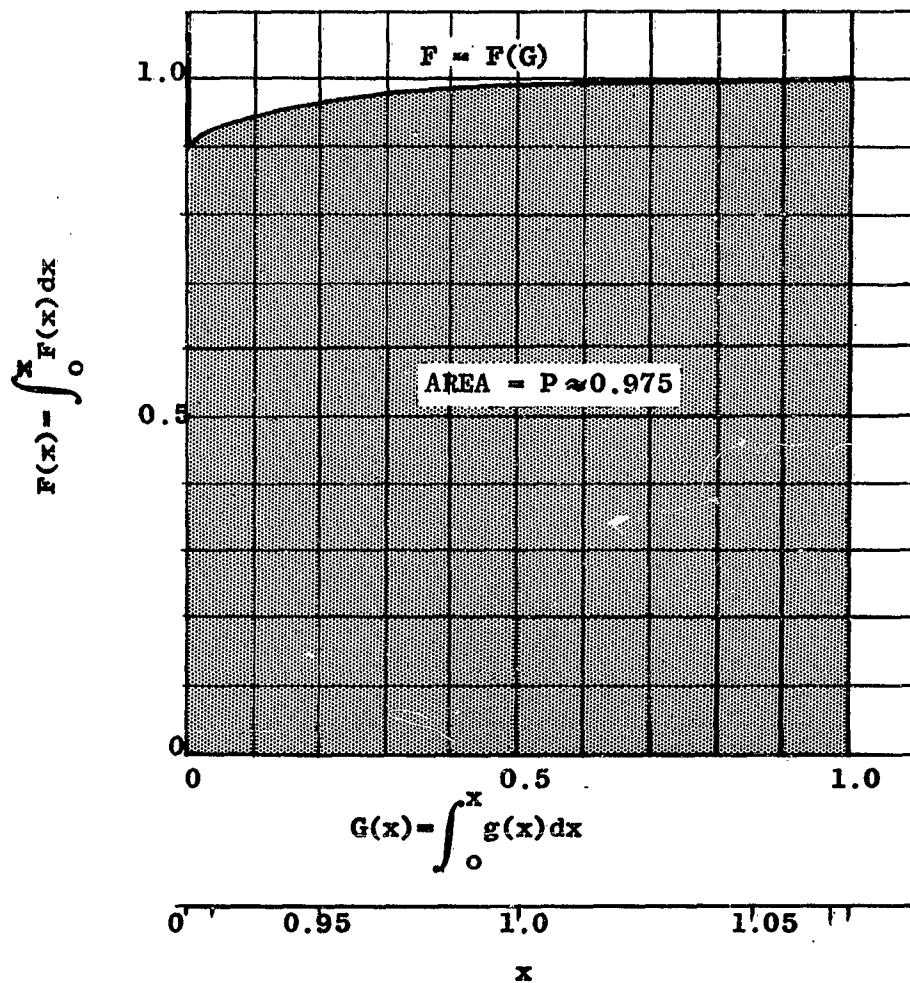


FIG. 7 GRAPHICAL METHOD OF EVALUATING RELIABILITY

The failure probability, that is, the probability that the difference between stress and strength is negative, or less than zero, may then be found by evaluating the integral:

$$P_f = \int_{-\infty}^0 \frac{1}{\sqrt{2\pi} \sigma} \exp - \left(\frac{(D-\mu)^2}{2\sigma^2} \right) dD$$

which can be done readily from standard statistical tables (Reference 6).

The application of this type of computational technique to the reliability analysis of a component which fails by a mechanism resulting from either excess load or severe environmental stress is relatively straightforward for point reliability estimates. It may be extended to interval-type reliability estimates on a somewhat more complex theoretical basis and by a more difficult computational method. */

SAMPLE SIZE AND CONFIDENCE INTERVAL

The proof of the pudding is in the eating and the demonstration of reliability involves the collection of experimental data. The problem arises how much experimental data is required before we can have confidence in our results. Phrased more precisely, what is the tradeoff between the sample size and the confidence coefficient? We can choose a very high confidence coefficient, i.e., have an extremely small risk of being wrong, at the price of very large sample sizes, or we can accept a very small number of tests at a much lower confidence. Engineering common sense and the system analysis provides appropriate guidance. If the component is relatively small, light and inexpensive, and the system can readily be designed to achieve redundancy, then a high system reliability can be attained with components of comparatively low individual reliability. Conversely, a critical and expensive component may merit very extensive effort. This decision is essentially a matter of economics. Figure 8 is a generalized plot of the relative cost of testing versus the desired confidence coefficient (Reference 7). It can be seen that

*/ See discussion in APJ Report 259-1, issued as WADD-TR 60-200 (Reference 1).

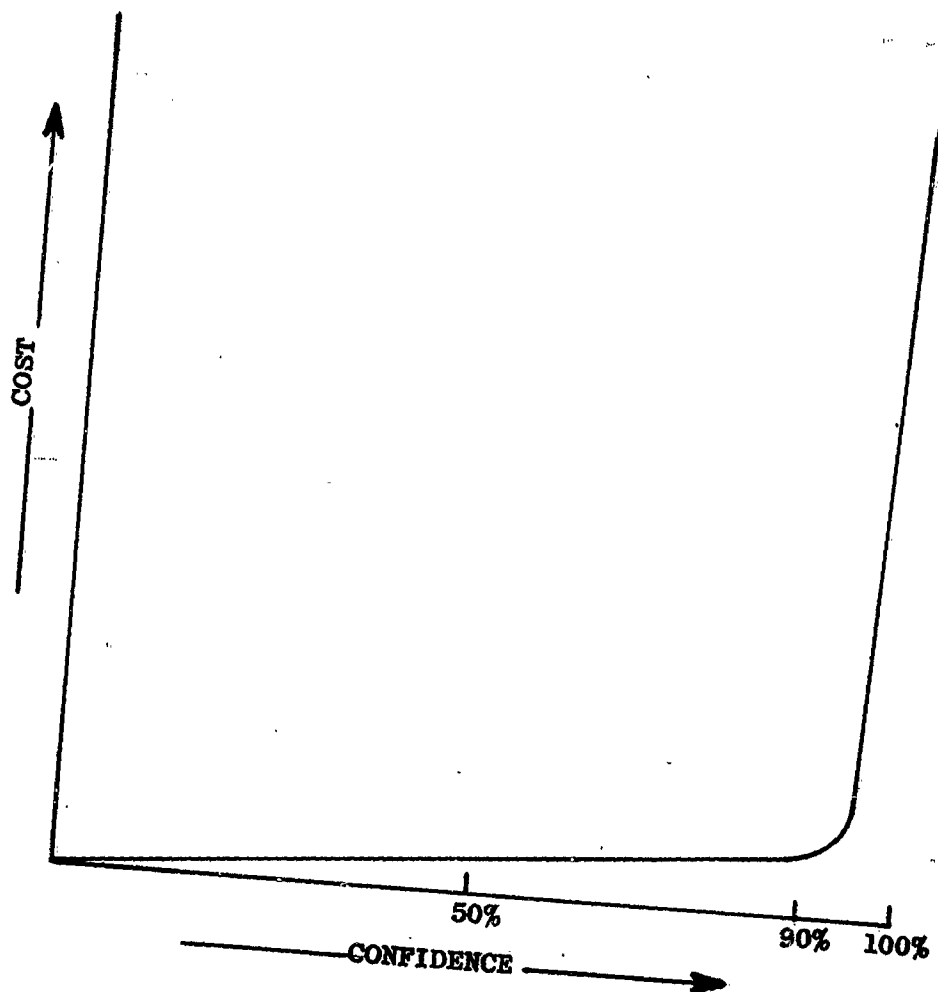


FIG. 8 COST OF TESTING TO A GIVEN
CONFIDENCE COEFFICIENT

the major increase in cost begins at about 90% confidence and rises very sharply thereafter. Obviously 100% confidence has no real meaning since its achievement requires an infinite number of tests.

From a system point of view, we may want to work to alternative confidence intervals for individual components so that the system cost as a whole is minimized.

An indication of the relative number of items which must be tested at 90% and 99% confidence levels in order to assert a given level of reliability is an indication of the level of effort required and is given in Figure 9.

For example, if no failures whatsoever are encountered in testing, over 20 systems must be tested to be sure of .90 reliability at a 90% confidence level. If assurance of .98 reliability is desired at 90% confidence, approximately 100 systems must be tested without a single failure. Increased confidence levels, of course, will increase the number of systems to be tested. For example, at 99% confidence, 50 systems must be tested without failure to assure .90 reliability; no failures in the testing of 100 systems will assure only .93 reliability.

By the use of sequential procedures, the number of tests which must be performed can be reduced to some extent, possibly by as much as 50%, but the required amount of testing remains quite considerable.

Testing facility and budget limitations are practical constraints. However, the procedures which we have outlined provide a practical measure for the degree of uncertainty which is a built-in consequence of a given budgetary or testing decision. The acceptability of this risk is a matter for decision by the weapon system manager.

SUMMARY

USES OF RELIABILITY

The result of the determination of reliability of a decelerator system can be used to evaluate the long run

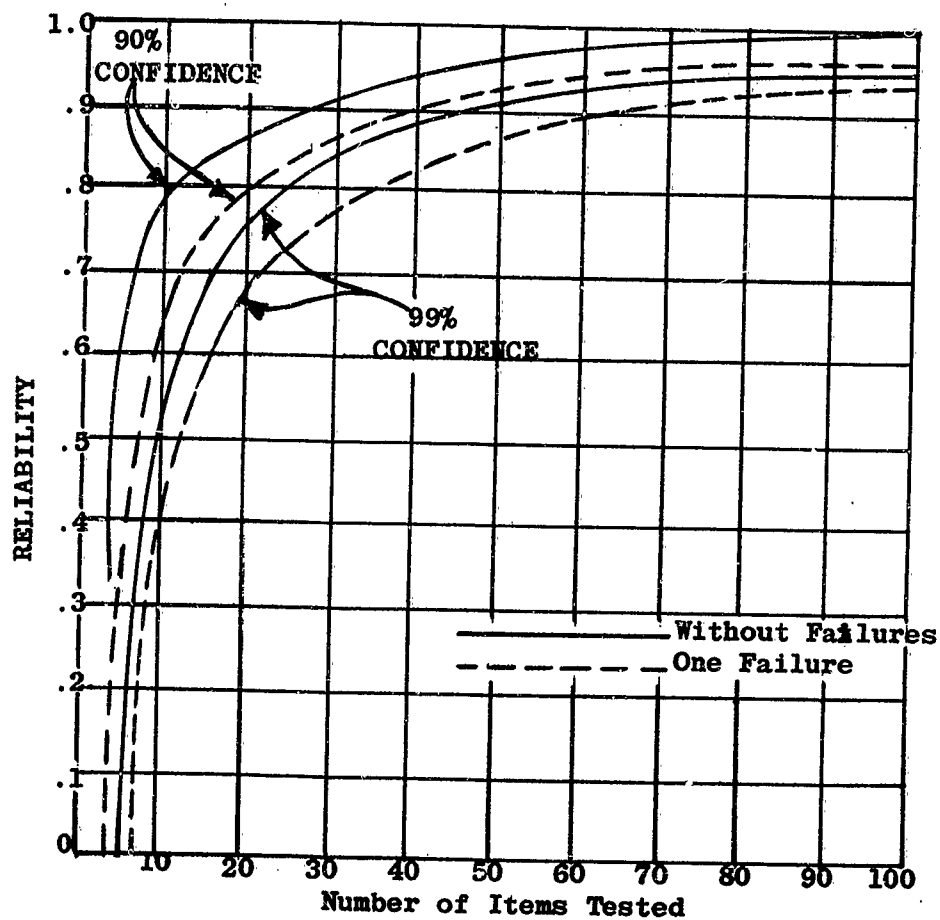


FIG. 9 RELIABILITY LEVELS FOR A SERIES OF TESTS
WITH AND WITHOUT FAILURES

performance which can be expected in large number of such systems. It should be remembered that this reliability value does not reflect the absolute performance of any individual system in a specific single mission; it gives the "odds" that an individual trial of the parachute will be successful. However, the process of reliability evaluation has broader and possibly more valuable applications than this single number for the overall development of the potential system.

In the process of evaluation of the component reliability model, the individual components of the parachute system most likely to fail are evaluated, as well as operational, installation and human factors at each stage of the system life history. It is imperative that consideration be given to each of the sub-results in the development and increase of reliability of decelerator systems. Efforts should be concentrated on achieving the same approximate degree of reliability for all components, as well as the areas which are influenced by human factors. Effort expended in this manner has the greatest payoff in increasing the reliability of the overall system.

The level of system reliability is influenced primarily by the components with the highest expected failure rate. Since the process of reliability analysis detects these components explicitly, it can be of major value in locating those portions of decelerator systems upon which further developmental effort will most improve the overall system reliability.

Reliability analysis can be used in the development of a unified physical design. Based on the experience of many organizations which have successfully integrated reliability with system design and fabrication, the following is a suggested outline of factors which should be considered:

1. Governing specifications.
2. Design conditions.
 - a. Description of physical characteristics (size, weight, configuration limits, etc.).
 - b. Description of installation provisions.

- c. Environmental requirements (to include natural and induced environments under operating, storage, handling, and transport conditions).
- 3. Construction requirements.
 - a. Standardization
 - b. Material
 - c. Maintainability requirements
 - d. Inspection procedures
 - e. Design efficiency controls
- 4. Production controls.
 - a. Reliability
 - b. Life
 - c. Protection and safety
 - d. Cost
 - e. Quality assurance

RELIABILITY AS A FIGURE OF MERIT

Reliability requirements on decelerator systems are, in general, very high. The difference between a reliability of 0.999 and 0.9999 is not only difficult to measure (it implies one failure in 10,000 trials!), but conveys very little "feel" to the analyst or design engineer concerned with the system. It is advantageous for such high reliability systems to consider the calculated reliability as a Figure of Merit. As a first approximation, we may think of the "number of significant figures" as indicating the Figure of Merit. Thus, the numerical comparison may be taken as having a Figure of Merit of four in comparison with three.

The Figure of Merit approach squares well with intuitive judgment of the engineering realities and can take advantage of the other data presentations which aid in indicating the degree to which we may rely on a given system.

RELIABILITY IMPROVEMENT

As previously noted, a major use of reliability analysis is to indicate the source of greatest pay-off in overall system performance. Component-by-component reliability analysis isolates those portions of the system

which require attention. Depending on the particular component, a decision can be made for the redesign, selection of other materials, etc., and the proposal evaluated in the light of its probable effect on system reliability.

A factor often ignored in reliability improvement is the maintenance of good records of test results and operational performance. The incompleteness and frequent inadequacy of these records is apparent to anyone who has attempted practical work in this area. It should be borne in mind that the effort made to record and store complete and accurate data is small in comparison with the time and costs that went into the creation of the information. It is even smaller in comparison with the consequence of making the same error twice or duplicating work.

A unified reliability point of view applied to decelerator systems is a tool of major potential value to reducing the lead times for the decelerators of the future.

ACKNOWLEDGEMENT

This report is, in a true sense, the joint effort of an American Power Jet Company team, the Retardation and Recovery Branch of ASD, Air Force, Army and Navy using agencies and parachute manufacturers. Their support and cooperation is gratefully acknowledged.

APPENDIX A

PARACHUTE RELIABILITY EXPERIENCE

The body of this paper is concerned with the underlying logical structure and methods applicable to establishing aerodynamic decelerator reliability. Reliability considerations include those concerned with items of construction and hardware, human, and operational factors. The following sections present a brief summary of parachute reliability experience considerations and data based on American Power Jet Company Report 259-1 "Analysis of Heavy-Duty Parachute Reliability" (Reference 1).

I. MATERIALS AND HARDWARE

The application of the stress-strength analysis technique requires an estimate of both the mean strength and standard deviation of parachute materials. Tests performed by manufacturers record not only that the material passed the specification, but also give the stress at failure. These results are given in Table I. It should be noted that the acceleration loads imposed on the fabric in actual operations are much higher than those of fabric testing devices in large scale use. This aspect may not be too serious, however, as shown by a study of the break strength of nylon materials at accelerations varying from two inches per minute to 48 feet per second. The small difference suggests that the results are quite stable.

Reefing line cutter reliability has both an operational and a design aspect. For example, failure data instances were encountered in which the cutters were not armed. Performance data on reefing line cutters based on actual parachute use are not generally available since most parachute systems employ more than one cutter; any one successful cutting operation will disreef the canopy.

The analysis of laboratory tests results on reefing line cutters indicates that high temperature, high relative humidity will result in the lowest reliability. This is due principally to the fact that many reefing line cutters employ a nylon ball which holds the firing pin in place until the firing wire is pulled. Upon removal of

TABLE I. MEASURED MEAN AND STANDARD DEVIATION OF BREAK STRENGTH, NYLON PARACHUTE WEBBINGS, TAPES AND CORDS */

| Specification | Type | Strength (lbs.) | Mean Meas. Strength (lbs.) | Standard Deviation (lbs.) |
|------------------|-------|--------------------|-------------------------------------|---------------------------------|
| <u>Webbings:</u> | | | | |
| MIL-W-4088C | I | 500 | 576 | 27.8 |
| " | II | 600 | 796 | 97.9 |
| " | III | 800 | 976 | 84.4 |
| " | IV | 1800 | 2461 | 39.7 |
| " | V | 3000 | 3135 | 76.6 |
| " | VI | 2200 | 2868 | 89.9 |
| " | VII | 5000 | 6659 | 181 |
| " | VIII | 3600 | 4492 | 171 |
| " | IX | 8200 | no data | |
| " | X | 8700 | 9502 | 307 |
| " | XI | 2400 | 3168 | 132 |
| " | XII | 1200 | 1527 | 145 |
| " | XIII | 6000 | 7893 | 410 |
| " | XIV | 1200 | 1963 | 21.7 |
| " | XV | 1500 | 2861 | 94.2 |
| " | XVI | 4500 | 5262 | 321 |
| " | XVII | 2400 | 3159 | 88.7 |
| " | XVIII | 6000 | 7486 | 272 |
| " | XIX | 10,000 | 11,699 | 1563 |
| " | XX | 9000 | 10,016 | 461 |
| " | XXI | 3600 | 4216 | 137 |
| MIL-W-4088D | XXII | ? | 8556 | 36 |
| MIL-W-005625C | 1/2" | 1000 | 1387 | 218 |
| " | 9/16" | 1500 | 1855 | 119 |
| " | 6/8" | 1850 | 2095 | 171 |
| " | 3/4" | 2300 | 3019 | 98.7 |
| " | 1" | 3500 | 4311 | 181 |
| MIL-W-5666 | 1- | | | |
| | 5/16" | 500 | 630 | 23.7 |
| MIL-T- | | | | |
| 005038B | IV-1" | 1000 | 1209 | 49.1 |
| " | IV-1- | | | |
| | 1/2" | 1500 | 1773 | 107 |

*/ Data presented are for undyed (natural) and condition "U" materials.

TABLE I. MEASURED MEAN AND STANDARD DEVIATION OF BREAK STRENGTH, NYLON PARACHUTE WEBBINGS, TAPES AND CORDS

| <u>Specification</u> | <u>Type</u> | <u>Strength (lbs.)</u> | <u>Mean Meas. Strength (lbs.)</u> | <u>Standard Deviation (lbs.)</u> |
|----------------------|-------------|----------------------------|---|--|
| <u>Tapes:</u> | | | | |
| MIL-T-005038B | II-1" | 900 | 1058 | 77.4 |
| " | III-3/8" | 200 | 226 | 5.6 |
| " | III-1/2" | 250 | 282 | 16.6 |
| " | III-3/4" | 400 | 466 | 15.9 |
| " | III-1" | 525 | 605 | 32.0 |
| " | V-9/16" | 500 | 550 | 19.0 |
| " | VI-3/4" | 425 | 478 | 24.5 |
| MIL-T-5608E | clB-III | 70 | 73.7 | 2.0 |
| " | clC-III | 90 | 96.9 | 2.9 |
| " | clC-V | 300 | 317 | 25.7 |
| " | clD-II | 460 | 477 | 18.2 |
| " | clE-II | 1000 | 1173 | 36.1 |
| " | clE-III | 1500 | 1727 | 43.1 |
| " | clE-IV | 2000 | 2314 | 109 |
| " | clE-V | 3000 | 3361 | 12 |
| MIL-T-6134A | 1" | 525 | 646 | 34.3 |
| <u>Cords:</u> | | | | |
| MIL-C-5040B | I | 100 | 121 | 3.98 |
| " | IA | 100 | 140 | 7.53 |
| " | II | 375 | 440 | 19.6 |
| " | III | 550 | 603 | 11.2 |
| " | IV | 750 | 771 | 16.5 |

the firing wire, the nylon ball is allowed to move back in a channel releasing the firing pin against the detonator. The distortion of the nylon ball due to high temperature and high humidity may retain the ball and cause it to move slowly back into the channel. Although not always resulting in a complete failure of the cutter, it often causes considerably lengthened delay times in actuation.

Laboratory tests of the effects of acceleration (or deceleration) on the operation of the reefing line cutter indicate that there are no adverse effects under operationally encountered accelerations. The magnitude of the forces in the operation of the reefing line cutter are more than required to compensate for acceleration forces. The only exception to the above was in the case of an exaggerated centrifugal acceleration test on one cutter. In this particular test, the cutter was subjected to 154 g's with the forces opposing the direction of the firing pin movement. Twelve cutters failed from 100 tested.

Of several reefing line cutters analyzed, the reliability with a 90% confidence ranged from .931 to .998. The lower reliability range was caused by one cutter which was quite susceptible to the effects of high temperature and high humidity (a total of twelve failures from 260 test items). These were due principally to the distortion of the nylon ball used in the assembly of the cutter. In all other tests, there were no other components of the reefing line cutter which caused failures.

HUMAN FACTORS

The reliability model and calculation procedure requires the attainment of stable independent estimators. It is tacitly assumed that the results of our observations of laboratory tests and field operations are representative. Actually, of course, they are performed by different human beings under different conditions and it is therefore necessary to consider this factor. Three major areas of possible error should be distinguished:

1. Errors in manufacturing not caught by inspection procedures.

2. Errors in rigging.
3. Errors in packing.

The possibility of human error in the manufacturing process is difficult to evaluate. It is primarily a function of the manufacturer's quality control and depends on proper training of manufacturing personnel and on thorough an effective inspection. In a study of over 5000 parachutes, no manufacturing errors of this type were isolated.

A distinction is made between human error in rigging and in packing. A rigging error involves both the load and the parachute while the packing error relates solely to the parachute. For example, parachute rigging errors in air-drop applications may occur with the deployment of irregularly shaped loads. In many such failures, the actual cause of failure was the snagging or tangling of some portion of the deployment canopy or lines on a portion of the load.

However, even though this type of failure causes system unreliability in a mission, considering such failures as parachute unreliability is open to question. In general, the rigging of the parachutes for a cargo drop is not under the control of the parachute design or engineering agency. Thus, the unreliability due to rigging error can be corrected primarily by operational discipline rather than by processes which can be truly said to be under engineering control.

Unlike many mechanical or electronic systems, parachutes require extensive human participation in "set up", i.e., packing. Studies of extensive parachute drop records and field interviews with military personnel indicate that the human problem in parachute packing is a major source of system failure. This is particularly true where the parachute is used for cargo drops and other heavy duty applications.

Two distinct portions of the packing process can be recognized from the viewpoint of error control: (1) the canopy lay-out, folding, tying, and stowing and (2) the installation of hardware and auxiliary devices required for parachute operation. In a survey of records of

parachute failure, most human error failures in packing was not in the canopy portion of the operation, but rather in the auxiliary device installation.

Observation of the packing process for large complex parachute systems suggests that the basic cause of this error is probably in the installation of the hardware items; quality control measures applied to the parachute packing process requires constant inspection at each stage of the packing. Much of the hardware and auxiliary devices, such as reefing line cutters, are usually quite small. Upon completion of the packing, it is difficult for the inspector to see all portions of the part clearly. Thus, inspection becomes very difficult and it is entirely possible that a highly qualified inspector might miss an error in the process which could eventually cause failure in the parachute in its mission.

It would appear that more inspection and closer inspection would not be the key to eliminating entirely failures of this type. Rather, it is necessary to design the parachute system for inspection of the packing operation. The design engineer must consider the problem of the inspector who must determine whether the packing or installation of each device had been done properly.

In Reference 1, a total of 5,563 drops of a complex parachute system were analyzed, each with an estimated 100 possible opportunities for error in each complete packing. This constitutes over 1/2 million chances for error. The results of these analyses were interesting in two respects: (1) the failure rates experienced in parachute operations and (2) causes of failures in packing.

The observed failure rate is extremely small. In the total sample of 5,563 drops (several groups of data), 15 packing failures were observed. This established an observed failure rate of between 1.6 and 3.6 per thousand parachute packings. In terms of a reliability model, this could be specified as a reliability of .9962, .9958, and .9952 at a confidence coefficient of 90, 95, and 99% respectively.

The 15 packing failures were analyzed individually to determine the actual cause of failure. The results

of these analyses have indicated that six failures occurred in which the reefing line cutters were not armed, one case in which the cut reefing line had not slipped through the reefing rings to release the canopy skirt, one case in which the canopy was packed in such a manner that it emerged from the bag twisted, three cases in which improper cut knife installation prevented deployment, one case of the use of too strong a break cord, one case in which the canopy was not attached to the bridle, and two cases of static lines improperly attached to the pack.

From the above, it can be seen that human error has entered into 14 out of 15 packing failures analyzed in approximately 5500 drops. There was only one failure due to the canopy packing itself. Even in this case, it is conceivable that a human error was involved in the actual stowing of the canopy in the bag.

OPERATIONAL FACTORS

The reliability model included an operational term which represents the probability of correct error-free packing of the parachute into its deployment bag and its correct stowage on the flight vehicle. It should be noted in this connection that the model deliberately stops short of the flight vehicle aspect of operation; i.e., the probability that the vehicle will be at the correct altitude, velocity, and attitude at the time deployment is initiated. This logical separation is for convenience in generalizing a given parachute analysis so that it may be applicable to a variety of weapon systems. In the overall weapon system analysis, this last factor must never be neglected.

At the design stage, prior to system construction, the analysis of operational reliability implies that if the decelerator is properly stowed in its container, the deployment process will proceed successfully. This must, of course, be confirmed by testing.

REFERENCES

1. Jailer, R. W., Freilich, G. and Norden, M. L., "Analysis of Heavy-Duty Parachute Reliability", American Power Jet Company Report No. 259-1, WADD TR 60-200, June 1960.
2. "Tables of the Binomial Probability Distribution", Department of Commerce, National Bureau of Standards, Applied Mathematics Series No. 6.
3. "Tables of the Individual Cumulative Terms of Poisson Distributions", Defense Systems Department, General Electric Company, Van Nostrand 1962.
4. Kendall, M. G. and Stuart, A., "The Advanced Theory in Statistics", 2 Vols., Revised 1960-1962, Griffin, London.
5. Hoel, P. G., "Introduction to Mathematical Statistics", John Wiley & Sons, New York, 1954.
6. Dixon, W. J. and Massey, F. J., "Introduction to Statistical Analysis", Second Edition. McGraw-Hill, New York, 1957.
7. Ruther, F. J. and Smith, L. D., "Proof of Reliability", WADC TN 58-87, May 1958.
8. Coplan, M. J. and Bloch, M. G., "A Study of Parachute Seam Design Criteria, Part I, Investigation of Strength of Nylon and Rayon Cloth Seams", WADC TR 56-313 Part I, Fabric Research Laboratories, Inc., June 1956 AD 110406
9. Miller, C. R., "A Study of Parachute Seam Design Criteria, Part II - Investigations of the Strength of Nylon Webbing Joints", WADC TR 56-313 Part II, Pioneer Parachute Co., June 1956, AD 110407.
10. Seshadri, V. and Odell, P. L., "A Method for Determining Unreliability Using Data from Life Tests", NAVORD Report 6618, U.S. Naval Nuclear Ordnance Evaluation Unit. Albuquerque, N. M., July 1959, AD 220841.

11. "United States Air Force Parachute Handbook", WADC TR 55-265, Dec. 1956, AD 118036.
12. Chorafas, D.M. "Statistical Process and Reliability Engineering", Van Nostrand, Princeton, 1960.
13. Resnikoff, G. J. and Lieberman, G. J., "Tables of the Non-Central t-Distribution", Stanford Univ. Press, Stanford, Calif., 1957.

WATER SURFACE WAVE ANALOGY AND APPLICATIONS TO PROBLEMS
OF AERODYNAMIC DECELERATION*

Shukry K. Ibrahim**

Department of Aeronautics and Engineering Mechanics
University of Minnesota

The Aerodynamic Deceleration Group at the University of Minnesota has been applying the Water Surface Wave Analogy to a variety of research problems since 1957.

This paper briefly reports the chronological development of the analogy, presents a summary of its basic theory, describes the facilities developed with particular emphasis on the recently completed moving water channel, outlines the experimental procedures adopted and discusses some of the results achieved and potential lines for further development.

*This work was sponsored jointly by the U.S. Army, Air Force, and Navy. Messrs. R. J. Berndt and J. H. DeWeese were the WADD Project Engineers.

** Messrs. D. Nordwall, R. Friestad and other students of the University of Minnesota also participated in the construction of equipment, performance of experiments and reduction of experimental data.

WATER SURFACE WAVE ANALOGY AND APPLICATIONS TO PROBLEMS OF AERODYNAMIC DECELERATION

INTRODUCTION

The water surface wave analogy to compressible gas flow, sometimes referred to as the gas-hydraulic analogy is one analogical method that has proven of great value in the study of transonic and supersonic flow phenomena. Other analogies such as the electro-hydrodynamic and the magnetohydrodynamic analogies have also found many interesting applications.

One of the objectives of a continuing research program on Aerodynamic Deceleration conducted at the University of Minnesota is the establishment of the flow patterns and corresponding velocity and pressure distributions that occur when two bodies are immersed in a fluid and one of them is located in the wake of the other. The primary and secondary bodies investigated in the program are basic forms representing actual or contemplated configurations of flying objects and trailing aerodynamic deceleration devices.

The entire program is rather large and would be very expensive if all interesting combinations were to be investigated in subsonic and supersonic wind tunnels. Therefore, studies by means of the water analogy method were conceived initially as a means of exploring the principal flow phenomena and narrowing down the number of configurations to be tested in wind tunnels.

Brief Historical Summary

The existence of the analogy was pointed out by Riabouchinsky in 1932 (Ref 1). In 1935, Ippen and Knapp (Ref 2) demonstrated experimentally the application of the methods of supersonic gas dynamics to hydraulic problems.

In 1938, Preiswerk (Ref 3) extended the theory of the hydraulic analogy for both isentropic flow and flow with shocks and conducted some experiments to show the applicability of the analogy to aerodynamic problems and hence its usefulness as a research tool.

In 1941, Johnson and Whitbeck (Ref 4) reported the use of a water table for the study of airflow into ram-jets and other aerodynamic devices. In this and in the previous tests, the water flowed past stationary models or through fixed ducts. In the same year, the North American Aviation Company (Ref 5) reported a series of tests on the analogy

where the water was stationary and the models were attached to a towing carriage. Variations in Mach number were obtained by controlling the speed of the carriage and the static depth of the water.

In 1946, the NACA conducted a research program designed to test the hydraulic analogy for flow around circular cylinders. In these tests, the initial Mach number was in the subsonic range, but, in some of the tests, the local Mach number extended into the supersonic range. Good quantitative results were obtained thus verifying the analogy for the subsonic and transonic velocity ranges (Ref 6).

Since 1947, work on the analogy was conducted in the Department of Civil Engineering at M.I.T. under Dr. A. T. Ippen. This led to a comprehensive study of the theory of supercritical flow of water in open channels which corresponds to the two dimensional supersonic flow of gas. The work conducted at M.I.T. was presented in a comprehensive report by Ippen and Harleman (Ref 7).

Since 1957, the Aerodynamic Deceleration Group at the University of Minnesota has been applying the gas-hydraulic analogy to investigate an increasing number of aerodynamic problems. Reference 8 presented the wave patterns for a wide range of configurations involving a number of primary and secondary bodies placed in tandem to represent existing or potential shapes of flying objects and aerodynamic deceleration devices at a simulated Mach 2. In these early tests, interest centered primarily on the overall wave pattern. The towed models were in sliding contact with the channel floor. There was reasonable agreement with regards to the shape of the detached shock waves obtained in the water tank and that calculated from existing theories. However, the standoff distances obtained experimentally were much larger than those calculated from theory. Some preliminary conclusions regarding optimum L/D values (separation distance over primary body diameter) for efficient operation of the retardation devices were obtained and later applied and verified in wind tunnel tests.

In September 1958, the author suggested a modification of the analogy aiming at extending its scope in testing aerodynamic deceleration devices. Instead of a rigid model mount producing a sliding contact with the channel floor, the models were freely mounted with a very small clearance (about 0.010 in) from the channel floor. The models were free to pivot about a vertical axis and, because of the hydrostatic pressure which is directly related to the depth distribution around the model, it tended to move to a stable position, i.e.; a position for which $C_m = 0$ and $dC_m/d\alpha$ is positive.

Preliminary tests with freely suspended rigid models indicated the potential value of such pendulum tests,

particularly as regards investigating the stability characteristics of various canopy shapes in transonic and supersonic flow.

Early in 1959, Dr. Heinrich suggested a further extension of the analogy permitting studies of the behavior of flexible parachute models. In order to more adequately exploit the ideas and possibilities mentioned above and avoid some limitations and shortcomings of the existing water tow channel, a new water tow channel was built during 1959. Since its completion, this facility has been extensively used and a wealth of information about wave patterns, stability characteristics of rigid and flexible canopy configurations, free canopy shapes, etc., was obtained.

Late in 1960, the author suggested complementing the conventional water tow experiments with studies in a moving water channel indicating that such an additional facility offered definite possibilities particularly as regards quantitative applications of the analogy and improved visualization techniques including the shadowgraph and schlieren methods. This channel is now in operation and has already proven of great value in our overall program of investigations.

After outlining the mathematical basis for the gas-hydraulic analogy and indicating its limitations, this paper will be devoted mainly to the design, operation and instrumentation of the moving water channel, a presentation of some of the experimental results recently obtained with it and a discussion of the gas-hydraulic analogy and its present and potential applications to aerodynamic decelerator problems.

THEORY OF THE GAS-HYDRAULIC ANALOGY

Analogies are constantly used in the physical world. In everyday language, they make for more picturesque speech. In science and engineering, analogies are valuable experimental tools by means of which one system may be compared with another that may be better known, more convenient, more flexible or less expensive to test.

Experimental analogies must rest on a solid mathematical foundation and since the mathematical formulation of any physical problem generally involves some assumptions and idealizations, it is important to constantly keep in mind, not only the mathematical equations and analogous quantities of the two systems, but also the assumptions and idealizations involved for each system.

The following summarized presentation of the mathematical theory of the analogy is largely based on Ref 3.

Water Flow Equations

The following assumptions are made in the derivation of the water flow equations:

1. The flow is frictionless, i.e., there is no conversion of energy into heat.
2. The flow is incompressible and irrotational; this last assumption implies the existence of a velocity potential.
3. The pressure on the free surface is constant and the vertical accelerations of the water are negligible compared with the acceleration of gravity. It follows from this assumption that the pressure in the fluid at any point depends only on the height of the free surface above that point (hydrostatic pressure).

Energy Equations

The energy equation simply states that the sum of the potential and kinetic energy of a water particle is constant during its motion.

If one considers a flow filament originating at the point $P_0 (x_0, y_0, z_0)$ (Fig 1) at which the velocity is assumed to be zero (Stagnation Condition), then Bernoulli's Equation applied to any point $P (x, y, z)$ on the same filament that originates at P_0 gives:

$$p + \frac{1}{2} \rho V_w^2 + \rho g z = p_0 + \rho g z_0 \quad (1)$$

where V_w represents the resultant water velocity at P .

Equation 1 may be written as

$$V_w^2 = 2g(z_0 - z) + \frac{2}{\rho} (p_0 - p) \quad (2)$$

From assumption 3, there follows:

$$p_0 = \rho g(d_0 - z_0) \quad (3)$$

$$\text{and } p = \rho g(d - z) \quad (4)$$

By substitution into Eqn 2 there follows:

$$V_w^2 = 2g(d_0 - d) \quad (5)$$

This is a simple form of the energy equation and it indicates that the velocity at any internal point is independent of z and hence constant over the entire depth.

The maximum velocity is given by:

$$V_{w_{\max}} = \sqrt{2gd_0} \quad (6)$$

and the velocity ratio

$$\left(\frac{v}{V_{\max}}\right)_w = \sqrt{\frac{d_0 - d}{d_0}} \quad (7)$$

Continuity Equation

The equation of continuity is given by:

$$\frac{d}{dx} \left(\frac{du}{dx} \right) + \frac{d}{dy} \left(\frac{dv}{dy} \right) = 0 \quad (8)$$

which may be expanded into:

$$d \frac{du}{dx} + u \frac{dd}{dx} + d \frac{dv}{dy} + v \frac{dd}{dy} = 0 \quad (9)$$

Potential Function

The energy equation (5) may be written in the form

$$d = d_0 - \frac{V_w^2}{2g} \quad (10)$$

Since $V_w^2 = u^2 + v^2$

Then

$$\frac{dd}{dx} = -\frac{1}{g} \left(u \frac{du}{dx} + v \frac{dv}{dx} \right) \quad (11)$$

and

$$\frac{dd}{dy} = -\frac{1}{g} \left(u \frac{du}{dy} + v \frac{dv}{dy} \right) \quad (12)$$

By substitution from 11 and 12 into 9 there is obtained:

$$\frac{du}{dx} \left(1 - \frac{u^2}{gd} \right) - \frac{uv}{gd} \left(\frac{du}{dy} + \frac{dv}{dx} \right) + \frac{dv}{dy} \left(1 - \frac{v^2}{gd} \right) = 0 \quad (13)$$

The assumption of irrotationality (Assumption 2) is expressed mathematically by:

$$\frac{dv}{dx} - \frac{du}{dy} = 0 \quad (14)$$

It implies the existence of a velocity potential function $\phi(x,y)$ such that

$$u = \frac{d\phi}{dx}; \quad v = \frac{d\phi}{dy} \quad (15)$$

By substitution from 15 into 13, the differential equation for the velocity potential of the free surface water flow is obtained, namely,

$$\phi_{xx} \left(1 - \frac{\phi_x^2}{gd} \right) - 2\phi_{xy} \frac{\phi_x \phi_y}{gd} + \phi_{yy} \left(1 - \frac{\phi_y^2}{gd} \right) = 0 \quad (16)$$

Two-Dimensional Compressible Gas Flow Equations

These equations and the assumptions underlying their derivation are well known and are given in many textbooks on Compressible Fluid Flow. Only the equations directly relevant to the present analogy are listed below.

The equation of state for an ideal gas is given by:

$$p = gR\rho T \quad (17)$$

The assumption of adiabatic flow, i.e., that no heat is added or removed from the flow yields the relations:

$$\frac{p}{p_0} = \left(\frac{\rho}{\rho_0} \right)^\gamma \quad (18)$$

$$\frac{\rho}{\rho_0} = \left(\frac{T}{T_0} \right)^{\frac{1}{\gamma-1}} \quad (19)$$

$$\frac{p}{p_o} = \left(\frac{T}{T_o} \right)^{\frac{\gamma}{\gamma-1}} \quad (20)$$

Energy Equation

Using the concept of enthalpy given by:

$$h = C_p T \quad (21)$$

The energy equation may be written in the forms

$$gh + \frac{1}{2} V_A^2 = gh_o \quad (22)$$

$$\text{or } gC_p T + \frac{1}{2} V_A^2 = gC_p T_o \quad (23)$$

where subscript _o refers to stagnation conditions and V_A, T represent the resultant air velocity and temperature at any specified point P in the flow.

Hence, the air flow velocity at P is given by

$$V_A^2 = 2g(h_o - h) = 2gC_p(T_o - T) \quad (24)$$

The maximum velocity is given by

$$V_{A_{\max}} = \sqrt{2gh_o} = \sqrt{2gC_p T_o} \quad (25)$$

and the velocity ratio:

$$\left(\frac{V}{V_{\max}} \right)_A = \sqrt{\frac{T_o - T}{T_o}} = \sqrt{\frac{h_o - h}{h_o}} \quad (26)$$

Continuity Equation

This is given by

$$\frac{d}{dx} (\rho u) + \frac{d}{dy} (\rho v) = 0 \quad (27)$$

Potential Function

The equation for the velocity potential of a two-dimensional compressible flow is given by:

$$\phi_{xx} \left(1 - \frac{\phi_x^2}{a^2}\right) - 2\phi_{xy} \frac{\phi_x \phi_y}{a^2} + \phi_{yy} \left(1 - \frac{\phi_y^2}{a^2}\right) = 0 \quad (28)$$

Correspondence Between the Water Flow Equations and the Two-Dimensional Compressible Gas Flow Equations

Comparison between Eqns 7 and 26 shows that the non-dimensional velocity ratios for water and gas flow will be the same if

$$\frac{d_o - d}{d_o} = \frac{T_o - T}{T_o} = \frac{h_o - h}{h_o} \quad (29)$$

$$\text{i.e.,} \quad \frac{d}{d_o} = \frac{T}{T_o} = \frac{h}{h_o}$$

For analogy, the water depth ratio would correspond to the gas temperature ratio or the enthalpy ratio.

Equations 8 and 27 expressing the continuity condition for the two flows have the same form and since the velocities are analogous, a further conditions for the analogy is that the water depth be identified with the air density, namely,

$$\frac{d}{d_o} = \frac{\rho}{\rho_o} \quad (30)$$

By using 29, it follows that

$$\frac{d}{d_o} = \frac{\rho}{\rho_o} = \frac{T}{T_o} \quad (31)$$

However, the adiabatic condition specified that

$$\frac{\rho}{\rho_o} = \left(\frac{T}{T_o}\right)^{\frac{1}{\gamma-1}} \quad (19)$$

Equations 19 and 31 can be consistent only if

$$\frac{1}{\gamma-1} = 1 \quad \text{i.e., } \gamma = 2$$

Thus, an intrinsic limitation of the analogy is that it is correct only for a gas having $\gamma = 2$.

Such a gas does not exist but fortunately, there are many flow problems which are not greatly affected by a change of γ and for these problems, the analogy can be very fruitful.

Equations 16 and 28 for the velocity potentials of the two flows indicate that the quantity \sqrt{gd} in the water flow is identifiable with a , the velocity of sound in the gas flow.

Physically, the quantity \sqrt{gd} represents the velocity of propagation of surface waves having wave lengths that are large in comparison to the water depth.

The ratio $\frac{V_w}{\sqrt{gd}}$ or Froude number in the liquid flow corresponds to the Mach Number $\frac{V_A}{a}$ in the gas flow.

Two flow regimes can be distinguished:

- a. The case $\frac{V_w}{\sqrt{gd}} < 1$ corresponding to $\frac{V_A}{a} < 1$, i.e., subsonic flow.
The water flow in this case is termed "streaming."
- b. The case $\frac{V_w}{\sqrt{gd}} > 1$ corresponding to $\frac{V_A}{a} > 1$, i.e., supersonic flow.
This water flow is known as "shooting."

Hydraulic jumps occur in shooting flow and Eqn 30 shows that the jump in depth corresponds to the step function in the density.

Small intensity hydraulic jumps are propagated with the velocity $c = \sqrt{gd}$ thereby creating a wave pattern which corresponds to the Mach waves in a gas flow.

From the equation of state (Eqn 17), it follows that:

$$\frac{P}{P_0} = \frac{\rho T}{\rho_0 T_0} \quad (32)$$

The analogy has already established that

$$\frac{T}{T_0} = \frac{d}{d_0} \quad (29)$$

and

$$\frac{\rho}{\rho_0} = \frac{d}{d_0} \quad (30)$$

Hence

$$\frac{p}{p_0} = \left(\frac{d}{d_0} \right)^2 \quad (33)$$

Thus the pressure ratios in the compressible gas flow field are analogous to the square of the depth ratio in the incompressible water flow field.

Some Limitations of the Analogy

One inherent limitation of the analogy is that it applies to a so-called "hydraulic gas" having $\delta = 2$. It is necessary therefore to keep in mind the possible changes of flow characteristics resulting from the difference between the actual and hypothetical values.

Another important limitation of the analogy is that since the water depth (direction of z axis) represents the density, only two other dimensions remain for the geometric representation of the flow field and hence only two-dimensional shapes can be geometrically represented.

In a critical examination of the analogy, Laitone (Ref 9) has discussed some additional limitations and restrictive assumptions of the analogy. One of these restrictions stems from the fact that the actual velocity of wave propagation is not given exactly by $c = \sqrt{gd}$ as assumed, but more accurately by:

$$c = \sqrt{\frac{g\lambda}{2\pi} + \frac{2\pi\sigma}{\rho\lambda}} \tanh \frac{2\pi d}{\lambda} \quad (34)$$

by expanding $\tanh \frac{2\pi d}{\lambda}$ as a power series in $\frac{2\pi d}{\lambda}$ and substituting into 34 one obtains

$$c = \sqrt{gd} \left[1 + \frac{4\pi^2\sigma}{g\rho\lambda^2} + \text{terms of order } \frac{d^2}{\lambda^2} \text{ or higher} \right]^{1/2} \quad (35)$$

Thus, the actual wave propagation velocity depends not only on the liquid depth d , but also on its surface tension σ and the wave length λ .

For the case $d \rightarrow 0$, the middle term in 35 containing the surface tension will become predominant for small λ ; these wave lengths correspond to the capillary waves and should be disregarded since they form no part of the analogy. The third term in 35 indicates that the vertical acceleration is not negligible unless $d \ll \lambda$, i.e., the water depth is very much smaller than the wave length. The disturbance wave length in shallow water is proportional to the model size and hence relatively large models should be used to reduce the capillary ripples.

Another restriction of the analogy discussed by Laitone arises in the investigation of shock waves. Equation 29 indicates that the local water depth directly corresponds to the local value of the enthalpy or temperature in the two-dimensional compressible gas flow. In an adiabatic gas flow, there is no change in the stagnation temperature across a shock wave. In the hydraulic jump, however, there exists a certain loss in the stagnation water depth due to the formation of eddies that eventually increase the water temperature. This additional loss of available energy has no counterpart in the analogous case of ordinary shock waves in gas flow. The analogy, therefore, should be restricted to that range of Mach numbers and flow deflections where the loss of stagnation depth is negligible.

Modification of the Analogy for Quantitative Application

The ultimate aim of gas-hydraulic analogy method of investigation is to predict with reasonable accuracy the aerodynamic characteristics of a given shape by means of results obtained in a water channel. It has already been indicated that the analogy was imperfect for two basic reasons:

First, $\gamma = 1.4$ for air while the analogy requires $\gamma = 2$.

Second, the change in internal energy for gas is not equivalent to the change in internal energy for water.

As an example (Ref 7), an oblique shock flow with an initial Mach number ranging between 1 and 9 and a flow deflection of 9° and its water analogue will be used for comparison. Figure 2 shows the theoretical correlation between the aerodynamic ratios of density, pressure and temperature as calculated from aerodynamic theory and the analogous hydraulic depth ratio for $\theta = 9^\circ$. The best agreement is obtained between the depth ratio and the density ratio.

If the desired aerodynamic quantities are determined from hydraulic data according to the relationships 29, 30, and 33, varying degrees of agreement will be obtained

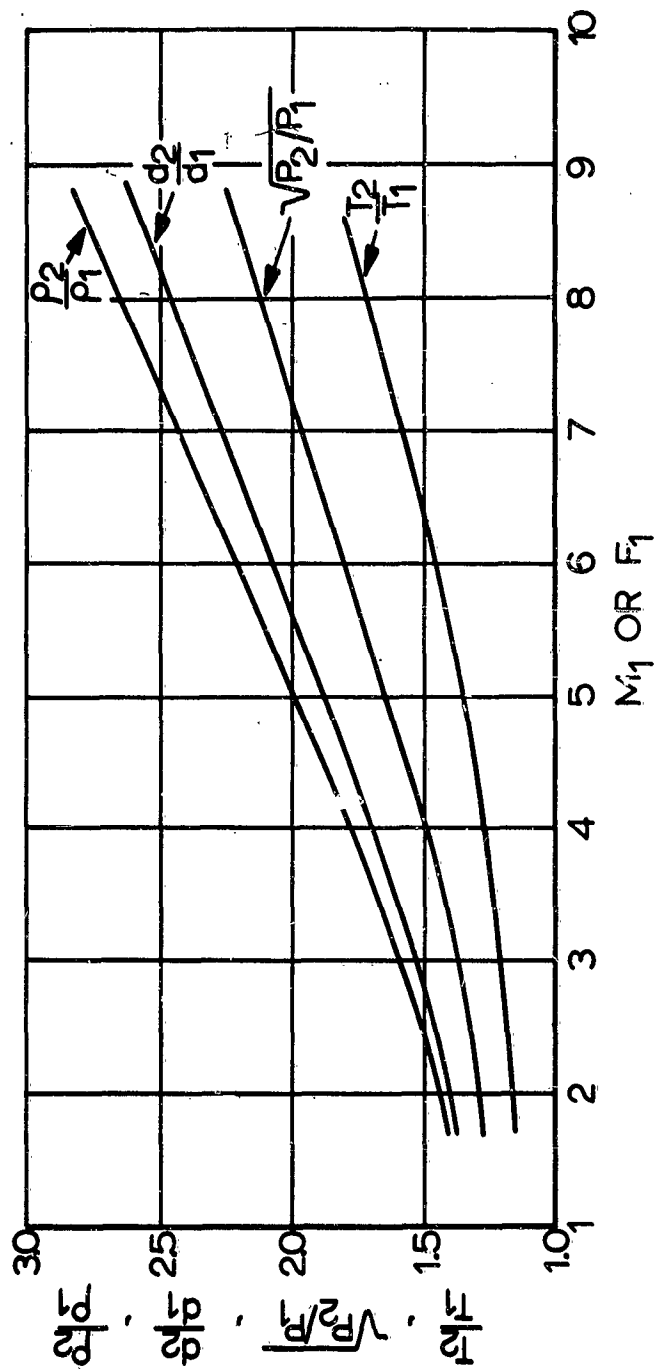


FIG 2. THEORETICAL CORRELATION BETWEEN ANALOGOUS WATER AND AIR CHARACTERISTICS FOR $M_1=F_1$ AND $\theta = 9^\circ$ (REF 7)

depending on the quantities desired. The modification, proposed by Ippen and Harleman (Ref 7) consists in obtaining the density ratio from the water depth ratio and then calculating all the other characteristics such as temperature, pressure, and Mach number from the aerodynamic relations which apply to the region in question. Table 1 compares the results obtained by using the direct analogy and the analogy with modification for the case of the 9° wedge with $M_1 = 2.5$.

EXPERIMENTAL EQUIPMENT

There are two general types of water channels used in gas-hydraulic analogy investigations. One type has placid water of a specified static depth and the model is towed through it at a controlled velocity. This will be referred to as a water tow channel. The other has a fixed model with the water flowing past it; the velocity and depth of the water can be controlled; often the slope of the channel is adjustable. This type will be called a moving water channel.

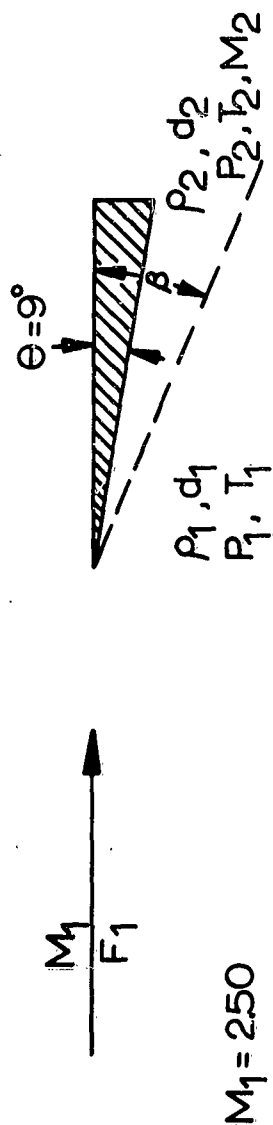
The moving water and the water tow channels may be considered as the analogy counterparts of the wind tunnel and the sled type test track.

Water Tow Channels

Figure 3 illustrates the water tow channel used in the early studies and Fig 4 is a typical illustration of our first application of the analogy to problems of aerodynamic deceleration.

The model mounting assembly used initially to investigate freely suspended models in the water tow channel is illustrated in Fig 5. Figure 6 shows the equilibrium position for a model of a hollow half cylinder in stable position in subsonic flow.

The early water tow channel shown in Fig 3, while quite suitable for the initial applications reported in Ref 8, was inadequate for the more sophisticated investigations envisioned. In the short run length of 6 ft, it was questionable whether a steady state condition of the free model was attained. Furthermore, the clearance between the glass and the model was not constant and this tended to produce secondary flows under the model, altering the two-dimensional nature of the flow and casting some doubts on the observed results.



| Initial Mach No. = 2.5 = Initial Froude No. $\theta = 9^\circ$ | | | | | | |
|--|--------------------|-----------|------------------|-------------------|-------------------|-------------------|
| Method of Analysis | Wave Angle β | d_2/d_1 | ρ_2/ρ_1 | p_2/p_1 | T_2/T_1 | M_2/M_1 |
| Aerodynamic Theory | $30^\circ 54'$ | --- | 1.489 | 1.759 | 1.181 | 0.852 |
| Direct Hydraulic Analogy | $32^\circ 30'$ | 1.465 | 1.465 (-1.6%) | 2.146 (+22.0%) | 1.465 (+24.0%) | 0.753 (-11.6%) |
| First Mod. Hyd. Analogy | $32^\circ 30'$ | 1.465 | 1.465 (-1.6%) | 1.718 (-2.3%) | 1.173 (-0.7%) | 0.858 (+0.8%) |

TABLE 1. THEORETICAL CORRELATION OF AIR-WATER
DATA BY MODIFICATION OF THE ANALOGY
(REF 7)

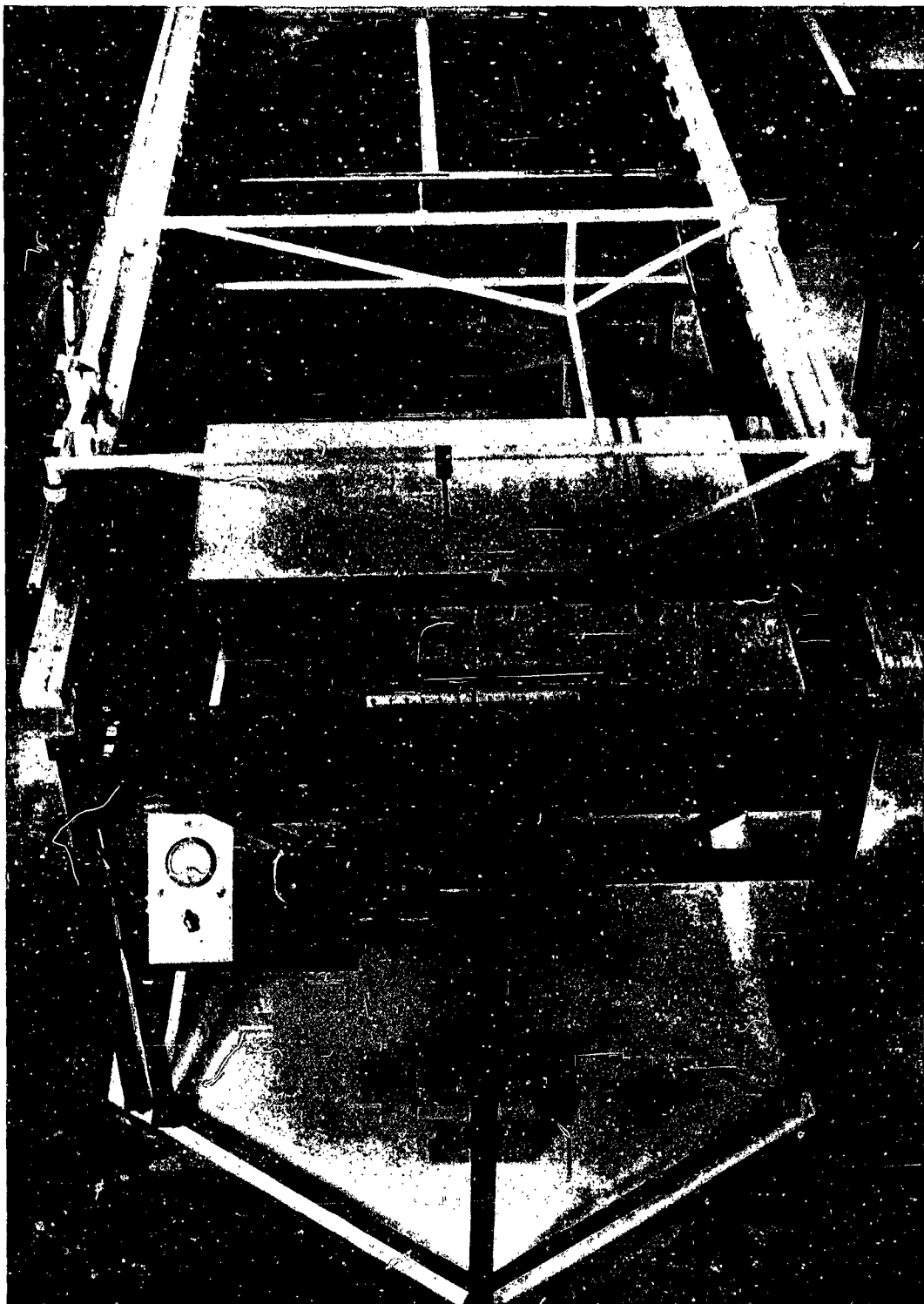


FIG 3 FIRST WATER TOW CHANNEL



(A) $L/D = 2$



(B) $L/D = 4$



(C) $L/D = 6$



(D) $L/D = 8$

FIG 4 REPRESENTATION OF OGIVAL NOSE CYLINDER WITH TRAILING SPHERE

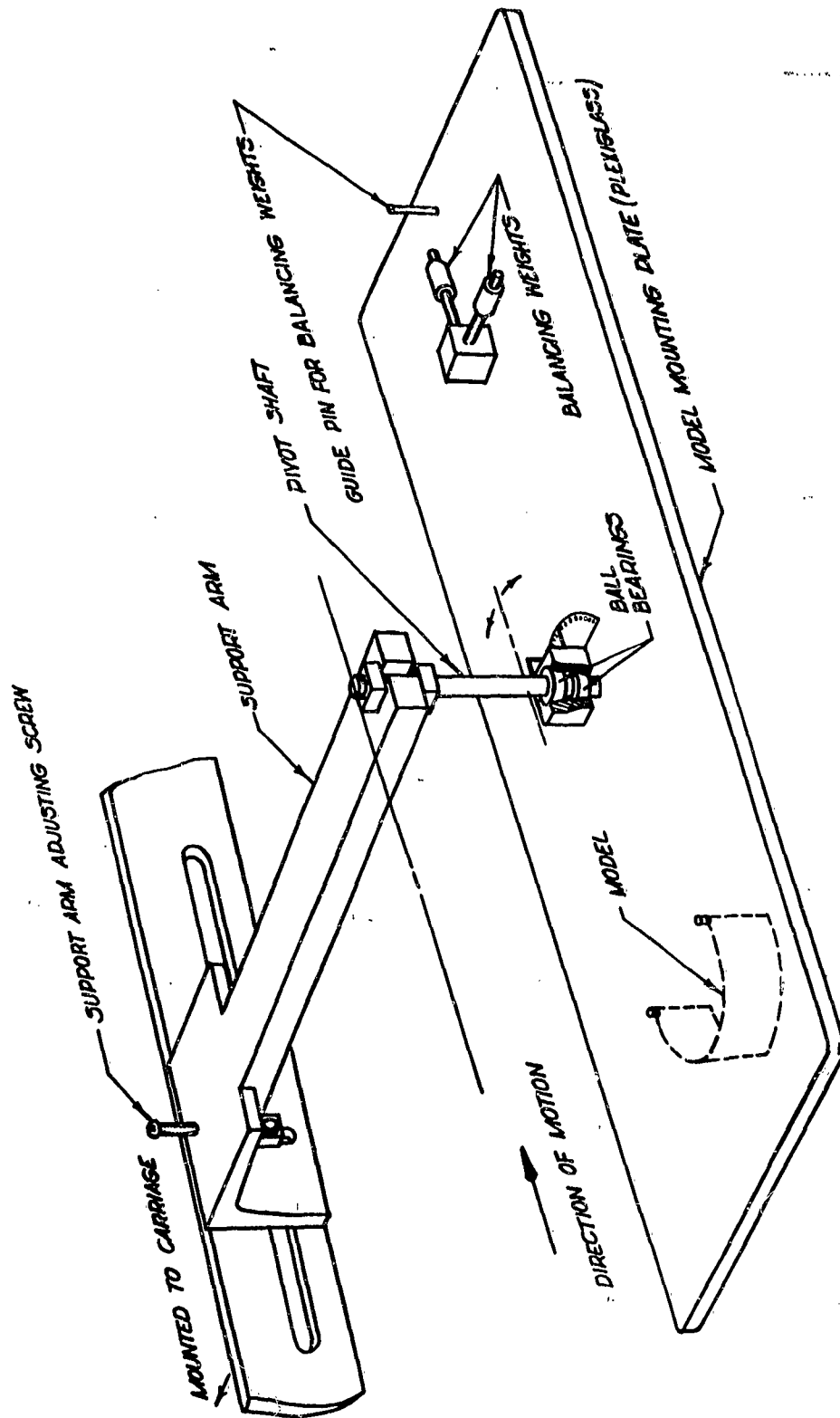


FIG. 5 PICTORIAL VIEW OF MODEL
MOUNTING ASSEMBLY



FIG 6 EQUILIBRIUM POSITION OF HOLLOW HALF CYLINDER
IN SUBSONIC FLOW

The second water tow channel, designed to overcome these shortcomings and limitations is illustrated in Figs 7 and 8. It is 30 ft long, $4\frac{1}{2}$ ft wide, and 3 ft high and has a usable length of run for testing purposes of 24 ft. The supporting table is constructed of welded, structural steel. The 26 legs supporting the structure are adjustable, thereby allowing the table to be levelled to $\pm 1/8$ in.

The floor of the channel consists of two pieces of high grade, mirror finish plate glass. Each piece of glass is 15 ft long, 52 in. wide, and $1/2$ in. thick. The surface of this glass is accurate to ± 0.001 in. The glass is supported by 120 adjustable jack pads used for fine adjustments in leveling its surface.'

The edges of the glass are sealed by cementing thin sheets of rubber between the glass and the structure as shown in the inset of Fig 7.

The moving carriage is shown in Fig 9. It is made of light weight metal tubing and provides for mounting the models, the camera, and the light source. It is supported by four "Teflon" wheels mounted on the corners. The wheels are wedge shaped and are machined to a tolerance of ± 0.001 in.

The velocity of travel of the carriage is controlled by a variable speed electric motor. The speed range is such that a wide range of Mach numbers may be simulated for a given depth of water. Limit switches are installed at each end of the table to automatically switch off the motor as the carriage approaches the end of its travel. The camera used to photograph the wave and model phenomena is mounted on the carriage approximately $3\frac{1}{2}$ ft above the model and is operated by a solenoid controlled from the main switchboard. In addition, two types of movie cameras have been used to photograph the model and wave phenomena. One operates at a film speed of 16 to 64 frames per second and the other at 128 frames per second.

The velocity of the carriage is determined by an experimental arrangement using a modified automobile ignition system. One lead is taken from the distributor to a spark plug. The spark is gapped between the tip of the plug and the carriage rail. A strip of sensitive paper (Stylograph), which runs the length of the rail, is put between the spark plug and the rail and the spark produces a small mark on the paper where it jumps. By knowing the rpm of the distributor rotor and measuring the distance between successive marks, the actual carriage velocity may be accurately determined.

Figure 10 illustrates the supporting mechanism used for testing two-dimensional flexible canopy models in the water tow channel.

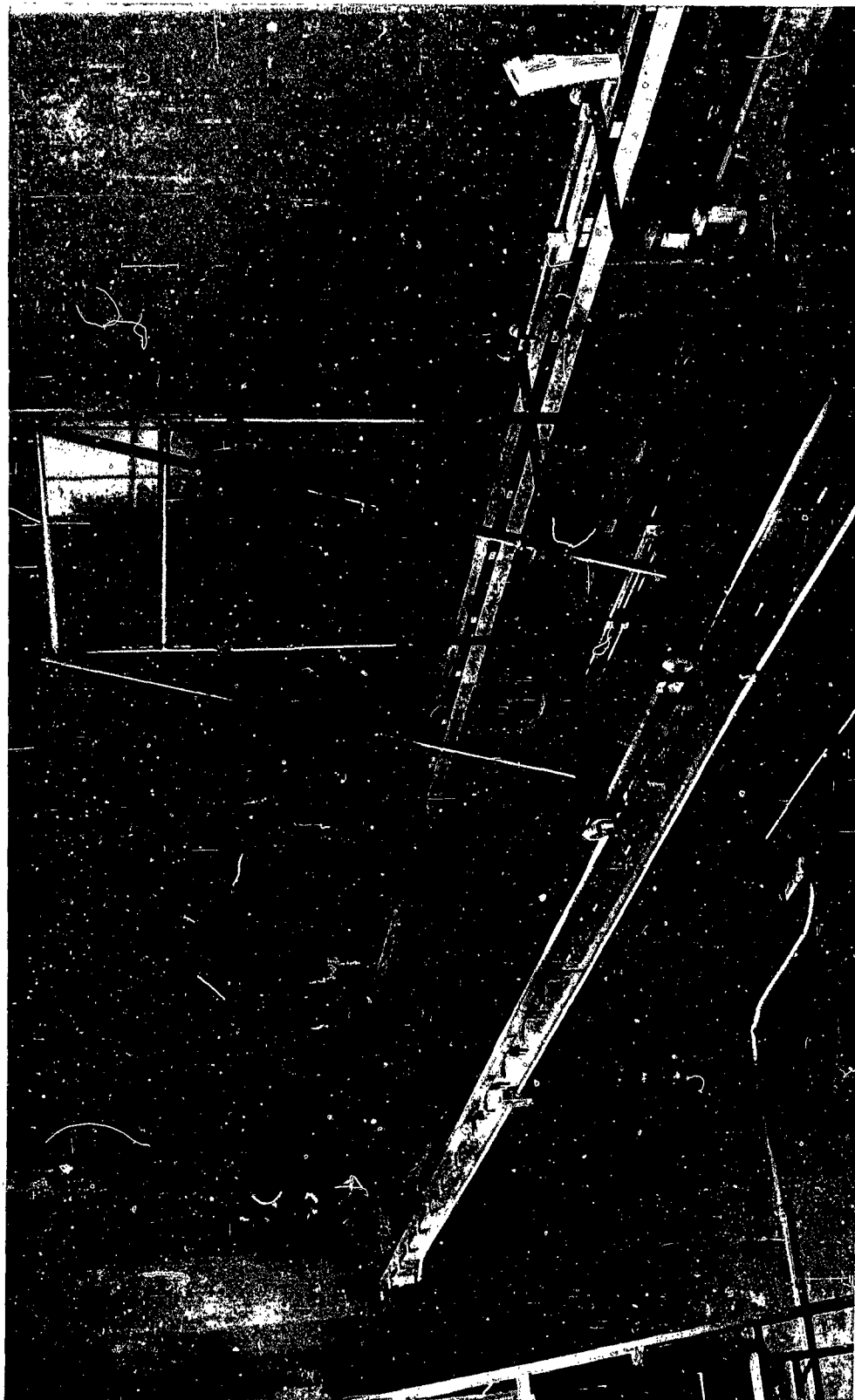


FIG 7 PHOTOGRAPH OF THE SECOND WATER TOW CHANNEL

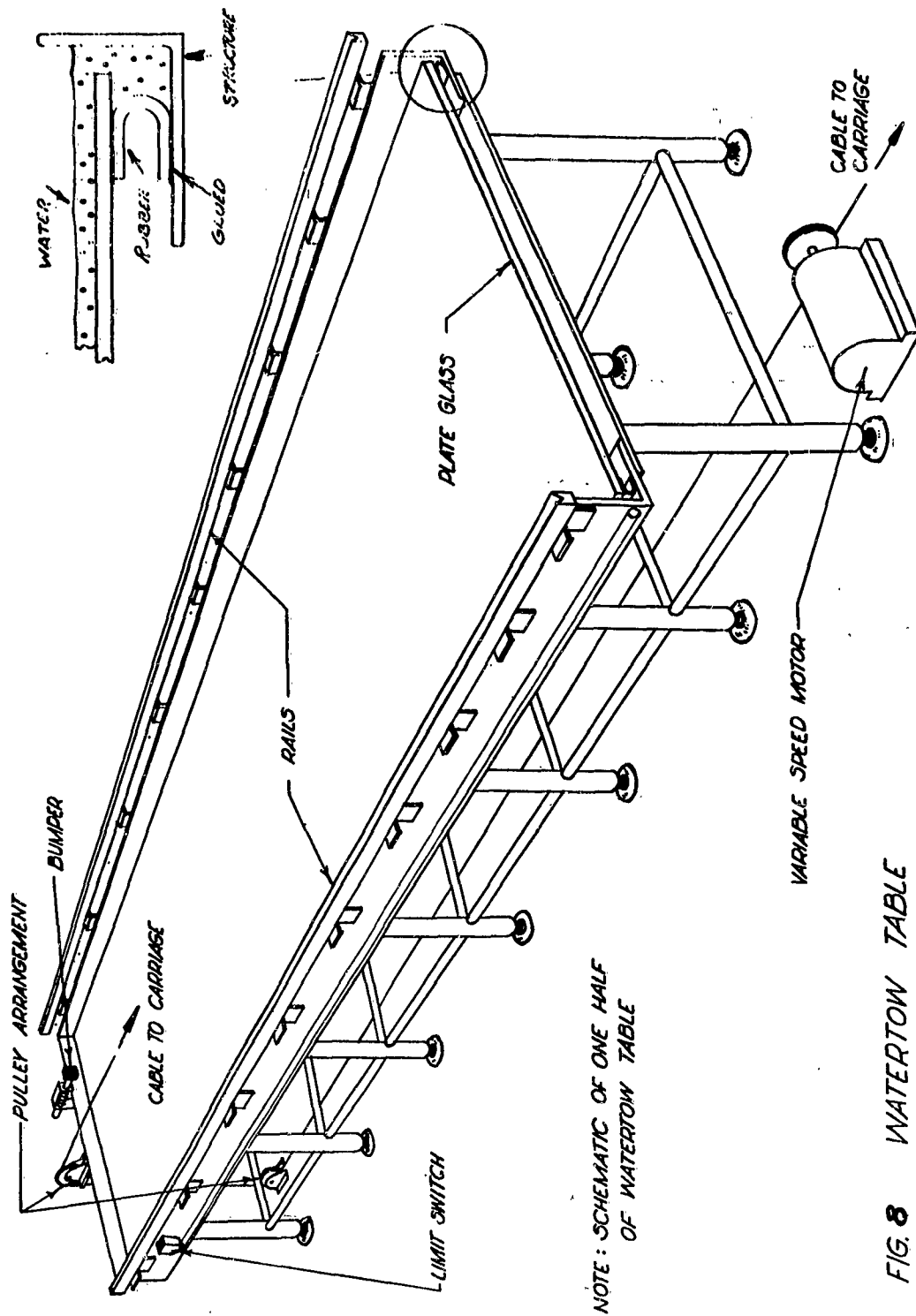


FIG. 8 WATERTOW TABLE

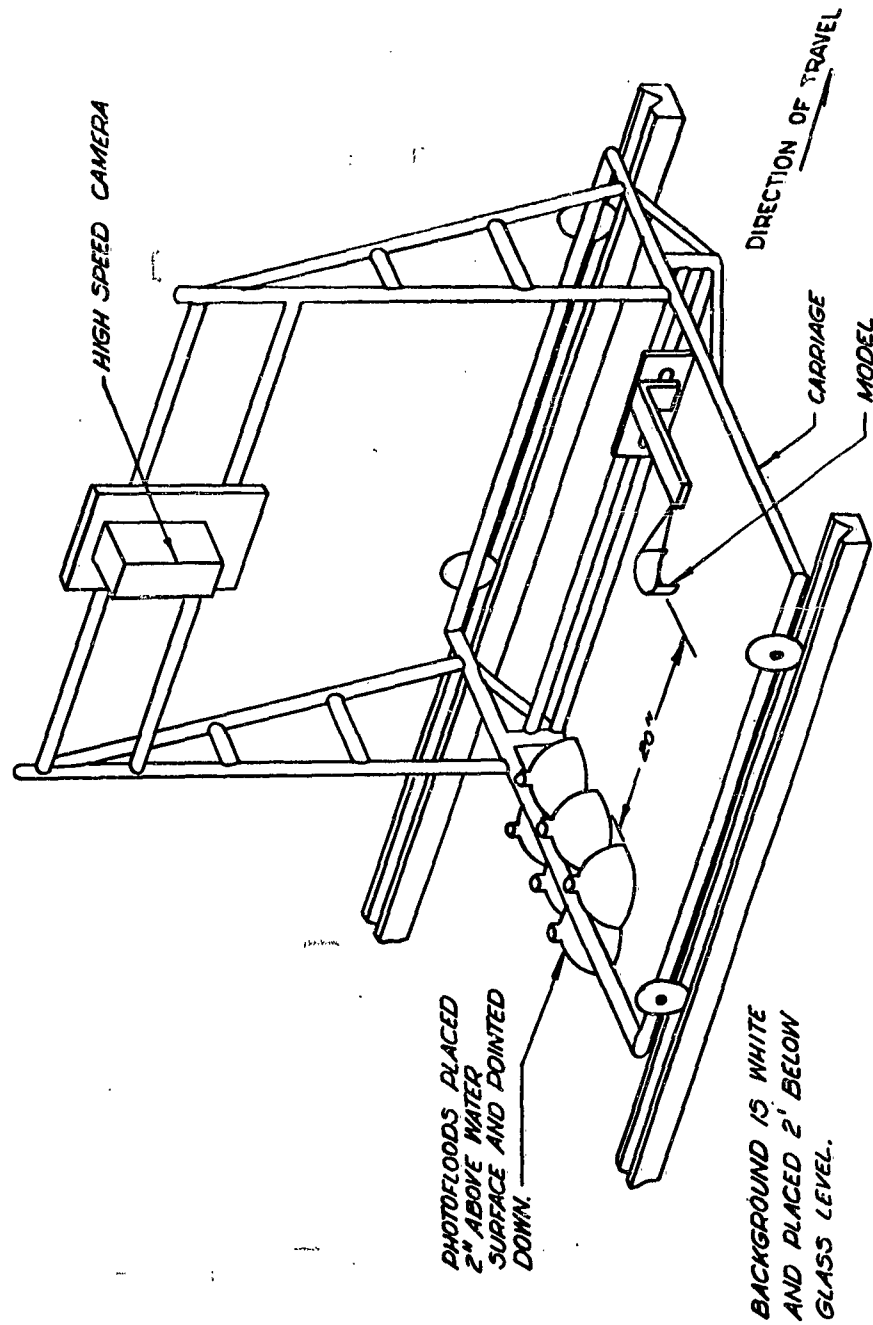


FIG. 9 LIGHTING ARRANGEMENT USED FOR PHOTOGRAPHING
FLOW AROUND MODELS WITH THE HIGH SPEED CAMERA.

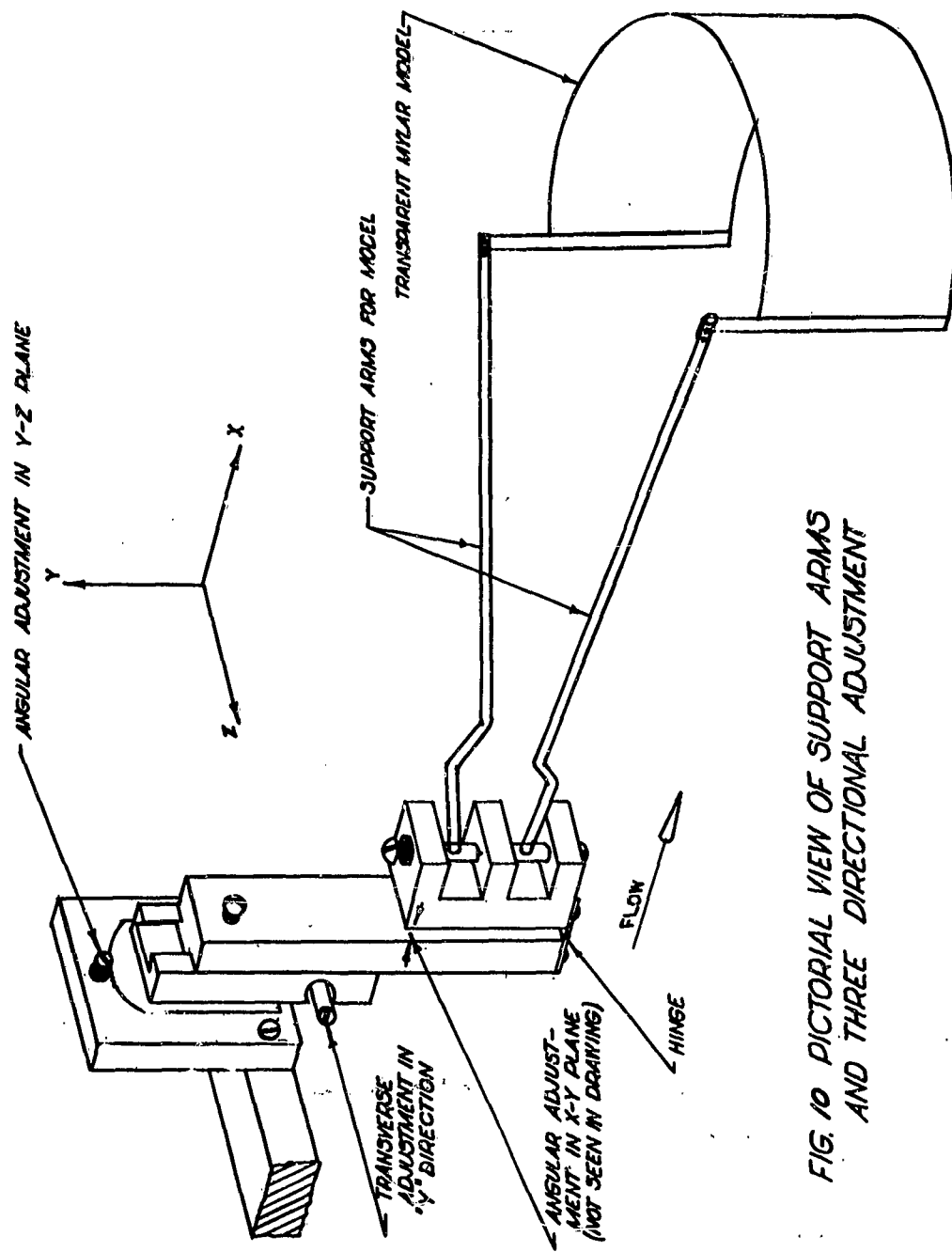


FIG. 10 PICTORIAL VIEW OF SUPPORT ARMS
AND THREE DIRECTIONAL ADJUSTMENT

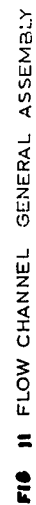
The important improvements incorporated in the new water tow facility are:

- 1) The channel length was increased from 12 ft to 30 ft thereby increasing the testing distance from 6 ft to 24 ft. This gives the model a sufficiently long run to reach a steady state condition and allows ample time for visual observations or photographic recording.
- 2) The 2000 lb supporting structure provides the mass and rigidity necessary to reduce vibrations induced by external disturbances or by the initial acceleration of the carriage.
- 3) The relatively thick mirror finish plate glass and its supporting system of adjustable jack pads allows the channel floor to be set to a tolerance of ± 0.005 in. and enables very small clearances between the freely suspended models and the channel floor.
- 4) The V-groove guide rails and the wedge shaped wheels have eliminated any lateral motion of the carriage.

Moving Water Channel

Figure 11 is a general assembly drawing of this channel showing its main features and dimensions and Fig 12 is a photograph of the channel during construction. The rectangular channel is 20 ft long, 52 in. wide, and 5 in. deep. A single piece of mirror finish plate glass 15 ft long and 1/2 inch thick forms the channel floor. The glass rests on Plexiglas support pads mounted on swivel head adjusting screws. This arrangement allows a precision adjustment of the glass surface.

The vertical side walls of the channel are made of 6 x 3 1/2 x 3/8 in. right angle structural steel attached to the top chord of the supporting structure. The channel is supported by two parallel steel trusses 2 1/2 ft deep; its top chords consist of 4 x 2 1/2 in. steel channel sections running the entire length of the structure. The lower chord is made 4 ft shorter at the downstream end to provide space for the pump and motor drive. At 2 1/2 ft intervals, there are cross ties joining the two top and the two bottom chords. The swivel screws and plastic pads which support the glass floor of the channel are screwed at intervals into the ties between the top chords. Ties at the lower panel joints support the water supply pipe and ducting. Horizontal diagonal bracing members were avoided in order to have large, unobstructed panels directly beneath the glass floor for photographic purposes.



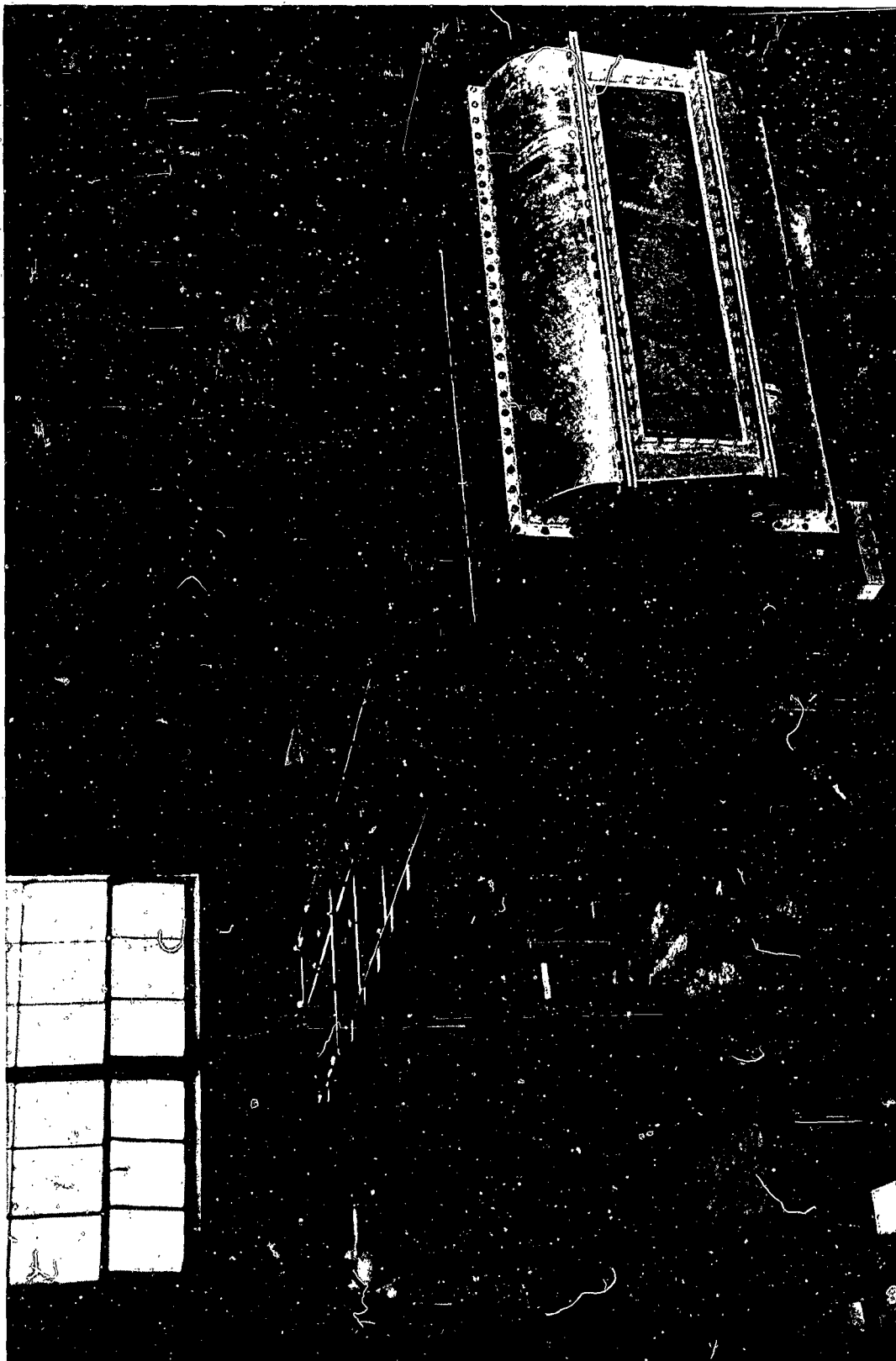


FIG 12 MOVING WATER CHANNEL DURING CONSTRUCTION

Channel Tilting Mechanism

A uniform slope of the channel is necessary to secure uniform flow velocity. This slope must be adjustable in order to attain the water flow velocity representing a certain Mach number. Variation of the longitudinal slope of the channel is provided by means of the tilting mechanism illustrated in the general assembly drawing (Fig 11). At the downstream end of the lower chord, the trusses are mounted on hinge pins. Near the upstream end of the channel, a one inch diameter bar is welded transversely to the bottom of the upper chord members. This bar will be carried by two hydraulic rams, one on each side. The hydraulic rams are connected to a hand operated hydraulic pump by means of flexible pressure tubing and shut-off valves. The hydraulic rams have a graduated travel; they can be operated in unison or independently to obtain the desired longitudinal slope and transverse levelling of the channel.

Water Supply System

The water supply and storage system consists of a steel tank $10\frac{1}{2} \times 3 \times 2\frac{1}{4}$ ft with a capacity of 500 gallons, placed on the floor at the downstream end of the channel so that its length is perpendicular to the channel's longitudinal axis. The pumping equipment consists of a $7\frac{1}{2}$ hp Westinghouse constant speed, three phase induction motor driving a Worthington Centrifugal pump rated at 250 gallons per minute and a total head of 45 ft. The motor and pump are mounted on a bed plate set transversely under the downstream cantilever portion of the truss. The discharge side of the pump feeds into a short flanged diffusing section which increases the diameter from 4 to 6 in. The water flows through a 6 in. Walworth gate valve to regulate the flow, and then to a rubber expansion joint which takes up the displacement resulting from tilting of the table and prevents the vibrations of the pump from being transferred to the trusses. The water then flows through a sequence of diffusers and 90 degree bends until it reaches the nozzle approach section which has a constant cross section of 4×52 in. The nozzle approach section is provided with large removable framed panels for observation of the flow, and incorporates flow straighteners. It leads to the variable nozzle made of a $1/4$ in. thick aluminum plate hinged to the top of the approach section and converging to any desired opening at the lip. The water flow returns to the reservoir by overflowing the downstream end of the channel.

The final assembly of the water channel involved mounting and anchoring in place the main structural framework of the water channel and connecting and sealing the various flanged sections which form part of the water circuit. The plate glass forming the test section floor was mounted on 54 adjustable Plexiglas jack pads suitably spaced.

For levelling the glass surface, the supporting frame was initially levelled and the table was filled to about 1 in. of water. A depth micrometer was used to check the depth at various points and the jack pads were systematically adjusted until the glass surface was everywhere within ± 0.003 in.

The method of sealing the glass was somewhat similar to that used previously in the water tow channel. However, it was necessary to add flexible rubber tubing squeezed between the glass edges and the channel side walls and running the full length of the glass plate on both sides. 3-M Super Weatherstrip adhesive was used for the rubber to glass seal and aquarium cement was used for filling the voids. At the downstream end of the channel, a $1/4$ in. thick, $52\ 1/4$ in. wide and 36 in. long aluminum plate was added to form an extension of the flow channel beyond which the water sheet falls into the 500 gallon capacity reservoir.

At the upstream end of the channel, a $1/4$ in. thick aluminum plate $52\ 1/4$ in. wide and $18\ 3/4$ in. long was hinged to the top plate of the nozzle approach section. By changing the height of the opening at the discharge end, it is possible to vary the water depth up to 2 in. The water flow velocity and corresponding simulated Mach number is controlled by means of the 6 in. Walworth gate valve on the discharge side of the constant speed centrifugal pump.

Initial runs of the water channel were carried out at a water depth of 0.5 in. It was noticed that the slight roughness of the steel angles forming the channel sides and the small irregularities at the corners created disturbances which appeared in the flow as weak oblique waves (simulated Mach waves). To reduce this effect and obtain sharply defined corners for the water flow section, Plexiglas strips $1/2$ in. wide and $2\ 1/2$ in. high were attached to the steel angles along the length of the channel to form the effective sides of the water flow section. This arrangement resulted in a noticeable improvement of the flow.

The two hydraulic jacks used to obtain a longitudinal slope of the channel were adjusted until the glass channel floor was horizontal. This was checked by ensuring the uniformity of the placid water depth throughout the channel using the micrometer depth gage. Two gunners' quadrants obtained from government surplus were mounted on the table near the hydraulic jack supports and adjusted to zero when the channel floor was horizontal. In order to set the channel to any desired slope to correspond to the desired Froude number (simulating the Mach number), it is now only necessary to set the two quadrants to the desired elevation and operate the hydraulic jacks until the level gages of the quadrants are centered.

Next, the carriage guide rails were realigned to be parallel to the glass surface. This was done by means of an Ames dial gage mounted on the triangular stand of the micrometer depth gage. The guide rails were adjusted to be parallel to the glass surface near the corresponding side of the table to within ± 0.001 in.

The multi-probe carriage with traversing mechanism is illustrated in Fig 13. It makes use of a standard optical bench bedplate to which extension pieces fitted with bevelled wheels were added. The bevelled wheels ride on two V-groove guide rails and provision is made for locking the carriage in any longitudinal position and indicating the position by means of a scale attached to one of the guide rails. The use of a standard optical bench bedplate affords good traversing accuracy for the probe carriages and flexibility in varying the number and location of the probes.

Figure 14 is a view of the structural framework of the channel looking towards the reservoir end. It shows the probe carriage and traversing mechanism and part of the lower water ducting mounted in place. Figure 15 shows the main reservoir with internal transverse stiffeners and drain pipe. Figure 16 shows the mounting of the centrifugal pump, reducing section, gate valve and part of the flexible coupling which attaches to the lower part of the water ducting.

Instrumentation

The design of the shadowgraph system is shown diagrammatically in Fig 17. The light source is a carbon arc lamp with the center of the arc positioned at the focal point of a 14 in. diameter, 14 in. focal length plastic Fresnel lens which is located directly under the test section. The lens produces a parallel beam of light through the test section. The shadowgraph image is formed on a frosted glass screen mounted horizontally above the model, on a frame attached to the model carriage.

This image can be viewed directly or photographed by still or movie cameras.

The design of the Schlieren system was integrated with that of the shadowgraph to enable a quick change over from one system to the other. As shown diagrammatically in Fig 7, the Schlieren system shares the same light source and Fresnel lens located underneath the channel test section but the horizontal viewing screen directly above the model is removed and an optical assembly, lens, and turning prism are mounted in its place. The parallel light beam through the test section is condensed by the second Fresnel lens and impinges on the knife edge, is turned 90° by the prism and is then projected onto a frosted glass screen mounted vertically in a frame attached to the carriage. Figure 18 is a photograph

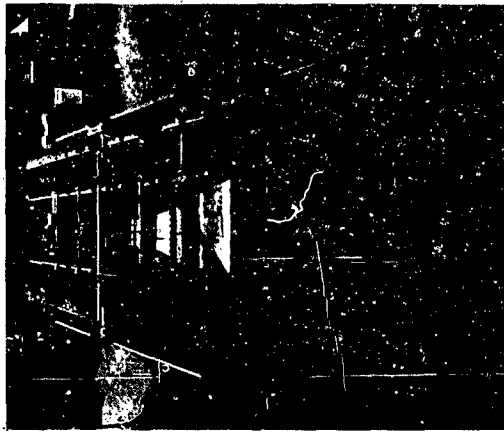


FIG 14 STRUCTURAL FRAMEWORK

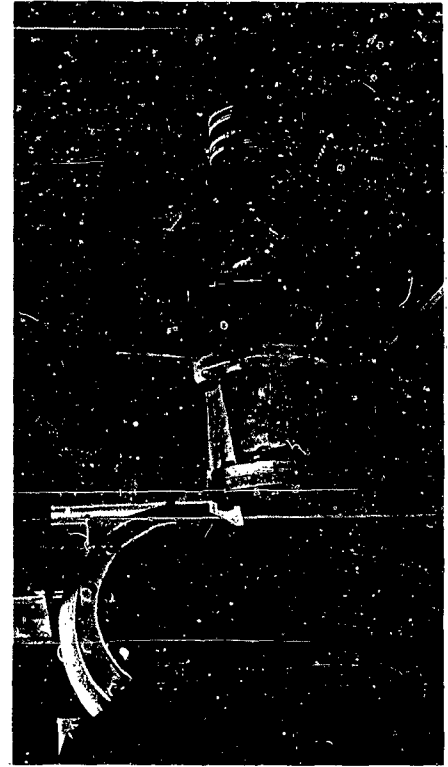


FIG 16 PUMP AND GATE VALVE



FIG 13 MULTI-PROBE CARRIAGE



FIG 15 RESERVOIR

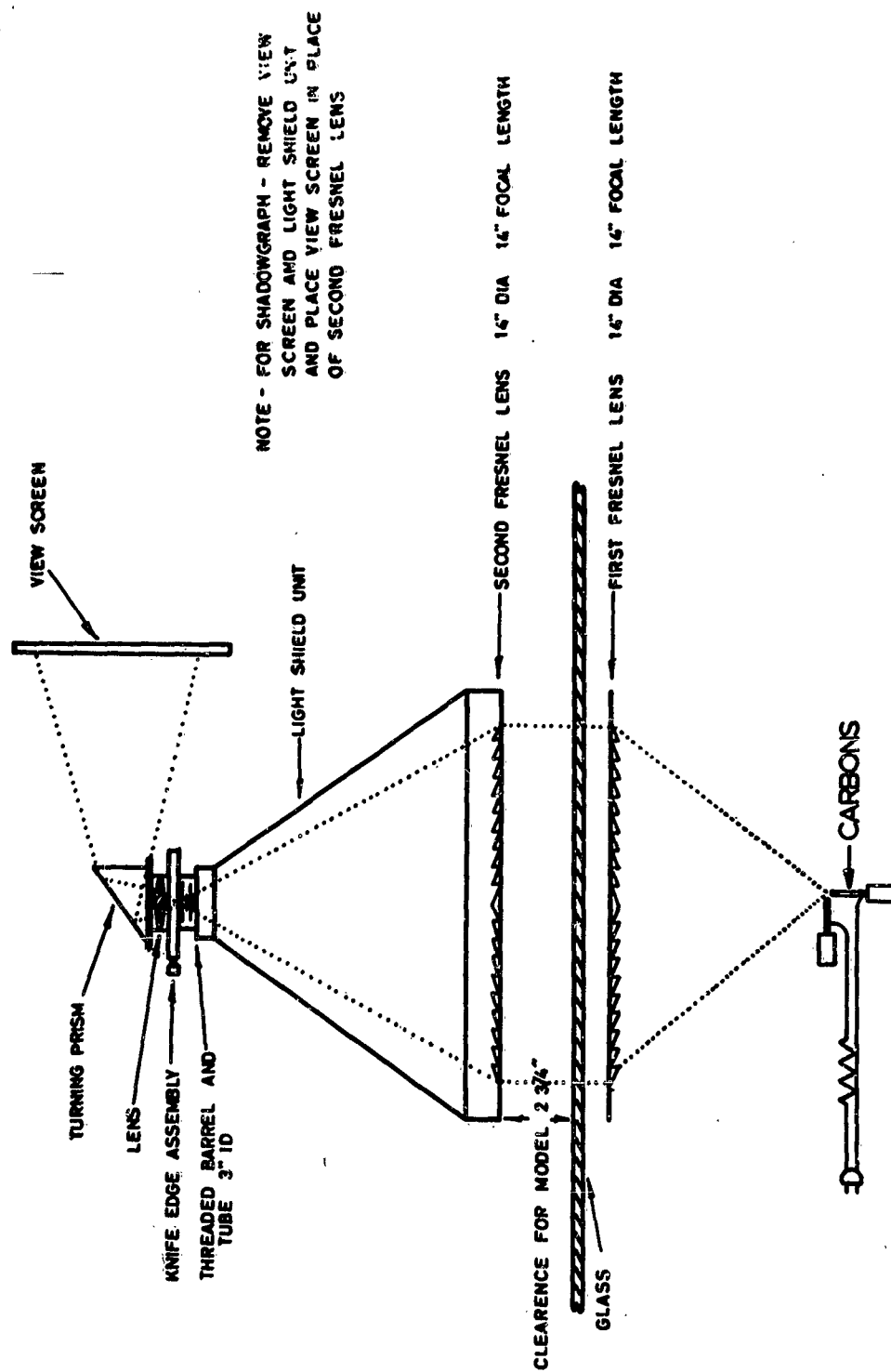


FIG 17 SKETCH OF SCHLIEREN AND SHADOWGRAPH

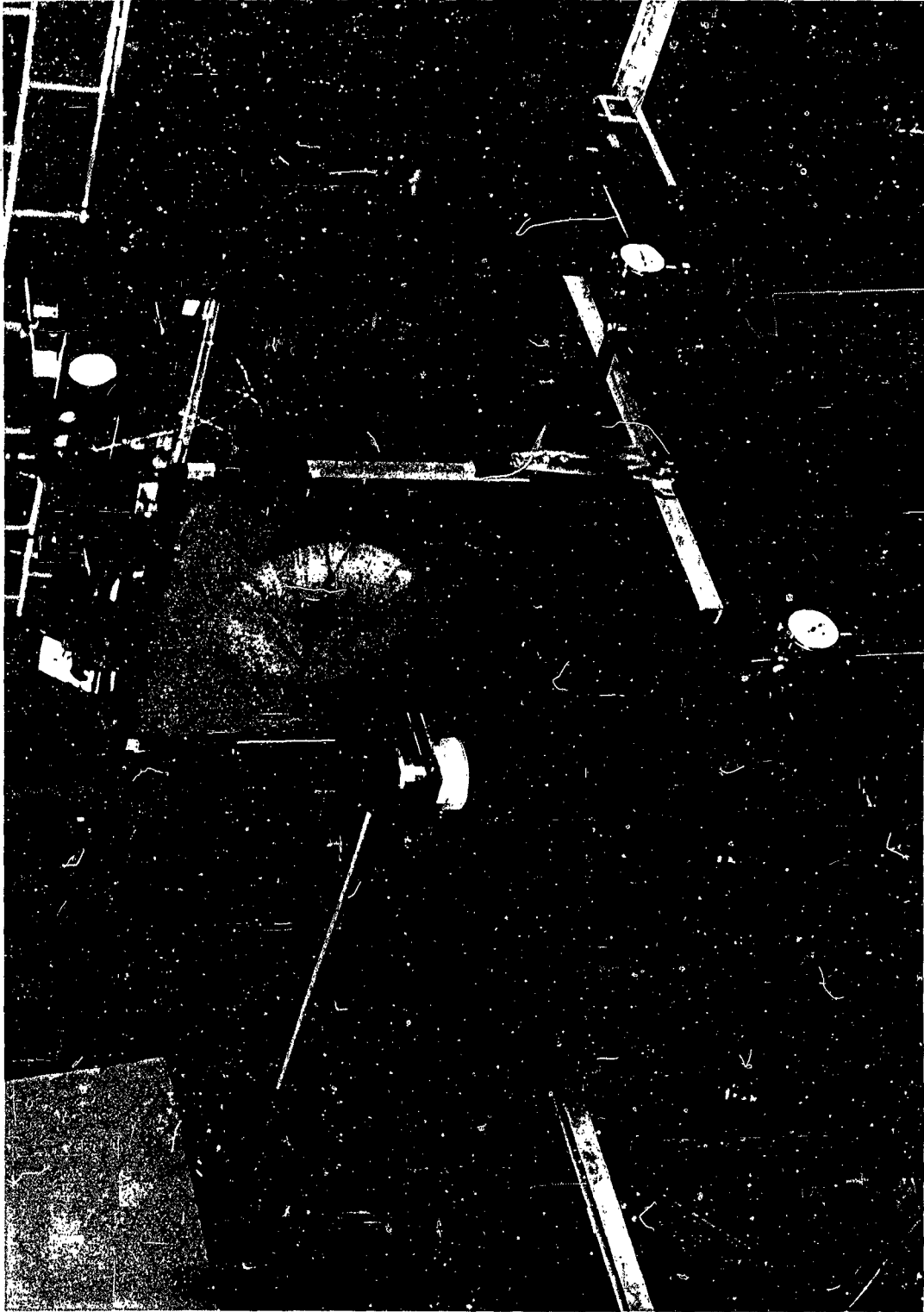


FIG 18 VIEW OF SCHLIEREN SYSTEM IN OPERATION

of the general arrangement of the upper assembly of the Schlieren system, and shows the Schlieren image of a diamond airfoil projected on the viewing screen. The thin plastic Fresnel lenses were found to be much improved by mounting them between two sheets of single weight window glass to avoid warping of their surfaces and consequent distortions of the flow image.

It is of interest to note that in photographing the shadowgraph and Schlieren patterns, it is possible to minimize random changes in the flow images obtained by using relatively long exposures of one or two seconds.

Two pointed probes attached to standard 1 in. travel Ames dial gages were designed for mounting on the traversing carriage. These probes were used for measuring the water depth distribution and calculating the simulated pressure coefficient field surveys presented later.

A special nozzle depth gage to enable a quick setting of the opening of the variable nozzle to the desired free stream water depth was constructed. It consists of a Plexiglas wedge with a rise of 1 in. over a length of 10 in. and is graduated along the length in 0.1 in. divisions, corresponding to a 0.01 in. rise.

A large piece of clear plastic, covering the field of view of the 14 in. diameter lens, was ruled off in $1/2$ in. squares and attached to the glass under the test section area, providing a reference grid which aids in the initial positioning of the model, defines clearly the probe positions in the flow field, and helps interpret the shadowgraph and Schlieren images.

A recently developed pressure sensitive paint (Celab Pressure Sensitive Paint No 9-A) appeared to hold great promise for use as a simple transducing element for hydrostatic and total pressure probes. Preliminary tests with this paint were carried out to evaluate its general operating characteristics such as sensitivity, repeatability, and drift. Gages have been constructed on pieces of plastic 0.015 in. thick. Unfortunately, all gages constructed thus far have shown a marked zero drift and it appears that the design of a satisfactory pressure transducer of this type for water channel application may require rather extensive developmental work. Some preliminary tests with a water pressure probe consisting essentially of an impact or pitot tube connected to a micromanometer showed the necessity for minimizing the size of the probe and a careful choice of its dimensions. Brass tubing with various small diameters ranging from $1/8$ in. to less than $1/32$ in. O.D. are being used to develop small impact probes to be hooked up to a sensitive water column manometer using a connecting tube filled with water. This eliminates any erroneous readings due to air water interfaces in the connecting tubes.

Before conducting any quantitative tests with the analogy, a depth survey of the channel test section area was carried out to determine the tolerance margins on depth measurements. For this purpose, the depth probes described above were used. With the channel floor set horizontally in both the longitudinal and transverse directions, the water depth in the test section area was found to be within ± 0.003 in. from the reference value.

Experimental Procedure

In a moving water channel, the quantities that may have to be measured are the rate of water flow, the values and directions of local flow velocities, the angles formed by hydraulic jumps and weak waves with respect to the direction of the flow velocity and the water depths at different points of interest of the flow field.

The rate of water flow may be obtained from standard hydraulic measurements. The measurement of local velocity may be made by a pitot-static or Prandtl tube; this may be inconvenient on account of the small water depths and relatively large diameter of the Prandtl tube and a more effective way of obtaining the local water velocity involves the use of an impact or pitot tube to measure the total head d_0 and simultaneously measuring the local water depth and obtaining the velocity from Eqn 5:

$$V_w^2 = 2g(d_0 - d) \quad (5)$$

At present, the flow Mach number to be simulated is set up by means of wave angle measurements using a symmetrical diamond airfoil with a wedge angle of 24 degrees at both leading and trailing edges. A more basic method setting up the simulated Mach number from direct measurements of the water velocity will be used when suitable miniature water pressure probes are developed.

The channel flow for simulating a desired Mach number is obtained by adjusting the nozzle flap to the desired opening height thus specifying the water depth, setting up the longitudinal channel slope to the required value as specified in Manning's formula given below and then adjusting the pump discharge by means of the Walworth gate valve until the oblique shock angle coming off the leading edge of the diamond airfoil equals the desired value for correct Mach number simulation at the water depth used.

The model is then placed in the test section, carefully aligned with respect to the reference grid, and water depth measurements taken at all grid points in the area of interest and also at points of intersection of the reference grid and the model surface as close to the model as the probes allowed.

These measurements are made by means of the depth probes mounted on the standard Ames dial gages with zero pre-setting and reading to 0.001 in. By pre-setting the zero to coincide with the channel floor, the water depth is obtained by setting the needle probe to touch the water surface. In placid water, a meniscus is formed when the needle probe touches the water but in flowing water, a system of waves is formed. The error involved in measuring the level of a liquid at rest is about 0.003, i.e., of the same order as the tolerance on the glass surface but, in the case of a flowing liquid, the error is larger, particularly for turbulent flow on account of the pulsations of the level. In order to obtain more consistent results, the depth is calculated from the arithmetic mean of the maximum and minimum depths where the maximum depth is measured at the instant when the tip first touches the water surface and the minimum depth is measured when the tip constantly touches the water surface. In order to avoid individual differences of interpretation, all the depth readings of a given test are made by the same operator. However, tests of the same model by different individuals produced substantially the same results. The measurements of water depth on the model itself are obtained by means of the Eosin dye technique described later. In this case, a correction factor for the meniscus was determined experimentally using the same model with placid water of known depth.

The flow rate in the channel is a function of the water depth and channel slope in the flow direction. The commonly accepted Manning formula for open channel flow (Ref 7) was employed to determine the channel slope necessary to produce a given Froude number (F). Hence, the velocity corresponding to different water depths is determined by,

$$V = \frac{1.49}{n} R_h^{2/3} S^{1/2} \quad (36)$$

where

V = water velocity in feet per second

R_h = hydraulic radius in feet; this is the ratio of flow cross-sectional area to the wetted perimeter

S = slope of the channel bed

n = roughness coefficient.

From Ref 7 a value of $n = 0.008$ was used for the smooth glass.

In the hydraulic flow, the Froude number (F) simulates the Mach number (M) of the aerodynamic flow. The quantitative tests reported here were for a Froude number $F = 2$.

Calculation of Simulated Pressure Coefficients from Water Depth Measurements

In a simple quantitative application of the analogy, one may derive the air density, temperature and pressure distributions directly from the water depth distribution using, in each case, the correspondence indicated earlier. It will then be found that varying degrees of agreement will result and that the best agreement obtained is that between the depth ratio and the density ratio as can be shown from Fig 2 taken from Ref 7. A modification of the direct analogy, originally proposed in Ref 7 produces greatly improved numerical results. The basis of this modification is the use of the depth ratio to determine the analogous density ratio only. All the other desired aerodynamic quantities are calculated from the density ratio by means of well known aerodynamic relations. In this way, the good agreement between air density ratio and water depth ratio is more fully exploited. The improvement in numerical interpretation of the analogy is illustrated in Table 1, taken from Ref 7.

Water Depth Distribution Around Models The Eosin Dye Method

In order to be able to calculate, by analogy, the pressure distribution on the surface of a given two-dimensional body in air, it is necessary to determine experimentally the water depth distribution around the hydrodynamic model. A simple experimental technique which would give the water depth profile (the watermark) around the fixed model immersed in the running water was needed. A technique using photographic paper wrapped around the model and exposed, for a brief period, to external lighting had been successfully used with the early water tow channel but that technique was inconvenient because it necessitated conducting the tests in a darkened room and involved manipulations of the model mounting, in the dark, prior to each test.

Experiments were conducted with commercial water colors and various water soluble dyes such as Methylene Blue, Saffranine, Aniline Blue, and Eosin applied to the model surface. The experiments were to determine certain desirable characteristics such as method of application, concentration of the dye, surface preparation of the model, time required for the dye to wash away from the immersed region, and sharpness of definition of the water mark. An aqueous and alcoholic solution of Eosin with Kodak Photo-Flo added as a wetting agent was very satisfactory, giving a sharply defined outline on the model surface. This solution is painted on the Plexiglas or aluminum model surface and it dries quickly.

Two slightly different experimental procedures were used. In the first, the dye painted model was lowered vertically in position into the flowing water until it made contact with the glass floor. In the second, the model was

set up in the test section prior to starting the water flow. In both cases, the dye was quickly washed away from the immersed portions of the model and a sharp water line obtained. Care was taken to use short test durations of the order of 4 or 5 seconds and to watch for any pulsations of the water flow since the water line obtained represented the maximum rather than the time average water depth at each point.

Another dye technique with the object of indicating the range of variation of water depth at every point of the boundary was tried. This method uses coloring agents which form a very thin film that floats on the water surface. The results were unsatisfactory because the dye marked only the stagnation region but separated from the rest of the model boundary and was quickly washed away downstream.

It must be noted, of course, that the capillary attraction of the model wall for the water surface will affect the local height of the water level and that corrections for these effects, based on separate experiments, should be applied.

Data Reduction Procedure

The procedure employed to calculate the desired aerodynamic quantities from water depth measurements is the following.

- 1) The values of ρ_{∞}/ρ_T , P_{∞}/P_T , and q_{∞}/P_T corresponding to the desired flow Mach number are taken from standard compressible flow tables such as Ref 12. Subscripts ∞ and T indicate the free stream and total stagnation conditions respectively.
- 2) From the experimental value of the local depth d and the free stream depth d_{∞} , the dimensionless water depth ratio d/d_{∞} is calculated and interpreted as the airdensity ratio ρ/ρ_{∞} .
- 3) The value of ρ/ρ_T is calculated by means of the simple relation:

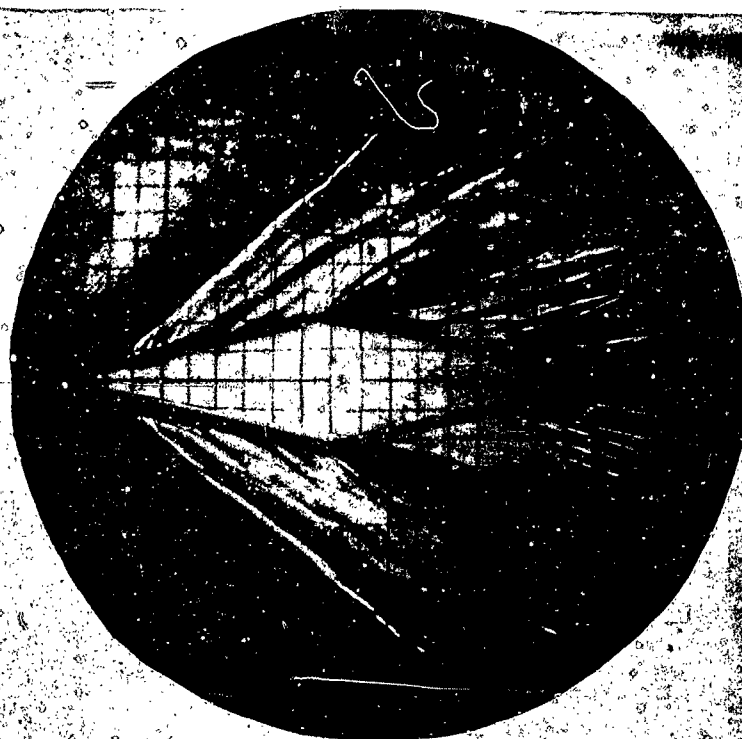
$$\rho/\rho_T = \rho/\rho_{\infty} \times \rho_{\infty}/\rho_T.$$

- 4) Using Ref 12, any aerodynamic property corresponding to ρ/ρ_T such as P/P_T , T/T_t or local Mach number can be obtained.
- 5) The local pressure coefficient can then be obtained by means of the relation:

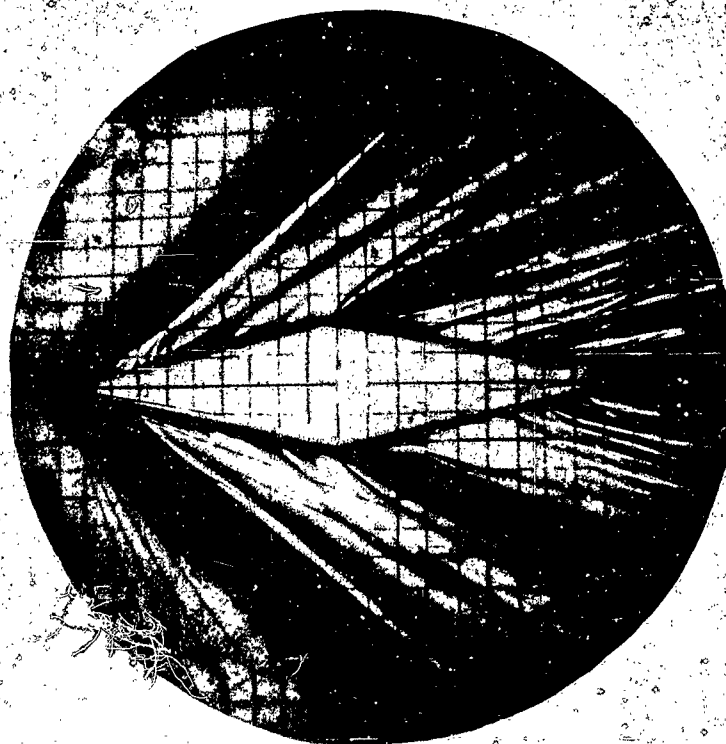
$$C_p = \frac{P - P_{\infty}}{q_{\infty}} = \left(\frac{P}{P_T} - \frac{P_{\infty}}{P_T} \right) \frac{P_T}{q_{\infty}}.$$



FIG 19 PLEXIGLAS MODELS USED IN MOVING WATER CHANNEL



(A) INSTANTANEOUS (1/25 SEC)



(B) TIME EXPOSURE (2 SEC)

FIG 20 SCHLIEREN PHOTOGRAPH OF A 12°
DIAMOND AIRFOIL AT $M_\infty = 2.0$



(A) SHADOWGRAPH

(B) SCHLIEREN PHOTOGRAPH

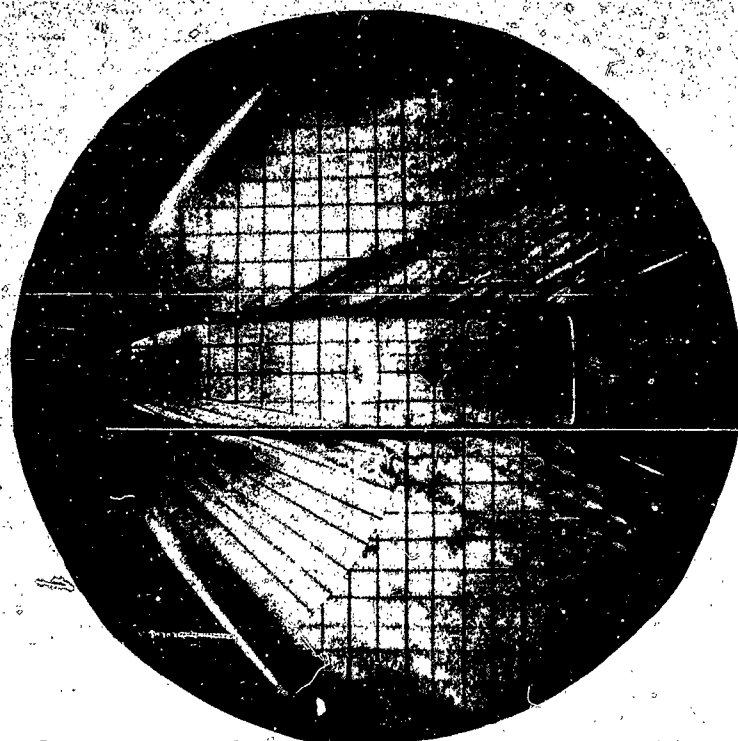
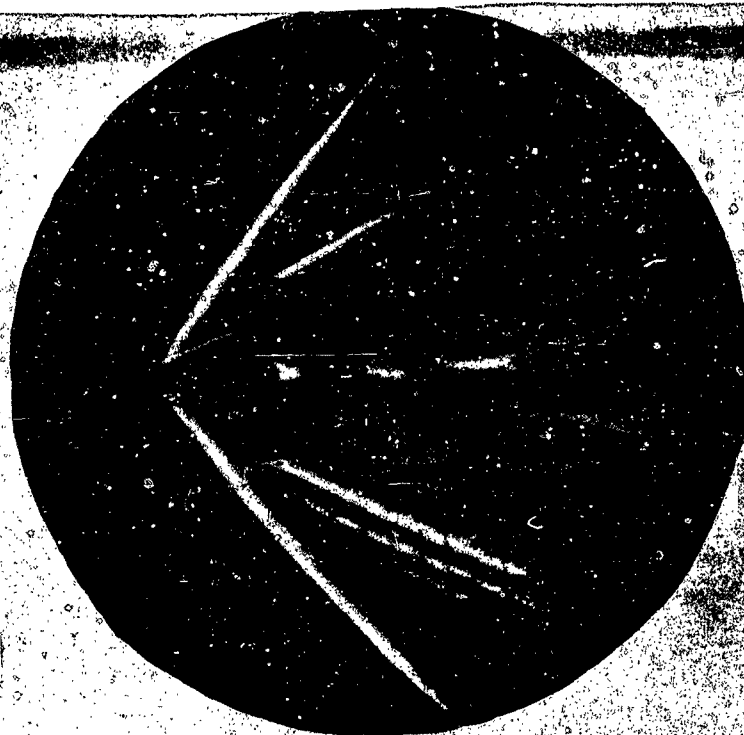


FIG 21 SHADOWGRAPH AND SCHLIEREN PHOTOGRAPH OF AN OGIVE CYLINDER AT $M_\infty = 2.0$



(A) SHADOWGRAPH

(B) SCHLIEREN PHOTOGRAPH

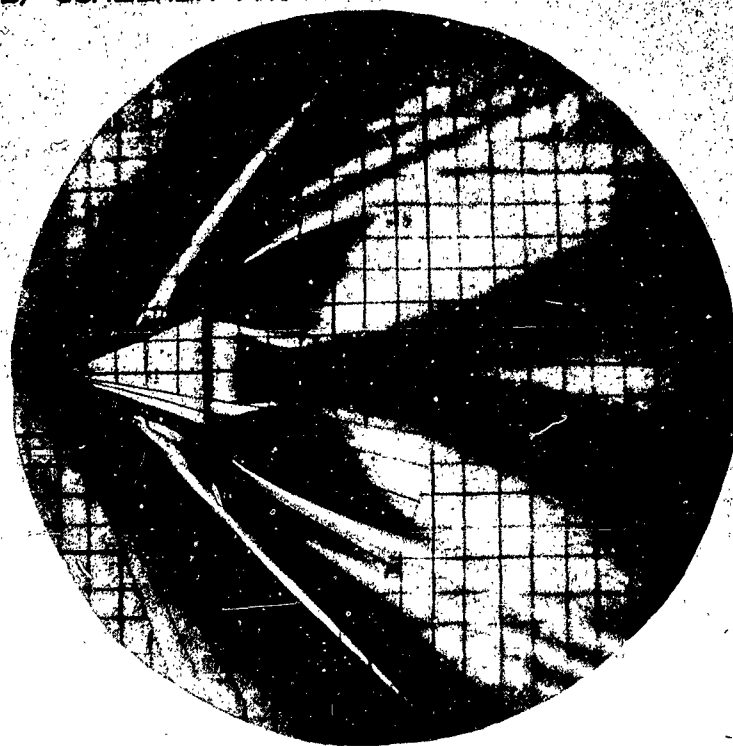


FIG 22 SHADOWGRAPH AND SCHLIEREN PHOTOGRAPH OF A 20° WEDGE AT $M_{\infty} = 2.0$

TEST CONDITIONS

FROUDE NUMBER: $Fr = 2.0$

FREE STREAM WATER DEPTH: $d_{\infty} = .304$ in

FROM NACA TR 1135 FOR $M_{\infty} = 2$

$R/\rho = .230$

$P_{\infty}/P_T = .128$

$q_{\infty}/P_T = .358$

| STA-TION | d (in) | d (ave) (in) | d/d _∞ (= d/d _∞) | ρ/ρ _T | P/P _T NACA TR 1135 | P/P _T - P _∞ /P _T | C _P |
|----------|--------|--------------|--|------------------|-------------------------------|---|----------------|
| 0 L | 0.334 | | | | | | |
| | | 0.332 | 1.09 | 0.251 | 0.145 | 0.017 | 0.048 |
| 0 R | 0.330 | | | | | | |
| 1 L | 0.552 | | | | | | |
| | | 0.542 | 1.78 | 0.409 | 0.284 | 0.156 | 0.436 |
| 1 R | 0.532 | | | | | | |
| 2 L | 0.523 | | | | | | |
| | | 0.506 | 1.66 | 0.382 | 0.261 | 0.133 | 0.372 |
| 2 R | 0.492 | | | | | | |
| 3 L | 0.492 | | | | | | |
| | | 0.484 | 1.59 | 0.366 | 0.246 | 0.118 | 0.330 |
| 3 R | 0.476 | | | | | | |
| 4 L | 0.499 | | | | | | |
| | | 0.488 | 1.60 | 0.368 | 0.246 | 0.118 | 0.330 |
| 4 R | 0.478 | | | | | | |
| 5 L | 0.426 | | | | | | |
| | | 0.423 | 1.39 | 0.320 | 0.203 | 0.075 | 0.210 |
| 5 R | 0.420 | | | | | | |
| 6 L | 0.204 | | | | | | |
| | | 0.207 | 0.68 | 0.156 | 0.074 | -0.054 | -0.151 |
| 6 R | 0.210 | | | | | | |
| 7 L | 0.196 | | | | | | |
| | | 0.196 | 0.64 | 0.147 | 0.068 | -0.060 | -0.168 |
| 7 R | 0.197 | | | | | | |
| 8 L | 0.199 | | | | | | |
| | | 0.202 | 0.66 | 0.152 | 0.072 | -0.056 | -0.156 |
| 8 R | 0.204 | | | | | | |
| 9 L | 0.205 | | | | | | |
| | | 0.201 | 0.66 | 0.152 | 0.072 | -0.056 | -0.156 |
| 9 R | 0.197 | | | | | | |
| 10 L | 0.239 | | | | | | |
| | | 0.232 | 0.76 | 0.175 | 0.087 | -0.041 | -0.114 |
| 10 R | 0.224 | | | | | | |

TABLE 2 EXPERIMENTAL DATA AND RESULTS FOR DIAMOND AIRFOIL MODEL

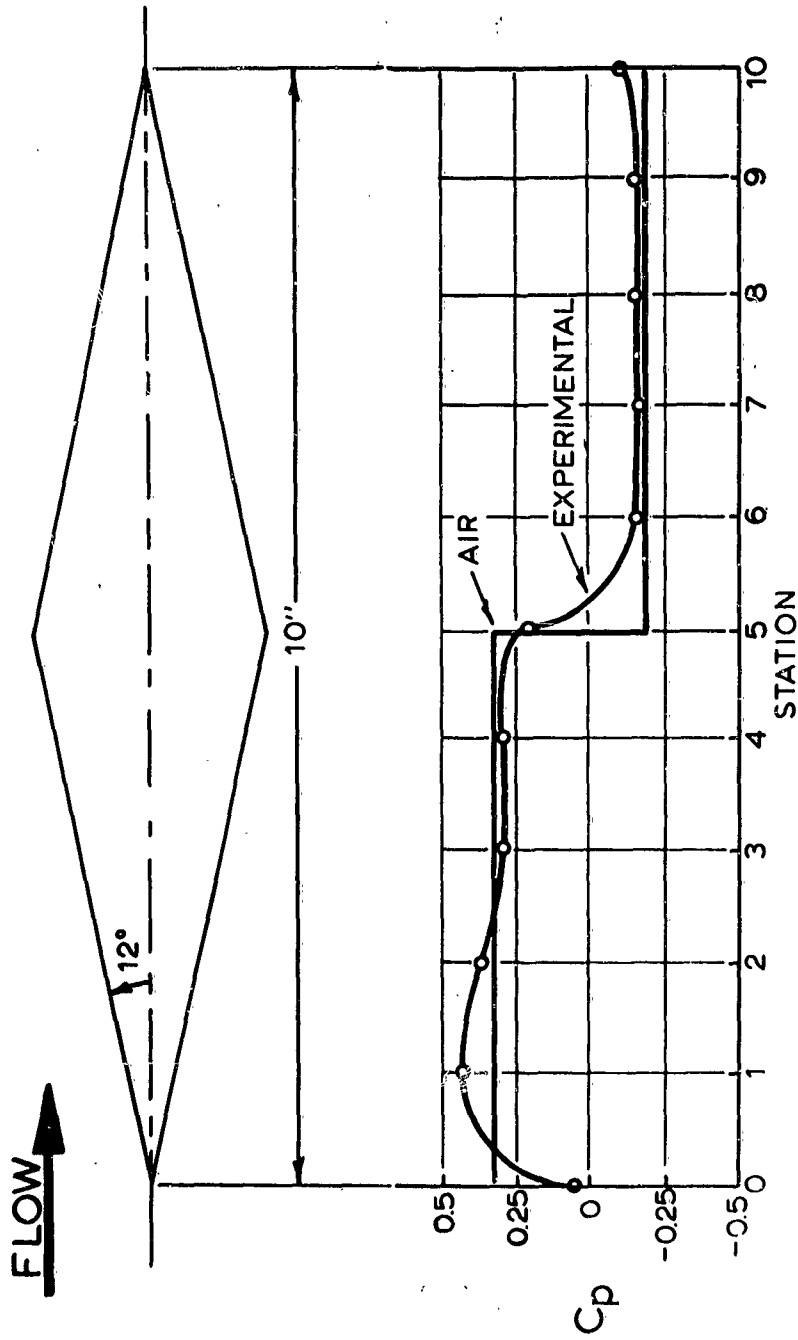


FIG 23 COMPARISON OF EXPERIMENTAL PRESSURE COEFFICIENTS WITH THEORETICAL VALUES FOR A SYMMETRICAL DIAMOND AIRFOIL AT $M=2$



FIG 24 PRESSURE COEFFICIENT FIELD SURVEY SUPER-
IMPOSED ON A SHADOWGRAPH OF A 20° WEDGE
AT $M_\infty = 2.0$

EXPERIMENTAL RESULTS

Shadowgraph and Schlieren Flow Patterns

The development of effective Schlieren and shadowgraph systems and suitable photographic techniques involved much experimentation with model materials, lighting, viewing arrangements and camera settings. As regards model material, the best results were obtained with Plexiglas models particularly for schlieren pictures. With opaque models, shadows around the contour prevented a clear delineation of the model outline. Figure 19 shows some of the models used. Figures 20A and 20B illustrate two schlieren images of the flow past a diamond airfoil at a simulated Mach 2. Figure 20A was taken with a short exposure of $1/25$ second and shows slight irregularities of the wave pattern while Fig 20B, taken with a long exposure of 2 seconds shows that the random fluctuations have been largely smoothed out and a much more regular pattern obtained. Figure 21A illustrates the shadowgraph of the flow past an ogive cylinder model at a simulated Mach 2 while Fig 21B is a schlieren image of the same model. Both photographs were taken with a 2 second exposure. Figures 22A and 22B show a shadowgraph and a schlieren image of the flow past a 20° wedge and clearly illustrate the difference between the two techniques. The shadowgraph is sensitive to the second derivative of the water depth while the schlieren is sensitive to the first derivative, i.e., the slope of the water surface; it therefore can show gradual depth changes such as correspond to the Prandtl-Meyer expansion at the rear corners of the wedge.

Water Depth Distribution Tests

Table 2 and Fig 23 present the experimental data and calculated results for the diamond airfoil model at a simulated Mach 2 and provide a comparison between the pressure coefficients obtained experimentally by means of the Eosin dye technique and the values calculated theoretically. The object of testing this simple configuration was to develop the experimental and data reduction procedures and to compare the experimental results with those of accepted aerodynamic theories. It is seen that there is reasonable agreement except perhaps at the corners of the model where the analogy indicates a rounded, more gradual change of pressure instead of the abrupt, step function change predicted by theory.

Figure 24 was obtained by superimposing the contour lines simulating the lines of constant pressure (isobars) as obtained from water depth measurements of the two-dimensional wedge on the schlieren pattern presented in Fig 21B. A modified experimental procedure, resulting in

an appreciable saving of time was adopted in this case. Instead of making depth probings at pre-selected grid points and then calculating the constant depth contour lines by interpolation, pre-selected values of the pressure coefficient were chosen, the corresponding depths calculated and, with the depth probes set at these values, the geometric coordinates of these contour lines obtained experimentally.

GENERAL REMARKS AND CONCLUSIONS

Desirable Features for a Gas-Hydraulic Analogy Facility

The experience gained with the water analogy over the past five years suggests the following characteristics to be very desirable features for a water analogy facility:

- a) Adequate width of channel to permit the study of models of relatively large size. Too large a width, however, would require overhead means of reaching the model section.
- b) Adequate length of the channel. For a moving water type, this should be sufficient to ensure uniform flow ahead of the model and provide sufficient length downstream to study the full wave pattern. For a water tow channel, the length should be such as to allow the flow to reach a steady state and provide enough time for flow observation or recording. An effective run of 24 ft was found to be quite adequate for our purposes.
- c) Adequate rigidity and mass of the supporting structure to minimize channel deflections and reduce vibrations induced by external disturbances.
- d) Smooth, transparent channel floor to reduce frictional losses and allow for adequate lighting and photography. The channel floor should preferably be mounted on adjustable supports to reduce channel floor sag and deflections to the minimum.
- e) Means for adjusting the longitudinal channel slope in the case of a moving water facility.
- f) Wide range of water depths and velocities to permit optimum choice for simulating a given Mach number.
- g) Avoidance of transverse disturbances in the flow field. This requires a very smooth finish to the channel sides and model surfaces.

Comparison of the Two Types of Water Channel

The main advantages of the water tow channel are:

1. Great reduction of the detrimental effects of viscosity on the flow field. Such effects act on the model surface whereas in the moving water channel, they act on the bottom and side surfaces of the channel as well as on the model surfaces.
2. Possibility and relative ease of simulating transient phenomena such as starting flow, accelerated or retarded flow.
3. Experimental flexibility and relative ease of simulating the Mach number range by varying the speed of the carriage and the still water depth.

The main advantages of the moving water channel are:

1. Ease of observation of the fixed models visually or by photographic means including more specifically the shadowgraph and schlieren techniques.
2. Relative simplicity of instrumenting the models and obtaining quantitative data including specifically means of measuring the depth distribution around the model and throughout the flow field and interpreting such measurements in terms of aerodynamic quantities.
3. Indefinite test duration made possible by the closed-cycle, continuous water flow.

General Conclusions

1. The gas-hydraulic analogy has proved to be an effective tool for investigating a number of aerodynamic decelerator problems in the transonic and low supersonic regimes. Specifically, overall wave patterns for single bodies and two-body combinations, the stability characteristics of rigid and flexible canopies, the inflation characteristics and free shapes of flexible canopies and the simulated pressure distribution were obtained.
2. The relatively simple nature of the experimental set up and the ease and rapidity of making models and modifying them when necessary make of the analogy a valuable "clearing house" for the preliminary evaluation of ideas concerning shapes and flow characteristics. In that respect, it is a guide to the correct approach for wind tunnel investigations and therefore more of an adjunct than a substitute for wind tunnel and high speed track tests.

3. The analogy has the additional essential merit of making it particularly easy to visualize the whole flow field and observe the changes resulting from a change of flow parameters.
4. The propagation speed of surface waves is of the order of 10^{-3} that of pressure waves in air and thus the observed phenomena in the channel are in effect, slow motion replicas of those taking place in air.
5. The size of model used in experiments has an important effect upon the results and large ratios of longitudinal dimensions to water depth should be used.
6. Effective use of the water channel as a research tool requires an intimate knowledge of its hydraulic characteristics and a judicious interpretation of its results. By means of certain modifications in the interpretation of the analogy, greatly improved conversion from hydraulic measurements to aerodynamic quantities is possible.
7. Theoretical considerations indicate the analogy to be equally valid for steady as well as for unsteady flow problems such as accelerated and retarded flow. Such investigations are particularly relevant to problems of aerodynamic deceleration and would be very difficult to conduct on conventional facilities. They appear to provide new and potentially fruitful fields of application of the analogy.
8. Another possible application of the analogy involves the measurement of forces and moments on models freely suspended in the water channel and interpreting such measurements in terms of aerodynamic force and moment coefficients.

SUMMARY OF THE ANALOGY

Two-Dimensional Compressible
Gas Flow

Liquid Flow with Free Sur-
face in Gravity Field

Flow Medium

Hypothetical Compressible Gas
with $\gamma = \frac{C_P}{C_V} = 2$

Incompressible Liquid

Field Geometry

Two-dimensional field with
model and side boundaries geo-
metrically similar to liquid
flow field

Shallow water with horizon-
tal bottom and free top
surface. Model and sides
geometrically similar to
gas flow field

Corresponding Quantities

Velocity ratio: $\left(\frac{V}{V_{\max}}\right)_A$

Velocity ratio: $\left(\frac{V}{V_{\max}}\right)_W$

Temperature ratio: $\frac{T}{T_0}$

Water depth ratio: $\frac{d}{d_0}$

Density ratio: $\frac{\rho}{\rho_0}$

Water depth ratio: $\frac{d}{d_0}$

Pressure ratio: $\frac{p}{p_0}$

Water depth ratio squared $\left(\frac{d}{d_0}\right)^2$

Velocity of sound: $a = \sqrt{\frac{\gamma p}{\rho}}$

Wave velocity: $c = \sqrt{gd}$

Mach number: $M = \frac{V_A}{a}$

Froude number: $F = \frac{V_W}{c}$

Subsonic Flow

Streaming Flow

Supersonic Flow

Shooting Flow

Shock Wave

Hydraulic Jump

REFERENCES

1. Riabouchinsky, D. Sur l'Analogie Hydraulique des Mouvements d'un Fluide Compressible, Compt. Rend. de l'Academie des Sciences, Paris, Vol. 195, 1932 and Vol. 199, 1934 (French).
2. Ippen, A. T. and Knapp, R. T.: A Study of High Velocity Flow in Curved Channels of Rectangular Cross Section, Trans. of the American Geophysical Union, 17th Annual Meeting, 1936, pp. 516-521.
3. Preiswerk, E.: Application of the Methods of Gas Dynamics to Water Flows with Free Surface, Parts I and II, NACA TM 934 and 935, 1940.
4. Johnson and Witbeck: Water Analogy to Two-Dimensional Air Flow, "General Electric Company, Report No. 55218.
5. North American Aviation, Inc.: Application of the Water Channel Compressible Gas Analogy, Report No. NA-47-87, March, 1947.
6. Orlin, W. J., Lindner, N. J., and Bitterly, J. G.: Application of the Analogy between Water Flow with a Free Surface and Two-Dimensional Compressible Air Flow, "NACA Report 875, 1946.
7. Ippen, A. T., Harleman, D. R. F., and Others: Studies on the Validity of the Hydraulic Analogy to Supersonic Flow, Parts I through V, M.I.T. AF TR No. 5985.
8. Heinrich, H. G., and Ibrahim, S. K.: Application of the Water Surface Wave Analogy in Visualizing the Wave Pattern of a Number of Primary and Secondary Body Combinations in Supersonic Flow, WADC TR 59-457, September, 1959.
9. Laitone, E. V.: A Study of Transonic Gas Dynamics by Hydraulic Analogy, Journal of the Aeronautical Sciences, Vol. 19, No. 4, April, 1952.
10. Heinrich, H. G.; Ibrahim, S. K. and others: Theoretical Parachute Investigations, WADC Contract No. AF 33(616)-6372, Quarterly Progress Reports, Department of Aeronautical Engineering, University of Minnesota.
11. Olson, R. M.: Essentials of Engineering Fluid Mechanics, p. 290, International Textbook Co., Scranton, Pa., 1961.
12. Ames Research Staff: Equations, Tables, and Charts for Compressible Flow, NACA TR 1135, 1953.

PARAVULCOON RECOVERY AND LANDING SYSTEM

A. J. Oberg

S. S. Sopczak

M. A. Sutton

Minneapolis Honeywell Regulator Company
Military Products Group
Ordnance Division

ABSTRACT

This paper presents the results of analyses and tests of a recovery and landing system combining the functional characteristics of a parachute and a hot gas balloon. The system components consist of a large Nylon-Mylar balloon which is ram air filled upon deployment by a pilot chute, a heat generator which warms the air within the balloon by convection, and a control system which modulates the heat generator to control the buoyant force.

The forces of drag and buoyancy are used to decelerate a falling payload to a zero vertical velocity. To land the payload, the controlled buoyant force is decreased.

Recovery and landing test data obtained from airdrops are presented along with laboratory test data. Consideration is also given for utilizing the PARAVULCOON System as a sky hook for exploration of Mars and Venus.

PARAVULCOON RECOVERY AND LANDING SYSTEM

A. J. Oberg

S. S. Sopczak

M. A. Sutton

Minneapolis Honeywell Regulator Company
Military Products Group
Ordnance Division

ABSTRACT

This paper presents the results of analyses and tests of a recovery and landing system combining the functional characteristics of a parachute and a hot gas balloon. The system components consist of a large Nylon-Mylar balloon which is ram air filled upon deployment by a pilot chute, a heat generator which warms the air within the balloon by convection, and a control system which modulates the heat generator to control the buoyant force.

The forces of drag and buoyancy are used to decelerate a falling payload to a zero vertical velocity. To land the payload, the controlled buoyant force is decreased.

Recovery and landing test data obtained from airdrops are presented along with laboratory test data. Consideration is also given for utilizing the PARAVULCOON System as a sky hook for exploration of Mars and Venus.

PARAVULCOON RECOVERY AND LANDING SYSTEM

INTRODUCTION

The results of analytical studies and test data have led to the definition of a potentially feasible recovery and landing system concept which has been aptly named "Paravulcoon." The principle feature of this system is the utilization of hot-gas generation to heat the air contained within a large balloon. Thus, the kinetic and potential energy of the appropriate payload is reduced by a combination of the aerodynamic drag force provided by the balloon size and shape and the buoyancy force resulting from the heated air within the balloon. With this system it is possible to actually float the payload at a controlled altitude above the surface. Thus, certain unique features such as (1) elimination of vertical impact loads, (2) prevention of water immersion, and (3) simplification of payload acquisition and recovery can be achieved. As an example, utilization of this recovery technique could considerably simplify the snatch recovery of Discoverer satellite payloads.

The Paravulcoon Recovery and Landing System is described in the following paragraphs. Typical system applications to air drops, re-entry vehicles, and planet exploration are considered.

DESCRIPTION AND OPERATION

Figure 1 illustrates the significant components of the Paravulcoon system. The system consists of a balloon, a heat generator, and a control system. A parachute may also be needed in the event the payload must be oriented and decelerated.

The balloon is deployed in a reefed condition by a pilot chute and is ram air filled. A large opening (throat) is provided at the bottom of the balloon for two purposes. First, to expedite ram air inflation and secondly to allow convective heat transfer from the heat generator to the gasses within the balloon. As the gas within the balloon is heated the gas density decreases and the balloon becomes buoyant. By controlling the heat transfer process, the buoyant force may be varied to control the motion of the suspended payload. The control system sensitivities and monitored inputs must be engineered to the desired payload mission. The payload mission may establish a critical landing velocity where the floatation feature of the system is not desired.

A more detailed description of the system components is given below for a large weight payload which is to be airdropped and gloated at 5000 feet altitude and then landed with a vertical velocity of less than 3 feet per second.

COMPONENTS

The major sub-systems of the Paravulcoon Recovery and Landing System are (1) parachute (s), (2) balloon, (3) control system, and (4) heat generator. A brief description of these major sub-systems is presented in the following paragraphs.

Parachute: A two stage parachute system may be used to orient and decelerate the payload and deploy the balloon. The size and particular type of parachute used is depended upon the Mach number, altitude, and potential and kinetic energy of the payload. The function of the parachute is to (1) decelerate the payload to subsonic velocities and (2) to deploy the balloon.

Balloon: The major sectional parts of the balloon are: (1) the crown, (2) the midsection and (3) the base section. See Figure 2. The meridional lines converge at the crown of the balloon. The base section extends a short distance up from the throat of the balloon. On a hot gas balloon as used on the Paravulcoon system, an opening is left at the bottom for the passage of ram air and hot gases into the balloon interior.

The balloon is fabricated from a composite of base fabrics, such as Nylon or Dacron, duPont HT-1 and Mylar. A composite material is selectively laminated on the basis of stress and thermal requirements consistent with minimum weight and packaging volume. The maximum surface temperature and stress occur at the crown which often requires the use of reinforced heat resistant fabrics such as Dacron or duPont HT-1 fabric. The close proximity of the burners to the base section may also require the use of higher temperature material in the area of the throat. A laminate of base fabric and aluminized Mylar will be used throughout the balloon if necessary. The aluminized Mylar serves to reduce permeability, protect the fabric from deteriorating effects of the hot gasses, and reduce radiant heat transfer. The loadlines of the balloon transfer the load from the payload into the balloon fabric. The loadlines can be continuous or segmented. The ends of the continuous loadline originate at the load ring on the payload; the leadline passes completely over the balloon through the meridional plane. In the segmented case fewer loadlines are fastened to the payload ring; additional balloon loadlines are coupled to crow foot risers near the throat of the balloon. These loadlines may be coupled to lower tensile strength webbing at the crown area. Loadlines converge at the balloon top end

fitting. Secondary load paths can be provided by use of meridional stress webs which transfer the load from the throat catenary into the balloon fabric in the midsection. The loadlines will be Nylon or Dacron cord rope depending upon the load to be transferred and/or webbing wrapped with aluminized tape or encased in asbestos sleeving in the throat area.

Control System: The control system provides (1) initiation and sequencing signals for recovery system operations, (2) burner control to insure that balloon materials are not over-heated, and (3) burner control to maintain proper balloon rate of descent and/or floatation altitude. Integration of the control system into the Paravulcoon recovery concept is shown in Figure 3. Specific control system functions are summarized below.

Sequencing signals are required to initiate (1) pilot and main parachute deployment, (2) balloon deployment, and (3) burner ignition. Accurate timing signals are necessary to insure payload recovery at a prescribed altitude.

Temperature sensors fastened to the balloon material at critical locations will provide warning signals to the control system if the material becomes over heated. In this case, the control system will throttle down or stop the burner to prevent material damage.

During buoyant flight conditions, the control system must function during landing operations to reduce impact velocity to a safe level when activated by either preset or remote command signals. If a winch-down landing is used the control system should function to provide a small positive buoyant force.

A block diagram of the control system which can fulfill all of the above requirements is shown in Figure 4. It consists of a timer, a high temperature sensor and an associated valve, a remote link, a presettable input, an altitude sensor, an altitude rate sensor, a signal conditioner, and a control motor, and associated fuel valves. Inter-connections, logic switching and a power supply will also be included in this system. Discussion of the illustrated control system components will be generalized below because specific hardware will vary with each application; however, all of the illustrated functions can be performed with the state-of-the-art components.

Timer: Control of the Paravulcoon recovery system will begin with the initiation of the timer. This initiation can be achieved in several ways: At release, at an inertially referenced position, at a peak deceleration point, or at a fixed deceleration point. The method of initiation will to a large extent depend upon the mission profile of the particular vehicle being recovered. At present time intervals after initiation, the timer will send the appropriate sequencing signals.

Solid state magnetic timers are available to perform the timing control function.

Remote Link: The remote control link will allow for command override of the control system. Provisions will be made for transmission of these signals through wire or radio transmission systems. Either method of remote control can be achieved with standard hardware.

Presettable Input: The presettable input will provide the selection of command signals which can be used to automatically control float altitudes and landing descent. A simple battery and voltage divider network with appropriate switching can perform this function.

Altitude Control Sensor: Altitude may be controlled by barometric or radar systems. The Honeywell PG10 Altitude Control can control altitude level to within one foot per second at an average altitude of 5000 feet. However, barometric systems are susceptible to deviations in atmospheric density; if the absolute value of buoyant flight altitude is not critical this system will prove satisfactory. For landing conditions, this system will control the altitude descent rate.

For those systems which require precise float altitude above terrain, a radar altimeter similar to the Honeywell Model 7091 will be required.

Signal Conditioner: Either preset or remote command signals in conjunction with altitude and altitude rate signals are combined in the signal conditioner. As presently envisioned the signal conditioner will not be required to modify or shape the incoming signals other than normal summing and amplification necessary to provide the required system gain. The output from the signal conditioner is then applied to the control motor.

Control Motor and Associated Fuel Valves: Several types of valve and methods of control can be used to modulate fuel flow in response to the output signals from the signal conditioner. A simple butterfly valve could be modulated to provide the desired control. An alternate method of fuel flow modulation can be achieved by varying the speed of a positive placement pump.

HEAT GENERATOR

A heat generator is required to supply heat to the air inside the balloon. This heating process is initiated after the balloon has been ram air filled. The terms, initial burner and control burner will be used to describe the heat generator behavior and/or requirements during the transisent, buoyancy controlled and descent flight conditions

experienced by the payload. The initial burner is ignited at a relatively high altitude. Sufficient heat is applied by this burner to establish buoyancy at altitudes above 5000 feet. The control burner supplies heat to overcome heat losses and maintain control. The throttling range for control burner operation is approximately six to one with a maximum heat rate output greater than twice the heat rate loss.

The development of a burner concept involves selecting a system which provides a maximum amount of heat with minimum weight and thrust penalties. The fuel must have a relatively high enthalpy of combustion and produce products which will not react with the air and/or balloon envelope material. The toxicity of fuels and their products of combustion should not present a lethal hazard to personnel. An analysis of rocket engines, nuclear heat generators, and fuel air systems has been conducted in Reference [1] but will not be presented here. Overall performance and economic considerations were considered for each concept investigated. It was concluded from this analysis that a propane burner is the optimum type of air heating system for a Paravulcoon Recovery System. Pressurized liquid propane is preheated in coils wound around a burner and is converted into a gas. The hot propane gas is expelled through a nozzle; thus including the required air flow for complete combustion. At high altitudes and for reliable ignition a supplementary oxygen system is provided. At lower altitudes and during buoyant flights, the supplemental oxygen will not be required. Major components of the burner system include the burner, fuel control valves, fuel supply tanks, ignition system, and the fuel system pressurization tank.

Having described the Paravulcoon Recovery and Landing System it is obvious that the principal feature of the system is the utilization of buoyancy to achieve a lifting force. But, buoyancy may also be achieved by the use of helium or hydrogen gas. Therefore, justification of the Paravulcoon System should be based upon a system analysis which compares the various means of obtaining a buoyant force. A meaningful comparison is presented in Table I in which tank weight, associated equipment, and the required size balloon for a specific lift are considered.

TABLE I
COMPARISON OF WEIGHT AND VOLUME PENALTIES
IMPOSED BY VARIOUS BALLOONS WHICH CAN LIFT
10,000 lb^(a)

| | <u>Hot Air^(b)</u> | <u>Helium</u> | <u>Hydrogen</u> |
|---|------------------------------|---------------|-----------------|
| Balloon Diameter - ft ^(c) | 111 | 75 | 71 |
| Weight of balloon fabric - lbs ^(d) | 403 | 188 | 173 |
| Fuel for 30 minutes - lbs ^(e) | 229 | None | None |
| Fuel for initial heat - lbs ^(f) | 123 | 55 | 59 |
| Weight of burner (st) + lbs | 138 | 7 | 8 |
| Weight of H _e or H ₂ - lbs ^(g) | None | 1,800 | 780 |
| Weight of tankage - lbs | 30 | 2,700 | 2,340 |
| Weight penalty - lbs ^(h) | 923 | 4,750 | 3,360 |
| Volume penalty - ft ³ (i) | 38 | 236 | 181 |

For clarification of the various items shown in this table, the following notes are included:

- (a) 10,000 lbs is the lift of the balloon gases (at 70° F ambient and 5000 ft altitude) minus the weight of fabric, fuel for flight, burners, and tanks.
- (b) Average internal air temperature of 250° F.
- (c) All balloons were assumed to have the "natural" shape for Hot-air.
- (d) Mylar-nylon laminate which weighs 0.013 lbs/ft².
- (e) Using propane at approximately 20,000 BTU/lb.
- (f) Using solid fuel for all three balloons.
- (g) Assumed to be liquid. No weight for insulating container is included.
- (h) Includes weight of balloon fabric, all fuel tanks, burners, and gases in the helium and hydrogen balloons.
- (i) Packed volume of fabric, all fuel tanks, burners, and helium or hydrogen gas (assumed to be liquified).

The hot-air balloon is approximately 50% larger in diameter than the balloons used in the other two systems. Even though this increases the fabrication task, the larger size may be advantageous because the balloon acts as a parachute to decelerate the load in the initial phase of the recovery operation.

A conservative estimate was made of the Paravulcoon burner assembly weight requirements by extrapolating present day hardware weights without allowing for refinements. As shown in the Table, both the weight and volume penalties for the hot air system are significantly smaller than those for helium or hydrogen systems. The principal reason for this advantage is that the hot air-system is not required to carry its lifting gas aloft.

Two other significant advantages of the hot-air system over the helium, hydrogen systems are (1) easier control and (2) relatively little effect on buoyancy due to balloon leaks. Experience indicates that heat modulation is vastly superior to ballast control and gas valving. Also, rather large leaks do not degrade lifting performance. For example, during a manned flight test a one foot diameter hole in the top of a 40 foot diameter hot-air balloon actually caused the balloon to rise. It was concluded that this was due to increased combustion efficiency.

Thus, from a performance standpoint, the hot-air balloon has significant advantages over helium or hydrogen balloons. That is, the hot-gas balloon system is lighter, requires less packaging volume, is easier to control, and is less effected by balloon skin rupture. Perhaps one disadvantage could be pointed out that the hot-air system possesses over the other systems. That is the limited amount of flight time. The hot air system flight time is dependent upon the fuel carried on board. The other systems are dependent primarily upon gas escapement which is normally small, resulting in long flight times.

PARAVULCOON SYSTEM WEIGHTS

A preliminary parametric study of the weight requirements of Paravulcoon Recovery Systems for various payload weights has been conducted. This study allows the prediction of the payload penalty imposed by the recovery system over the spectrum of payload weights from 5000 to 300,000 pounds. The results are based on heat input computations and burner and fuel system size estimates for gross weights

of 10,000, 50,000, 90,000 and 282,000 pounds. Equilibrium float durations of 1/2 and 1 hour at 5000 altitude have been considered.

The estimated recovery system weights and payload penalties are plotted in Figure 5 as functions of payload weight. For 1/2 hour float duration the system weight varies from 610 pounds for a 5000 pound payload to 32,000 pounds for a 300,000 pound payload. The corresponding payload penalties are 12.6 percent and 11.2 percent respectively. If a 1 hour float duration is considered, the corresponding weights are 810 and 35,500 pounds and the penalties are 16.4 and 12.2 percent. This shows clearly the greater importance of the control heat requirements with the smaller payloads where the steady state heat loss is a larger percentage of the total energy requirements. For the higher payloads where the balloon surface area is smaller in relation to the volume the initial heat requirement is the more significant parameter.

FLIGHT ANALYSIS

Utilization of the Paravulcoon Recovery System for any payload application involves two somewhat unique flight regimes. These are (1) the period during which the balloon is deployed and inflated and (2) the period during which heat is supplied to the balloon to achieve buoyancy. Assumptions and analytical techniques used to describe these two regimes are summarized below.

BALLOON INFLATION

Knowledge of the balloon inflation period is necessary to evaluate acceleration, velocity, and distance traveled. The analysis undertaken consists of the application of Newton's inertial laws to the balloon and payload. The influence of (1) the virtual mass phenomenon and (2) the air mass within the balloon are of special interest.

A number of basic assumptions were made

- . The descent path of the balloon and payload is vertical
- . The virtual mass of the balloon is appreciable and must be considered.
- . The linear velocity of the ingested air relative to the throat of the balloon is proportional to the descent velocity of the balloon until the balloon is fully inflated.
- . The ram jet effect of ingested air is negligible.

The following applicable equations of motion must be simultaneously solved. (See the sketch for clarification of terminology):

Balloon

$$(m_B + m_A) \ddot{x}_B + \dot{m}_A \dot{x}_B = m_B g - D_B + F_S \quad (1)$$

Payload

$$m_P \ddot{x}_P = m_P g - D_P - F_S \quad (2)$$

where

$$m_A = \rho V_{ia} \left(1 + \frac{1}{2} \frac{V_{ia}}{V_{ia_term}} \right) \quad (3)$$

= ingested air mass + virtual mass

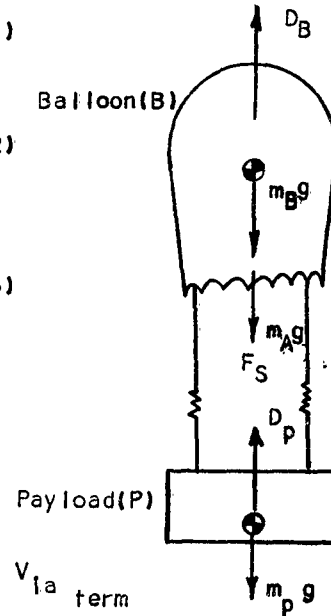
V_{ia} = volume of ingested air

ρ = density of ingested air

Differentiation of (3) gives

$$\dot{m}_A = \rho \left(1 + \frac{V_{ia}}{V_{ia_term}} \right) \dot{V}_{ia} \quad \text{when } V_{ia} < V_{ia_term} \quad (4)$$

$$= 0 \quad \text{when } V_{ia} \geq V_{ia_term}$$



The magnitude of F_S can be determined from the number and elastic properties of the shroud lines.

Solutions to these equations allow determination of payload motion and displacement history during this balloon inflation period.

BALLOON HEATING

One balloon inflation has been completed, the burner near the base is ignited thereby providing buoyancy to the system by heating the balloon contained air.

A general thermodynamic analysis has evolved from consideration of the appropriate flight regimes and associated problems. Based on this analysis a set of differential equations have been derived from which the altitude time histories of the descending balloon-payload can be predicted. From the problem conditions it is possible to estimate optimum balloon size, burner requirements, etc.

Once the balloon has been deployed and fully inflated by ram air, the aerostat drops vertically at equilibrium velocity. This velocity depends upon the ballistic coefficient $\frac{W}{C_D A_B}$. Buoyancy can be created to further reduce this descent velocity. It is desirable to accomplish this rapidly enough to allow the system to float in static equilibrium before it impacts the ground. The analysis of this portion of the flight must include simultaneous consideration of dynamic motion and thermodynamics.

A rather lengthy discussion of the thermodynamic problems involved herein is included in Reference 1. The resulting transient equations are

$$\underbrace{\ddot{y}}_{\text{acceleration}} + \underbrace{(g \ell_\infty / 2W_T) (C_D A_B)}_{\text{drag}} - \underbrace{V_B^2 / RT_B}_{\text{buoyancy}} + \underbrace{(g V_B \ell_\infty / W_T) (1 - T_\infty / T_B)}_{\text{weight}} - g = 0$$

where:

$$W_T = W_B + W_P + W_b + W_f - \int_0^t \dot{W}_f dt$$

Thermal:

$$\underbrace{\dot{W}_f}_{\text{burner}} + \underbrace{(V_B / J) \dot{p}_B}_{\text{compression}} = \underbrace{g C_P V_B \ell_\infty \left[\frac{T_\infty}{T_B} + \frac{1}{2gRT_B} \dot{y}^2 \right]}_{\text{thermal storage}} + \underbrace{K(T_B - T_\infty)}_{\text{convection - radiation}} + \underbrace{C_P \dot{W}_B \left(\frac{T_B - T_\infty}{T_B} \right)}_{\text{air mass movement}}$$

where:

$$\dot{p}_B = \left\{ \ell_\infty \left[g R \frac{\partial T_\infty}{\partial y} \ddot{y} \right] + \left[g R T_\infty + \frac{1}{2} \dot{y}^2 \right] \frac{\partial \ell_\infty}{\partial y} \right\} \dot{y}$$

$$W_B = g V_B \ell_\infty \left[\frac{T}{T_B} + \frac{1}{2gRT_B} \dot{y}^2 \right]$$

For the purpose of this analysis, the balloon is a pear-shaped plastic envelope with a large opening in its base. The envelope is subject to the ambient atmospheric pressure while the opening is subject to the ram air pressure created by the velocity of the dropping aerostat. This ram pressure maintains the rigid inflated shape of the envelope. Thus, while the mass of air in the balloon is subject to movement in and out of the opening, the volume of air in the balloon is constant. In fact, this analysis is not valid for a balloon which has significant stretch or which is partially deflated. In addition, since the Paravulcoon is usually of significant length, it is subject to a static-pressure gradient from top to bottom due to the atmospheric pressure gradient.

During the terminal descent regime, heat must be added to the air in the balloon to develop buoyancy. This is done with a heat generator or burner located in or near the opening at the base. As a result a rising column of hot air is formed in the center of the envelope. To study the temperature distribution caused by this movement, a preliminary laboratory investigation was conducted using a small tethered balloon and thermocouple probes. The results of this study are indicated in Figure 6. As would be expected, the highest temperature was observed directly over the burner with the readings decreasing with distance above the burner. Temperature in the upper third of the envelope was found to be nearly constant from the center to the outer edge while the values at locations near the skin become cooler as the distance from the bottom apex is reduced. This temperature pattern confirms the expectation that the hot-air introduced around the burner travels up through a central core, mushrooms over at the balloon crown, and moves downward along the inside surface of the balloon envelope. The hot central core gives off heat to the cooler downward flow while in turn this downwash is cooled by the outer skin.

It is seen that the highest skin temperature was recorded at the crown and the lowest at the throat. This suggests that if a high limit temperature sensor is used in the control system it should be located at the crown. Also the skin temperature pattern suggests some possibilities for efficient Paravulcoon envelope design. These include the use of a high temperature material for the upper third of the envelope and the throat edge region (for possible flame impingement), and a less exotic material for the mid and lower sections of the envelope. Thus, a thorough understanding of the heat flow and temperature distribution within the balloon envelope is desirable for an optimized design.

In addition to these static considerations, energy is added to the balloon air by compression from the atmospheric pressure gradient as the aerostat drops. The balance of all of these geometric and thermal factors governs the aforementioned movement of air in and out of the balloon as it descends through the atmosphere.

It is evident that conditions inside the balloon consist of a swirling mass of air encompassing a wide range of temperatures, pressures, and densities. These state properties are seen to be functions of both location and time giving a situation which might be very difficult to treat analytically. For this analysis a single average condition which is a function of time only has been assumed in order to make possible the prediction of the aerostat performance in both the transient and equilibrium regimes. This average is chosen in such a way, that a single pair of time dependent values of temperature and density will result in the same Paravulcoon buoyancy as the summation of the actual spatially distributed values.

Similarly, for the purposes of this analysis, ambient conditions over the entire balloon surface are assumed constant. This single condition is that corresponding to a standard atmosphere at an average time dependent altitude which is considered the balloon altitude. As a result of the use of these two average conditions, an assumed discontinuity between them at the Paravulcoon opening must be made even though the actual conditions vary over a continuous gradient. In the analysis, the interior condition is balanced by ambient ram conditions at this plane.

In addition to the heat required to warm the cold air during the transient regime, heat is required to make up for the energy losses during both the transient and equilibrium regimes. These losses are heat transfer through the balloon envelope and energy transfer associated with the air movement through the balloon opening. The latter is referred to as ventilation. Again for analytical convenience, it is necessary to consider these losses in terms of the difference between the average ambient and average balloon temperature discussed above.

Heat transfer through the balloon envelope occurs by a combination of radiation and convection from the warm air to the envelope material, conduction through the material, and convection and radiation from this material to the surroundings. Since the envelope material is thin, its resistance to conduction is negligible compared to the other factors. The convection - radiation factors on each side are functions of local adjacent temperatures; local boundary layer conditions; and, for radiation, the envelope material characteristics. Due to the variety of interior air conditions it is difficult to predict this factor. A preliminary analysis, however, plus the results of early tests, on small hot-air balloons, indicate that an over-all heat transfer coefficient of 0.75 to 1.1 BTU/HR^{OF} FT², based on the difference between the average interior and the average ambient temperature, may be expected. These values are just slightly higher than the usual rule of thumb values for simple free convection over the same temperature difference. Tests indicate that the use of a reflectorized material could reduce this factor by as much as 20 to 30 percent.

Ventilation heat loss is the energy required to raise the temperature of the subject mass of air from the ambient temperature, at which it enters the balloon, to the Paravulcoon air temperature at that instant. Since this energy is not recovered from air leaving the balloon, a net energy loss due to ventilation occurs to the system whether the air moves in or out. Ventilation is caused by three mechanisms, two predictable and one unpredictable. The first has been described above and is due to unbalance between interior and exterior air conditions. The second is due to the combustion air required for the burner. Assuming all the combustion products enter the balloon this factor can be predicted on the basis of the fuel-air ratio utilized for the burner. It has been found to be less than 20 percent of the higher heating value of the fuel when 200 percent excess combustion air is used. Finally, ventilation could be created by random gusts blowing into the opening and "pumping" created by small scale altitude oscillations during the equilibrium float regime. This effect is unpredictable and can be allowed for by a judgment factor applied to the overall heat transfer coefficient.

The heat transfer by convection-radiation and ventilation is of particular importance during the equilibrium float regime. The steady state values of these factors determine the total heat input required to maintain equilibrium float and thus are important design parameters for the system. While these factors also contribute to the transient regime heat requirement their evaluation is of lesser importance in this regime for two reasons. They are significantly smaller than the heat required to raise the temperature of the balloon air, and since they are functions of the temperature difference, they start at zero and increase to their steady state value during the transient flight.

As an example of the application of these equations, consider the results shown on Figure 7. As indicated, the total weight was assumed to be 282,500 pounds. The balloon volume of 14.65×10^6 ft³ (311 ft diameter) is available for supplying buoyancy to the system. A terminal velocity of approximately 185 ft/sec was assumed and for the various altitudes indicated (at time zero) it was assumed that the burner is ignited and supplies the indicated heat inputs to the system. The temperatures in parentheses indicate the maximum balloon material temperature. From the figure it can be seen that with the burner ignited at 20,000 feet altitude, a heat input of 200,000 BTU/sec will result in floatation at an altitude of 5,000 feet. The maximum balloon material temperature is 264° F.

The preceding equations were utilized to establish a feasible C-5 booster recovery system which is subsequently discussed.

FLIGHT TESTS

A model of a Paravulcoon Recovery System was designed, built and successfully tested twice by Raven during 1961. The test model consisted of a capsule containing a balloon, a burner assembly, a fuel tank, and a simple control system interconnected as shown in Figure 8. In addition, a drogue parachute was included to stabilize the test-package during free fall and to deploy the balloon.

Characteristics of the test balloon are presented in Table 2. Altitude versus time histories of the balloon during the two flight tests are shown in Figures 9 and 10. Data for the two graphs was obtained from a barograph attached to the flight package during each flight.

Significant results obtained from the two tests are summarized in Table 3.

TABLE 2

BALLOON MODEL CHARACTERISTICS

| | |
|---|---------------|
| Ballon diameter | 25 ft. |
| Gore length | 39.4 ft. |
| Balloon volume | 7,650 cu. ft. |
| Theoretical gas lift (70° ambient, 250° F gas temperature and 5,000 ft. altitude) | 121 lbs. |
| Area of envelope fabric (0.004 inch thick and 0.011 lbs/sq ft) | 1880 sq. ft. |
| Weight | 22 lbs. |
| Packed volume | 2.08 cu. ft. |

In the first test conducted on August 29, 1961, the Paravulcoon model was loaded as an external store on an aircraft and subsequently released at an altitude of approximately 11,500 feet. In the second test conducted on September 26, 1961, the model was elevated to approximately 6700 feet by a helium mother balloon and then released. Motion picture coverage of this test is available and clips from the film are shown in Figure 11.

The balloon ram air inflation inlet was not structurally forced to an open position as may be accomplished with various devices such as an inflated torus which could be constructed in the inlet throat. Also, in order to keep the control system simplified, burner modulation control for maintaining a given float altitude was not included. The burner heated the gas to higher temperatures than needed, thereby creating an excess buoyancy which forces the aerostat to higher altitudes as shown in the altitude histories.

It was concluded from these results that the Paravulcoon concept for floating aerial loads is feasible because:

1. The Paravulcoon deployed, inflated, and heated up properly.
2. The air was heated quickly enough to float the aerostat before it descended more than 2500 feet.

TABLE 3

SIGNIFICANT PARAVULCOON MODEL TEST RESULTS

| <u>Item</u> | <u>Test #1</u> | <u>Test #2</u> |
|---|----------------|----------------|
| Weight of entire models | 78.50 lbs | 87.00 lbs |
| Balloon | 22.00 lbs | 22.00 lbs |
| Drogue chute | 3.64 lbs | 3.64 lbs |
| Tank, burner, and instrumentation | 52.86 lbs | 61.36 lbs |
| Average descent velocity before a deployment of the balloon | 110 ft/sec | 48.8 ft/sec |
| Average descent velocity between balloon deployment and burner ignition | 19.7 ft/sec | 26.2 ft/sec |
| Time for burner to stop descent | 1 min.35 sec | 1 min.17 sec |
| Average descent velocity during gas warm up | 7.2 ft/sec | 11 ft/sec |
| Altitude descent during warm up | 683 ft. | 966 ft. |
| Total altitude descent from release to float | 2,340 ft. | 2,689 ft. |
| Climb rate of hot balloon | 11.3 ft/sec | 7.07 ft/sec |

TABLE 3 (continued)

| <u>Item</u> | <u>Test #1</u> | <u>Test #2</u> |
|---------------------------------------|----------------|----------------|
| Total climb of hot balloon | 4,089 ft. | 4,296 ft. |
| Burner fuel weight | 7.0 lbs | 7.5 lbs |
| Burner-on-time | 6.5 min. | 8.63 min. |
| Average fuel consumption rate | 1.08 lbs/min. | 0.87 lbs/min. |
| Total time in air (release to impact) | 19.5 min. | 20.15 min. |

BOOSTER RECOVERY SYSTEM

The feasibility of a Paravulcoon Recovery and Landing System for booster recovery was investigated and established in Reference 1 for the Saturn C-5 booster which is illustrative of a large weight, high energy re-entry vehicle.

The following paragraphs indicate some basic considerations which were utilized to establish the C-5 recovery system as is subsequently presented.

To determine if the Paravulcoon System could be utilized as a recovery and landing system for large payloads, preliminary analyses were conducted which considered various re-entry vehicles and associated missions. The primary motive was to establish the feasibility of the Paravulcoon Recovery System. However, because the Saturn C-5 booster is typical of a high energy re-entry vehicle most of the analysis is centered about the recovery of this size payload.

To establish specific recovery requirements point mass ballistic re-entry trajectories were computed for Apollo, Mercury, and Discoverer class of vehicle and for Redstone and Saturn boosters. Nominal missions were determined and estimates were made of vehicle weights, drag coefficients, re-entry velocities, and path angles. A model for trajectory simulation with a CDC-1604 computer was selected from an established library computer program. Point mass trajectory simulation was performed in two degrees of freedom on a spherical earth with a 1959 ARDC standard atmosphere. Since the Paravulcoon System is used primarily to dissipate residual energy prior to landing, comparison of altitude-velocity profiles as shown in Figure 12 was made to evaluate the energy levels. Although a large variation in initial velocity exists for the various vehicles, atmospheric drag rapidly decelerates all of the vehicles to a sub-sonic impact velocity. The G5 booster is representative of a high energy vehicle for recovery by the Paravulcoon System.

Since the main objective of the study was to determine the feasibility of the Paravulcoon Recovery System, a detailed analysis which would consider recovery operations initiated at booster separation was not undertaken. However, a limited analysis was conducted to determine subsequent low atmosphere recovery criteria as affected by high altitude recovery operations.

It was concluded that the sole use of retro rockets or drag modulation would not be satisfactory engineering approaches and that drag and lift modulation would be required to obtain feasible inertial and heat loads during booster re-entry.

In an effort to place stringent requirements on the Paravulcoon System, the low altitude environment of the C-5 booster without initial recovery operation was selected. In this manner higher velocities associated with lower altitudes are obtained. See Figure 13.

With a booster re-entry trajectory established for a ballistic parameter ($W/C_D A$) equal to 182 psf, it became evident that the booster becomes subsonic at an altitude of about 35,000 feet. With balloon deployment occurring at subsonic payload velocities it was assumed desirable to employ a parachute decelerator to decrease subsequent event time sensitivities. The requirement of the parachute decelerator is marginal because deployment of the balloon results in a large drag area ($C_D S = 15,000 \text{ ft}^2$) upon inflation. But, the time to deploy and inflate the balloon is questionable. A parametric trajectory analyses was conducted to establish parachute sizes to obtain a subsonic velocity at the required balloon deployment altitude. Deployment Mach numbers of less than 3.0 were considered with parachute drag characteristics taken from Reference 2. Analyses utilizing the previously established equations of motion were conducted to optimize a paravulcoon deployment velocity in conjunction with a feasible heat generator. This led to the selection of a required parachute system. A brief component and operational description is given below for the C-5 Booster Paravulcoon Recovery and Landing System.

PARAVULCOON RECOVERY SYSTEM FOR THE SATURN C-5 BOOSTER

The Paravulcoon Recovery System for the Saturn C-5 booster as established in Reference 1 is briefly described here. In summary, the hot-gas balloon is deployed by a drogue parachute. After deployment, the balloon is inflated by ram air which further decelerates the payload. Burners heat the air within the balloon envelope, the hot air provides lift for buoyant flight. A control system regulates the burner output to maintain the buoyant flight altitude.

The estimated weight of this recovery system is 29,133 pounds, or 11.2% of the empty C-5 booster weight of 260,000 pounds. This system

weight provides fuel for one hour of buoyant flight. Additional weight summary information is presented in Table 4 .

DESCRIPTION

The major subsystems of the recovery system include:

1. The parachutes
2. The hot air balloon
3. The burner
4. The control system
5. The structure

All components of the recovery system are packaged in the booster interstage structure. The component arrangement within the interstage structure and the packaging criteria and assumptions used to develop this arrangement are discussed below:

The heat generator which consists of six units is symmetrically located 60 degrees apart adjacent to the interstage shell. Three spherical propane fuel tanks are spaced 120 degrees apart with one fuel tank supplying two burners. Oxygen and pressurant fuel tanks would be located adjacent to the propane tanks to minimize length of fuel lines and necessary connections. Other components such as electronic and mechanical controls, sequencing explosive components, and search equipment occupy a relatively small volume and can be packaged within expedient locations as required.

To establish an efficient packaging arrangement, various design parameters need to be considered. The overall objective is to package the required recovery system components for minimum volume and minimum weight consistent with the functional requirements. Certain assumptions have been made and these assumptions along with the principal considerations that will influence the final design are itemized below.

- During re-entry the booster is oriented with its rocket engines pointed downward and the recovery system is not subjected to severe heating conditions. Therefore, provisions for affording thermal insulation to the various components within the recovery system are not extensive.
- In the design of the support structure for the various recovery components, the design load factors to be considered are ± 6.0 G's in a longitudinal direction and ± 1.5 G's in a lateral direction.

- The loadline arrangement as conceived for the balloon consists of attaching the lines to appropriately spaced fittings that are located around the inner circumference of the interstage shell. Design of the loadlines and attachment fittings include consideration of anticipated shock loads associated with the deployment of the balloon.
- A highly reliable device for ejection of the pilot chute is required. An explosive linear actuator ejects the pilot chute canopy to which the pilot chute is attached.
- It may be necessary to augment the influx of air within the interstage area to provide a sufficient flow of air for efficient burner operation. If further studies show that more air is necessary, a linear explosive network can be placed adjacent to the interstage shell to cut appropriate sections for venting, explosively actuated mechanical air scoops can be considered as a possible solution.
- Design and analysis work required to integrate the Paravulcocon Recovery System components into the C-5 booster must be very closely coordinated with the booster structural and performance design effort. This is necessary to insure an integrated design approach.

DESCRIPTION OF MAJOR SUBSYSTEMS

A brief discussion of the function, a description of the components, and a summary table of the weight and volume for each of the major subsystems is presented in the following paragraphs.

a. Parachute System - The parachute system is composed of a pilot chute and a parachute decelerator. The requirement for a 50-foot diameter supersonic parachute decelerator appears to be beyond the current state of the art. For engineering purposes, the following physical characteristics have been established.

Parachute Decelerator

| | |
|--------------|--------------------------|
| Type | 20 degree conical ribbon |
| Porosity | 30% (geometric) |
| Diameter | 50 feet (nominal) |
| Riser length | 70 feet |
| Total weight | 1600 pounds |

From the supersonic sled tests, the following pilot chute characteristics have been proved feasible.

Pilot Chute

| | |
|--------------|--------------------------|
| Type | 15 degree conical ribbon |
| Porosity | 30% (geometric) |
| Diameter | 6.5 Feet (nominal) |
| Riser length | 70 feet |
| Total weight | 25 pounds |

A brief description of the parachute system is presented below. This is followed by a weight and volume summary.

The pilot chute is deployed from the booster during an inertial booster deceleration of about 4 g's. Successful deployment therefore requires the use of a deployment gun. Detailed design of the gun will have to be established, but, based upon existing guns, a 25 pound deployment gun using smokeless black powder propellant appears feasible. The pilot chute design is based upon conical ribbon parachutes recently developed by USAFASD (Reference 3). The parachute is constructed of 16 gores with 10 horizontal ribbons and 3 vertical ribbons. Specially treated Dacron is used for the riser line to decrease the high elasticity associated with Nylon risers. The lower elasticity of the Dacron riser will tend to decrease parachute dynamic instabilities which are predominate at supersonic speeds.

The parachute decelerator design is based upon an extrapolation of the parachute technology. This appears to be justifiable since drogue parachute deployment is expected near Mach number 1.5 with a dynamic pressure of 609 lbs/ft². Aerodynamic heating should not be a problem since deceleration to subsonic velocities is expected to occur in less than 4 seconds.

The following parachute and inflation Mach number values were obtained from USAFASD as indicative of engineering achievement:

| Parachute Diameter | Deployment Mach Number |
|------------------------------------|------------------------|
| 120 ft. | 0.8 |
| 24 ft. | 1.2 |
| 40 ft. | 1.2 |
| 8 ft. | 2.0 |
| 6 ft. | 1.48 |
| 4.78 ft. (cluster of 3 parachutes) | 1.53 |

The critical design load established for the parachute decelerator is the opening shock which is the maximum force encountered during inflation. An opening shock of 504,340 pounds, based upon an inflation time of 1.04 seconds, was obtained by the method of Reference 14 and compares favorably with the method presented in Reference 5 when using the opening shock factors presented in Reference 3.

A detailed analysis of decelerator requirements should be considered prior to future development programs. Due consideration will be given to the ASD Ballute which has been flight tested with a Cree missile forebody as the payload. Here, a 9 foot diameter balloon was inflated near the base of the payload and reeled out a riser line; thus eliminating snatch forces. Inflation of the balloon at the payload base minimizes the initial presented drag area which is then increased by reeling out the riser line. Employing a ballute as a booster decelerator instead of the 50 foot parachute would eliminate the requirement for a pilot chute.

Analyses of decelerator requirements and weight trade-off should be considered prior to development efforts since initial estimates of the required ballute system result in a ballute system weight of 1200 pounds with a packing volume of 150 ft³. The proposed parachute system weight is estimated at 1707 pounds with a packing volume of 84.6 ft³.

b. Hot Air Balloon (Paravulcoon) - The balloon is fabricated primarily of two major components; The envelope and the loadlines. The envelope is made of Nylon fabric pressure sealed with Mylar. Nylon webbing is used for the loadlines.

The physical parameters for the balloon are summarized below:

- . Volume = 14,688,000 ft³
- . Height of inflated envelope = 293 feet
- . Diameter of throat = 77.8 feet
- . Diameter of inflated envelope = 311 feet
- . Length of exposed loadline = 33.8 feet
- . Total weight = 11,827 pounds.

The hot air balloon is designed for a factor of safety for 2. This factor provides adequate margins of safety through the sewing.

Included in this section are summary discussions on the following subjects:

. Description of Balloon Components

. Balloon Packing

. Weight and Volume

1) Description of Balloon Components

The two major components of the balloon are the envelope and the load lines.

Envelope - When fully inflated, the balloon envelope will be 311 feet in diameter and will contain 14,688,000 cubic feet of air. Lifting forces developed by the air within the envelope will be transferred from the fabric to the loadlines. The envelope will be designed so that only meridional loads occur in the fabric. Since the gores are forced outward due to internal pressure between the loadlines, large hoop-tension loads are prevented from developing due to the relatively small radius of curvature of the fabric between the loadlines.

The loads in the balloon fabric are greatest in the area of the throat and at the top of the balloon. In the midsection of the balloon, loads from the loadlines are transferred to the fabric to reduce the weight of loadlines. At the crown of the balloon, the load in the fabric will be transferred back into the loadlines.

Nylon will be used for the basic fabric of the balloon. The Nylon fabric will be covered with Mylar on the inner side to form a gas tight seal. If the temperatures of the fabric prove to be high at the crown or near the throat, Dacron or possibly HT-1 material will be substituted for Nylon.

Load-lines - The loadlines (shroud lines) transfer the load from the balloon envelope to the payload. In the proposed design, the loadlines extend continuously over the balloon in a meridional plane.

Two hundred and forty (240) Nylon webbing type loadlines will be used. Each loadline will be divided into three sections as follows:

Loadlines of 10,000 lbs. strength will extend from the booster load-ring to about 8 feet above the balloon throat.

- Loadlines of 6,000 lbs. strength will extend from the throat to 55 feet from the top.
- Loadlines of 8,000 lbs. will overlap the midsectional loadlines and extend to the top of the balloon.

At the top of the balloon, the load in the loadlines and fabric will be transferred to a circumferential ring. A heavier fabric cap will close the top of the balloon envelope.

20 Balloon Packing

The final packing design will result from experimental tests conducted to evaluate material folding techniques, container shapes, and envelope materials. The accordion fold method, appears to be the most feasible at this time since this folding technique should induce less whipping of the material during deployment. Friction will be reduced by lining the inner surface of the container with Teflon.

High altitude flight and deployment of the balloon present some unique problems in packing the envelope. In packaging, small amounts of entrapped air will expand at high altitude. This expansion might result in serious damage to the envelope.

Merely sealing the balloon pack at sea level pressure will protect the packed envelope for apogee altitude but will not protect it when the seal is broken for deployment at 30,000 ft. The breaking of the seal will result in rapid expansion of the entrapped air which will damage the envelope prior to deployment.

To resolve this problem it is possible to evacuate the envelope as it is being packed. The container will be evacuated to the deployment altitude pressure.

c. Burner - The burner is provided to (1) heat the cold air within the balloon envelope to develop buoyancy and (2) to overcome heat loss of the balloon in order to maintain the buoyant altitude. These two heating phases are called the Initial Burner and Control Burner phases, respectively.

For the proposed C-5 Booster design, six (6) burners providing a total heating rate of 255,000 BTU/sec will be required for the Initial Burner phase.

Each of the six burner systems provides an output of 37,500 BTU/sec during the Initial Burner phase.

The burner system uses propane as fuel. Oxygen is provided to insure ignition at high altitude and to supplement the free air flow to insure complete combustion of the fuel. Major components of the burner system include (1) the fuel ejector system, (2) the oxygen ejector system and (3) the burner.

The burner concept combines the desirable features of liquid bi-propellant and fuel-air systems into a single design. Liquid oxygen is introduced into the burner during the initial, 225,000 BTU/sec, burning phase at 25,000 feet altitude to provide the stoichiometric mixture required for complete combustion. Ignition of the burner is initiated at 25,000 feet so that the maximum heating rate of 225,000 BTU/sec will be available at the required altitude of 20,000 feet. The flow rate of oxygen is decreased as altitude decreases. During control burning, no liquid oxygen is required.

d. Controls - The recovery control system for the C-5 Booster provides the necessary signals to initiate the deployment of the pilot and drogue parachutes and the balloon. Following deployment of the balloon, the control system will ignite the burners and provide the necessary control functions to maintain the aerostat at a constant altitude or provide a fixed descent rate. During burner operation, over-temperature conditions in the balloon will also be monitored. The total control system weight is 67 pounds.

1. Control System Sequence

Timer initiation - Following separation of the booster from the launch vehicle, recovery system safing circuits will be de-energized to permit activation of the recovery system. To activate the recovery system, some predictable booster environmental parameter must be sensed. This parameter may be peak deceleration, a fixed value of deceleration, velocity, temperature, etc. It may also be a signal from an inertial sensor or a fixed time after a thorough study of the booster flight path and its environmental parameters has been made.

Timer functions - Initiation of the timer will start the deployment functions of the control system. At fixed times after timer initiation the control system will

- . Deploy pilot parachute
- . Deploy drogue parachute
- . Deploy balloon
- . Energize radio beacon

. Ignite Initial and Control burners

If a visual beacon aid is desired, the timer could also be employed to actuate a high intensity light similar to the Minneapolis Honeywell Atkins Light. This would aid in visual location of the recovered booster.

Control to float altitude - Following initiation of the Initial and Control Burners, the control system will continually monitor descent rate. At a predetermined descent rate, the control system will shut off the Initial Burner and the Paravulcoon will then be controlled at this descent rate until the Initial float altitude is reached. The initial float altitude will be programmed into the recovery control system prior to launch.

Float control - After reaching the initial float altitude the Paravulcoon will be maintained at this altitude by the control system until a new float altitude or a descent rate command is received via the remote radio link. If the Paravulcoon has been attached to a towing helicopter, command signals could also be sent to the control system through signal wires which are an integral part of the tow cable.

Letdown - When the Paravulcoon has been positioned over a suitable landing berth, letdown will be accomplished by winching against a small buoyancy or by a controlled descent rate. In either case, the control system will provide the necessary control to the sustainer burner to provide the correct lift. At touchdown the control system will provide a signal to appropriately placed squibs to release the Paravulcoon loadlines and/or vent the Paravulcoon to remove all lift.

Over-temperature control - At the time the Initial and Control burners are ignited, and until touchdown, an over-temperature control circuit will be energized. Strategically placed sensors on the balloon fabric will continuously monitor temperature. If a temperature high enough to damage the fabric should occur, the over-temperature control will reduce the burner output to a fixed minimum value until the over-temperature ceases to exist.

2. Major Components

Altitude and altitude rate sensor - As presently envisioned, altitude and altitude rate would be sensed by a barometric type sensor, such as the M-H PG10 Altitude Controller. At the float altitudes and descent rates required by the recovery system, accuracies of ± 20 feet and ± 1 ft/sec. can be expected.

Sequence Timer - The sequence timer is required to furnish the appropriate signals to various control circuits at fixed times after timer initiation. There are several available timers which will satisfactorily perform this operation. The M-H XM-5 interval timer could be readily adapted to this application.

Remote Link - A remote link is required in the control system to provide a means of changing the float altitude and commanding descent rates. The remote link will also allow ground or air control of the other control functions. Presently available FM-FM telemetry receivers are readily adaptable to this application.

Electronic Circuitry - As in any electronic system, coupling and amplification between the various sensors input signals, and output signals will be required. None of these applications require an extension of present state-of-the-art in electronic circuitry.

Control Motors and Solenoids - The output of the control system will be applied to one or more motors which are used to drive the burner valves. Because of the additional complexity and weight in the power supply necessary to provide AC, every attempt will be made to use DC motors for this application.

Solenoid valves will be required in the control system to provide over-temperature control, burner initiation, etc. These will be DC solenoids and are available as off-the-shelf items.

Beacon Transmitter - The beacon transmitter serves only as a means of locating and identifying the recovered package. Any of several UHF or VHF transmitters would be suitable for this purpose.

Antennas - Antennas will be required for the beacon transmitter and the remote link receiver. Since it will be very difficult to locate one antenna to provide complete coverage for these functions, it is planned to locate 3 antennas for the transmitter and 3 antennas for the receiver in the sides of the booster package to provide adequate coverage. The antennas will be internally mounted with suitable openings in the side of the booster package to provide adequate coverage. The antennas will be internally mounted with suitable openings in the side of the booster.

Power Supply - Because of the long periods of operation which may be required of the control system, thermal batteries do not appear feasible as a primary power supply, storage batteries of the nickel-cadmium type would appear to be of a much more logical choice.

While the use of DC components will be considered whenever possible some AC voltages will be required in the control system. Solid state inverters will be used to obtain the required AC power.

3. System Weight & Volume Summary

Table 4 presents a weight and volume summary for each of the major subsystems of the Paravulcoon Recovery System.

TABLE 4
PARAVULCOON RECOVERY SYSTEM
WEIGHT AND VOLUME SUMMARY

| <u>Item</u> | <u>Weight - lbs.</u> | <u>Volume - ft.³</u> |
|--|----------------------|---------------------------------|
| <u>Basic System</u> | | |
| Parachutes | 1,707 | 84.6 |
| Hot Air Balloon | 11,827 | 784 |
| Burners (*1) | 15,032 | 655 |
| Control System | 67 | 1 |
| Structure | 500 | |
| Total System (*1) | 29,133 | 1,524.6 |
| Additional Fuel for 2 hours of flight | 5,890 | |
| Total weight for 2 hours of flight (*2) | <u>35,023</u> | |
| Addition Fuel for 3 hours of flight | 5,890 | |
| Total weight for 3 hours flight (*3) | <u>40,913</u> | |

* NOTE: 1) The burner weight of 15,032 lbs includes fuel for a controlled flight of one (1) hour in addition to the fuel required to decelerate the recovery system to buoyancy.

2) Total System weight for 2 hours of controlled flight.

3) Total System weight for 3 hours of controlled flight.

PERFORMANCE

The required functions of the recovery system are based upon the following C-5 booster characteristics. The residual propellants are expelled prior to atmospheric re-entry resulting in a booster empty weight of 260,000 lbs. Modulated drag and lift trajectory control is required to limit aerodynamic loading associated with atmospheric ballistic re-entry. The Paravulcoon Recovery System environmental design parameters associated with ballistic re-entry are relaxed when re-entry is accomplished with drag and lift modulation. Therefore, to be conservative, the recovery system was designed to function with an uncontrolled ballistic booster re-entry associated with a nominal Saturn mission. The functional requirements and environmental design criteria associated with the various subsystems are discussed in the following paragraphs.

The recovery system sequence of events is shown as a time history of the trajectory parameters in Figure 14. A 6.5-foot pilot chute is deployed from the booster by a deployment gun and is used to deploy a 50-foot ribbon type parachute which is packed in a deployment canister. The parachute is attached to a 70-foot riser line that is structurally attached through the balloon container to the booster. Upon deployment, the parachute is snatched out of the deployment canister by the riser line. The parachute snatch force carried by the riser line is estimated to be 35,000 pounds and does not appear as a significant rise in Figure 14. The parachute inflates immediately after snatch and decelerates the booster from 1440 ft/sec to 600 ft/sec. The opening shock due to parachute inflation is estimated to be 504,340 pounds during a time interval of 1.04 seconds. After 17 seconds of parachute deceleration, balloon deployment is initiated. The balloon container is released from the booster by explosively rupturing structural restraint fittings. The 50 foot parachute then acts as a pilot chute and deploys the balloon. The balloon snatch force of 810,000 to 1,540,000 pounds is transferred to the booster by 240 loadlines, the 50 foot parachute is released prior to balloon snatch.

The time required to deploy and snatch the balloon is about 3 seconds. Balloon inflation by ram air begins immediately after snatch and requires an inflation time of 25 seconds. The opening shock force associated inflation is 910,000 pounds. The balloon also acts as an aerodynamic decelerator, decelerating the booster from a velocity of 600 ft/sec to 180 ft/sec at an altitude of 20,000 feet. When the balloon is fully inflated, the heat generators are ignited. The buoyant force generated by heating the air within the balloon is

additive to the total drag. The heat generators are composed of six propane fuel burners and supply 225,000 BTU/sec to raise the internal temperature of the balloon. A burning time of 160 seconds is required to decelerate the booster to an aerostatic buoyant altitude of 5,000 feet. The maximum buoyant force is 285,000 pounds. Burner modulation, which decreases the buoyant force, occurs 6 seconds prior to reaching the 5,000 foot altitude. Burner modulation is self-controlled to give an altitude hunt amplitude of no more than 40 feet (± 20 feet). Depending upon the mission requirements the booster will remain at the aerostatic buoyant altitude or descend to ground contact. The total time at the buoyant altitude is dependent upon the "onboard fuel" which in this case is for one hour. In the event total fuel consumption is imminent, the control system will automatically land the booster. Contact velocity and dispersion of the aerostat is, of course, dependent upon prevailing winds. Self controlled landing is accomplished with a vertical velocity of $1 \text{ ft/sec} \pm 1\frac{1}{2} \text{ ft/sec}$. Retrieval of the buoyant system is initiated by search aircraft. Acquisition aids of an ID transmitter and flashing light beam are provided. Once the booster location is determined, helicopters may be summoned. The helicopter snatches a tow cable transfer line which is suspended from the booster. This transfer line is used to transfer the towing cable and in-air fueling lines from the helicopter to lock fittings on the booster. The helicopter then tows the booster to a landing site and provides in-flight burner refueling. Assuming no winds, the maximum true air speed while towing at a 5,000 foot altitude is 25 fps with one helicopter and 36 fps with two helicopters.

The landing site will provide the necessary landing bed and ground equipment to safely land the recovered booster.

PLANET EXPLORATION

In the near future the United States will be sending instrumented payloads to Venus and Mars. In fact, Mariner II should be transmitting, within a few short weeks, needed information to define the environment of Venus. Prior to manned flights, orbital probes will be required and even these will be followed by the soft landing of instrumented packages. As noted in Reference 2, initial exploration of Venus and Mars may be accomplished by a balloon with controlled descent through the planet atmosphere. By close observation of the surface terrain, decisions can be made on the type of vehicle to be used for further exploration. To obtain close observation, photographic surveys will have to be conducted.

To determine if the Paravulcoon system could be considered to perform this exploration function a brief analysis has been conducted. The following discussion indicates the ability of the Paravulcoon System to be adapted to this mission.

Since the principal feature of the Paravulcoon System is buoyancy, a comparison of an earth system is made relative to the atmosphere of Mars and Venus. To float a payload, the buoyant force must equal the payload mass times the local gravitational acceleration. To obtain the buoyant force, a density differential must be obtained by heating the gas within the balloon.

The pertinent atmospheric characteristics are presented in Table 5 as obtained from Reference 6 for the planets to be considered.

TABLE 5
PLANET CHARACTERISTICS

| Planet | Surface Gravity (Relative) | Surface Temperature R | Atmospheric Density (relative) | Atmospheric Gases (Major) |
|--------|-------------------------------|--------------------------|-----------------------------------|--|
| EARTH | 1.0 | 443 | 1.0 | N ₂ , O ₂ , H ₂ O CO ₂ |
| MARS | 0.383 | 391 | 0.13 | CO ₂ , N ₂ O |
| VENUS | 0.866 | 412 | 1.47 | CO ₂ , N ₂ , H ₂ O |

As pointed out in Reference 6, the available information on Mars and Venus in many cases is contradictory, especially for Venus. At best, any comparison based upon the data shown in Table 5 is speculative. A comparison of the buoyant lifting efficiency is made in Table 6 based upon the following assumptions using the characteristics presented in Table 5

1. The Paravulcoon internal temperature is 710° R for required envelope tensile strength.
2. The stored energy to obtain 710° R is the same for all cases. (Expended fuel mass is the same.)

Since the balloon volume will vary for the atmospheric gas constituents, based upon the above assumptions, the relative balloon volumes are also indicated.

TABLE 6

EFFICIENCY COMPARISON

| <u>Planet</u> | <u>Relative Buoyancy</u> | <u>Relative Balloon Volume</u> |
|---------------|--------------------------|--------------------------------|
| EARTH | 1 | 1 |
| VENUS | 1.17 | 0.67 |
| MARS | 1.15 | 7.9 |

From Table 6 it can be concluded that for the same level of energy input from a heat generator 17% more buoyancy is obtained on Venus with a Paravulcoon System which has a smaller balloon than a comparable system on earth. It should also be noted that the heat loss through the smaller balloon envelope during sustained flight would be somewhat less than on earth since the balloon temperature differential is comparable. This would require a lower fuel consumption.

The system efficiency relative to Mars is considerably reduced based upon the balloon size. This is due to the extremely low atmospheric density of 0.13.

If the heat generator requires oxygen, then an oxidizer will have to be carried for Venus and Mars exploration since only limited, if any, free oxygen is available. The weight penalties associated with a nuclear heat generator should be established during any design which would consider a float time of several days or months.

It is concluded that the Paravulcoon System should be considered as a tool for planetary exploration since the system will function in any atmosphere and will provide a space platform from which data could be obtained that would be difficult for a satellite or land station to obtain.

CRITICAL DESIGN AND DEVELOPMENT AREAS

There are several critical design and development problems associated with the use of this recovery system. The degree of criticality, of course, depends upon the specific application. Without regards to application, however, the following itemizes these problem areas.

Balloon Deployment - Very little, if any, study has been given to the maximum dynamic pressure and thermal conditions to which a balloon could be subjected during deployment. Considerable experimentation and analysis is required.

- Transient Thermodynamics - The principles involved in the transient heating of the air in the balloon are understood. However, the qualitative and quantitative aspects of the heating mechanism within the balloon must be more fully tested and understood.
- Burner Design - For maximum system efficiency, the burner should have minimum weight. Large size burners for the recovery of large payloads are not available.
- Burner Controls - While the controls and sensors for this system have not been specified in detail, it is felt that with a nominal amount of study and experimentation the control system would be a state-of-the-art device.
- Recovery System Weight - Detail designs and associated experimentation should be made to determine optimum weight for a large range of practical recovery devices. Overall system weight should be compared with other recovery system along with functional operational requirements associated with various recovery problems.

ACKNOWLEDGEMENT

The authors wish to acknowledge the contributions and research efforts of Messers. L. Norman (M-H Warhead Electronics Group) and R. Pohl (Raven Industries - Research Group).

REFERENCES

1. Minneapolis-Honeywell, "PARAVULCOON Recovery System for the Saturn C-5 Booster," Ordnance Division TD 87762 Serial 55060, 28 March 1962.
2. Koelle, H. H., (Editor) Handbook of Astronautical Engineering, McGraw Hill, N. Y., c. 1961.
3. Pederson, P. E., "Study of Parachute Performance at Low Supersonic Deployment Speeds; Effects of Changing Scale and Clustering," ASD TR61-186, July 1961.
4. Heinrich, H. G., "Notes from Aerodynamic Decelerator Course," Presented at the University of Minnesota, Institute of Technology, July 1961.

5. USAF, "United States Air Force Parachute Handbook," WADC TR 55-265, December, 1956.
6. "Proceeding of the Recovery of Space Vehicles Symposium," August 31-September 1, 1960, IAS, N.Y.
7. Raven Industries and Minneapolis Honeywell, "High Altitude PARAVULCOON Recovery System Airdrop Tests," September 1961, 16 mm Silent Colored Movie available upon request from Minneapolis Honeywell, Ordnance Division, Hopkins, Minnesota, Attn: Mr. R. L. Seaberg.
8. Minneapolis Honeywell, "Engineering Design Study and Test Program for PARAVULCOON Recovery Systems," Ordnance Division TD 87862, Serial 55061, 28 March 1962.

Nomenclature

A = Cross-sectional area
 C_d = Drag coefficient
 D = Drag force
 F = Force
 g = Gravitational acceleration
 H_f = Heating value of fuel
 J = Mechanical equivalent
 k = Heat transfer factor
 m = Mass
 p = Pressure
 R = Gas constant
 T = Temperature
 t = Time
 V = Volume
 W = Weight
 x, y = Linear displacement
 (y is positive downward)
 η = Burner thermal efficiency
 ρ = Air density

Subscripts and superscripts:

() B Balloon
 () b Burner
 () f Fuel
 () P Payload
 () S Shroud force
 () ∞ Average free stream
 (), (') Differentiation with respect to time.

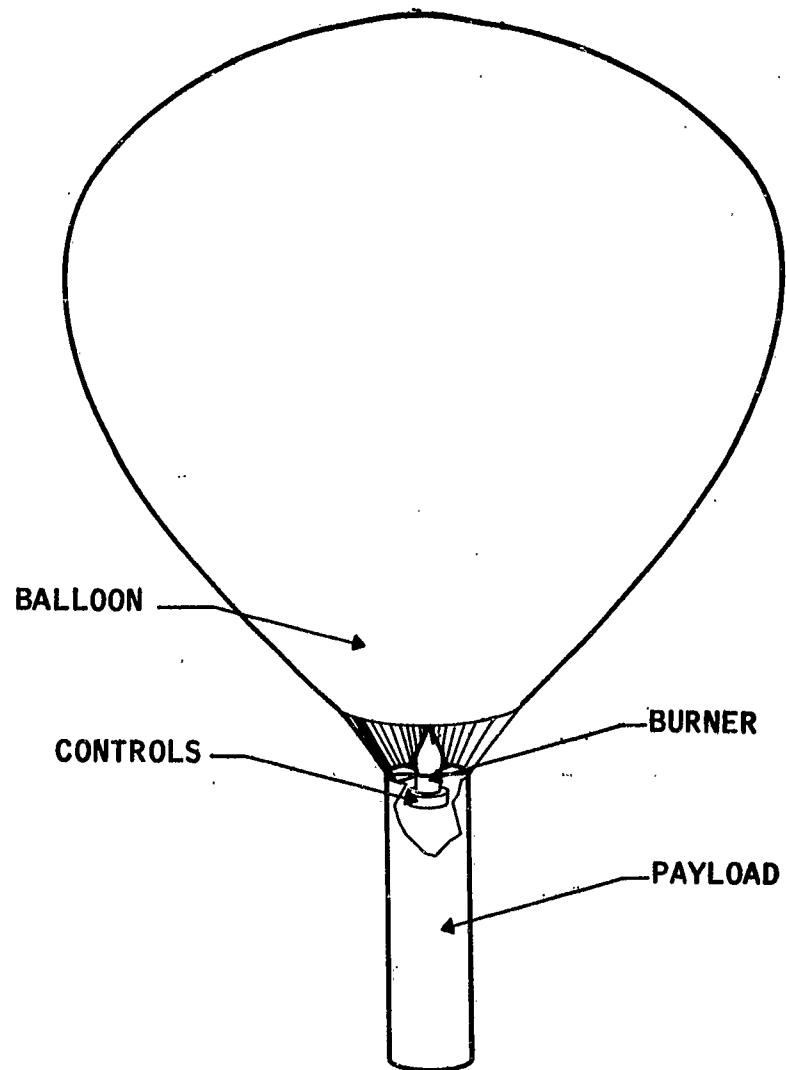


Figure 1. Paravulcoon Concept

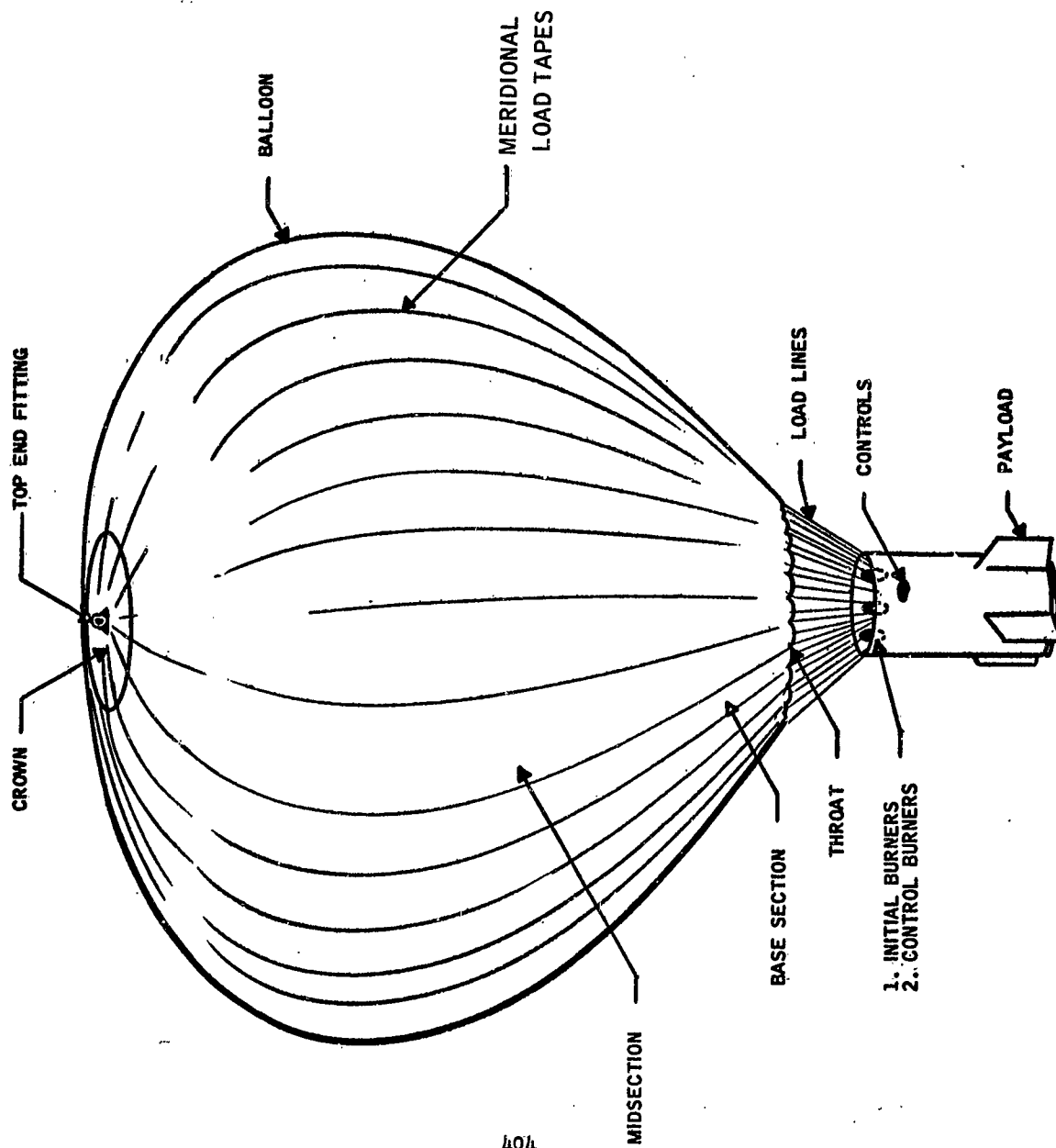


Figure 2. Faravulcoon Recovery System - Terminology

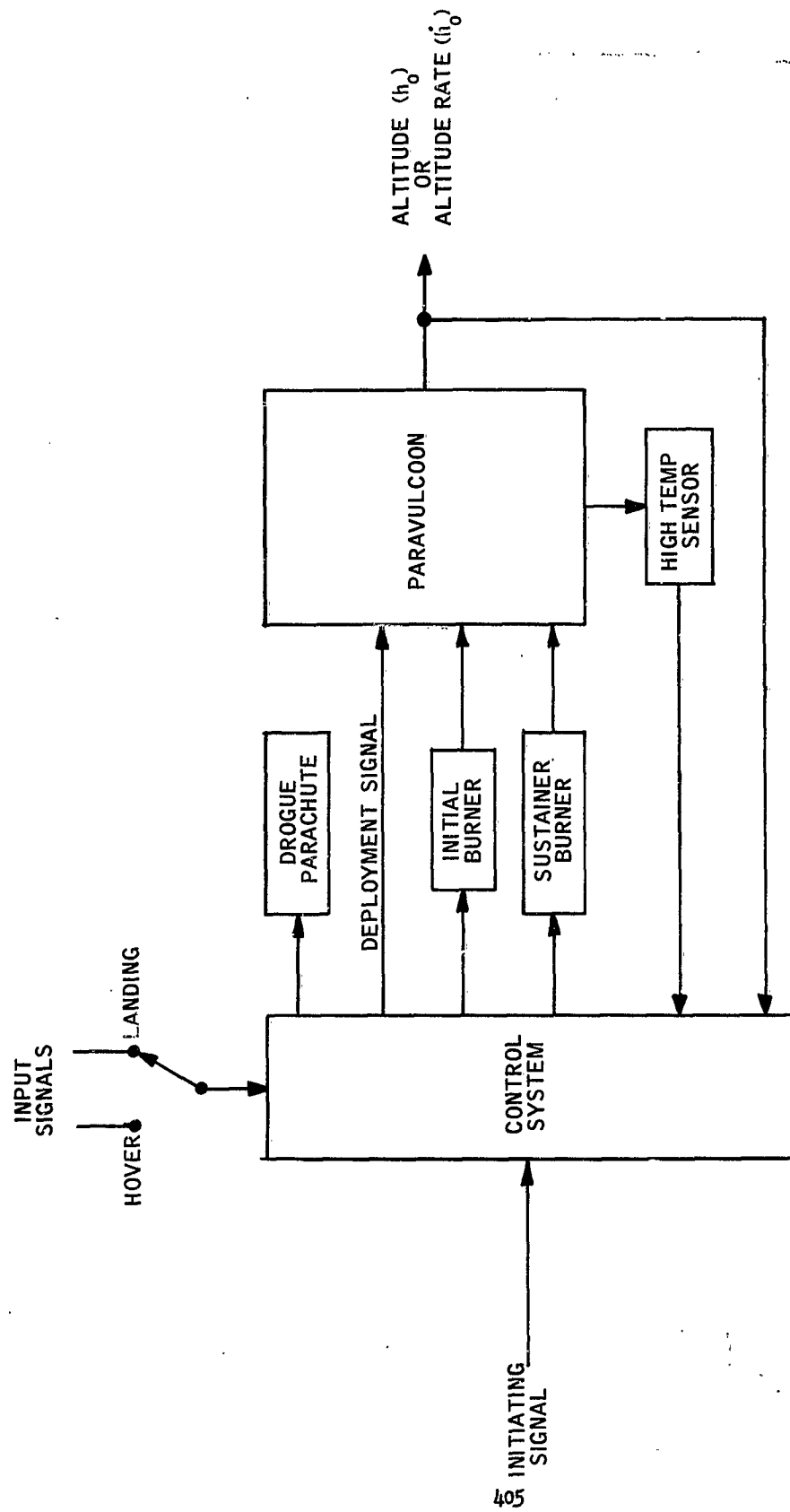


Figure 3. Integrated Control System

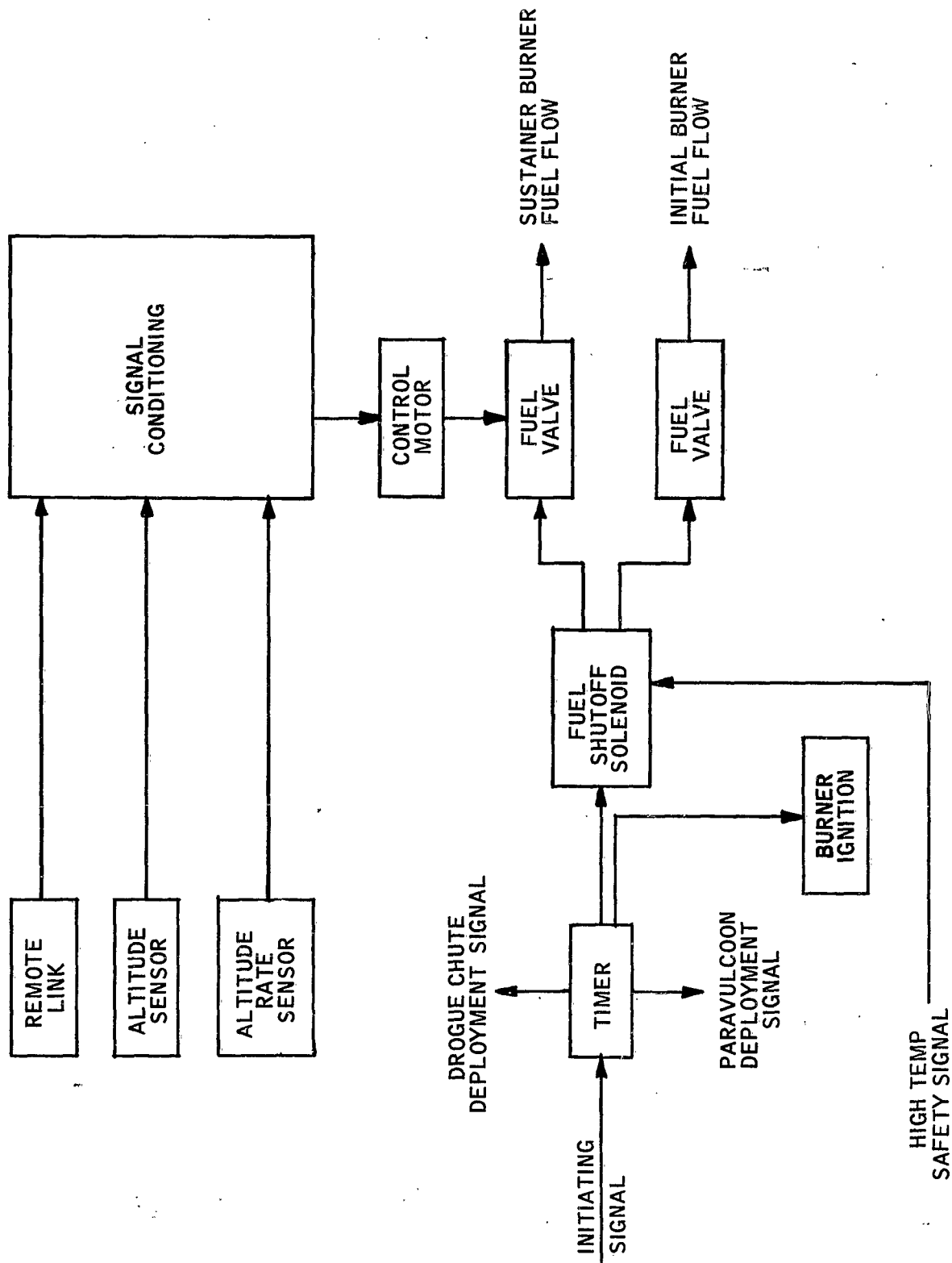


Figure 4. Control System Block Diagram

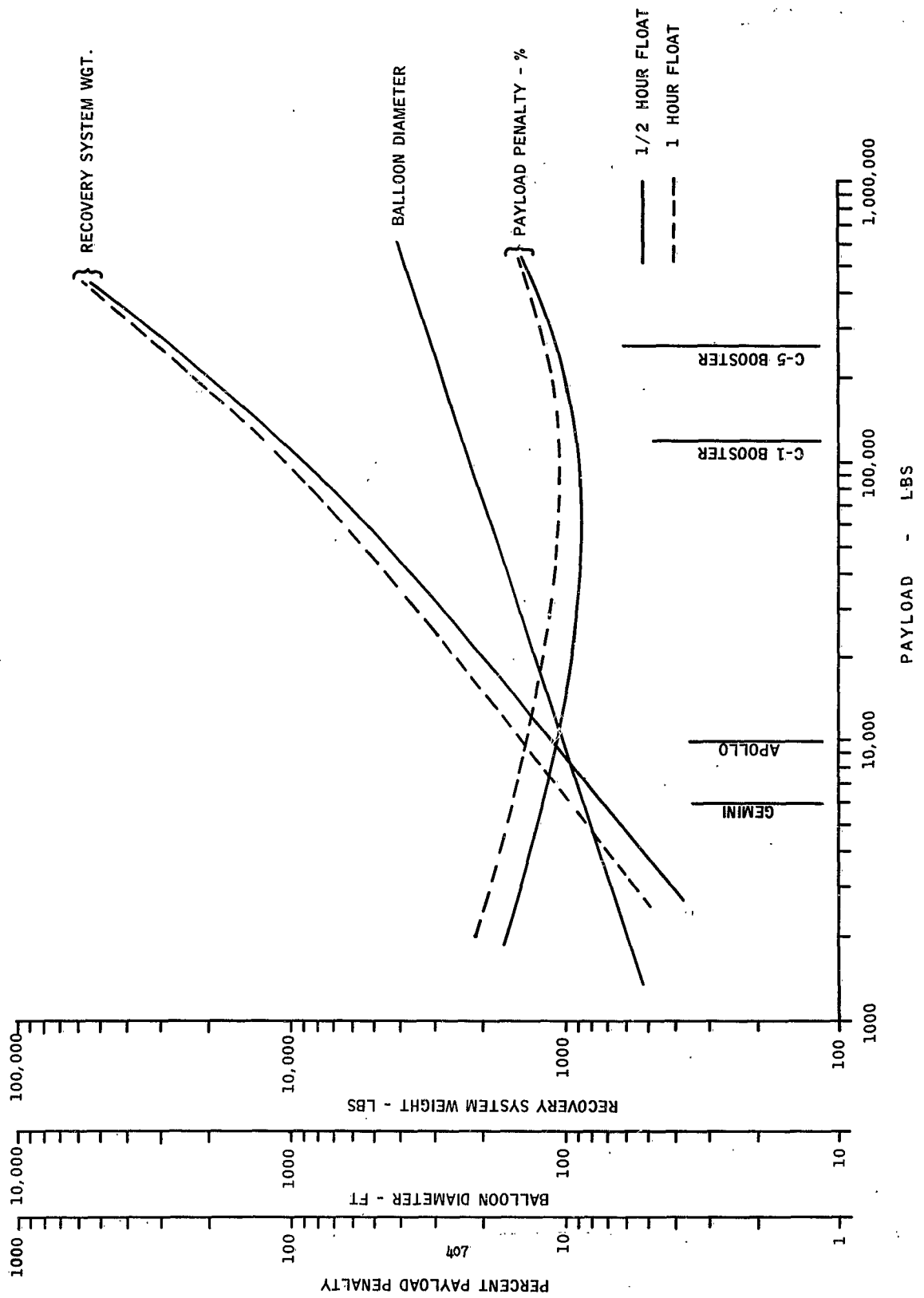
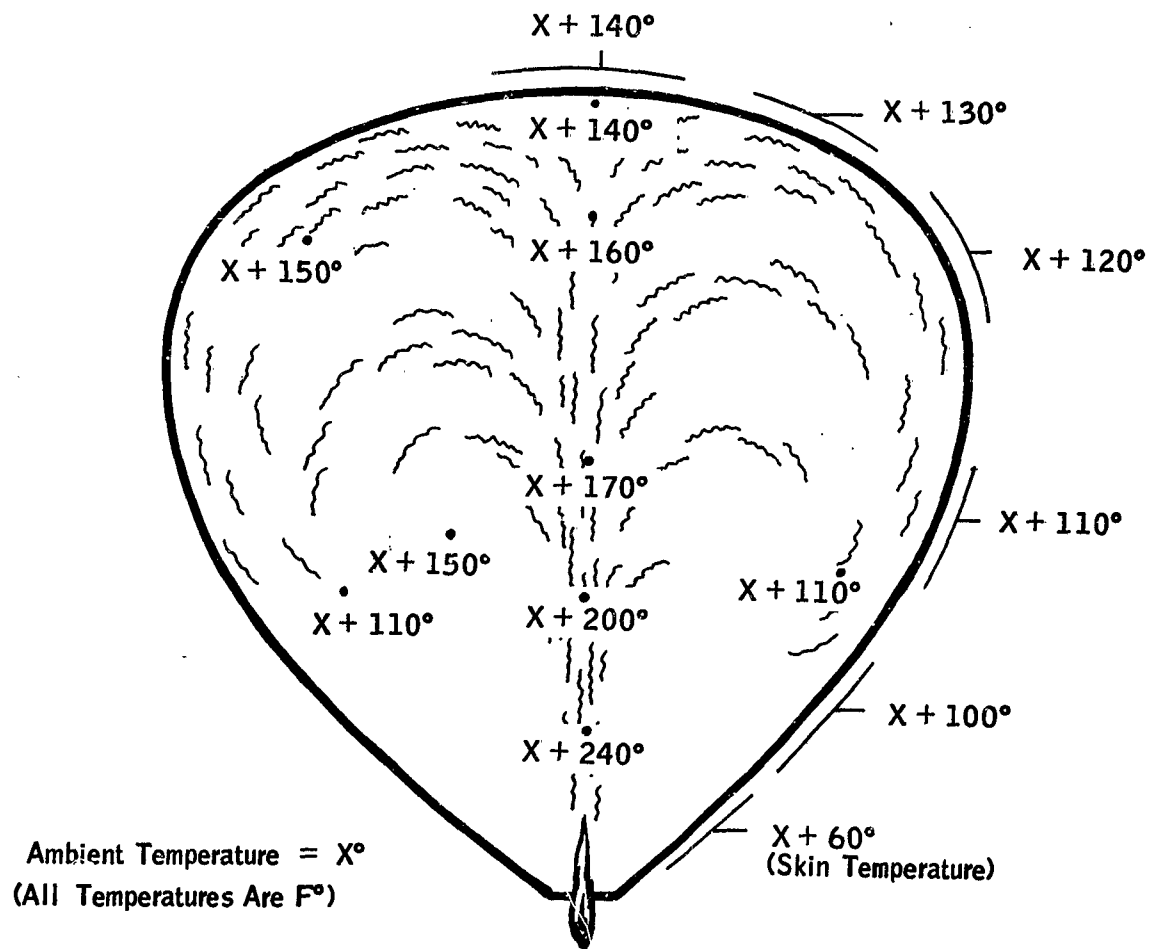


Figure 5. Paravulcon Recovery System Weights vs Payload Weights



Average Temperature Differential
 In This Illustration Is 140°F

Figure 6.

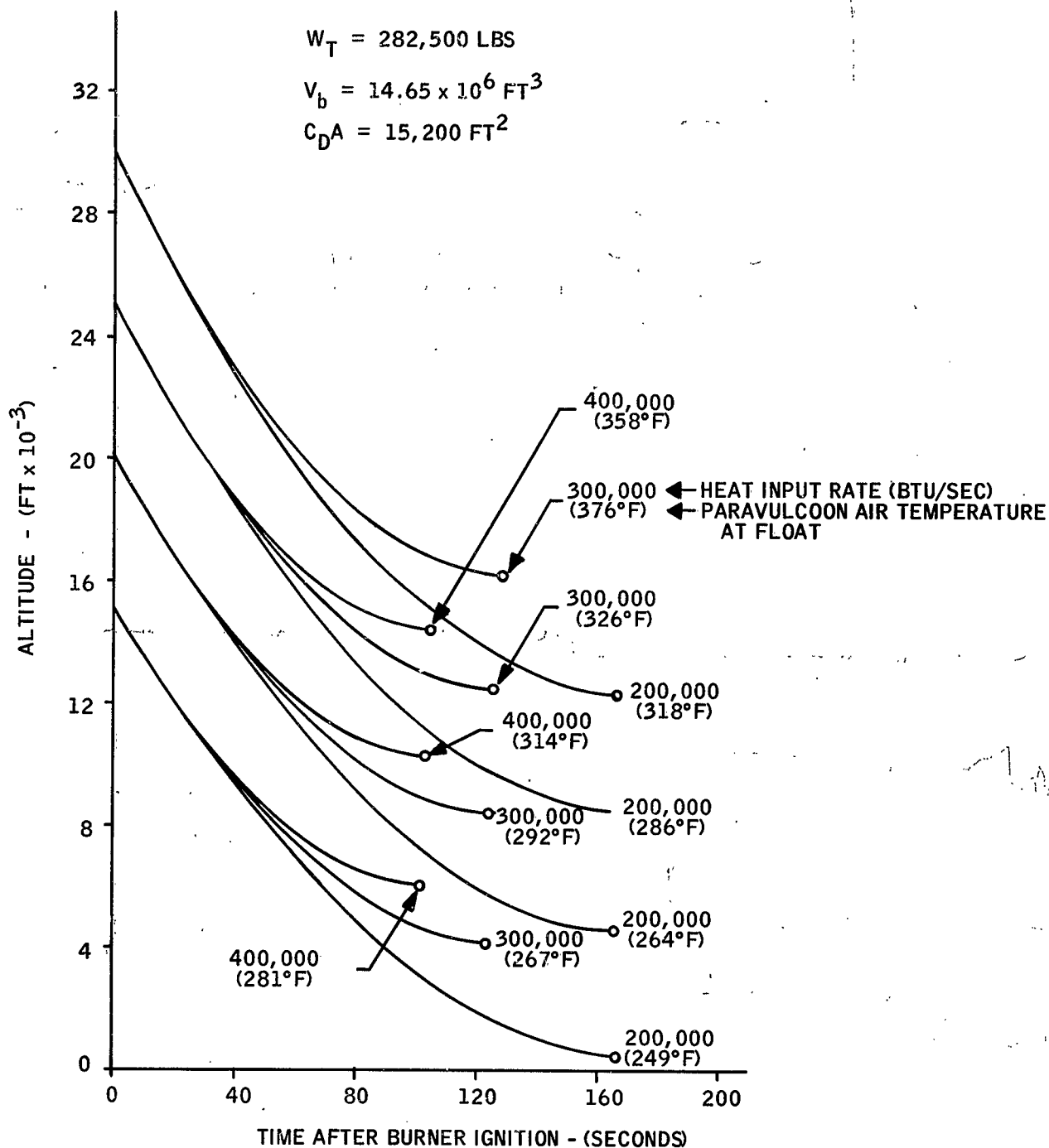


Figure 7.

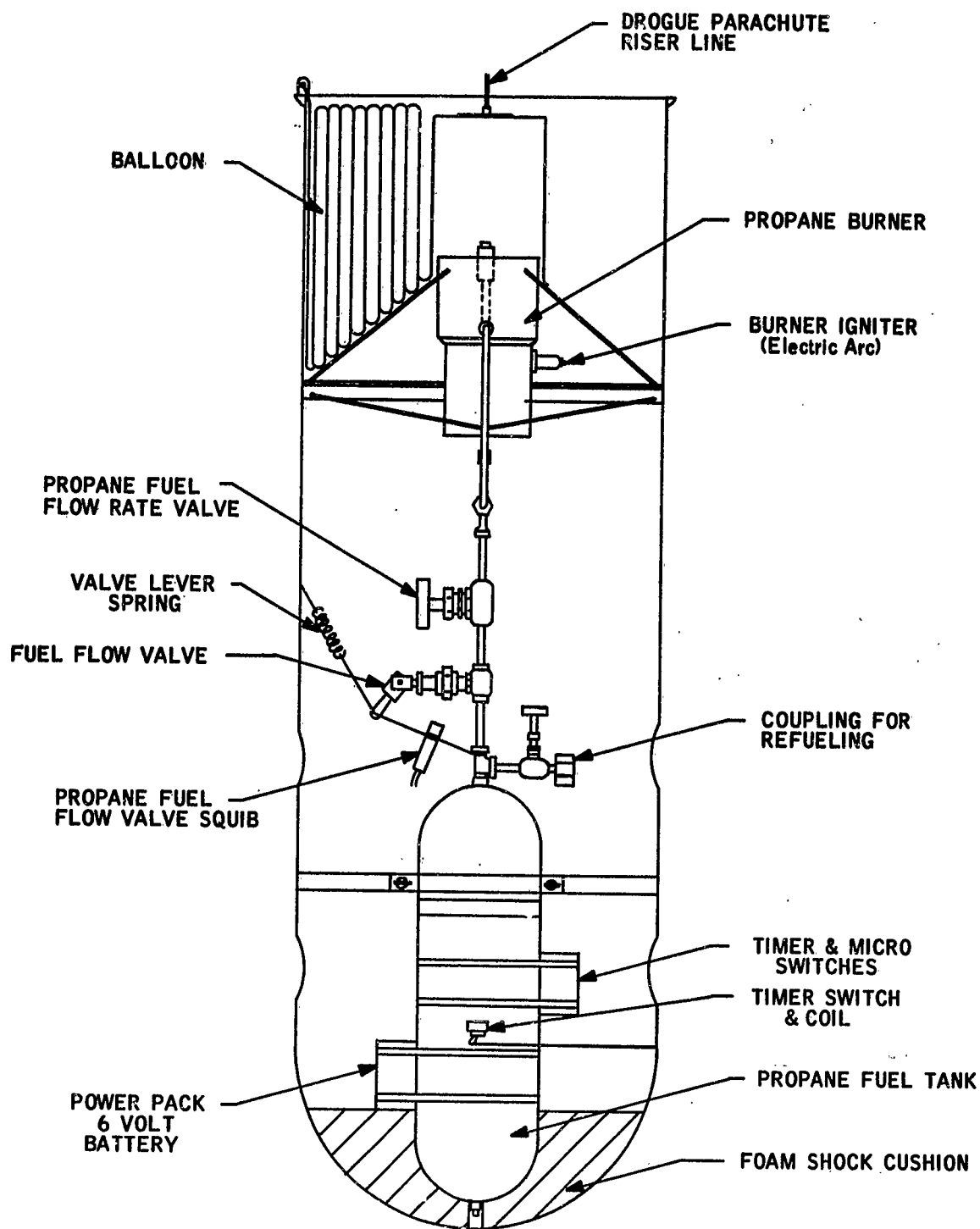


Figure 8. Raven Test Model Packaging Configuration

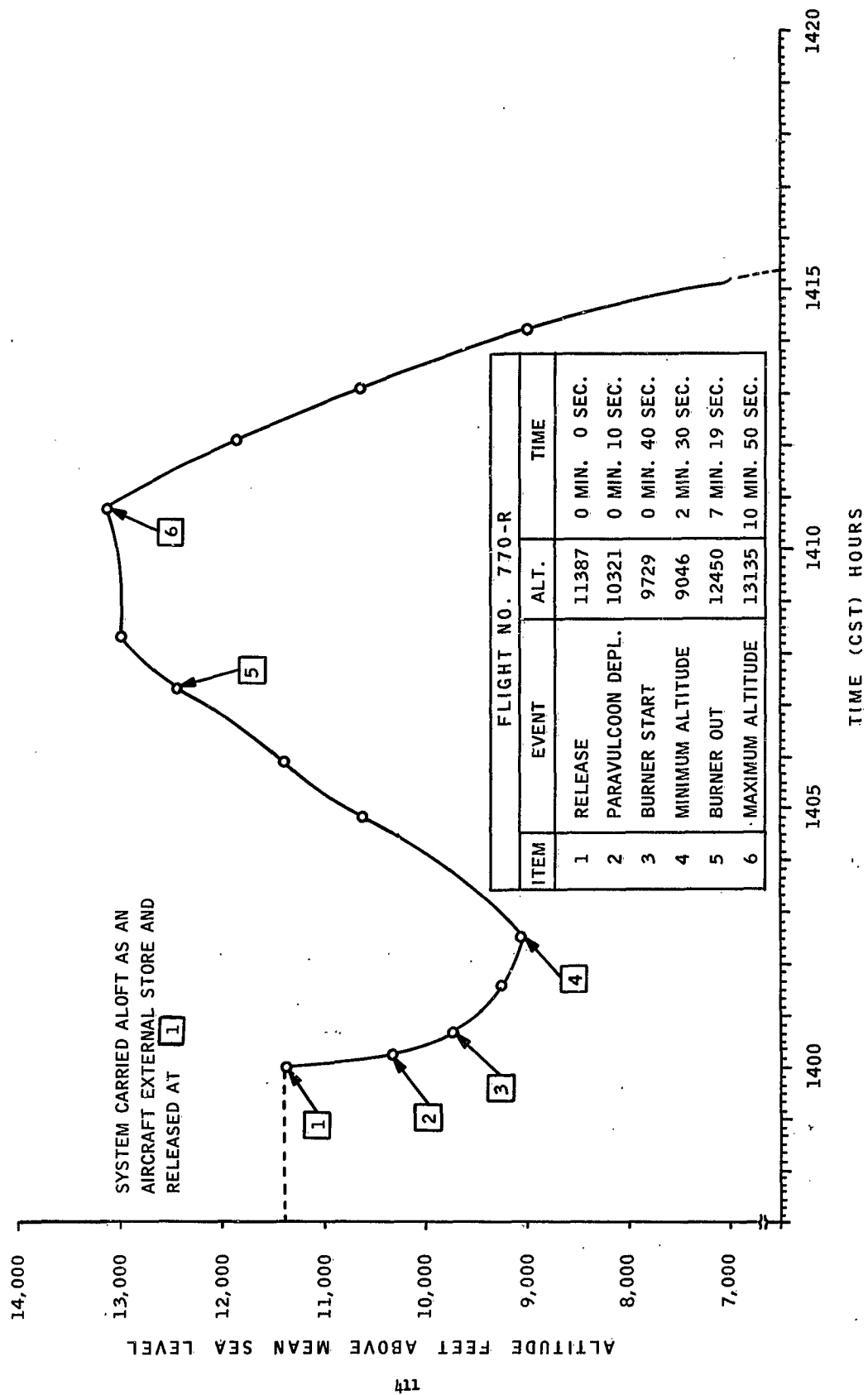


Figure 9. Altitude Time History - Aircraft Drop Recovery System Flight Test

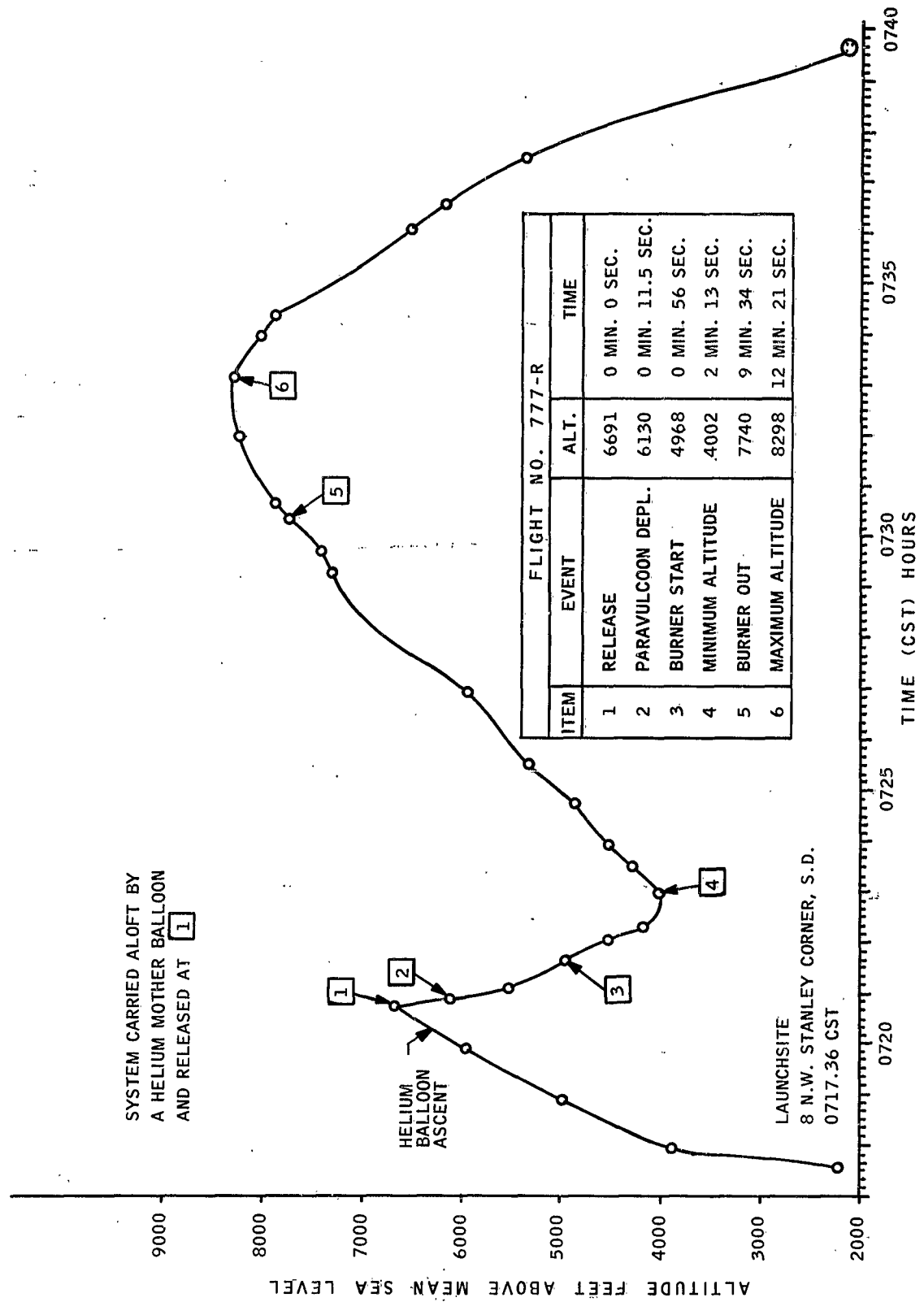


Figure 10. Altitude Time History - Balloon Drop Recovery System Flight Test

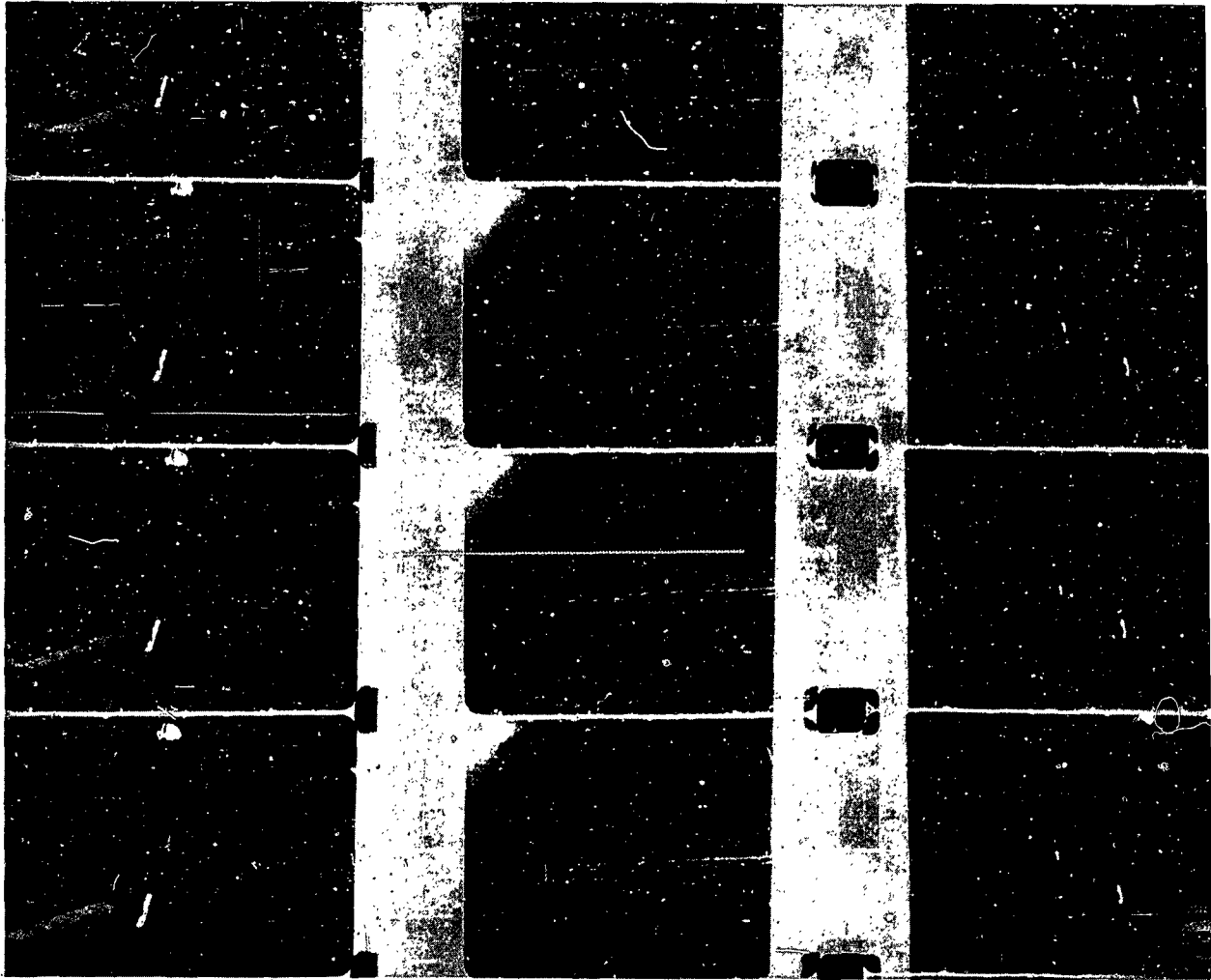
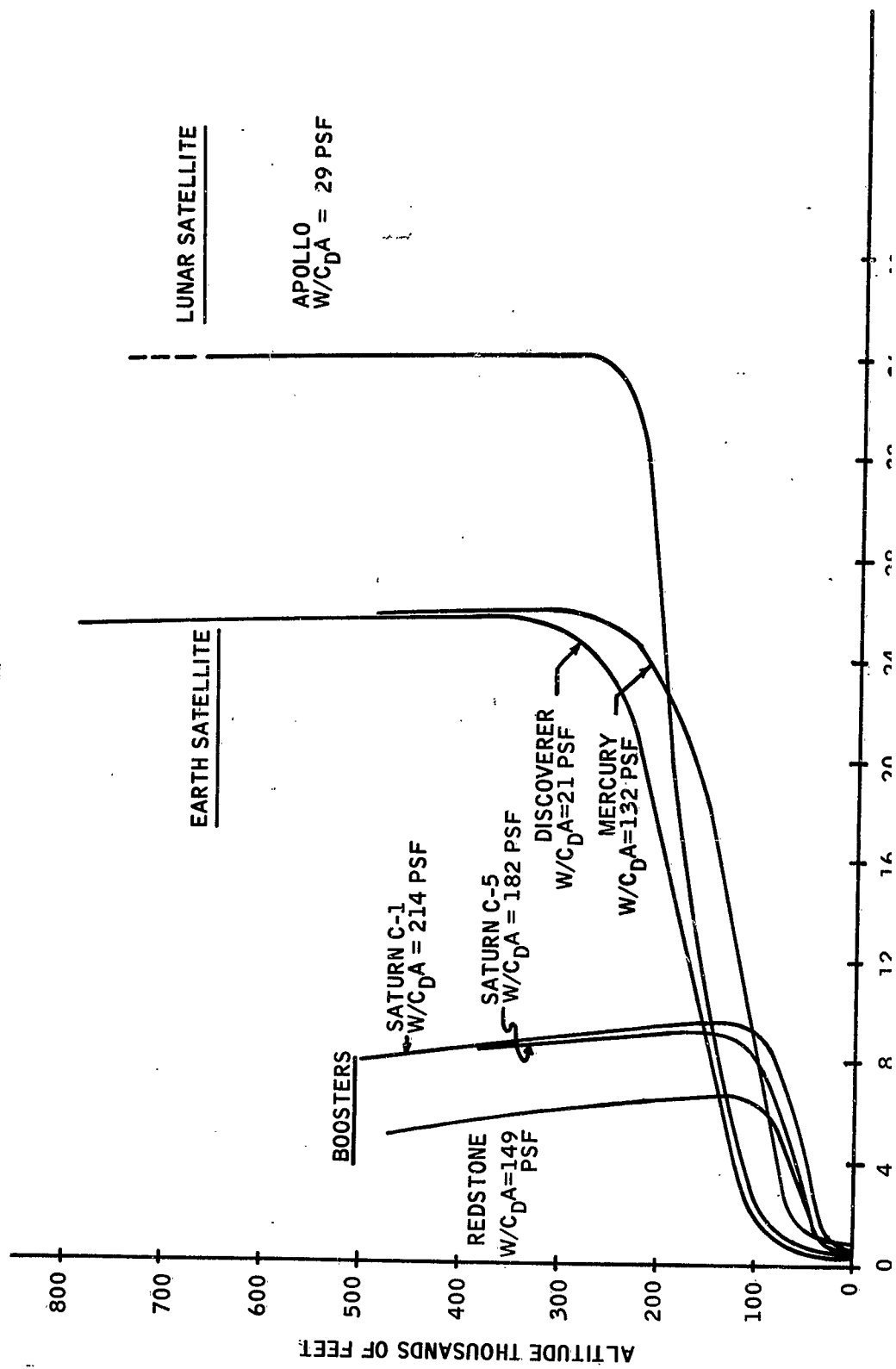


Figure 11. Motion Pictures of Raven's Test Flight



Spherical non-rotating Earth with a gravitational field as a function of latitude, longitude, and altitude. (At $t=0$, Latitude= 45.0°N , Longitude= 85.0°W with Heading= 90.0°E .)

1959 ARDC Standard Atmosphere
Drag coefficient varies as a function of flight Mach number with $\alpha = 0$ degrees.

Weight = 282,500 pounds
 $\gamma_{B.O.} = 19.4$ degrees
 $V_{B.O.} = 9200$ feet per second
 $Z_{B.O.} = 213,265$ feet

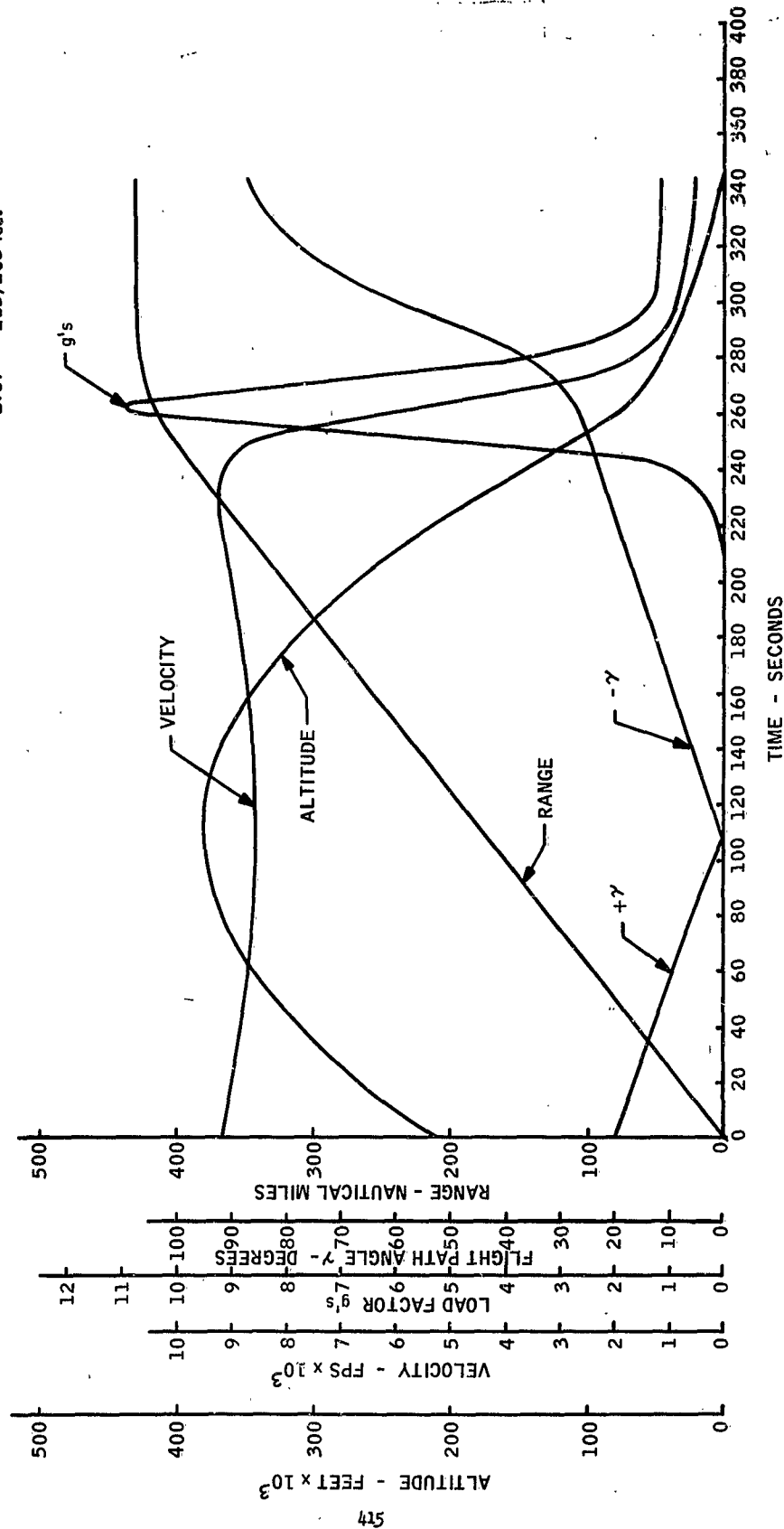


Figure 13. Spherical Nonrotating Earth With a Gravitational Field as a Function of Latitude, Longitude, and Altitude. (At $t=0$, Latitude= 45.0°N , Longitude= 85.0°W With Heading= 90.0°E .)

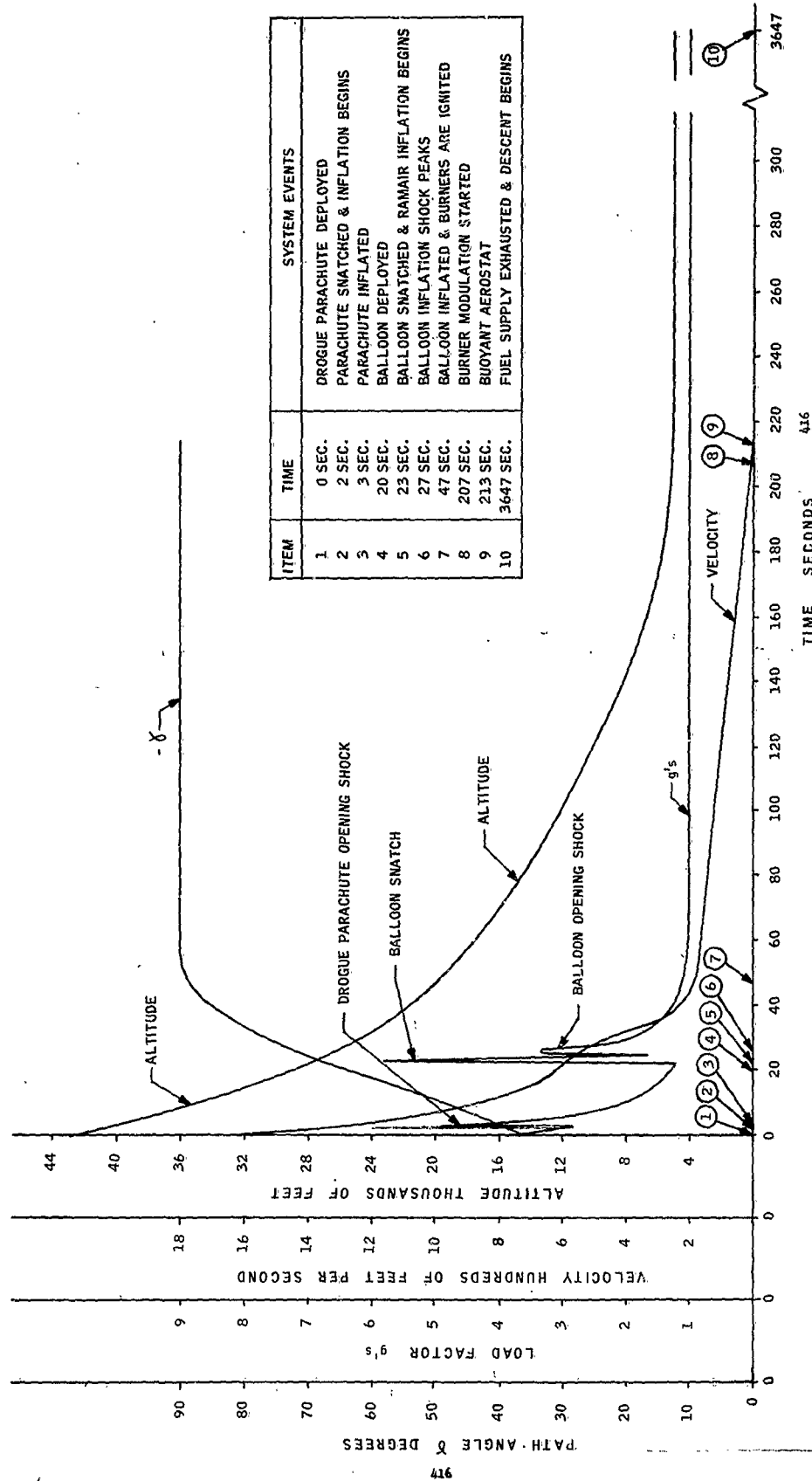


Figure 14.

Session IV

GENERAL CONSIDERATIONS SESSION

Chairman: LT COL J. E. MURRAY
Hq USAF
Washington, D. C.

SYSTEMS CONSIDERATIONS

Theodore W. Knacke

Chief of Technical Staff
Paradynamics Systems Section
Northrop Corporation, Ventura Division

ABSTRACT

Recovery means return of the vehicle, after completed mission, to its home base undamaged by boost, environment, landing, or retrieval. Parachutes today form a subsystem part of the total recovery system. Requirements for reliability have been increased by an order of magnitude. New methods are being developed for force determination. Sequencing and reliability of the recovery cycle are an important factor. New approaches are desirable for location aids. Self-inflating flotation bags have recently been developed and used successfully. Numerous areas are outlined that demand more research, development, and improved equipment.

SYSTEMS CONSIDERATIONS

INTRODUCTION

Not too many years ago people would come to us and say, "I need a parachute about thirty (30) feet in diameter for about one hundred fifty (150) miles per hour, and it should provide a rate of descent of approximately twenty (20) feet per second!" When we pointed out politely that recovering an item after flight requires somewhat more than just a parachute, people were surprised that there were different types of parachutes, different means of deploying and opening parachutes, or that we thought we could calculate parachute forces.

Today, we still use parachutes for lowering personnel, equipment, and vehicles, but mostly as part of a complete recovery system. On the other hand, parachute reliability requirements have increased by several orders of magnitude for projects Mercury and Apollo where parachutes provide the standard means for descent and landing after completion of the space mission.

Parachutes, together with deployment, sequencing, impact absorption, flotation, location, and retrieval equipment, form the recovery system. This is well demonstrated in the recovery package for the Echo II balloon data capsule that brought the pictures of the inflating balloon back from nine hundred (900) miles altitude. The total package, including re-entry heat shield, retardation, flotation, and location subsystem, carries a price tag of approximately twenty-six thousand dollars (\$26,000) with the parachute priced at only five hundred dollars (\$500). Recovery today means undamaged return of the payload to home base and protection against hostile environment from take-off to landing. Completion of this cycle documents a successful recovery. Figure 1 on Page 3 illustrates pictorially the recovery cycle of a reusable booster using one of the various proposed recovery concepts. Inclusion of all recovery equipment and environmental protection will increase the empty booster weight by twenty (20) to thirty (30) per cent, a figure that is considered unacceptable for present boosters. However, the requirement for booster re-use, that means for booster recovery, remains unchanged, see References 1, 2, and 3.

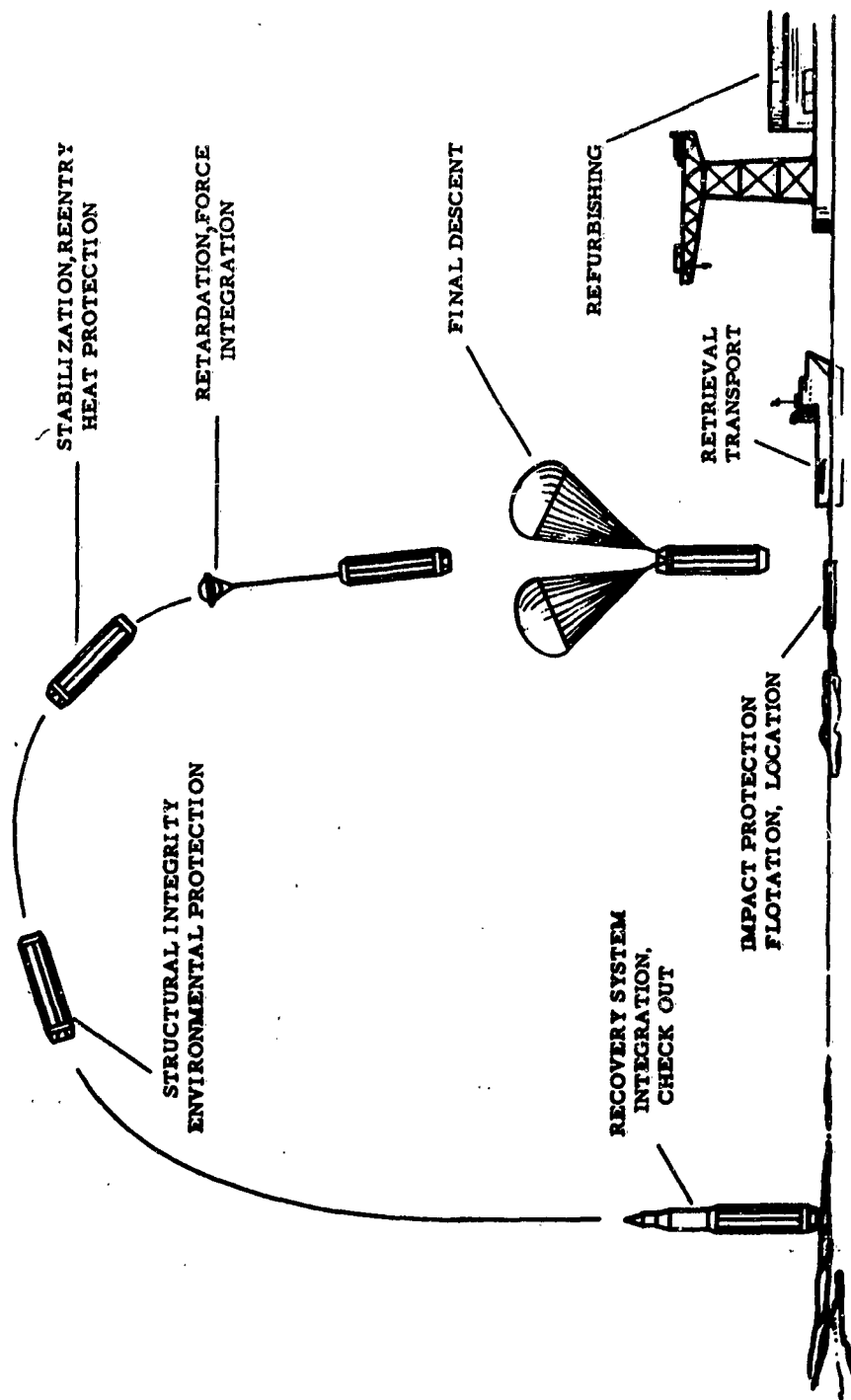


FIGURE 1. RECOVERY CYCLE OF A RE-USABLE BOOSTER

RECOVERY CONCEPT

Recovery boundaries extend today from zero forward speed at on-the-deck escape for military aircraft to recovery of space vehicles re-entering the earth's atmosphere at an angle of ninety degrees (90°) and a velocity of thirty-six thousand (36,000) feet per second. Figure 2 on Page 5 illustrates the various phases of space vehicle recovery: orbit transfer; de-orbiting; atmospheric re-entry; deceleration; descent and landing; and location and retrieval. The recovery concepts used in projects Mercury and Apollo are marked as Path 1 and Path 2, respectively. Looking toward the future, it stands to reason that two (2) recovery concepts may become the predominant means for landing of space vehicles. These two (2) concepts are indicated in Path 3 and Path 4. Path 3 refers to the spaceplane that lands and takes off like an airplane; its development is a foregone conclusion and only a question of time and funds. However, for a number of technical and economical reasons, the concept outlined in Path 4 may emerge as the most practical solution for unmanned logistics space vehicles. The vehicle re-enters on a ballistic or low L/D path similar to project Apollo and lands with a steerable parachute or a deployable rotor with controlled glide and horizontal and vertical descent capability. This approach may lack the pinpoint accuracy of the spaceplane, but may more than compensate for this with its lower weight resulting in a twenty (20) to thirty (30) per cent gain in payload and a substantially lower price.

Use of large, low W/C_D .A inflatable and deployable drag or drag/lift devices at re-entry has been proposed as early as 1952 (References 4 to 7). However, the de-orbiting and atmospheric re-entry phase and its associated problems of deceleration, stabilization, and heat management are not the subject of this paper.

RECOVERY ENVELOPE

Four important areas of recovery applications are shown in Figure 3 on Page 6. Included are space capsules of the Mercury type, ballistic missiles, re-entry research vehicles, and emergency escape from military aircraft. The space capsule landing problem is the least difficult one, judging from a performance point of view. Aircraft emergency escape is unique in the required recovery range from zero on-the-deck velocity to Mach 3 at eighty thousand (80,000) feet. This requires extremely balanced retardation sequencing throughout the recovery envelope and skillful recovery engineering.

| | | | |
|--|---|---|--|
| 1. ORBIT TRANSFER | | | |
| 2. DEORBITING Retro-rockets | | | |
| 3. ATMOSPHERIC REENTRY | | | |
| 1. <u>Ballistic</u> Blunt Body Nose Cone | 2. <u>Low Lift/Drag</u> Eggers-Type Body L/D Body | 3. <u>High Lift/Drag</u> Spaceplane, High L/D Vehicle, Dyna-Soar | |
| 4. DECELERATION | | | |
| 1. <u>Ballistic</u> Drag Brake Retro-rocket Supersonic Parachute | 2. <u>Low Lift/Drag</u> Eggers-Type Body (Glide-Parachute) | 3. <u>High Lift/Drag</u> Spaceplane Parawing | |
| 5. DESCENT, LANDING | | | |
| 1. <u>Hard Ballistic</u> Drag Vehicle Retro-rocket | 2. <u>Soft Ballistic</u> Parachute Retro-rocket Impact Attenuator | 3. <u>Steep Guide</u> Glide-Parachute with Impact Attenuator | 4. <u>Aircraft-Type</u> <u>Landing</u> Spaceplane Parawing |
| 6. LANDING AREA, LOCATION, RETRIEVAL | | | |
| 1. <u>Large - Semiflat</u> <u>Ocean, Desert</u> Maximum Location and Retrieval Aids | 2. <u>Large - Flat</u> <u>Ocean, Test Range</u> Medium Location and Retrieval Aids | 3. <u>Small - Flat</u> <u>Water, Range</u> Farmland Limited Location and Retrieval Aids | 4. <u>Prepared Area</u> <u>Airfield</u> Dry Lake Minimum Location and Retrieval Aids |
| (1)(2) | | (2A) (3) | (3) |

(1) MERCURY, (2) APOLLO, (2A) APOLLO, (3) SPACEPLANE, (4) UNMANNED SPACE VEHICLE

FIGURE 2. SPACE FLIGHT LANDING PHASES AND MEANS

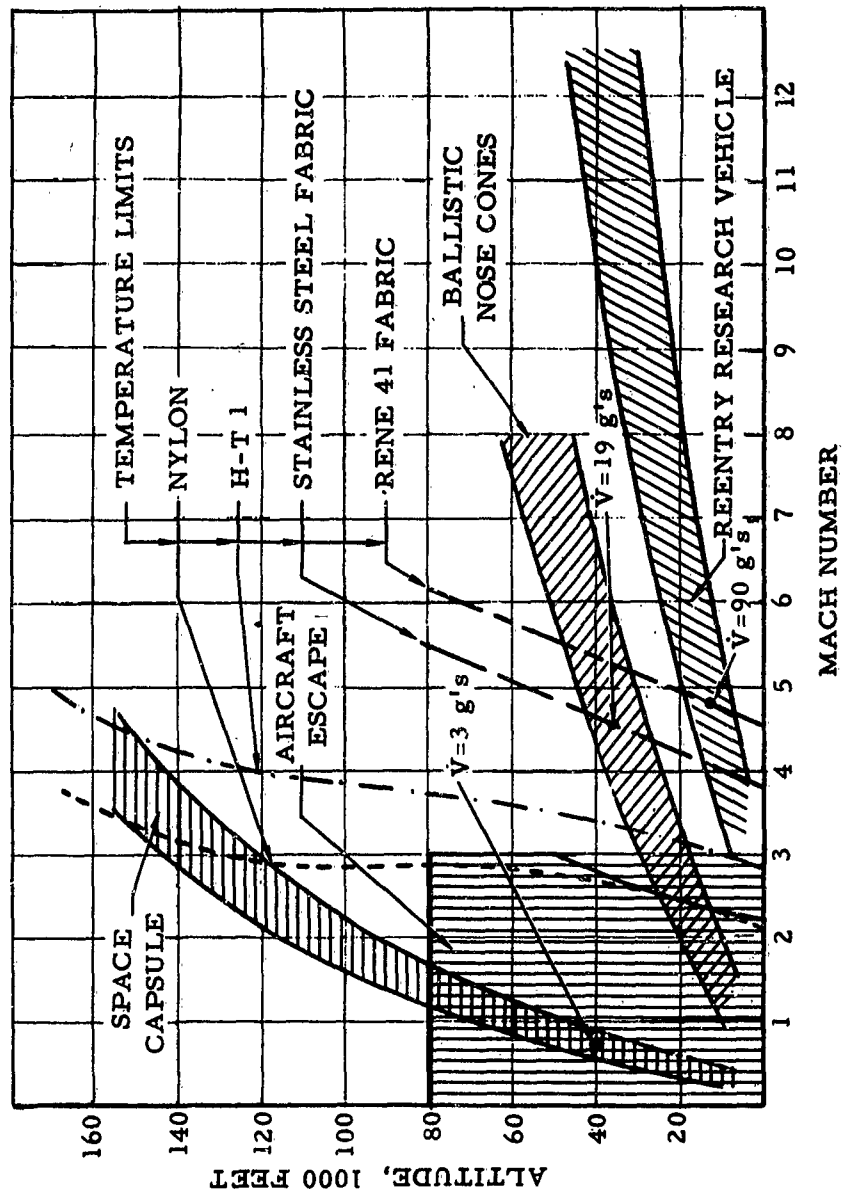


FIGURE 3. TYPICAL RECOVERY REGIONS, MATERIAL LIMITS & PEAK DECELERATIONS V

Recovery of re-entry research vehicle, with its related deceleration and heating problems, is obviously way beyond the range of textile parachutes.

The fact that parachute landing is part of the normal mission places reliability requirements of the space craft recovery system an order of magnitude above the aircraft emergency escape system and the recovery of ballistic missiles and research vehicles.

Aerodynamic heating is a matter of major concern. Thermal material stress and self-inflation problems place a limitation on nylon parachutes at about Mach 2.5 to 3.0 depending on altitude, velocity, and recovery vehicle re-entry characteristics. This limit presents no problem for the space capsule, but can present a problem for aircraft emergency escape and is clearly beyond the recovery capability of the research vehicle. HT-1 textile fiber extends the range to approximately Mach 3 to Mach 4. This increase solves the aircraft escape problem and the majority of recovery requirements for ballistic missiles. Use of inflatable deceleration devices fabricated from coated metal cloth with stainless steel or Rene 41 filament material will allow recovery of re-entry research vehicles with medium ballistic coefficients. Ablation or combined sublimation transpiration cooled retardation devices will be required for vehicles entering the earth's atmosphere at escape velocity.

Applied forces and decelerations are frequently predominant design factors. Maximum forces during the recovery and landing phase are limited for the man-rated space capsules to twenty (20) g-units for such short duration events as drogue parachute opening and landing impact. Final landing parachute systems seldom produce forces in excess of four (4) g-units during opening through use of reefing, thus greatly reducing parachute weight and volume.

Recovery of ballistic missiles and research vehicles from low altitude and high velocities necessitates high average decelerations. Decelerations \bar{v} of nineteen (19) and ninety (90) g-units are required for stepwise opening retardation devices suitable for recovery of ballistic missiles or re-entry research vehicles, see Figure 3. These deceleration values are based on the assumption that recovery starts at the operational limits of stainless steel or Rene 41 metal fabrics.

RETARDATION AND DESCENT

Good operational data are available on hemisflo ribbon parachutes at velocities up to Mach 2.4 and some data up to Mach 2.9 (References 8 and 9). Design, performance, and

fabrication methods of these parachutes are reasonably well defined. Work is under way to extend this range to higher velocities. Other supersonic retardation devices including paraballoon, deployable drag cone, and other drag devices are discussed in References 7, 10, 11, and 12.

The technology of final descent devices is in a progressing state of development. This refers to textile parachutes as well as to other suitable retardation devices. Parachutes still dominate the field; however, parawings; steerable parachutes; and rotating, deployable, and storable decelerators present an ever increasing challenge and may, within the next few years, replace the conventional parachute for some applications. Figure 4 on Page 9 shows the performance of commonly used final descent parachutes. The data are brought up-to-date from those presented by the author in Reference 13.








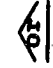






A qualitative and quantitative comparison of final descent devices is presented in Figure 5 on Page 10. This comparison includes the rogallo wing or parawing; deployable rotors; storable rotors; steerable or gliding parachutes; and regular parachutes. Storable rotors are defined as rotor systems with foldable or extendable blades. Deployable rotors are defined as having flexible or inflatable blades that can be stored and deployed similar to parachutes.

The comparative analysis includes deployment and opening characteristics; weight; volume; and the capability to glide, to flare out, and to land horizontally or vertically. The comparison results in a high rating for the rotor type decelerators. However, a workable, stowable, or deployable rotor of sufficient size and reliability is presently far from reality. Development of deployable rotors should be accelerated by an order of magnitude.

Extensive effort is presently devoted to the parawing development. The nature of the parawing classifies it as an aircraft wing type device requiring reasonably prepared landing areas for a glide landing; whereas, the flexible rotor or high L/D parachutes are more comparable to Convertaplanes having both the capabilities to land vertically and to perform an aircraft type glide landing.

RECOVERY RELIABILITY

Reliability, defined as the capability of a system to perform its required mission within encountered environment, has become an integral part of any recovery systems analysis. Reliability requirements for the three main types of recovery systems: primary, man-rated landing system (Mercury); secondary, man-rated landing system (Aircraft Escape); and recovery systems for unmanned vehicles vary roughly by an order of magnitude.

| PARACHUTE TYPE | PLAN VIEW | CROSS-SECTION | DRAG CO-EFFICIENT C_{D_0} | STABILITY \pm O | OPENING SHOCK FACTOR X_0 | VELOCITY RANGE KNOTS | SPECIFIC DRAG AREA $\frac{C_{D_0} \cdot S_0}{W_p} \text{ FT}^2/\text{LB}$ |
|----------------|---|---|-----------------------------|-------------------|----------------------------|----------------------|---|
| RIBBON |  |  | .47 - .55 | 0 - 3 | ~ 1.05 | 300 - 400 | ~ 25 |
| RING SLOT |  |  | .55 - .70 | 0 - 10 | ~ 1.05 | 250 - 350 | ~ 35 |
| RING SAIL |  |  | .69 - .80 | 5 - 15 | ~ 1.30 | 200 - 300 | 50 |
| SOLID FLAT |  |  | .7 - .90 | 15 - 40 | 1.7 | 200 - 350 | 50-55 |
| HEMISPHERICAL |  |  | .65 | 5 - 15 | 1.25 | UNKNOWN | UNKNOWN |
| GUIDE PERSON. |  |  | .72 | 8 - 20 | 1.20 | 250 - 375 | 48 |
| EXTEND. SKIRT |  |  | .8 - .9 | 10 - 20 | ~ 1.25 | 250 - 375 | 60 |

(1) FACTOR GIVES SQUARE FOOT OF PARACHUTE DRAG AREA $C_{D_0} \cdot S_0$ PER POUND OF PARACHUTE WEIGHT W_p

FIGURE 4. RECOVERY PARACHUTE TYPES

| PERFORM. PHASE | LANDING DECELERATOR | ROGALLO-SAIL S = 1200 FT ² V _{horizontal} = 75 FPS | DEPLOYABLE ROTOR (2) | STORABLE ROTOR (2) | GLIDING PARACHUTES V _{vert.} = 30 FPS (3) V _{hor.} = 30 FPS | STAND. PARACHUTE SYST. CLUSTERS |
|---|---------------------------------------|--|-------------------------------|---------------------------------|---|--|
| DEPLOYMENT | FAIR | FAIR | FAIR | NO PROBLEMS ANTICIPATED | GOOD | GOOD |
| INFLATION | DIFFICULT | DIFFICULT | DIFFICULT | RIGID ROTORS | GOOD | GOOD |
| SYSTEM COMPLEXITY | FAIR | FAIR | HIGH | MEDIUM | FAIR | LOW |
| GLIDE CHARACTERISTICS | GOOD | GOOD | MEDIUM | GOOD | MEDIUM | NONE |
| FLARE-OUT CAPABILITY | MEDIUM | MEDIUM | MEDIUM | GOOD | LOW | NONE |
| ZERO HORIZONTAL VELOCITY | NO | NO | GOOD | GOOD | GOOD | GOOD |
| EMERGENCY SYSTEM REQUIRED | 100% | 100% | 100% | 100% | PARTIAL (CLUSTER) | PARTIAL (CLUSTER) |
| SYSTEM WEIGHT (4) | HIGH | HIGH | MEDIUM | HIGH | MEDIUM | LOW |
| SYSTEM VOLUME | HIGH | HIGH | LOW | HIGH | MEDIUM | LOW |
| LANDING WITHOUT GROUND WIND | | | | | | |
| LAND | V _v (5) = 0-15 FPS FAIR(6) | V _v (5) = 0-15 FPS FAIR(6) | V _v = 0 GOOD (6) | V _v = 0 FPS GOOD (7) | V _v = 30 FPS IMPACT. ATTN. REQUIRED V _h = 0 FPS GOOD | V _v = 30 FPS IMPACT. ATTN. REQUIRED V _h = 0 FPS GOOD |
| WATER | V _h = 75 FPS (CRITICAL)(8) | V _h = 75 FPS (CRITICAL)(8) | V _h = 0 GOOD | V _h = 0 FPS GOOD | V _h = 0 FPS GOOD | V _h = 0 FPS GOOD |
| | V _v = 0-15 FPS GOOD | V _v = 0-15 FPS GOOD | V _v = 0 GOOD | V _v = 0 FPS GOOD | V _v = 30 FPS GOOD | V _v = 30 FPS GOOD |
| | V _h = 75 FPS (CRITICAL) | V _h = 75 FPS (CRITICAL) | V _h = 0 GOOD | V _h = 0 FPS GOOD | V _h = 0 FPS GOOD | V _h = 0 FPS GOOD |
| LANDING WITH GROUND WIND (30 KNOTS, 50 FPS) | | | | | | |
| LAND | V _v = 0-15 FPS (6) FAIR | V _v = 0-15 FPS (6) FAIR | V _v = 0 FPS GOOD | V _v = 0 FPS GOOD | V _v = 30 FPS IMPACT. ATTN. REQUIRED | V _v = 30 FPS IMPACT. ATTN. REQUIRED |
| | ΔV _h = 25 FPS (9) FAIR | ΔV _h = 25 FPS (9) FAIR | ΔV _h ≤ 25 FPS FAIR | ΔV _h = 0 FPS GOOD | ΔV _h = 20 FPS FAIR | ΔV _h = 50 FPS POOR |
| WATER | V _v = 0-15 FPS GOOD | V _v = 0-15 FPS GOOD | V _v = 0 FPS GOOD | V _v = 0 FPS GOOD | V _v = 30 FPS GOOD | V _v = 30 FPS GOOD |
| | ΔV _h = 25 FPS POOR | ΔV _h = 25 FPS POOR | ΔV _h ≤ 25 FPS POOR | ΔV _h = 0 FPS GOOD | ΔV _h = 20 FPS FAIR | ΔV _h = 50 FPS POOR |

WEIGHT OF LOAD = 8000 LBS.

(1) ROGALLO SAIL W/A = 6.7 REF. L/D = 5.
(2) ROTOR EQUIPPED WITH GLIDE AND FLARE CAPABILITY, L/D = 5.
(3) GLIDING PARACHUTES, L/D = 1.0.
(4) INCLUDES DECELERATION, DESCENT, IMPACT ATTENUATION, AND CONTROL.
(5) ΔV REFERS TO VELOCITY BETWEEN VEHICLE AND SURFACE.
(6) FLARE OUT DEPENDS ON EFFECTIVENESS OF CONTROL SYSTEM & OPERATOR.
(7) FLARE OUT SAMPLE THROUGH TIP ADDED ENERGY.
(8) ANTICIPATES LANDING IN UNPREPARED TERRAIN.
(9) ΔV REFERS TO VELOCITY BETWEEN VEHICLE AND SURFACE.

FIGURE 5. PERFORMANCE COMPARISON OF SPACECRAFT LANDING DECELERATORS

Logical model setup and mathematical treatment of reliability are readily accomplished for sequencing subsystems, location aids, and similar units, but encounter some problems in the analysis of parachute systems. Each parachute assembly necessitates the consideration of three reliability functions: the parachute itself; the parachute deployment process with its related components; and the parachute installation which may interfere with the proper deployment. Parachutes properly designed, installed, and deployed have an extremely high reliability.

The United States Army, which performs three hundred thousand (300,000) paratrooper jumps a year, stopped reporting parachute malfunctions due to the scarcity of occurrence. Accidents happen, but they are caused by static lines hanging up; jumpers being towed behind the aircraft; dragging in surface winds; drowning; and similar causes, but not due to malfunctioning parachutes. Using the same troop parachute in a different installation and deployment arrangement, however, can result in anomalous parachute operation and serious impairment of the reliability record of this parachute.

Adherence to experience and common practice as part of the "Parachute Art" makes known concepts work, but may provide considerable resistance to new approaches and methods; for example, the reliability comparison of recovery systems. Figure 6 on Page 12 shows the reliability analysis of a cluster of three (3) different arrangements. It is assumed that two (2) parachutes will meet the performance requirements with the third (3rd) parachute serving as a backup parachute in case of failure of one (1) of the other two (2). System I in Figure 6 uses independent deployment of the deceleration parachute and all three (3) main landing parachutes. The deceleration parachute, as a deceleration device is not included in this reliability consideration with the exception of System III, where the deceleration parachute deploys the main parachute cluster. The following reliability factors have been assigned to the various components:

- | | |
|--------------------------------------|---------------|
| 1. Deployment mortar | (P M) = .9995 |
| 2. Pilot parachute | (P C) = .999 |
| 3. Deceleration parachute | (D C) = .998 |
| 4. Deceleration parachute disconnect | (D D) = .9999 |
| 5. Main parachute | (M C) = .998 |

The influence of such related equipment as bridles and deployment bags is included in the reliability factors.

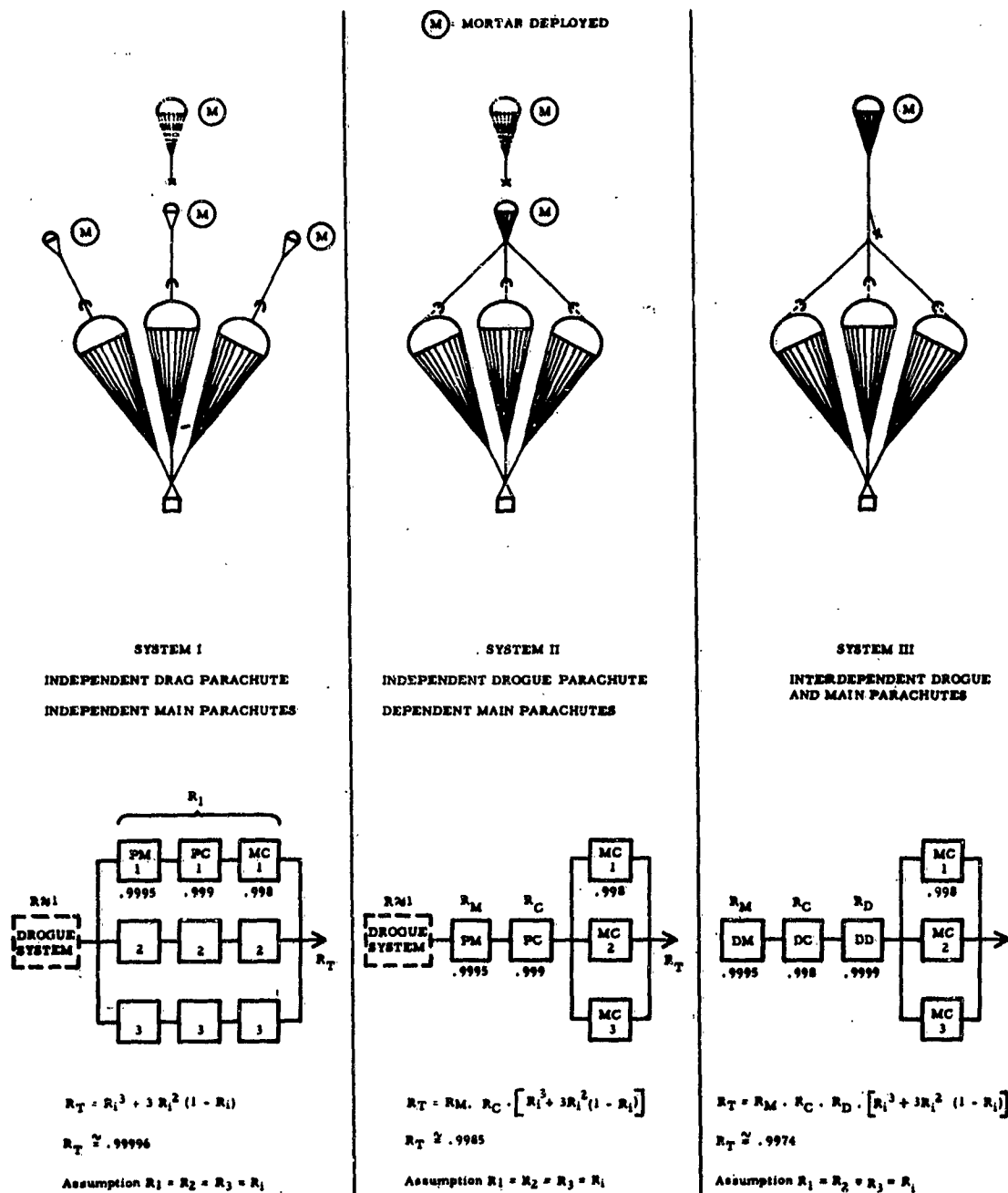


FIGURE 6. RELIABILITY COMPARISON OF PARACHUTE CLUSTER SYSTEMS

System II deploys the three (3) main landing parachutes by means of a single mortar-ejected pilot chute. The main landing parachute deployment, therefore, is independent of drogue parachute operation or disconnect. System III uses the disconnected drogue chute for deployment of the main landing parachute cluster; this sequence is commonly used for missile recovery.

The reliability figures for the three (3) systems clearly show the two (2) orders of magnitude higher reliability of System I. This analysis does not include failure modes which may change the reliability factors. However, this example clearly demonstrates the fact that a mathematical reliability analysis can outline the approach to a reliable system.

PARACHUTE FORCES

Exact prediction of parachute forces and load factors is of prime importance for space vehicle recovery systems in order to accomplish the maximum weight savings. This requires:

1. A precise determination of the velocity-altitude-deceleration force-time history of the recovery sequence.
2. An exact determination of all design and environmental factors effecting the recovery system and the ratio of actual loads to ultimate strength of required materials.

Most man-carrying and cargo parachutes have ratios of actual force to ultimate design strength of three (3) to six (6). These high safety factors compensate for considerable variations in parachute opening forces and opening behavior. Such high safety margins are unacceptable for spacecraft systems where parachute forces must be predicted within an accuracy of \pm ten (10) per cent or better. No analytical, closed solution method for calculating parachute forces, especially reefed parachute forces, has been developed that meets this requirement. Introduction of modern high speed computers has eliminated the need for a closed solution due to the computers' capability of solving complex problems by stepwise computations. A method, developed in 1961 for extended skirt parachutes, has proven equally useful for Ringsail parachutes and is presently applied to determine parachute forces for projects Apollo and Gemini, see Reference 14.

The general approach to the computer analysis is shown in Figure 7, Page 16. The drag area of the parachute increases during the opening procedure from a minimum value at canopy line stretch in a continuous or stepwise function and a known time sequence to its fully open value. Formulating

equations for the various time steps and the drag area increase versus time allows a computer determination of the time-velocity-altitude-force history. This method is useful if the drag area increase during parachute opening is a known, repeatable process for a particular parachute type. Analysis of a large number of drop tests with good, time co-ordinated velocity-altitude-force records has shown this to be true for the extended skirt parachute and the Ringsail parachute. Drag area, determined as instantaneous force divided by instantaneous dynamic pressure, is not drag area in the classical sense, but it includes such variables as, apparent mass, effective porosity, and other factors that influence the parachute opening process. The equations for parachute opening times assume that parachutes open in approximately the same traveled distance. This conclusion, which is based on the continuity law, has been confirmed from evaluation of a large number of drop tests. It was found that the specific types of parachutes have similar canopy filling time characteristics.

This calculation method is now in preliminary use at Northrop Ventura and has produced good agreement with drop test. Efforts are continuing to improve this method and to obtain analytical expressions for filling time and drag area increase versus time. The equations for filling time and drag area increase versus time for extended skirt parachutes are shown in Figure 7. The drag area increase was found to be a power function. The drag area increase of Ringsail parachutes was found to be linear with time similar to previous evaluations of Ribbon parachutes. An interesting point on large Ringsail parachutes is the fact that the drag area increases at a factor of approximately fifteen (15) to twenty (20) per cent per second. Using Figure 7 as reference, the following equations have given good results for Ringsail parachutes.

Filling times:

$$t_{f1} = \frac{n_1 \cdot D_o}{V_s} \cdot \left[\frac{(C_D \cdot S)_R}{(C_D \cdot S)_o} \right]^{\frac{1}{2}} ; n_1 \approx 20 \quad (5)$$

$$t_{f2} = \frac{n_2 (D_o - D_r)}{V_r} , \text{ with } D_r = \left[\frac{(C_D \cdot S)_R}{(C_D \cdot S)_o} \right]^{\frac{1}{2}} \cdot D_o ; n_1 \approx 1.5 \quad (6)$$

Drag area increase versus time:

$$(C_D \cdot S)_{x_1} = (C_D \cdot S)_R \cdot \frac{t_{x_1}}{t_{f_1}} \quad (7)$$

$$(C_D \cdot S)_R = (1 + .2t_r) \cdot (C_D \cdot S)_R \quad (8)$$

$$(C_D \cdot S)_{x_2} = (C_D \cdot S)_R + \left[(C_D \cdot S)_O - (C_D \cdot S)_R \right] \cdot \frac{t_{x_2}}{t_{f_2}} \quad (9)$$

Nomenclature:

t_{f_1} = reefed fill time - seconds

t_{f_2} = disreefed fill time - seconds

t_{r_c} = reefing device time - seconds

t_r = reefing time = $t_{r_c} - t_{f_1}$ - seconds

V_s = line stretch velocity - FPS

V_R = reefed opening velocity - FPS

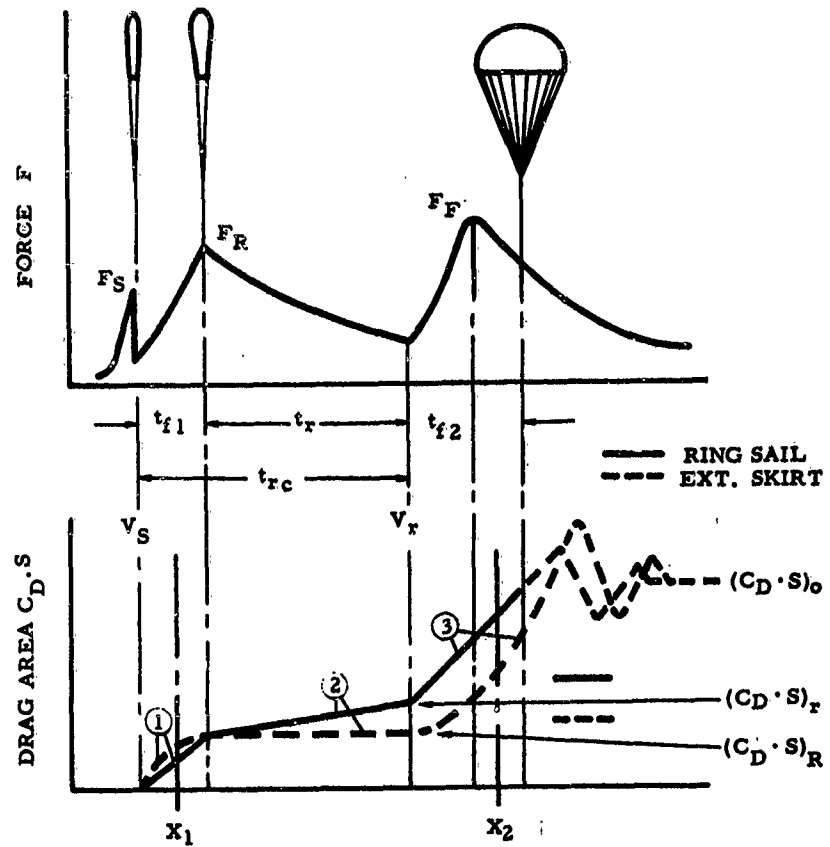
V_r = disreef velocity - FPS

D_O = nominal parachute diameter - feet

$(C_D \cdot S)_O$ = drag area of fully open parachute - sq. feet

$(C_D \cdot S)_R$ = drag area of reefed parachute - sq. feet

$(C_D \cdot S)_r$ = drag area at point of disreef (used only for Ringsail parachutes) - sq. feet



$$\textcircled{1} \quad t_{f1} = \frac{n_1 \cdot D_o}{V_S \cdot 9} \cdot \left[\frac{(C_D \cdot S)_R}{(C_D \cdot S)_o} \right]^{1/2} \quad (1) \quad 14 < n_1 < 20$$

$$\textcircled{3} \quad t_{f2} = \frac{n_2 \cdot D_o}{V_r \cdot 9} \cdot \left[\frac{(C_D \cdot S)_o - (C_D \cdot S)_R}{(C_D \cdot S)_o} \right]^{1/2} \quad (2) \quad 4 < n_2 < 7$$

$$\textcircled{1} \quad (C_D \cdot S)_{X_1} = (C_D \cdot S)_R \cdot \left(\frac{t_{x1}}{t_{f1}} \right)^{m_1} \quad (3) \quad m_1 = .5$$

$$\textcircled{3} \quad (C_D \cdot S)_{X_2} = (C_D \cdot S)_R + \left[(C_D \cdot S)_o - (C_D \cdot S)_R \right] \cdot \left(\frac{t_{x2}}{t_{f2}} \right)^{m_2} \quad (4) \quad m_2 = 3 - 5$$

FIGURE 7. PARACHUTE OPENING SEQUENCE

The following design and environmental conditions should be considered for parachute systems:

1. Safety factor (SF): A factor of 1.35 to 1.5 is presently used for suspension line and canopies of final landing parachutes.
2. Line geometry factor:
3. Humidity loss:
4. Fatigue loss: Applicable for nylon parachutes after more than a hundred uses
5. Abrasion loss: This factor depends on parachute installation and deployment.
6. Material connection losses: This loss factor applies to connection of suspension lines to canopy, suspension lines to riser, and riser to metal attachment fittings.
7. Radiation loss:
8. Temperature loss:
9. Hard vacuum loss:
10. Uneven canopy loading:
11. Uneven load distribution in parachute clusters:

These factors will vary for canopies and suspension lines of reefed and unreefed parachutes; risers; pilot chute; bridles; and other parachute components. The exact determination of these figures will decisively influence the selected material strength and, consequently, the weight of the parachute assembly.

A degrading influence of hard vacuum on nylon material has recently been found. Data on this phenomenon will be published after completion of tests.

RECOVERY SEQUENCE

The start of recovery and the selection of the various steps of the recovery cycle is greatly influenced by: the vehicle trajectory, which determines the start of the trajectory cycle; by the allowable payload deceleration, which effects the parachute opening sequence and rate of descent; and by requirements for landing, location aid, retrieval, and transport conditions.

Start of recovery at high speeds, at still high levels of trajectory deceleration, from an unstable body, or from low altitude will always produce the most severe recovery conditions. The required development testing of the recovery systems under actual environmental and performance conditions is directly related to the selected recovery sequence and is frequently higher in cost than the engineering development phase. A detailed analysis must be conducted in order to obtain the most practical recovery cycle that requires the minimum amount of design, development, and development testing commensurate with meeting the recovery requirements.

Northrop Ventura recently conducted an extensive systems analysis for a re-entry recovery project. It was found that by adding an additional recovery step the recovery altitude and velocity could be reduced from twenty-four thousand (24,000) feet altitude and a Mach 3.2 velocity to fifteen thousand (15,000) feet and Mach 1.5. This change resulted in replacing a HT-1 material hemisflow ribbon parachute with an already qualified conical Ribbon parachute. Mortar ejection of the hemisflow parachute against forty-five (45) g's deceleration could be reduced to ejection against fifteen (15) g's deceleration. Both changes had a deciding influence on recovery system weight, volume, and the necessary amount of environmental and aerial testing. A substantial saving was achieved in development time, in funds, and in unit price.

Figure 8 on Page 19 shows a typical sequencing system for recovery of a re-entry vehicle. The master switch allows work on the recovery package during pre-flight tests, installation and check-out. The acceleration switch activates the recovery system during re-entry at increasing acceleration; the time function makes sure that this acceleration has been effective for several seconds. This method prevents activation of the system due to short time accelerations caused by shocks before take-off, boost irregularities, booster separation shocks, re-entry oscillation, and similar shocks. Opening the deceleration switch on the decreasing branch of the re-entry deceleration starts the actual recovery cycle. Barometric switches are generally used for main parachute deployment. A second generation of g-switches, timers, barometric switches, and similar components is emerging with greatly reduced weights and dimensions.

Redundant electrical sequencing systems with independent power sources and mechanical or electrical initiators are a must unless the desired reliability figures of components have been proven in tests at an acceptable confidence level. Transfer function units for continuation of redundant signals, in case of component failure, may be advisable, but have to be designed with care to avoid circuit problems.

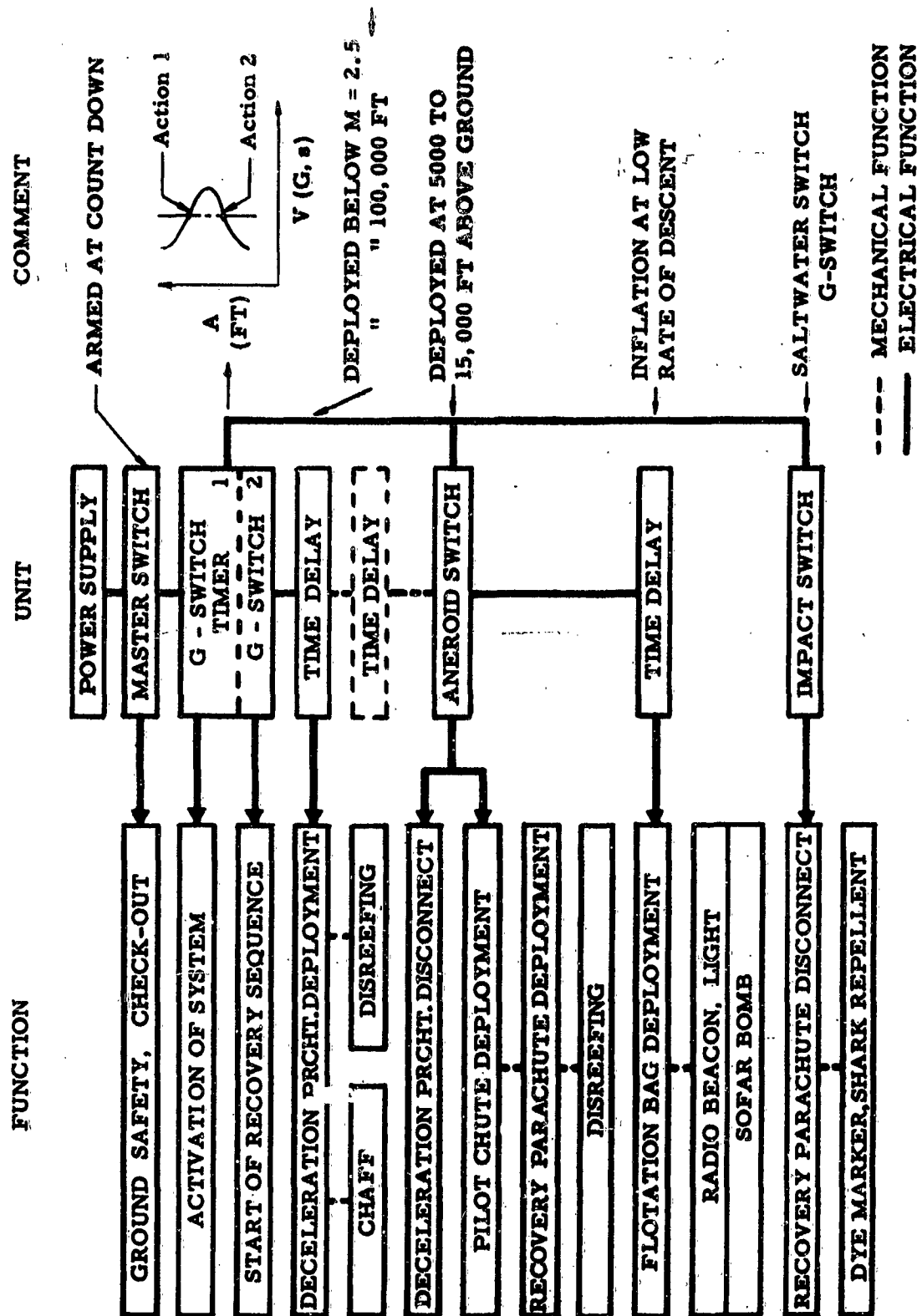


FIGURE 8. SEQUENCING SYSTEM FOR REENTRY VEHICLE RECOVERY

Check-out leads are desirable for circuit continuity check, polarity check, battery check and squib continuity check. Provision should be made for easy replacement of power supplies, radio beacons, and squibs. Location of all sequencing elements in a single unit is advisable; this allows for simple environmental protection as well as for easy visual and electrical inspection and check-out.

Pyro-actuation of mechanical functions has been developed to a high degree of reliability and perfection. Single squibs with double bridge wires or complete parallel units are used in most recovery systems. Figure 9 on Page 21 shows the reliability analysis of a common type of electro-pyro initiator. The reliability values assigned to the various components are:

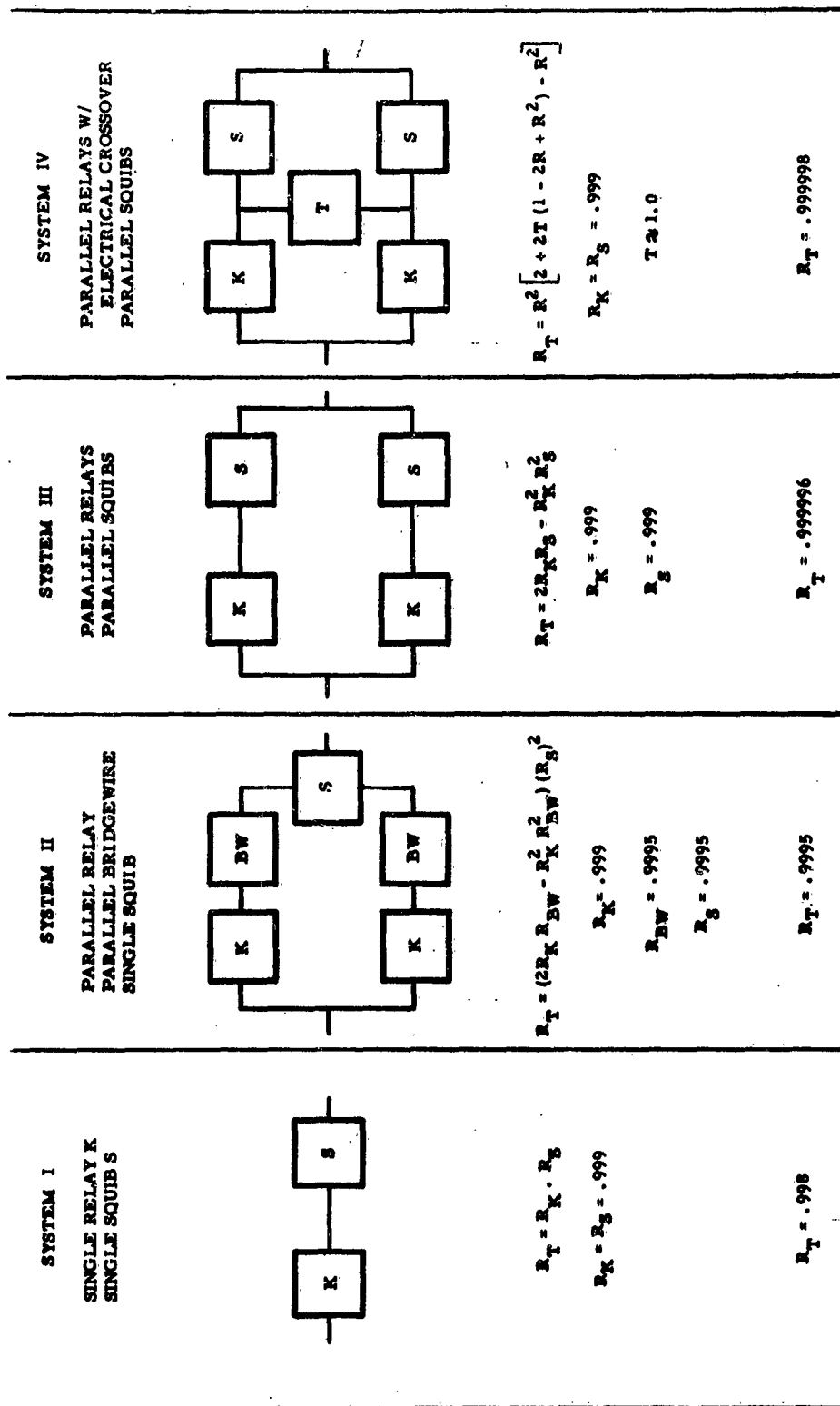
- | | |
|---------------------|---------|
| 1. Relay (K) | = .999 |
| 2. Squib (S) | = .999 |
| 3. Bridge wire (BW) | = .9995 |

The analysis shows that the crossover link provides only small benefits due to the high individual component reliability. Before deciding on pyrotechnical components, it is advisable to check on the safety requirements of the Test Ranges where the unit will be flown. Squib safety levels of one (1) Amp. no-fire and three (3) to four (4) Amp. sure-fire are required by most Test Ranges. This affects the peak output of required power supplies, especially if several pyrotechnic units are fired at the same time.

LANDING-LOCATION-FLOTATION

Little progress, except in minor refinements, has been made in location aids during the last decade. Radio beacons, flashing lights, and dye markers have become standard equipment, with tracking beacons, reflecting parachutes, SOFAR bombs and SONAR equipment used for special applications. A real need exists for a long range, long duration, light weight beacon with low power demands.

Impact shock absorption systems for land and water landings have recently been extensively treated by H. W. Bixby, see Reference 15. It can be expected that retro-rockets in various forms will be used more and more for landing shock absorption. The use of retrorockets in connection with parachute landing systems has resulted in minimum landing system weight. This weight advantage is especially pronounced in systems where a low impact deceleration is required at a high rate of descent. Rocket systems are now under development that use the GEM principle. These units should effect considerable weight saving and good versatility.



SINGLE BRIDGE WIRE USED FOR EACH SQUIB.
CROSSOVER FUNCTION T CANNOT BE IGNORED FOR COMPONENT VALUES $R < .999$
NO FAILURE MODES CONSIDERED

FIGURE 9. RELIABILITY COMPARISON OF ELECTRO-PYRO INITIATORS

Flotation bags utilizing ambient pressure inflation have recently been developed by Northrop Ventura and are being used successfully for several applications. Figure 10 on Page 23 shows tower drop tests of such a self-inflating flotation bag. A one-third ($1/3$) weight saving has been obtained, and the complexity is greatly reduced by the elimination of the stored gas and the complex inflation equipment.

Several aerial pick-up methods for air and water pick-up have been developed in the last few years, mainly, under the sponsorship of the United States Air Force, Space Systems Division; however, only sketchy data are available. It is recommended that the Air Force publish the present state of development of these methods for general use.

CONCLUSIONS AND RECOMMENDATIONS

It appears that, besides new approaches to landing of space vehicles, ballistic and semi-ballistic recovery parachutes, will be used for some time to come. However, many approaches, subsystem, and components are not sufficiently developed for customarily requested shelf-item approach to recovery. It is, therefore, considered appropriate to make recommendations concerning some of the urgent requirements that we in industry are faced with today or can predict in the foreseeable future.

1. Accelerated applied research is necessary in flexible, deployable decelerators usable at velocities up to Mach 4 to Mach 5.
2. Accelerated applied research is necessary on final descent retardation devices with glide and flare-out capability.
3. Support is required for Company-started work on practical methods for determination of parachute opening forces on multiple step parachute systems.
4. The influence of hard vacuum on fibrous textile materials needs investigation.
5. Applied research work should be started on in-place foaming of plastic shapes suitable for re-entry heat protection, deceleration, impact shock absorption, flotation, and environmental protection.
6. Long range, long duration location equipment should be developed with lower power demands.
7. Conduct more applied research in landing shock absorption systems.

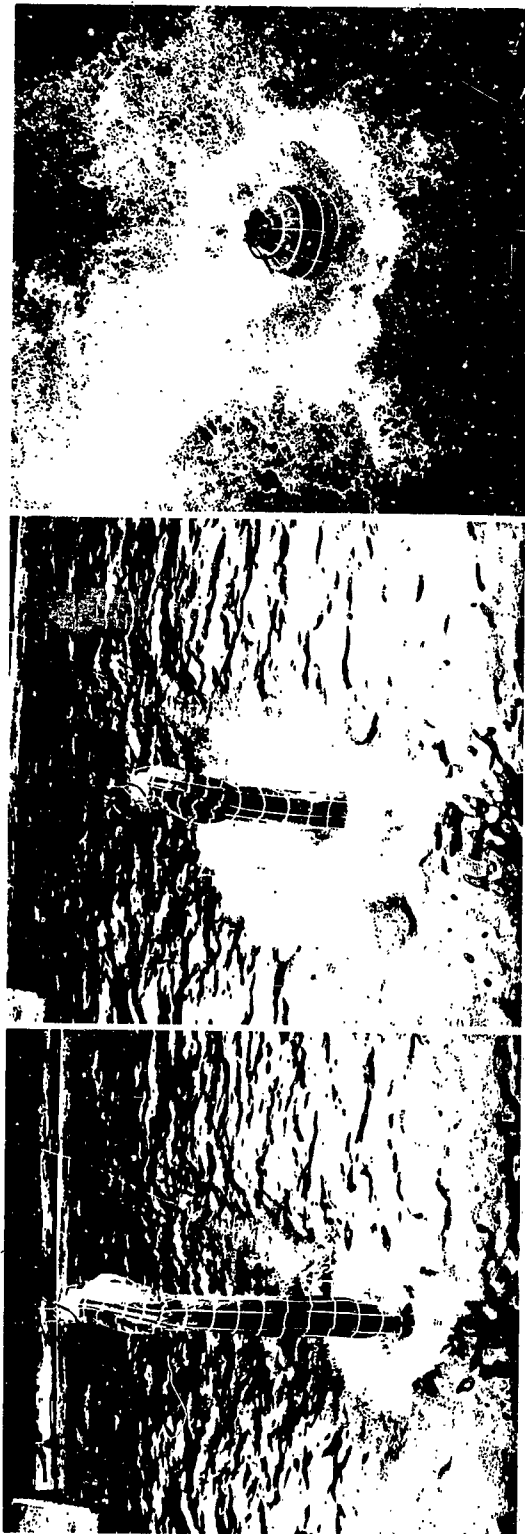
Flotation bags utilizing ambient pressure inflation have recently been developed by Northrop Ventura and are being used successfully for several applications. Figure 10 on Page 23 shows tower drop tests of such a self-inflating flotation bag. A one-third ($1/3$) weight saving has been obtained, and the complexity is greatly reduced by the elimination of the stored gas and the complex inflation equipment.

Several aerial pick-up methods for air and water pick-up have been developed in the last few years, mainly, under the sponsorship of the United States Air Force, Space Systems Division; however, only sketchy data are available. It is recommended that the Air Force publish the present state of development of these methods for general use.

CONCLUSIONS AND RECOMMENDATIONS

It appears that, besides new approaches to landing of space vehicles, ballistic and semi-ballistic recovery parachutes, will be used for some time to come. However, many approaches, subsystem, and components are not sufficiently developed for customarily requested shelf-item approach to recovery. It is, therefore, considered appropriate to make recommendations concerning some of the urgent requirements that we in industry are faced with today or can predict in the foreseeable future.

1. Accelerated applied research is necessary in flexible, deployable decelerators usable at velocities up to Mach 4 to Mach 5.
2. Accelerated applied research is necessary on final descent retardation devices with glide and flare-out capability.
3. Support is required for Company-started work on practical methods for determination of parachute opening forces on multiple step parachute systems.
4. The influence of hard vacuum on fibrous textile materials needs investigation.
5. Applied research work should be started on in-place foaming of plastic shapes suitable for re-entry heat protection, deceleration, impact shock absorption, flotation, and environmental protection.
6. Long range, long duration location equipment should be developed with lower power demands.
7. Conduct more applied research in landing shock absorption systems.



$$\frac{\text{WEIGHT RATIO}}{\text{PRESSURE INFLATED FLOTATION BAG}} = \frac{2}{3}$$

FIGURE 10. SELF-INFLATING FLOTATION BAG TEST

References

1. Barraza, R. M., "Launch Vehicle Recovery System Requirements", SAE Paper No. 5900, October 1962
2. Koelle, H. H., "On the Economy of Large Booster Recovery", ASME Paper No. 59-AV-1, June 1959
3. Shipps, P. R., "On the Methods and Economics of Recovering Boosters for Orbital Vehicles", IAS Paper No. 60-29, January 1960
4. Knacke, T. W., "High Altitude Parachute Recovery" "Physics and Medicine of the High Atmosphere", Press, University of Mexico
5. Hoglund, R., Thale, "Recovery from Satellite Orbit", 1960, Cook Research Laboratory Report
6. Haynes, J. E., Rose, P. H., and Vander Velde, W. E., "Analytical Study of a Drag Brake Control System for Hypersonic Vehicles", WADD Technical Report No. 60-267
7. AVCO - Everett Research Laboratory, AVCO Corporation, "Study of a Drag Brake Satellite Recovery System", WADD Technical Report No. 61-348, January 1962
8. Engstrom, B. A., "Performance of Trailing Aerodynamic Decelerators - Part I to V", 1958 to 1962, WADC Technical Report No. 58-284
9. Etherton, B. D., Burns, F. T., and Norman, L. L., "B-58 Escape Capsule Stabilization, Parachute System Development", February 1962, Report No. FZA-4-408, General Dynamics/Ft. Worth
10. Wiant, H. T., and Fredette, R. O., "A Study of High Drag Configurations as First Stage Decelerators", WADC Technical Note No. 56-320
11. Charczenko, N., and McShera, J. T., "Aerodynamic Characteristics of Towed Cones Used as Decelerators at Mach Numbers from 1.57 to 4.65", December 1961, NASA TN D-994
12. McShera, J. T., and Keyes, T. W., "Wind Tunnel Investigation of a Balloon as a Towed Decelerator", NASA Technical Note No. D-719
13. Koelle, H. H., "Handbook of Astronautical Engineering", McGraw-Hill, 1961
14. Bixby, H. W., "Impact Attenuation Methods for Manned Space Craft", "Proceedings of National Meeting on Manned Space Flight", April 1962, NASA

NEW PARACHUTE DEVELOPMENT ASPECTS

Alfons M. Hegerle
Charles E. Carroll
Herman Engel, Jr.

Parachute Branch
Crew Equipment Division
Directorate of Operational Support Engineering
Aeronautical Systems Division
Wright-Patterson Air Force Base, Ohio

During the last 10 years, the requirements and applications of parachutes for personnel emergency escape, air drop of equipment and personnel, aircraft deceleration, special weapon retardation, and space vehicle recovery have considerably changed and become more complex. Consequently, studies and investigations of new or improved designs and construction methods of parachutes and related equipment became essential. This paper describes the development programs which have been lately conducted as in-the-house projects by the Parachute Branch or under contract by the industry to improve the design and performance of parachute assemblies and related equipment with the aim to provide safer and more reliable items, and to define the progress made in the air drop of equipment.

I. INTRODUCTION

Since the actual use of conventional parachutes in 1916, when fighter pilots were equipped with solid flat circular parachutes, a variety of parachute designs have been developed to satisfy specific parachute applications because individual performance requirements could not be combined in any one single type of parachute. The progress in the field of parachute technique made in the last few decades has indeed been fascinating. The parachute, initially designed as a life saving device for flying personnel, is now used as the most economical and efficient device for deceleration of aircraft, air drop of equipment, retardation and trajectory control of bombs, mines, and nuclear weapons, stabilization of emergency ejection seats and capsules and recovery of manned and unmanned satellite capsules and instrument packages. Today, aerodynamic decelerator systems in one form or another have become one of the important subsystems in any flight vehicle.

Parallel with the expanding applications, the performance requirements for and the complexity of the design and operation of parachutes have steadily increased, necessitating extensive research and development efforts by the Armed Forces, colleges and private industry.

The purpose of this paper is to report certain development programs and investigations which have been undertaken by the Parachute Branch, Crew Equipment Division, Aeronautical Systems Division as in-the-house projects or under contract by the industry during the last few years to improve the design and performance of parachute assemblies, to provide safer and more reliable items, and to define the progress made in the air drop of military equipment. These work efforts have been conducted to comply with the ever changing flight conditions and delivery or recovery requirements.

II. PERSONNEL EMERGENCY PARACHUTES

In the field of personnel emergency parachutes, investigations are regularly conducted to improve the design and performance of the various personnel parachute styles by changing the conventional design, packing method and deployment sequence. These improvements have been conducted to reduce the extensive training, familiarity, and dexterity now required of the pilots in order to attain the skill for most effective operation of the parachute assembly.

Presently, there are three emergency personnel parachute configurations which are individually worn by aircrewmembers, depending on the aircraft they are flying: The back, seat, and chest style.

The back style parachute, by far the most commonly used parachute in the USAF, has undergone changes which have improved or will improve wearer comfort, usage, and reliability. The major changes are the incorporation of dual canopy releases on the harness, low friction power transmission components on the automatic parachute ripcord release, a windblast resistant ripcord grip, and a harness strap tensioning device.

1. The incorporation of a second canopy release on the harness has been initiated based on reports of difficulties encountered during helicopter rescue and the boarding of life rafts by escapees. It is anticipated that this change will reduce injury rates and drowning as a result of being dragged over the ground or through the water after landing in high surface winds.

2. The effective power transmitted from the automatic parachute ripcord release, Type F-1B, has been increased in the order of 60% as a result of the incorporation of low friction components. These are a teflon lined power cable housing and a single sheave pulley to change cable direction.

3. The windblast resistant ripcord grip is a "T" shaped handle, which replaces the former "D" ring in the fabric pocket. This handle fits into a metal socket similar to that used on the automatic arming ball.

4. A clip (tensioner) has been incorporated on all parachute harness strap adjusters to prevent harnesses from creeping out of the tight adjustment during body movements in the cockpit. This tensioner does not interfere with the ordinary harness adjustment required to insure a comfortable fitting.

In addition to the above equipment changes the following four items are representative of current developments:

1. A pack opening cutter. The cutter consists of movable razor sharp blades positioned near the pack locking cords so that the automatic parachute ripcord release will trigger the pack opening by shearing the locking cords rather than withdrawing ripcord pins from loops. The pull required from the automatic release with low friction components to open the pack with a cutter is reduced from about 27 pounds to approximately 10 pounds. It is anticipated that this installation will not only provide greater pack opening reliability but will also help alleviate the problems of premature and uncontrolled parachute deployment, because the pack can be closed in a much tighter fashion with no increase in friction affecting the actuating forces. In fact, the greater the tension on the pack closing cords the more positive and reliable becomes the cutting of this cord.

2. A heat resistant personnel parachute pack. It appears that the ability of the recently developed HT-1 fibre to remain

functional after exposure to temperatures far above the melting point of nylon (80% strength retention after exposure to 600°F) will make this an ideal material for parachute packs. Tests conducted by the Fibrous Materials Branch, Materials Central, ASD (Ref 1), indicate that HT-1 packs will provide sufficient protection to nylon canopies so they will satisfactorily function after exposure of the packed parachute to flash fire where parachute assemblies completely made from nylon material become useless.

3. An improved canopy release. The proposed AF Type J-1 parachute canopy release assembly (Figure 1) is considered for replacement of the familiar squeeze button operation with a popout cable loop lanyard stowed under the safety clip. Following the release of the safety clip a pull on the cable loop actuates camming members which in turn depress the release buttons without the need for the squeeze motion which is particularly difficult with cold or gloved hands. It is believed that, with this change, the escapee will be provided with a device which more easily disconnects the parachute canopy from his harness under a much wider range of environmental conditions.

4. An integrated ripcord handle incorporating a semi-automatic "zero" lanyard connector. Reports of fighter pilots state that the complete manual method of connecting or disconnecting the hook of the present "zero" lanyard causes a dangerous diversion from primary flight procedures, especially in an emergency. Figure 2 shows the zero lanyard coupler currently under development to replace the manual 1 & 0 lanyard hook. A semi-automatic procedure permits shifting from a "Connect", 1 & 0 low altitude low speed escape mode, to "Disconnect", 1 & 1 high speed high altitude escape mode, by a simple switch type motion.

To further advance the performance of the back style personnel parachutes, particularly in low speed performance, a test program has been initiated to investigate and compare the performance of four different parachute configurations under identical and closely controlled conditions: (1) standard automatic back style parachute assembly, P/N50C7024-18; (2) standard back style parachute assembly, P/N50C7024-20; (3) standard back style parachute assembly, P/N. 50C7024-20, incorporating the "Hatton" reefing system; (4) standard automatic back style parachute assembly, P/N50C7024-18, with an internal parachute. The program objective is to obtain a quicker opening parachute at low speed with a minimum compromise of high speed performance. The tests will be conducted by the 6511th Test Group at El Centro, California, using the whirtower and C-130 and B-66 aircraft.

The seat style parachute has undergone changes similar to those taking place on the back style parachute. Other changes generally concern the comfort of this parachute. Following are two examples which are considered to be advantageous improvements over the present configuration.

1. The pack of the standard automatic seat style parachute is prone to being packed oversize in relation to the space provisions provided in the T-33 aircraft ejection seats. Care and time consuming packing procedures must be practiced to prevent the pack width from exceeding the seat bucket compartment size in the aircraft. Control of the pack width leads to increased pack thickness which in turn leads to excessive seated height for taller pilots and the hazards accompanied with limited pilot vision and head clearance in the cockpit. Redesign of the pack will be aimed at easier handling and maintenance of the parachute, and subsequent comfort improvement.

2. The automatic parachute ripcord release used in the seat pack is armed by withdrawal of the arming pin from one end of the device which makes it necessary to mount the arming control on the right side of the man's body as he wears the parachute. This arrangement, opposite to that used with the back style parachute, requires encumbering extra length lanyards to facilitate the necessary interconnection of the parachute actuating controls with the automatic ejection seat safety belt. It forces the pilots to reverse the habit patterns they may have established flying other aircraft equipped with back style parachutes. A redesign of the automatic parachute ripcord release is being investigated which will allow arming of the release from either the right or left side permitting control installation on the left side of the seat style parachute harness.

The chest style parachute has been changed the least during the last 10 years because of its limited and specific application in crew and passenger positions, which are not equipped with ejection seats, and as a reserve parachute for premeditated jumping. A program to incorporate an explosive type pilot chute with this style parachute, for possible use by the Army on troop reserve parachutes, was recently conducted. The configuration consisted of the replacement of the conventional pilot chute coil spring with a bladder and an explosive cartridge to more forcefully catapult the pilot chute into the airstream. No significant improvement in the performance of the pilot chute was noted when tested under conditions simulating main parachute malfunction.

III. NUCLEAR WEAPONS RETARDATION SYSTEMS

In the field of nuclear weapons retardation, the complexity of the delivery methods of those weapons has steadily increased. The anticipated use of parachutes for the delivery of nuclear weapons at supersonic velocities under low altitude conditions has re-emphasized the requirement of improvements in parachute canopy design, packing method and test procedures to assure efficient and reliable operation of parachute retardation systems deployed at high dynamic pressures. In view of the limited volume allocated to retardation systems for nuclear weapons, new textile materials with higher strength to weight characteristics and new packing methods have been considered to

minimize the volume of the parachute systems. Unfortunately, classification prevents the discussion of parachute system details due to possible compromise.

In a study (Ref. 2) conducted by the Space Recovery Systems, Inc. under an ASD contract, pressure packing has been established as an effective method to reduce the volume of parachutes. The general conclusions which may be drawn from this study, have been substantiated by actual packing of heavy duty nuclear weapons retardation systems and are as follows:

1. The degree of volume reduction or pack density achieved by hydraulic or mechanical devices is primarily dependent upon the pressure applied (Figure 3). Volume reduction of 50% and pack densities of 45 pounds per cubic feet are about the maximum values which can be obtained without too much difficulty. Applied pressures in excess of 100 PSI are not advantageous.

2. The volume reduction achieved by pressure packing is virtually independent of the type and construction of the canopy and the method of pressure application.

3. The volume reduction which can be obtained by the vacuum packing method is small and a function of the external atmospheric pressure acting on the vacuum bag.

4. The parachute bag shape affects the ultimate volume reduction. The further the shape departs from the most desirable cylindrical shape, the more difficult is the attainment and retention of the reduced volume.

5. The parachute system growth after pressure packing can be limited by selecting bag and lacing materials with low elongation characteristics. Bags made from nylon material may stretch up to 10% under the constant expansion force of the contained parachute.

In the past two years significant weight reductions in heavy duty ribbon canopies have been achieved by changing the construction of the drag producing surface of the canopy. Figure 4 shows the conventional standard gore "ladder" construction where each horizontal ribbon is cut to overlap at all radial seams. The progress in ribbon canopy production techniques permitted the use of continuous horizontal ribbons resulting in the elimination of the horizontal ribbon overlaps at each radial seam (Figure 5). The elimination of the laps permits a reduction in the horizontal and radial ribbon strength since the horizontal ribbon strength needs only to be equal to the strength of the original horizontal ribbon splice and the radial ribbons are only required to space the horizontal ribbons. Table 1 contains two examples of weight savings which may be achieved.

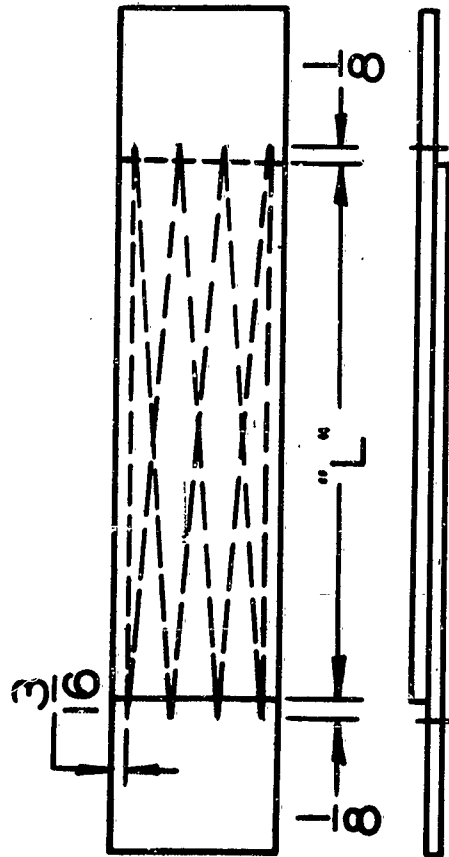
| Construction | 14 ft. dia. | 50 ft. dia. |
|----------------------|-------------|-------------|
| Standard Gore Ladder | 70 lbs. | 664 lbs. |
| Continuous Ribbon | 56 lbs. | 575 lbs. |

TABLE 1 - WEIGHT OF HEAVY DUTY RIBBON CANOPIES

In trying to further reduce volume, an investigation of a proprietary (patent pending) suspension line load attachment fitting is currently in process (Figure 6). This attachment fitting is a plastic material molded to the end of the suspension line. Preliminary tests indicate a 100% joint efficiency between webbing and fitting. The fitting may be molded to any shape suitable for hooking or sliding into slots on the parent vehicle. The fittings represent potential weight savings by eliminating loops at the ends of suspension lines and connector links, and providing a better distribution of loads into the parent structure.

Concurrently with the development of new parachute materials and construction techniques, a continuous program of testing connections, joints, and overlaps is being pursued. Following are some results of a study (Ref 3) which was conducted by Pioneer Parachute Company under an ASD contract. These data should be considered in the design of parachutes.

1. By incorporating the right size thread and number of stitches per inch, seam efficiencies in the average of 90% have been obtained under expert workmanship conditions. Normally, a factor of 0.8 or 80% efficiency should be chosen in order to allow for a low efficiency which may occur during the manufacturing process by less than expert but still acceptable workmanship. As an example, in Table 2, variations in efficiencies are presented for an overlap of 1 inch wide 6000 and 3000 lbs nylon webbings versus various thread sizes, length of overlap, and number of stitches per inch. Each figure represents an average of five test samples. As shown in this table, the use of 5 cord thread in place of 6 cord does not appreciably affect the strength of the overlap. Shortening the stitching length of the overlap from 6 to 4 inches decreases the efficiency by about 10%, in this case from 90 to 81% which cannot be tolerated and must be corrected. The last three lines show the efficiency as affected by variation of the number of stitches per inch on a joint of two 3000 lb webbings. It shows an efficiency reduction of about 5 to 8% if too few or too many stitches are used. At the same time, the effect of a worn needle point on the seam efficiency in comparison with a new needle point was investigated and revealed that the difference in the strength of the joint or seam is insignificant. Generally, it can be concluded that, by normal maintenance and parts replacement of the sewing machines, the strength of the textile sewing connections will not be below the allowable factor of 0.8 and should not be the cause of parachute damage and failure if the parachute manufacturer is complying with the requirements of the applicable drawings. Breaking strength data from samples being taken from canopies undergoing pro-



| Nylon Webbing | Thread Size Cord | ST/IN | "L" in. | Joint Efficiency % |
|------------------------------|---------------------|-------|------------|-----------------------|
| MIL-N-4088 1" Wide, 6,000 | 6 | 6 | 6 | 90.0 |
| | 6 | 6 | 4 | 84.0 |
| | 5 | 6 | 6 | 90.7 |
| | 5 | 6 | 4 | 81.1 |
| MIL-N-5625 1" Wide, 3,000 | 3 | 5 | 4 | 79.7 |
| | 3 | 8 | 4 | 86.9 |
| | 3 | 11 | 4 | 82.0 |

TABLE 2 - JOINT EFFICIENCY VS THREAD SIZE, OVERLAP LENGTH,
AND NUMBER OF STITCHES

longed storage under environmental conditions substantiate this conclusion.

2. Materials should be selected on the basis of their rated breaking strengths specified in the applicable materials specification. Although the actual breaking strength is usually higher than the minimum value in the specification, the strength calculation must be based on the value stated in the specification.

3. Because fabrication methods can vary with each parachute manufacturer and the fact that cloth, ribbons, and webbings will "draw up" during the sewing process, the drawings and specifications should specify that the parachute manufacturer must compensate for the shortening in length during the sewing process by making the cut length appropriately longer, in order to meet the finished dimensions within the specified tolerances.

IV. AIR DROP OF EQUIPMENT AND PERSONNEL

The initial operational requirements for air drop specified that the equipment and troops delivered by air drop should be concentrated into small areas for most effective support. In order to meet these requirements the dropping of equipment is presently accomplished from cargo aircraft flying in formation at an altitude between 1000 and 1500 ft.

To facilitate the loading and extraction of heavy loads, a "skate" wheel conveyor system was developed and used operationally. In the course of training and operational type missions it became apparent that the lack of guidance and the use of manual tie-downs and restraints to secure the loads in the aircraft became occasionally hazardous. To overcome this deficiency, a dual rail aerial unloading kit was developed. The kit consists of four roller conveyors with a restraint and guide rail outboard on each outside conveyor. The rails provide vertical and lateral guidance for loading and extraction and have locks which the pallet pins engage to form the fore and aft restraint. In the dual rail system the pilot has complete control of the load release thereby eliminating the hazard of manually removing tie-downs prior to drop and having a free load in the aircraft prior to parachute inflation and extraction of the load. The dual rail system is currently being installed in USAF cargo aircraft. Still, this delivery method of troops and cargo leaves, in certain instances, much to be desired in accuracy of hitting the drop zone and in dispersion of men and equipment due to the altitude of delivery and time intervals required between individual troopers and equipment loads.

In compliance with repeatedly stated requirements for higher accuracy, a low level, ground proximity, delivery program has been undertaken. Feasibility tests (Ref 4) have been conducted extracting loads up to 13,000 pounds from a C-130 aircraft with the wheels on the ground during touch-and-go landings (Figure 7) and with the low-

fly-by method while the aircraft was flying approximately 5 feet above the ground (Figure 8). The equipment consists of a trailing hook attached to the load engaging a cable perpendicular to the aircraft flight path. The cable is attached to a ground installed energy absorbing system which permits extraction of the load from the aircraft and deceleration of the load longitudinally with a predetermined G force. The evaluation of the limited tests revealed that it is possible to satisfactorily extract and stop heavy cargo loads with the above method within a few hundred feet when sliding on unprepared surface free of major obstructions. It appears that based on these feasibility tests the operational range of air drop can be greatly extended and that low altitude drops can successfully be accomplished under certain defined conditions. The following filmclip shows the recently conducted tests at Georgetown, Delaware.

This concludes my presentation on new aspects in the parachute and air drop development area. The presented efforts to enhance personal comfort, improve manned escape systems, provide larger drag surfaces in smaller volumes, and deliver equipment with higher accuracy represent a small but significant contribution in the overall parachute technology. In conclusion it should be noted that reliability whether it be as a result of added relaxation permitted by comfort or the accuracy of personnel and equipment emplacement is the undercurrent in all parachute development efforts.

LIST OF REFERENCES

1. Little, C. D., Jr. Capt., USAF; Ross, J. H. Fire Resistant Materials for Personnel Parachute Packs, ASD TR 61-515. Directorate of Materials and Resources, ASD. December 1961
2. Study of Pressure Packing Techniques for Parachutes, ASD-TR-61-426. Space Recovery Systems, Inc. for Aeronautical Systems Division, WPAFB, Ohio. June 1962
3. Miller, C. R. A Study of Parachute Seam Design Criteria, Part II Webbing Joints, WADC TR 56-313, Part II. Pioneer Parachute Co., Inc. for Wright Air Development Center, WPAFB, Ohio. June 1956
4. Report on Feasibility Demonstration of Ground Proximity Aerial Cargo Delivery, AF-186. All American Engineering Company for Aeronautical Systems Division, WPAFB, Ohio. September 1962.

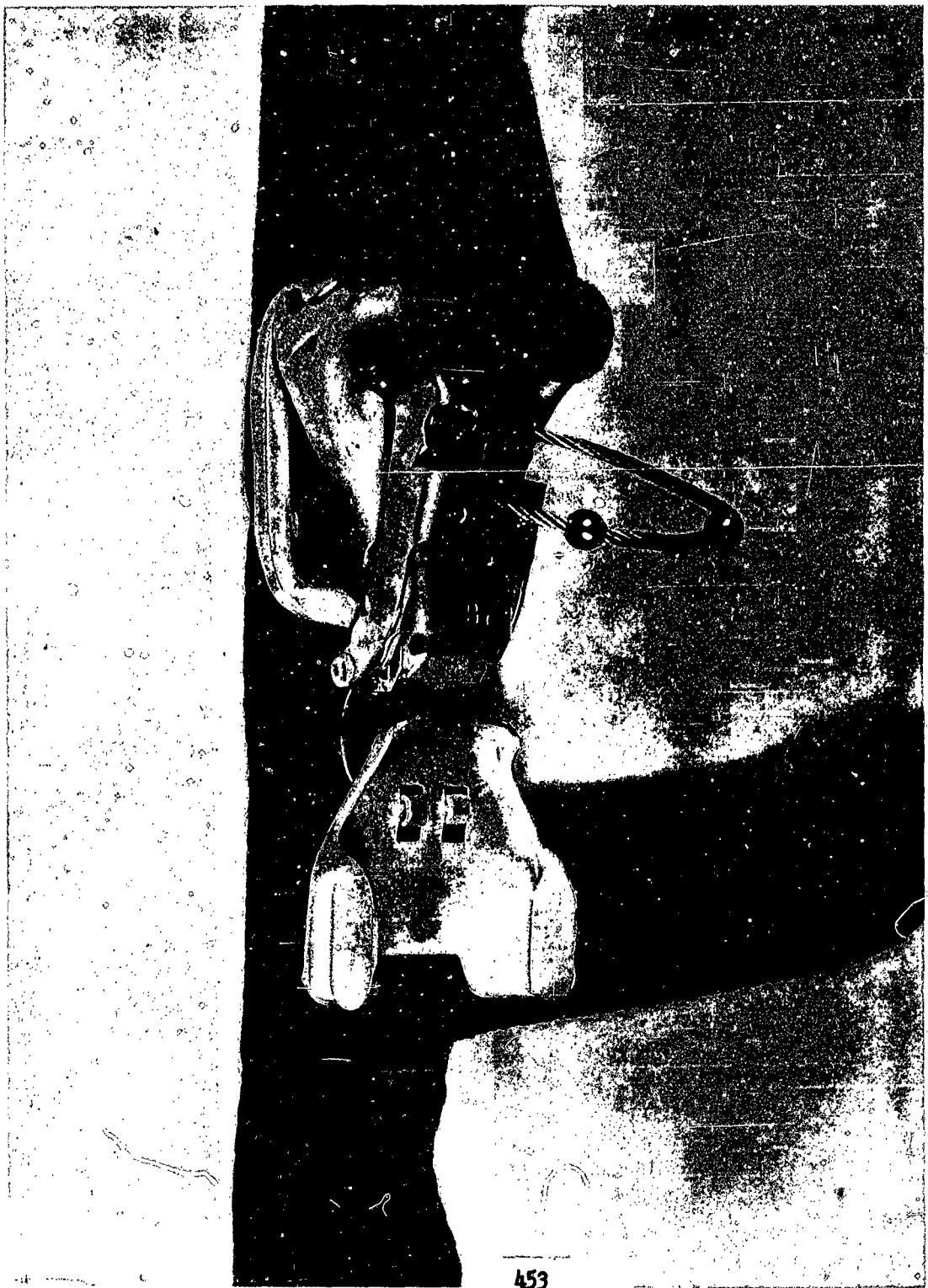


FIGURE 1 - CANOPY RELEASE ASSEMBLY WITH CABLE LOOP

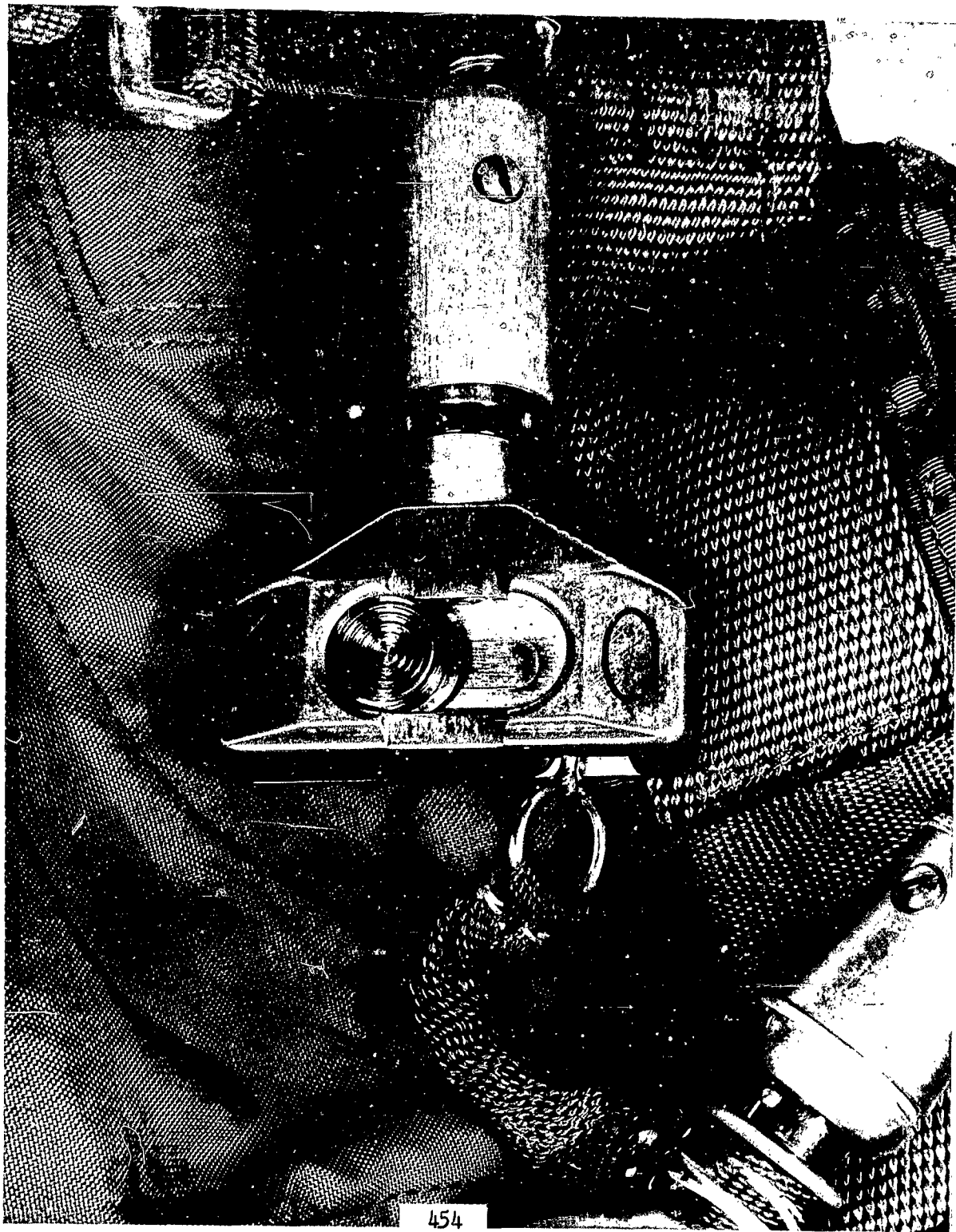
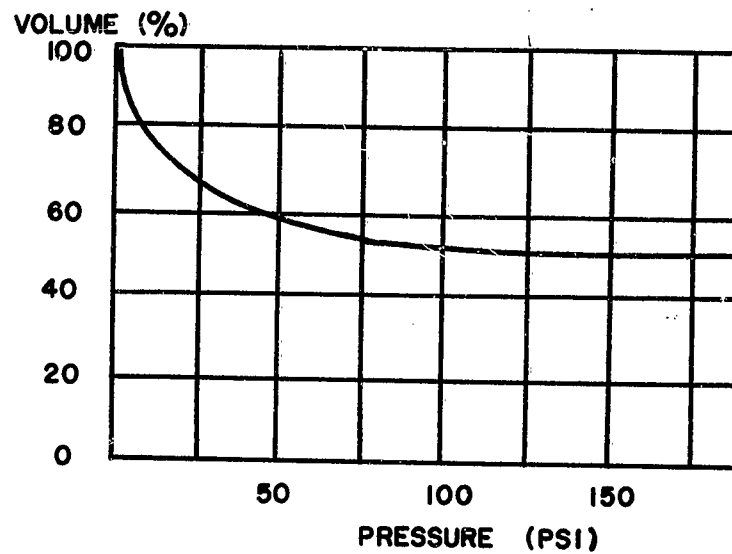
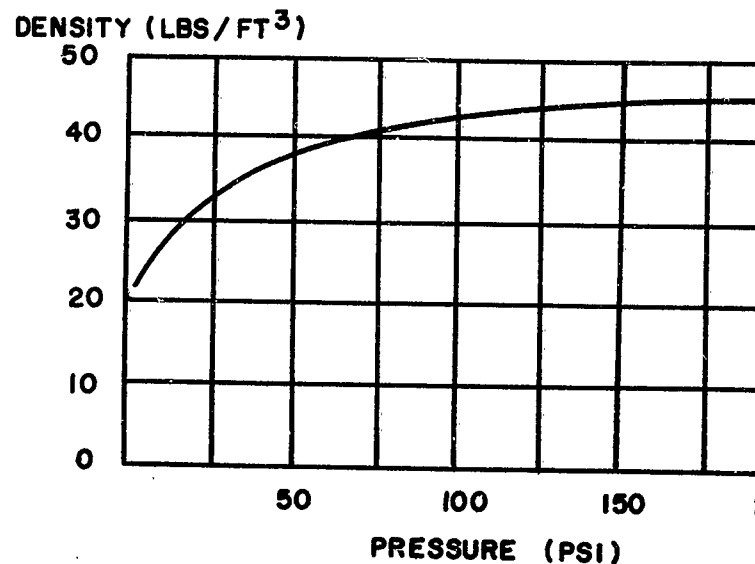


FIGURE 2 - "ZERO" LANYARD COUPLER

PRESSURE PACKING



VOLUME VS. PRESSURE



DENSITY VS. PRESSURE

FIGURE 3

ORIGINAL CONSTRUCTION

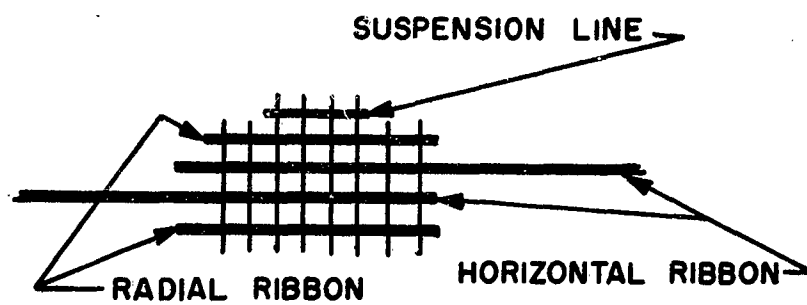
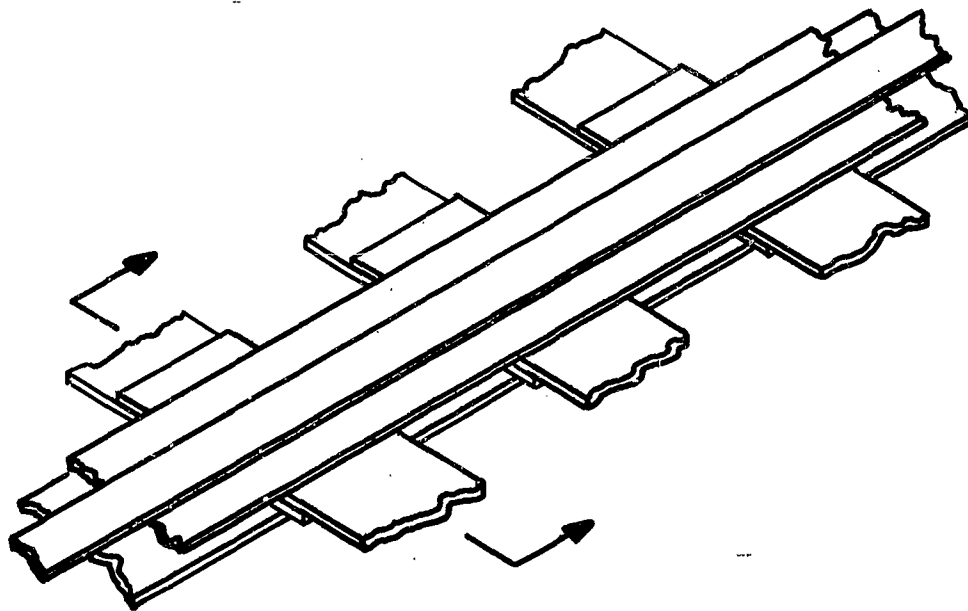


FIGURE 4

CONTINUOUS RIBBON CONSTRUCTION

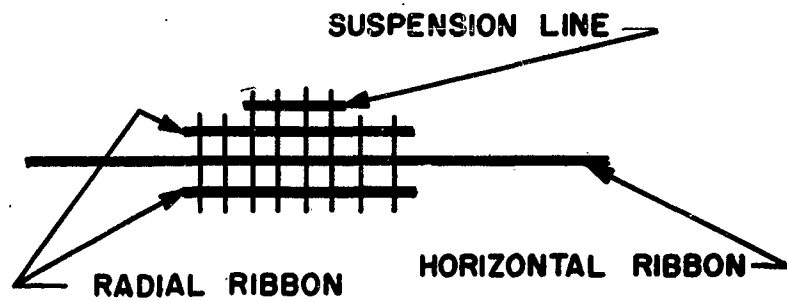
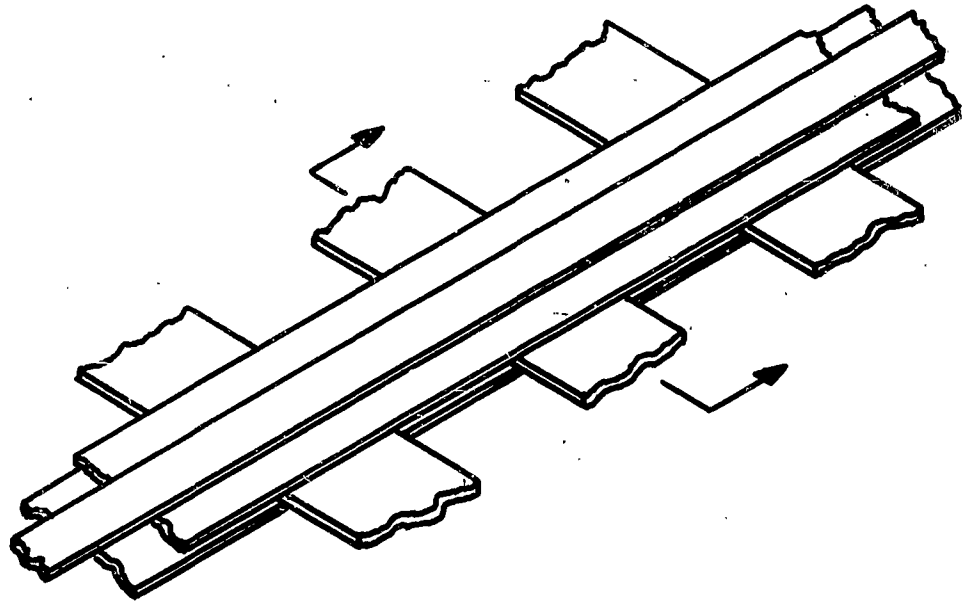


FIGURE 5

PLASTIC SUSPENSION LINE - LOAD ATTACHMENT FITTINGS

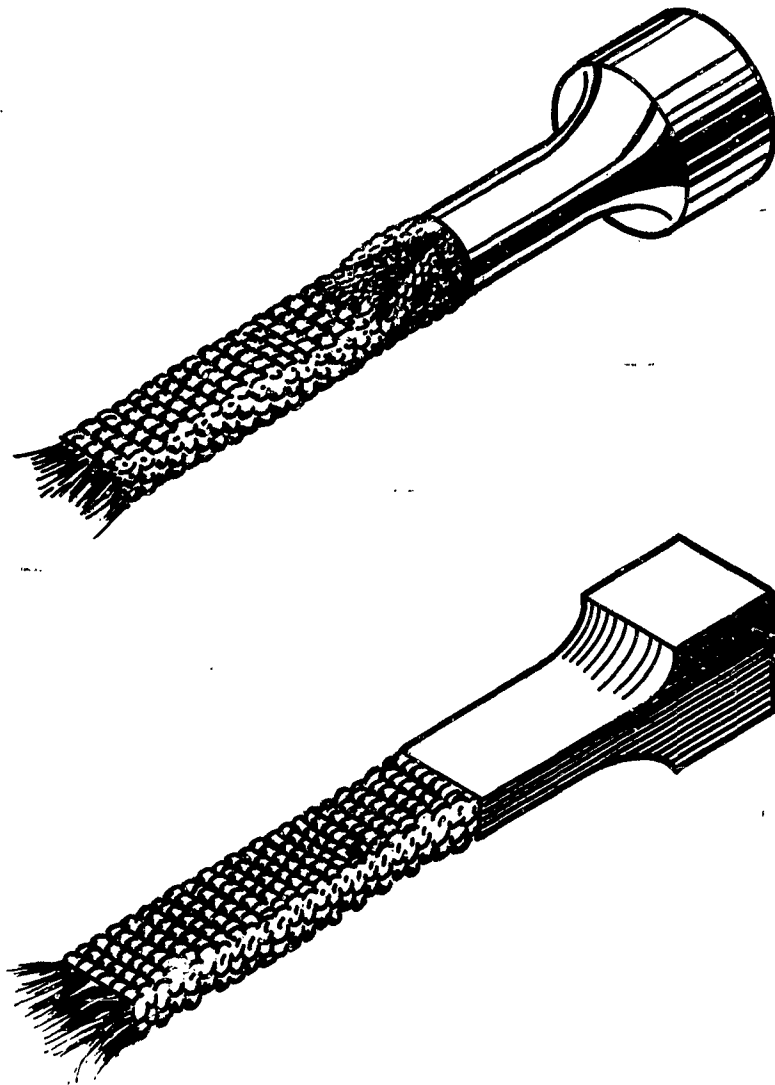


FIGURE 6



FIGURE 7 - TOUCH-AND-GO DELIVERY



FIGURE 8 - LOW-FLY-BY DELIVERY

TECHNICAL AREA OF

GEORGE A. SOLT.

Chief, Retardation and Rec
Flight Accessories Lab
Wright-Patterson Air Force

AERODYNAMIC DECELERATOR: THEIR USE AND FUTURE

INTRODUCTION

The parachute is serving a vital role in man's attempt to travel farther from the surface of the earth and safely return home and to satisfy his scientific curiosity of the unknowns beyond our planet. It is also used to save lives, to improve the performance of military flight vehicles, as a device for exciting but safe sports, and even as a sea anchor. The deployable aerodynamic decelerator, of the parachute is one form, is not particular as to the nature of the body moving through an atmosphere to which it is applied for retardation or recovery purposes. Therefore, its potential as a useful aerodynamic device on future bodies in flight is high. This discussion deals with military and scientific objectives in which the decelerator will serve as a useful and sometimes mandatory tool to assure successful achievement of the objectives and discusses the decelerator capabilities required for the future.

A FAMILY OF DECELERATORS

The deployable aerodynamic decelerator, with its functions of retardation and recovery, can be compared in one sense with that of fire extinguishing systems on flight vehicles. Neither of these capabilities are required to be in operation throughout the duration of a flight. The fire extinguishing system is on a stand-by status until the fire detectors signal the indication of a fire at which time the successful operation of the extinguishing system becomes extremely vital to eliminate an emergency condition. The deployable aerodynamic decelerator also plays a vital role on bodies moving through an atmosphere not only under emergency conditions but also as the most effective or only means of satisfying certain flight or mission requirements.

The parachute is the popular symbol of the textile device which provides retardation and recovery benefits. However, the performance requirements forecast for the future dictate the need for capabilities beyond the practical limit of parachutes in the configurations we have known them in the past. The expression "deployable aerodynamic decelerators," or simply decelerators, is now used to denote those devices including the parachute which will be required to perform retardation and recovery functions.

As the name implies, decelerators do not encompass all of the potential sources for achieving retardation and recovery. The decelerator family retains the basic parachute characteristics, namely, the achievement of its function by exertion of an aerodynamic drag force on a body and by the use of flexible materials to provide an efficient stowage capability.

The determination that a family of decelerators would be required in the future was not predicated upon an assumption or fact that parachutes were not or could not be efficient retardation and recovery devices in the future. The self-inflating parachute will continue to play vital roles on future vehicles including those traveling in the atmosphere of other planets. However, as in the case of other technologies, performance requirements are becoming more ambitious in magnitude, greater versatility in operation is desired, and the necessity for greater reliability, lower bulk, and lower weight is ever present. In the interest of efficiency, simplicity, and reliability, self-inflating parachutes will continue to be the most effective decelerator under certain flight conditions. On the other hand, the requirements for decelerators of the future will range in deployment speeds from near zero to superorbital, in altitude of operation from extreme low altitude to the limits of the sensible atmosphere, and will include efficient steerability and other capabilities for controlled descent and landing. Parachutes will not be the most efficient decelerator throughout these speed and altitude regimes. Below a dynamic pressure of one pound per square foot, the parachute becomes increasingly inefficient in relation to predictable performance and to the drag-to-bulk and drag-to-weight ratios. Also, extremely difficult if not insurmountable problems are envisioned in an attempt to maintain structural integrity of the parachute at dynamic pressures above 10,000 psf. Other potential decelerator concepts also exist within the actual or potential capability of the parachute and the parachute may not be the best decelerator choice for certain applications within its capability. Thus, the necessary technology for a family of decelerators required to best satisfy future flight and mission needs must be established.

FUNCTIONS

In order to forecast the decelerator technology required to satisfy future applications, the potential decelerator benefits should be recognized and then related to the future.

The general public has observed the application of parachutes to save men, to deliver cargo, to decelerate aircraft, and to recover orbital vehicles although the actual functions or benefits of the parachute may not be recognized. For example, the public may conclude that the wheel brakes on military aircraft are "no good" because a landing deceleration parachute is used on fighters and bombers. It is not recognized that there

| BODY TYPE | DECELERATION | STABILIZATION | FLIGHT PATH CONTROL | EXTRACTION | AIR DROP OR RECOVERY |
|-------------------------|--------------|---------------|---------------------------|------------|----------------------------|
| HUMAN ESCAPE SYSTEMS | | X | | X | X |
| AIRCRAFT | X | | X | X | |
| WING TANKS | | X | X | X | |
| WHEELS | X | | | | |
| ORBITAL VEHICLES | | X | | X | X |
| PROBES, ETC. | | | | X | X |
| AIR DROP LOADS | X | X | X | X | X |
| WINGED MISSILES | | | | X | X |
| MAN | | X | | X | X |

FIGURE 1
INDIVIDUAL PARACHUTE FUNCTIONS REQUIRED ON PAST AND CURRENT APPLICATIONS

is a marriage of deceleration techniques on modern aircraft and that the parachute is substituting for controllable propellers or thrust reversers which are employed extensively to supplement brake action. Nor are the added benefits of reduced wear and tear on tires and brakes, and thus reduced maintenance and replacement time and costs, generally recognized.

The expressions "retardation" and "recovery" are generalized terms which do not provide much of an insight to the functions of decelerators. Figure 1 reflects a breakdown of these expressions in relation to arbitrarily established types of bodies moving through an atmosphere. The body types reflect both complete flight vehicles as well as representative payloads or components which have been ejected, extracted, or released from a primary flight vehicle in past or current decelerator applications.

The functions of controlled deceleration and stabilization can be easily understood. Flight path control can take several forms. The ballistic trajectory of an unpowered body can be altered for some particular purpose or, in the case of the B-47, the approach angle was increased to improve flight characteristics together with a desirable increase in throttle setting to name two examples. Extraction of air droppable cargo by parachute is widely known and parachutes have been observed extracting other parachutes from containers or packs. Extraction and stabilization of B47 and B52 wing tanks by the use of parachute is not common knowledge. Aerial delivery, officially termed air drop in the Air Force, differs from recovery by the fact that the payload accomplishes its mission during or after the controlled descent to the ground whereas a recovered payload has completed its primary mission or task prior to the final descent. The tool used to achieve all of these functions is the decelerator's drag force or, more specifically, an aerodynamic force exerted on the body in flight in a direction opposite to the direction of flight.

THE LONG LINE OF POTENTIAL APPLICATIONS

What of the future? With technical advancements being made in every quarter, will there be a useful service to be performed by decelerators?

The considerations should not be restricted to an operational outlook. Decelerators of the past have proven to be valuable and sometimes vital during research programs such as the X-7 and during the development phase of the flight vehicles as in the case of the Matador missile. Training versions of flight vehicles which are not normally recoverable can effectively use decelerators as the means for recovery, the situation which also existed on the Matador. The purpose of the decelerator in these cases is to permit post-flight evaluation of equipment to an

extent and accuracy which is not usually possible by the use of telemetering or to provide a re-use capability in the interest of economy.

If Figure 1 is reexamined, it can be easily recognized that all decelerator functions could apply in some manner to a body in flight. In some cases, the possibility of a certain function being required on a particular body may appear to be remote. However, fifteen years ago, many applications now taken for granted were considered to have only a remote possibility for actual use. This fact is understandable because it is difficult to forecast the specific requirement for components or subsystems which are not obviously contributing or vital to the success of flight or a mission.

The need for propulsion or flight vehicle power is obvious. The situation with decelerators is different. In order to forecast the potential future requirements, it is sometimes necessary to make assumptions from which, in turn, decelerator requirements can be established. Take the case of orbital vehicles of the future. If the assumptions are made that the vehicle defined only by mission will be manned and that a separable return escape system is involved, the need for decelerators arises to support the escape system.

Due to unknowns or to certain anticipated undesirable characteristics during flight, a decelerator may be incorporated on lifting re-entry vehicles particularly during the development phase. This can be compared today to the use of spin recovery parachutes during development tests of fighters.

In spite of the advantages of maneuverable, high lift re-entry vehicles, it can be safely predicted that ballistic and semi-ballistic bodies will be used for certain future applications. The general advancement in space flight technology which will occur in the future together with decelerator advancements will provide for relatively small preselected landing areas, a degree of maneuverability during descent, obstacle avoidance, and soft landing at a point selected during final descent with a ballistic configuration.

The degree of maneuverability of ballistic bodies using decelerators will not be as great as that of a high lift vehicle nor will a preselected runway landing capability be provided. On the other hand, high maneuverability and runway landing capabilities will not be firm requirements for all future bodies descending to the ground. The relative systems simplicity and associated high reliability in a decelerator controlled return will justify the use of ballistic vehicles to achieve certain missions in the future. Consider the recovery of an orbital vehicle to secure recorded data or samples subjected to particular environments. Consider, also, the "aerial delivery" of pay loads on an

orbital vehicle for which physical acquisition is desired or required either from a non-recoverable vehicle or at an intermediate time during an orbital life. A sophisticated return and landing capability would not be required except if the time between initiation of return and the presence of the vehicle or its payload at a specific location beyond decelerator maneuvering capabilities was a critical factor.

Decelerators can be used to support exploration and achieve aerial delivery on other planets having an atmosphere. A space vehicle passing close to a planet can eject a payload which enters the atmosphere and transmits information such as cloud and atmospheric composition, density, and temperature during its slow decelerator-controlled descent. Delivered softly to the planet's surface, its sensitive equipment can act as a mechanical scientist by conducting experiments and transmitting the results. The value of possessing reliable, detailed information concerning other planets prior to manned landing and exploration needs no explanation.

The recovery of the Matador missile during development tests was mentioned previously. The purposes for recovering the Matador can apply equally well to unmanned boosters. Although telemetering is a useful method of obtaining information, it cannot provide the variety and detail of information that can be gained by inspection and post-flight tests of the recovered items. There are mixed feelings on the advisability of recovering unmanned boosters for operational reuse. If the requirement does arise, decelerators could successfully recover at least vital booster subsystems in the interest of economy or to make more boosters available within a given time period by reducing the total manhours required to fabricate components and assemble each booster. The total weight of a booster into which a recovery system and possibly a trajectory control system is incorporated may increase. In spite of this, certain problems or circumstances could justify recovery.

The forecast of decelerator application to aircraft is fairly clear cut. Parachutes are applied almost exclusively to combat aircraft except for individual human escape parachutes which are employed extensively on most military aircraft. A few military cargo aircraft have used parachutes to provide short field landing and take-off capabilities. Parachutes or other decelerators will be used in the future on military aircraft primarily as a component of escape systems and for landing roll deceleration. Any other applications will be dictated by conditions peculiar to each aircraft under development or in service and, therefore, cannot be forecast with any degree of accuracy.

Many items of equipment cannot successfully withstand ground impact under free fall conditions. The delivery of items to the ground from

aircraft in flight has been accomplished extensively since World War II. Anything which can be successfully air transported and can fall or be pushed or pulled out of an aircraft in flight without damage to the aircraft or the item is a potential air droppable load.

The requirement for air drop capabilities in the future may be questioned in view of the availability of helicopters and the activity in the STOL area. There is no doubt that helicopters and STOL aircraft could deliver cargo directly to a small, cleared area. However, place these aircraft in modern combat situations and we will see that air dropping is still mandatory or most efficient for many missions. Clearings on which these aircraft could land are not always available and the time or opportunity may not exist to prepare a clearing. In the case of operations near or in unfriendly territory, helicopters and other aircraft moving at relatively slow flight speeds or required to approach the ground to discharge cargo are extremely vulnerable to loss from small arms and anti-aircraft fire. As a result, helicopter and STOL potentials to support ground troop operations near or in an unfriendly territory must be augmented with a capability for effective air drops.

By eliminating the necessity to fly close to the ground or to land, vulnerability of the drop aircraft to unfriendly fire can be reduced by conducting higher speed, in flight air drops. Unit loads up to 41,000 pounds have been successfully air dropped; however, improvements are still desired in air drop characteristics. The cost of air drop equipment should be reduced although this fact is easier stated than accomplished. A decelerator design with demonstrated adequate performance and high reliability must be employed together with the materials and fabrication techniques required to assure structural integrity during operation. At present, the cheapest adequate materials and most efficient fabrication techniques which are available are used on those parachute designs considered acceptable for air drop purposes.

The ground dispersion of air dropped loads should be reduced. The inherent uncontrolled gliding tendencies of certain parachutes do not provide sufficient assurance of achieving a landing within a reasonable distance of the desired landing point. A load which lands an appreciable distance from its intended landing point may be lost or the excessive time for retrieval may prevent its use as a vital tool for achieving a military objective. Equipment could be delivered to a desired spot on the ground and obstacles avoided by use of steerable gliding decelerators. It is possible that the number of loads under controlled descent at any moment might have to be minimized and involve only the most vital loads in the interest of reducing the possibility of mid-air collisions between loads. The steerable gliding decelerator capability for air drop will also have application to ballistic and semi-ballistic re-entry bodies during final descent.

FUTURE CAPABILITIES

It is obvious that the decelerator capabilities of today will not satisfy many of the ambitious applications of the future. In the case of human escape, aircraft will be traveling at greater supersonic velocities. An escape capability within the atmosphere will be required on future space craft. The small, first stage decelerator required for escape system stabilization or deceleration will be required to operate successfully with predictable performance to at least Mach 25. Today, the capability for small decelerators is in the parachute with performance and design criteria available to Mach 2.5 and a dynamic pressure of 3700. Obviously, higher speed and dynamic pressure capabilities must be established.

In the area of controllability in decelerators, we know that certain man-carrying parachutes for special applications can be controlled to a limited degree in direction and glide by human manipulation. Air drop and recovery exercises could greatly benefit from the use of a canopy with a high lift to drag ratio and a steering capability. An L/D of 2 in a specially shaped canopy which would provide a high glide ratio is not a technically unreasonable target. It will be necessary to move away from canopy ideas involving open spaces or slots and emphasize the aerodynamics of a canopy by increasing lift or decreasing drag.

One benefit of value in the future decelerator is that of soft landing which would eliminate, or at least minimize, the ground impact problem. Stored energy rotors have the potential of providing efficient controllability during descent and, by use of collective and cyclic pitch, a near zero velocity vertical landing. In many applications, the advantages of rotor capabilities and the elimination of ground impact attenuators will overshadow the complexity introduced in a control system.

The potential of decelerators to satisfy future requirements associated with flight programs sponsored by government agencies is extremely broad and technical programs are being conducted to advance the capabilities of decelerators in every useful aspect in order to provide the necessary technology. As in the past, decelerators will be applied to a great variety of bodies moving through an atmosphere to provide life saving, a tool for efficient research and development, combat support, economy by reuse, improved flight conditions, recovery, or to support exploration.

The variety of tasks which a decelerator could perform, either independently or in combination with retro-rockets, shock attenuators, or other devices, is limited only by the imagination. The decelerator will continue to contribute either directly or indirectly to the success of flight and the accomplishment of military and exploratory missions.

| CONSIDERATIONS | HELICOPTER (LANDING) | STOL | TOUCH AND GO OR LOW FLY-BY | DECELERATOR AIR DROP |
|------------------------------------|--------------------------|---------------------|----------------------------------|------------------------------|
| SITE REQUIREMENTS | SMALL, ROUGH CLEARING | "RUNWAY" SURFACE | "SHORT RUNWAY" AREA | VARIABLE (NONE-DROP ZONE) |
| VULNERABILITY | HIGH | HIGH | MEDIUM-HIGH | MEDIUM |
| PAYLOAD DELIVERED (LA/C-1 PASS) | LOW | MEDIUM | LOW MEDIUM | MEDIUM-HIGH |
| DELIVERY WHERE SPECIFIED | EXCELLENT | FAIR- EXCELLENT | FAIR- EXCELLENT | FAIR- EXCELLENT |
| SPECIAL EQUIPMENT | NONE | NONE | EXTRACTION SYSTEM | AIR DROP SYSTEM |

AERIAL DELIVERY (AIR LIFT) VS AIR DROP IN COMBAT AREAS

CLOSING REMARKS

by

MR. L. H. HILDEBRANDT
Technical Director
Flight Accessories Laboratory
Aeronautical Systems Division

Gentlemen, I am a substitute and this would open the way for that much overworked story which I am not going to tell you. If you haven't heard it, ask your neighbor.

The program indicates, "closing remarks". I don't know what closing remarks are. I thought I had something to say, but this able gentleman just took away the last thing I had to say. To recap this symposium, both General Ascani and Mr. Murray, threw some challenges out at the outset of this meeting and I think if we will look at what has transpired in the last two days you have addressed the meeting to these challenges. We covered significant advances in the field of development, of test, of applied research, advanced technology, reliability, and system application. I think you all are to be congratulated as a collective Government-Industry group. Certainly this area has enjoyed as much, if not more, technological advancement, than other areas have engaged in the last four or five years.

I had hoped that our Captain Bud Gerzina could be here. I do not believe he is because he is attending graduate classes at Ohio State. He is a very industrious young man and he was the Project Officer for this symposium. To him and a lot of assistants who I will not mention, goes the credit for this meeting.

We were on a trial balloon here, the first time a symposium was held in this technical area. We feel real pleased with it. We would like to have your comments. Don't go home now and forget about it. Mail your comments in with suggestions for improvement. Do you want this symposium again? Mail comments to George Solt, or Capt. Gerzina. If there are no further comments, I declare the first symposium in the retardation and recovery area closed. Whereupon at 1630 hours, 14 November 1962 the symposium adjourned.

CLOSING REMARKS

by

MR. L. H. HILDEBRANDT
Technical Director
Flight Accessories Laboratory
Aeronautical Systems Division

Gentlemen, I am a substitute and this would open the way for that much overworked story which I am not going to tell you. If you haven't heard it, ask your neighbor.

The program indicates, "closing remarks". I don't know what closing remarks are. I thought I had something to say, but this able gentleman just took away the last thing I had to say. To recap this symposium, both General Ascani and Mr. Murray, threw some challenges out at the outset of this meeting and I think if we will look at what has transpired in the last two days you have addressed the meeting to these challenges. We covered significant advances in the field of development, of test, of applied research, advanced technology, reliability, and system application. I think you all are to be congratulated as a collective Government-Industry group. Certainly this area has enjoyed as much, if not more, technological advancement, than other areas have engaged in the last four or five years.

I had hoped that our Captain Bud Gerzina could be here. I do not believe he is because he is attending graduate classes at Ohio State. He is a very industrious young man and he was the Project Officer for this symposium. To him and a lot of assistants who I will not mention, goes the credit for this meeting.

We were on a trial balloon here, the first time a symposium was held in this technical area. We feel real pleased with it. We would like to have your comments. Don't go home now and forget about it. Mail your comments in with suggestions for improvement. Do you want this symposium again? Mail comments to George Solt, or Capt. Gerzina. If there are no further comments, I declare the first symposium in the retardation and recovery area closed. Whereupon at 1630 hours, 14 November 1962 the symposium adjourned.

HYPERSONIC SESSION
QUESTION AND ANSWER PERIOD
13 NOVEMBER 1962

"Heating Problem for Supersatellite Re-entry" - MR. PETER H. ROSE

Question - Mr. Demele, NASA - Ames Research Center

I noticed that you had curves of equal radiative and convective heating on a plot. Actually, in terms of ablative weight penalties, shouldn't one look at total heat, and would the picture be somewhat different if you did include the integrated heat as opposed to stagnation heating rates?

Answer - Mr. Rose

The curve, as you noted, was purely a rate curve and certainly, from any design point of view, you want to look at integrated, but in general, all re-entry shapes are sort of similar, and if you then take the peak rates and use those as a sort of figure of merit, you also get a rough idea of integrated rates.

Question - Mr. Demele

But the rate of heating drops off more rapidly than does the convective.

Answer - Mr. Rose

Certainly, you have different curves for the two. Again, the ablating material, as you point out, you have a different mechanism whereby they reject heat. It's a completely different story, but not the total story. I'm purely talking about the input data to an ablation calculation.

Question - Mr. Love - General Dynamics Corporation

Perhaps I should ask this question of Mr. Scala. I don't know whether he's here or not. I'll ask you anyway. Have you people resolved the Scala data? Is it all convective or is it possible that it's a combination of radiative and convective? Is it their explanation that they do include radiation?

Answer - Mr. Rose

Let me make one separation. The theory -- The Scala data was collected by a gentleman by the name of Warren. Theory does not consider anything but convection but the data collected by Warren attempts to account for radiation, and it is felt by everybody that conditions at which these tests are made, radiation is not a

significant contributor. It's a five or ten per cent kind of effect. But, there are, as I pointed out, on one of the curves five or six data points which are not explained and consequently I can't state categorically that there are no radiative effects, but it is generally felt there is no radiative effect in this data.

"Hypervelocity Re-Entry Configurations" - MR. M. L. BUCK

Question - Mr. Lloyd - Lockheed Missile and Space Co.

Much of your information regarding conclusions as relating to required L/D is dependent on the lateral maneuverability you can obtain with different L/D vehicles. You didn't show any maneuvering envelopes or lateral capability. I wonder what data you based your maneuverability on, that is, maneuverability as a function of L/D.

Answer - Mr. Buck

Well, this is, I think, on the first order type of relationship that we get where the cross range is a function of just the lift to drag ratio.

Question - Mr. Lloyd

You mean a simple exponential relationship?

Answer - Mr. Buck

Yes.

Question - Mr. Rose

In your composite design, you gave the impression that the combination of low speed performance, high speed performance, a supersatellite re-entry and radiative cooling were compatible. You did not mention the temperature range at which your vehicle was operating. Would -- Could you state that?

Answer - Mr. Buck

I'm not sure that we stated they were compatible here. I think you are referring to the chart with the figure -- with the various constraints, vehicle constraints, as a function of the velocity.

Question - Mr. Rose

Yes, I understood you to say that it was possible to find a vehicle which had sufficient hypersonic L/D, subsonic L/D and was capable of radiative cooling.

Answer - Mr. Buck

No, that was for the sub-orbital case, For super-orbital, we would have to look into ablation type of cooling or solution to the heating problem, at least, for the first generation type of vehicles.

Question - Representative of Douglas Aircraft Company, Inc.

You had two conical slides about the rather hot landings associated with the low L/D's and you made allusion to increasing L/D to approximately five or six, subsonic. With this increased L/D, what would be your landing technique?

Answer - Mr. Buck

I'm afraid I couldn't answer that question. We haven't looked into what the landing technique would be. We are directed primarily at a conventional type of landing such as one would experience with the X-15 type of vehicle.

Question - Representative

My question is really with increased L/D, what you are looking for, is decreased sink rates, decreased landing speeds, or the 270 approach.

Answer - Mr. Buck

Right. I think we would have to examine what the vehicle can do for us. We would like to achieve not only the low sink speeds but the low landing speeds as well. In addition to this, a high lifting capability of the low angles of attack and the approach. I think this would have to be worked out. I couldn't say right here what the type of approach would be. In this, we are not really concerning ourselves with the approach.

Question - Mr. Johnson - Aeronautical Research Laboratory

Aren't you seeking maneuverability? Isn't this the point?

Answer - Mr. Buck

He is talking about the terminal phase of flight.

Question - Mr. Johnson

At these L/D's you do have certain maneuver characteristics.

Answer - Mr. Buck

However, we are still talking about unpowered flight and he still is going to have only this one pass at making this successful landing. However, by giving these high L/D's we are able to decrease the sink speed, landing speed, and give more time for the pilot reaction. It therefore increases his capability in the area.

Question - Mr. Myron - Rand Corporation

I was wondering if you could make some comment about the stability of some of the various shapes in the transonic and hypersonic regimes that you have looked at. It is my understanding that some of these don't fair too well under this criteria.

Answer - Mr. Buck

Well, on the MDF configuration we showed you, wind tunnel test indicates this vehicle has fairly descent stability across the Mach number range it was tested, and this was from about, I believe, .2 to -- Well, we tested up to 18 on this.

Question - Mr. Myron

Are there other shapes particularly unstable?

Answer - Mr. Buck

Well, we have looked at just a pure lifting body at the low speeds, but we didn't take any stability data in the tunnel tests. Now, we would expect that there are stability problems in this region and some sort of fix or some change in the design is going to be required to solve this problem. But, you may be able to accomplish this by using these expandable surfaces because on the pure lifting body, your lift to drag ratio at the subsonic velocities isn't going to be sufficient to give you good landing characteristics. It seems probable, if you're going to attempt to land these

vehicles in a conventional manner, you would want to use an expandable surface at the lower speeds, terminal portion of flight. Utilizing these, of course, many problems are associated with these expandable structures, but you could be able to design these to take care of the stability problem, I think, through this same increment in the velocity spectrum.

"Hypersonic Drag Devices" - MR. S. R. METRES

Question - Mr. Baier - Armour Research Foundation

Will your data be published in an ASD Technical Note?

Answer - Mr. Metres

It will be published. The program has just been completed and we have the reproducible in hand right now. We expect it to be out by January, we hope.

Question - Mr. Ross - Fibrous Materials Branch - ASD

On the 17 1/2 ounce fabric you're talking about, what was the weight or the coating?

Answer - Mr. Metres

It was ten ounces.

Question - Mr. Ross

That's per square yard?

Answer - Mr. Metres

Right.

Question - Mr. Pepper - Sandia Corporation

I was just wondering on your tubes that collect air, does this present any problem in packing in a small volume?

Answer - Mr. Metres

The aft inflating probe configuration resulted from the questionable inflation pressures available from nose inflation in the non-convergent wake of the primary body. The probes in a free flight test model would have to be repositioned to possibly the burble fence for efficient packing.

Question - Mr. Coplan - Fabric Research Laboratory

What do you visualize as the optimum compaction ratio for deployed and undeployed configurations?

Answer - Mr. Metres

This is something I don't know. Do you have any comments on that Fred?

Answer - Mr. Nebiker - Goodyear Aircraft Corporation

The packaging ratio will be around 7. It comes out about 35 lbs. per cubic foot.

SUPERSONIC SESSION
QUESTION AND ANSWER PERIOD
13 NOVEMBER 1962

"Supersonic Parachute Research" - MR. R. J. BERNDT

Question - Mr. Fredette - Hayes International Corporation

I would like to ask a question myself, Mr. Berndt. Do you have any comments on the maximum diameter, the diameter ratio to which you would expect these configurations to perform satisfactorily?

Answer - Mr. Berndt

Well, we don't really have any conclusive indication of whether or not limit really exists, but from the tests that we have conducted, we have seen that a deterioration in inflation stability and static stability occurs if the diameter ratio becomes larger than 2.5. This doesn't mean that the parachute is unstable but there is a slight deterioration in overall performance if it becomes larger than 2.5. We have tested up to 3.37 and it performed reasonably well.

Question - Mr. Fredette

Is this reduction in performance primarily due to reduction in the inflated diameter?

Answer - Mr. Berndt

No, the inflated diameter remained essentially constant. The reason why the performance changes, has as yet not been resolved.

Question - Mr. Knacke - Northrop Ventura

I have a question. When can we expect data from the larger model tested in free flight?

Answer - Mr. Berndt

As we have it programmed now, the first free flight test is a ribbon roof hyperflo canopy, and it should come off in about three weeks.

Question - Mr. Knacke

What diameter?

Answer - Mr. Berndt

Well, we haven't really determined the diameter. Between 2 1/2 and 4 feet in diameter.

Question - Mr. Baier - Armour Research Foundation.

You showed an example of 34 degrees angle. Why is this?

Answer - Mr. Berndt

Why was this angle chosen? For operation of Mach Nr. 3.

"Application of Axisymmetric Flow Analysis to Inflation Stability of Supersonic Flexible Parachutes" - MR. J. K. BUCKNER

Question - Mr. Fredette

I might ask one question. Have you considered the approach here to determine how these considerations might be modified by depending upon flow ahead of the canopy as you might encounter in a wake condition?

Answer - Mr. Buckner

No, I haven't done that, insofar as it pertains to the flow ahead of the chute. In interpreting data used to get the inlet area ratio as a function of Mach Number, we did calculate wake of the payload which was used at this time. I might add, payload diameter -- diameter ratio of the filled canopies to the payload was about 2 in all cases.

Question - Mr. Fredette

Was that also true of low porosity configurations?

Answer - Mr. Buckner

Three particular tests which were used in the development of the method were all medium porosity, a range between 20 and 30% total porosity.

Question - Dr. Heinrich - University of Minnesota

As I recall, there was a graph which indicated certain

boundaries which divide stable and unstable regions. If one would lay out a supersonic parachute, say Mach 3, full inflation at Mach number 3, and recovery would take place at 3, and then proceed down to maybe .9, would such a chute stay inflated and remain stable?

Answer - Mr. Buckner

Such a chute in which region of operation?

Question - Dr. Heinrich

If the chute is laid out for Mach 3 for full inflation and stability and then the recovery takes place at Mach 3, and during the recovery and speed decreases to .9, would the chute stay inflated and remain stable?

Answer - Mr. Buckner

Well, it's my opinion that it would. Somewhere, in the case of the hemisflo parachute, it was reasoned that it would probably only semi-inflate in the deployed condition, simply because it was above this boundary 3 which I calculated, and as it decelerates it will increase in inflation until it becomes choked, and the normal shock would come through the parachute and form in front. In this transition period, there may be some instability, but it is my opinion it would be a very short period of time.

Question - Dr. Heinrich

Well, I think my question is, if they design the chute for full inflation at Mach 3 -- I gather you can do that -- would that chute stay inflated and remain stable when the speed reduces to Mach .9?

Answer - Mr. Buckner

I presume, yes, you could design a parachute that would do that. Yes.

Question - Mr. Fredette

Do you recall what the porosity for stability was at Mach 3? That might help.

Answer - Mr. Buckner

No, I can get it.

Question - Mr. Fredette

I would hazard a guess that if the porosity, so defined, is low enough to insure subsonic inflation, it would probably stay inflated. As I recall, porosity for Mach 3 was lower than necessary for 1.501.

Answer - Mr. Buckner

Yes, that's true. If you have a partial porosity which I defined of about 20% or less, and we aren't bothered by the violent oscillations for very low porosity parachutes. In other words, boundary one for the violent oscillations hasn't been defined, so that might be causing trouble. However, if we have a partial porosity of 20 then it should work at Mach 3.

Question - Dr. Heinrich

And it would inflate fully at Mach 3?

Answer - Mr. Buckner

That I'm not sure of. This depends upon the analysis of the higher boundary between the semi-inflated parachute and inflation instability.

Question - Mr. Arnold - Boeing Company

Would you care to define further the specific canopy configuration and the porosity selected for the B-58 stabilization chute, or can you do this?

Answer - Mr. Buckner

Yes. It is a total porosity of 21.2% and it's a 10% extended skirt, hemisflo, which is the third design that I considered.

Question - Mr. Johnson - Arthur D. Little, Inc.

Would the stable and unstable conditions you showed as the equilibrium condition, you can go back and forth, have you established that experimentally for a given set porosity?

Answer - Mr. Buckner

No, nothing has been established experimentally to my knowledge.

Question - Mr. Johnson

When you open the chute, don't you have to automatically start from Mach zero? Even if you're in flight, say at Mach 3, in the opening process it goes from zero on up to the Mach number we are talking about? How do you deploy at Mach 3 without going from Mach zero?

Answer - Mr. Buckner

I see your point, yes. You don't, I guess.

"Rogallo Wing" - MR. F. M. ROGALLO

Question - Representative from Rand Corporation

I was wondering if you could indicate the extent of any research that may have gone on in the past year or two on the flexible wing or your flexible paraglider in the hypersonic or supersonic regime. Could this ever be extended for recovery from orbit?

Answer - Mr. Rogallo

In the past year I believe the only supersonic tests that we made were some at near Mach 5 of a model of the micro meteoroid paraglider. We had previously completed a number of tests up to about Mach 5 on earlier models. These data are already published. You are probably familiar with them. We haven't been working on anything recently applicable to recovery from orbit. There hasn't been any funded program on that phase of it and we have been busy getting out information for the other programs such as the ones that I showed you today which are all subsonic applications.

Question - Dr. Heinrich

When you deploy the parawing, do you absorb, in the first instance, a force which is higher than the steady state force, something like an opening shock of a parachute?

Answer - Mr. Rogallo

I'm sure there is something like this that happens, but there are many methods of deploying these wings though, and the shock

loading depends on the method. In one case that I have heard about, where it is deployed first as a parachute and then converted to a paraglider, a shock loading of about 8G was mentioned to me. In another case with a different kind of deployment, tests done in our 19 Ft. Tunnel at Langley, a figure of about 1.3 was quoted, a preliminary figure. It is entirely, I think, a matter of how you do it, but there is certainly the possibility of getting high loads.

Question - Mr. D'Annunzio - General Dynamics Corp./Astronautics

I have a couple of questions I'd like to ask. In connection with deployment for recovery of devices such as Gemini, is there any problem associated with deploying the parawing at rather high dynamic pressures?

Answer - Mr. Rogallo

I think there is. This is one of the principal problems to be worked out yet. So far, the experimental work has only included the stability and control and landing capability of the model after deployment, and the next step is to deploy it, that is, the half-scale models and full scale models, under actual conditions to be expected with the Gemini. Now, we have done some wind tunnel deployments that are somewhat like those anticipated for the Gemini, with some success. I wouldn't say just how difficult this is going to be and how reliable it will turn out to be.

Question - Mr. D'Annunzio

Could you also comment on the structural weight fractions associated with the Rogallo recovery wings for these applications? Do you have enough data to mention them?

Answer - Mr. Rogallo

No, I don't. I have heard that the weights and volumes are in pretty good shape relative to parachutes.

Question - Mr. D'Annunzio

You mentioned one figure of 3,000 pounds for the Mercury. Was this for the 2,000 pound?

Answer - Mr. Rogallo

That was with the standard boiler plate Mercury capsule. We added -- The 2,000 pound capsule and we added another thousand pounds of weight in it, and this was a pretty crude wing we built ourselves out of material we had on hand. It was about a hundred pounds of cloth. We had expected to inflate the tubes, to a pressure of 4 lbs. per sq. in., but we found that the material wasn't strong enough to take it, so we were restricted to about a pound and a half of pressure. The flight you saw there, and it had some leakage, we had to pump up to a pound and a half and then by the time we picked up on the ground it would be down to a pound. So, we figure it had about a pound and a quarter in the flight. We thought that we would run out of its lifting capability before we ran out of the helicopter's lifting capability which was about the 3,000 pounds that you saw in that flight, but the paraglider looked better the higher weight we put on it. This flight you saw looked better than any of the lighter weight flights. I don't know what the limit would be on that one, but that was 3,000 lbs. carried by a hundred pounds of cloth. The ropes, etc., the rigging, and some fairly heavy aluminum plates that we attached to it to tie the ropes to it, weighed another hundred pounds, so that the cloth and all the rigging weighed about 200 pounds.

Question - Mr. Arnold - Boeing Company

You showed some pictures of L/D's going from 6, 8, 12 and 14 depending on the configurations concerned. Just what does a practical rigging factor do for L/D rigging, for example, such as used on Gemini or Apollo?

Answer - Mr. Rogallo

I know what you're asking; I don't know how to answer it. Certainly, it cuts it down some but I don't have a figure on how much. The Ryan airplane was tested in our full scale tunnel and the estimate on that was that the wing alone would add L/D of close to 7, and the complete machine will drop down to five and a half, as I recall. The Gemini half-scale model was tested in the Ames wind tunnel, but I don't recall any results there. Anyway, they probably didn't determine that because they only tested the complete model.

Question - Mr. Whitney - ASD

Have you had any problems with flutter in any of the configurations that you worked with?

Answer - Mr. Rogallo

Well, the trailing edges frequently flutter, if you don't take steps to prevent it, that is, put a little rope and tighten it up a little at the trailing edge to put a little load on it. If it's unloaded, it will shake a little. Now, subsonically, this doesn't bother; it can shake for hours without doing any damage. Supersonically, however, it could be pretty violent. In the tests we made supersonically, we always took precautions to keep them from fluttering. The first glider they built at Edwards had quite a bit of trailing edge flutter. When they re-built it, they tailored the canopy a little differently and eliminated the flutter, so I would say that you can encounter flutter and you can take steps to eliminate it.

"High Temperature Fibrous Material for Decelerators" - MR. J. H. ROSS

Question - Mr. Shichman - U. S. Rubber Co.

I wonder if you could mention some typical temperature-time environments you might encounter for flexible structures on re-entry, or that you would like to withstand, and you might also mention how some of these systems described this morning such as the paraglider or some of the new parachute designs might affect these temperature-time environments.

Answer - Mr. Ross

I'm afraid that's one question I can't answer. The work that we do, doesn't get us into any specific time-temperature histories. We pick at random, let's say, or we pick a series of time-temperatures to study with the anticipation that one of these will be within the regime of some system when it's built. Probably the answer could come better from the deceleration people rather than from myself.

Answer - Mr. Bernat

It depends a great deal on what you're shooting for. I can't give you real values.

Question - Mr. Shichman

Well, for example, we have talked about metal alloys withstanding 2,000 degrees. I presume this is after rocket deterioration. Is this something that you envision as required in the design that you have been looking at?

Answer - Mr. Berndt

Well, 2,000 degrees. We are looking at, I think, 1500 degrees for circular re-entry, and probably 2,000 - 2500 for supercircular, if you put a decelerator on those of large enough size.

Question - Mr. Fredette

Any more questions? If not, I believe there have been several questions on the status of the parachute handbook that Mr. Berndt would like to comment on at the moment.

Answer - Mr. Berndt

As you know, we are rewriting the parachute handbook, that is, WADD Tech. Report 55-265. We now hope to have it in publication by the end of February and at that time it should go into the mail.

DECELERATOR INVESTIGATIONS SESSION

QUESTION AND ANSWER PERIOD

14 NOVEMBER 1962

"Reliability of Recovery Systems" - MR. G. CHERNOWITZ

Question - Mr. Baier - Armour Research Foundation

Mr. Chernowitz, you stated when setting up goals, instead of stating the absolute goals that one required, you should give acceptable results. I was wondering if you would comment about this. When you were talking in the area of the design and manufacture of the envelope, you stated that ordinarily absolute goals are given; however, you would like acceptable results to be given. I was wondering if you would comment on that.

Answer - Mr. Chernowitz

I should really have said, an envelope of acceptable goals, rather than absolute goals, that is to say, when we set a specification we should state the tolerances on that specification, and that specification, you see will be stated and should be stated in as many of the environments as possible. If I used the word "results" I meant "goal".

"Water Surface Wave Analogy" - MR. S. K. IBRAHIM

Question - Mr. Kieth - University of Dayton

One question for Mr. Ibrahim. You mentioned several times the importance of keeping the size of the model relatively large compared to the depth. What size did you find to be sufficiently adequate on this? In other words, how small is too small?

Answer - Mr. Ibrahim

The size has to be related to the water depth. The whole thing comes from the fact that you have to separate, more or less, capillary waves from the main waves you want to study. As a practical answer and from our own experience, we have used models of maybe between 10 and 20 inches long and water depth of about one third to one-half of an inch for the transonic regime, up to Mach 2.

GENERAL CONSIDERATIONS SESSION

QUESTION AND ANSWER PERIOD

14 NOVEMBER 1962

"Systems Consideration" - MR. T. W. KNACKE

Question - From the Floor

Mr. Knacke was stressing the potential of the rotor, and thinking at the time, from Germany as we know, I had heard that they use some kind of rubber or kind of material propellers or airplanes or something, is this true? Did they ever use this?

Answer - Mr. Knacke

Yes, I had been told by a professor of mine when I went to college, he was a zeppelin designer and a gentleman who worked with Dr. Armski from Goodyear, that they used flexible rotors for power. They were textile rotors with steel cables inside. They were chopped back at the ends and used a little bit as-- it is interesting of course to tell how the rotor used to warp up once in a while around the hub and someone had to go out during flight and stop the ship midway during flight and go out and unravel them and start the motor again and continue flying, but this was back in 1905, 1906, 1907, Dr. Armski from Goodyear may know about this. These two gentlemen, Dr. Swinger, Dr. Armski and my professor worked together on that one.

"New Parachute Development Aspects" - MR. A. M. HEGELE

Question - Dr. Heinrich - University of Minnesota

I have two questions for Mr. Hegele. What was the vertical distance those trucks dropped out; and, Nr. 2: What type of parachute did the driver of the truck wear, back, seat, or chest type?

Answer - Mr. Hegele

At first he asked how high was the altitude at which the load dropped out of the aircraft during flyby. Now it was between five and ten feet. Probably you noticed on this one run where we had a failure, it took quite a while until the load came out, so they are striving to get it out about five feet above the surface. Fortunately in no vehicle was a man involved. On the other hand, we are already considering how we can get these drivers or troops down with a similar method. That is already a requirement, true, to deliver personnel at such low altitude.

Question - From the Floor

Would you discuss the placing problem there. In other words, would you have to hold your cables, anchored in at either end? Is this revited in by a wedge or is this mechanically done? I'm talking about anchoring the cable that stretches across the runway.

Answer - Mr. Hegele

In this case the all-American system, water twist was used which was located, one item each, on the side of the runway. Now these water twisters, they were put in the ground by sticks or however you call it so they hold together. Now they have various sizes of water twisters depending on the loads they want to retract from the aircraft. You cannot use this method under all conditions. Sometimes you are not able to put a ground station beforehand on the ground, so consideration is given as to whether there could be used another method without any ground station. But, nothing has been accomplished as of yet.

A STATEMENT MADE BY: MR. G. CHERNOWITZ

This is not really a question. I think I would voice the sentiment of everyone here if I said that one is truly impressed by the technical quality of the meeting, but also of what could be described as superlative logistics. Very rarely have I attended a symposium where all things were handled so well and were made to come out so well. I don't know whether it will be dealt with formally before the meeting ends, but certainly someone from the floor should take the opportunity to say that.

APPENDIX - LIST OF ATTENDEES

ATTENDEES AT THE "RETARDATION AND RECOVERY SYMPOSIUM"

ADAMS, K.
AFANASIEF, I. P.
AICHINGER, G. E.
ALEXANDER, W.
ANDERSON, A. D.
ARNOLD, A. M.
ASCANI, F. J., BRIG. GEN.

Chrysler Corporation
McClellan AFB, California
ASW / ASD
Goodyear Aircraft Corp.
Cook Electric Company
Boeing Company
Deputy Commander/B-70

BABISH, C. A., III
BAIER, W. H.
BALOK, R. S.
BARISH, D. T.
BARZDA, J.
BEASLEY, M. D., JR.
BELL, R. N., LT.
BENJAMIN, R., DR.
BERESFORD, T.
BERNDT, R. J.
BERNSTEIN, F. L.
BEYERSDORFF, L. E.
BLOETCHER, F.
BOESKOOL, I. L.
BOWDEN, J. R.
BRADY, C. C.
BRAUN, J. F.
BRENT, F. T.
BROWN, B. N. P.
BRUMIT, C. D., CAPT.
BUCK, M. L.
BUCKNER, J. K.

ASD(ASRMFD-1)
Armour Research Foundation
Autonetics Company
Barish Associates, Inc.
Kaman Aircraft Corporation
McDonnell Aircraft Corp.
ASD(ASZR)
Cook Electric Company
Cook Electric Company
ASD(ASRMFD-1)
RCA, Camden N. J.
Goodyear Aircraft Corp.
Goodyear Aircraft Corp.
Lear Siegler, Inc.
ASD(ASR00-1)
Rocket Power, Inc.
Technology, Inc.
Fairchild-Stratos, Inc.
Northrop Corporation
ASD(ASNPPSP-1)
ASD(ASRMDF)
General Dynamics Corporation

CAMPBELL, C. C.
CARROLL, C. E.
CHAGARIS, W. J.
CHERNOWITZ, G.
CHUNG, J.
CHURCH, A. S.
COPLAN, M. J.
COX, T. J.
CREASEY, F. E.

NASA - Manned Spacecraft Center
ASD(ASNPPSP-3)
Douglas Aircraft Co., Inc.
American Power Jet Company
Republic Aviation Corporation
Northrop-Ventura
Fabric Research Laboratory
ASD(ASORC)
Chance-Vought Corporation

D'ANNUNZIO, M. G.
De DONATO, G. O.

General Dynamics/Astronautics
North American Aviation, Inc.

DEI, J.
DELL'AMICO, F.
DELURGIO, P. R.
DEMELE, F. A.
DEUTSCHMAN, J. N.
DeWEESE, J. H.
DIBBLE, H. L., DR.
DICKSON, G. G.
DIETZ, A. E.
DOBSON, T. H.
DOUGHERTY, J. P.
DRAPER, A. C.
DUFFY, J. H.

EDWARDS, H. H.
EICHEL, D. A.
ELIAS, G. M.
ENGEL, H.
ERB, L. H.
EVERETT, W.

FARINHA, C.
FARQUHAR, B. S.
FINNEY, R. M., CAPT.
FISH, H. C.
FISHER, P.
FLOOD, D. L., MAJ.
FREDETTE, R. O.
FREESTON, W. D., JR.
FREY, L. J., JR.

GEORGE, T. W.
GERVAIS, R. L.
GERZINA, A. W., CAPT.
GIBSON, J. E.
GIMALOUSKI, E. A.
GOODE, J. E.
GORTON, C. A.
GRAN, W.
GREENE, J. E.
GRINDSTAFF, C. E.
GROSS, R. J.

HAAK, E. L.
HARRIS, G.
HARRISON, R. T.
HASTINGS, R. P., LT.

Chrysler Corporation
Cornell Aeronautical Lab., Inc.
Irving Air Chute Company
NASA - Ames Research Center
Flight Sciences Laboratory
ASD(ASRMFD-1)
Autonetics Company
ASD(ASZR)
Hayes International Corp.
General Electric Company
Chemstrand Company
ASD(ASRMDF)
Frank Ix and Sons

Chance-Vought Corp.
General Electric Company
Narriocot Corporation
ASD(ASNPS-4)
Bell Helicopter Company
Pioneer Parachute Co., Inc.

Space Vehicle/M
E. I. duPont de Nemours & Co.
MCFL / AFLC
U. S. Naval Parachute Facility
U. S. Naval Ordnance Laboratory
Hq. USAF (AFRAE-S)
Hayes International Corporation
Fabric Research Laboratory
U. S. Army Munitions Command

Celanese Corporation
Douglas Aircraft Co., Inc.
ASD(ASRMFD-2)
Rand Corporation
Pioneer Parachute Co., Inc.
General Dynamics Corp./Fort Worth
Hoskins Manufacturing Company
Cook Electric Company
NASA
ASD(ASNPS-4)
ASD(ASRMFD)

University of Minnesota
Amerotron Company
Minneapolis-Honeywell Reg. Co.
6511th Test Group (Parachute)

HAWKENS, E. A., COL. —
 HEDGEPEETH, J. M., DR.
 HEGELE, A. M.
 HEINRICH, H. G., DR.
 HEITCHUE, R. D.
 HERDRICK, W. F., CAPT.
 HESS, S. R.
 HILDEBRANDT, L. H.
 HILL, W. R.
 HOLTON, H. F.
 HUG, W. B.
 HUNTER, W. C.
 HURTT, W. W.

IBRAHIM, S. K.

JACKSON, J. T.
 JACKSON, S. W.
 JAREMENKO, I. M.
 JELLISON, R. P., LT.
 JOBE, C. E.
 JOHNSON, D. E.
 JOHNSON, E. G.
 JONES, D. J.
 JOSHI, K.

KAGAN, M. G.
 KANOWSKI, M. B., CWO
 KATZ, G. D.
 KEISTER, P. H., PROF.
 KEPLER, G. H.
 KENNEDY, R. M.
 KENNET, H.
 KIETH, R.
 KIRCHNER, O.
 KLINE, J. E.
 KNACKE, T. W.
 KOOCHEMBERE, C.
 KRAMER, J. F.

LANGENDERFER, K. S.
 LEONARD, P. A.
 LEWIS, W. R.
 LIEFKE, A.

ASD(ASRMP)
 Martin-Marietta Corporation
 ASD(ASNPPSP)
 University of Minnesota
 Douglas Aircraft Company
 Kirtland AFB, N. Mex.
 University of Minnesota
 ASD(ASRMF)
 All American Engineering Co.
 ASD(ASNPPSP-4)
 Frank Ix and Sons
 ASD(ASRMFD)
 Lockheed Missile and Space Co.

University of Minnesota

General Dynamics Corp./Convair
 QM R&E Command
 Goodyear Aircraft Corporation
 6511th Test Group (Parachute)
 ASD(Flight Dynamics Laboratory)
 Arthur D. Little, Inc.
 Aeronautical Research Laboratory
 General Dynamics Corp./Convair
 Technology, Inc.

Pioneer Parachute Company
 6511th Test Group (Parachute)
 GE - MSD
 MCLI-SE/Dept. of Mechanics
 Thiokol Company
 Grumman Aircraft Eng. Corp.
 Boeing Co./ Aerospace Division
 University of Dayton
 Boeing Co./Aerospace Division
 ASD(ASNPPSP-1)
 Northrop Ventura
 Naval Air Material Center
 Cook Electric Company

ASD(ASNDSR)
 North American Aviation, Inc.
 QM R&E Command
 Cook Electric Company

LIBBEY, C. E.
LINDGREN, M. J.
LLOYD, J. T.
LOOK, B. C.
LORENZ, L.
LOVE, C. C., JR.
LOZAR, W. R.

MARTIN, D.
MATSUO, J. T., MAJ.
MATTESON, H. C.
MAZZOLA, L. L.
McFARLAND, S.
McGRATH, J.
MEEK, T. B., JR.
MELVIN, B. W.
MESSNER, J.
METRES, S. R.
MILLIKEN, S. A.
MINARDI, J.
MITCHELL, N. E.
MORISSET, B.
MURRAY, J. E., LT. COL.
MURRAY, P. R.
MUTIMER, G. R.
MUZZEY, C.
MYERS, E. C.
MYRON, MR.

NEBIKER, F. R.
NICCUM, R. J.
NIELSEN, J. N.
NYLAND, F. S.

PATTON, E. L.

PEDERSON, P.
PEPPER, W.
PERCARPIO, E. P.
PERKINS, J. M.
PINNELL, W. R.
POHL, R. A.
PRUYN, R. R.
PUDDYCOMB, R. H.

RABER, N.
RAY, P.
REGETZ, J. D.

NASA, Langley Research Center
Lockheed Missile and Space Co.
Lockheed Missile and Space Co.
NASA - Ames Research Center
Cook Electric Company
General Dynamics Corporation
U.S. Rubber Company

R.D.P. Associates
ASD(ASNFPSP-4)
General Dynamics Corp./Convair
Arthur D. Little, Inc.
ASD(ASRMFD-2)
ASD(ASRCNF)
Sikorsky Aircraft Corp.
E. I. duPont de Nemours & Co.
Olmsted AFB, Pa.
ASD(ASRMFD-2)
General Dynamics Corp.
University of Dayton
Douglas Aircraft Corp.
Chrysler Corporation
Hq. USAF /Wash. D. C.
ASD - Deputy for Technology
Northrop-Ventura
Cornell Aeronautical Lab.
6511th Test Group (Parachute)
Rand Corporation

Goodyear Aircraft Corp.
University of Minnesota
Vidya, Inc.
Rand Corporation

Southern Utilization Research
and Development Division
Cook Electric Company
Sandia Corporation
U. S. Rubber Company
U. S. Naval Missile Center
ASD(ASRMFD-2)
Raven Industries, Inc.
Kellett Aircraft Corp.
6511th Test Group (Parachute)

Olmsted AFB, Pa.
Technology, Incorporated
NASA

REITZ, R.
RHODES, A. S.
RICLES, R.
RIFFLE, A. B.
ROGALLO, F. M.
ROSE, P. H.
ROSS, J. H.
ROSWURM, LT. COL.
RUBLE, F.

SANDERSON, R. J.
SCESA, S.
SCHAUWEKER, J. E.
SCHMALHOFFER, J. E., JR.
SCHMARGE, D. P., LT.
SCHULTZ, E.
SCOTT, C. J.
SCULLEY, L. J.
SEPP, O. W.
SHAPLAND, D., DR.
SHICHMAN, D.
SHINE, A. J., DR.
SINGLETON, R. W.
SLAGLE, C. V.
SLOAN, G. J.
SNAVELY, R. C., CAPT.
SOLT, G. A., JR.
SOPCZAK, S. S.
SPARROW, W. T.
SPENCER, J.
SPINNER, MR.
SPINOSA, D.
STAUBER, E.
STEINTHAL, M. B., JR.
STONE, B. T.
STOODY, H. A.
SULLIVAN, T.

TENTE, A. S.
THOMAS, J.
THOMASSON, F. T.
TROTT, MR.
TURNER, C.
TYNDALL, R.

ASD(ASRM00)
Kelly AFB, Texas
Republic Aviation Corp.
ASD(ASRMFD-1)
NASA - Langley Research Center
AVCO-Everett Research Lab.
ASD(ASRCNF)
6511th Test Group (Parachute)
Goodyear Aircraft Corp.

Stanley Aviation Corporation
Rand Corporation
ASD(ASR00-1)
ASD(ASRMFD-2)
6511th Test Group (Parachute)
Kaman Aircraft Corporation
University of Minnesota
Irving Air Chute Co., Inc.
M. Steinthal and Co., Inc.
Stanley Aviation Corporation
U. S. Rubber Company
Air Force Institute of Technology
Celanese Corporation
Temco Aerosystems
U. S. Naval Ordnance Lab.
Hq. Space Systems Division
ASD(ASRMFD)
Minneapolis-Honeywell Reg. Co.
Martin Company
General Electric Company
Hoskins Manufacturing Co.
Rocket Jet Engineering Co.
N. Mexico State University
M. Steinthal and Co., Inc.
NASA - Lewis Research Center
Kaman Aircraft Corporation
Cook Electric Company

Fairchild-Stratos Company
N. Mexico State University
Bureau of Naval Weapons
U. S. Naval Missile Center
General Dynamics Corp./Pomona
ASD(ASNDFD)

UJIHARA, B.

North American Aviation, Inc.

VARBLE, A. E.
VELKOFF, H.

ASD(ASNPSP-1)
ASD(ASRMPE)

WALCOTT, W.
WALKER, J. J.
WALKER, R. H., JR.
WATSON, L. L.
WEAVER, MR.
WEINTRAUB, P. L.
WHATLEY, W.
WHITFORD, D.
WHITNEY, J.
WILES, H. O., CAPT.
WINEBRENNER, L. E., LT. COL.
WINKER, J. A.
WOOD, J.
WOODIS, W.
WONG, L.
WRIGHT, N. A.

Technology, Incorporated
General Dynamics Corp./Fort Worth
ASD(ASRMFD-2)
ASD(ASRMFD-1)
Owens-Corning Co.
6511th Test Group (Parachute)
ASD(ASRM00)
University of Dayton
ASD(ASRCNF)
AFSWC(SWVWP)
ASD(ASRMF)
Raven Industries, Inc.
R. D. P. Associates
Martin Company
Hughes Aircraft Company
All American Engineering Co.

YOUNGMAN, MR.
YUSKA, J. A.

General Electric Company
NASA - Lewis Research Center

ZELINSKAS, G. A.
ZIMMER, G. F.

ASD(ASNPSP-2)
Lockheed Corporation

Aeronautical Systems Division, Dir/Aero-
mechanics, Flight Accessories Lab, Wright-
Patterson AFB, Ohio.
Rpt No. ASD-TDR-63-329, PROCEEDINGS OF
RETARDATION AND RECOVERY SYMPOSIUM. Final
report, May 63, 500p. incl illus., tables,
and refs.

Unclassified Report

This report contains the proceedings of the
Retardation and Recovery Symposium sponsored
by ASD 13 and 14 Nov 62. The Introductory
Session was opened with the Keynote Address
which reviewed the use and applications of
deployable aerodynamic decelerators through-

(over)

out the past 50 years and noted the areas in
which additional work had to be accomplished.
The four Technical Sessions deal with the
latest significant developments in the retard-
ation and recovery area. They begin with pre-
sentations and discussions of investigations
in hypersonic and supersonic flight regimes;
technical analyses of transonic and supersonic
flow phenomena follow. New aerodynamic decel-
erator designs and discussion of the wind
tunnel tests pertaining to them, as well as
overall reliability of recovery systems, are
also presented. The final Technical Session
concludes with a discussion of the military,
scientific, and general objectives for decel-
erators intended for future use.

1. Hypersonic Regime
2. Supersonic Regime
3. Deceleration In-
vestigations
4. Recovery Systems
I. A.W. Gerzins, Capt,
USAF, Monitor
II. Aval fr OTS
III. In ASTIA collection

Aeronautical Systems Division, Dir/Aero-
mechanics, Flight Accessories Lab, Wright-
Patterson AFB, Ohio.
Rpt No. ASD-TDR-63-329, PROCEEDINGS OF
RETARDATION AND RECOVERY SYMPOSIUM. Final
report, May 63, 500p. incl illus., tables,
and refs.

Unclassified Report

This report contains the proceedings of the
Retardation and Recovery Symposium sponsored
by ASD 13 and 14 Nov 62. The Introductory
Session was opened with the Keynote Address
which reviewed the use and applications of
deployable aerodynamic decelerators through-

(over)

out the past 50 years and noted the areas in
which additional work had to be accomplished.
The four Technical Sessions deal with the
latest significant developments in the retard-
ation and recovery area. They begin with pre-
sentations and discussions of investigations
in hypersonic and supersonic flight regimes;
technical analyses of transonic and supersonic
flow phenomena follow. New aerodynamic decel-
erator designs and discussion of the wind
tunnel tests pertaining to them, as well as
overall reliability of recovery systems, are
also presented. The final Technical Session
concludes with a discussion of the military,
scientific, and general objectives for decel-
erators intended for future use.

1. Hypersonic Regime
2. Supersonic Regime
3. Deceleration In-
vestigations
4. Recovery Systems
I. A.W. Gerzins, Capt,
USAF, Monitor
II. Aval fr OTS
III. In ASTIA collection